Systematic Study of OX40 Ligand Context-Dependent Function on Human T Helper Cell Polarization

Léa Karpf

université PARIS-SACLAY

Systematic study of OX40 Ligand context-dependent function on human T helper cell polarization

Thèse de doctorat de l'université Paris-Saclay

École doctorale n°582, Cancérologie, Biologie, Médecine, Santé (CBMS)
Spécialité de doctorat : Aspects moléculaires et cellulaires de la biologie
Unités de recherche : U932, Institut Curie & U976, Institut de Recherche Saint-Louis
Référent : Faculté de Médecine

Thèse présentée et soutenue en visioconférence totale, le 27 novembre 2020, par

Léa Karpf

Composition du Jury

Jean-Christophe Bories Directeur de recherche, Hôpital Saint-Louis (UMR-976 INSERM)	Président du jury
Claire Hivroz Chef d'équipe, HDR, Institut Curie (UMR-932 INSERM)	Rapporteur et examinatrice
Lars Rogge PhD, HDR, Institut Pasteur (URA-1961 CNRS)	Rapporteur et examinateur
Géraldine Schlecht-Louf PU, Université Paris-Saclay (UMR-996 INSERM)	Examinateur
Vassili Soumelis Chef d'équipe, Hôpital Saint-Louis (UMR-976 INSERM)	Directeur de thèse

Thèse de doctorat

NNT : 2020UPASL044

TABLE OF CONTENT

ACKNOWLEDGMENTS

Je tiens tout d'abord à remercier les membres de mon jury d'avoir accepté d'évaluer ce travail de thèse. Je remercie chaleureusement le Dr Claire Hivroz et le Dr Lars Rogge d'avoir pris le temps d'évaluer mon manuscrit de thèse et je remercie également le Dr Géraldine Schlecht-Louf et le Dr Jean-Christophe Bories d'avoir accepté d'examiner mes travaux de thèse.

Un très grand merci à mon directeur de thèse, Vassili, de m'avoir accueilli au sein de son équipe et de m'avoir donné l'opportunité d'enrichir mon parcours scientifique. Merci de m'avoir permis d'intégrer cette équipe, de m'avoir fait confiance et de m'avoir donné la liberté de tester mes idées pendant ces trois ans de thèse.

Je tiens à remercier l'Université Paris Saclay et l'École Doctorale de Cancérologie, Biologie, Médecine et Santé de m'avoir donné l'opportunité et de m'avoir financé pour effectuer cette thèse. Je remercie également le Dr Sebastian Amigorena de m'avoir accueilli au sein de l'unité U932 à l'Institut Curie pendant mes deux premières années de thèse et Dr Armand Bensussan et Pr Vassili Soumelis au sein de l'unité U976 à l'Hôpital Saint-Louis pour ma dernière année.

Beaucoup de personnes m'ont aidé et soutenu pendant cette thèse, dans l'équipe et à l'extérieur, la liste est longue !

Tout d'abord, je tiens à remercier du fond du cœur Coline « ma maman de labo », sans qui cette thèse aurait eu une bien autre tournure ! Mille mercis pour ton soutien et ton aide tout le long de cette thèse (je ne sais pas ce que j'aurais fait sans toi !). Je suis vraiment heureuse qu'on ait eu l'occasion de travailler ensemble sur ce projet OX40L, notre chouchou ! Tu m'as énormément apporté en termes de réflexion scientifique, d'organisation d'expériences, d'écriture de papier et de manuscrit, et en plus j'ai eu la chance d'être formée par la Queen des manips. Merci d'avoir relativisé des erreurs que je voyais comme catastrophiques, de m'avoir motivé à mieux organiser ma hotte en la comparant à la tienne (non je ne vois pas la différence…), de m'avoir soutenu psychologiquement (et expérimentalement) dans les moments plus difficiles, ça a été extrêmement formateur pour moi. Et pour finir, merci pour ta patience (cf : « Mais comment on va faire pour la manip je ne suis pas là ce week-end !!! Mais si Léa, c'est le week-end prochain où tu n'es pas là (x4)…), et bien sûr pour ton amitié (qui elle durera évidemment après la thèse !). Vive le houmous, les pizzas et les rires ! Un peu moins les manips à 250 conditions, LA journée de la mort, et les manips avec 15 plaques de culture… Mais bon la difficulté rapproche ! Enfin bref, merci pour tout !

Je tiens à remercier Max pour toute l'aide qu'il m'a apporté pendant cette thèse, que ce soit pour la réflexion scientifique, la mise en place des expériences, le pratico-pratique des manips et toutes les rigolades dans le L2 ! Merci du fond du cœur d'avoir pris tout ce temps alors que tu étais en fin de thèse, d'avoir toujours répondu à mes questions (calmement…ou pas) et d'avoir pris le temps pour me former, ça a été un tremplin vraiment essentiel pour ma thèse.

Je tiens à remercier Philémon qui a aussi été une personne essentielle de ce doctorat. Merci d'avoir été mon mentor cancer (un peu glauque dis comme ça) ! Merci de m'avoir appris toutes les techniques nécessaires pour l'analyse des tumeurs, de m'avoir appris à les distinguer et à mieux percevoir leurs caractéristiques spécifiques, d'avoir sauvé des catastrophes (qui n'étaient parfois que dans ma tête !). Et bien sûr pour toutes les looongues discussions sur la vie en général, et pour nos déjeuner Fricadelle, tu m'as beaucoup manqué à Saint-Louis !

Je tiens à remercier chaleureusement Lilith, ma super-héroïne des biostats ! Tu m'as presque appris à les aimer (presque) ! Merci pour toute l'aide que tu m'as apporté pendant cette thèse, que ce soit sur le projet checkpoints tumeur ou le projet OX40L. Tu as été un moteur essentiel à l'avancée de ces projets et je suis très heureuse d'avoir pu travailler avec une personne aussi talentueuse, raisonnée et appliquée que toi !

Un immense merci à Justine qui apporté une touche de bonheur lors de cette thèse ! Avec toi, le « Général Caché » est devenu un lieu incontournable, nécessaire et essentiel à nos santés mentales de thésardes. Il a été le QG de discussions professionnelles et personnelles intenses, riches en confidences, en rires et en émotions ! Je suis extrêmement heureuse que nos thèses respectives nous aient mis sur le chemin l'une de l'autre.

Je souhaite bien évidemment également remercier tous les anciens et nouveaux membres de l'équipe : Camille, Caroline, Pierre, Sarantis, Charlotte, Elise, Floriane, Maude, Arturo, Faezeh, Omar, Rabie, Alain, Fanny, Lucile, Jasna, Alba, Iris, Mélissa, Anne-Sophie, Maëva et Sara. Merci pour votre soutien et vos commentaires constructifs tout le long de cette thèse !

Je tiens ensuite à remercier des personnes de Curie qui m'ont été chères pendant ce doctorat. Tout d'abord, un énorme merci à Alice, qui est très rapidement passé de voisine de bureau à amie. En plus de nos entraides thésardes, ce doctorat nous a permis de passer de longues soirées de discussions et de rires à la montagne et d'exceller en danse d'agence immobilière (à défaut ne pas voir été assidues en zumba (en même temps entre la zumba et la montagne le choix est vite fait) et en moderne jazz pour ma part).

Je tiens également à remercier de tout mon cœur Anastasia, la gentillesse, la spontanéité et l'attention, et Émeline, la gentillesse, la sagesse et l'assurance, un petit duo qui a enrichi ce doctorat en sciences et en rires et qui m'ont aussi soutenu sans faille dans les moments plus difficiles.
Et bien sûr merci à tous les membres du bureau étudiant, the place to be !

Je tiens à remercier Mélanie, qui m'a également beaucoup aidé en début de thèse et qui a pris beaucoup de son temps pour répondre à mes nombreuses questions sur les petites cellules T. Même si entendre « Mélanie, j'ai une petite question » a fini par te donner de l'urticaire, merci pour tes précieux conseils et d'avoir persévérer même lorsqu'une même question revenait plusieurs fois en une semaine… Et merci d'avoir apporté de la joie dans le L2 en le transformant en dancefloor !!
PS : Pour Mélanie et Max, sachez que je ne suis plus stagiaire !!!

Je tiens aussi à remercier chaleureusement Hélène pour sa présence et son soutien. J'ai été extrêmement heureuse que tu rentres en France et de te retrouver à Curie, après avoir eu la chance de travailler avec toi à Mont Sinai. Merci pour toute l'aide que tu m'as apporté, qu'elle soit professionnellement ou personnelle, pour ton écoute, ton soutien, ta disponibilité à tout moment, et pour ton amitié.

Et enfin il y a bien sur la famille et les amis qui aident énormément !
Merci à mes parents et ma sœur, d'avoir toujours été là pour moi et de m'avoir soutenu de toutes les manières possibles pendant ces trois ans (même quand vous n'en pouviez plus de m'entendre râler pour la énième fois !).
Merci à Sylvain pour ton amour, ta sagesse d'esprit et ton soutien inébranlable.
Merci à tous mes amis, et principalement Élise (avec qui on a en plus pu travailler ensemble, et travailler avec ses meilleurs amis c'est le top !), Thibaut (entre Paris, Londres et Berlin, loin de yeux mais proche du cœur), Lola (amitié retrouvée et réconfortante, autour de délicieux verres de vin), Inès (rayon de soleil souvenir du « bon vieux temps »), Camille (une énergie positive et attentionnée à l'état pur), Tiffany (évasion de rire, TSFS j'ai retenu je crois), Malina (entre copines thésardes on se soutient !)…

Finalement, cette thèse a été un cocktail de hauts et de bas, de persévérances et de découragements, d'euphories et de déceptions, de moments joyeux et d'autres plus difficiles mais on y arrive ! Je suis très heureuse et fière de pouvoir vous présenter à tous ces trois années de travail.

LIST OF FIGURES AND TABLES

LIST OF ABBREVIATIONS

AD: atopic dermatitis

AHR: aryl hydrocarbon receptor

APC: antigen presenting cell

Ascl2: Achaete-Scute homologue 2 transcription factor

BAFT3: basic leucine zipper ATF-like transcription factor 3

Bcl6: B cell lymphoma 6

BCR: B cell receptor

bDC: blood DC

CD: cluster of differentiation

cDC: conventional DC

CTLA-4: cytotoxic T-lymphocyte associated protein 4

CXCR: CXC Chemokine Receptor

DAMP: damage-associated molecular pattern

DC: dendritic cell

EAE: experimental auto-immune encephalomyelitis

E. coli: Escherichia coli

FBS: fetal bovine serum

FDA: U.S Food and Drug Administration

FDC: follicular dendritic cells

FoxP3: forkhead box transcription factor

FRC: fibroblastic reticular cell

HCV: hepatitis C virus

HEV: high endothelial venule

HHV-8: human herpes virus 8

HNSCC: head and neck squamous cell carcinoma

IBD: inflammatory bowel disease

ICOS: inducible T cell co-stimulator

ICOSL: inducible T cell co-stimulator ligand

IDO: indoleamine 2,3-dioxygenase

IFN: interferon

Ig: immunoglobulin

IL: interleukin

IL-2R: IL-2 receptor

iTreg: induced regulatory T cell

KO: knock-out

KS: Kaposi Sarcoma

LAG-3: Lymphocyte-activation gene 3

LC: Langerhans cell

LCMV: lymphocytic choriomeningitis virus

LFA-1: lymphocyte function associated antigen 1

LMM: linear mixed model

LPS: Lipopolysaccharides

MHC: major histocompatibility complex

MLR: mixed-lymphocyte reaction

MoDC: monocyte-derived dendritic cell

NK: natural killer

NKT: natural killer T

nTreg: nature regulatory T cell

OX40L: OX40 Ligand

Pam3: Pam3Csk4

PAMP: pathogen-associated molecular pattern

PCA: principal component analysis

PD-1: programmed cell death 1

pDC: plasmacytoid DC

PolyI:C: polyinosinic:polycytidylic acid

RA: rheumatoid arthritis

rhOX40L: human recombinant OX40L protein

SLE: systemic lupus erythematosus

SLO: secondary lymphoid organ

STAT: signal transducer and activator of transcription

TRAF: TNFR-associated factors

Tbx: T box transcription factor

TCR: T cell receptor

Tfh: T follicular helper

Th: T helper

TIGIT: T Cell Immunoreceptor With Ig And ITIM Domains

TIL: tumor-infiltrating lymphocyte

TIM-3: T-cell immunoglobulin and mucin-domain containing-3

TLR: toll-like receptor

TLS: tertiary lymphoid structure

TME: tumor microenvironment

TNFRSF: Tumor necrosis factor receptor superfamily

TNFSF: tumor necrosis factor superfamily

TRC: T cell zone reticular cells

TSLP: thymic stromal lymphopoietin

Treg: regulatory T cell

WT: wild-type

YFV: yellow fever virus

INTRODUCTION

I) CD4 T cell: a central player of adaptive immunity

1) CD4 T cell ontology

a) Immunology basic concepts

The immune system can be defined as our “body bodyguard”. Indeed, it has a protective role and defends our body against non-self-pathogens. More precisely, this system is divided into two different immune mechanisms, with specific functions: innate and adaptive immunities.

On the one hand, the innate immune system acts as a first barrier to provide an immediate response against an identified exogenous pathogen. It is composed of phagocytic cells that can recognize and kill non-self-organisms rapidly and unspecifically. Different cell types are found according to the anatomical location. Granulocytes (neutrophils, eosinophils and basophils) and monocytes are present in the blood whereas macrophages and mast cells are present in tissues. Moreover, natural killer (NK) cells have important functions in innate immunity.

On the other hand, adaptive immunity is longer to set up, but that is the price for developing a specific response against pathogens. CD4 and CD8 T cells and B cells belong to this second type of immunity. Contrary to innate cells that recognize antigens unspecifically, these cells recognize specific pathogenic antigen through particular receptors: T cell receptor (TCR) and B cell receptor (BCR). In the T cell lineage, CD4 T cells are also called CD4 T helper (Th) cells. As their name suggests, these cells help other cell types by providing them signals that impact their activation and behavior. Thus, CD4 T cells orchestrate immune response and guide it according to the encountered pathogen. CD8 T cells are specialized in fighting against intracellular pathogens such as viruses by killing infected cells. Finally, B cells that differentiate into antibody-producing plasma cells, are specialized in extracellular pathogen elimination.

Between innate and adaptive immunities, one cell type orchestrates this complex organization: dendritic cells (DCs).

This manuscript will be principally focused on CD4 T helper cells and their polarizing capacities.

b) CD4 T cell: from thymus to lymph node

T lymphocyte precursors migrate from the bone marrow to populate the thymus and undergo their maturation. During the thymic development, TCR gene rearrangement and thymocyte proliferation occur. Moreover, this is the step where the TCR co-receptor is chosen. Cell-surface molecule modifications allow distinguishing the thymocyte population at different stages of maturation. Beyond these molecules, T cells notably express both CD4 and CD8 co-receptors at the beginning of their development and, after different steps of selections based on recognition of major histocompatibility complex (MHC) I or II, they will exit the thymus expressing only one of them.

After becoming a mature naive CD4 T cell, the next step is to access secondary lymphoid organs, mainly lymph nodes. Particulate antigens, antigen-presenting cells (APC) and some leukocytes coming from peripheral tissues migrate to lymph nodes through the lymphatic system. On their side, naive CD4 T cells circulate in the bloodstream and enter lymph nodes by following a CCL19/CCL21 chemokine gradient and via specialized structures called high endothelial venules (HEV). Then, they gather in the paracortex, also called the T cell zone. Paracortex microarchitecture is supported and organized by a subset of fibroblastic reticular cells (FRC), the T cell zone reticular cells (TRC). These cells are essential to T cells homing, survival and migration by expressing a large panel of adhesion molecules and secreting the chemoattracting chemokines CCL19 and CCL21, and the survival factor interleukin (IL) 7. They also form a very dense meshwork all along the T cell zone, allowing DC and T cell migration and thus promoting their interaction [1].

Afterwards, T cells have to get activated by a DC. T cells screen MHC-peptide complexes at the surface of DCs present in the same lymph node zone, looking for their specific antigen. Since one naive CD4 T cell is specific for one particular antigen, the screening has to be very efficient to set up an adaptive immune response as quickly as possible. A T cell encounters a multitude of DCs, with which it transiently interacts using adhesion molecules such as lymphocyte function-associated antigen 1 (LFA-1). If a T cell does not find its specific MHC-peptide complex, it reaches the bloodstream to start again in another lymph node [1].

2) T cells and antigen presenting cells encounter in the lymph node

a) Dendritic cell patrolling and activation

Three different cell types can present antigen to T cells: DCs, macrophages and B cells. Here, the focus will be on dendritic cells, which are the most efficient to activate T cells. One of the reasons why DCs are professional antigen presenting cells (APCs) is that display more MHC and co-stimulatory molecules than the others [2].

DCs migrate from bone marrow to tissue through blood, seeking non-self-agents throughout the body. They are specialized in the uptake of broad variety of pathogens such as bacteria, fungi, parasites and viruses.

To detect a wide range of pathogens from different natures, they display extracellular and intracellular signaling receptors. Immature DCs express pattern recognition receptors (PRRs), that can recognize pathogen-associated molecular patterns (PAMPs) and damage-associated molecular patterns (DAMPs). PRRs include mainly two groups of receptor: transmembrane proteins such as toll-like receptors (TLR), cytoplasmic proteins such as NOD-like receptors (NLRs) and C-type lectin receptor (CLR) [3].

Immature DCs continuously patrol throughout tissues. The encounter between circulating immature DCs and danger signals (pathogens or inflammatory signals) engages a process of maturation, and their migration to the lymph node. Moreover, antigens that have been captured by DCs are processed as peptides and presented on MHC molecules, constituting a peptide-MHC complex. Thus, upon arrival in the lymph node, they highly express peptide-MHC complexes and co-stimulatory molecules, to be fully competent to prime naive T cells [4]. In absence of pathogen or inflammatory signal (steady-state), DCs can present self-antigens instead of exogenous antigens from pathogens. The goal of this process is to prevent immunization against self-proteins, which is also known as tolerance. In the case of tolerance, self-antigen presentation leads to the induction of regulatory T cells (Treg). Instead of producing inflammatory signals to activate downstream immune effectors, Treg will secrete anti-inflammatory signals to dampen the inflammation. Recognition of self-antigen could also lead to anergy, which means that T cells are unable to mount a complete immune response. This is illustrated in Figure 1.

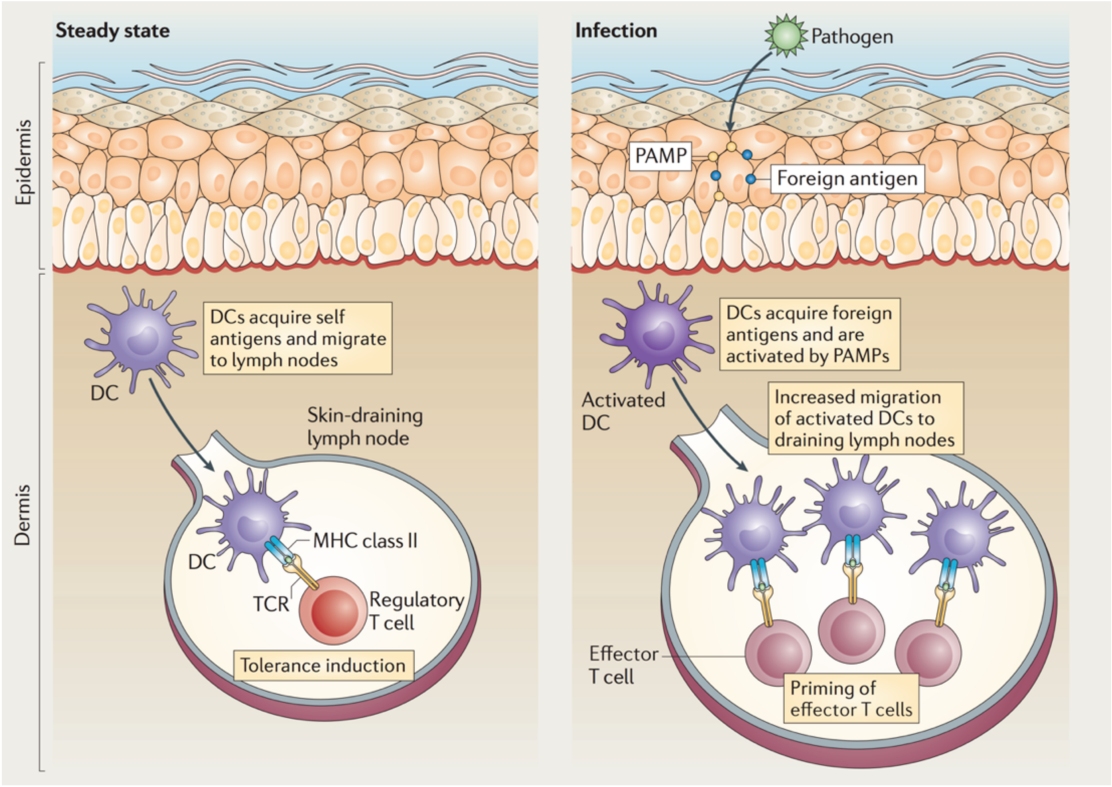

Figure 1: T cell-mediated adaptive immune response initiation

(Illustration from Summer DeLuca et al. Nat Rev Immunol, 2012 [5])

b) T cell polarization by dendritic cells: the three-signal theory

As described above, naive CD4 T cells are screening MHC-peptide complexes, seeking their specific antigen. When they find the right match, DC activates and differentiates the T cell in a specific way, according to the peptide it presents. This is described by the three-signal theory depicted in Figure 2.

The first activating signal for T cell consists of TCR activation. The TCR recognizes peptide presented on the DC MHC. Nevertheless, this signal is not sufficient to ensure Th differentiation.

A second signal is necessary for T cells to begin clonal expansion, develop their effector functions and avoid becoming anergic. This co-stimulatory signal is mediated by CD28 on the T cell, binding to CD80/CD86 molecules on the DC. It allows CD40 Ligand (CD40L) expression but also IL-2 receptor (IL-2R) expression and IL-2 cytokine secretion. IL-2 fixation on IL-2R ensures T cell survival and proliferation, in an autocrine and paracrine way.

Finally, the T cell needs a third signal to bifurcate in the appropriate T cell polarization program. Thus, DCs secrete different cytokines and express a large set of surface molecules that constitute the last signal for T cell activation and differentiation, allowing CD4 T helper cells to be polarized in a subset with specific functions, consistent with the pathogen to eliminate [6].

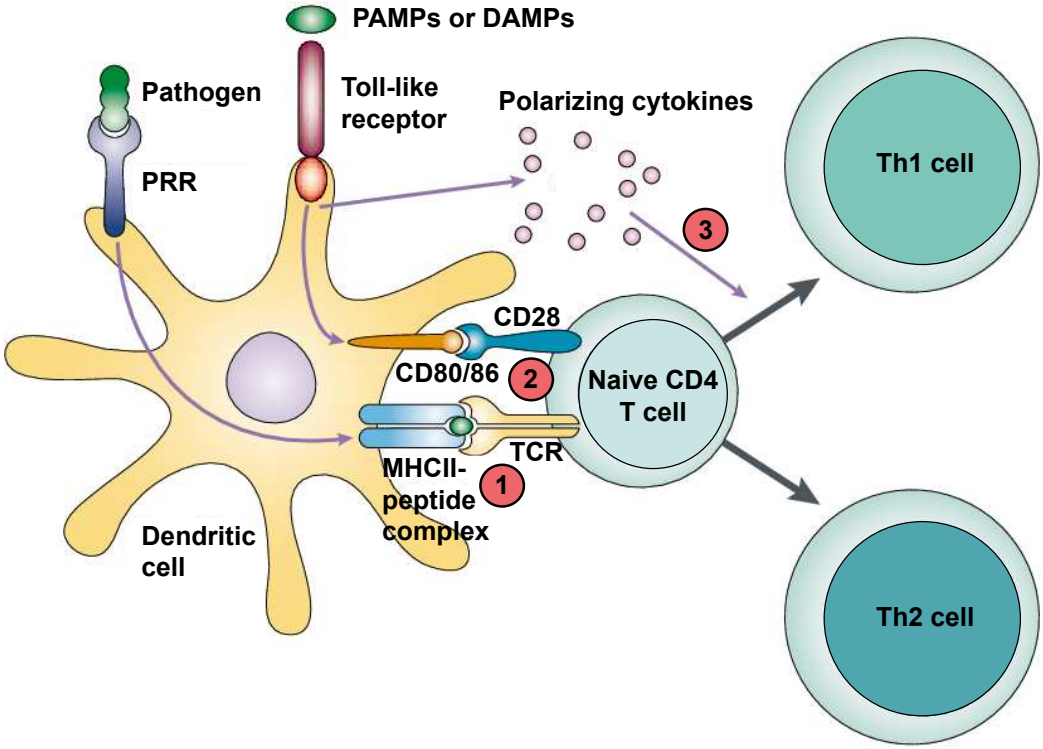

Figure 2: The three-signal theory of naive CD4 T cell activation

1: TCR activation signal; 2: co-stimulatory molecule signal; 3: cytokine signal (Illustration adapted from Medzhitov et al. Nat Rev Immunol, 2001 [7])

A naive CD4 T cell can therefore mature into different types of T helper cell subsets, that will be studied in more detail in the next part.

This Th differentiation model is very useful to have a clear idea of how do naive CD4 T cells polarize. However, many different views were published over the years, contradicting this theoretical version. Its limits will be reviewed in the second part of this introduction.

3) T helper cell diversity

a) Historical highlight on the function of Th cells

In the '60s, T lymphocytes started to be distinguished from B lymphocytes, but their functions were reduced to help B cells in their antibody production [8,9].

In the '70s, T lymphocytes were classified according to their surface markers in either helper cells or cytotoxic cells [10].

Finally, in the '80s, Mosmann and Coffman were the first to highlight the concept of Th subsets. After immunizing mice with antigen proteins, they managed to derive *in vitro* two Th clones: Th1 and Th2 [11]. They differentiated Th1 and Th2 mostly according to the cytokines (at the time called lymphokines) they secreted. Th1 cells are specialized in secreting IL-2 and interferon (IFN) γ and Th2 in secreting IL-4, IL-5 and IL-13 [12].
Three years later, they described in greater detail in the Annual Review of Immunology that, within T lymphocytes, subsets had distinct characteristics suggesting that T lymphocytes could have other functions apart from helping B cells. They hypothesized that Th1 led to cytotoxic mechanisms resulting in the elimination of intracellular parasites and tumor cells, whereas Th2 led to an antibody response [13].

From this arose the concept of division of labor between Th subsets, allowing to efficiently fight against a large variety of pathogens.

b) Th subset phenotypes and functions

As described before, CD4 T helper subsets are defined principally by the cytokines they secrete. In this part, what is characterizing each Th subsets will be studied in detail. T helper cells are currently classified according to the three following parameters. First, how are they induced, what are the necessary signals to polarize a naive T cell in Th1 for instance? A second important factor distinguishing subsets is the transcription factor they express. Finally, they are separated according to the effector cytokines they produce.

i) Th1 and Th2 paradigm

As seen previously, Th1 and Th2 were the first studied subsets. The main role of Th1 is the clearance of intracellular pathogens by different mechanisms such as helping macrophage activation [14] and cytotoxic CD8 T cell response [15]. Based on this last function, Th1 is a major actor in antitumor immunity [16].

A key signal that initiates Th1 polarization is the IL-12 cytokine. This integration induces the signal transducer and activator of transcription 4 (STAT4), following which the transcription factor T-bet is downstream activated to allow IFNγ production [17,18]. Additionally, IFNγ can bind to its receptor at the T cell surface, leading to STAT1 activation, which also has the ability to interact with the Tbx21 gene (T-bet gene). This creates a positive feedback loop enhancing IFNγ production and Th1 commitment. Other molecules can activate STAT1 such as type I IFN and IL-27, an IL-12 cytokine family member [19].

T-bet has a second pro-Th1 role. Indeed, it downregulates the Th2 master regulator GATA-3 not only in developing Th2 cells but also in established ones: the addition of a retroviral T-bet in T-bet knock-out (KO) mice decreases GATA-3 levels [20]. Additionally, Djuretic et al showed that T-bet can also form a complex with the transcription factor Runx3. This cooperation activates the Ifng gene, inhibits Il4 gene [21] and interacts with GATA-3 to suppress its activity [22].

Moreover, besides IFNγ master Th1 secreted cytokine, these cells also produce IL-2, TNF-α and TNF-β [23].

In addition to secreted cytokines, specific surface chemokine receptors have been identified on Th1 cells: CCR5 and CXCR3 [24].

Contrary to Th1 cells that induce cell-mediated immunity, Th2 cells act to help antibody production by B cells and elimination of extracellular pathogens such as parasites. They are induced by the IL-4 cytokine, which activates STAT6 and then GATA-3 [25]. This molecular mechanism leads to IL-4, IL-5, IL-6, IL-9, IL-13 and IL-31 cytokine secretion. Eventually, secreted IL-4 enhanced Th2 profile by creating a feedback loop [26]. Another GATA-3 activating pathway exists through IL-2-induced STAT5 [27].

Th2 cells also express specific surface markers: CCR3 and CCR4 [24].

Principal Th1 and Th2 differentiation mechanisms are summarized in Figure 3.

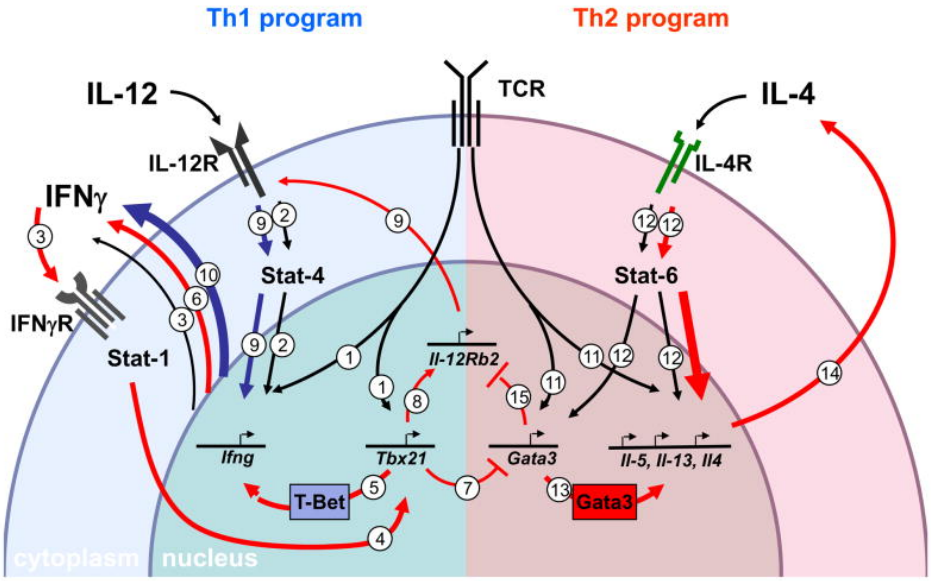

Figure 3: Th1 and Th2 induction model

(Scheme from Amsen et al. Curr Opin Immunol, 2009 [28])

In line with Mosmann and Coffman's work, studies on Th1 and Th2 provided evidence that CD4 T helper cells were composed of several subsets with different functions. This idea has been heightened by the discovery of new subsets, that will be studied in the next subparts.

ii) Th17 cells

The discovery of Th17-related cytokines led to the definition of Th17 cells as an independent CD4 Th subset. The first important breakthrough occurred in 2000. IL-23, constituted of IL-12p40 chain and a new p19 chain, is discovered [29]. A few years later, using experimental auto-immune encephalomyelitis (EAE) mouse model, two different studies demonstrated that IL-23 plays a critical role in the pathology, by driving the development of T cells secreting IL-17 [30,31]. The fact that these cells secreted IL-17 but low level of IFNγ suggested that IL-17-producing T cells could be a distinct lineage from Th1 cells, despite the p40 chain common to IL-12. They were called Th17 cells.

Later on, inducer signals and transcription factors were associated with Th17. For mice, TFG-β and IL-6 were described as the principal inducer cytokines [32,33].

In human models, some teams tried to determine polarizing factors of the subset, a lot of contradictory results came out and it took a while to have a clear idea about how to induce Th17 cells. Some cytokines were highlighted as participating in the differentiation: IL-23, IL-1β, IL-6, TFG-β, IL-21. But cytokine combinations to obtain Th17 cells remained unclear, especially because the combination of TFG-β and IL-6 was not capable of polarizing human Th17 cells, like in mice [34,35]. This raised another issue: human Th17 human differentiation seemed to be different from the mouse one, blurring the characterization even more [34]. Finally, the role of TGF-β and the other cytokines in Th17 differentiation were clarified. Manel et al. showed that TFG-β, IL-1β and IL-23 were required in human Th17 polarization. They also combined successfully TFG-β, IL-1β and IL-6 or IL21 [36]. Their idea of adding IL-21 came up because this cytokine was secreted in response to IL-6 and this allowed Th17 differentiation in mice. This combination was also confirmed by Yang et al [37]. Thus, IL-21 is not necessary but is an important stabilizer of Th17 cells. IL-21 is probably creating a positive feedback loop that enhances Th17 polarization. Eventually, Volpe et al. showed that adding TFG-β in an environment containing IL-23 and pro-inflammatory cytokines (IL-1β and/or IL-6) induced Th17 differentiation [38].

Concerning transcription factors, RORγt as well as RORα were identified as being major transcriptional regulators in Th17 differentiation [36,39,40]. IL-6 and IL-21 can induce RORγt and RORα. IL-23, IL-6 and IL-21 can also activate STAT3, which is necessary for RORγt induction [41,42].

Moreover, regarding surface markers, Th17 cells express CCR6 and CCR4 [43].

Finally, Th17 cells produce different cytokines. Some of them have an important pro-inflammatory role such as IL-17A, IL-17F and IL-22. It has been demonstrated that these cytokines can induce antimicrobial peptide secretion by keratinocytes and epithelial cells [44,45]. Moreover, IL-17A and IL-17F can impact directly neutrophils and enhance their recruitment [46]. Thus, Th17 cells protect against fungi and bacteria at the mucosal and epithelial surfaces.

iii) Th22 cells

Th22 cells have come a long way before being considered as a fully-fledged subset.

IL-22, the master cytokine of Th22 cells, belongs to IL-10 family [47]. In the beginning, this cytokine was associated with Th1 cells since it was the first cell to be identified as an IL-22 producer. Wolk et al. studied the production of this recently described cytokine in human-polarized Th1, Th2 and regulatory T (Treg) cells and showed that Th1 was highly producing IL-22 [48].
Th17 were also described to produce IL-22. As seen above, IL-22 is commonly co-expressed with IL-17A and IL-17F Th17 cytokines. But actually, the Th17 context is not the optimal environment to obtain IL-22 production, because it is inhibited by TGF-β [49,50].

Th22 as an independent subset was established after some studies described IL-22-producing Th cells, in the absence of IL-17, IL-4 or IFNγ. Trifari et al. showed that naive CD4 T cells cultured with IL-1β and IL-23, in the presence or absence of IL-6, led to the production of IL-22 but not IL-17 [51]. Moreover, Volpe et al. demonstrated that IL-17 and IL-22 were differentially regulated and that IL-12 and IL-23 induced high levels of IL-22 [52].
Furthermore, Eyerich et al. provided evidence about Th22 cell phenotype stability. When re-cultured with Th1, Th2, Th17 and Treg-polarizing cytokines, Th22 cells clones, established from psoriasis patient, kept producing IL-22 [53].

In addition to IL-22 production, Th22 cells express CCR6, CCR4 and CCR10 at their surface [51].

Regarding transcription factors, despite a common regulator with Th17 cells, STAT3, the master transcription factor of Th22 cell is AHR [54].

Th22 cells have similar effector functions than Th17 cells. Indeed, Th22 cells induce the production of antimicrobial agents by keratinocytes and epithelial cells, protecting against bacteria and fungi at mucosal and epithelial surfaces. A function that Th22 cells do not share with Th17 cells is that they participate in wound healing [53].

iv) Th9 cells

Th9 case is similar to the Th22 one in the sense that IL-9 was primarily defined as a Th2-associated cytokine [55].

Th9 cells were discovered in 2008, when a study demonstrated that adding TGF-β on Th2 cells induced a new Th subset, producing IL-9. Th2 cells lost their capacities to secrete IL-4 and express

GATA-3, and only kept IL-10 production [56]. At the same time, another study showing similar results added that IL-4 associated with TGF-β could directly differentiate naive CD4 T cells in Th9 cells, without passing through Th2 polarization. Additionally, they demonstrated that Th9 cells did not have suppressive activity despite IL-10 production [57]. Moreover, it has recently been shown in mice that TNF-α promoted polarization, survival and proliferation of Th9 cells *in vitro* [58].

Th9 cells require different transcription factors. The specific one for Th9 cells is PU.1 [59]. It has been described that PU.1 could interact directly with the IL-9 promoter region and interfere with GATA-3 to inhibit Th2 polarization [60,61]. However, GATA-3 and STAT6 also have an indirect role which seems consistent with the importance of IL-4 in Th9 differentiation. Although their role is not clearly established, they seemed to impact by downregulating FoxP3 (that is promoted by TGF-β) [62,63].

Th9 cells have been shown to impact mast cell recruitment and activation. In 2009, Veldhoen et al described an IL-9-induced mast cell activation against helminths, an intestinal nematode [56]. This effect on mast cells showed also positive results on antitumor immunity. Purwar et al. showed that decrease of tumor growth correlated with IL-9 production and Th9 cells among tumor-infiltrating lymphocytes (TILs) and with the presence of mast cells in mice melanoma and lung cancer. It was confirmed by adoptive transfer experiments [64]. Moreover, another study supported the idea that Th9 cells played a role in antitumor immunity, without involving mast cells [65].

v) Regulatory T cells

First of all, regulatory T cells (Treg) are classified into two categories. On the one hand, naturally occurring Treg (tTreg) cells develop in the thymus over different selections. On the other hand, induced Treg (iTreg) cells are differentiated from naive CD4 T cells under tolerogenic conditions and TCR stimulation, outside the thymus. Here the focus will be only on iTreg polarization.

Treg phenotype is commonly described ad $CD4^+CD25^+FoxP3^+$, FoxP3 being the major transcription factor of this subset. Treg cells also express some characteristic, but not specific, surface molecules such as CTLA-4 and GITR [66,67].

A lot of studies described that iTreg generation depends on a high strength TCR signaling and the presence of IL-2 and TFG-β in the microenvironment. Indeed, a suboptimal TCR activation enhanced FoxP3 induction [68]. This TCR activation goes along with the appropriate co-stimulation. CD28 binding to CD80/CD86 has been described to inhibit Treg differentiation. On the contrary, CTLA-4, CD28 competitor, promoted TGF-β-induced FoxP3 [66]. Moreover, TGF-β and IL-2 play a critical role in iTreg differentiation. TGF-β is required for FoxP3 induction and IL-2 for TGF-β-mediated induction of FoxP3 [69–71].
FoxP3 inhibits pro-inflammatory cytokine production such as TNF-α, IFNγ, IL-17, IL-4, by Treg. Treg cells secrete characteristic immunosuppressive cytokines such as IL-10 and TFG-β [72].

Treg cells are essential actors of immune tolerance. They are indispensable to control autoimmunity and inflammation through the body by inducing tolerance. As seen above, immunosuppressive cytokines and co-inhibitory molecules play a role in inhibiting pro-inflammatory responses of T cells and B cells but also dendritic cells, macrophages and NK cells [72,73]. More recently, a study highlighted the role of IL-2 receptor in suppressive mechanisms, showing that IL-2 consumption by Treg helped to control CD8 response [74].

vi) T follicular helper cells

T follicular helper cells (Tfh) were first described in 2000 as CD4 T cell with special features, which were a high CXC Chemokine Receptor (CXCR) 5 expression and the ability to help B cell immunoglobulin (Ig) production directly into germinal center follicles [75]. Besides, CXCR5 is also expressed by B cells that allow them to respond to CXCL13 and form follicles. With this same chemokine receptor, Tfh cells are capable to migrate at the T-B border to meet B cells. Nonetheless, it remains a challenging marker because it rapidly downregulated *in vitro* [76].

Bcl6 and Ascl2 are the master transcription factors of Tfh cells. Bcl6 represses Blimp1, which is known as a Bcl6 antagonist and as an inhibitor of Tfh differentiation [77]. Ascl2 also acts as a suppressor of Th differentiation [78].

The optimal cytokine context for Tfh differentiation is difficult to identify. In mice, IL-6 and IL-21 have been described as important cytokines in this process [79]. In human, some studies showed that IL-12 induces IL-21 secretion [80,81]. Others showed an important role for IL-12 but also TFG-β

and IL-23 [82]. It has also been observed that IL-2 was a limiting factor for Tfh development contrary to its positive effect on other Th subsets [83,84]. In addition to cytokines, co-stimulatory molecules have been identified as important for Tfh induction, such as OX40 [85,86] and inducible T cell co-stimulator (ICOS) [87,88]. Thereby, a clear pathway remains very difficult to establish since Tfh polarization seems to be the result of multiple steps and multifactorial mechanisms.

To distinguish Tfh from Th cells, a first marker is CXCR5. Tfh cells also upregulate programmed cell death 1 (PD-1) and ICOS molecules and secrete IL-21, IL-4 and CXCL13, CXCR5 ligand [89,90].

Tfh cells have different functions related to B cell help. They participate in B cell survival, proliferation, differentiation and maturation. Moreover, Tfh cells have been described to be involved in the germinal center formation and maintenance [91,92].

All CD4 T helper cell characteristics are summarized in the following Table 1.

CD4 T helper subset	Cytokine inducer signals	Master transcription factors	Secreted cytokines	Effector functions
Th1	IL-12 IL-27 IFN	T-bet STAT4 STAT1	IFNγ IL-2 TNF-α TNF-β	Intracellular pathogen clearance Antitumor immunity
Th2	IL-4	GATA-3 STAT6	IL-4 IL-5 IL-6 IL-9 IL-13 IL-31	Extracellular pathogen clearance Humoral response
Th9	IL-4 TFG-β	PU.1 GATA-3 STAT6	IL-9 IL-10	Parasite clearance Mast cell recruitment Antitumor immunity
Th17	TFG-β IL-1β IL-23 IL-6 IL-21	RORγt RORα	IL-17A IL-17F IL-21 IL-22	Antimicrobial properties against extracellular pathogen Neutrophil recruitment
Th22	IL-1β IL-23 IL-6 IL-12	AHR STAT3	IL-22	Antimicrobial properties Wound healing
Tfh	Unclear, possibly a lot of different signals	Bcl6 Ascl2	IL-21 IL-4 CXCL13	B cell help
Treg	TFG-β IL-2	FoxP3	IL-10 TGF-β	Immune tolerance Anti-inflammatory function

Table 1: Characteristics of human CD4 T helper cell subsets

c) Th subset distinction: an old way of thinking?

In the previous part, the classical view of T helper subsets has been shown. This "separatist" vision is useful and necessary to better understand each subset functions and specificities. The idea of distinct subsets arose at the time when Mosmann and Coffman discovered Th1 and Th2, since before that CD4 T lymphocytes were considered only as a cell type helping B cells. It led to a dualistic view of Th subsets. After that, the identification of new subsets increased more and more the Th classification complexity.

Figure 4 shows an overview of the Th subsets in perspective.

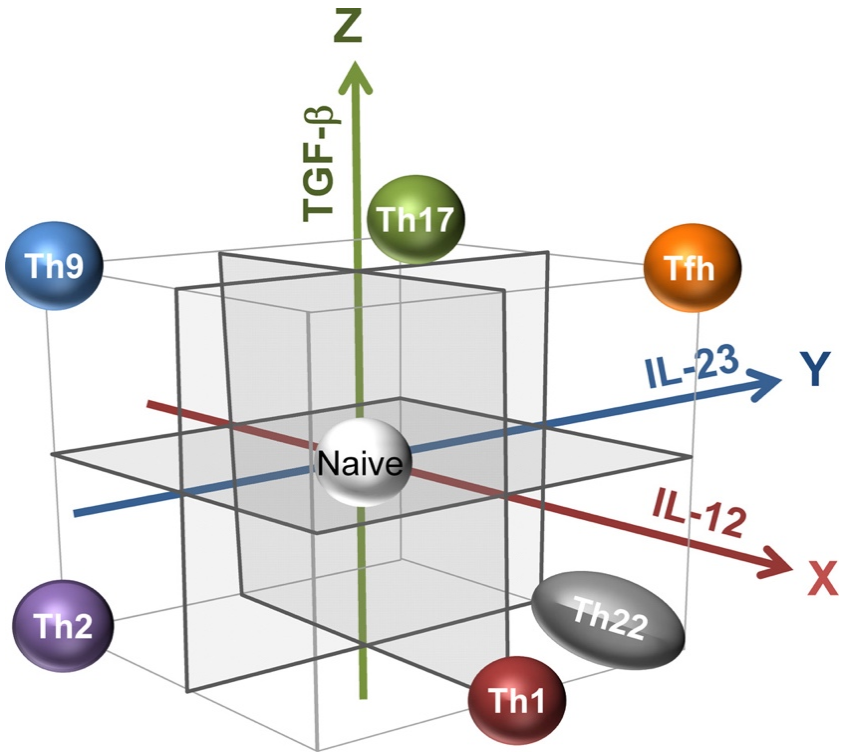

Figure 4: Regulation of human Th differentiation by IL-12, IL-23 and TGF-β

(Illustration from Schmitt et al. Curr Opin Immunol, 2015 [93])

This figure highlights two contradictory ideas. On the one hand, it draws attention to the fact that each subset can be easily classified according to only three cytokines IL-12, IL-23 and TFG-β. On the other hand, the fact that only three molecules can drive such different profiles with such distinct effector functions seems illusory.

As seen previously, subsets such as Th9 or Th22 were recognized after being associated with other subsets. Th2 and Th9 subsets are quite close on the three-dimensional cube. The only difference is the absence or presence of TFG-β. However, for the Th22 subset, that was blended with Th17, it appears that they localize further apart from each other. Contrary to Th2 and Th9 cells, that were separated by one dimension, Th17 and Th22 are separated by two dimensions: Th17 in presence of TFG-β and absence of IL-12 and Th22 in absence of TFG-β and presence of IL-12. Two out of the three dimensions of difference seems like a lot to define two subsets, considering that both produce IL-22 and that they share some of their effector functions.

Similarly, Th2 and Tfh cells are localized on the opposite side of the cube whereas they both produce IL-4.

Therefore, a lot of complexity is generated with the discoveries of new subsets and consequently, it becomes more and more difficult to classify Th subsets and determine the criteria on which to base the classification.

Are inducer and secreted cytokines enough to explain this complexity? If not, how to explain this complexity and how is it generated?

In the next part, the multiplicity of signals integrated by T cells that can impact Th polarization will be detailed.

II) Underlying mechanisms of T helper cell polarization

In the early years of Th1/Th2 regulation, cytokines were commonly described as the only actors inducing Th polarization. However, other signals can be involved. In this section, the multiplicity of signals leading to T helper cell polarization will be examined.

T cells integrate many different signals. At the T cell level, the complexity of Th differentiation can be dissected at different stages, from large to small:

- The cellular impact: how DC parameters affect Th polarization?
- The molecular impact: how molecular pattern diversity on DCs can influence Th polarization?

Moreover, based on these parameters, the concept of context-dependency which can influence Th polarization and many, if not all, biological mechanisms, will be introduced. Indeed, naive CD4 T cells respond to specific environments and Th polarization will be influenced by the signals specific to this particular environment.

1) Influence of dendritic cell diversity on Th polarization

a) Human DC ontology basics

DCs constitute a complex cell family of APCs. Several subtypes, phenotypically and functionally distinct, have been identified.

First, DCs have been classified according to their migratory capacities. Non-lymphoid tissue-migratory DCs patrol peripheral tissues, seeking for antigens, and migrate to lymph nodes after activation to present antigenic peptides to T cells. Lymphoid tissue-resident DCs reside in lymph nodes, capture circulating antigens and directly present them to T cells [94].

Secondly, DCs have been classified into two distinct groups: conventional DCs (cDCs) and plasmacytoid DC (pDCs). In human, within cDCs, two subsets have been identified: cDC1 and cDC2, defined as $CD11c^{+}$ $CD123^{-}$. On the one hand, cDC1 have been characterized by the expression of

BDCA-3 (also called CD141), XCR1 and CLEC9A. They have been described to highly cross-present antigens to CD8 T cells, and both resident and migratory cDC1 have been found [95]. On the other hand, cDC2 have been characterized by the expression of BDCA-1 (also called CD1c) and CD11b. cDC2 can also be both resident or migratory and they are known for their capacity to polarize naive CD4 T cells [95].

pDCs have been defined, in opposition to cDC, as expressing $CD11c^-$ $CD123^+$. They have been shown to express BDCA-2 (also called CD303) and BDCA-4 (also called CD304) and to produce high amounts of type 1 IFN in response to viral infection [96].

Furthermore, only present in the epidermis, another specific type of DC has been described: the Langerhans cells. They were the first DCs to be discovered and have been shown to express CD1a and Langerin. This particular phenotype makes them easily distinguishable from the other subsets.

Moreover, another DC type, monocyte-derived DCs (MoDCs), has been firstly reported in mice. MoDCs have been described to be rare at steady-state and to arise during inflammation, such as in Leishmania-induced intestinal inflammation mouse model [97]. Indeed, Leon et al. showed that MoDCs were differentiated from CD14 monocytes recruited on the inflammation site, as opposed to cDC and pDC that derived from a common DC progenitor. For this reason, they have also been called inflammatory DCs (infDC). They have been later observed in human, in physiopathological conditions in breast cancer ascites [98], and in physiological conditions in peripheral tissue [99].

Based on MoDC differentiation, two teams showed that $CD14^+$ monocytes could be differentiated into MoDC-like cells by GM-CSF and IL-4 stimulation [100,101]. Although these *in vitro*-derived cells are less physiological and are known to be considerably different compared to primary DCs [102], this *in vitro* model is helpful due to the limited availability of DCs in blood and tissue.

DC subset diversity is described in Figure 5.

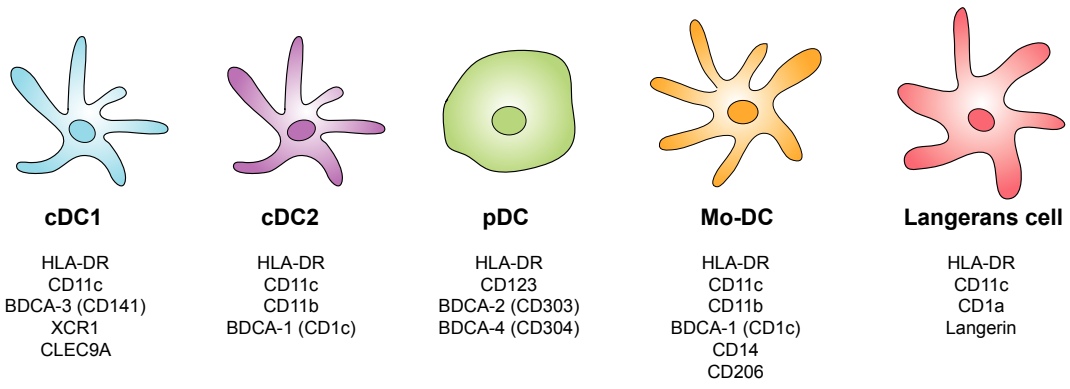

Figure 5: DC subset diversity

Recent studies have dug in more detail in DC classification thanks to single-cell RNA sequencing and mass cytometry technologies. Indeed, although flow cytometry and microscopy provided a lot of information on DCs at steady-state and in diseases, these methods were restricted regarding the number of analyzed parameters and the necessity to have prior knowledge on studied molecules. Thus, several papers came out recently, bringing a novel view of DC subsets [103–106]. Notably, the cDC2 population has been particularly discussed concerning its heterogeneity and the possible existence of subpopulations.

In this manuscript, the first definition of cDC2, in other words, cDC2 as one DC subtype, will be taken into consideration. Indeed, depending on the study: 1) the number of cDC2 subpopulations was variable, 2) the subpopulations were identified based on different markers and 3) identified subpopulations were either described as subsets or variability among donors. In this end, cDC2 precise characterization remains controversial. Moreover, since these studies are very recent, evidence of a differential impact of these possible subpopulations on Th polarization are very limited.

b) Impact of DC parameters on Th polarization

i) Role of the DC subset on Th polarization

DCs belong to a very broad family, with highly different subsets in regards to their markers and their migratory capacities, but also their morphology. In this part, many studies focusing on the role of these different DC subsets on CD4 T cells, notably on Th proliferation and polarization will be presented.

Firstly, several studies compared the role of cDC1 and cDC2 on Th polarization. For instance, Segura et al. compared polarizing capacities of cDC1 and cDC2 from healthy donor blood and breast cancer noninvaded lymph nodes. They showed first that all DC subsets, migratory and resident, were equally competent in inducing CD4 T cell proliferation. Secondly, they showed that cDC1 and cDC2 were both inducing production of the Th1 cytokine IFNγ by CD4 T cells, but poor production of the Th2 cytokine IL-5 and IL-13 [107]. Yu et al. also described that both cDC1 and cDC2 were able to induce IFNγ-producing CD4 T cells, but they added that cDC1 were more efficient to

induce Th2 polarization than cDC2, by measuring IL-4 and IL-13 T cell secretion [108]. On the contrary, Jongbloed et al showed that blood cDC1 induced more Th1 responses compared with cDC2 [109].

Additionally, Durand et al. isolated DC subsets from human tonsils and compared their ability to polarize naive CD4 T cells into Tfh cells. They looked at Tfh surface markers, such as PD-1 and CXCR5, and secreted cytokines and chemokines, such as IL-21 and CXCL13. They observed that cDC2 population was the most efficient subset, compared to cDC1 and pDC, to induce Tfh polarization [110].

Concerning inflammatory DCs, Segura et al. showed that this subset was highly competent in polarizing Th17 cells [98].
Some studies were also conducted using the MoDC differentiation model. In a mouse study, Chow et al. compared the capacity of MoDC and cDC to influence Th polarization and proliferation. They showed that, although cDC were more competent in inducing CD4 T cell proliferation, MoDCs were more efficient at inducing Th1 and Th17-associated cytokines than cDC. They also added that MoDCs were efficient at inhibiting Th2 polarization via CCR2 [111].

Some studies were also conducted on DCs from the skin. Klechevsky et al. demonstrated that Langerhans cells were more efficient to induce a Th2 profile compared to dermal $CD14^+$ DCs and cDC2. Moreover, they showed that dermal $CD14^+$ DCs were the most potent to induce Tfh cells, followed by cDC2 and Langerhans cells [112]. Furio et al. confirmed that Langerhans cells were more capable than cDC2 to induce a Th2 profile, but also a Th1 profile [113].
To finish on Langerhans cells, two other studies showed that this subset was the most efficient to polarize naive CD4 T cells into Th22 cells, producing IL-22 in the absence of IL-17 [114,115].

ii) Role of the DC-activating stimulus on Th polarization

The cellular impact on Th polarization can be due to the DC subset, as previously described. Moreover, this cellular impact can also be composed of a second important parameter, the DC-activating stimulus. DCs express a broad variety of receptors, allowing them to recognize a wide range of pathogens, that can affect Th subset induction.

First, a lot of studies have been conducted *in vivo* in mouse models. Using OVA mouse model, Pulendran et al. showed that *Escherichia coli* (*E. coli*) lipopolysaccharides (LPS) predominantly

induced Th1 polarization. However, *Porphyromonas gingivalis* LPS were not efficient in inducing Th1 but induced a Th2 response. Moreover, in line with these observations, they described that IL-12 secretion by $CD11c^+$ $CD8\alpha^+$ DCs, the equivalent of human cDC1, was only induced by *E. coli* LPS [116].

Using the same model, Dillon et al. confirmed *in vitro* that *E. coli* LPS stimulation was highly efficient in inducing IL-12 secretion by DCs and a Th1 response with IFNγ production. Additionally, they used Pam3Csk4 (Pam3) stimulation and showed that it was efficient in inducing IL-10 secretion by DCs and Th2 response, by measuring IL-4 and IL-5. Interestingly, they also performed *in vivo* analysis showing an interest in the impact of these stimuli on DC cytokine secretion. $CD11c^+$ $CD11b^+$ DCs (including cDC2) were more potent to secrete IL-10 and $CD11c^+$ $CD11b^-$ (including cDC1) to secrete IL-12 [117].

In human, several studies also demonstrated an impact of these DC-activating stimuli on Th polarization.

Agrawal et al also studied E. coli LPS. They showed that *E. coli* LPS stimulation induced high IL-12 and TNF-α secretion by MoDCs. On the contrary, Pam3-stimulated MoDCs did not induce Th1-polarizing cytokines. By co-culturing MoDCs with allogeneic CD4 T cells, they showed that *E. coli* LPS-stimulated MoDCs induced more IFNγ secretion by T cells and that Pam3-stimulated MoDCs induced more IL-5 and IL-13 secretion by T cells [118]. These results corroborated those in mice. A few years later, they stimulated human MoDC with other stimuli: Zymosan, prepared from yeast cell walls and stimulating TLR2 and dectin-1 CLR, and Curdlan, a dectin-1 agonist bacterial polysaccharide. They observed that Curdlan favored IL-23 secretion and both Curdlan and Zymosan favored IL-1β and IL-6 secretion by MoDCs. Consistent with these results, they showed that both dectin-1 stimuli promoted Th17 polarization of CD4 T cells [119]. Interestingly, different pathogen stimuli on the same DC subset could lead to different Th polarizations.

In addition to microorganism-derived stimuli, cytokines can also activate DCs and indirectly affect Th polarization. For instance, thymic stromal lymphopoietin (TSLP) is an IL-7-like cytokine belonging to the IL-2 cytokine family. It is produced by epithelial cells or other stromal cells and can activate DC-mediated inflammation in allergic diseases. In atopic dermatitis patients, it is especially secreted by keratinocytes [120].

Soumelis et al. showed that $CD11c^+$ DCs (including cDC1 and cDC2) stimulated with TSLP primed Th2 response by CD4 T cells by measuring IL-4, IL-5 and IL-13. Moreover, they observed that TSLP-activated DCs induced TNF-α but inhibited IFNγ and IL-10 production by CD4 T cells [121]. Ito et al

confirmed these observations by demonstrating that TSLP-stimulated DCs promoted TNF-α^+ IL-10^- Th2 cells from naive CD4 T cells [122]. Moreover, TSLP-activated $CD11c^+$ DCs have been described to induce Tfh differentiation. Indeed, TSLP-DC-polarized Tfh cells secreted high levels of IL-21, IL-4 and IL-13, expressed Tfh markers such as CXCR5, PD-1 and ICOS, and were able to help B cells to secrete class-switched IgE [85].

In addition to the DC subset and the DC-activating stimulus, another interesting parameter affecting Th polarization was identified. Tanaka et al. observed that Th polarization could be influenced by the number of DCs. In their study, they showed that *in vitro* stimulator/responder cell ratio could impact the differential regulation of Th1 and Th2 polarization. Using MoDC, they found that a low ratio (meaning few DCs compared to T cell number) induced preferentially a Th2 profile, with IL-4, IL-5 and IL-13 secretion, whereas a higher ratio (meaning higher DCs number in the co-culture) induced preferentially a Th1 profile, with IFNγ and IL-2 secretion [123].

In conclusion, DC parameters, such as the DC type, the DC-activating stimulus and the DC/T cell ratio, can have an impact on Th polarization. In the next part, below the cellular impact, the molecular impact on Th polarization will be described.

2) Influence of molecular pattern diversity on Th polarization

In this part, surface molecules influencing Th differentiation will be studied. Indeed, in the first part of this introduction, the cytokine signal impact in the three-signal theory of T cell differentiation was mainly described but the two other signals were not lingered: TCR signaling and co-stimulatory molecule signals.

a) Impact of TCR signal on Th polarization

It has been recently shown that TCR signaling can importantly influence Th polarization. A critical point is that this influence can be quantitative, but also qualitative.

In the ‘90s, several studies came out revealing the importance of the TCR signaling strength on Th1 and Th2 differential polarization. By using altered peptide ligands and wild-type peptides

coding for some residues of tobacco moth cytochrome c, two studies observed a high IL-4 production in the case of naive CD4 T cell in the presence of the altered peptide ligand or a low dose of WT peptide, and on the contrary, a high IFNγ production in the presence of the WT peptide [124,125]. Thus, Th1 cell induction required a stronger TCR signal strength than Th2 cell differentiation. One hypothesis was that, in naive CD4 T cells stimulated with a high concentration of peptides, the ERK pathway was induced at a high level, which led to GATA-3 suppression, transient blocking of STAT5 and Th2 failure [126]. Another study using OVA peptide corroborated these data by showing Th2 induction with low antigen doses and Th1 induction with increasing antigen doses. They also added that increasing antigen doses can also lead to Th2 polarization, which complexifies even more the concept [127].

Furthermore, Boyton et al. greatly illustrated Th polarization according to TCR affinity. The experimental system involved a bulk of CD4 T cells with a receptor of low or high affinities, and two microenvironments, one containing the Th1-polarizing cytokine IL-12 and the other containing the Th2-polarizing cytokine IL-4. In a "Th1 microenvironment", Th1 polarization occurred only for CD4 T cell clones with high-affinity receptors. On the contrary, in a "Th2 microenvironment", both CD4 T cell clones, with high and low-affinity TCRs, could be differentiated into Th2 cells, with a preferential expansion of clones with low-affinity receptors (Figure 6) [128].

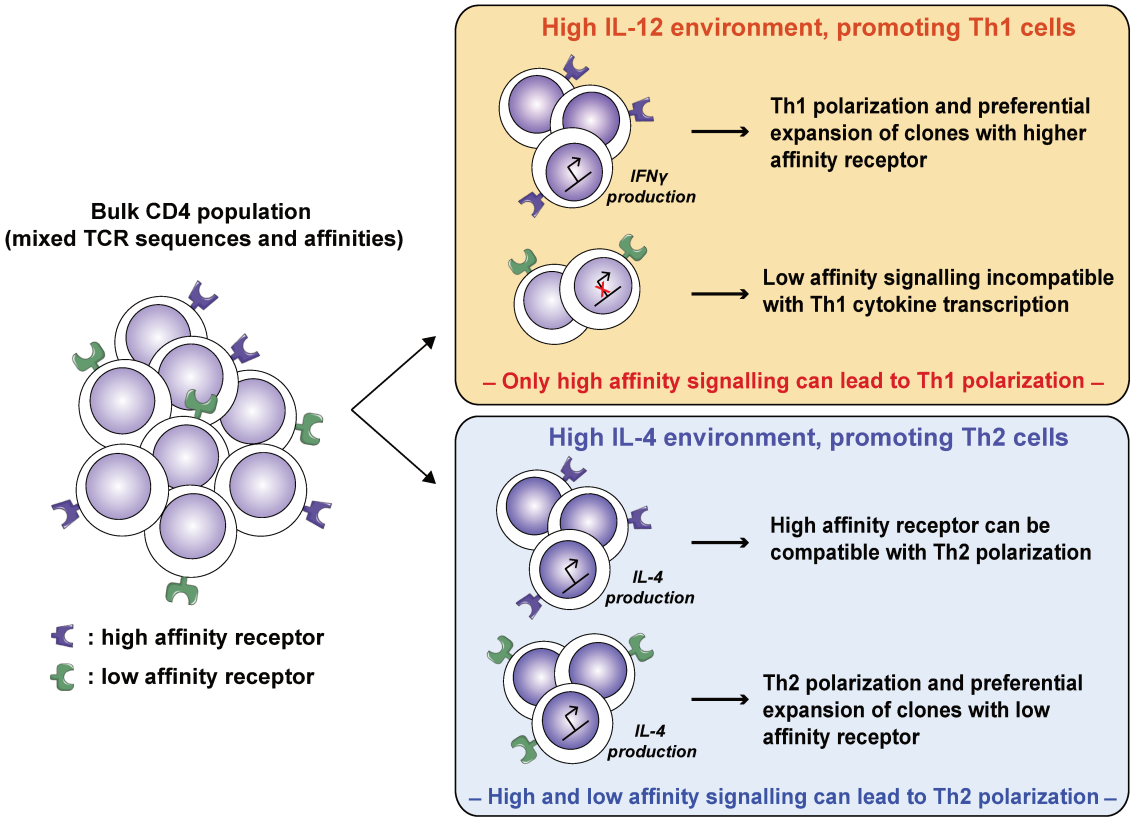

Figure 6: Th1 and Th2 differentiation depending on TCR signaling affinities

(Illustration adapted from Boyton et al. Trends Immunol, 2002 [128])

Thus, both antigen dose and TCR affinity are involved in TCR strength and seem to have a major impact on Th1 and Th2 differential polarization.

Similar to Th1 and Th2 differentiation, TCR strength has been described to play a role in Th17 versus Treg polarization. Turner et al used two types of antigen and demonstrated that a low antigen dose preferentially expanded Treg cells [129]. Using OVA peptide, another team corroborated these data showing that high dose TCR stimulation reduced iTreg differentiation, and on the contrary, Th17 cells failed to develop with a weak TCR signal [130].

Moreover, focusing on Th17 polarization, another study showed differential regulation of Th17 cytokines depending on TCR stimulation. IL-17A production was more sensible to anti-CD3 doses compared to IL-17F and a decrease of TCR stimulation led to a decrease of IL-17A production, but not IL-17F [131].

b) Impact of co-signal molecules on Th polarization

Co-signals are composed of co-stimulatory and co-inhibitory molecules. They play a critical role in immune response activation and regulation. Nowadays, they are commonly called immune checkpoint molecules, since their preferential targeting in immunotherapies, mostly in cancer therapies. They include over thirty molecules, belonging to various molecular and structural subfamilies. Functionally, co-stimulatory molecules can boost T cell activation, whereas co-inhibitory molecules play a role in the regulation of T cell responses. Immune checkpoints will be discussed in more detail in the last part of this introduction.

Co-stimulatory and co-inhibitory molecules constitute the second signal of the three-signal theory of T helper cell differentiation. These molecules can both affect the strength and nature of the signal transmitted to T cell and thus, promote or inhibit specific subset differentiation. Most studies about co-signals influencing Th polarization have been conducted in mouse models, principally using knock-out mice of co-signal of interest. Given the large number of co-signals, few important ones, that illustrated well their impact on Th polarization, will be dissected in this part.

CD28 constitutes a first essential signal, belonging to co-stimulatory signals. It is constitutively expressed on T cells and is essential for T cell survival, proliferation and differentiation. CD28 commitment is related to TCR strength and can lead to both Th1 and Th2 cell polarization. In presence of high TCR affinity or high antigen doses, it has been shown to promote Th1 polarization [132]. On the contrary, extended CD28 commitment tended to favor Th2 polarization [133,134]. Similarly to Th1 polarization, CD28 could also promote Th17 cells in the context of a strong TCR stimulation [131,135].

Moreover, CD28 has the interesting role of promoting Th differentiation via another co-stimulatory molecule named ICOS [136,137]. ICOS is a CD28 homolog and is also essential for T cell activation and differentiation [138]. Their signals have been described to be synergic for the induction of specific cytokines and complementary for others. In the case of *Staphylococcus aureus* enterotoxin B-infected mice, it has been described that ICOS was important for TNF-α and IL-10 secretion whereas CD28 was important to induce IL-2, IFNγ and IL-4 [139].
Independently of CD28, several studies highlighted that ICOS deletion led to a lack of Th1 cells. For instance, in ICOS-deficient mouse model, *Salmonella enterica* infection took over because of Th1 response defect [140]. Besides, ICOS-deficiency inducing Th1 cell impairment protected NOD

mice against diabetes [141]. However, opposite effects have also been reported, showing that ICOS-deficient mice developed exacerbated Th1 immune responses and enhanced IFNγ production in many infection models such as *Mycobacterium tuberculosis*, *Plasmodium chabaudi chabaudi* or *Schistosoma mansoni* [142–144]. Thus, ICOS influences Th1 cells but its impact stays controversial and seems to be highly dependent on the context.

Contrary to its differential contributions to Th1 cells, ICOS has been clearly described to promote Th2 and Tfh polarizations. High ICOS expression has been observed on Th2 cells compared to Th1 cells, blocking of ICOS importantly decreased IL-4 production [145,146] and impaired GATA-3 expression has been noted in ICOS-deficient mice [147]. Moreover, ICOS KO mice resulted in reduced Tfh cell number and germinal center collapse [148]. Thus, ICOS seems to be greatly involved in polarization acting on B cell help.

Moreover, ICOS promoted IL-21 production in Tfh cells, essential for their development and maintenance, but also in Th17 cells. However, ICOS was described to not be crucial for Th17 polarization but to be a great enhancer [149,150].

Finally, according to Akbari et al, ICOS was necessary for iTreg induction in hyperreactivity model [151]. Other papers connected ICOS to iTreg functionality. $ICOS^+$ CD4 T cells, but not $ICOS^-$, were described to prevent naive CD4 T cells proliferation in mixed-lymphocyte reaction (MLR) experiments [152]. Moreover, $ICOS^{hi}$ CD4 T cells have been associated with IL-10 anti-inflammatory cytokine secretion [153].

Therefore, ICOS influence on Th polarization is complex. ICOS has the ability to prevent immune responses but also to induce pro-inflammatory Th cells. Its function seems to vary a lot according to the studied context and the signal promoting ICOS Ligand (ICOSL) on the APC. Furthermore, although co-signal molecule impact on Th cells is clearly demonstrated, it remains difficult to understand when they exactly impact. For instance, in the case of ICOS playing a role in Th1 cells, does ICOS affect the Th1 polarization process itself, or the Th1 cell expansion? When a decrease of Th1 cells and/or decrease of IFNγ production is observed in mouse models, did we attend to a direct impact on naive T cell polarization or a Th plasticity after polarization?

CD40L is also a co-stimulatory molecule described as important in Th polarization. As opposed to CD28 and ICOS, its contribution is indirect since the ligand is expressed on T cells. CD40-CD40L interaction induces an effect on the DC, which impacts the T cell afterwards.

First, CD40L ligation has been shown to induce IL-12 secretion by DCs, promoting Th1 polarization [154,155].

Moreover, some studies described the role of CD40-CD40L axis in Th17 polarization, which increased IL-6 and IL-23 secretion by DCs [156]. Again, CD40-CD40L interaction allowed creating a beneficial cytokine environment for Th17 differentiation but did not impact CD4 T cell in a cell-intrinsic manner. Iezzi et al corroborated these results and added that a strong TCR signaling strength up-regulated CD40L on T cells, promoting this phenomenon [157].
Acting on DC cytokine secretion, the role of CD40L in Th polarization seems more straightforward than ICOS impact.

Finally, co-inhibitory molecules can also impact Th polarization but in an opposite manner. T Cell Immunoreceptor With Ig And ITIM Domains (TIGIT) is an example of a co-inhibitory molecule. TIGIT shares the same ligands CD155 (PVR) and CD112 (nectin-2) with the co-stimulatory molecule CD226 (DNAM-1), similarly to CD28 and CTLA-4 which share the same ligands CD80 and CD86 [158,159]. TIGIT is highly expressed on Treg cells but is also expressed by the others Th subsets after activation.
TIGIT was shown to inhibit pro-inflammatory Th1 and Th17 cells, but interestingly not Th2 cells [160]. Another paper even showed that TIGIT could promote Th2 polarization in an *in vitro* Th polarization system and an allergic disease mouse model [161]. These results corroborate with what has been observed for TIGIT competitor, CD226, which promotes Th1 and Th17 axis [162,163]. Even though few papers came out about TIGIT impact on Th polarization, it underlines that co-inhibitory molecules can also do more than just inhibit T cell activation and functions.

Of course, many other co-signal molecules have been reported to impact Th polarization such as CD30 and CD27/CD70 impacting Th17 polarization [164–166], or Notch receptor impacting Th9 polarization [167].

It should be noted that OX40 has also an important role in Th polarization. The last part of the introduction will be dedicated to this co-stimulatory molecule that will occupy a central position in this manuscript.

Thus, it appears that many co-signals are involved in the polarization of several subsets. This highlights that the same molecule can have different roles and functions depending on the context in which the T cell is evolving.

3) Complex signal integration involves context-dependency

It has been shown in the previous parts that many different signals, from different origins and different natures can be involved in a Th polarization process.

Given this multiplicity of signals integrated by T cells when communicating with DCs (Figure 7), the three-signal theory of T cell differentiation seems a bit obsolete.

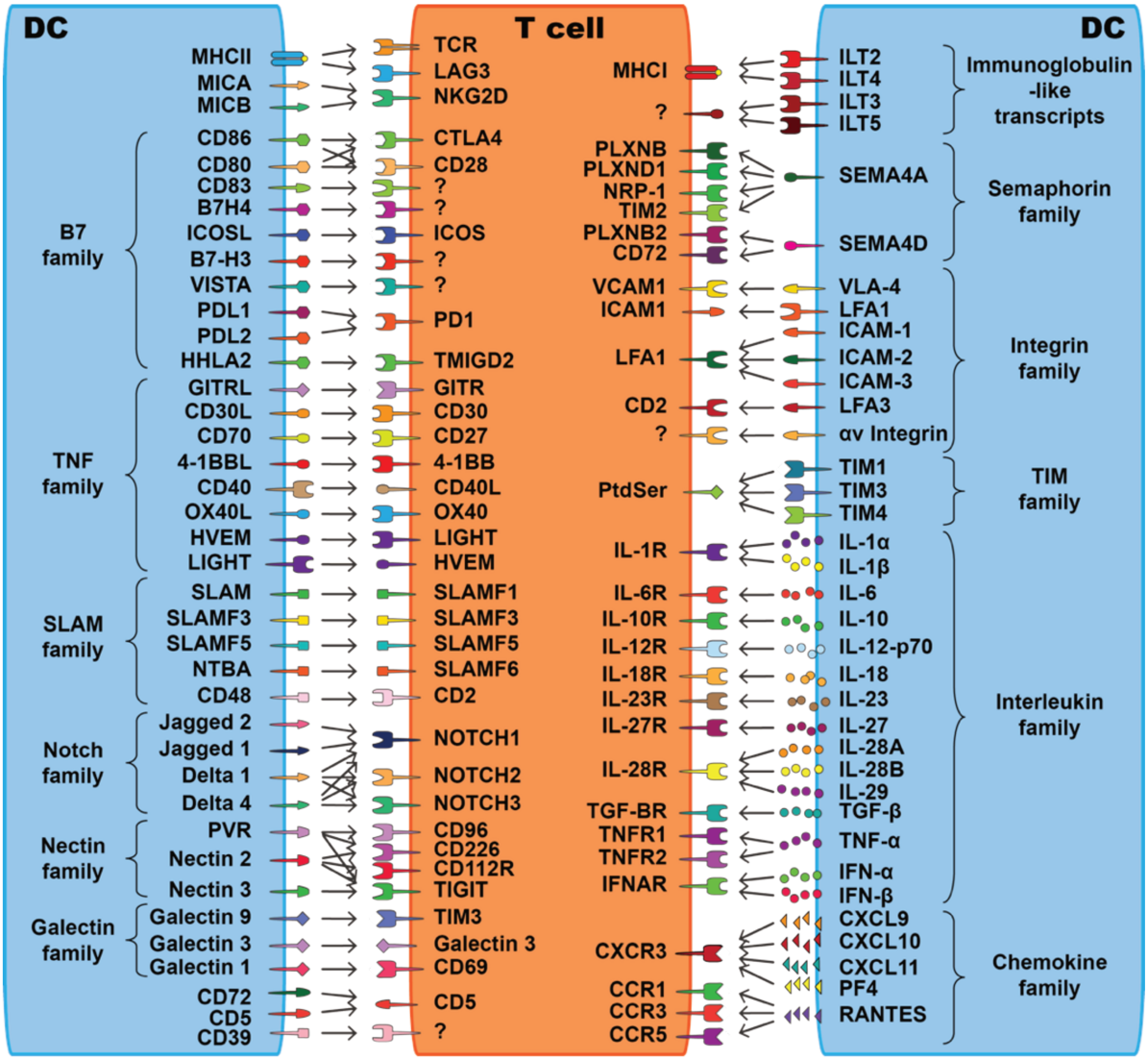

Figure 7: Signal multiplicity and diversity integrated by CD4 T cell during DC/T communication

(Schematic illustration of DC/T cell communication molecules designed by Coline Trichot)

The concept of context-dependency can be defined “in real life” as the following. One person evolves in different environments, is surrounded by many different people, etc. According to these elements and many others, the same person can behave and react differently in a situation. For instance, the same person may respond to the same question differently whether she is in her professional or personal environment. This concept can be applied to biology as well. A cell, a molecule can have different behaviors or functions depending on the context in which it is evolving.

Cytokines frequently exhibit context-dependent functions. This is the case of TGF-β that can differentiate naive CD4 T cells into different Th subsets when it functions within specific cytokine environments. In conjunction with IL-2, TGF-β was shown to promote Treg [168]. TGF-β was also a key inducer of Th17 cells, when it co-operated with IL-6, IL-1β and IL-23 [38]. In combination with IL-4, TGF-β was involved in the polarization of Th9 cells [57]. Moreover, Schmitt et al. showed that TGF-β in presence of IL-12 and IL-23 could induce several Tfh markers from naive CD4 T cells such as CXCR5, ICOS, Bcl-6 and IL-21 [82].
IFN has also been studied in this perspective because of its pleiotropic functions. Touzot et al. explored the context-dependency of this cytokine in Th-polarizing cytokine contexts: Th0, Th1 (IL-12), Th2 (IL-4) and Th17 (TGF-β, IL-6, IL-1β, IL-23). They showed that IFNα induced distinct transcriptional signatures in each of these Th contexts [169].
These two examples illustrate that a single cytokine can drive multiple effects in target cells, here different Th polarizations or signatures, when it is combined with different other cytokines.

Co-stimulatory molecules can also induce differential effects in target cells according to the immunological context.
This can be illustrated by CD28 that induced functionally diverse Th cytokine secretion depending on the MoDC-activating stimuli. For instance, blocking of CD28 induced quantitatively different secretion of IL-6, IL-21 and IL-17A by CD4 T cells in co-culture with MoDC activated with LPS and Zymosan, compared to MoDC activated with Influenza virus [170].
Moreover, multifaceted ICOS is a good example of the context-dependent role of a molecule for two reasons. First, concerning Th1 subset, it was presented above that ICOS can have opposite effects and that the physiopathological environment seems to highly influence either promotion or inhibition of Th1 cells. Besides, the fact that ICOS appears to be involved in many different cytokine secretions and many, if not all, Th subsets, is second evidence of the potential role of the context on ICOS functions.

In addition, Yu et al. compared Th polarization capacities between cDC1 and cDC2 activated with four different stimuli: Influenza virus, TSLP, Curdlan or Poly I:C. It can be assumed that the combination of DC types and DC-activating stimuli create 8 cellular contexts (*e.g.* influenza-cDC1, influenza-cDC2, TSLP-cDC1, TSLP-cDC2, etc.). Interestingly, they observed that both DC type and DC-activating stimuli impacted CD4 T cell secretion of IFNγ and IL-13 [108].

These examples highlighted that microenvironmental contexts can influence T cell behaviors and T cell-activating molecule functions.

4) Context-dependency in pathology: example of cancer

The concept of context-dependency leads to consider differently immune responses in physiopathology and to grant more importance to the context. The example of cancer will be taken. Indeed, cancer is a very diverse pathology since it can have various tissue origins and tumor locations. Hence, given the number of cancer types that can be considered as different contexts in one single pathology, it is a great example to illustrate the concept of context-dependency.

In this part, how Th subsets and Th cytokines are linked with specific tumor microenvironment in different cancer types and their associated context-dependencies will be studied.

a) Tumor microenvironment composition

The tumor microenvironment (TME) is a dense and complex cell network (Figure 8). It influences cell functions and interactions between cell types in their environment. But from another point of view, it is the result of many interactions and crosstalk between different cell types.

Fibroblasts are a key element in the TME that greatly illustrates this crosstalk idea. Fibroblasts are specialized in extracellular matrix (ECM) synthesis, a dense macromolecule network supporting surrounding cells. On the one hand, TME signals modify fibroblast phenotype and these “activated” fibroblasts are commonly called cancer-associated fibroblasts (CAFs). On the other hand, CAFs impact TME and promote cancer progression by providing additional pro-tumoral signals [171]. For instance, CAFs can remodel ECM and act on different parameters such as its

composition, structure, compactness, etc. In terms of antitumoral immunity, this affects T cell access to the tumor core by retaining them into the stroma [172].

In addition to stromal cells, immune cells are a critical cell component in TME. T cells, NK cells, B cells, dendritic cells, macrophages, neutrophils, among others, are pieces of cancer heterogeneity. Regarding tumor-infiltrating T cells (TILs), $CD8^+$ and $CD4^+$ T cells under different differentiation states are found. The fact that Th polarization is also affected by TME signals will be shown later.

TME sometimes includes tertiary lymphoid structures (TLSs). They resemble secondary lymphoid organs (SLOs) and can be found in several pathophysiological conditions and diseases. In cancer, they are more abundant in the stroma or the invasive margin than in the tumor core. As SLOs, they are composed of immune cells such as T cells, B cells and DCs, and stromal cells such as follicular dendritic cells (FDCs) organizing the lymphoid follicles [173].

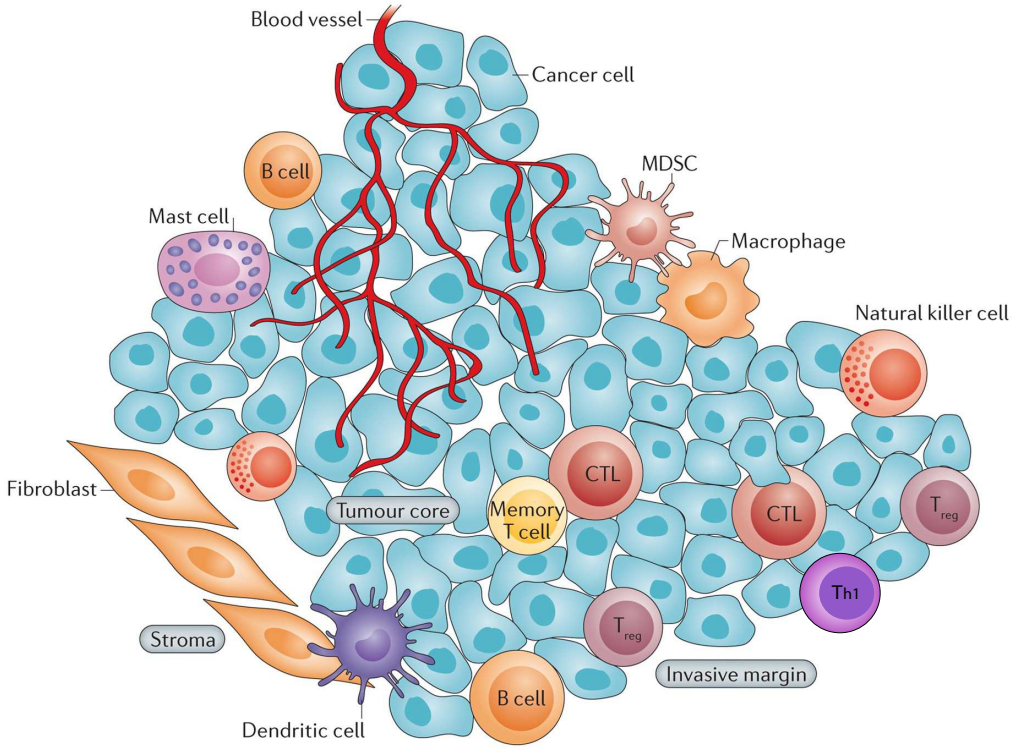

Figure 8: Schematic representation of TME cellular composition

(Illustration adapted from Hackl et al. Nat. Rev. Genet, 2016 [174])

b) Th subsets and cancer immunoediting

Cancer immunoediting theory states that cancer evolves in three phases: elimination, equilibrium and escape. TME is an essential actor for success in this process, by providing the necessary signals to the escape. A simplified view is often proposed.

During the first phase, elimination, the immune system successfully fights against the tumor. On the tumor site, the pro-inflammatory microenvironment induces innate cell recruitment such as macrophages that produce IL-12, and NK cells that produce IFNγ, critical cytokines for antitumor immunity. In tumor-draining lymph nodes, naive CD4 T cells are activated by mature DCs presenting tumor antigens, inducing Th1 polarization. These Th1 cells are necessary to help tumor-specific $CD8^+$ cytotoxic T cell (CTL) development via cross-presentation of tumor antigens on DC MHC I [175,176]. On the tumor site, Th1 cells and CTL are fundamental providers of IFNγ. IFNγ downstream antitumoral effects are various and include for instance macrophage tumoricidal activity or CTL and NK cell enhancement, which can directly kill tumor cells [177]. Th1 cells also release IL-2 that is essential for CTL survival and function [178].

The second phase, the equilibrium, is highly dynamic, contrary to what is suggested by its name. T cells and innate cells fight against the tumor, tumor growth is contained but it is not enough to completely eradicate it.

Finally, during the escape phase, tumor cell variants, which resisted the equilibrium phase by increasing resistance and reducing their immunogenicity, dominate the immune response [179]. CTLs become less responsive and less efficient in eliminating cancer cells. Regarding CD4 T cells, this phase goes along with modifications in the TME that affect Th polarization. They also become less responsive and inefficient in providing suitable T cell help while TME promotes Treg cell induction. TME-driven regulatory phenotype occurs through different processes such as immunosuppressive cytokine secretion (*e.g.* TGF-β and IL-10) [180,181] and co-inhibitory molecule expression (*e.g.* PD-L1) [182], among many others. Thus, the TME delivers signals that can affect Th polarization to favor malignancy progression. There is a lack of specific target to specifically deplete or functionally impair Treg, without affecting T helper cells and CTLs.

Following this perspective, Treg cells have been reported to be a bad prognosis in breast cancer and melanoma for instance [183–185]. However, they were also reported to be a good prognosis in head and neck cancer and colorectal cancer [186–188]. The fact that Th subsets in cancer are not black

and white and that context can highly influence T cell cytokine secretion, will be seen in the next part.

c) Th subset and Th secreted cytokine context-dependencies in cancer

Th cells and their functions are highly diverse; thus, it is not surprising that all Th subsets cannot be efficient in the antitumor immunity process. The focus will be on Th1 and Th17, which have been importantly studied in cancer.

As previously described, Th1 subset is for now the principal one widely correlated with a good prognosis in solid cancer, although other subsets have been studied. The positive involvement of Th1 master cytokine IFNγ is broadly recognized since multiple studies showed IFNγ-dependent antitumor immunity by various pathways [177,189–191]. Additionally, a study using adenocarcinoma and sarcoma mice models showed that IL-12 treatment induced IFNγ-dependent tumor regression [192]. Braumuller et al added more recently that TNF, also played a critical role in tumor control [193]. In human, high infiltration of Th cells, exhibiting Th1-associated genes such as T-bet, was correlated with good prognosis in several cancer types [194–196], as well as Th1-circulating cytokines [197].

Nevertheless, it has also been described that IFNγ could have pro-tumoral effects in certain conditions. In colorectal carcinoma mouse model, mice deficient for SOCS-1, a tumor suppressor gene, spontaneously developed tumors, contrary to SOCS-1$^{-/-}$ IFNγ$^{-/-}$ mice that did not develop any colon tumors or strong colitis. This suggested that IFNγ could be a key actor in tumorigenesis [198]. IFNγ has been shown to be involved in papilloma development by increasing Th17 response [199]. IFNγ has also been described to upregulate PD-L1 in several cancer cell lines [200].

These few examples, among many others, on IFNγ in cancer highlight that the same molecule can have opposite effects in a singular pathology. Although IFNγ has been mostly associated with antitumor benefits, it shows the importance of considering the context to study a molecule function.

Opposite role in tumor immunity has also been described for other Th subsets. For instance, different studies associated Th17 cells with either a good or bad prognosis. On the one hand, several studies positively correlated a high level of Th17 cells or IL-17 cytokines with better patient outcomes in colorectal, cervical and ovarian human cancer types [201–203]. Among these studies,

Kryczek et al showed in mice and human ovarian cancer that Th17 cells were positively correlated with IFNγ-producing T cells, and that Th17 cells were negatively correlated with Treg cells in human [204,205]. Moreover, two studies on adoptive transfer in B16 melanoma mouse model even showed that Th17 cells were even more efficient for tumor rejection than Th1 cells [206,207]. However, melanoma is a great model illustrating the paradox of Th17 cells in cancer since Th17 and IL-17 have also been associated with melanoma progression. IL-17 has been shown to promote tumor growth and more TILs and IFNγ were observed in IL-17 KO B16 mice [208]. Moreover, in other models and in human, several studies described protumoral effects of IL-17 [199,209,210]. Although it was not always very clear whether IL-17 cytokines were produced by Th17 cells, these articles show that the TME can enforce a differential regulation of Th17 function or at least IL-17 function.

All these studies show that Th subsets, or their secreted cytokines, can have different roles according to the tumor type, and even sometimes different roles within the same tumor type. It highlights the importance of the context on Th subsets in cancer. It also brings light on the fact that some TME parameters are either not enough understood yet, or not enough taken into consideration.
Moreover, it leads to reconsider the way patients are treated, by better considering each TME context within tumor types, but also each patient as individual-specific contexts.

In the next and final part of this introduction, the focus will be on an interesting immune checkpoint molecule influencing T cell activation and polarization: OX40 Ligand (OX40L).

III)OX40-OX40L: biology of a co-stimulatory immune checkpoint

1) General concepts of immune checkpoint molecules

Immune checkpoints are defined as regulator molecules of the immune system and play a key role in T cell biology as they accompany TCR signaling. Because of their targeting in immunotherapies, the term “immune checkpoint” is commonly used to describe immune checkpoint blockade in cancer therapy and therefore associated with inhibitory immune checkpoints. In this manuscript, the term “immune checkpoint” refers to both co-stimulatory molecules that stimulate immune processes, such as CD28 or ICOS (Figure 9a), and co-inhibitory molecules that inhibit immune processes, such as PD-1 or CTLA-4 (Figure 9b). In this line, immune checkpoint molecules are usually seen as the “brake” and “gas” of the immune system. However, interestingly, their definitions continuously evolve with the discovery of new co-inhibitory and co-stimulatory molecules, their biochemical characterization, their signaling pathways and their immunological functions.

Co-signal interactions can be unidirectional, only affecting T cell fate, but can also be bidirectional, affecting the T cell carrying the receptor and the cell carrying the ligand. For instance, this is the case for CTLA-4. CTLA-4 can inhibit T cell activation and functions through its interaction with B7-1 (CD80) and B7-2 (CD86). Moreover, this interaction induces indoleamine 2,3-dioxygenase (IDO) expression by the APC, which can suppress T effector cell activation and promote Treg function (Figure 9b). Bi-directional action of CTLA-4 can also occur during effector T cell and Treg interaction. On the one hand, CTLA-4 suppresses effector T cell functions and on the other hand, it increases Treg suppressive capacity (Figure 9c). PD-1 follows a similar pattern by suppressing effector T cell functions and promoting proliferation, survival and maintenance of Treg (Figure 9c) [211].

In addition, CTLA-4 is a great example of co-inhibitory and co-stimulatory molecule competition. Several co-signal receptors can bind to the same ligand and vice versa. CTLA-4 and CD28 can both bind to B7-1 and B7-2. Recently, it has been shown that CTLA-4 and CD28 could also bind to a third ligand named B7-H2 (ICOSL) (Figure 9d) [211].

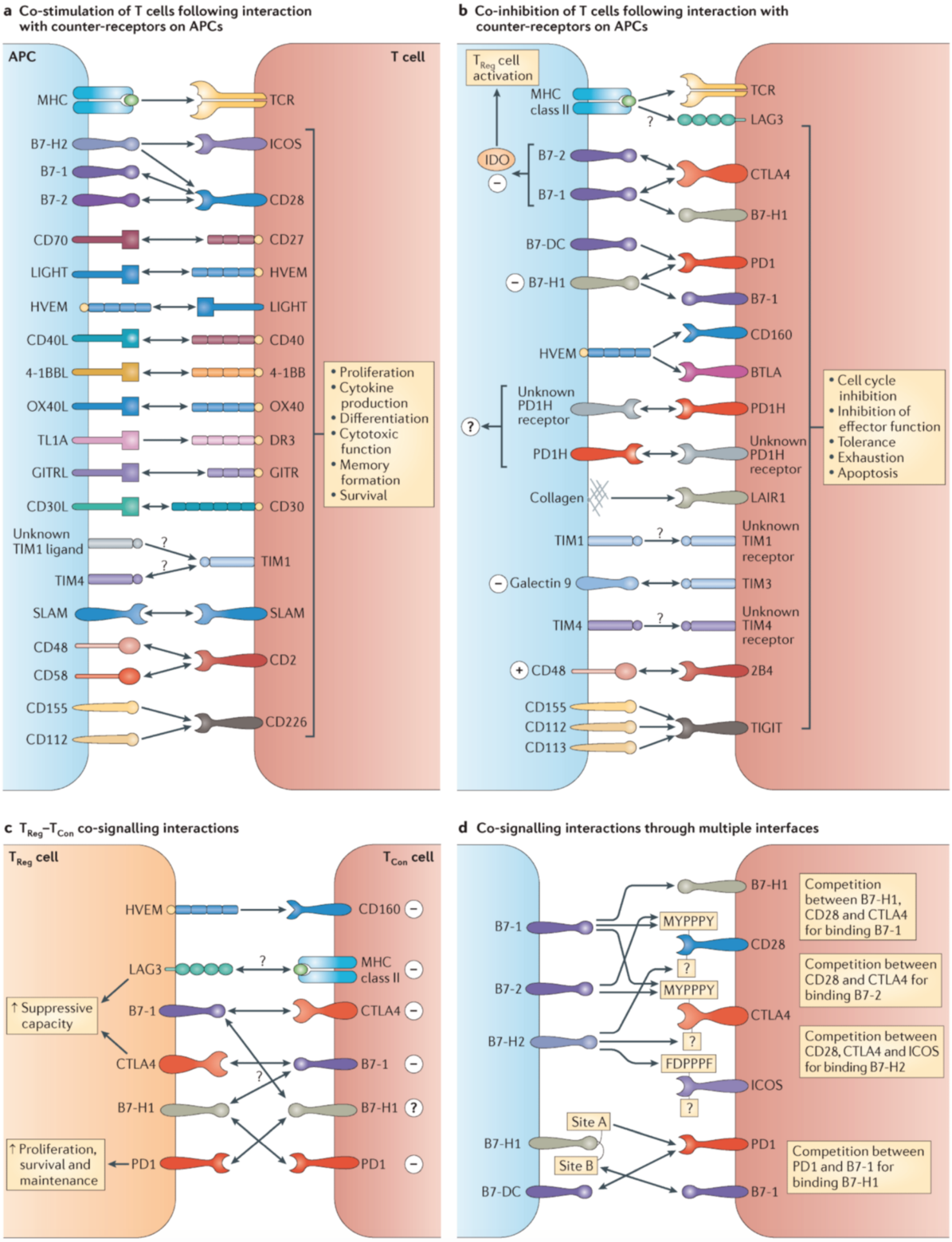

Figure 9: Receptor and ligand co-signal interactions in T cells

(Illustration from Chen et al. Nat Rev Immunol, 2013 [211])

In cancer, immune checkpoint blockades have remarkably changed the landscape of antitumor therapy. Immune checkpoint immunotherapies aim to restore immune response against the tumor. Several monoclonal antibodies directed against inhibitory immune checkpoints, anti-PD-1, anti-PD-L1 or anti-CTLA-4, have been approved by the U.S Food and Drug Administration (FDA) in various types of cancer. Other candidates, such as TIGIT (*e.g.* NCT03563716), T-cell immunoglobulin and mucin-domain containing-3 (TIM-3) (*e.g.* NCT03489343) and Lymphocyte-activation gene 3 (LAG-3) (*e.g.* NCT03005782), are being actively tested. However, in the majority of cancers, less than 20% of patients develop objective and durable responses to co-inhibitory immune checkpoint blockade. Co-stimulatory immune checkpoint agonists are also developed and tested in clinical trials [211,212].

In the last part of this manuscript, a specific co-stimulatory immune checkpoint couple will be dissected: OX40 and OX40L.

2) OX40-OX40L couple function on T cell activation

a) OX40 and OX40L discovery and classification

OX40 was first discovered by Paterson et al. during the '80s at Oxford University. Using activated rat T cells and mouse monoclonal antibodies, Alan Williams team showed that one monoclonal antibody, MRC OX-40, recognized a new antigen of 50000 molecular mass on CD4 T cells, and increased their proliferation [213]. In the '90s, OX40 antigen cDNA was cloned, sequenced and classified as a member of the tumor necrosis factor receptor superfamily (TNFRSF) [214].
OX40L was discovered within the same period as OX40 [215] but was confirmed to be its ligands only during the '90s [216,217].

Later on, in 2006, murine and human crystal structures of the OX40-OX40L complex were described by Compaan et al. OX40L is a homotrimer and displays unusual features compared to its counterparts. Indeed, OX40L shares only 40% sequence identity and its trimer interface is highly compact compared to many other tumor necrosis factor superfamily (TNFSF) ligands. In contrast, OX40 is more similar compared to other members of the TNFRSF [218]. Due to its expression under a trimeric form, OX40L binds to three OX40 molecules.

The tumor necrosis factor receptor and tumor necrosis factor superfamily, to which belong OX40 and OX40L, plays an important role in cell activation, proliferation, differentiation and function of immune cells, in synergy with TCR and CD3 signaling. It is composed of about 30 receptors and 20 ligands, such as CD40L/CD40 or 41BB/41BBL. TNF and its receptors are the most studied molecules in this superfamily and are targeted by therapeutic blocking antibodies in several inflammatory diseases [219].

Moreover, OX40 and OX40L encoded genes, respectively TNFRSF4 and TNFSF4, are located on chromosome 1 [220].

b) OX40 and OX40L expression

OX40 is predominantly expressed on activated T cells, CD4 including all Th subsets and Treg cells and CD8. Unlike the CD28 co-stimulatory molecule, it is not constitutively expressed on naive CD4 and CD8 T cells, but only after activation. It has been described that TCR stimulation was sufficient to induce OX40 expression, but CD28 co-stimulation highly enhanced it. It is consistent with the fact that OX40 acts sequentially after CD28 [221,222].

Additionally, memory T cells do not express OX40 at baseline, but it can be rapidly re-expressed after activation. OX40 is also observed on NK cells, NKT cells and neutrophils, but at lower levels compared to activated T cells [223–225].

OX40L is predominantly expressed on APCs. Indeed, it has been observed on blood DCs (bDCs) and MoDCs, but also on B cells and macrophage [226–228]. Similar to OX40, OX40L is expressed after APC activation. Various stimulations can induce OX40L expression on APCs, for instance, inflammatory cytokines such as TSLP and IL-18 [122,229].

OX40L is also expressed on various other cell types including NK cells, mast cells, smooth muscle cells and vascular endothelial cells [230–233].
Interestingly, OX40L has also been observed on activated T cells [234,235]. Mendel et al. showed that OX40L was expressed on activated T cells after 6 days of *in vitro* culture with anti-CD3 and that it depended on anti-CD3 doses [236].

c) OX40 signaling pathway in CD4 T cells

Figure 10 describes the OX40 signaling pathway after stimulation with OX40L by APC.

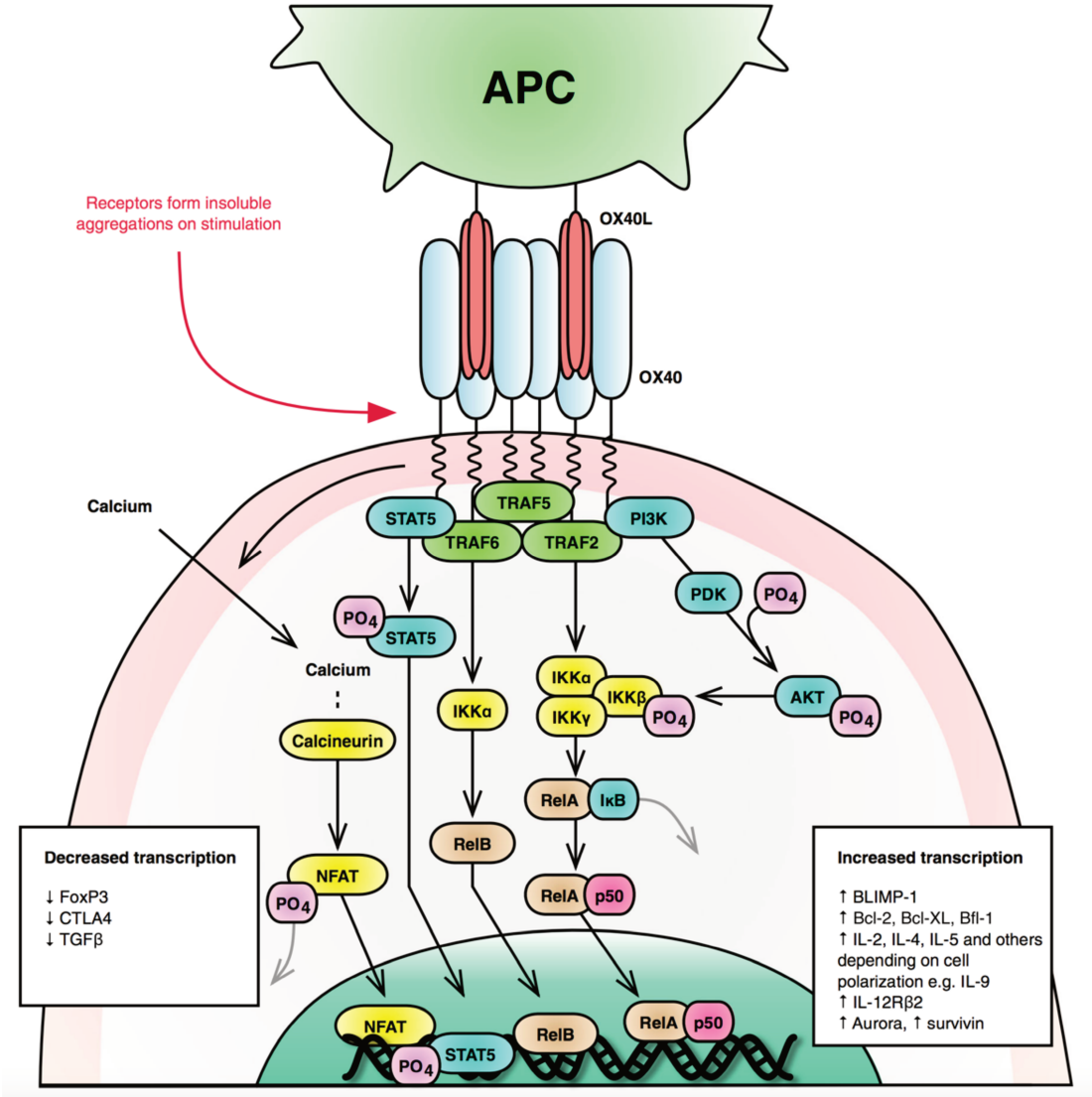

Figure 10: OX40 signaling pathway in T cells

(Illustration from Webb et al. Clin Rev Allergy Immunol, 2016 [237])

OX40L expressed at the surface of an APC binds to three OX40 molecules on the T cell. Following this ligation, OX40 molecules are recruited into lipid rafts and form a complex with TNFR-associated factors (TRAF) adaptor proteins, namely TRAF2, 5 and 6, and IKKα, IKKβ and IKKγ. TRAF2, 5 and 6 are involved in NFκB activation among others and interestingly, TRAF6 is also involved in IL-9 production by CD4 T cells.

As a result of this complex formation, IκB is degraded and RelA, a sub-unit of NFκB, and p50 can enter the nucleus. In another process, dependent on TRAF6, IKKα can induce RelB entrance in the nucleus.

OX40 complex can also phosphorylate STAT5 that can then enter the nucleus.

Moreover, OX40 can increase AKT, by constituting a complex with PI3K and in a PDK-dependent manner. AKT is able to enhance signaling through IKK.

Finally, OX40 can increase calcium entry into the T cells and activate calcineurin. As a result, NFAT is dephosphorylated and can enter the nucleus [237].

All these signals promote T cell survival and maintenance of the immune response by, for instance, up-regulating genes coding for Bcl-XL, survivin (anti-apoptotic molecules) and Th cytokines, and down-regulating genes coding for FoxP3, CTLA-4 and TGFβ. OX40-OX40L interaction functions will be described more in detail in the next part.

d) OX40-OX40L interaction functions on CD4 T cells

The first important function of OX40-OX40L was established upon OX40 discovery. OX40 agonist monoclonal antibodies on rat CD4 T cells amplified their proliferation [213]. The same observation was made on mouse and human models [217].
In line with its function on T cell proliferation, OX40 ligation has been shown to increase Th polarization and Th cytokine secretion [238]. This function will be discussed in more detail in the next part.

OX40L has also been described to be involved in CD4 T cell longevity by lengthening their activation, not through APC-T cell but T cell-T cell interaction. Indeed, Sorrosh et al. observed *in vivo* and *in vitro* that OX40L expressed on T cells promoted their survival by binding to OX40. They suggested that this allowed T cells to maintain OX40 signal after they separated from DCs, in an autocrine or paracrine manner, and thus to maintain their activation [235].

In addition, it has been shown that OX40L deficiency or blocking was impairing memory CD4 T cell population, in terms of expansion and survival [239,240].

Moreover, OX40 signaling has been shown to promote IL-2 secretion from T cells and enhance IL-2Rα expression at the surface of the cell during the effector phase. In contrast, for naive CD4 T cells, this is mainly controlled by CD28 [222,239].

OX40 and OX40L have also been associated with adhesion function. OX40 has been shown to be involved in activated T cell adhesion to vascular endothelial cells [233]. They have also been shown to be implicated in migration function by promoting chemokine and chemokine receptors up-regulation such as CXCR5, CXCR4 and CCL5 [221,241–243].

OX40 ligation functions on CD4 T cells are summed up in Figure 11.

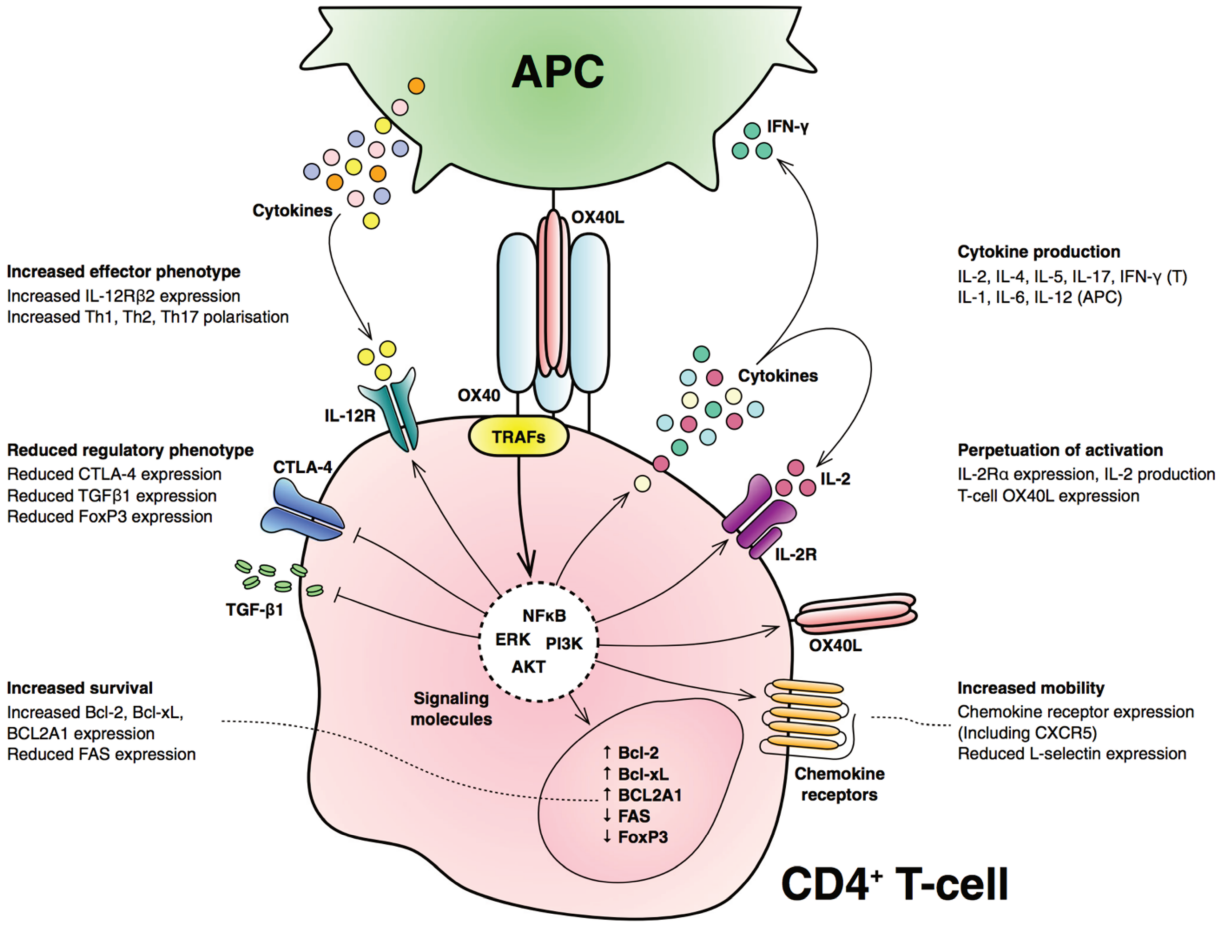

Figure 11: OX40 ligation functions on CD4 T cells

(Illustration from Webb et al. Clin Rev Allergy Immunol, 2016 [237]

Interestingly, some studies also described the role of OX40L on the APC expressing it, even if it was less studied than the effect of the receptor. OX40L ligation has been shown to increase

inflammatory cytokine secretion and co-stimulatory molecule expression on DCs [226]. Regarding B cells, Stüber et al. described OX40L as necessary for differentiation in plasma cells and Ig production [244,245].

OX40L ligation functions on non-CD4 T cells are summed up in Figure 12.

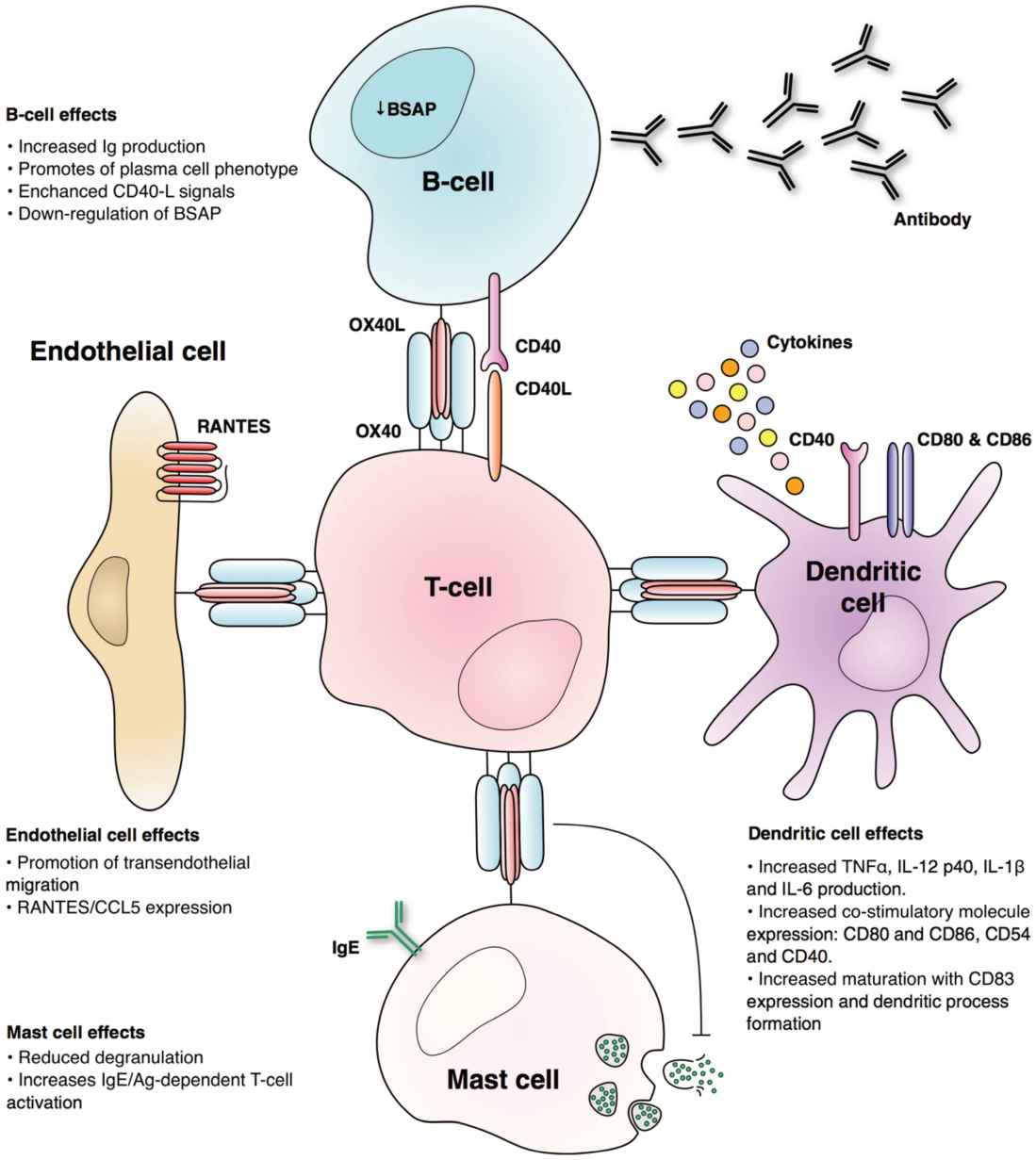

Figure 12: OX40L ligation functions on non-CD4 T cells

(Illustration from Webb et al. Clin Rev Allergy Immunol, 2016 [237])

3) Control of Th polarization and cytokine secretion by OX40L

OX40 and OX40L are primarily described as a T cell co-stimulator couple that maintains T cell proliferation and survival. Consequently, this characteristic is for instance targeted in cancer immunotherapies to increase antitumoral T cell response. However, their role in T cell is much broader than the regulation of activation. In this part, what is known about OX40-OX40L effect on Th polarization will be explained in detail.

a) OX40-OX40L and Th1/Th2 subsets

OX40L has been reported to regulate both Th1 and Th2 subsets. Th1 and Th2 cytokine production are usually studied together.

In naive CD4 T cells, OX40L was described as an inducer of Th2 polarization. This was observed in both mouse and human models, by measuring Th2 cytokine production [246,247].

In *Leishmania major* infected mouse model, Akiba et al. also showed that the decrease of Th2 cytokine in presence of OX40L blocking went along with an increase of IFNγ Th1 cytokine production, *in vitro* and *in vivo* [247]. So et al. described similar results under physiological conditions by comparing WT and OX40-deficient mice T cells *in vitro* [248]. On the contrary, under physiological conditions as well, Murata et al. showed that the absence of OX40L led to IFNγ inhibition [249]. Finally, in a murine model of asthma, Jember et al. saw a decrease of Th2 cytokines in OX40-deficient mice but they did not report any impact of OX40 absence on IFNγ production [250].
It seems that OX40L preferentially leads to Th2 differentiation and that OX40L-induced effect on Th1 polarization highly depends on the context of the experimental condition.

In human studies, it has also been shown that OX40L promoted Th2 responses. Two studies showed that OX40L blocking in a TSLP-activating bDC context induced a decrease of IL-4, IL5 and IL-13 Th2 cytokines [122,251]. They also both observed a decrease of TNF-α and an increase of IL-10. Regarding IFNγ, Inagaki-Katashiba et al. did not see any effect of OX40L blocking whereas Ito et al. saw a little decrease (but it remained difficult to compare since Ito et al. did not perform any statistical analysis and showed only replicates of one unique donor on their graphs). These results were established using total $CD11c^+$ bDCs. In another model of influenza virus-activated bDCs, Yu

et al. described that OX40L blocking during co-culture with naive CD4 T cells led to a decrease of Th2 cytokines, but only for co-culture with cDC1. Besides, they did not see any impact on IFNγ production [108].

b) OX40-OX40L and Th17 subset

Opposite effects of OX40L on Th17 cell differentiation and Th17 cytokine secretion have been shown in different *in vivo* and *in vitro* models.

First, in mouse models of Th17-associated diseases, OX40-OX40L induced positive effects. For instance, in EAE or rheumatoid arthritis (RA) mouse models, blocking antibody against OX40 or OX40L led to dramatic amelioration of disease severity [252–254]. However, these studies, performed at the beginning of 2000, did not make any specific link between OX40-OX40L blocking positive effect on the disease and a decrease of Th17 cells. A few years later, another study showed that IL-17 production and RA disease were enhanced through OX40-OX40L interaction [255].

Moreover, in a mouse uveitis disease model, it has been demonstrated that an up-regulation of OX40 enhanced Th17 cell functions and increased ocular inflammation. They also showed that blocking IL-17 improved the disease outcome. Regarding OX40, they showed that its activation with an agonist antibody increased IL-17 and IL-21 production, but they did not try to improve the disease using an anti-OX40 antagonist antibody [256].

Finally, in a mouse intestinal inflammation model using *Candida albicans*, Xin et al. described the impact of Treg population ablation in WT and B7-deficient mice. After Treg depletion, they observed an expansion of IL-17-producing CD4 T cells in B7-deficient mice, but not in WT mice. In contrast, they observed an expansion of IFNγ-producing T cells in WT mice. Adding an anti-OX40L antagonist antibody allowed to decrease the percentage of IL-17-producing cells, but not IFNγ-producing T cells in both WT and B7-deficient mice [257].
This study highlights again the role of OX40L in promoting Th17 differentiation but it also remarkably shows how Th polarization can be context-dependent. Indeed, in the absence of Treg, Th1 and Th17 are differentially induced according to the presence or absence of B7 molecule. It demonstrates that two molecular contexts (here defined by the presence and absence of a molecule) can differentially affect one readout.

In contrast with all these studies, Remedios et al. recently described that OX40L attenuated the polarization of Treg cells exhibiting a Th17 phenotype [258]. Indeed, it has been established that Treg cells can secrete IL-17 under inflammatory conditions. [259,260]. They showed that, within the Treg cell population, FoxP3$^+$ Treg cells were drastically diminished in OX40 KO mice, whereas they observed an increase of RORγt$^+$ Treg cells. The same phenomenon was observed in CD27 KO mice, another TNFSF member [258].

This system is a bit different from the previous one because they studied IL-17 and RORγt expression in the Treg population and not in the Th17 population, but it illustrates that OX40L might have a differential role on a given molecule, here IL-17, according to the context, here a cellular context (Th17 or Treg).

In addition, it has also been shown that OX40 stimulation inhibited IL-17 production by CD4 T cells *in vivo* and *in vitro*, through histone activation and chromatin repression at the IL-17 locus [261].

In human *in vitro* model, it has been shown that OX40L inhibited Th17 differentiation. Li et al. observed that OX40L down-regulated IL-17 production by CD4 T cell through up-regulation of IFNγ production [262].

c) OX40-OX40L and Th9 subset

Two studies demonstrated an important role of OX40-OX40L in inducing Th9 cells.

Xiao et al. cultured mouse naive CD4 T cells in Th9-polarizing cytokine condition (IL-4 + TGFβ) in the absence or presence of an OX40L transgenic presenting cells or an agonist anti-OX40 antibody. When stimulating OX40, they showed an important increase of Th9 cell percentage, by looking at intracellular IL-9 staining. They described that this induction was independent of PU.1, Th9 transcription factor, and occurred through TRAF6 and the non-canonical NF-κB pathway. In an *in vivo* airway inflammation model, they demonstrated that the injection of an anti-OX40 agonist antibody enhanced inflammation in WT mice whereas it had no impact on IL-9-KO and OX40-KO mice [263].

In addition, they looked at the impact of OX40L not only in Th9 but also in Th17 and Treg-polarizing conditions. Interestingly, they observed that OX40L increased Th9 cell percentage but it dramatically decreased Treg and Th17 cell percentage in their respective polarizing contexts [263].

Corroborating Xiao et al. observations, another study showed that OX40L was a key contributor of naive CD4 T cell polarization into Th9 cells when primed by dectin-1-activated DCs. Still in mice, but this time in cancer models, the authors showed that dectin-1 directed Th9 polarization via the contribution of OX40L and another member of the TNFSF, and induced an antitumoral response *in vivo* that relies on IL-9 [264].

d) OX40-OX40L and Tfh subset

OX40-OX40L interaction has been observed to highly influence Tfh development. Just before 2000, studies came out suggesting that OX40 could play a role in Tfh response. For instance, OX40L was shown to promote the expression of the chemokine receptor CXCR5 and to be involved in CD4 T cell migration into B cell zone and GC development [221,265]. Then, a lot of studies reported a positive impact of OX40-OX40L on Tfh cells, in mouse and human models.

In mouse model, Vogel et al. showed that OX40 and ICOS degradation by Roquin-1 and Roquin-2 proteins controlled Tfh cells and that Roquin-1 and Roquin-2 deletion increased OX40 signaling and Tfh differentiation [266].

More recently, in a vaccinia virus infection mouse model, Tahiliani et al. observed that OX40-deficient mice displayed a huge decrease (about 70%) of Tfh cells in comparison with WT mice. In this line, they showed that OX40 signaling was crucial for GC development and antibody production. Finally, in addition to its action at the initial phase of Tfh response, OX40 was shown to maintain mature and GC Tfh cells [267].

Regarding human studies, Jacquemin et al. showed that a human soluble recombinant OX40L protein induced characteristic Tfh-associated genes, IL-21, CXCR5 and Bcl-6 among others, by both naive and memory CD4 T cells from healthy donors, stimulating with anti-CD3/anti-CD28 [86]. These results were confirmed by Pattarini et al., this time in a co-coculture system. They demonstrated that co-culturing TSLP-activated $CD11c^+$ DCs and allogeneic naive CD4 T cells with an anti-OX40L blocking antibody decreased key features of Tfh cells, such as IL-21 and CXCL13 secretion and Bcl-6 expression [85].

However, some papers showed that OX40-OX40L negatively regulated Tfh population.
In murine infection model, Boettler et al. described that OX40-deficient mice lacked GC, were

impaired for T cell anti-viral response and failed to control lymphocytic choriomeningitis virus (LCMV) infection, suggesting that Tfh responses might be negatively affected [268]. However, one year later, they published that treating LCMV infected mice with an anti-OX40 agonist antibody at the early phase of infection inhibited LCMV-specific humoral response and enhanced viral replication. They added that Tfh population was reduced in the anti-OX40 treated mice compared to the control group, most probably because OX40 induced Blimp-1 and T-bet expression and thus drove Th1 differentiation [269].
On the other hand, Marriott et al. did not see any impact of OX40-OX40L interaction on Tfh cell number in *Listeria* infection mouse model [270].

Another study described that anti-OX40L antagonist antibody treatment did not impair GC and $CXCR5^+$ Tfh development, as opposed to anti-ICOSL antagonist antibody [271].

e) OX40-OX40L and Treg subset

OX40 ligation impact on Treg is a worthwhile topic, in particular since anti-OX40 agonist antibodies are being developed for cancer immunotherapies, where Treg promotion would be counter-productive. Indeed, Treg cells in tumors are known to upregulate OX40 and up to 80% of Treg cells can express OX40 in some cancers [272].

In mice, a lot of studies showed that OX40 induced a negative regulation of FoxP3 and thus Treg subsets and their suppressive functions in several models such as cancer or graft [273–276].

More recently, Zhang et al. described how OX40 signaling led to $FoxP3^+$ cell inhibition and thus Treg cell inhibitions through two molecular pathways, one involving basic leucine zipper ATF-like transcription factor 3 (BAFT3) that acted on chromatin compaction at the Foxp3 locus, and the other involving the AKT-mTOR pathway that excluded Foxo1/3, essential for FoxP3 transcription [277].

In human, Ito et al. demonstrated that OX40 stimulation abrogated IL-10-producing Treg (also called Tr1 cells) from naive and Tr1 memory CD4 T cells induced by dexamethasone and vitamin D3. OX40 also inhibited the generation of Tr1 cells from naive CD4 T cells induced by ICOSL or by the co-culture with immature DCs [278].

Voo et al. confirmed these observations by showing that anti-human OX40 agonist antibody inhibited Treg induction and suppressive function [279].

Many articles also related OX40 molecule as a positive regulator of Treg cells and important for their homeostasis. The first straightforward evidence was that OX40 was highly expressed on Treg cells and on top of that, higher compared to non-Treg cells.

In an OX40-deficient mouse model of colitis, it has been shown that OX40 promoted the accumulation of Treg cells in the colon and was required to inhibit T cell-induced intestine inflammation [280].

Recently, Polesso et al. showed that anti-OX40 agonist treatment did not impair Treg function and actually enhanced CD4 T cells (including Treg) proliferation, *in vitro* and *in vivo* in tumor-bearing mice [281]. This study is in line with a study from Takeda et al. showing that OX40 positively influenced Treg development, homeostasis and suppressive function [282].

Thus, OX40-OX40L impact on Treg seems to highly depend on the context and this is greatly illustrated by Ruby et al. They showed in mice that Treg differentiation from naive CD4 T cells, induced by TGFβ and OX40L, was dependent on the cytokines present in the medium. In addition, blocking IFNγ and IL-4 increased Treg cell subset percentage [283].

4) OX40 / OX40L in pathologies and clinical trials

a) Cancer

As described in the previous part, cancer is a very complex pathology. In contrast with chemotherapy, that kills tumor cells by targeting rapidly-dividing cells in the body, immunotherapy aims at boosting the patient immune system, for it to recognize and eliminate tumor cells. For now, only a few antagonist antibodies against co-inhibitory immune checkpoints were granted FDA licensure in specific cancer type but agonist antibodies against co-stimulatory immune checkpoints, such as anti-OX40, are under development.

An interesting fact was reported in an OX40-deficient patient. So far, a single human has displayed homozygous recessive mutations in the OX40 gene, TNFRSF4, leading to very few OX40 at the T

cell surface and thus few OX40-OX40L interactions. In addition, this woman was diagnosed with a Kaposi Sarcoma (KS), a rare type of cancer affecting cells with an endothelial origin. KS is caused by the human herpes virus 8 (HHV-8), which is asymptomatic in almost all cases. This patient had a higher percentage of naive CD4 T cells, a lower percentage of non-naive T cells subsets in blood and an impaired memory CD4 T cell response. They correlated the loss of function of OX40 alleles with KS development [284].

In the end, the rationale of targeting OX40 pathway in cancer is based on its ability to increase T cell proliferation, migration and survival, to enhance cytokine production and to increase memory T cell generation, useful features for antitumor immunity.

An OX40 monoclonal antibody was tested in phase I clinical trial in advanced cancer (NCT01644968). It showed promising effects in 12 out of 30 patients, with at least one metastatic lesion regression and a significant increase of non-Treg CD4 and CD8 T cell proliferation [285].

MedImmune launched several clinical trials with anti-OX40 agonist antibodies, in monotherapy or combination. MEDI6469, a murine agonist antibody, was tested in advanced solid tumors (NCT02274155). Its administration was safe and increased proliferation and activation of T cells in TME and peripheral blood of some patients [286]. MEDI6469 was also tested in combination with chemotherapy or radiotherapy (NCT01303705, NCT01862900). MEDI0562 is also an anti-OX40 monoclonal antibody, but a humanized form of MEDI6469. It was tested on advanced solid tumors in phase I (NCT02318394) and is now tested more specifically on head and neck squamous cell carcinoma (HNSCC), melanoma and ovarian cancer patients (NCT03336606, NCT03267589). Both MEDI6469 and MEDI0562 have been tested in combination with Durvalumad or Tremelimumab, monoclonal antibodies against PD-L1 and CTLA-4 respectively (NCT02205333, NCT02705482). Other humanized anti-OX40 agonist antibodies have been developed and tested in clinical trials by other companies, MOXRO0916 from Genentech (NCT02410512, NCT03029832) and GSK3174998 from GlaxoSmithKline and Merck (NCT02528357), and a fully human monoclonal antibody, PF-04518600, was created by Pfizer (NCT02315066).

In addition to monoclonal antibodies, recombinant proteins have been conceived. MEDI6383 is a human OX40L fusion protein, tested in advanced solid tumors, alone or in combination with an anti-PD-L1 (NCT02221960).
Moreover, recently, Shattuck Labs started a clinical trial using a PD-1-Fc-OX40L in advanced solid tumors and lymphomas (NCT03894618). This is a two-sided human fusion protein that can bind

to PD-L1/L2 and block PD-1 signaling, and stimulate OX40. PD-1-Fc-OX40L was observed in immune synapses and enhanced T cell proliferation and cytokine production. Interestingly, its functional activity was superior to anti-PD-1 antagonist antibody, anti-OX40 agonist antibody and the combination of both antibodies [287].

b) Allergic diseases

Allergies are defined by an allergic inflammation, caused by the patient immune system interacting with its environment. Allergy is composed of a sensitization phase and a specific immune response development against the allergen. Allergies can occur against several components, natural or chemical, it can be food, drug, a substance in the air such as pollen, dust mite, etc. They can be acute or chronic and are maintained by different mechanisms such as histamine, pro-inflammatory mediator and IgE release, eosinophils activation and mast cell degranulation [288].

Allergic diseases have been rapidly associated with IL-4 cytokine and thus IL-4 producing Th2 and Tfh cells [289,290]. Although OX40L functions on Th polarization seems to be highly dependent on the context, it has been shown previously that a lot of studies reported OX40L as a Th2 and Tfh promoting molecule. Hence this pathway is interesting to target in allergy, intending to block OX40 and OX40L interaction, in contrast with agonist antibodies developed for cancer treatment.

Atopic dermatitis (AD) is a chronic allergic disease. It is the most common form of eczema, in which the patient skin becomes red, dry and itchy. AD affects essentially children and usually disappears within a few years, but in 10% of cases, it can continue during adulthood. OX40 and OX40L have been shown to be up-regulated in AD patient skin lesions, even though they were not associated with disease severity [291].

Several blocking antibodies against OX40 were conceived in this pathology. GBR830 is a monoclonal antagonist antibody targeting OX40 from Glenmark Pharmaceuticals. A first clinical trial phase, to assess the safety and the activity of the compound, was completed in May 2020 (NCT02683928) and showed efficacy in moderate-to-severe AD. GBR830 was well tolerated by patients and around 75% of patients showed an improvement of eczema and severity index score. This antagonist also induced a decrease of Th1, Th2 and Th17 inflammatory markers, such as IFNγ, IL-31 and IL-23 respectively [292]. It is now in phase IIb clinical trial and was renamed ISB830

(NCT03568162).
Another blocking antibody, KHK4083, produced by Kyowa Kirin Pharmaceutical Development, completed phase I (NCT03096223) and is now in phase II (NCT03703102).

Another clinical trial, this time using an anti-OX40L monoclonal antibody, has also been conducted by Genentech, for mild asthma, on patients with allergen-induced airway responses (NCT00983658). The treatment was well-tolerated and induced a decrease of serum IgE level and sputum eosinophil numbers. However, OX40L blockade showed no significant effect on blood eosinophil numbers and allergen-induced airway hyperresponsiveness, and in the end, did not attenuate asthmatic hyperresponsiveness [293].

c) Autoimmune diseases

Autoimmune diseases are defined by an activation of T cells and/or B cells, in absence of foreign antigen. This abnormal activation is usually associated with the presence of autoantibodies targeting self-antigens. It can be either organ-specific, such as type I diabetes, or systemic, such as systemic lupus erythematosus (SLE) [294].

OX40/OX40L-deficient mice or OX40/OX40L blockade revealed an important role of these molecules in autoimmune diseases, such as gastrointestinal autoimmune diseases including ulcerative colitis and Crohn's disease, commonly named inflammatory bowel disease (IBD). Gastrointestinal autoimmune diseases are defined by an exacerbated immune response in the gastrointestinal tract [295]. In IBD mouse models, blocking OX40-OX40L interactions have shown promising effects. Indeed, the authors described a clinical amelioration, associated with a decrease of T cell infiltration and inflammatory cytokine production in the colon [296,297]. In humans with IBD, an increased density of $OX40^+$ cells compared to healthy controls have been reported in the colon [298,299].

The monoclonal antagonist antibody targeting OX40, KHK4083, the same one tested in AD, has been tested in moderate ulcerative colitis patients and is now in phase II (NCT02647866). For now, although targeting the OX40 pathway appears promising, this is the only clinical trial targeting OX40-OX40L pathway in autoimmune diseases.

OBJECTIVES

CD4 T helper cells and their representative secreted cytokines play a central role in setting up an appropriate adaptive immune response against foreign pathogens. In the introduction, the complexity of the current CD4 Th cell subset classification, the polarization mechanisms of these subsets and how OX40L, a co-stimulatory immune checkpoint with the ability to boost T cell response, act on this polarization, have been presented. Moreover, it has been shown that the context in which a cell type, here CD4 T cells, is evolving can affect their global behavior at a large-scale (at the population or cellular level) and at a smaller scale a molecule function.

Regarding immune checkpoint molecules, current immunotherapies constitute a major advance for patient treatment in several pathologies, and particularly cancer. However, the positive rate response stays low and much remains to be done on the understanding of their mechanisms. In most studies, immune checkpoint functions were established by studying them individually, in specific conditions. However, the context may dramatically influence the function of biological molecules on a given output. For instance, it has been shown in the team that type I interferon response in CD4 T cell was highly dependent on the cytokine context [169].

There is currently no framework to properly analyze the context-dependency of a molecule function in biological systems. In biology among other disciplines, context-dependency can be more difficult to study because of several reasons. In *in vivo* systems, the cause inducing a molecule context-dependent function can be difficult to determine at the level of a whole organism. *In vitro*, it requires highly controlled systems and a sufficient number of contexts for the detection and quantification of context-dependency to be relevant.

To develop such a framework, we used the immune system as a model, because of the multiplicity of stimuli immune cells may sense, and the complexity of possible contexts. We established an experimental system including a stimulus of interest, applied to a specific immune cell type in several contexts. We chose to study OX40L function on CD4 Th cell differentiation, in four molecular and 11 cellular contexts. As described in the introduction, OX40L is an important immune checkpoint molecule in immunology and therapeutics. Moreover, CD4 Th cells are essential in physiological and physiopathological responses. As output response, we measured 17 Th cytokine secretion because:

- it has been shown that OX40L can modulate Th polarization and their specific cytokine secretion

- Th polarization is a major feature of CD4 T cells, and these 17 output cytokines are characteristic of Th subset responses
- Both molecular and cellular contexts have the ability to induce Th polarization

Thus, this work tried to address the following questions:

- How to evaluate context-dependency of a biological molecule function?
- Is it possible to quantify context-dependency? How?
- What would be the best method to quantify context-dependency of a molecule? How statistical modeling can be applied to this concept and its quantification?
- When several parameters define a context, how to determine their respective importance in context-dependent function of OX40L?

Then, regarding the data themselves, other questions came out:

- How to choose the experimental systems in which accurately quantify context-dependency?
- How to represent a large quantity of data without losing information? In other terms, how to reduce dimensionality with minimal information lost in systems with many parameters?

RESULTS

Publication

Quantitative modeling of OX40 ligand context-dependent function on human T helper cell polarization

Léa Karpf, Coline Trichot, Iris Legbre, Lilith Faucheux, Maximilien Grandclaudon, Charlotte Lahoute, Hamid Mattoo, Benoit Pasquier and Vassili Soumelis

Submitted at Plos Biology

Immune checkpoints are part of a broad signal diversity integrated by T cells. Immune checkpoints are known to play a key role during T cell activation and regulation. This family includes about thirty molecules and is divided into two functional categories. Co-stimulatory immune checkpoints, such as CD28, have the ability to boost T cell activation whereas co-inhibitory immune checkpoints, such as PD-1, play a role in T cell response regulation.

In this study, we use CD4 T helper polarization as a model to highlight how microenvironment parameters can have an impact on internal parameters, such as a biomolecule function on a given output. We wanted to further explore this aspect of context-dependency and its possible impact on Th polarization and particularly on Th cytokine secretion. Moreover, we chose OX40L as an interesting immune checkpoint molecule to study this concept. As presented in the introduction, there are already clues on OX40L functions on Th polarization and cytokine secretion. However, how the context can influence its function has never been described. In addition, tools were available to study OX40L in our two experimental systems: human recombinant OX40L protein (rhOX40L) and human anti-OX40L blocking antibody.

Consequently, we first decided to use a systematic approach by applying several cytokine contexts on T cells in the presence or absence of rhOX40L. To this aim, we used Th polarization culture system, with anti-CD3/anti-CD28 beads for TCR stimulation and Th polarizing-cytokines to induce Th0 (no cytokine), Th1 (IL-12), Th2 (IL-4) and Th17 (IL1β + IL-6 + IL-23 + TGF-β). A trimeric soluble rhOX40L protein was added to the culture to stimulate OX40 on T cells.

In a second step, we wanted to integrate a cellular context in our external parameters applied to T cells, to see the impact on OX40L function. These cellular contexts are composed of two parameters, the DC type and the DC-activating stimulus. We used two types of DCs: blood cDC2, directly isolated from healthy donor blood, and MoDCs, differentiated with IL-4 and GM-CSF from $CD14^+$ monocytes, also isolated from healthy donor blood. To extend the number of contexts, each subset was activated using different stimuli, with broad physiopathological relevance to bacterial (LPS, HKSA, Curdlan) and fungal (Zymozan) infections, and to allergy (TSLP). In this case, we added an antagonist monoclonal antibody against OX40L to block DC-T communication through OX40-OX40L interaction.

In our two experimental systems, we analyzed the major 17 Th secreted cytokines (output cytokines), in the presence or absence of OX40L, with the hypothesis that context-dependency may occur on different output cytokines. These output cytokines were measured in 302 observations to create a large dataset. By combining experimental systems and statistical modeling, we quantified and scored OX40L context-dependent functions on Th polarization, characterized by Th cytokine secretion.

In terms of mathematical methods for data integration, we used two main statistical modeling tools in this work: linear mixed model (LMM) and Lasso analysis. To establish a relevant context-dependency score, statistical modeling developments have been done first on Th molecular contexts since they are more simplistic compared to cellular contexts. We applied a linear mixed model on our Th dataset, independently for each output cytokine (Equation 1). In equation 1, Y (the variable we want to explain by the model) represents the OX40L-induced relative difference for a specific cytokine, in other terms, the OX40L-induced variation for a specific cytokine.

$$Y = \alpha_{\text{donor}} + \sum_{\text{context } k} \beta_k \mathbb{1}_k + \varepsilon \qquad (1)$$

Using this LMM, we estimated a β coefficient for each context, which represents the effect of the context on OX40L-induced cytokine variation, whilst taking into account the donor effect (α coefficient estimation). β coefficients correspond to the mean of OX40L-induced cytokine variation of donors for each context. Then, β coefficients were used to calculate OX40L context-dependency scores, also independently for each output cytokine. To this end, we calculated the

distances between β' (β/standard deviation) of each context two by two and the score was defined as the mean of these distances.

This same statistical strategy was then applied to bDC and MoDC cellular contexts. As described previously, contexts were composed of two parameters. In this line, when several parameters define a context, how to determine their respective importance in the context-dependent function of OX40L? To answer this question, we used a Lasso model to perform variable selection. By applying increasing penalties on variables, the Lasso model forces the model to keep only the most important variable, which best explains OX40L context-dependency.

To summarize, our mathematical modeling strategies allowed us to:

1) Identify the cytokines for which OX40L context-dependency was the most important in each of our systems (LMM and OX40L context-dependency score).

2) Define two different types of context-dependency, namely quantitative and qualitative context-dependencies.

3) Classify each context according to OX40L context-dependency (principal component analysis (PCA) and lollipop plot).

4) Identify the most important parameter influencing OX40L context-dependency between the DC type and the DC-activating stimulus (Lasso analysis).

Thus, among Th contexts, Th2 appeared as the one with the most influence on OX40L function, while in the bDC contexts, TSLP was by far the most influential. Finally, among cellular contexts, the DC type was found dominant in controlling OX40L context-dependency as compared to DC-activating stimulus.

In the end, our statistical model can be applied to any biomolecule, to decipher and quantify its context-dependency and evaluate its impact on the biomolecule function.

Title: Quantitative modeling of OX40 ligand context-dependent function on human T helper cell polarization

Authors: Léa Karpf[1,2,7], Coline Trichot[1,2,3,7], Iris Legbre[2,8], Lilith Faucheux[2,4,8], Maximilien Grandclaudon[1], Charlotte Lahoute[3], Hamid Mattoo[5], Benoit Pasquier[3], Vassili Soumelis[1,2,6,*]

Author affiliations

[1] Institut Curie, PSL University, INSERM U932, F-75005, Paris, France

[2] Université de Paris, Institut de Recherche Saint-Louis, INSERM U976, F-75010 Paris, France

[3] Immunology and Inflammation Therapeutic Area, Sanofi, Vitry-sur-Seine, France

[4] Université de Paris, Institut de Recherche Saint-Louis, INSERM UMR-1153, ECSTRRA Team, F-75010 Paris, France

[5] Immunology and Inflammation Therapeutic Area, Sanofi, Cambridge MA, USA

[6] Assistance Publique-Hôpitaux de Paris (AP-HP), Hôpital Saint-Louis, Laboratoire d'Immunologie, F-75010, Paris, France

7 These authors contributed equally to this work: Léa Karpf, Coline Trichot

[8] These authors contributed equally to this work: Iris Legbre, Lilith Faucheux

Contact information: vassili.soumelis@aphp.fr

Keywords: Immune checkpoints, T helper cell polarization, dendritic cells, OX40 ligand, context-dependency, statistical modeling, immunotherapy

Abstract

Context-dependency may explain large parts of the functional variability of physiopathological and pharmacological stimuli. Currently, there is no framework to analyze and quantify context-dependency over multiple contexts and response outputs. We studied OX40 ligand (OX40L) function on T helper (Th) cell differentiation, in four molecular (Th0, Th1, Th2, and Th17), and 11 dendritic cell (DC) contexts (5 monocyte-derived DC, and 6 cDC2 conditions). We measured 17 Th cytokines in 302 observations, and developed a statistical modeling strategy to quantify OX40L context-dependency. This revealed highly variable quantitative context-dependency scores, depending on the output cytokine and context type. Among Th contexts, Th2 was the most influential on OX40L function. Among DC contexts, DC type rather than activating stimuli was dominant in controlling OX40L context-dependency. This work unveils the complex determinants of OX40L function, and provides a unique framework to decipher and quantify the context-dependent functional variability of any biomolecule or drug.

Introduction

Context-dependency may induce tremendous variability in the function of any biomolecule or drug [1, 2]. It could explain large parts of the patient-to-patient variability in drug response [3, 4]. Although studies in the past 5 to 10 years have brought increasing evidence of its potential impact, the context-dependency of major functional molecules, such as growth factors, cytokines, and immune checkpoints (IC), remains mostly unknown.

Progress in the field has been hampered by the underlying complexity [5, 6]. First, a large number of possible molecular and cellular contexts may influence the function of a biomolecule of interest. For example, TNF-α in the context of rheumatoid arthritis may act differently than TNF-α in the context of cancer microenvironment. Second, context-dependency can be of different types, depending on the quantitative or qualitative differences observed across different contexts. The same type of output response (such as induction of protein X) observed at different magnitudes, would correspond to a quantitative context-dependency. Conversely, opposite effects observed in two different contexts would be qualitative context-dependency. Third, the nature and magnitude of the context-dependency may depend on the functional outputs. There is currently no systematic framework to decipher and quantify context-dependency by taking into account these different levels of complexity.

IC include over thirty molecules, and play a key role in T cell activation and regulation. Most IC functions were established by studying checkpoints individually, focusing on one function, in one stimulatory condition. However, IC act in variable microenvironmental contexts, at steady state and in pathologies, which might impact their function. Studies of IC context-dependency are scarce. The cytokine context was shown to impact the function of OX40 ligand (OX40L), a co-stimulatory IC, on Th2 [7] and Tfh [8, 9] differentiation. We have recently shown that CD28 harbored different functions depending on variations in DC-expressed molecular contexts [10]. These studies contributed to a proof-of-concept for IC context-dependency. Additionally, OX40/OX40L-targeting antibodies have been used in preclinical and clinical studies in allergy, autoimmune diseases and cancer [11, 12, 13]. Hence, OX40L context-dependent functions may impact its biological role in immune responses, as well as the therapeutic response to OX40L targeting.

In this study, we used OX40L as a model to dissect the impact of multiple molecular and cellular contexts on IC function. By combining experimental systems and statistical modeling, we were able to quantify and score OX40L context-dependency, and to specifically determine the impact of Th and DC contexts. Our integrated statistical framework has broad applicability to any biomolecule, and revealed potential mechanisms to tailor OX40L targeting based on individual inflammatory contexts.

Results

OX40L modulates multiple Th-derived cytokines in distinct Th-polarizing contexts

IC molecules co-stimulate or co-inhibit T cells in different microenvironmental contexts that may influence their function. We sought to address the impact of the cytokine context on IC function in Th polarization. We focused on OX40L as a model costimulatory IC because of its known ability to influence Th polarization [7, 8, 9]. We studied the function of OX40L in four prototypical Th-polarizing cytokine contexts: Th0 (no added cytokine), Th1 (IL-12), Th2 (IL-4), and Th17 (IL-1β+IL-6+IL-23+TGF-β). Naive CD4 T cells purified from healthy donor blood were cultured in these four contexts, in the presence of anti-CD3/anti-CD28 beads. We verified OX40 expression on T cells by flow cytometry. OX40 is not constitutively expressed on naive CD4 T cells but is expressed as early as 24 hours culture upon TCR stimulation (Figure S1a). OX40 triggering was obtained by using a soluble trimeric recombinant human OX40L (rhOX40L) protein in each of the Th cytokine context. We assessed the Th responses after 5 days of culture by protein level measurement of all 17 major Th-derived cytokines (hereafter "output cytokines") in T cell culture supernatants. This generated a dataset composed of 17 Th output cytokine levels in four Th contexts, from 13 independent donors (Figures 1a and S2, Step 1).

Each of the four Th contexts induced expected lineage-defining output cytokine secretion: IFNγ for Th1, IL-4, IL-5 and IL-13 for Th2, IL-17A and IL-17F for Th17. Of the remaining output cytokines, some were detected in all contexts, such as IL-2, IL-21 and TNF-α, and others in one or two specific contexts, such as IL-31 in Th2, and IL-9 in Th2 and Th17 (Figure S1b).

In each of the Th contexts, we analyzed the expression of the 17 output cytokines in presence and absence of rhOX40L. Because of the large number of measurements (17 cytokines in 8 conditions for 13 donors), we represented the results in the form of a heatmap. We calculated absolute differences of each output cytokine concentration between presence and absence of rhOX40L, in each Th context (Figure S2, Step 2). This established whether each output cytokine was induced (red), inhibited (blue) or not impacted (white) by rhOX40L (Figure 1b). For example, rhOX40L decreased IL-10 secretion in all contexts, with a stronger decrease in Th2 context. rhOX40L also decreased GM-CSF production in Th0, Th1 and Th17 contexts, but not in Th2 context. Moreover, rhOX40L increased IL-21 secretion in Th0, Th2 and Th17 contexts but not in Th1 context (Figures 1b and 1c).

Next, we addressed the impact of rhOX40L on the global Th profile, by integrating all 17 output cytokines in a principal component analysis (PCA). On the basis of the 17-output cytokine profile, we could clearly distinguish Th0, Th1, Th2 and Th17 conditions, as represented by their barycenter distributed in the PCA space. Presence of rhOX40L induced a shift in the global output cytokine profile, representing its functional impact. The smaller shifts were observed in Th1 and Th17 contexts, and projected along PC2 and PC1, respectively. The largest shifts occurred in Th2 along

PC1, and in Th0 along both PC1 and PC2 (Figures 1d and S2, Step 3). Shifts induced by rhOX40L were quantitatively and qualitatively different for each context. Hence, rhOX40L induced a differential effect on output cytokine secretion according to the Th context in which T cells were evolving, establishing a context-dependent effect of rhOX40L on output cytokines.

OX40L induces a significant context-dependent effect on five output cytokines

In this first multivariate description, we noticed that OX40L context-dependent effects were also depending on the nature of the output cytokine. We developed a method to quantitatively score context-dependency of a biological stimulus on multiple output response variables.

In order to compare the score across the different output cytokines, we transformed the dataset to obtain OX40L-induced relative differences, taking into account donor effect and normalized concentration levels between output cytokines (Figure S2, Step 4.1). For each output cytokine, we applied a Linear Mixed-effects Model (LMM) (Figure S2, Step 4.2). Then, we calculated the mean distances between the different Th contexts re-scaled estimate, β' (i.e. $\hat{\beta}/\hat{\sigma}$), to score context-dependency (Table S1). Finally, we tested statistical significance of this context-dependency with a likelihood ratio test (Figures 2a and S2, Step 4.3).

This method can generally be applied to any dataset, even if the output is not expressed in all contexts. However, in our Th settings, some cytokines were produced only under certain contexts, such as IL-4, IL-5, IL-9, IL-17A, IL-17F and IL-31, which are specific Th2 and Th17 lineage cytokines. In addition, they were not de novo induced in the presence of OX40L. Thus, taking into account these output cytokines would induce a bias in the final score, because they would appear as strongly context-dependent, only due to their very narrow expression pattern. To avoid this bias, we included in the analysis only the 11 output cytokines detected in all Th contexts.

As previously, we represented the estimated OX40L-induced relative difference for the 11 output cytokines in the form of a heatmap (Figure 2b). Strikingly, we observed that OX40L effects on a given output cytokine were highly dependent on the Th context. We defined two types of context-dependency: the first when OX40L was increasing or decreasing a given output cytokine concentration in all contexts but in different magnitudes ("quantitative context-dependency"), as was the case with IL-6 or IL-10 (Figure 2b); the second when OX40L had qualitatively different effects on a given output cytokine according to the context ("qualitative context-dependency"), as was the case with IL-22 or GM-CSF (Figure 2b). A combination of qualitative and quantitative context-dependencies could be observed.

Such statistical modeling strategy enabled to 1) directly compare OX40L context-dependency for different Th output cytokines, 2) assess the type of context-dependency, 3) assess its statistical significance (Figure 2c). Likelihood ratio tests highlighted significant context-dependencies for five output cytokines: IL-10, IL-22, IL-13, TNF-α, and IL-3 (Figures 2c and 2d). OX40L decreased IL-10, IL-13 and IL-3 in all contexts (one-way variation: black bars in Figure 2c), indicating quantitative

context-dependency. On the contrary, IL-22 and TNF-α secretion increased or decreased in presence of OX40L according to the Th context (two-ways variation: black bars indicate dominant variation, Figure 2c), indicating qualitative context-dependency. This quantitative analysis of context-dependency demonstrated that 1) the molecular context (represented by distinct Th conditions) could heavily impact the function of the IC OX40L, and 2) the intensity and type of context-dependency was highly variable for distinct OX40L functions. This implies that a context-dependent effect for a given function may not necessarily apply to another function.

The impact of cellular blood DC contexts on OX40L function

OX40L may be expressed by DC in various phenotypic and functional states, characterized by differences in multiple molecular signals delivered to T cells. We addressed the impact of such cellular contexts on OX40L functions in DC-T cell crosstalk. Immature primary cDC2 blood DC (bDC) were FACS-sorted from healthy donors and activated with 6 different stimuli, each defining one "bDC context": Zymosan, PAM3CSK4 (PAM3), LPS, Heat-killed Staphylococcus aureus (HKSA), Curdlan or TSLP. These conditions were selected for inducing distinct DC activation states [10]. We measured OX40L expression on bDC after 24 and 48 hours activation. OX40L was expressed in all bDC contexts even bDC cultured without stimulation (NT) (Figure S3a). After 24 hours stimulation, activated bDC were co-cultured with allogeneic naive CD4 T cells in presence of an anti-OX40L blocking antibody or matching isotype. As in Th context experiments, the output cytokines were measured after 6 days of co-culture and 24 hours restimulation (Figures 3a and S2, Step 1).

We performed the same type of analysis as in Th contexts, and calculated absolute differences in cytokine concentrations between absence (anti-OX40L antibody) and presence (isotype control) of OX40L at the DC surface, in each bDC context (Figures 3b and S2, Step 2). As for Th contexts, results were represented in the form of a heatmap given the large number of measurements (17 cytokines in 12 conditions for 9 donors). OX40L significantly increased IL-13 and TNF-β in 4 out of 6 bDC contexts (PAM3, LPS, HKSA and Curdlan-bDC), but increased IL-22 only in LPS-bDC context (Figures 3b and 3c). We noticed that OX40L had a minor overall impact on output cytokines in the Zymozan-bDC context, as compared to the five other contexts. Strikingly, OX40L-induced effects on output cytokines in the TSLP-bDC context had a very different pattern, as compared to the five other contexts (Figure 3b). This observation was corroborated by a PCA showing that the directional shift from "TSLP+anti-OX40L" to "TSLP" conditions was in an opposite direction when compared to the shift in the other bDC-contexts. The PCA also revealed that the larger OX40L-induced shifts were observed in the PAM3, and Curdlan bDC contexts (Figures 3d and S2, Step 3).

The TSLP-bDC context determines a qualitatively different OX40L-induced effect

Next, we applied the same analysis strategy than in Th contexts to quantify OX40L-induced context-dependency in bDC contexts (Figure S2, Step 4). The heatmap of estimated OX40L-induced relative difference for the 17 output cytokines revealed different patterns of output cytokine behaviors due to

OX40L presence, across the 6 bDC contexts (Figure 4a). We found again both quantitative and qualitative context-dependencies. For example, OX40L effects on IL-21 and IL-9 were quantitatively context-dependent (one-way variations, different in magnitude), and OX40L effects on IL-22 and IFNγ were qualitatively context-dependent (two-ways variations) (Figures 4a and b). The likelihood ratio tests highlighted significant context-dependency for four output cytokines (Figures 4b and 4c), including IL-3 (quantitative context-dependency), GM-CSF, IL-2 and IFNγ (qualitative context-dependency). In order to identify the contexts that were inducing these context-dependencies, we performed post-hoc likelihood ratio tests (Figures S3b and S2, Step 5 and Table S2). Confirming the PCA observation, they indicated that these qualitative context-dependent effects were mostly due to OX40L impact on output cytokines in the TSLP-bDC context, which was very different from the others.

Thus, OX40L-induced effect on output cytokines was dependent on the bDC context, with a strikingly different pattern in the TSLP-bDC context.

DC subsets differentially impact OX40L-induced effects on output cytokines

We have started by defining cellular contexts based on distinct stimuli given to the same DC subset. Next, we assessed whether the DC type could also determine context-dependent OX40L functions. To answer this question, we compared OX40L-induced effects on output cytokines in bDC versus monocyte-derived DC (MoDC) contexts, each stimulated in the same 5 conditions (Zymosan, PAM3, LPS, HKSA or Curdlan). Since TSLP receptor was not expressed on MoDC [14, 15], we did not use TSLP to activate MoDC. We verified OX40L expression on MoDC after 24 and 48 hours activation in each of the MoDC contexts. OX40L expression was significantly higher in all MoDC contexts compared to MoDC cultured without any stimulation (NT) (Figure S4). After 24h stimulation, activated MoDC were co-cultured with allogeneic naive CD4 T cells in presence of an anti-OX40L blocking antibody or corresponding isotype. The same output cytokines as previously were measured in the supernatants after 6 days coculture, and 24 hours anti-CD3/CD28 restimulation (Figures 5a and S2, Step 1).

To get a global view of OX40L effects on output cytokine secretion, we calculated absolute differences of cytokine concentration between absence and presence of anti-OX40L, in each MoDC context (Figure S2, Step 2). OX40L increased IL-13 in all MoDC contexts but in different magnitude, similar to bDC contexts (quantitative context-dependency). This was also observed for TNF-β, but this time it was not concordant with what was observed in bDC contexts. For IL-22, both MoDC and bDC contexts determined qualitative context-dependency (Figures 3b/c and 5b/c). PCA performed on MoDC contexts revealed a large shift in all MoDC contexts when comparing the presence and absence of OX40L (Figures 5d and S2, Step 3). Thus, OX40L-induced effects on Th output cytokines were more evenly distributed across MoDC contexts, as compared to bDC contexts.

Next, we compared OX40L context-dependency scores for each output cytokine between bDC and MoDC contexts. Scores for bDC were re-computed without considering TSLP-bDC context, since MoDC were not stimulated with TSLP (Figures 6a, 6b, 6c and S2, Step 4). Interestingly, OX40L context-dependency scores showed different patterns in bDC and MoDC contexts (Figure 6b). The likelihood ratio tests highlighted significant context-dependency for four output cytokines in MoDC contexts and none in bDC contexts (Figures 6b and 6c). In MoDC contexts, OX40L induced an increase in IL-31 and GM-CSF concentrations in all contexts, which indicated that context-dependencies were defined by a quantitative effect. IL-4 and IL-5 secretion increased or decreased in presence of OX40L according to the MoDC context, indicating qualitative context-dependency (Figure 6b). These behaviors were not observed in the corresponding bDC contexts.
Thus, in addition to DC stimuli, DC type also had an impact on OX40L-induced effects on output cytokines. This established that the cellular context determined by either different activating stimuli, or different subsets, both affected OX40L function.

DC type has more impact than DC-activating stimuli on OX40L context-dependent function

Finally, we wanted to determine which parameter had the most impact on OX40L-induced modulation of Th output cytokines. We compared the impact of the Th contexts, bDC contexts and MoDC contexts on OX40L function. Based on the previous PCA, we first calculated the Euclidean distances in each context between presence and absence of OX40L. In the Th contexts, Euclidean distance calculations revealed a higher distance between Th2 and Th2+rhOX40L than in Th0, Th1 and Th17. This suggested that OX40L had a greater impact on output cytokines within Th2 context, followed by Th0 context (Figure 7a). In bDC contexts, OX40L had a greater impact on output cytokines within TSLP-bDC context, as compared to the five other bDC contexts (Figure 7b). Finally, in MoDC contexts, we saw fewer striking differences than in Th and bDC contexts. Still, LPS-MoDC contexts conferred higher OX40L-induced impact on output cytokines (Figure 7b). This confirmed what we observed above, using only the first two components of the PCA.

In addition, we went deeper in the analysis within DC contexts. In the previous analysis, we considered the DC context as bDC or MoDC activated with different stimuli. DC contexts were composed of two variables: the DC type and the DC-activating stimuli. Therefore, we sought to understand which of these two variables, composing DC context, revealed the strongest context-dependent effect of OX40L. To this end, for each cytokine independently, we applied a LMM to remove intra-donor correlations, followed by a group-lasso model on the residuals. We displayed the model's coefficients values according to the lasso penalty, so that the main variable involved in OX40L context-dependency would be the last to fall to zero (Figure 7c and d). We observed two distinct groups of cytokines, one for which OX40L context-dependency was predominantly due to the DC type (Figure 7c), and one for which OX40L context-dependency was predominantly due to the DC-activating stimuli (Figure 7d). However, for the majority of output cytokines (13 out of 17),

the DC type was the main variable involved in OX40L context-dependency (Figure 7c). Thus, within tested cellular contexts, OX40L context-dependency on output cytokines was mostly due to the DC type.

Discussion

Context-dependency refers to the variability in the function of a biomolecule when acting in different contexts. A major challenge in studying context-dependency lies in the tremendous diversity of possible contexts, which can be viewed at several levels: different individuals, organs, sub-anatomical locations or microenvironmental niches. Considering anatomical sites, it is known that the lung microenvironment promotes the development of Th2 responses [16], whereas the brain promotes regulatory T (Treg) cell responses [17]. However, to our knowledge, there is no direct comparison of the function of the same biomolecules acting within lung versus brain microenvironments. This would allow to precisely determine the extent of that function that may depend on the anatomical microenvironment. Similar questions may be asked when considering different types of inflammatory contexts: is a given molecule functioning differently when expressed in distinct types of inflammation. We and others have shown that TSLP is expressed in atopic dermatitis and activates DC to promote a Th2 response [7, 15]. However, in the context of skin psoriasis, TSLP may promote IL-23 production by DC, which would favor Th17 responses [18]. This can only occur due to the lack of IL-4, which can inhibit DC-derived IL-23 [18].

Studies at the level of an organism, an organ or tissue may be important to raise the possibility of context-dependent functions, but cannot be used to definitely demonstrate and quantify context-dependency. In order to do so, a controlled experimental system is required, in which specific output functions of a molecule of interest would be assessed in distinct contexts. This strategy was used to establish important functional dichotomies of cytokines. For example, the differential effect of TGF-β on mouse CD4 Th cell polarization was demonstrated by comparing the absence and presence of IL-6, which promoted Treg cells and Th17 differentiation, respectively [19, 20]. The importance of the cytokine context in human Th cell polarization was also established for Th17-promoting cytokines [21], and type I Interferon [6]. However, the limited number of contexts (usually two) did not allow to quantify context-dependency, and to identify possible qualitative variations in a systematic manner. In our study, we considered 15 different contexts, which necessitated the use of quantitative statistical methods in order to precisely quantify context-dependency in the form of a score. This score could be assessed for various output functional response markers, which enabled to rank them according to context-dependency. This revealed that IL-10 was the most sensitive to OX40L context-dependency in Th-polarizing contexts, meaning that the impact of OX40L stimulus on IL-10 production was highly variable. If the inhibition of T cell-derived IL-10 would be a target function of antagonistic anti-OX40L antibody, we would expect high patient-to-patient variability. Conversely,

the impact of OX40L on some other T cell-derived cytokines (IL-6, IL-21, TNF-β) was very robust to the context, suggesting a more consistent effect across patients and inflammatory contexts.

Most studies evaluating the context-dependent effects of a molecule have used molecularly defined contexts [7, 8]. Although useful in proof-of-concept studies, using the presence and absence of a cofactor to define a biological context has several limitations. First, it creates extreme scenarios of complete absence versus high concentrations of the molecular context. This would not reflect slight variations that may be observed in physiopathology. Second, it does not reflect the complexity of inflammatory contexts, which may involve variations in several contextual molecules of different nature. In our study, we have introduced the concept of "cellular context", represented by different cell types, in different activation states. It is known that distinct DC-activating stimuli are associated to very different DC molecular and functional states [10]. However, the impact of the DC state on the function of a given IC was never addressed. By studying the function of OX40L systematically across 11 DC states, we could precisely quantify the impact of the cellular context on OX40L effects in T helper cell polarization. The use of group-lasso models allowed us to deconvolute the respective contribution of DC type versus DC-activating stimuli in the control of OX40L function. This revealed that the DC type was the most influential variable. This should encourage future studies of cell-derived biological stimuli to consider the cellular context as a potentially key determinant of functional variability.

OX40L context-dependency was very different when comparing molecular and cellular contexts. In molecular contexts, OX40L could enhance or decrease the production of an output cytokine (IL-22, TNF-α), depending on the Th-polarizing context considered. It also revealed previously unknown functions of OX40L, in particular the differential regulation of IL-17A versus IL-17F in the Th17 context. On the contrary, OX40L preferentially increased output cytokines across cellular contexts. An exception was the TSLP-bDC context, which influenced OX40L in a qualitatively different manner, as compared to the other bDC contexts. Post-hoc tests and the analysis of bDC contexts without TSLP-bDC demonstrated that the TSLP-bDC context was the most impactful on OX40L context-dependency (Table S2). This emphasizes the peculiarity of the TSLP-bDC context, and shows that the function of an IC cannot be dissociated from the state of the DC expressing it.

The large variability of molecular and tissue contexts during inflammation raises the question of how broadly they may be represented and mimicked in experimental systems. In our study, we considered four molecular and 11 DC contexts, as defined by the combination of DC type and activating stimulus. This represents a large diversity of contexts, with broad physiopathological relevance to bacterial (LPS, HKSA, Curdlan) and fungal (Zymosan) infections, and to allergy (TSLP). However, number of inflammatory conditions may induce different DC states. In cancer, the microenvironment induces peculiar DC programs, which may either promote or control tumor

development [22]. Such complex tissue microenvironments are difficult to recapitulate in controlled systems, and require dedicated studies. The availability of data resources on tumor DC states [23, 24], and biological resources from human tumors, should facilitate the generation of tumor "DC contexts" for systematic studies. Our results suggest that distinct DC contexts may influence the function of various IC, and possibly modify the efficiency of IC targeting strategies.

OX40 has been considered as a drug target to enhance or inhibit T cell responses for over 20 years [25]. OX40 blockade demonstrated promising effects in mouse models of rheumatoid arthritis [12, 26]. Interestingly, OX40 agonists used in tumor models increased mice survival and tumor-specific CD4 memory T cells in a manner that was dependent on cancer type model and anatomical site, suggesting that the context could significantly influence treatment efficiency [27, 28]. More recently, OX40 agonists associated with PD-1 blockade increased antitumor immunity in a transplanted mouse mammary tumor model [29]. In human clinical trials, OX40 targeting has yet to demonstrate an efficacy, although promising results were obtained in early stage studies [13, 30]. Variable patient response to OX40 agonists in cancer echoes previous studies showing contextual effects in mouse models [27, 28], and in human Th polarization assays with limited number of contexts [7, 8]. Our study now definitely establishes the context-dependency of OX40L function in molecular and cellular contexts, with a precise quantification and identification of the complex underlying determinants. Applying our conceptual and methodological framework to other IC in a systematic manner, could help quantifying their context-dependency, and identifying their most contextual functional outputs. Together, such new knowledge could help in a rational selection of IC to target in a given tumor type, and to identify the determinants of drug response variability in individual patients. On the contrary, ignoring major context-dependent effects may create an obstacle to the efficient targeting of highly contextual molecules and pathways.

Methods

PBMCs purification

Fresh apheresis blood from healthy human blood donors was obtained from Etablissement Français du Sang (French Blood Establishment) after written informed consent, under an ethically-approved convention with Institut Curie and INSERM, according to national regulations. PBMCs were isolated by centrifugation on a density gradient (Lymphoprep, Proteogenix).

Naive $CD4^+$ T cells purification

Naive $CD4^+$ T cells were purified from PBMCs using the EasySep™ Human Naive $CD4^+$ T Cell Isolation Kit (StemCell Technologies) to reach 95% purity as $CD4^+CD45RA^+CD45RO^-$ cells.

Cytokine contexts for Th cell polarization

Naive CD4 T cells were cultured for 5 days with only anti-CD3/anti-CD28 Dynabeads (Life Technologies) to obtain Th0, or in combination with either 10 ng/mL IL-12 (R&D Systems) (Th1), 25 ng/mL IL-4 (R&D Systems) (Th2), or a cocktail of 100 ng/mL IL-23 (R&D Systems), 10 ng/mL IL-1β, 1 ng/mL TGF-β and 20 ng/mL IL-6 to obtain Th17 (Peprotech) as already published [6]. When indicated, 600 ng/mL rhOX40L (R&D Systems) was added to the T cell culture. At the end of the culture T cells were washed, counted and reseeded at 10^6 cells/mL and restimulated with anti-CD3/CD28 Dynabeads (Life Technologies) for 24 hours before collecting supernatants for cytokine measurement.

Monocyte-derived dendritic cells generation

$CD14^+$ cells were selected from PBMCs using magnetically labeled anti-CD14 Microbeads and MACS LS columns following manufacturer's instructions (MiltenyiBiotec). $CD14^+$ cells were then cultured with IL-4 (50 ng/mL) and GM-CSF (10 ng/mL) (MiltenyiBiotec) for 5 days in RPMI 1640 Medium, GlutaMAX (Life Technologies) with 10% Fetal Calf Serum.

Blood dendritic cells purification

Blood DC were purified using the EasySep Human Myeloid-DC Enrichment Kit (Stem Cell Technologies). cDC2 dendritic cells were sorted on a MoFlo Astrios sorter (Beckman Coulter) to reach 98% purity as Lineage (CD3, CD14, CD16, CD19, CD20, CD56)$^-$, $CD4^+$ (BD), $CD11c^+$ (Biolegend), $BDCA1^+$ (ThermoFisher), $BDCA3^-$ (Miltenyi Biotec).

DC and MoDC activation

MoDC and sorted cDC2 were seeded at 10^6 cells/mL in a flat bottom 96-well plate and activated for 24 hours using 10 µg/mL PAM3CSK4 (Invivogen), MOI 10 Heat-killed Staphylococcus aureus (Invivogen), 10 µg/mL Zymosan (Sigma-Aldrich), 10 µg/mL Curdlan (Invivogen) or 100 ng/mL LPS (Invivogen) in RPMI 1640 Medium, GlutaMAX (Life Technologies) with 10% Fetal Calf Serum (Hyclone) 100 U/mL Penicillin/Streptomycin (Gibco), MEM Non-Essential Amino Acids (Gibco) and 1 mM Sodium Pyruvate (Gibco). cDC2 were also activated using 50 ng/mL TSLP (R&D Systems).

DC/T coculture

After 24 hours activation, bDC and MoDC were counted and cocultured with allogeneic naive CD4 T cells, at a ratio of 1 DC for 5 T cells, in serum-free X-VIVO 15 medium (Lonza). When indicated, 10 µg/mL anti-human OX40L monoclonal antibody (Oxelumab, Absolute Antibody) or matching human IgG1 isotype were added to the coculture and maintained for the whole duration of the coculture. After 6 days of coculture, T cells were washed and live cells were counted. T cells were reseeded at 10^6 cells/mL and restimulated with anti-CD3/CD28 Dynabeads (LifeTechnologies). 24 hours later supernatants were collected to measure the T cell cytokines.

Flow cytometry analysis

For surface flow cytometry analysis, dead cells were first stained using Live/dead fixable yellow dead cell stain kit (ThermoFisher). T cells were stained with an antibody recognizing OX40 (Biolegend), while MoDC and bDC were stained with an antibody recognizing OX40L (BD). Cells were acquired on a ZE5 instrument (BioRad).

Cytokine quantification

Cytokines from T cell supernatants were quantified using CBA flex set for IL-2, IL-3, IL-4, IL-5, IL-6, IL-9, IL-10, IL-13, IL-17A, IL-17F, TNF-α, IFNγ and GM-CSF (BD), and Luminex for IL-21, IL-22, IL-31 and TNF-β following the manufacturer's protocol.

Data availability

All data generated and analyzed during this study are included in Supplementary material Code_and_Data.

Software and code availability

FACS data were analyzed using the FlowJo software (TreeStar).

Software used for CBA analysis was FCAP Array v3.

Statistical analysis was performed using the Prism software (GraphPad) and R software (version 3.5.3).

Code to reproduce the results is available in Supplementary material Code_and_Data.

Cohorts description

For the cytokine-induced Th cell polarization experiments, 13 independent donors were included, in five independent experiments.

In each bDC-T cell and MoDC-T cell coculture experiment, one single bDC or MoDC donor was coupled to a different naive CD4 T cell donor. For the MoDC-T coculture experiments, 9 independent MoDC donors were included, and cocultured with 9 different T cell donors, in 3 independent experiments. For the bDC-T coculture experiments, 9 independent bDC donors were included, and cocultured with 9 different T cell donors in 6 independent experiments. The 9 TSLP-bDC donors were processed in different experiments than the 9 donors of the other bDC contexts, so the donors are different from the other bDC contexts.

Statistical analysis

All concentration values below the limit of detection (LOD): 10 pg/mL were set to LOD/2 (5 pg/mL). Luminex measurements (four cytokines) were realized later than CBA measurements (13 cytokines). Because of the limited amount of material in some donors, we prioritized measurements

of the output cytokines by CBA over Luminex. Supernatants from 12 samples (out of 108 samples) of the bDC-T coculture experiments and from 10 samples (out of 90 samples) of the MoDC-T coculture experiments were missing and measurement of four cytokines (IL-21, IL-22, IL-31 and TNF-β) could not be performed. To handle missing values, stochastic single imputation was performed using MICE (Multiple Imputation by Chained Equations). Absolute and relative differences in concentration induced by OX40L were computed. Two-sided paired Wilcoxon tests were used to compare raw concentrations and absolute differences across stimulation contexts; mean and standard deviation are displayed.

Context-dependency score

The following steps were used to compute the context-dependency score, for each output cytokine independently: (i) using the relative differences in concentration induced by OX40L, the estimated effect for each stimulation context ($\hat{\beta}_{context\ k}$) and its standard deviation ($\hat{\sigma}_{context\ k}$) were obtained from a Linear Mixed Model (LMM) featuring the different contexts as fixed effects and donor-specific intercepts as random effects (equation (1)) ;

$$Y = \boldsymbol{\alpha}_{\mathbf{donor}} + \sum_{\text{context } k} \beta_k \mathbb{1}_k + \boldsymbol{\varepsilon} \qquad (1)$$

where Y is the relative difference in concentration induced by OX40L presence for a given cytokine ; $\mathbb{1}$ is the indicator function, $\boldsymbol{\beta}_{\boldsymbol{k}}$ is the fixed effect for stimulation context k ; $\boldsymbol{\alpha}_{\mathbf{donor}}$ is the random intercept associated to each donor, with $\alpha_{donor} \sim \mathcal{N}(0, \nu^2)$; and $\varepsilon \sim \mathcal{N}(0, \sigma^2)$ is the residual error term (Figure S2, Step 4.2); (ii) Pairwise Euclidean distances between the context-specific estimated effect divided by their standard deviation $\left(\frac{\hat{\beta}_{context\ k}}{\hat{\sigma}_{context\ k}}\right)$ were computed (Figure S2); (iii) Last, the context-dependency score was obtained by taking the mean of the pairwise Euclidean distances. A likelihood ratio test, between the LMM with and without the context variable as a fixed effect, was performed to evaluate the significance of the context-dependency (Figure S2, Step 4.3).

The scores were then represented according to the OX40L-induced effect on the different contexts: when OX40L effect was in the same direction for all contexts (output cytokine production either always induced or always inhibited), the score was represented with a positive value in black, however, when OX40L effect went in both directions (inducing or inhibiting the output cytokine production, depending on the context), the score was represented in two parts: a positive value in black, representing the main proportion of contexts affected in the same direction by OX40L, and a negative value in grey, representing the minor proportion of contexts affected in the other direction by OX40L.

To evaluate difference in OX40L effect between pairs of contexts, likelihood ratio tests, between the LMM with and without the pair of context variable as a fixed effect, were performed (only observations for the two contexts were used).

Relative importance of DC-type-context and stimuli-context on the context-dependent effect of OX40L was evaluated with a two-steps method, for each cytokine relative difference independently: (i) first a LMM including only an intercept as fixed and random effect was fitted; (ii) the residuals from this model were used as the response in a group-lasso model. All stimulation contexts were defined as one group in the lasso model in order to compare the two types of context: DC type and stimuli.

Acknowledgments

We thank Annick Viguier and Sophie Grondin from the Institut Curie cytometry platform for cell sorting. We wish to thank Pierre Tonnerre for his critical review of the data and manuscript. CT was supported by ANRT, LK and LF were supported by a fellowship from the French Ministry of Research. This study was supported by the Institut National de la Santé et de la Recherche Médicale HTE2016, by Agence Nationale de la Recherche under grants ANR-10-IDEX-0001-02 PSL*, ANR-11-LABX-0043, ANR-16-CE15-0024-01, ANR-15-CHIN-0002, by CIC IGR-Curie 1428 and by Ligue Nationale contre le cancer EL2016.LNCC/VaS.

Author Contributions

LK, CT and MG designed experiments. LK and CT performed experiments. IL and LF conducted statistical analyses. LK, CT, LF and VS wrote the manuscript. VS, CL, HM and BP supervised the study.

Competing Interests

CL, HM and BP are full time employees at Sanofi and CT was full time employee at Sanofi for part of the study. The rest of the authors declare that they have no relevant competing interests.

References

1. Chen F, Beezhold K, Castranova V. Tumor promoting or tumor suppressing of NF-kappa B, a matter of cell context dependency. *International reviews of immunology* 2008, **27**(4)**:** 183-204.

2. Volkow ND, Wang GJ, Fowler JS, Ding YS. Imaging the effects of methylphenidate on brain dopamine: new model on its therapeutic actions for attention-deficit/hyperactivity disorder. *Biological psychiatry* 2005, **57**(11)**:** 1410-1415.

3. Chiou VL, Burotto M. Pseudoprogression and Immune-Related Response in Solid Tumors. *Journal of clinical oncology : official journal of the American Society of Clinical Oncology* 2015, **33**(31)**:** 3541-3543.

4. Dona I, Blanca-Lopez N, Torres MJ, Garcia-Campos J, Garcia-Nunez I, Gomez F*, et al.* Drug hypersensitivity reactions: response patterns, drug involved, and temporal variations in a large series of patients. *Journal of investigational allergology & clinical immunology* 2012, **22**(5)**:** 363-371.

5. Cappuccio A, Zollinger R, Schenk M, Walczak A, Servant N, Barillot E*, et al.* Combinatorial code governing cellular responses to complex stimuli. *Nature communications* 2015, **6:** 6847.

6. Touzot M, Grandclaudon M, Cappuccio A, Satoh T, Martinez-Cingolani C, Servant N*, et al.* Combinatorial flexibility of cytokine function during human T helper cell differentiation. *Nature communications* 2014, **5:** 3987.

7. Ito T, Wang YH, Duramad O, Hori T, Delespesse GJ, Watanabe N*, et al.* TSLP-activated dendritic cells induce an inflammatory T helper type 2 cell response through OX40 ligand. *The Journal of experimental medicine* 2005, **202**(9)**:** 1213-1223.

8. Jacquemin C, Schmitt N, Contin-Bordes C, Liu Y, Narayanan P, Seneschal J*, et al.* OX40 Ligand Contributes to Human Lupus Pathogenesis by Promoting T Follicular Helper Response. *Immunity* 2015, **42**(6)**:** 1159-1170.

9. Pattarini L, Trichot C, Bogiatzi S, Grandclaudon M, Meller S, Keuylian Z*, et al.* TSLP-activated dendritic cells induce human T follicular helper cell differentiation through OX40-ligand. *The Journal of experimental medicine* 2017, **214**(5)**:** 1529-1546.

10. Grandclaudon M, Perrot-Dockes M, Trichot C, Karpf L, Abouzid O, Chauvin C*, et al.* A Quantitative Multivariate Model of Human Dendritic Cell-T Helper Cell Communication. *Cell* 2019, **179**(2)**:** 432-447 e421.

11. Gauvreau GM, Boulet LP, Cockcroft DW, FitzGerald JM, Mayers I, Carlsten C*, et al.* OX40L blockade and allergen-induced airway responses in subjects with mild asthma. *Clinical and experimental allergy : journal of the British Society for Allergy and Clinical Immunology* 2014, **44**(1)**:** 29-37.

12. Yoshioka T, Nakajima A, Akiba H, Ishiwata T, Asano G, Yoshino S*, et al.* Contribution of OX40/OX40 ligand interaction to the pathogenesis of rheumatoid arthritis. *European journal of immunology* 2000, **30**(10)**:** 2815-2823.

13. Aspeslagh S, Postel-Vinay S, Rusakiewicz S, Soria JC, Zitvogel L, Marabelle A. Rationale for anti-OX40 cancer immunotherapy. *European journal of cancer* 2016, **52:** 50-66.

14. Akamatsu T, Watanabe N, Kido M, Saga K, Tanaka J, Kuzushima K*, et al.* Human TSLP directly enhances expansion of CD8+ T cells. *Clinical and experimental immunology* 2008, **154**(1)**:** 98-106.

15. Soumelis V, Reche PA, Kanzler H, Yuan W, Edward G, Homey B*, et al.* Human epithelial cells trigger dendritic cell mediated allergic inflammation by producing TSLP. *Nature immunology* 2002, **3**(7)**:** 673-680.

16. Voehringer D, Shinkai K, Locksley RM. Type 2 immunity reflects orchestrated recruitment of cells committed to IL-4 production. *Immunity* 2004, **20**(3)**:** 267-277.

17. Ito M, Komai K, Mise-Omata S, Iizuka-Koga M, Noguchi Y, Kondo T*, et al.* Brain regulatory T cells suppress astrogliosis and potentiate neurological recovery. *Nature* 2019, **565**(7738)**:** 246-250.

18. Volpe E, Pattarini L, Martinez-Cingolani C, Meller S, Donnadieu MH, Bogiatzi SI*, et al.* Thymic stromal lymphopoietin links keratinocytes and dendritic cell-derived IL-23 in patients with psoriasis. *The Journal of allergy and clinical immunology* 2014, **134**(2)**:** 373-381.

19. Bettelli E, Carrier Y, Gao W, Korn T, Strom TB, Oukka M*, et al.* Reciprocal developmental pathways for the generation of pathogenic effector TH17 and regulatory T cells. *Nature* 2006, **441**(7090)**:** 235-238.

20. Veldhoen M, Hocking RJ, Atkins CJ, Locksley RM, Stockinger B. TGFbeta in the context of an inflammatory cytokine milieu supports de novo differentiation of IL-17-producing T cells. *Immunity* 2006, **24**(2)**:** 179-189.

21. Volpe E, Servant N, Zollinger R, Bogiatzi SI, Hupe P, Barillot E*, et al.* A critical function for transforming growth factor-beta, interleukin 23 and proinflammatory cytokines in driving and modulating human T(H)-17 responses. *Nature immunology* 2008, **9**(6)**:** 650-657.

22. Veglia F, Gabrilovich DI. Dendritic cells in cancer: the role revisited. *Current opinion in immunology* 2017, **45:** 43-51.

23. Michea P, Noel F, Zakine E, Czerwinska U, Sirven P, Abouzid O*, et al.* Adjustment of dendritic cells to the breast-cancer microenvironment is subset specific. *Nature immunology* 2018, **19**(8)**:** 885-897.

24. Dudek AM, Martin S, Garg AD, Agostinis P. Immature, Semi-Mature, and Fully Mature Dendritic Cells: Toward a DC-Cancer Cells Interface That Augments Anticancer Immunity. *Frontiers in immunology* 2013, **4:** 438.

25. Sugamura K, Ishii N, Weinberg AD. Therapeutic targeting of the effector T-cell co-stimulatory molecule OX40. *Nature reviews Immunology* 2004, **4**(6)**:** 420-431.

26. Jiang J, Liu C, Liu M, Shen Y, Hu X, Wang Q*, et al.* OX40 signaling is involved in the autoactivation of CD4(+)CD28(-) T cells and contributes to the pathogenesis of autoimmune arthritis. *Arthritis research & therapy* 2017, **19**(1)**:** 67.

27. Weinberg AD, Rivera MM, Prell R, Morris A, Ramstad T, Vetto JT*, et al.* Engagement of the OX-40 receptor in vivo enhances antitumor immunity. *Journal of immunology* 2000, **164**(4)**:** 2160-2169.

28. Kjaergaard J, Tanaka J, Kim JA, Rothchild K, Weinberg A, Shu S. Therapeutic efficacy of OX-40 receptor antibody depends on tumor immunogenicity and anatomic site of tumor growth. *Cancer research* 2000, **60**(19)**:** 5514-5521.

29. Messenheimer DJ, Jensen SM, Afentoulis ME, Wegmann KW, Feng Z, Friedman DJ*, et al.* Timing of PD-1 Blockade Is Critical to Effective Combination Immunotherapy with Anti-OX40. *Clinical cancer research : an official journal of the American Association for Cancer Research* 2017, **23**(20)**:** 6165-6177.

30. Curti BD, Kovacsovics-Bankowski M, Morris N, Walker E, Chisholm L, Floyd K*, et al.* OX40 is a potent immune-stimulating target in late-stage cancer patients. *Cancer research* 2013, **73**(24)**:** 7189-7198.

Figure Legends

Figure 1: OX40L impact on Th cell polarization depends on the cytokine polarizing-context. a) Experimental design of the Th cell polarization assay. b) Heatmap representing OX40L-induced scaled absolute difference on the 17 output cytokines measured in each Th context. The absolute difference corresponds to the concentration of a given cytokine in a Th context in the presence minus absence of rhOX40L. The mean over 13 donors is represented. Paired Wilcoxon's test was used to evaluate significance of OX40L effect. c) IL-10, GM-CSF and IL-21 production in each Th context in the presence (red dots) or absence (black dots) of rhOX40L. The mean ± SD, and individual values from 13 donors are represented. Paired Wilcoxon's test was used for statistical analysis. d) Principal component analysis representing the barycenters of the four Th-polarizing contexts in the presence (red dots) and absence (black dots) of rhOX40L. * P ≤0.05; ** P ≤0.01; *** P ≤0.001.

Figure 2: OX40L context-dependency across molecular contexts is the strongest on IL-10. a) Simplified mathematical modeling strategy used to quantify the context-dependent role of OX40L on output cytokine production (illustrated in b), and scoring of OX40L context-dependency (depicted in c). In the following analyses, IL-4, IL-5, IL-9, IL-17A, IL-17F and IL-31 were excluded to avoid bias because they were produced in only one or two contexts. b) Heatmap representing the estimated OX40L-induced relative difference for the 11 output Th-cytokines measured in each Th context, calculated using Linear Mixed-effects Models (LMM) on 13 independent donors. The estimated coefficients for the fixed effects from the models are represented. For a given cytokine, in a given Th context, the LMM's fixed effect coefficient corresponds to the mean over donors of the concentration in the presence minus absence of rhOX40L, divided by the concentration in the absence of rhOX40L. c) Scoring of the context-dependency across the four Th-polarizing contexts ranked according to statistical significance. Black bars represent the variation of a considered output cytokine in one direction (increase or decrease) in the majority of the Th contexts in presence of OX40L. When present, grey bars indicate variation of an output cytokine in the opposite direction in at least one Th context due to the presence of OX40L. The scores were computed from 13 independent donors. Likelihood ratio tests, between the LMM with and without the context variable as a fixed effect, were performed to evaluate the significance of the context-dependency. * P ≤0.05; ** P ≤0.01; *** P ≤0.001. d) Statistical significance (likelihood ratio test) of the context-dependency across the four Th-polarizing contexts. 13 independent donors were used in the analysis. Negative signs for context-dependency scores were attributed to cytokines for which OX40L effect was positive (induction) for some contexts and negative (inhibition) for others.

Figure 3: OX40L influence on Th cell differentiation varies depending on the bDC-activating stimulus. a) Experimental design of the bDC-T coculture. b) Heatmap representing the OX40L-induced scaled absolute difference on the 17 output Th-cytokines measured in each bDC context.

The absolute difference corresponds to the concentration of a given cytokine in a bDC context in the presence of the isotype (DC cont.) minus the concentration of the cytokine in that bDC context in the presence of anti-OX40L antibody (DC cont. +anti-OX40L mAb). The mean is represented. Paired Wilcoxon's test was used for statistical analysis. c) IL-13, IL-22 and TNF-β production in each bDC context in the presence of anti-OX40L blocking (black dots) or isotype (red dots). The mean ± SD and individual values are represented. Paired Wilcoxon's test was used for statistical analysis. d) Principal component analysis representing the barycenters of the six bDC contexts in the presence (black dots) and absence (red dots) of anti-OX40L blocking antibody, meaning absence and presence of OX40L on bDC, respectively. 9 independent donors were used in each analysis. * P ≤0.05; ** P ≤0.01.

Figure 4: TSLP-DC context determines a specific OX40L functional impact on Th output cytokines. a) Heatmap representing the estimated OX40L-induced relative difference on the 17 output Th-cytokines measured in each bDC context, calculated using Linear Mixed-effects Models. The estimated coefficients for the fixed effects from the models are represented. For a given cytokine, in a given bDC context, the LMM's coefficient corresponds to the mean over donors of the concentration in the presence of the isotype (DC cont.) subtracted by the concentration in the presence of anti-OX40L antibody (DC cont. + anti-OX40L mAb), divided by the concentration in the presence of anti-OX40L antibody (DC cont. + anti-OX40L mAb). b) Scoring of the context-dependency across the six bDC contexts, ranked according to statistical significance. Black bars represent the variation of a considered output cytokine in one direction (increase or decrease) in the majority of the bDC contexts in presence of OX40L. When present, grey bars indicate variation of an output cytokine in the opposite direction in at least one bDC context due to the presence of OX40L. Likelihood ratio tests, between the LMM with and without the context variable as a fixed effect, were used to assess the significance of the context-dependency. c) Statistical significance (likelihood ratio test) of the context-dependency across the six bDC contexts. Negative signs for context-dependency scores were attributed to cytokines for which OX40L effect was positive for some contexts and negative for others. 9 independent donors were used for the analysis. * P ≤0.05; ** P ≤0.01; *** P ≤0.001.

Figure 5: High and variable impact of OX40L on Th cell polarization in the different MoDC-activating contexts. a) Experimental design of the MoDC-T coculture. b) Heatmap representing the OX40L-induced scaled absolute difference for the 17 output Th-cytokines measured in each MoDC context. The absolute difference corresponds to the concentration of a given cytokine in a MoDC context in the presence of the isotype (DC cont.) subtracted by the concentration of the cytokine in that MoDC context in the presence of anti-OX40L antibody (DC cont. +anti-OX40L mAb). The mean is represented. Paired Wilcoxon's test was used for statistical analysis. c) IL-13, IL-22 and TNF-β production in each MoDC context in the presence of anti-OX40L blocking (black dots) or isotype (red

dots). The mean ± SD and individual values are represented. Paired Wilcoxon's test was used for statistical analysis. d) Principal component analysis representing the barycenters of the five MoDC contexts in the presence (black dots) and absence (red dots) of anti-OX40L blocking antibody, meaning absence and presence of OX40L on MoDC, respectively. 9 independent donors were used in each analysis. * P ≤0.05; ** P ≤0.01.

Figure 6: The cellular context highly impacts OX40L context-dependency effects on Th cytokine secretion. a) Heatmaps representing the estimated OX40L-induced relative difference for the 17 output Th-cytokines measured in each of the five bDC and MoDC contexts, calculated using Linear Mixed-effects Models. The estimated coefficients for the fixed effects from the models are represented. For a given cytokine, with a given DC type and in a given DC context, the LMM's coefficient corresponds to the mean over donors of the concentration in the presence of the isotype (DC cont.) subtracted by the concentration in the presence of anti-OX40L antibody (DC cont. + anti-OX40L mAb), divided by the concentration in the presence of anti-OX40L antibody (DC cont. + anti-OX40L mAb). b) Scoring of the un-ranked context-dependency across the five bDC and MoDC contexts. Black bars represent the variation of a considered output cytokine in one direction (increase or decrease) in the majority of the bDC or MoDC contexts in presence of OX40L. When present, grey bars indicate variation of an output cytokine in the opposite direction in at least one bDC or MoDC context due to the presence of OX40L. Likelihood ratio tests were used to evaluate the significance of the context-dependency. c) Statistical significance (likelihood ratio test) of the context-dependency across the five DC contexts. Negative signs for context-dependency scores were attributed to cytokines for which OX40L effect was positive for some contexts and negative for others. The TSLP-bDC context was removed for these analyses to compare the same contexts between bDC and MoDC. 9 independent donors were used in each analysis. * P ≤0.05; ** P ≤0.01; *** P ≤0.001.

Figure 7: OX40L context-dependency depends mainly on the DC type. a) Euclidean distance between presence and absence of rhOX40L for each Th context based on a PCA of the 17 Th-cytokines measured. 13 independent donors were used in the analysis. b) Euclidean distance between presence (isotype) and absence (OX40L blocking) of OX40L on DC for each bDC and MoDC context based on a PCA of the 17 Th-cytokines measured. 9 independent donors were used in the analysis. c-d) For each of the 17 output Th-cytokines measured in DC-T cocultures, group-lasso coefficients as a function of the penalization parameter (lambda) are represented. c) Cytokines for which OX40L context-dependency was predominantly due to the DC type. d) Cytokines for which OX40L context-dependency was predominantly due to the DC contexts.

Supplementary Figure Legends

Figure S1: Control Th cell profiles. a) Quantification of OX40 MFI on Th0, Th1, Th2 and Th17 at Day 0 (D0), 1, 2, 3, 4 and 5 of culture. Mean ± SD and individual values from 3 donors are represented. b) Output cytokine production in each of the four Th contexts. Mean ± SD and individual values from 13 independent donors are represented. Two-sided paired Wilcoxon's test was used for statistical analysis. Statistical significance was annotated as follows: ns P >0.05; * P ≤0.05; ** P ≤0.01; *** P ≤0.001.

Figure S2: Detailed analysis strategy. Detailed mathematical modeling strategy used for data analysis and context-dependency scoring.

Figure S3: OX40L expression on bDC. a) Quantification of OX40L MFI on bDC activated for 24 or 48 hours without stimulation (NT), or with zymosan, PAM3, LPS, HKSA, Curdlan or TSLP. Mean ± SD and individual values from 3 donors are represented. Paired student's test was used for statistical analysis. Statistical significance was annotated as follows: ns P >0.05; * P ≤0.05; ** P ≤0.01. b) Difference in OX40L-induced effect between pairs of contexts, evaluated by likelihood ratio tests, between the linear mixed models with and without taking into account the contexts. This analysis is associated to the context-dependency scores represented in Figure 4b. 9 independent donors were used for the analysis. Statistical significance was annotated as follows: * P ≤0.05; ** P ≤0.01; *** P ≤0.001. Only P≤0.05 are displayed.

Figure S5: OX40L expression on MoDC. Quantification of OX40L MFI on MoDC activated for 24 or 48 hours without stimulation (NT), or with zymosan, PAM3, LPS, HKSA or Curdlan. Mean ± SD and individual values from 3 donors are represented. Paired student's test was used for statistical analysis. Statistical significance was annotated as follows: * P ≤0.05; ** P ≤0.01.

Supplementary Table Legends

Table S1: Detailed rescaled estimates. Table showing the detailed rescaled estimates (estimates divided by their standard deviation) for each experimental setting: Th contexts, MoDC contexts, bDC contexts with and without TSLP context.

Table S2: Context-dependency post-hoc tests. Table displaying the results of the likelihood ratio tests performed to evaluate the difference in OX40L effect between pairs of contexts, between the LMM with and without the pair of context variable as a fixed effect. One tab per experimental setting: Th contexts, bDC contexts, bDC contexts without TSLP context and MoDC contexts.

Table S3: Detailed p-values. Table recapitulating p-values for each figure panel.

Supplementary Material

Code_and_data. Zip file containing all data and scripts used in this study.

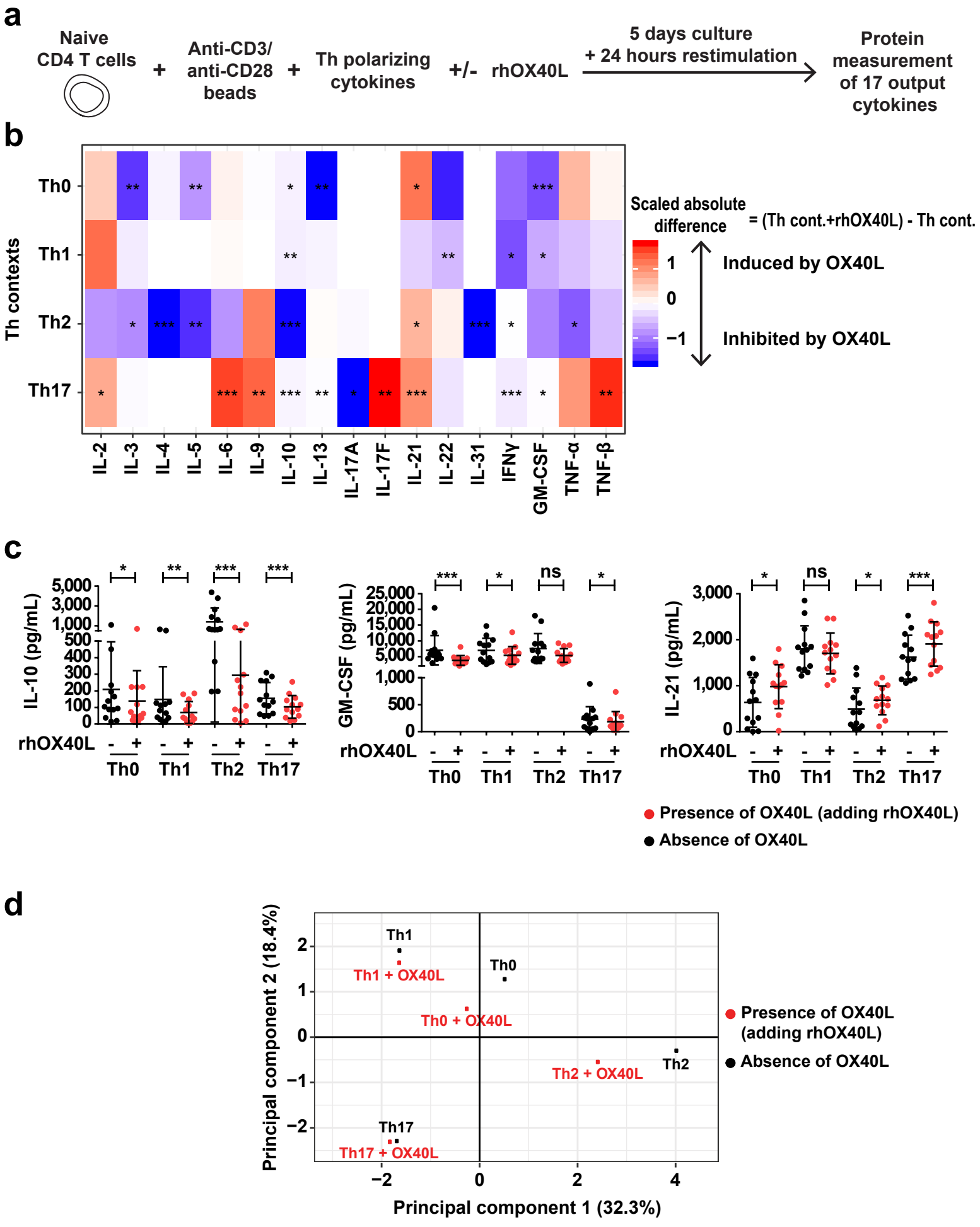
a
Naive CD4 T cells
+
Anti-CD3/ anti-CD28 beads
+
Th polarizing cytokines
+/-
rhOX40L
5 days culture + 24 hours restimulation
Protein measurement of 17 output cytokines
b
Th contexts
Th0
Th1
Th2
Th17
IL-2
IL-3
IL-4
IL-5
IL-6
IL-9
IL-10
IL-13
IL-17A
IL-17F
IL-21
IL-22
IL-31
IFNγ
GM-CSF
TNF-α
TNF-β
Scaled absolute difference
= (Th cont.+rhOX40L) - Th cont.
1
0
−1
Induced by OX40L
Inhibited by OX40L
c
IL-10 (pg/mL)
GM-CSF (pg/mL)
IL-21 (pg/mL)
rhOX40L
Th0
Th1
Th2
Th17
ns
Presence of OX40L (adding rhOX40L)
Absence of OX40L
d
Principal component 2 (18.4%)
Principal component 1 (32.3%)
Th1
Th1 + OX40L
Th0
Th0 + OX40L
Th2
Th2 + OX40L
Th17
Th17 + OX40L
Presence of OX40L (adding rhOX40L)
Absence of OX40L

FIGURE 1

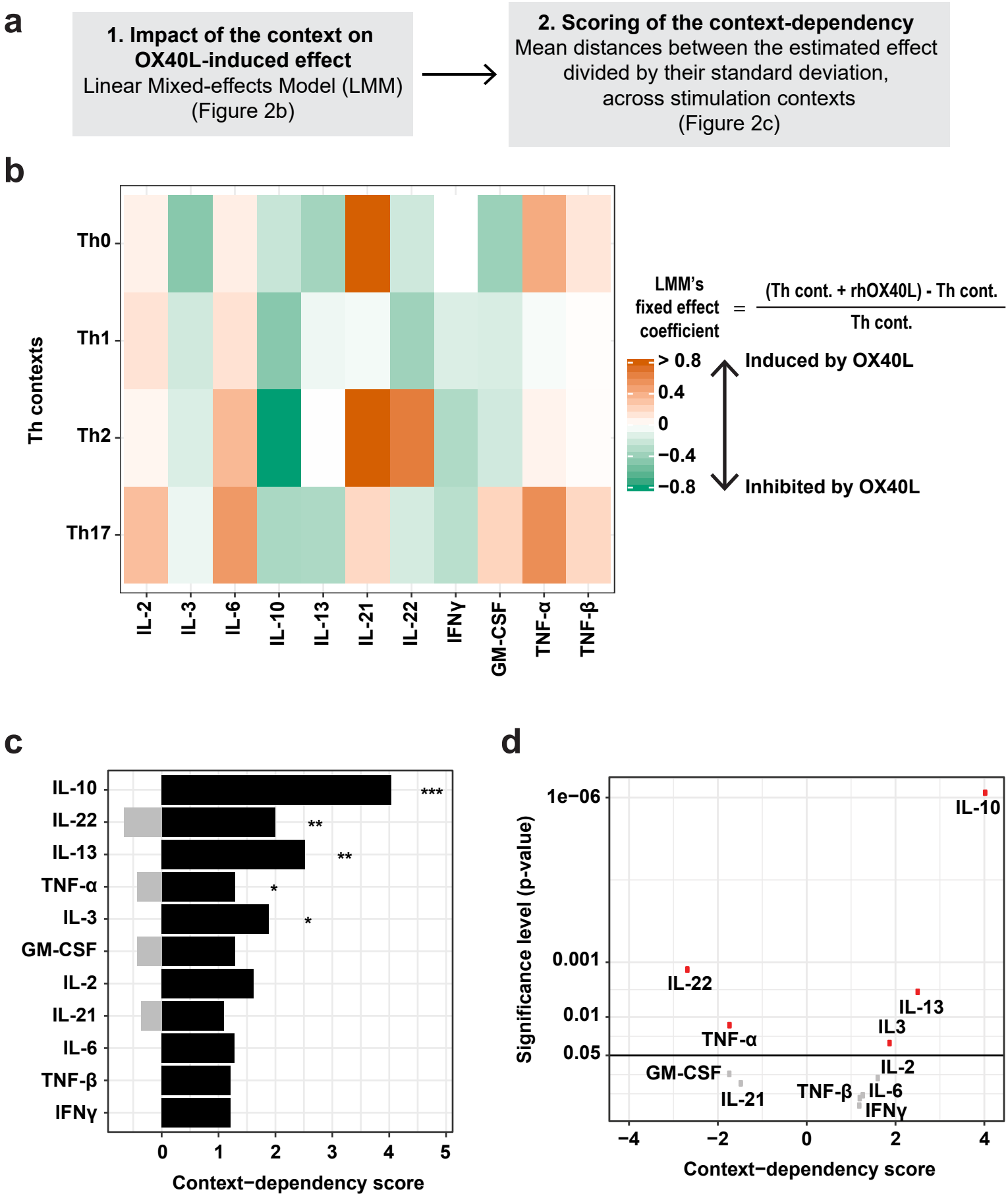
a
1. Impact of the context on OX40L-induced effect
Linear Mixed-effects Model (LMM)
(Figure 2b)
2. Scoring of the context-dependency
Mean distances between the estimated effect divided by their standard deviation, across stimulation contexts
(Figure 2c)
b
Th contexts
Th0
Th1
Th2
Th17
IL-2
IL-3
IL-6
IL-10
IL-13
IL-21
IL-22
IFNγ
GM-CSF
TNF-α
TNF-β
LMM's fixed effect coefficient
(Th cont. + rhOX40L) - Th cont.
Th cont.
> 0.8
0.4
0
−0.4
−0.8
Induced by OX40L
Inhibited by OX40L
c
IL-10
IL-22
IL-13
TNF-α
IL-3
GM-CSF
IL-2
IL-21
IL-6
TNF-β
IFNγ
***
**
**
*
*
0
1
2
3
4
5
Context−dependency score
d
Significance level (p-value)
1e−06
0.001
0.01
0.05
IL-10
IL-22
IL-13
IL3
TNF-α
IL-2
GM-CSF
IL-21
TNF-β
IL-6
IFNγ
−4
−2
0
2
4
Context−dependency score

FIGURE 2

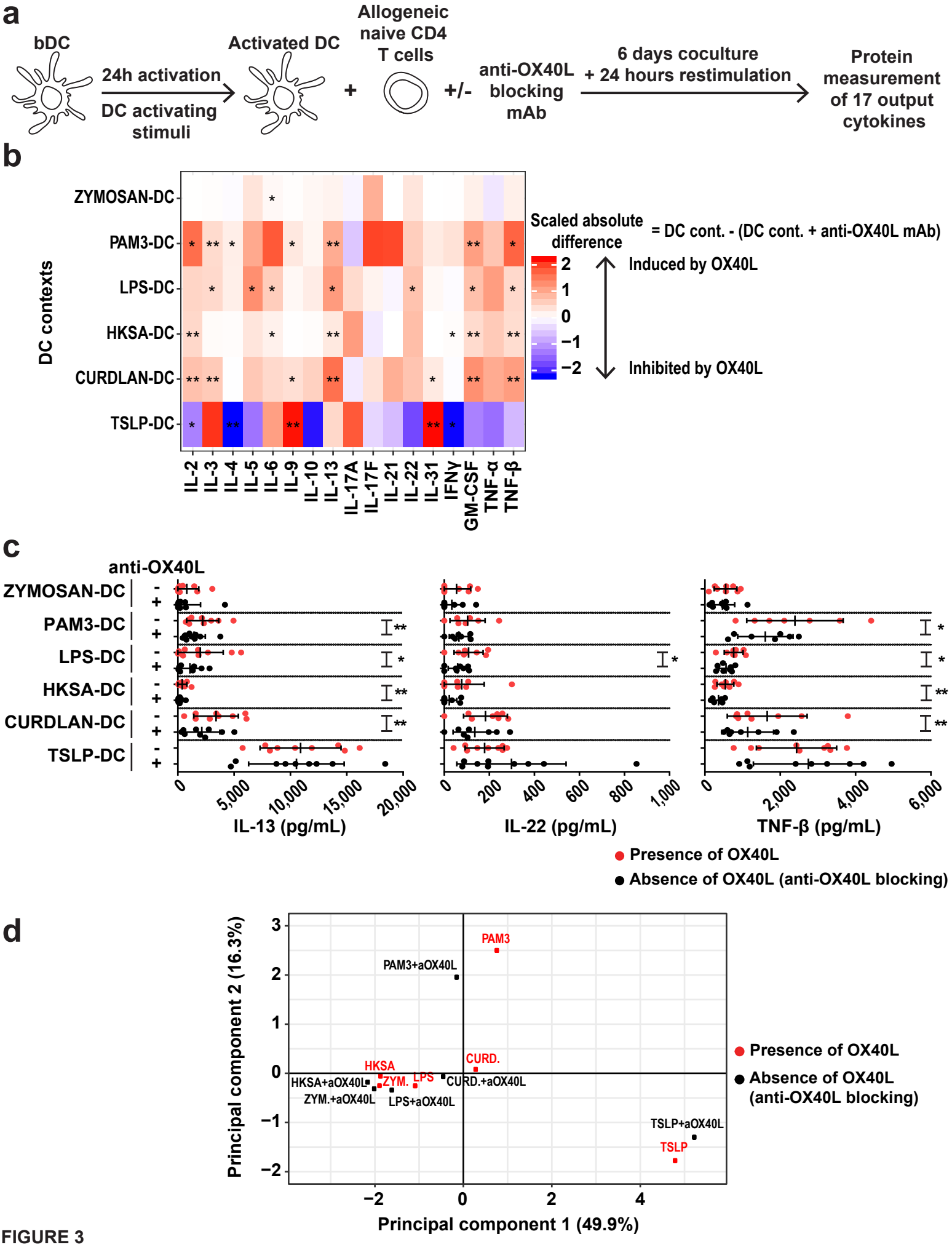
a
bDC
24h activation
DC activating stimuli
Activated DC
Allogeneic naive CD4 T cells
+
+/-
anti-OX40L blocking mAb
6 days coculture + 24 hours restimulation
Protein measurement of 17 output cytokines
b
DC contexts
ZYMOSAN-DC
PAM3-DC
LPS-DC
HKSA-DC
CURDLAN-DC
TSLP-DC
IL-2
IL-3
IL-4
IL-5
IL-6
IL-9
IL-10
IL-13
IL-17A
IL-17F
IL-21
IL-22
IL-31
IFNγ
GM-CSF
TNF-α
TNF-β
Scaled absolute difference
= DC cont. - (DC cont. + anti-OX40L mAb)
2
1
0
−1
−2
Induced by OX40L
Inhibited by OX40L
c
anti-OX40L
IL-13 (pg/mL)
IL-22 (pg/mL)
TNF-β (pg/mL)
Presence of OX40L
Absence of OX40L (anti-OX40L blocking)
d
Principal component 2 (16.3%)
Principal component 1 (49.9%)
PAM3
PAM3+aOX40L
CURD.
CURD.+aOX40L
HKSA
HKSA+aOX40L
ZYM.
ZYM.+aOX40L
LPS
LPS+aOX40L
TSLP
TSLP+aOX40L
Presence of OX40L
Absence of OX40L (anti-OX40L blocking)

FIGURE 3

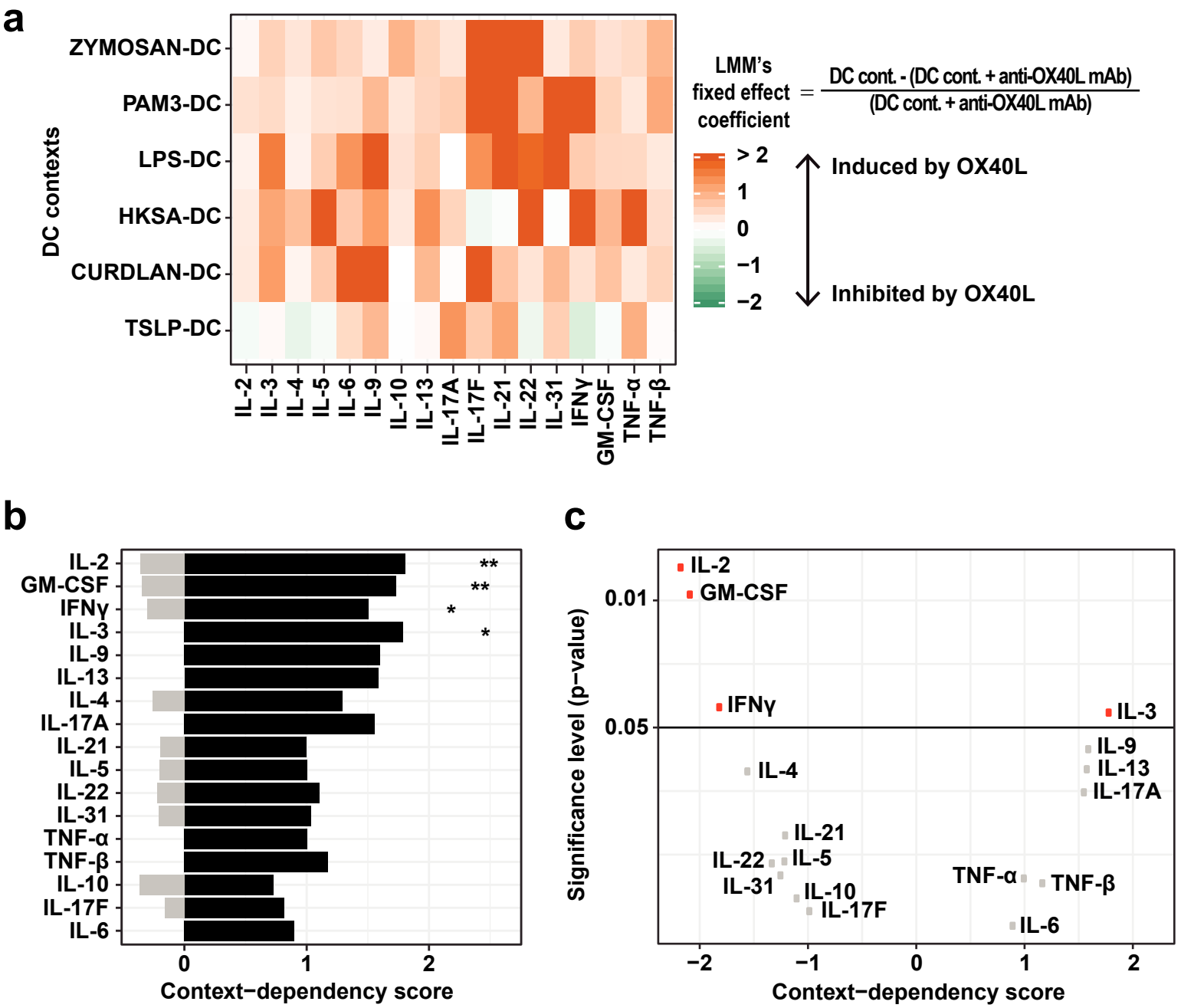
a
ZYMOSAN-DC
PAM3-DC
LPS-DC
HKSA-DC
CURDLAN-DC
TSLP-DC
DC contexts
IL-2
IL-3
IL-4
IL-5
IL-6
IL-9
IL-10
IL-13
IL-17A
IL-17F
IL-21
IL-22
IL-31
IFNγ
GM-CSF
TNF-α
TNF-β
LMM's fixed effect coefficient = DC cont. - (DC cont. + anti-OX40L mAb) / (DC cont. + anti-OX40L mAb)
> 2
1
0
−1
−2
Induced by OX40L
Inhibited by OX40L
b
IL-2
GM-CSF
IFNγ
IL-3
IL-9
IL-13
IL-4
IL-17A
IL-21
IL-5
IL-22
IL-31
TNF-α
TNF-β
IL-10
IL-17F
IL-6
**
**
*
*
0
1
2
Context−dependency score
c
Significance level (p−value)
0.01
0.05
IL-2
GM-CSF
IFNγ
IL-3
IL-9
IL-13
IL-17A
IL-4
IL-21
IL-22
IL-5
IL-31
IL-10
IL-17F
TNF-α
TNF-β
IL-6
−2
−1
0
1
2
Context−dependency score

FIGURE 4

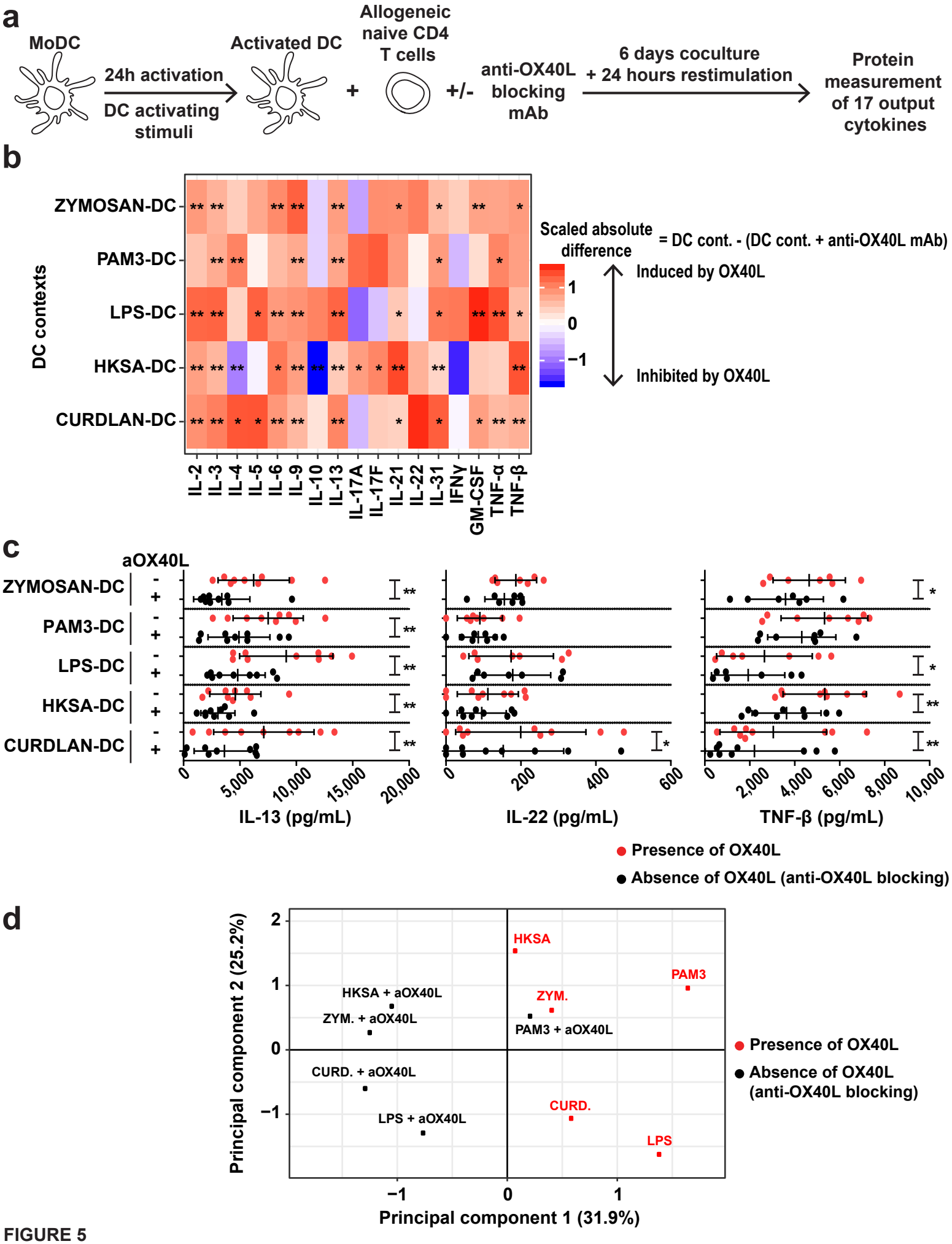
a
MoDC
24h activation
DC activating stimuli
Activated DC
+
Allogeneic naive CD4 T cells
+/-
anti-OX40L blocking mAb
6 days coculture + 24 hours restimulation
Protein measurement of 17 output cytokines
b
DC contexts
ZYMOSAN-DC
PAM3-DC
LPS-DC
HKSA-DC
CURDLAN-DC
IL-2
IL-3
IL-4
IL-5
IL-6
IL-9
IL-10
IL-13
IL-17A
IL-17F
IL-21
IL-22
IL-31
IFNγ
GM-CSF
TNF-α
TNF-β
Scaled absolute difference
= DC cont. - (DC cont. + anti-OX40L mAb)
Induced by OX40L
Inhibited by OX40L
1
0
−1
c
aOX40L
ZYMOSAN-DC
PAM3-DC
LPS-DC
HKSA-DC
CURDLAN-DC
IL-13 (pg/mL)
IL-22 (pg/mL)
TNF-β (pg/mL)
Presence of OX40L
Absence of OX40L (anti-OX40L blocking)
d
Principal component 2 (25.2%)
Principal component 1 (31.9%)
HKSA
PAM3
ZYM.
HKSA + aOX40L
ZYM. + aOX40L
PAM3 + aOX40L
CURD. + aOX40L
LPS + aOX40L
CURD.
LPS
Presence of OX40L
Absence of OX40L (anti-OX40L blocking)

FIGURE 5

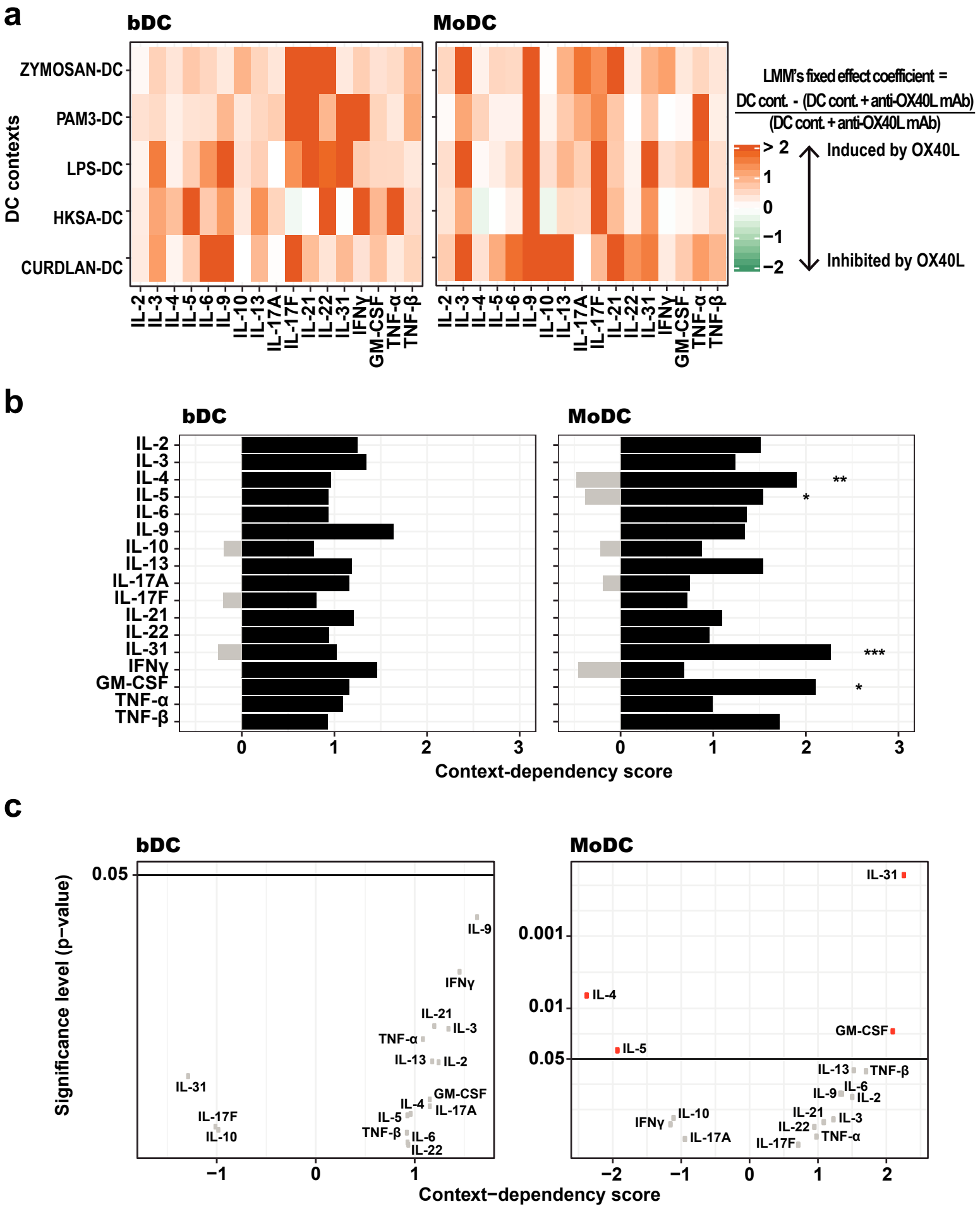
a
bDC
MoDC
ZYMOSAN-DC
PAM3-DC
LPS-DC
HKSA-DC
CURDLAN-DC
DC contexts
IL-2 IL-3 IL-4 IL-5 IL-6 IL-9 IL-10 IL-13 IL-17A IL-17F IL-21 IL-22 IL-31 IFNγ GM-CSF TNF-α TNF-β
LMM's fixed effect coefficient =
DC cont. - (DC cont. + anti-OX40L mAb)
(DC cont. + anti-OX40L mAb)
> 2
1
0
−1
−2
Induced by OX40L
Inhibited by OX40L
b
bDC
MoDC
IL-2 IL-3 IL-4 IL-5 IL-6 IL-9 IL-10 IL-13 IL-17A IL-17F IL-21 IL-22 IL-31 IFNγ GM-CSF TNF-α TNF-β
**
*
***
*
0 1 2 3
Context-dependency score
c
bDC
MoDC
Significance level (p−value)
0.05
0.001
0.01
0.05
IL-9 IFNγ IL-21 IL-3 TNF-α IL-13 IL-2 IL-31 GM-CSF IL-4 IL-17A IL-5 IL-17F IL-10 TNF-β IL-6 IL-22
IL-31 IL-4 GM-CSF IL-5 IL-13 TNF-β IL-9 IL-6 IL-2 IL-10 IFNγ IL-21 IL-3 IL-22 TNF-α IL-17A IL-17F
−1 0 1
−2 −1 0 1 2
Context−dependency score

FIGURE 6

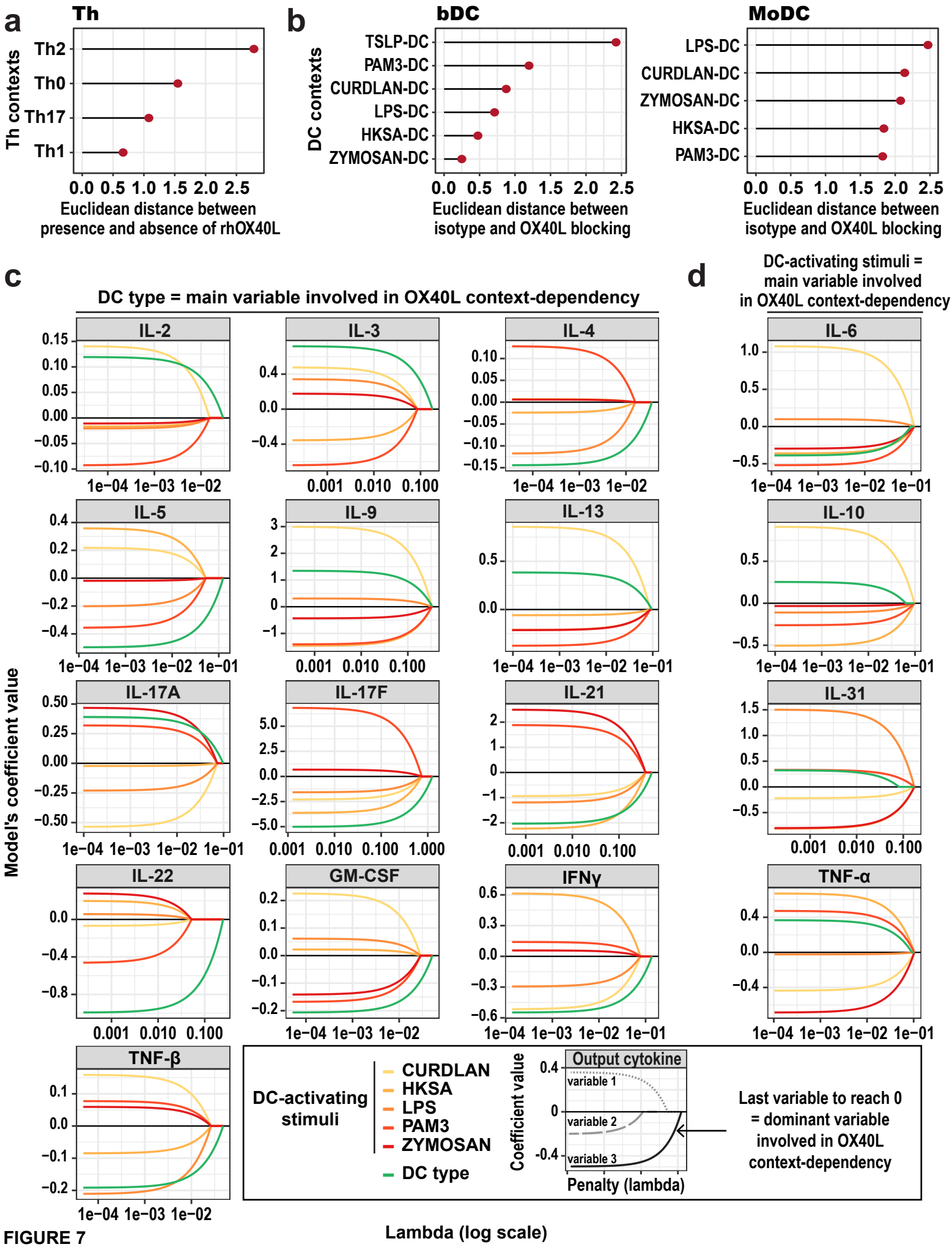
a
Th
Th contexts
Th2
Th0
Th17
Th1
0.0 0.5 1.0 1.5 2.0 2.5
Euclidean distance between presence and absence of rhOX40L
b
bDC
DC contexts
TSLP-DC
PAM3-DC
CURDLAN-DC
LPS-DC
HKSA-DC
ZYMOSAN-DC
0.0 0.5 1.0 1.5 2.0 2.5
Euclidean distance between isotype and OX40L blocking
MoDC
LPS-DC
CURDLAN-DC
ZYMOSAN-DC
HKSA-DC
PAM3-DC
0.0 0.5 1.0 1.5 2.0 2.5
Euclidean distance between isotype and OX40L blocking
c
DC type = main variable involved in OX40L context-dependency
d
DC-activating stimuli = main variable involved in OX40L context-dependency
Model's coefficient value
IL-2
IL-3
IL-4
IL-6
IL-5
IL-9
IL-13
IL-10
IL-17A
IL-17F
IL-21
IL-31
IL-22
GM-CSF
IFNγ
TNF-α
TNF-β
1e-04 1e-03 1e-02
0.001 0.010 0.100
1e-04 1e-03 1e-02 1e-01
0.001 0.010 0.100 1.000
DC-activating stimuli
CURDLAN
HKSA
LPS
PAM3
ZYMOSAN
DC type
Output cytokine
variable 1
variable 2
variable 3
Coefficient value
Penalty (lambda)
Last variable to reach 0 = dominant variable involved in OX40L context-dependency
Lambda (log scale)

FIGURE 7

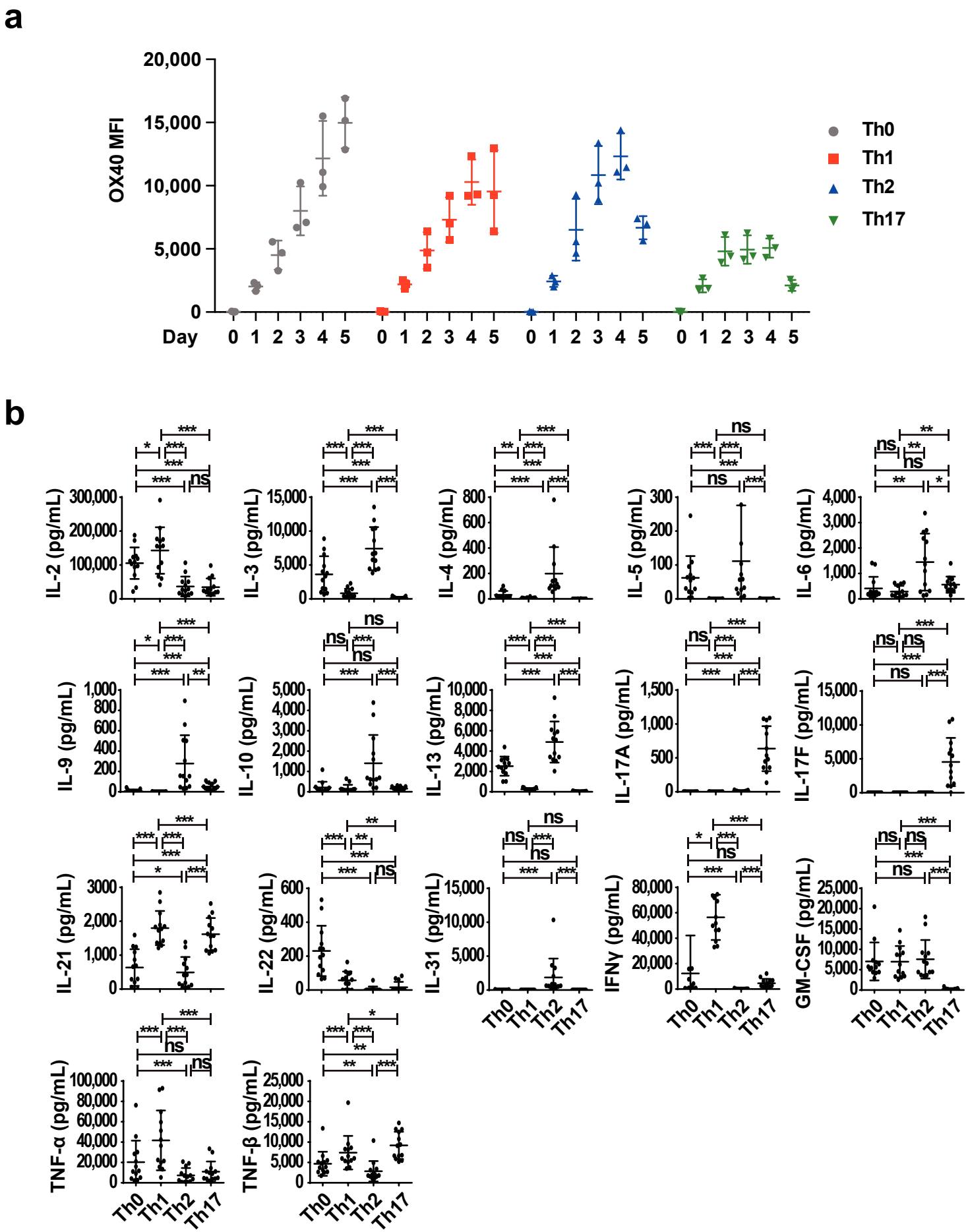
a
OX40 MFI
20,000
15,000
10,000
5,000
0
Day
0 1 2 3 4 5
Th0
Th1
Th2
Th17
b
IL-2 (pg/mL)
IL-3 (pg/mL)
IL-4 (pg/mL)
IL-5 (pg/mL)
IL-6 (pg/mL)
IL-9 (pg/mL)
IL-10 (pg/mL)
IL-13 (pg/mL)
IL-17A (pg/mL)
IL-17F (pg/mL)
IL-21 (pg/mL)
IL-22 (pg/mL)
IL-31 (pg/mL)
IFNγ (pg/mL)
GM-CSF (pg/mL)
TNF-α (pg/mL)
TNF-β (pg/mL)
Th0
Th1
Th2
Th17

FIGURE S1

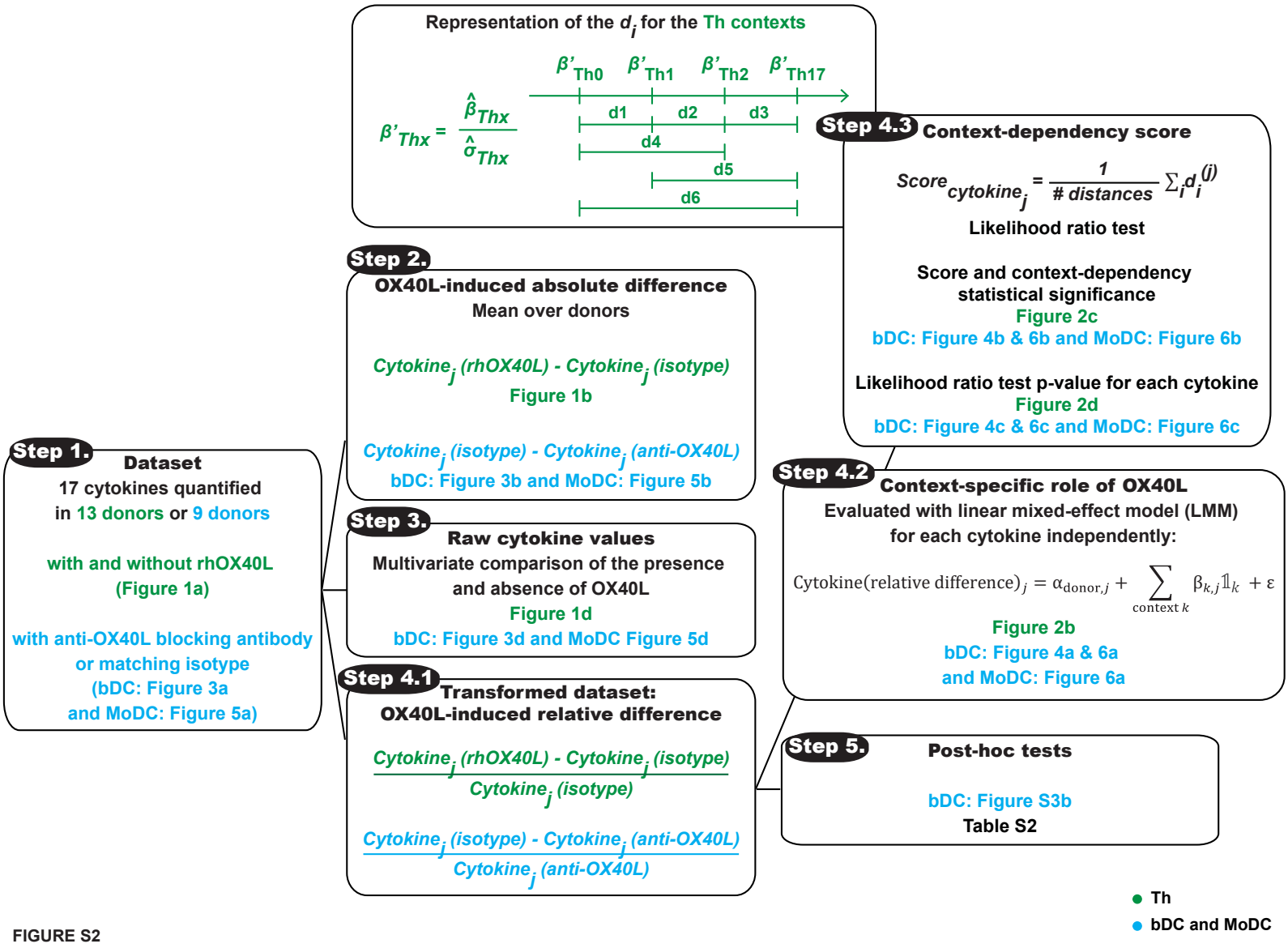
Representation of the d_i for the Th contexts
β'_{Th0} β'_{Th1} β'_{Th2} β'_{Th17}
$\beta'_{Thx} = \frac{\hat{\beta}_{Thx}}{\hat{\sigma}_{Thx}}$
d1 d2 d3 d4 d5 d6
Step 1.
Dataset
17 cytokines quantified
in 13 donors or 9 donors
with and without rhOX40L
(Figure 1a)
with anti-OX40L blocking antibody
or matching isotype
(bDC: Figure 3a
and MoDC: Figure 5a)
Step 2.
OX40L-induced absolute difference
Mean over donors
$Cytokine_j$ (rhOX40L) - $Cytokine_j$ (isotype)
Figure 1b
$Cytokine_j$ (isotype) - $Cytokine_j$ (anti-OX40L)
bDC: Figure 3b and MoDC: Figure 5b
Step 3.
Raw cytokine values
Multivariate comparison of the presence
and absence of OX40L
Figure 1d
bDC: Figure 3d and MoDC Figure 5d
Step 4.1
Transformed dataset:
OX40L-induced relative difference
$\frac{Cytokine_j \text{ (rhOX40L)} - Cytokine_j \text{ (isotype)}}{Cytokine_j \text{ (isotype)}}$
$\frac{Cytokine_j \text{ (isotype)} - Cytokine_j \text{ (anti-OX40L)}}{Cytokine_j \text{ (anti-OX40L)}}$
Step 4.3
Context-dependency score
$Score_{cytokine_j} = \frac{1}{\#\ distances} \sum_i d_i^{(j)}$
Likelihood ratio test
Score and context-dependency
statistical significance
Figure 2c
bDC: Figure 4b & 6b and MoDC: Figure 6b
Likelihood ratio test p-value for each cytokine
Figure 2d
bDC: Figure 4c & 6c and MoDC: Figure 6c
Step 4.2
Context-specific role of OX40L
Evaluated with linear mixed-effect model (LMM)
for each cytokine independently:
$\text{Cytokine(relative difference)}_j = \alpha_{\text{donor},j} + \sum_{\text{context } k} \beta_{k,j} \mathbb{1}_k + \varepsilon$
Figure 2b
bDC: Figure 4a & 6a
and MoDC: Figure 6a
Step 5.
Post-hoc tests
bDC: Figure S3b
Table S2
Th
bDC and MoDC

FIGURE S2

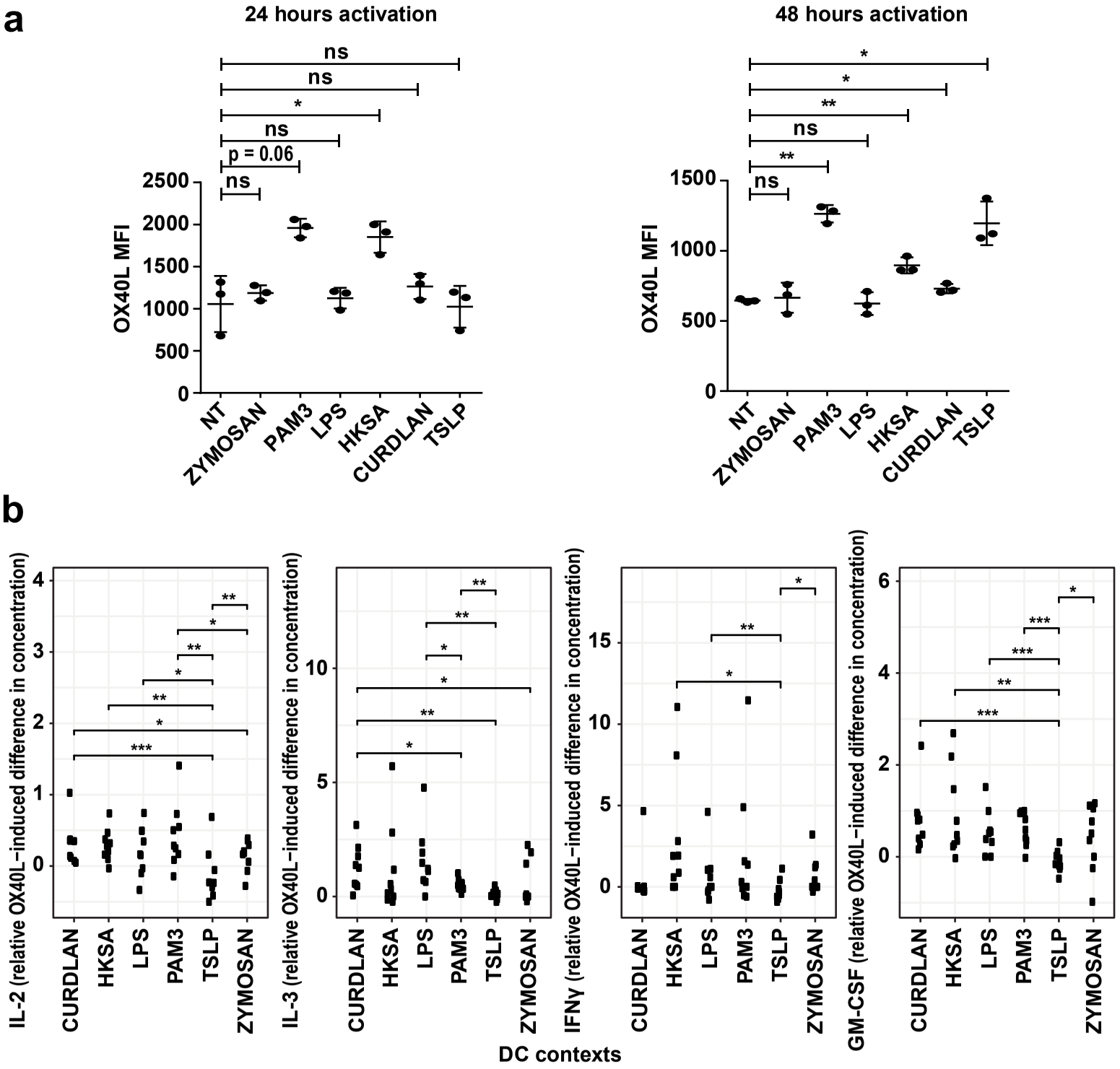
a
24 hours activation
48 hours activation
OX40L MFI
NT
ZYMOSAN
PAM3
LPS
HKSA
CURDLAN
TSLP
p = 0.06
ns
b
IL-2 (relative OX40L−induced difference in concentration)
IL-3 (relative OX40L−induced difference in concentration)
IFNγ (relative OX40L−induced difference in concentration)
GM-CSF (relative OX40L−induced difference in concentration)
DC contexts

FIGURE S3

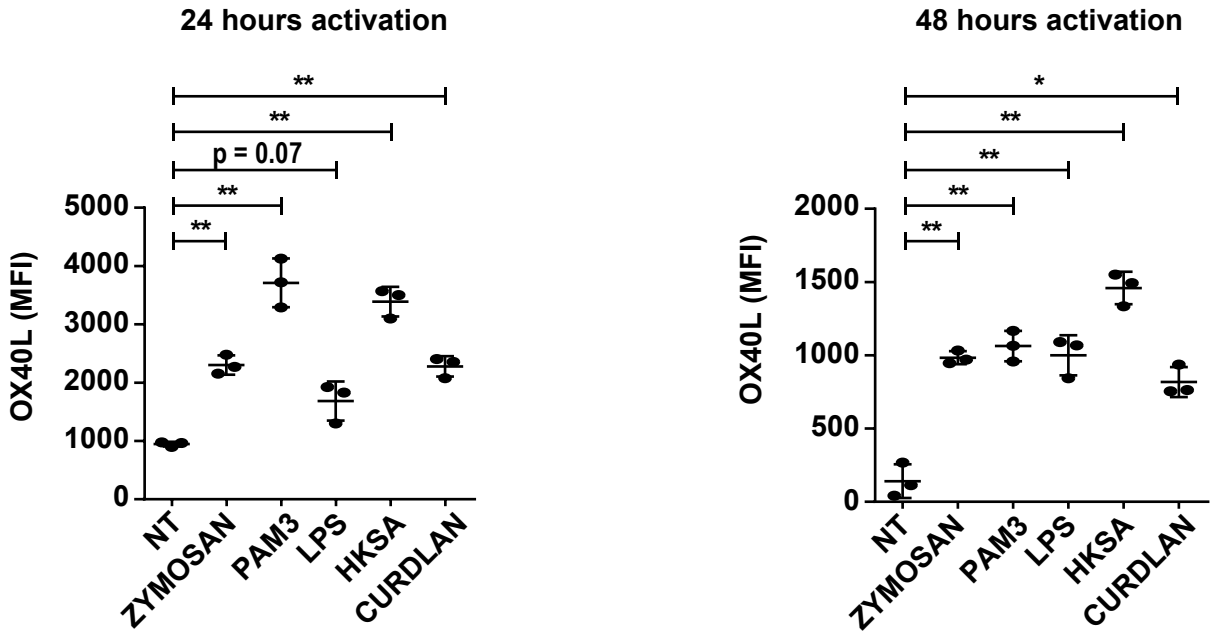
24 hours activation
48 hours activation
OX40L (MFI)
p = 0.07
**
*
NT
ZYMOSAN
PAM3
LPS
HKSA
CURDLAN
0
1000
2000
3000
4000
5000
500
1500

FIGURE S4

GENERAL DISCUSSION AND PROSPECTS

I) Context-dependency concept

1) Multidisciplinary importance of context-dependency

The concept of context-dependency has been identified in many scientific fields and some papers tried to better understand its consequences very recently.

Egushi et al. reflected on the importance of the context-dependency concept in the field of genetics and focused more specifically on the context-dependency of genetic mutation on phenotypes [300]. The authors demonstrated that a genetic mutation function on a phenotype could vary according to several parameters such as genetic background, cell type, age, etc. They highlighted that context-dependency complicated phenotypic prediction from a mutation. As an aside, this is particularly interesting to consider at a time when single-cell RNA sequencing is very popular; measurement at the protein level remains highly important. Then, they interrogated how to predict a phenotype from a mutation when the context can actually influence it. They reviewed different approaches to study genetic context-dependency, for instance, measuring the phenotypic impacts of many gene deletions across many contexts in yeast, or quantifying the impact of several mutations ("mutation contexts") on phenotypic impacts of a single protein mutation. Interestingly, this latter method is in the same frame of mind as our method.

Context-dependency has also been studied on drugs, on animal models. Jackson et al. studied the context-dependent off-target effects of an antidiabetic compound, the dipeptidyl peptidase 4 (DPP4) inhibitor [301]. This drug is associated with frequent comorbidities, such as chronic kidney disease and hypertension, and it is of particular interest to understand the context in which these different comorbidities appear. In preclinical *in vivo* studies with animal models, they showed that long-term DPP4 inhibitor treatment increased arterial blood pressure in genetically hypertensive rats and on the contrary was antihypertensive in rats with metabolic syndrome and did not affect genetically normotensive rats. This greatly illustrated the impact of the context on disease side-effect outcomes and its importance in therapy.

Also interesting, a study from 1981 focused on the impact of the environmental conditions on rat behavior injected with cocaine [302]. They observed differences in rat behaviors and tolerance according to the environment in which they received the cocaine.

Context-dependency has been highly studied in ecology, compared to other disciplines. For instance, it has been studied by quantifying trait variance and repeatability, to better understand evolutionary processes. Killen et al. focused on the context-dependent trait of wild fish populations [303]. As for humans, animal populations are constituted of many individuals, each with different behavior and physiology. Thus, they questioned whether the best fish in a population (regarding swimming performances, stress responsiveness, metabolic rate, etc) is always the same one, or whether the best fish differs according to the environmental context, composed of several parameters such as temperature, pollutants, food and oxygen availability, etc. In other words, does an individual that has the greatest fitness in one context, will still be the best in another one? Until now, in animal populations, context-dependency has been applied to evolutionary ecology and to a lesser extend to ecology management and conservation.

In another recent ecology article, Perring et al. studied the context-dependency of nitrogen deposition effects on forest understorey plant population responses [304]. They demonstrated that the environmental context, defined by parameters such as pH or light, impacted how plants respond to nitrogen deposition. Here, the context-dependency concept is applied to plant physiological response to better understand and predict nitrogen deposition in understorey plant populations, with the aim to better conserve forest biodiversity.

Finally, context-dependency has also been of interest in neuroeconomics, for instance in terms of valuation affected by context-dependent perception [305].

2) Originality of our context-dependency statistical model

All these articles highlight the importance of considering context-dependency in many disciplines. Some team built prediction models trying to include context-dependency in the equation [306]. But although context-dependency has been examined and studied in many fields as seen above, few studies allow us to comprehensively quantify it directly. Context-dependency in its entirety is a difficult problem because it is actually the combination of an uncountable number of parameters,

each including many variant combinations. Therefore, such complexity needs to be formalized using an integrated mathematical modeling approach. As proof of concept, our study illustrates that context-dependency can be measured and quantified by a new statistical method strategy.

About Th polarization, some studies looked at the induction of Th subsets in different contexts [82,86,122]. For instance, Schmitt et al. described that TGFβ is a critical signal in Tfh cell induction, and that the cytokine context accompanying TGFβ affected the polarization [82]. However, the number of contexts was limited and context-dependency was not the focus of the study. An interesting study from Cano-Gamez et al. focused on characterizing naive and memory CD4 T cell responses to five different cytokine combinations [307]. They observed the acquisition of distinct phenotypes according to the context but did not focus on context-dependency.

Thus, to our knowledge, no study has quantitatively evaluated the context-dependency of a molecule functions, in a systematic manner and across many contexts. Moreover, more specifically, OX40L context-dependent effects on Th polarization and Th cytokine secretion had never been addressed, in various molecular and cellular contexts. As described throughout this manuscript, the notion of context-dependency refers to the variable function of molecules depending on the context. In this case, it means that OX40L can impact differently Th polarization according to the context in which the T cell is evolving. It can allow the description of some OX40L effects that would not be observed in a "mono-context" experiment. For example, IL-13 is a cytokine principally secreted by Th2 cells and as a consequence, it is mainly studied in Th2 cell-focused studies. In our Th contexts, we observed that rhOX40L had no significant impact on IL-13 secretion by T cells in a Th2 context. However, we observed that rhOX40L decreased IL-13 secretion in Th0 and Th17 context, and it was associated with a significant context-dependency score. Here, context-dependency reflects the complex T cell signal integrations that act on Th polarization and Th cytokine secretion.

To study OX40L context-dependent functions on Th polarization we used two experimental methods, a DC-free Th polarization system and a T cell-DC co-culture system. These methods, as well as tools to agonize or antagonize OX40L, were highly controlled since they were well established in the literature and the team [85,86,122,169,170]. This allowed us to elaborate our model on well-known experimental systems. Moreover, it was also useful to already have available data about OX40L effects on Th polarization and Th cytokine secretion [85,170]. As previously discussed, the study of context-dependency involves high numbers of parameters and combinations, and

thus, it calls initially for well-established experimental systems and trustable data to go beyond a standard experiment in one specific context.

These aforementioned experimental systems were the base of our two types of contexts: molecular, using the presence of Th-polarizing cytokines, and cellular contexts. Both contexts conferred different advantages and drawbacks. For the few studies that observed different effects of OX40L on Th polarization, molecularly defined contexts were used [86,122]. They are easier to control because each context induces a very specific panel of secreted cytokines by T cells, while contexts using activated DCs induced a mixed cytokine panel. We will discuss this aspect more in detail in the last part of the discussion. With cellular contexts, in which T cells are activated and polarized by DCs, we added complexity in our contexts and tried to get closer to physiological conditions compared to molecular contexts.

For all this diversity of contexts applied to CD4 T cells, we measured systematically a big quantity of Th secreted cytokines, 17 output cytokines, compared to most studies which selected few cytokines of interest. We obtained a huge dataset containing 5046 data points:
(302 conditions x 17 cytokines) - 88 missing values = 5046 data points
(missing values are due to a lack of supernatants to perform Luminex for four cytokines (IL-21, IL-22, IL-31 and TNF-β); CBA for the 13 other cytokines have been performed in all conditions).

Regarding the mathematical and statistical modeling, we worked in close relationship with biostatisticians. The model was established in the first place on the Th molecular contexts because there are easier to control and involve less parameter. To understand the impact of the context on cytokine variation due to OX40L, we used LMM. This classical model in statistics allowed us to determine and quantify the link between the variable to be explained and explanatory variables. LMM was applied to each cytokine individually. The model estimated β coefficients, that quantify this impact of the context on the cytokine variation due to OX40L for each context. Then, for the context-dependency score, we first calculated a β' value (β/standard deviation) for each context. This allowed us to consider the standard deviation, in other terms, the confidence in β coefficients estimated by the model. Subsequently, we calculated the distance between each β' for each context two by two and our context-dependency score was defined as the mean of these distances. We made the decision to use the mean of these distances to define the context-dependency score. Indeed, the mean enabled to consider β' extreme values. We could have used the median but it would have excluded β' extreme values while there are interesting in our setting

because they show different context impacts on OX40L function (the definition of context-dependency).

The second type of model we used in this study was Lasso analysis. Lasso model is used to perform variable selection principally in omics disciplines in biology, such as genomics, proteomics or metabolomics. It is commonly used in two types of analysis to improve accuracy [308,309]:

- In the case that a lot of variables are present compared to the number of samples/individuals. When we are confronted with a huge number of variables, the Lasso model allows finding the ones that could explain a variable to explain. By applying penalties, it forces variable coefficients to zero, meaning that these variables are removed from the model, hence sparsity.
- In the case it is necessary to perform variable selection before applying a classical statistical model (*i.e.* linear model), to identify the best model to understand a variable to explain. Here, we look for the best penalty, associated only with explained variables.

In our case, we used the Lasso model in a non-classical and original way to determine the variable that had the most importance in OX40L context-dependency. In cellular contexts, namely bDC and MoDC, contexts were composed of two parameters: the DC type and the DC-activating stimuli. By applying increasing penalties and forcing their coefficients to zero, the Lasso model helped us to identify the most influential parameter on OX40L context-dependency for each output cytokine, which was the DC type for 13 output cytokines on 17 totals.

3) Context-dependency model applications

In this study, we described an original approach to comprehensively and specifically analyze context-dependency and to better understand how the context influences the function of OX40L on Th polarization. We have analyzed the context-dependency of OX40L in various molecular and cellular contexts representing different immune and inflammatory microenvironments.
In our model, we focused on molecular cytokine contexts and cellular DC contexts, we could also have included molecular immune checkpoint contexts for instance (Figure 13).

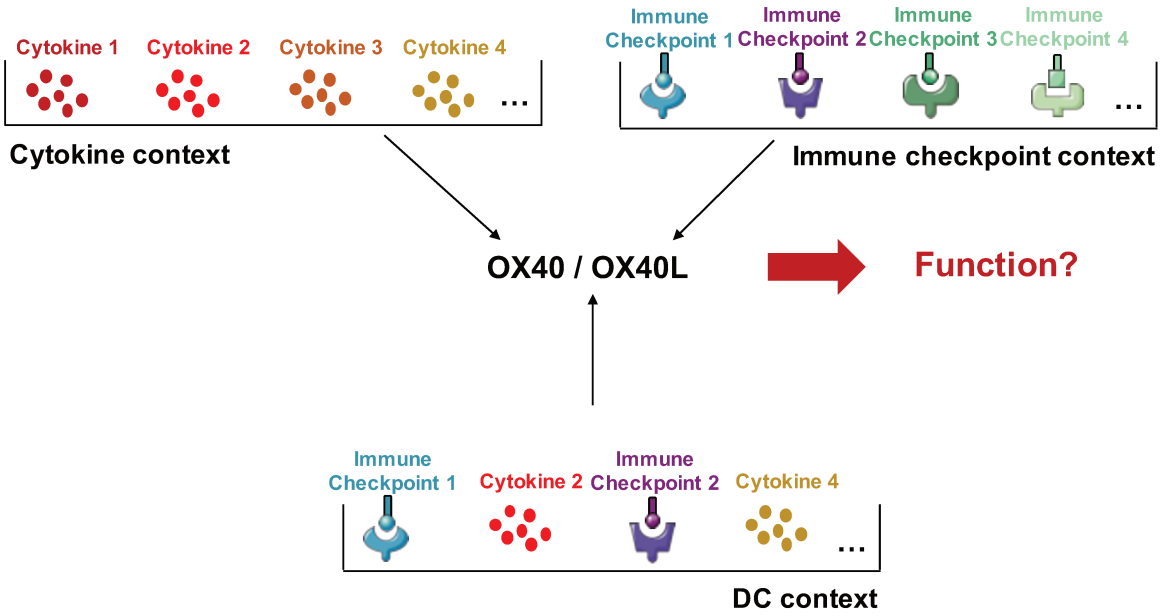

Figure 13: Context-dependency of OX40L functions

DC context is a cellular context and is the combination of many factors including the DC type, the DC-activating stimuli, secreted cytokines, immune checkpoint surface molecules, etc. Cytokine context is a molecular context that we illustrated throughout this manuscript with Th polarizing cytokines. Another possible molecular context could be an immune checkpoint context, where OX40L function is evaluated in the presence or absence of another immune checkpoint molecule.

This model can be applied more broadly to other molecules (*e.g.* a cytokine, a glucocorticoid, etc), in other contexts (*e.g.* immune checkpoint contexts, other cellular contexts, etc). Thus, although it was established in human Th cell polarization, the same conceptual and methodological framework may be applied to dissect other molecule functions in contexts associated with a given physiopathological situation. Context-dependency is not a rare phenomenon and should be more systematically taken into account, notably for drugs that can impact many cell types in many microenvironmental contexts.

Therapies using immune checkpoint monoclonal antibodies have been more and more developed in the last decade, principally targeting PD-1 and CTLA-4 co-inhibitory immune checkpoints. They have shown promising results but one of the main issues is that clinical efficacy is limited to a few patients in the majority of cancer types. One attractive and instinctive solution is to combine therapeutic agents [310]. Our model can be interesting to use in this situation. As an example, the question can be what is the impact of an anti-PD-1 monoclonal antibody in combination or not with an anti-TIGIT on T cell proliferation? Context-dependency can be measured at different

levels. First, the context can be defined by the presence or not of the second therapeutic agent. In the case of two co-inhibitory molecules, does PD-1 monoclonal antibody impact on T cell proliferation can be different in presence of another antagonist antibody? Synergic, antagonistic, dominant impact? (Figure 14).

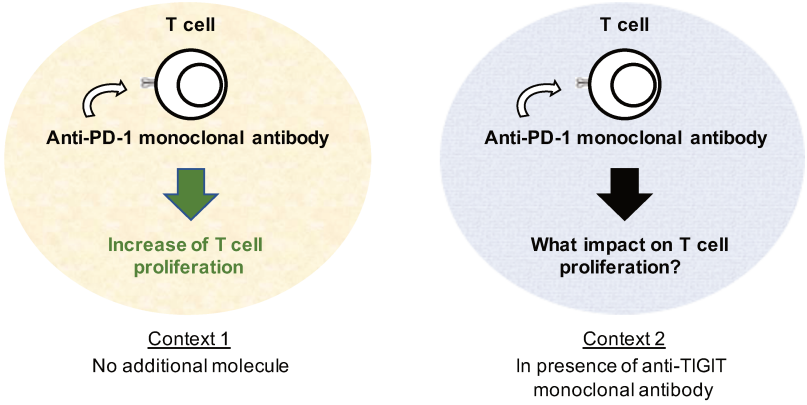

Figure 14: Scheme illustrating context-dependency of monoclonal antibodies effect on T cell proliferation in relation to each other

As an example, here, the impact of anti-PD-1 monoclonal antibody is tested on T cell proliferation, in different contexts defined by the presence or the absence of an immune checkpoint (e.g. anti-TIGIT).

Then, if we admit that combination induces synergic interaction, does the combination of two co-inhibitory immune checkpoints induces synergistic function in different broader contexts? For instance, does PD-1 and TIGIT monoclonal antibodies or their combination have the same impact in patients treated or not with chemotherapy? (Figure 15)

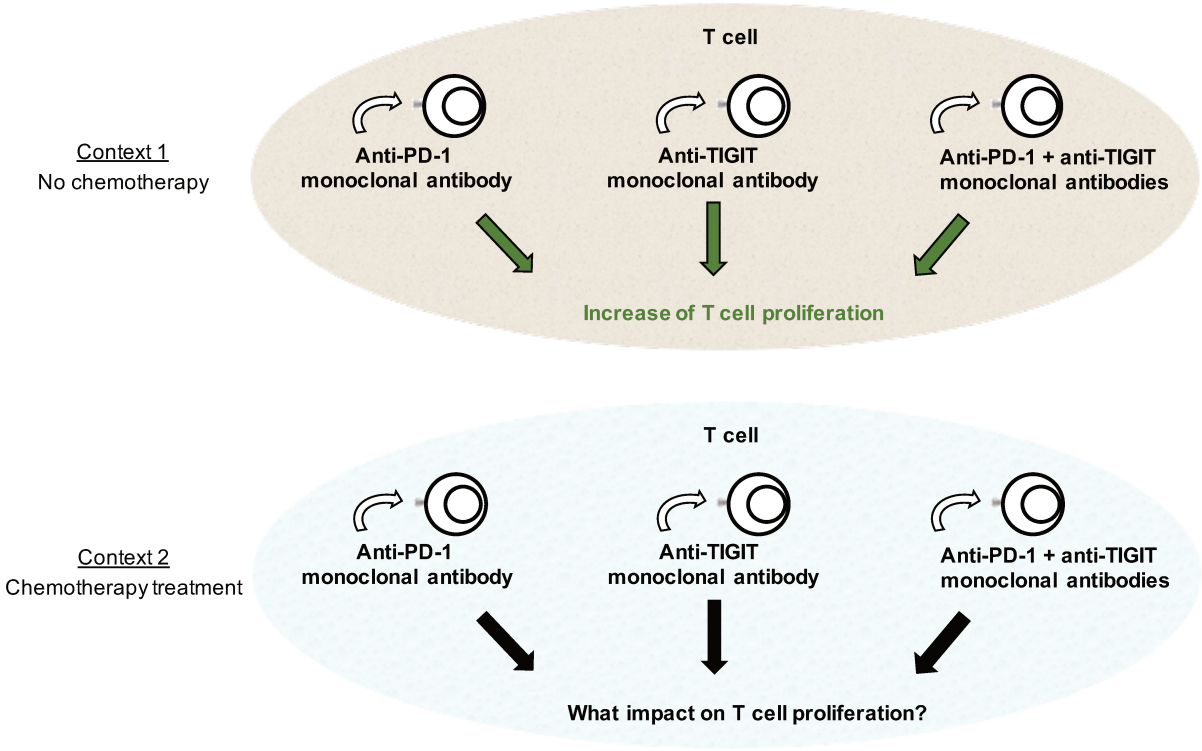

Figure 15: Scheme illustrating context-dependency of monoclonal antibodies effect on T cell proliferation according to the chemotherapy treatment

As an example, here, the impact of anti-PD-1, anti-TIGIT or a combination of these two monoclonal antibodies are tested on T cell proliferation, in different contexts defined by the fact that patients are treated or not with chemotherapy.

OX40 agonists are being developed as immune-stimulating agents in cancer. They are expected to function in various contexts, represented by the specific patient tumor microenvironment. Similarly, this raises the question of how much agonist OX40 effects would be modified by the context, specifically if it is combined with an antibody targeting a co-inhibitory immune checkpoint as PD-1.

In our cellular contexts, we included activating-stimuli with physiopathological relevance to bacteria (LPS, HKSA, Curdlan), fungus (Zymozan) and allergy (TSLP). It would have been interesting to include a tumoral context in our panel since we are working on the functions of a molecule with potential for immunotherapy. DC programs induced by tumor microenvironment is peculiar and can either promote or control cancer development. There are some data resources about DC states in tumors [311,312]. However, such complex tissue microenvironments, highly variable between patients, are difficult to recapitulate in controlled systems and require dedicated studies. An interesting experiment would be to culture T cells in tumor supernatants. The different

contexts can be defined as several parameters, first, it can be simply the same tumor type from different patients, that have their own tumor microenvironment. Then it can go deeper, including different tumor types, different tumor treatments, etc. Pieces of tumor tissue could be placed in culture for 24 hours in an appropriate medium. The day after, the supernatants would be recovered and used to culture T cells in presence of an immune checkpoint agonist or blocking antibody. Measuring and quantifying the context-dependency of an immune checkpoint function would be very interesting. In the case of one context defined by one patient tumor microenvironment, this kind of analysis might be the first step in better understanding the variable efficacy of immune checkpoint blockade.

In line with defining one patient tumor microenvironment as one specific context, it could be interesting to address this question more globally, where the donor could be a context itself. For instance, in our setting, could some OX40L impact on output cytokines be controlled first by the donor effect before the DC activating stimulus or the DC type? This could draw a major conclusion useful for the community about the donor effect, which is usually removed from the analysis, including ours. To evaluate the context-dependency of OX40L function on Th polarization across donors, we would need to have several data points per donor for each condition (in the same way that we have several data points for TSLP-bDC for example in our model).

To finish on context-dependency applications in cancer, we will discuss the use of organoids in preclinical studies. Organoids are three-dimensional *in vitro* cell culture. This model is more and more used to test immunotherapy treatment because they can recapitulate realistic microarchitecture of the TME. In mice and human models, some studies tested PD-1 blockade in organoids [313–315]. Patient-derived organoids are also considered as a tool for personalized cancer treatments, to evaluate and choose the most efficient drug for each patient [316]. It could be very interesting to quantify context-dependency in this model, still in the idea that one context is defined by one patient tumor microenvironment.

Moreover, technically, it exists several methods for organoid generation, for instance hanging drop culture, matrix embedding culture or culture in low adherence plate [317]. However, this parameter can influence the output response. Saitakis et al. studied T cell functions in polyacrylamide gels and generated three contexts defined by different stiffness values (0,5kPa, 6,4kPa or 100kPa). They demonstrated that the stiffness of the environment to which T cells are exposed modulated their functions, including their morphology, migration, gene expression and

cytokine secretion. For instance, they showed IFNγ and TNF-α secretion increase with the gel stiffness [318]. Thus, in the case of organoids with potential use in personalized medicine, it is important to consider that the physical properties of the surfaces can influence T cell functions. It would be interesting to apply our context-dependency model across physically different contexts defined by the stiffness to quantify the context-dependent function of an immune checkpoint, like OX40L, on cytokine secretion, and see the impact on the different cytokines.

4) Context-dependency model limitations

In this part, we will focus on the limits of our model and the rationale of these limits.

The first limitation of context-dependency studies is of course the number of contexts. As said previously, a context can be composed of a multitude of parameters, which cannot all technically be considered in one experimental study. In our case, we first decided to take into account the cytokine context, because they are commonly described to be a major signal in Th polarization. We used a recombinant OX40L protein (rhOX40L) in a simplified experiment of polarization, without any DC intervention, using anti-CD3/anti-CD28 beads for T cell activation and synthetic cytokines for polarization. This setting allowed us to well-control all quantities of compounds. In addition, the fact that T cells come from one donor and react to a precise concentration of synthetized recombinant protein in a controlled cytokine context generates less donor variability. However, “extreme” scenarios can be created due to the simplification of the polarization process, in which only polarizing cytokines are present in high concentrations or not at all, and it obviously does not reflect the complexity of inflammatory contexts.

Our second experimental setting using DCs to activate and polarize T cells aims to “upgrade” our contexts to get closer to the reality of Th polarization in lymph nodes. Nevertheless, increasing our context complexity goes along with decreasing controlled systems. Indeed, co-cultures imply one donor of T cell and one donor of DC, inducing more variability due to histocompatibility between two random donors. Secondly, although an excess of OX40L blocking antibody is added to the co-culture, the initial quantity of OX40L protein on DCs varies according to the DC activating stimulus, so it is different across contexts and this cannot be controlled.

Within cellular contexts, we could have done plenty of other choices for the contexts such as choose other DC activating stimuli for example. Unfortunately, adding more DC activating stimuli would have been difficult in regards to the number of DCs we obtained from a blood pocket.

In terms of DC type, we only include two types of DCs, cDC2 and MoDCs. Co-cultures with these two subsets were routinely done in the team. We thought about adding co-cultures with cDC1 and pDC, to increase our number of cellular contexts and have more diversity. However, both subset percentages in blood are very low [319] and it would have been difficult to perform experiments in the same conditions as with cDC2 and MoDCs. As we need a minimum number of 50000 T cells to performed cytokine secretion analysis, we would not have been able to have all DC contexts for each donor. In addition, in the case of pDCs, Xvivo15, the medium we used for our experiments, is not optimal for co-culture with T cells. In the team and in the literature, pDCs and T cells are usually co-cultured in Yssel medium containing 10% of fetal bovine serum (FBS). We expressly chose to use a medium without FBS for our experiments to not induce a bias linked to the serum composition. Adding pDCs in the model would have compelled us to use Yssel + 10% FBS medium for all our experiments to have the same settings in all contexts and be able to compare them. It is known that the medium highly impacts cellular interaction in culture and plays a significant role in the reproducibility of results [320]. Having a systematic study on context-dependency related to medium could be very helpful for the scientific community. It would be interesting to include medium contexts in our model to determine how much the medium and the presence/absence of serum and even the type of serum (human versus fetal calf serum) can influence the function of OX40L on Th polarization (and it could be applied to other molecules and outputs).

Overall, we summarized high quantity and diversity of data in understandable and various ways. We began with 32 dimensions (17 cytokines + 15 contexts) but managed to show them into two dimensions representations:

- Simple graphs: cytokine concentrations versus contexts
- PCA: with two principal components for global cytokine analysis
- Lollipop plots: Euclidian distances between presence and absence of OX40L versus contexts
- Heatmaps: one for absolute differences OX40L impact on cytokine concentrations and one for β coefficients estimated by the LMM

- Graphs of context-dependency scores: context-dependency scores versus output cytokines

In these 2D representations, we tried to lose as little information as possible, but it remained difficult in some cases considering the quantity of information. On heatmaps of absolute differences, we lost information about donor variability because the mean across donors are represented. We added some simple graphs showing cytokine concentrations versus contexts for few cytokines.

For OX40L context-dependency scores: we defined two types of context-dependencies, namely quantitative and qualitative. We determined quantitative context-dependency, meaning that for the same output response, OX40L induced either an increase or a decrease of a cytokine concentration by Th cells at different magnitudes across contexts. Conversely, if opposite effects were observed for the same output response, we defined it as qualitative context-dependency (cf. article manuscript). In contrast, what we defined as context-independency was when OX40L had the same effect in all contexts (Figure 16).

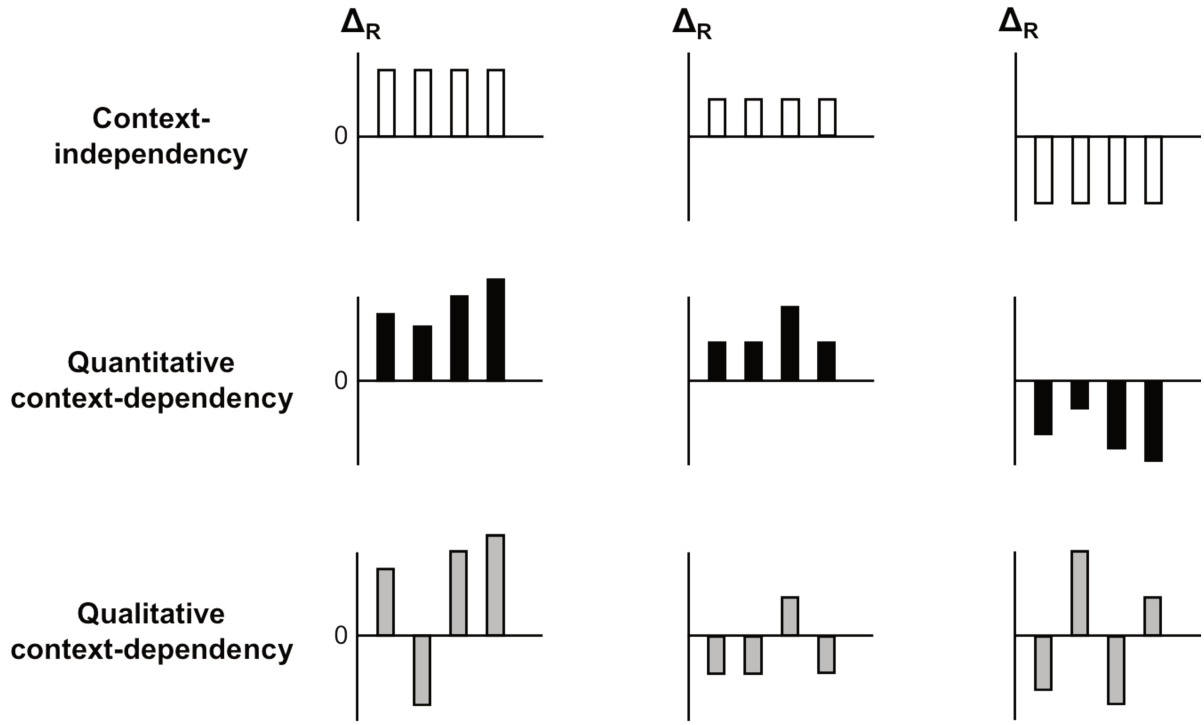

Figure 16: Context-dependency definitions

Within this type of context-dependency, we could also observe quantitative context-dependency, this important information is missed in our graphs representing context-dependency scores. For an easier comprehension of complex data, we decided to represent only qualitative context-dependency when both were present. We considered qualitative context-dependency more important than quantitative context-dependency. Indeed, the fact that OX40L (or other biomolecules) can have opposite effects in different contexts is more impactful than different magnitudes of action.

Although we took all precautions to avoid variability, we observed inter-donor variability (hence evaluating the context-dependent function of a molecule across donors, as previously suggested, can be very interesting). This inter-donor variability can be linked to many parameters that we cannot control, such as environmental factors. Indeed, although they are healthy donors, they are exposed to factors initiating immune responses and their accumulation modulates immune system responses [321]. Thus, the historical immune reaction varies between an individual and another and can lead to variable responses in our experiments. Moreover, ethnic and social origins but also age and gender can also contribute to variability [322,323].

The Immune Variation (ImmVar) is a project that aims to understand immune response variation among healthy donors. Among other things, they showed that a minor but meaningful percentage of RNA expression variation (around 20%) between two individuals from different origins can be explained by genetic factors [322]. Moreover, Patin et al. showed that genetic factors, but also external parameters such as smoking, could alter immune system homeostasis [324].

In our work, the donor effect was taken into account to calculate our context-dependency scores for each type of context (Th, cDC2 and MoDC contexts). Moreover, in the last figure of the paper, the donor effect was even removed from the Lasso analysis to not bias the analysis (otherwise it would have been considered as a parameter like the DC type and the DC-activating stimulus).

II) OX40L impact on Th cytokine secretion and its context-dependent effects

As described in the introduction, OX40L role on Th polarization is very diverse and has been described on many Th subsets. In this part, we will discuss its role on specific cytokines and its context-dependent (or independent) impact on others.

1) OX40L impact on Th main cytokines

a) OX40L and IL-4 secretion

Context-dependency may also be interesting to consider in the case of paradoxical results between different studies. In the case of OX40L, we were interested in IL-4 since a lot of studies linked OX40L to allergy, Th2 and Tfh cells [290]. In our Th2 context, we observed a decrease of IL-4 in presence of rhOX40L protein, as well as a decrease of IL-5 and IL-31 Th2 cytokines. Along similar lines, in our TSLP-bDC context, we observed an increase of IL-4 in presence of the anti-OX40L blocking antibody, which means that OX40L decreased IL-4.

Up to now, OX40L has been classified as inducing Th2 in the literature. Ito et al. performed a prominent study, with settings close to ours, in which they used a co-culture system with human naive CD4 T cells and TSLP-bDC and described a decrease of IL-4 when blocking OX40L [122]. However, they used neither the same DC type nor the same medium for their experiments. They used total blood $CD11c^+$ DCs while we used blood $BDCA1^+$ cDC2, and they used Yssel medium with human serum while we used serum-free Xvivo15 medium. Another recent study (in which Ito is a co-author) showed that anti-OX40L blocking decreased IL-4 secretion by T cells when co-cultured with TSLP-bDC [251]. They still used total blood $CD11c^+$ DCs and RPMI medium with human serum. We determined that the DC type was a very important parameter that could influence OX40L function (cf. Figure 7 of the article manuscript). Indeed, it has a greater impact on OX40L function on cytokine secretion compared to the DC-activating stimuli for the majority of output cytokines. This might be an explanation of the difference between our study and these regarding OX40L effect on IL-4 secretion.

It can also be noted that in the study from Jacquemin et al., the authors performed intracellular

staining for IL-4 and showed a decrease of IL-4$^+$ cells in presence of a rhOX40L protein, in a Th0 context [86]. The settings were very similar to ours, activating naive CD4 T cells with anti-CD3/anti-CD28 and the same rhOX40L protein.

b) OX40L and IL-17A/IL-17F secretions

An interesting impact of OX40L in our data was observed on IL-17A and IL-17F cytokines. These two cytokines are only detected in the Th17 context because they necessitate a specific polarizing cytokine cocktail to be induced in absence of DCs [38]. Moreover, using a similar setting to ours, Jacquemin et al. could not detect IL-17 in Th0 and Th1 contexts, even in presence of rhOX40L [86]. As seen in the introduction, OX40L has been described to impact Th17 cell polarization. However, the majority of studies focused only on IL-17A [255–257,262] and the few ones measuring both IL-17A and IL-17F in mice models eventually focused on IL-17A [258,261].

In our Th17 context, we noticed that OX40L had a differential regulation of IL-17A and IL-17F. IL-17A concentration was decreased whereas IL-17F concentration was increased in presence of OX40L. Originally, *IL17A* and *IL17F* genes were proposed to be coordinately regulated [325]. Up to now, few studies have reported a differential regulation of IL-17A and IL-17F. In mouse model, Gomez-Rodriguez et al. observed that naive CD4 T cells secreted less IL-17A, but not IL-17F, in response to a low dose TCR stimulation or low dose of Calcineurin inhibitor. They noted normal levels of RORγt and RORα, however, they showed that IL-17A promoter had a binding site for Ca^{2+} sensitive Nuclear Factor of Activated T cell (NFAT) transcription factors, but not IL-17F [131]. A few years later, two papers from the same team showed that cAMP-responsive element modulator α (CREMα) transcription factor was responsible for increasing IL-17A and decreasing IL-17F in SLE patients [326,327]. Additionally, Adamik et al. described that distinct conditions mixing IL-1β, IL-23 and Prostaglandin E2 led to different induction levels of IL-17A and IL-17F in human primary memory Th17 cells. Moreover, they showed that *IL17A* and *IL17F* chromatin were differentially regulated because of divergent epigenetic architecture loci, which led to a preferential expression of *IL17A* [328]. Finally, Grandclaudon et al. demonstrated that the combination of IL-12 and IL-1β induced the production of IL-17F, but not IL-17A [170].
In the context of OX40L function on Th17 cells, no study reported yet a differential regulation of IL-17F and IL-17A cytokines. Our data provide new insights about OX40L role on these cytokines.

It could help to better understand how they are differentially regulated in humans by performing RNA sequencing on Th17 cells and Th17 cells treated with rhOX40L for instance. Indeed, although they have similar or even sometimes synergic actions due to high homology, their role can also differ in certain contexts [329–332], hence there is an interest in a better comprehension of their secretion mechanism to be able to target them individually.

c) OX40L and other Th cytokines

In the introduction, we reviewed that OX40L had a positive impact on Th9 cells [263,264]. In our data, we observed that IL-9 significantly increased or tended to increase in almost all Th and DC contexts. The only contexts in which OX40L had no impact is in Th0 and Th1 contexts. This is because IL-9 was not induced initially in these two contexts, it turned out that OX40L never induced a cytokine *de novo* in our settings.

Regarding Th1 polarization, some papers described an inhibiting effect of OX40L on IFNγ [247] and others showed a stimulating effect [249]. We suggested in the introduction that OX40L-induced effect on Th1 polarization varied depending on the context of the experimental condition.
In our Th contexts, IFNγ significantly decreased or tended to decrease in all contexts. However, in bDC contexts, we observed a significant context-dependency score for IFNγ, meaning that OX40L impact on IFNγ depended on the bDC-context. This is interesting given the heterogeneity of responses in the literature.

Before discussing context-dependency more in detail, it is interesting to notice that OX40L function in Th versus DC contexts is different at a global cytokine level. Although OX40L seems to increase and decrease cytokine concentrations more or less equally in Th contexts, we noticed that OX40L mainly increased cytokine concentrations in DC contexts. The only DC context in which OX40L induced clear concentration decrease for several cytokines is the TSLP-bDC context. It will be discussed more thoroughly in the next part.

2) OX40L context-dependent functions on Th cytokines

Our model reveals a new level of complexity of OX40L responses, in terms of context-dependencies. As previously detailed, we differentiated quantitative and qualitative context-dependencies.

In our Th contexts, we observed these two context-dependency types. On the one hand, OX40L increased or decreased IL-22 and TNF-α across contexts, hence OX40L has a qualitative context-dependent function on these two output cytokines. On the other hand, OX40L played a quantitative context-dependent function on IL-10 and IL-13. Among these output cytokines, IL-10 had the higher context-dependency score, meaning that it was the most sensitive, in a quantitative manner, to OX40L context-dependency in Th contexts, followed by IL-22, in a qualitative and quantitative manner. Interestingly, IL-10 and IL-22 both belong to the IL-10 cytokine family. The main function of this cytokine family is to protect organs and tissues from damage caused by infections and inflammatory responses [47]. Decrease of IL-10 in all Th contexts is interesting, for cancer treatment for instance. The fact that OX40L induced a quantitative context-dependent decrease of IL-10 could also suggest that we would expect patient-to-patient variability in the case of treatment with an OX40L agonist antibody.

Within bDC context, OX40L context-dependency on IL-2, GM-CSF, IFNγ and IL-3 output cytokines was highly dependent on the TSLP context. This is particularly obvious because after removing the TSLP context from the analysis to compared bDC and MoDC contexts, we could not observe context-dependency on any output cytokine (cf. Figures 4 and 6 of the article manuscript). At first sight, it looked coherent because the TSLP-bDC context is instinctively different from the five other ones. Indeed, in Zymozan, PAM3, LPS, HKSA and Curdlan-bDC contexts, the DC activating stimuli are mimicking an external pathogen, fungal or bacterial infections. On the contrary, TSLP is an inflammatory cytokine produced by epithelial cells or by other stromal cells, in a very distinct context that is allergy.

As for Th contexts, we observed the two types of context-dependency. OX40L played a qualitative context-dependent function on IL-2, GM-CSF and IFNγ. OX40L induced a decrease of these cytokines in the TSLP-bDC context, whereas it induced an increase in the five other ones. IL-2 and IFNγ are principally defined as Th1 cytokines (even if they are secreted by other Th cells, we will discuss it in the next part of the discussion). GM-CSF can be secreted by several Th cells and is

known to stimulate the proliferation and activation of many cells such as macrophages, dendritic cells and monocytes, and to enhance phagocytosis, antigen presentation and proinflammatory cytokine secretion [333]. Thus, the increase of these three cytokines by OX40L in fungal/bacterial infection contexts, and conversely the decrease in allergic contexts, seems consistent with the required immune response in these contexts.
Besides, OX40L played a quantitative context-dependent function on IL-3, which increased in all bDC contexts but at different levels.

The fact that TSLP-bDC context seems to be the main cause of OX40L context-dependency since this latter disappeared in absence of this context, could also let us think that Zymozan, PAM3, LPS, HKSA and Curdlan-bDC are contexts in which OX40L will always have the same function on output secreted cytokines. However, this idea is challenged by context-dependency scores obtained in MoDC contexts. As explained previously, we could not apply the TSLP stimulus on MoDC since they do not express the TSLP receptor [121,334]. Thus, context-dependency scores were calculated only across Zymozan, PAM3, LPS, HKSA and Curdlan-MoDC contexts. In contrast to bDC contexts without TSLP, context-dependency scores for certain cytokines were significant. This was the first evidence that the DC-activating stimulus could not be the only parameter influencing OX40L context-dependent functions. Cytokines impacted by OX40L context-dependency in MoDC contexts were mainly Th2 cytokines. OX40L influenced differently IL-4, IL-5, IL-31 and GM-CSF across the different fungal and bacterial contexts.

We could also have defined a “context-independent” behavior of OX40L on output cytokines. For instance, we observed no context-dependency of OX40L function on IL-21 secretion. OX40L similarly increased IL-21 cytokine in all our Th and DC contexts. The link between OX40L, IL-21 and Tfh cells has been well-established [85,86] and our model is consistent with the literature.

III)Relevance of Th cell classification

As we saw in the introduction, Th subset classification is based on several parameters, mainly their distinct secreted cytokines. In this last part of the discussion, we will reflect on how the cytokine secretion analysis at a large-scale triggered conclusion that modifies, through its quantitative and qualitative aspects, the general concepts of Th differentiation.

1) Narrow profile versus mixed profile of Th cytokine secretion

In our study, we performed the analysis of OX40L function, in a systematic manner across many contexts, on one output, which is Th polarization. We decided to also be systematic regarding our output and for that, we analyzed in each context the global Th cytokines production. Figures 17 and 18 gather together all the output secreted cytokines in Th1, Th2 and Th17 for Th contexts, and in PAM3-MoDC and TSLP-bDC for DC contexts (without any addition of rhOX40L in the Th contexts or OX40L blocking antibody in the DC contexts).

We observe that Th contexts induced a narrow Th profile, meaning that each Th subset mainly secreted their specific subset-defining cytokines. However, when complicating our contexts by introducing activated DCs, we observed that T cells secreted a mixed profile of cytokines.

In more details, in Th contexts, a first observation was that the cytokine secretion profiles were clear for each subset: Th1 context induced a high secretion of IL-2, IFNγ, TNF-α, TNF-β (Figure 17A); Th2 context induced IL-4, IL-5 (both in small quantity but present), IL-9, IL-10, IL-13, IL-31 (Figure 17B); Th17 context induced IL-17A, IL-17F, IL-6 (Figure 17C). Globally, it seems that the Th2 context was the most mixed between the three. To have a clearer Th2 profile, we could have added anti-IFNγ or anti-IL-12, but we did not want to have an even more “extreme” context by adding blocking antibodies. Moreover, we noticed that IL-21 was secreted in all Th-polarizing contexts. IL-21 is principally produced by Tfh and Th17 cells [91,335]. The fact that all subsets secreted IL-21 is interesting considering the sub-classification of human Tfh cells into Tfh1, Tfh2 and Tfh17 cells, we will look deeper into this in the next part. We also have substantial production of IL-3 and GM-CSF in Th1 and Th2 contexts only. Mosmann et al. noted that both of their Th1 and Th2 clones secreted IL-3 and GM-CSF [11]. IL-3 secretion by Th cells remains poorly described. GM-CSF

has been more described at that time and can be secreted by Th1, Th2 and Th17 [333]. Interestingly, two recent studies showed that IL-3 and GM-CSF were typically co-expressed [336,337].

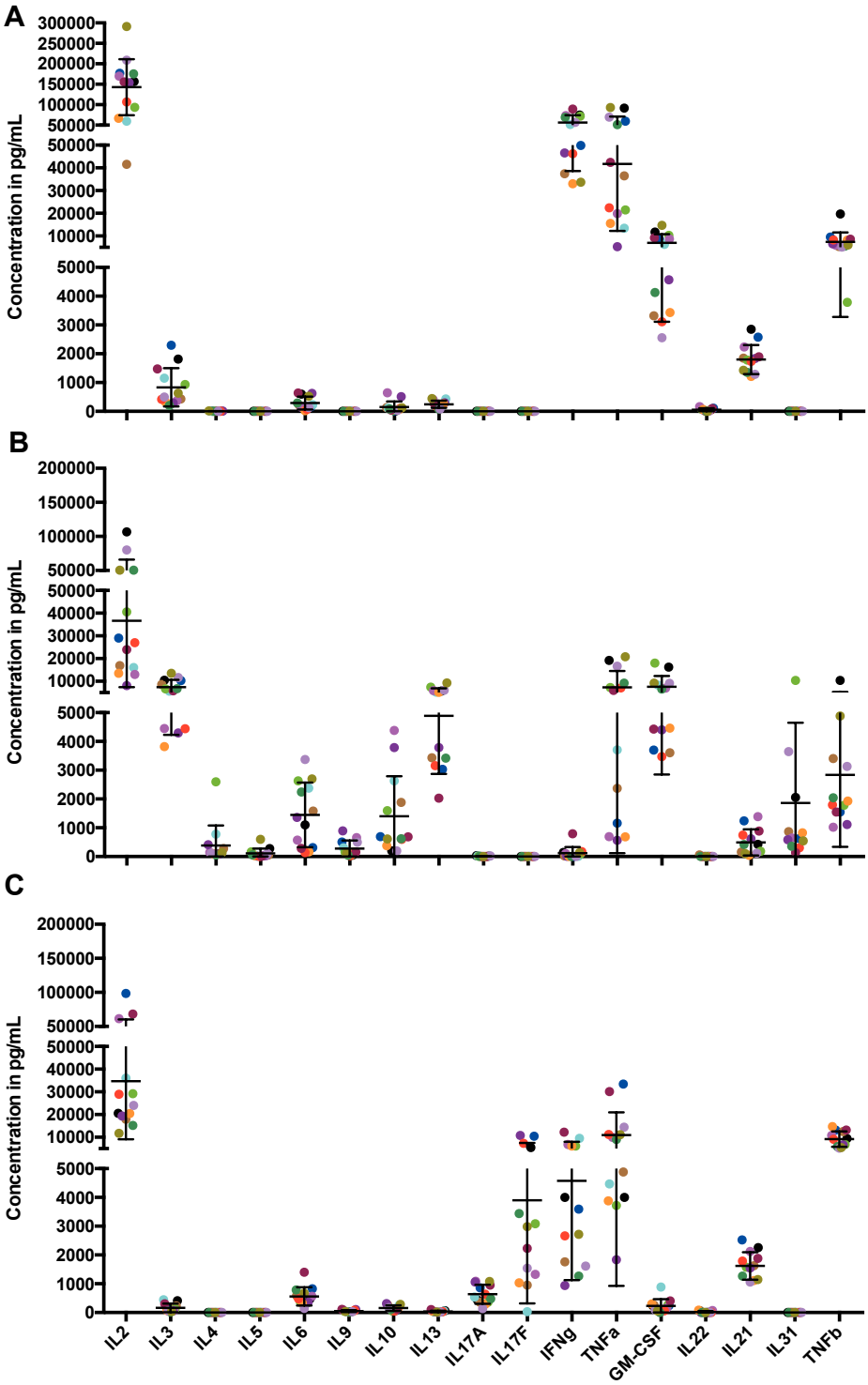

Figure 17: Concentrations of all secreted output cytokines in Th contexts

Concentrations of all secreted output cytokines in A) Th1 context, B) Th2 context and C) Th17 context. Each color represents one donor (n=13).

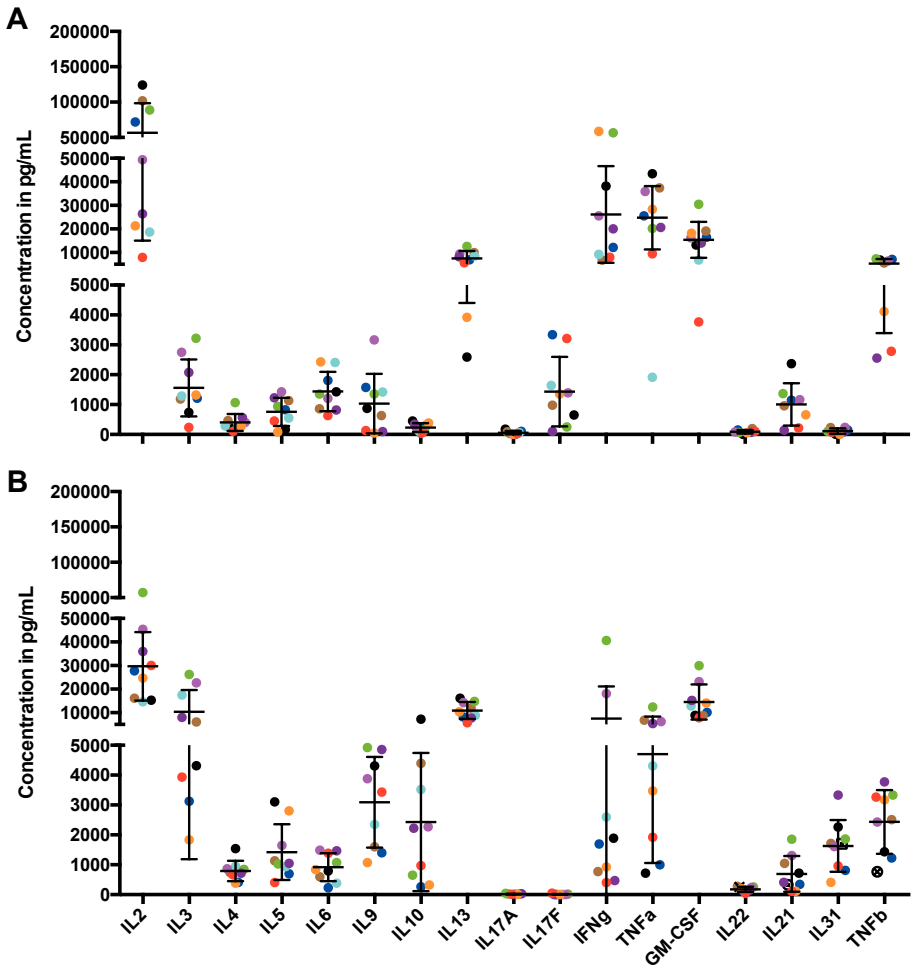

Figure 18: Concentrations of all secreted output cytokines in two very different DC contexts

Concentrations of all secreted output cytokines in A) PAM3-MoDC context and B) TSLP-bDC context. Each color represents one donor (n=9).

In Figure 18, for these two DC contexts that differ from the DC type and the DC-activating stimulus, we observed that the majority of cytokines are secreted in both contexts, but at different levels. For example, in the PAM3-MoDC context, we observed a high secretion of Th1 cytokines such as IFNγ, TNF-α, TNF-β, IL-2, but also a secretion of IL-17F and Th2 cytokines, IL-4, IL-5 and IL-13 (Figure 18A). In the TSLP-bDC context, we measured a lot of Th2 cytokines (IL-4, IL-5, IL-13, IL-31, GM-CSF), but also Th1 cytokines, although at a lower concentration than in the PAM3-MoDC context (Figure 18B). Although it seems that there is a dominance of certain cytokines compared to others in the different contexts, a mixed profile of cytokines from distinct Th subsets is observed.

Comparing these results of narrow versus mixed profile of secreted cytokine by Th cells with the literature is difficult for several reasons:

- Studies usually focus on specific Th subsets or specific cytokines and do not perform a systematic analysis of all main Th cytokines.
- When analyzing a large panel of cytokines, most studies look at gene expression by single-cell or bulk RNA sequencing, whereas we measured our cytokines at the protein level, and it has been shown by comparative studies that correlations between mRNA and protein levels can be relatively uncertain [338,339].

  Specifically in CD4 T cells, this was greatly illustration by Cano-Gamez study. They stimulated naive and memory CD4 T cells in a Th17 and iTreg stimulation contexts. For naive CD4 T cells, they observed 733 differentially expressed genes and only 455 differentially expressed proteins between the two contexts. In the same line, for memory CD4 T cells, they observed 42 differentially expressed genes and no differentially expressed proteins [307].

Wong et al. investigated the impact of tissue microenvironment on T cell differentiation. In this study, they used mass cytometry to measure many Th output parameters at the protein level, including cytokines and surface receptors. Interestingly, their data suggested that it is actually very difficult to distinguish distinct Th subsets across the different human tissues they studied. Similar to what we observed in DC contexts, they showed that Th cells could secrete multiple Th-associated cytokines. For instance, they showed a co-secretion of IFNγ, IL-17A and IL-22 [340].

The use of mass cytometry in this study has many advantages. First, it allows quantifying many different molecule expressions at the protein level. Secondly, this molecule expression quantification is done at the single cell level, and thus, it enabled them to look at cytokine co-expression at the single cell level. On the contrary, in our data, we can only look at a simultaneous secretion of cytokines, but we cannot determine whether they are secreted from a unique cell or distinct ones within a population. For example, in the PAM3-MoDC context (Figure 18A), does the same T cell co-secrete IL-17F and IL-13? Or is Th population constituted of IL-17F$^+$ cells and IL-13$^+$ cells? Does co-secretion of cytokines by the same cell or co-presence of cytokines at the same location induce different immune responses?
It would have been great to have this information in our systematic study that includes a lot of

cytokines to better understand global Th cytokine secretion. We could also have done intracellular cytokine staining, which is more easily accessible. However, it does not enable to include as many parameters in one panel compared to mass cytometry, and technically, to measure co-expression, they need to be assembled in one panel only.

In our work, we polarized a pool of naive CD4 T cells. This pool of naive CD4 T cells is actually a mix of many different naive antigen-specific CD4 T cells, that can recognize many different antigens. In the present results, we did not take into consideration antigen specificity since we did not add antigen in Th contexts and we were in allogeneic condition in DC contexts. It could be very interesting to identify if naive antigen-specific CD4 T cells secrete a narrower cytokine profile when activated by their specific antigen. Indeed, the mixed cytokine secretion profile could be explained by the multiplicity of T cell clones.

Rafi Ahmed team and Robert Thimme team are specialized in antigen-specific T cells, respectively of yellow fever virus (YFV) and hepatitis C virus (HCV). Akondy et al. characterized naive and memory YFV-specific CD8 T cells, from donors vaccinated or not against yellow fever [341]. They used YFV-specific tetramer to enrich and sort naive YFV-specific CD8 T cells in unvaccinated donors and memory YFV-specific CD8 T cells in vaccinated ones. Besides, Wieland et al. studied memory HCV-specific CD8 T cells in chronically HCV-infected patients [342]. Both focused on antigen-specific CD8 T cells, but the same principle could be applied to antigen-specific CD4 T cells.

The use of tetramer could be a great tool to apply in our study. The idea would be first to stimulate a pool of naive CD4 T cells isolated from blood (it would necessitate a large number of naive T cells since antigen-specific T cell frequency is very low) with an antigen, flu for instance. Stimulation could be done either directly on T cells, using a flu optimal epitope and complemented with an anti-CD28, or through flu-activated DCs (certainly, CD4 responses in each context could be different). After 6 days of activation, flu-specific CD4 T cells would be sorted with flu tetramer. Flu-specific CD4 T cells and the rest of the pool would be restimulated separately for 24 hours with anti-CD3/anti-CD28 beads and cytokine secretion measured by CBA and Luminex (same protocol as in the article manuscript). It would allow distinguishing whether flu-specific CD4 T cells activated by flu secrete a narrower cytokine profile compared to other antigen-specific CD4 T cells activated by flu.

2) Complexity of Th classification

Our data are providing additional evidence that the majority of Th cells have an important degree of plasticity. It is important to keep in mind that this plasticity is influenced by many parameters such as cytokine receptor and transcription factor expressions, the availability of polarizing signals in the T cell microenvironment, etc. Plasticity related to Th cells was used to define a switch in lineage commitment. This means that plasticity is considered at an "inter-subset" level, when the T cell is changing from one Th subset phenotype to another. Our work and reflections on mixed cytokine profile lead us to the idea that plasticity might even be defined at an "intra-subset" level. When considering all these aspects, the concept of plasticity can become counter-intuitive because if a Th cell is supposed to be committed to a specific subset, then it should not be plastic, otherwise it would not be a specific subset.

In our data, we saw for instance that the TSLP-bDC context induced a mixed profile Th population secreting IL-4 and IFNγ (Figure 18B), even if IFNγ is in lower concentration compared to other contexts like PAM3-MoDC (Figure 18A). As previously said, we miss information about cytokine co-expression because we do not perform intracellular staining. However, since TSLP is an important topic of our team, some intracellular staining data are available on T cells activated by TSLP-bDC (Figure 19).

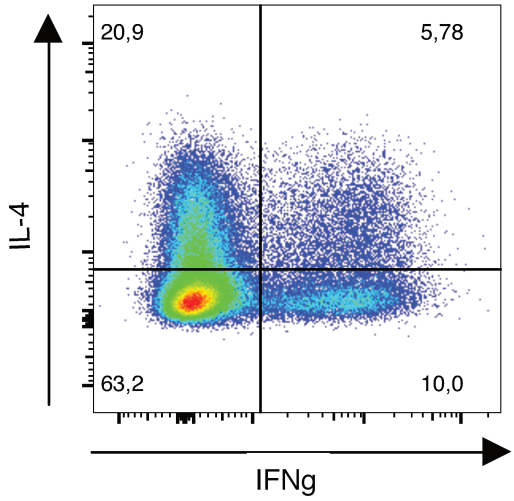

Figure 19: IL-4 and IFNγ intracellular staining on T cells activated with TSLP-bDC

This data has been generated by Coline Trichot.

In this plot, we can observe that 20,9% of Th cells only express IL-4, 10% of Th cells only express IFNγ and 5,78% of Th cells co-express both cytokines. If we consider classical Th subsets, we would say that we have 20,9% of Th2 cells, 10% of Th1 cells and 5,78% of Th1/Th2 cells. These double-positive cells are difficult to explain with the classical Th subset classification.

Another example of an increasing level of Th subset complexity has been described in Treg cells. Dong et al. showed that Treg subset could be subdivided into three subpopulations and that two of them ($CD4^+FoxP3^+CD45RA^-HLA\text{-}DR^-$ and $CD4^+FoxP3^+CD45RA^-HLA\text{-}DR^+$) were able to produce IFNγ and IL-17A (not both cytokines within the same cell) [343]. The secretion of pro-inflammatory cytokines by Treg cells that are supposed to induce tolerance greatly illustrates the growing complex heterogeneity of Th subsets.

We saw previously, in Figure 17, that IL-21 was secreted in all our Th contexts. IL-21 is produced in large amounts by Tfh cells and this observation seems consistent with Tfh cell plasticity. Indeed, looking at CXCR5, CCR6 and CXCR3 surface markers in the CD4 memory cell compartment, Morita et al. described that human Tfh cells isolated from peripheral blood, usually called circulating Tfh cells, can be subdivided into different sub-subset that mirror Th cells: Tfh1, Tfh2 and Tfh17 [344]. The main characteristic of these cells is that they express CXCR5 chemokine receptor and secreted the specific cytokines of Th1, Th2 and Th17 subsets respectively, in addition to IL-21 and CXCL13 secretion. Tfh2 and Tfh17 cells were capable of B cell help, contrary to Tfh1 cells that could not induce the secretion of Ig. But, this raises questions such as: is it coherent to name Tfh a cell that cannot provide help to B cells?

Moreover, a new sub-subset of Tfh13 cells has been identified very recently in mice and human and was described as responsible for the production of high-affinity anaphylactic IgE [345].
Mixed profiles of cytokine secretion by Th cells and new subset identification bring a main question: does the identification of new subsets or even sub-subsets is really relevant? Would it not be more relevant to reconsider Th cells by taking into consideration the global cytokine secretion (which would not exclude the fact that some cytokines can dominate compared to others)? In the example of Tfh13 cell study, only a few cytokines have been measured (principally IL-13 and IL-4). Does the identification of IL-13 not a bias toward a single cytokine inducing high-affinity anaphylactic IgE production (which is amplified by the name given to the subset)? More generally, is defining a new subset on a handful of effector cytokines not biased?

The global understanding of all these Th subsets and their derived cytokines leads to re-examine Th association to disease. At the time when only Th1 and Th2 were identified, Th classification of diseases was binary and related to a specific pathogenic Th subset and their specific cytokine secretion between those two. A clear example of this fact is multiple sclerosis. IFNγ-producing Th1 cells were described as playing a major role in multiple sclerosis, which was clearly classified as a Th1-associated disease [346–348]. Additionally, in line with the Th dichotomy described by Mossman and Coffman, EAE clinical improvements were correlated with the decrease of IFNγ but also the increase of IL-4, and Th2 cytokines were described as protective against exacerbated Th1 cells [349,350]. However, the discovery of Th17 changed the view of multiple sclerosis as a Th1-associated disease and helped the understanding of immune responses that were unexplained by the Th1 and Th2 paradigm [351], and after that, Th17 cells were shown to also play a pivotal role in multiple sclerosis disease [352].

Multiple sclerosis is one example among others in which a disease was associated with a specific subset and finally with many subsets. The evolution from a bipolar view to a multipolar view of multiple Th subsets involved in a single pathology led to growing complexity of Th cells and Th cytokine association to diseases and disease states. This brings many questions. First, related to the disease itself, is a disease associated with a specific pathogenic Th subset or several ones? In the second case, how the identification of several Th subsets involved in one pathology can help the understanding and therapy of this disease?

Moreover, Th plasticity questions what is the best strategy to treat patients when several Th subsets are involved? Targeting the signals in the microenvironment that induce pathogenic Th cells? Targeting directly these pathogenic Th cells? Targeting the pathogenic Th effector? As many questions that remain open on the classification of Th lymphocytes.

APPENDICES

1. Appendix 1

A quantitative multivariate model of human dendritic cell-T helper cell communication

Maximilien Grandclaudon*, Marie Perrot-Dockès*, Coline Trichot*, Léa Karpf, Omar Abouzid, Camille Chauvin, Philémon Sirven, Wassim Abou-Jaoudé, Frédérique Berger, Philippe Hupé, Denis Thieffry, Laure Sansonnet, Julien Chiquet, Céline Lévy-Leduc and Vassili Soumelis

Grandclaudon et al., 2019, Cell 179, 432–447

Article

Cell

A Quantitative Multivariate Model of Human Dendritic Cell-T Helper Cell Communication

Graphical Abstract

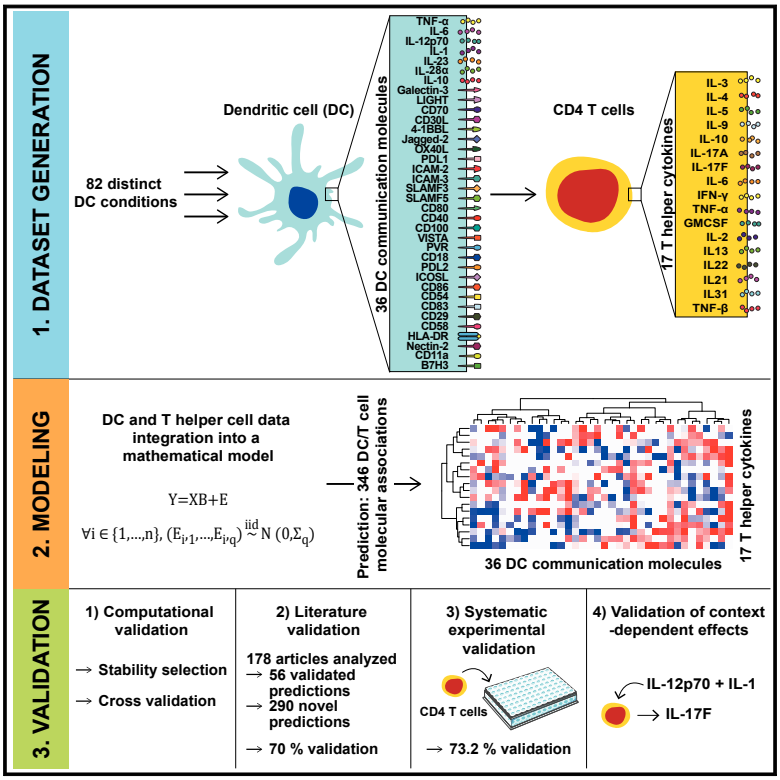

Highlights

- 428 protein-level measurements of 36 DC communication molecules and 17 Th cytokines
- Data-driven quantitative model of DC-T cell communication extensively validated
- Systematic and unbiased predictions of context-dependent mechanisms
- Validation of a new context-dependent role of IL-12p70 in Th17 differentiation

Authors

Maximilien Grandclaudon, Marie Perrot-Dockès, Coline Trichot, ..., Julien Chiquet, Céline Lévy-Leduc, Vassili Soumelis

Correspondence

vassili.soumelis@curie.fr

In Brief

Grandclaudon et al. show that combinatorial rules that explain communication between dendritic cells and T helper cells can be helpful in vaccine design and immunotherapy.

Grandclaudon et al., 2019, Cell *179*, 432–447
October 3, 2019
https://doi.org/10.1016/j.cell.2019.09.012

CellPress

Cell

Article

A Quantitative Multivariate Model of Human Dendritic Cell-T Helper Cell Communication

Maximilien Grandclaudon,[1,2,8] Marie Perrot-Dockès,[3,8] Coline Trichot,[1,2,8] Léa Karpf,[1,2] Omar Abouzid,[1,2] Camille Chauvin,[1,2] Philémon Sirven,[1,2] Wassim Abou-Jaoudé,[4] Frédérique Berger,[1,5,6] Philippe Hupé,[1,6,7] Denis Thieffry,[4] Laure Sansonnet,[3] Julien Chiquet,[3] Céline Lévy-Leduc,[3] and Vassili Soumelis[1,2,9,*]

[1]Institut Curie, Centre de Recherche, PSL Research University, 75005 Paris, France
[2]INSERM U932, Immunity and Cancer, 75005 Paris, France
[3]UMR MIA-Paris, AgroParisTech, INRA—Université Paris-Saclay, 75005 Paris, France
[4]Computational Systems Biology Team, Institut de Biologie de l'École Normale Supérieure, Centre National de la Recherche Scientifique UMR8197, INSERM U1024, École Normale Supérieure, PSL Université, 75005 Paris, France
[5]Institut Curie, PSL Research University, Unit of Biostatistics, 75005 Paris, France
[6]Institut Curie, PSL Research University, INSERM U900, 75005 Paris, France
[7]Mines Paris Tech, 77305 Cedex Fontainebleau, France
[8]These authors contributed equally
[9]Lead Contact
*Correspondence: vassili.soumelis@curie.fr
https://doi.org/10.1016/j.cell.2019.09.012

SUMMARY

Cell-cell communication involves a large number of molecular signals that function as words of a complex language whose grammar remains mostly unknown. Here, we describe an integrative approach involving (1) protein-level measurement of multiple communication signals coupled to output responses in receiving cells and (2) mathematical modeling to uncover input-output relationships and interactions between signals. Using human dendritic cell (DC)-T helper (Th) cell communication as a model, we measured 36 DC-derived signals and 17 Th cytokines broadly covering Th diversity in 428 observations. We developed a data-driven, computationally validated model capturing 56 already described and 290 potentially novel mechanisms of Th cell specification. By predicting context-dependent behaviors, we demonstrate a new function for IL-12p70 as an inducer of Th17 in an IL-1 signaling context. This work provides a unique resource to decipher the complex combinatorial rules governing DC-Th cell communication and guide their manipulation for vaccine design and immunotherapies.

INTRODUCTION

Cell-cell communication involves the exchange of molecular signals produced by a given cell and transmitting an effect through specific receptors expressed on target cells. This process requires integration of multiple communication signals of different nature during homeostatic or stress-related responses. For example, differentiation of pluripotent hematopoietic stem cells into mature myeloid or lymphoid blood cells requires the collective action of multiple cytokines, growth factors, and Notch ligands (Balan et al., 2018). In the context of stress, multiple signals need to be integrated by innate and adaptive immune cells, including cytokines, growth factors, inflammatory mediators, and immune checkpoints (Chen and Flies, 2013; Macagno et al., 2007). In most studies, these communication molecules have been studied as individual stimuli to a target cell by gain- and loss-of-function experiments. This provides important knowledge regarding the downstream effects of the signals but prevents us from widely addressing their function in various contexts of other co-expressed communication signals.

Context dependency is an important aspect of verbal language communication that can directly affect the meaning of individual words but also modify the logic of syntactic rules (Cariani and Rips, 2017; Kintsch and Mangalath, 2011). Similarly, context dependencies may dramatically affect the function of biologically active communication signals. For example, we have shown that 90% of the transcriptional response to type I interferon in human CD4 T cells depends on the cytokine context (T helper 1 [Th1], Th2, or Th17; Touzot et al., 2014). Other studies have identified major context-dependent functions of immune checkpoints, such as OX40-ligand (Ito et al., 2005), and regulatory cytokines, such as transforming growth factor β (TGF-β) (Ivanov et al., 2006; Manel et al., 2008; Volpe et al., 2008). These studies suggest that communication molecules function as words of a complex language with grammar defining combinatorial rules of co-expression and mutual influence of one signal over the function (meaning) of another signal.

Three levels of biological complexity need to be integrated to decipher those combinatorial rules: (1) the multiplicity of input communication signals to include as many possible contextual effects; (2) communication signals at their naturally occurring concentrations; and (3) a large number of output responses in target cells, reflecting the effect of cell-cell communication quantitatively and qualitatively. Those three levels create a bottleneck in deciphering cell-cell communication.

Here we developed an integrative approach combining (1) coupled protein-level measurement of multiple communication signals and output response molecules in target cells; (2) a multivariate mathematical modeling strategy enabling us to infer the input-output relationships for individual signals, taking into account the context and configuration of all other signals; and (3) experimental validation of model-derived hypotheses. We applied this framework to decipher human dendritic cell (DC)-Th cell communication, which potentially involves over 70 individual molecular stimuli (Chen and Flies, 2013), including cytokines, tumor necrosis factor (TNF) family members, integrins, nectins, Notch ligands, and galectins (Tindemans et al., 2017; Zhu et al., 2010; Zygmunt and Veldhoen, 2011). These molecules can all be expressed by DCs and function as communication signals to T cells (hereafter called Th stimuli). They can be measured at the protein level by highly specific assays to optimize biological relevance.

By using this unbiased data-driven approach, we could capture the simultaneous effects of large numbers of DC-T cell communication signals in naturally occurring patterns and expression levels. Our systems-level model revealed novel emergent and context-dependent mechanisms controlling Th cell differentiation. A similar framework can be applied to systematically decipher the communication of other cell types.

RESULTS

Generation of a Unique Multivariate Dataset of Human DC-Th Cell Communication

To induce a broad range of DC molecular states expressing various patterns of communication signals, human monocyte-derived DCs (MoDCs) and primary blood CD11c$^+$ DCs (bDCs), were activated for 24 h with a diversity of DC-modulating signals (hereafter called DC perturbators). These included 14 distinct stimuli that were grouped in three categories reflecting various physiopathological contexts: (1) the endogenous factors interferon β (IFN-β), GM-CSF, TSLP, and PGE2; (2) the Toll-like receptor ligands lipopolysaccharide (LPS) (a Toll-like receptor 4 [TLR4] agonist), PAM3CSK4 (a TLR1 and 2 agonist), Curdlan (a Dectin1 agonist), zymosan (a TLR2 and Dectin1 agonist), R848 (a TLR7 and 8 agonist), poly(I:C) (a TLR3 agonist), and aluminum potassium sulfate (Alum, an NLRP3 inflammasome inducer); and (3) the whole pathogens heat-killed *Candida albicans* (HKCA), heat-killed *Listeria monocytogenes* (HKLM), heat-killed *Staphylococcus aureus* (HKSA), heat-killed *Streptococcus pneumoniae* (HKSP), and influenza virus (flu). These 14 DC perturbators were used in distinct doses and combinations to further increase the diversity of DC communication molecules and downstream functional effects (Table S1). In each independent experiment, we included a medium condition as a negative control and LPS (100 ng/mL) and/or zymosan (10 μg/mL) as positive controls. A total of 66 perturbators were used on MoDCs and 16 on bDCs, totaling 82 distinct "DC conditions" (C1–C82; Table S1).

Under each DC condition, we measured 36 DC-expressed molecules that influence Th cell differentiation in at least one published study (STAR Methods) and can be measured with a highly specific antibody-based assay. Twenty-nine were measured by fluorescence-activated cell sorting (FACS) at the DC surface (Figure S1A), and 7 were measured in the 24-h DC culture supernatant (STAR Methods).

Following 24-h culture under each of the 82 DC perturbation conditions, the same DC batch was used to stimulate naive CD4 T cells in a heterologous co-culture system. On day 6 of co-culture, we measured Th cell expansion fold (Exp Fold) and a total of 17 distinct Th cytokines broadly representing the spectrum of Th cell output responses (STAR Methods). In total, we produced a unique dataset of coupled measurements of DC-derived Th stimuli and Th response cytokines from 428 independent observations from 44 independent donors (Figure 1A; Table S2).

Variability and Specificity of DC Communication Signals

We asked whether our systematic DC stimulation strategy could generate important variations in the expression of individual DC-derived Th stimuli. All Th stimuli were expressed over at least three logs (Figure 1B) with high coefficients of variation (>0.44; Figure 1C). Interleukins had higher variability (10^4–10^5) and high coefficients of variation from 2.72 for interleukin-12 (IL-12) p70 (IL-12) to 1.43 for IL-6. CD11a had a wide expression range (10^4) but the smallest coefficient of variation (0.44), with values distributed around the mean (Figure 1C). Hence, we were able to generate highly variable expression patterns for all Th stimuli.

We sought to identify conserved and specific patterns of Th stimuli in response to standard DC perturbators. We compared the expression levels of DC-derived Th stimuli under three conditions belonging to distinct classes of microbes—LPS (100 ng/mL, bacteria), zymosan (10 μg/mL, fungi), and flu (1×, Viruses)—that were used across at least 17 MoDC biological replicates (Figure 1D). Medium MoDCs (negative control) expressed lower levels of activation-associated communication molecules (Figures 1D and S1B). We confirmed previous findings, validating our experimental system: (1) zymosan induced specifically IL-10 and IL-23, (2) flu induced a large amount of IL-28α, and (3) LPS and zymosan induced a large amount of IL-12 (Figures 1D and S1B). In addition, we identified novel specific inductions of DC-derived Th stimuli: zymosan-treated MoDCs expressed the highest levels of CD54 and PVR, flu-treated MoDCs specifically induced ICOSL, and LPS-treated MoDCs induced the highest levels of CD30L and CD83 (Figure 1D). Specificity of expression of a given signal for a given DC stimulation was determined using Wilcoxon statistical test (Figure S1B). Hence, standard DC perturbators induced specific patterns of Th stimuli.

Defining the Spectrum of DC Communication States

Next we aimed to assess the spectrum of DC communication states, as defined by their expression pattern of communication signals, across the 82 DC conditions. We computed the mean expression of biological replicates for each DC-derived Th stimulus and performed unsupervised hierarchical clustering to identify classes of the most similar conditions (C1–C82, y axis) and DC-derived Th stimuli (x axis) (Figure 2A). This revealed five groups of DC conditions (Figure 2B). Each of the four standard DC conditions (Figure 1D) belonged to a different group (Figure 2A).

Group 1 was defined by high expression of adhesion molecules such as CD18, ICAM-2, ICAM-3, and CD29 and low levels

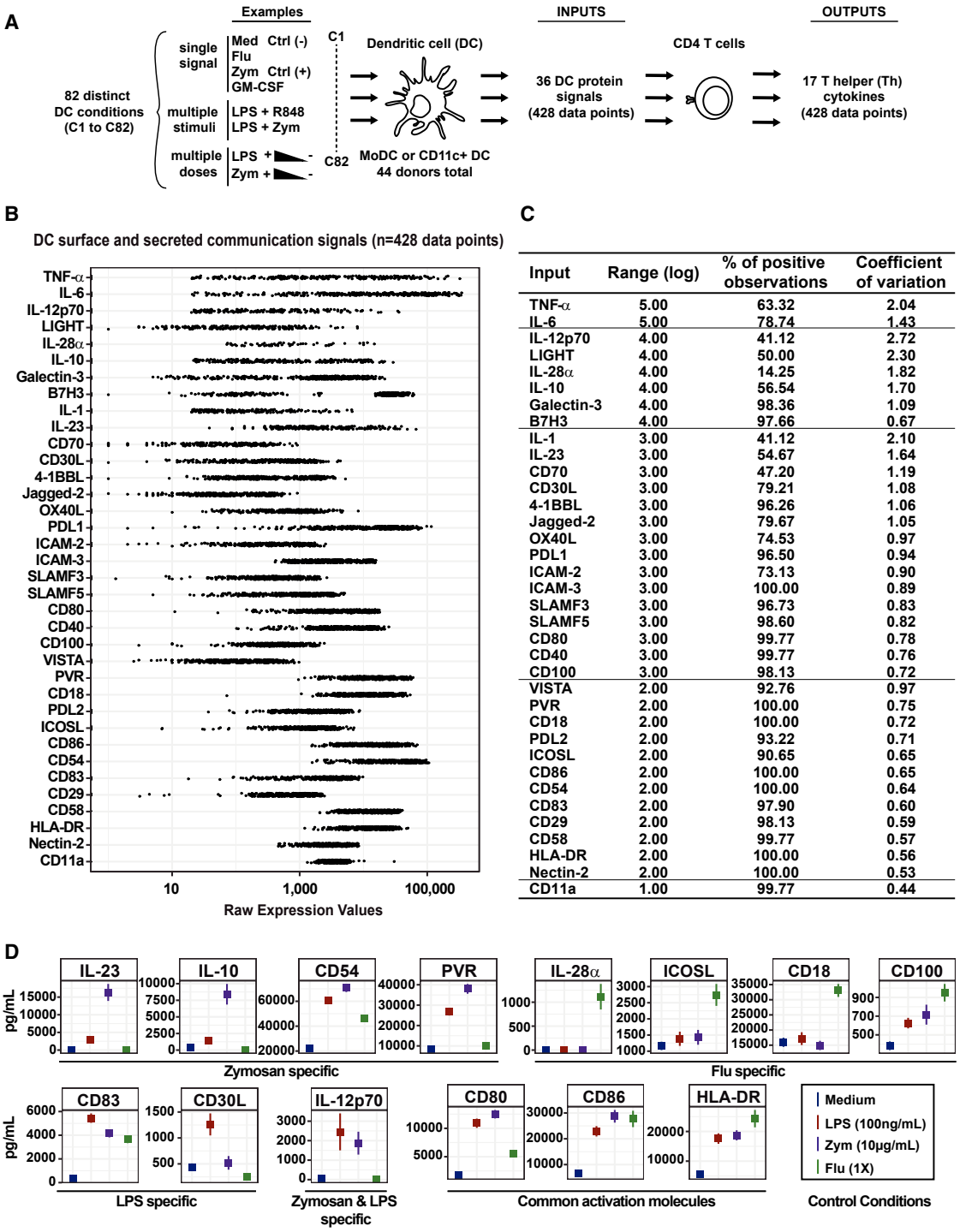

Input	Range (log)	% of positive observations	Coefficient of variation
TNF-α	5.00	63.32	2.04
IL-6	5.00	78.74	1.43
IL-12p70	4.00	41.12	2.72
LIGHT	4.00	50.00	2.30
IL-28α	4.00	14.25	1.82
IL-10	4.00	56.54	1.70
Galectin-3	4.00	98.36	1.09
B7H3	4.00	97.66	0.67
IL-1	3.00	41.12	2.10
IL-23	3.00	54.67	1.64
CD70	3.00	47.20	1.19
CD30L	3.00	79.21	1.08
4-1BBL	3.00	96.26	1.06
Jagged-2	3.00	79.67	1.05
OX40L	3.00	74.53	0.97
PDL1	3.00	96.50	0.94
ICAM-2	3.00	73.13	0.90
ICAM-3	3.00	100.00	0.89
SLAMF3	3.00	96.73	0.83
SLAMF5	3.00	98.60	0.82
CD80	3.00	99.77	0.78
CD40	3.00	99.77	0.76
CD100	3.00	98.13	0.72
VISTA	2.00	92.76	0.97
PVR	2.00	100.00	0.75
CD18	2.00	100.00	0.72
PDL2	2.00	93.22	0.71
ICOSL	2.00	90.65	0.65
CD86	2.00	100.00	0.65
CD54	2.00	100.00	0.64
CD83	2.00	97.90	0.60
CD29	2.00	98.13	0.59
CD58	2.00	99.77	0.57
HLA-DR	2.00	100.00	0.56
Nectin-2	2.00	100.00	0.53
CD11a	1.00	99.77	0.44

Figure 1. Variability and Specificity of DC Communication Signals

(A) Experimental strategy.

(B) Raw expression values of the 36 DC communication signals (n = 428 data points).

(C) Statistical descriptors of the 36 DC communication signals: expression range (log magnitude), percentage of positive observations among the 428 datapoints, and coefficient of variation.

(D) Average expression values and SD for the four indicated DC signals for MoDCs.

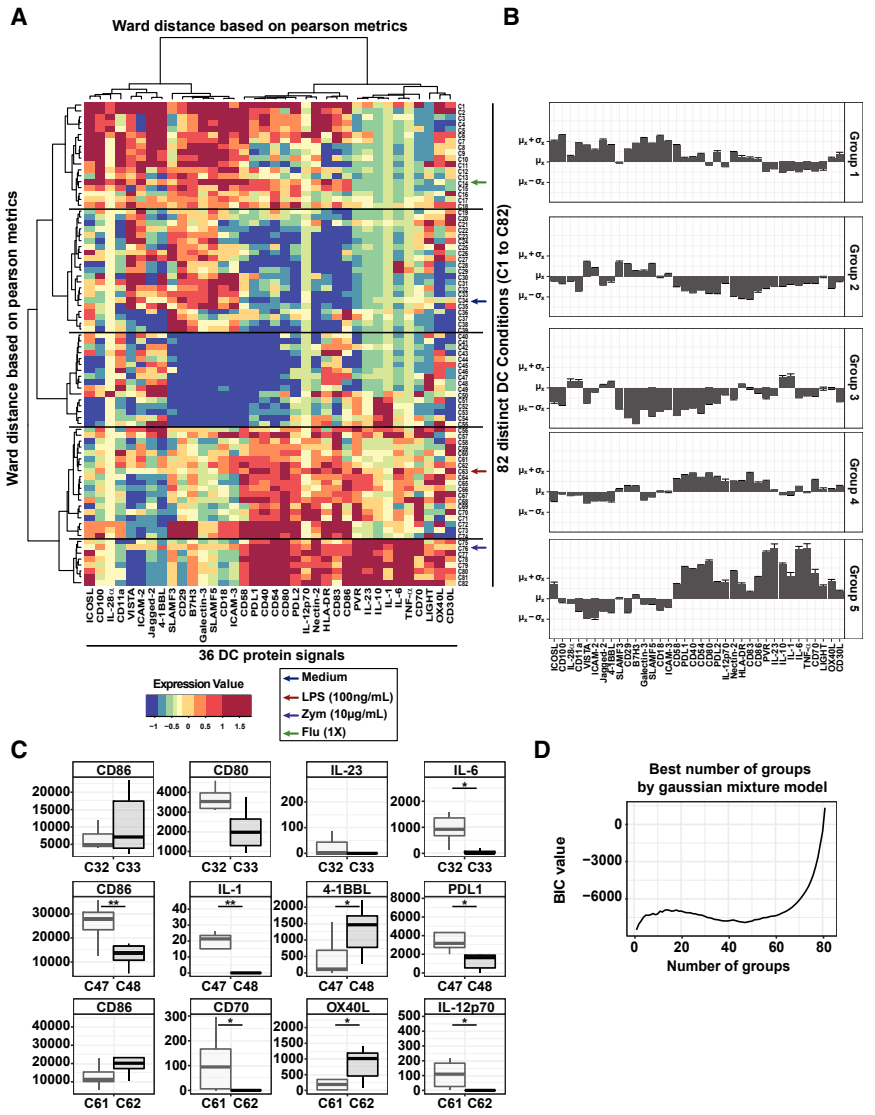

Figure 2. The Diversity of DC States Is Defined by Unique Combinations of Communication Molecules

(A) Heatmap showing expression values of each 36 DC-derived signal, performed with hierarchical clustering on Pearson metrics for the DC signals and Euclidian distances for the 82 DC conditions.

(B) Expression profiles (mean and SD) of the 36 communication molecules within the five groups of DC conditions, defined by hierarchical clustering. Expression data were logged and scaled so μ represents the mean and σ the SD of the expression of a given DC signal across the whole dataset.

(C) Boxplot of selected DC signals for pairs of stimulatory conditions defined as being the most correlated within our dataset by Pearson correlation (t test).

(D) Best number of groups by Gaussian mixture model, determined using the 428 points of the 36 DC parameters.

of co-stimulatory molecules and cytokines with the exception of high IL-28a. Group 2 showed low expression for most DC-derived Th stimuli but high levels of integrins, VISTA and B7H3, suggesting a capacity to interact with T cells and transmit co-inhibitory signals. Group 3 showed a complementary pattern, lack of group 1- and group 2-specific molecules, and intermediate or high levels of co-stimulatory molecules such as CD83, CD86, HLA-DR, 4-1BBL, and OX40L. This suggested potent T cell stimulating functions. Group 4 exhibited high levels of molecules from the B7 and TNF superfamilies, such as CD80, CD86, PDL1, PDL2, and CD40, but intermediate or low cytokine levels. In contrast, group 5 showed the highest level of cytokines and molecules of the B7 and TNF superfamilies (Figure 2B).

Next we sought to analyze intra-cluster heterogeneity. We selected three pairs of perturbators most closely related as defined by Euclidian distance (C32 [MoDC HKLM, MOI 1] and C33 [MoDC HKCA, MOI 1], C47 [bDC LPS, 100 ng/mL] and C48 [bDC HLKM, MOI 1], and C61 [MoDC R848, 1 µg/mL] and C62 [MoDC PAM3, 10 µg/mL]) and compared them regarding expression of the 36 DC-derived Th stimuli (Figure 2C). C32 and C33 did not exhibit significant differences in CD80 and CD86 expression, reflecting equal levels of DC activation. They were statistically different only for IL-6, with levels ranging from complete absence in C33 to over 1 ng/mL in C32 (Figure 2C). In contrast, the pairs C47/C48 and C61/C62 showed significant differences for multiple Th stimuli. C47 expressed significantly more CD86, PDL1, and IL-1 than C48. On the contrary, C48 expressed higher levels of 4-1BBL. C61 and C62 showed marked differences in CD70 and IL-12 (higher in C61) and OX40L (higher in C62) levels. Hence, each DC condition expressed unique combinations of DC-derived Th stimuli, suggesting different communication potential with CD4 T cells.

An unsupervised Gaussian mixture model showed that the highest Bayesian information criterion (BIC) value corresponded to 82 groups, confirming that each DC condition induced a unique profile of the 36 communication molecules (Figure 2D).

Using principal-component analysis (PCA), we showed that neither the date of the experiment nor the donor batch had a major effect on clustering (Figure S1C; STAR Methods).

The Heterogeneity of DC-Induced Th Cytokine Responses

We characterized the diversity of CD4 T cell output responses, as assessed by Th cytokine profiles, following co-culture of naive CD4 T cells with activated DCs across the 82 conditions described previously. Th cytokines exhibited important variations across the 428 observations (Figure 3A). Some cytokines, such as IL-2, TNF-α, GM-CSF, TNF-β, and IL-3, were always detected (Figure S2A).

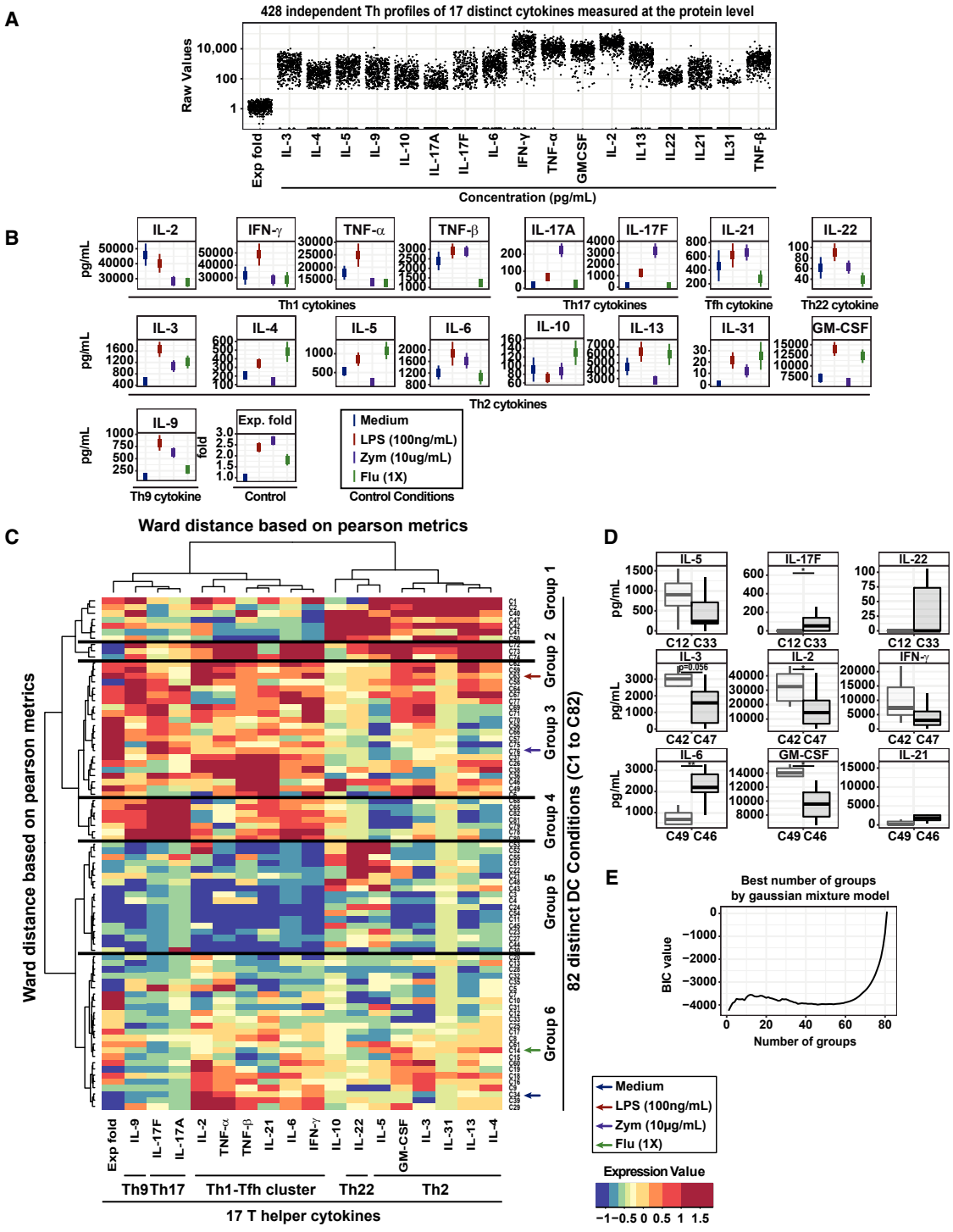

Figure 3. Th Cytokine Responses Mirror the Variability in DC Communication States

(A) Raw expression values of each of the 18 Th-derived parameters (n = 418 data points).

(B) Average expression values and SD for all Th-derived signals under the MoDC conditions medium, LPS, zymosan, and flu.

(C) Heatmap of expression values of each 18 Th parameters, performed with hierarchical clustering on Pearson metrics for the DC signals and Euclidian distances for the T cell conditions.

(D) Boxplot of Th signals for pairs of conditions selected as being the most correlated within our dataset by Pearson correlation (t test).

(E) Best number of groups by Gaussian mixture model, determined only using the 428 points of the 18 Th parameters.

To identify Th subset signatures, we compared cytokine expression under our four standard conditions: medium (negative control), LPS, zymosan, and flu. The Th17 cytokines IL-17A and IL-17F were induced predominantly in zymosan MoDCs. LPS MoDCs induced mixed Th1, Th2, and Th9 responses characterized by high IFN-γ, IL-13, IL-3, and IL-9 compared with medium. Flu MoDCs induced the Th2 cytokines IL-4, IL-5, and IL-31 (Figures 3B and S2B). These results indicate that, under the LPS, zymosan, and flu conditions, each DC state induced a distinct set of Th cytokine responses corresponding to prototypical Th signatures or mixed Th profiles.

Th Cytokine Responses Mirror the Variability in DC Communication States

We asked whether Th cytokine responses would reveal distinct patterns or a continuum of responses mirroring each of the DC communication states (Figure 2A). We performed hierarchical Pearson clustering on our 18 distinct Th-derived variables across the entire 82 DC-activating conditions (Figure 3C). This revealed 6 distinct groups, although intra-group heterogeneity was evident in almost all groups. Interestingly, DC perturbation conditions (C1–C82) did not appear in the same order compared with DC communication signal clustering (Figure 2A), indicating that closely related patterns of DC-derived Th stimuli did not necessarily induce the closest patterns in Th cytokine responses.

Group 1 was dominated by production of IL-10, IL-22, IL-5, GM-CSF, IL-3, IL-31, IL-13, and IL-4 (Figure S2C). Group 2 was the most heterogeneous and included the inflammatory cytokines TNF-α and IL-6 co-expressed with variable levels of the Th1 (IFN-γ) and Th2 (IL-4 and IL-13) cytokines (Figure S2C). Group 3 expressed IL-21, IFN-γ, and IL-17F but no or low IL-17A, suggesting the possibility of differential regulatory mechanisms (Figure S2C). Group 4 was dominated by the Th17 cytokines IL-17A and IL-17F, group 5 by IL-22, and group 6 by IL-2. Distinct sets of DC perturbation conditions and, hence, patterns of DC-derived communication molecules were associated with each of these groups (Figure 3C). This was the first suggestion of specific rules underlying input-output relationships in DC-Th communication.

Because of intra-group heterogeneity, we asked whether most correlated conditions within the same cluster would differ from each other (Figure 3D). C12 and C33 were associated to different levels in IL-17F, whereas C42 and C47 were different in IL-2 and C46 and C49 were different in IL-6 and GM-CSF levels (Figure 3D). As for the DC dataset, we found that 82 was the best number of groups in our Th-derived dataset, based on a Gaussian mixture model (Figure 3E). This suggested that a single DC profile of communication molecules would induce a unique set of Th cytokines.

A Data-Driven Lasso Penalized Regression Model Predicts Th Cytokine Responses from Combinations of DC-Derived Th Stimuli

Having generated distinct patterns of DC-derived communication signals associated with a diversity of induced CD4 T cell cytokine responses, the question of their relationship appeared to be critical to decipher DC-Th communication. Given the complexity of the dataset and the lack of clear hypotheses concerning the majority of DC-derived Th stimuli, we applied an unsupervised mathematical modeling strategy (Figure 4A).

The MultiVarSel strategy with stability selection performed similarly as the internal positive control and better than other methodologies tested (Figure S3A; STAR Methods). Therefore, we applied MultiVarSel to the modeling of our experimental data (Figure 4A). This methodology takes into account the dependencies that may exist among Th cell cytokines and combines Lasso criterion and stability selection to select associations between DC-derived signals (inputs) and Th cytokines (outputs) (STAR Methods).

Our multivariate model identified a large number of significant positive (red) and negative (blue) associations of the 36 DC-derived Th stimuli with the 17 Th-derived cytokines (Figure 4B). White squares represent the absence of significant association (Figure 4B). The frequency of selection obtained for each input-output association is provided in Figure S3B.

Our mathematical model revealed (1) the effect of each DC communication signal on Th output responses and (2) the critical regulators for each Th cytokine. For example, negative regulators of IL-10 were OX40L, 4-1BBL, IL-12, TNF-α, CD58, VISTA, Galectin-3, CD80, CD29, IL-1, ICAM-3, SLAMF3, IL-28α, and CD83, and positive regulators were Jagged-2, PDL1, IL-10, CD11a, HLA-DR, ICOSL, CD100, CD30L, CD18, ICAM-2, and CD86 (Figure 4B). Hence, the model can predict IL-10 production by responding Th cells for any DC, given the expression level of these molecules. It allows simulating loss or gain of function of an input. Similar insight can be obtained for each of the 17 Th cytokine responses, which may be explained by a combination of DC-derived communication signals.

We used computational cross-validation to evaluate the error of prediction of our model (Figure 4C). For all Th cytokines, the multivariate outperformed the best univariate model (Figure S3C). We ranked Th cytokines based on their prediction errors; the Th variables best explained by our model were IL-6, IL-17F, Exp Fold, and IL-3 (Figure 4C).

To address DC type specificity in model performance, we calculated the cross-validation error for each Th output of the MoDC and bDC dataset, respectively. Our model predicted equally well the majority of the outputs for the two DC types (Figure S3D). For a few outputs, mostly IL-22 and TNF-β, the model was more error prone in bDCs than MoDCs (Figure S3D). Interestingly, a higher prediction error was found for TNF-β in 5 of 118 observations (Figure S3E), where TNF-β levels were very high (range, 6.7–22.2). This suggested that a TNF-β-promoting input signal might be involved in those 5 cases but not included in our model. For IL-22, more observations had a higher prediction error in bDCs compared with MoDCs, but the prediction error range and distributions were similar, suggesting that the input-output relationship was conserved (Figure S3E).

We performed hierarchical clustering for both DC and T cell-derived variables to identify co-regulations between Th outputs. We retrieved relevant clusters of Th cytokines belonging classically to the same Th subset (Figure 4B). The Th2-related cytokines IL-13, IL-31, IL-5, IL-4, IL-10, and GM-CSF were found in the same cluster, suggesting that their induction would be controlled by similar mechanisms. IL-17A and IL-17F were also

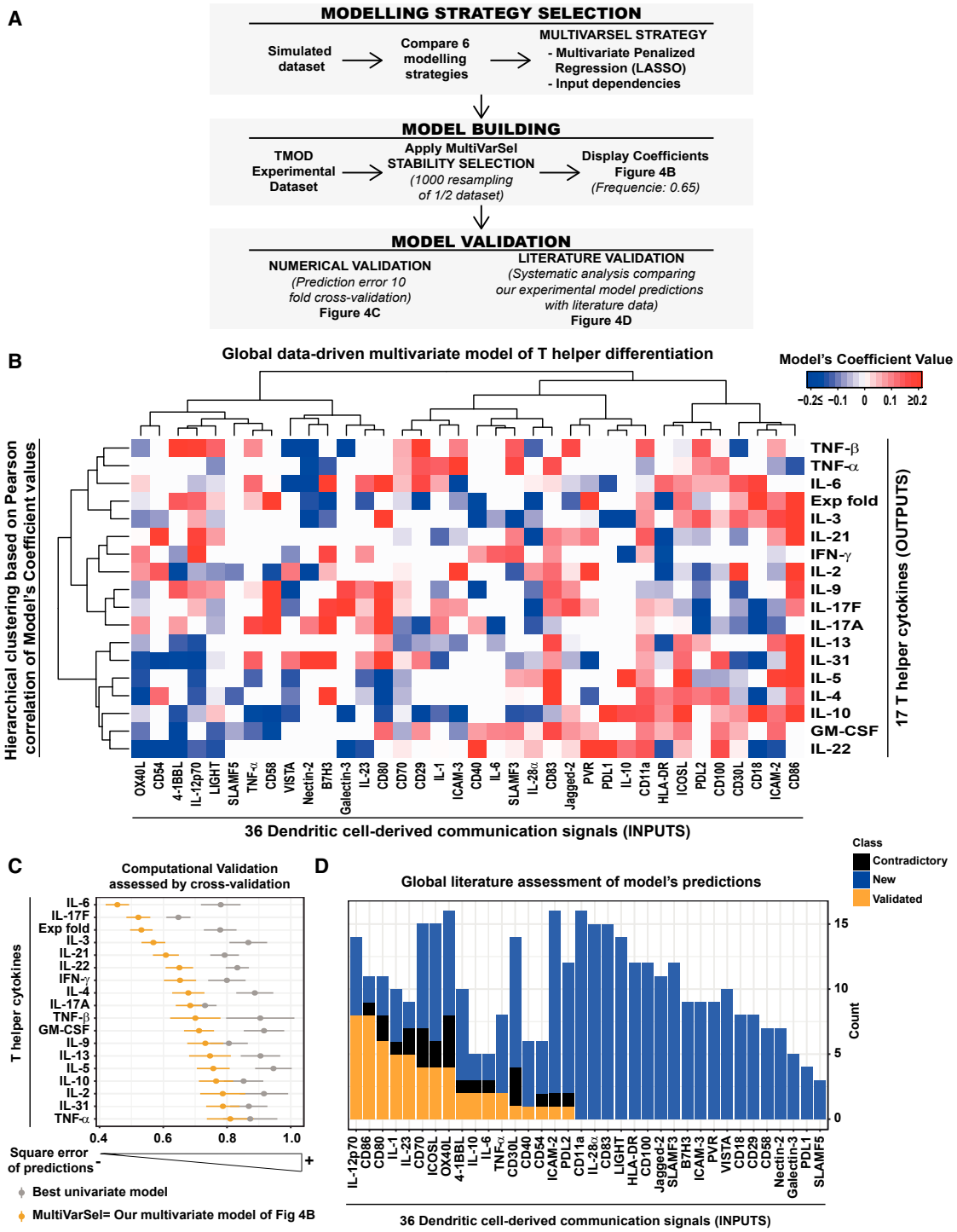

Figure 4. A Data-Driven Lasso Penalized Regression Model Predicts Th Differentiation Outcomes from DC-Derived Communication Signals

(A) Mathematical modeling strategy.

(B) Heatmap of the model's coefficient values of the MultiVarSel-derived model, explaining the 18 Th parameters based on the 36 DC-derived signals (Pearson correlation-based hierarchical clustering).

(C) Mean and SE of prediction error values obtained by 10-fold cross-validation for Th parameters using the multivariate model (yellow) and the best univariate model (gray) within the 36 DC signals.

(D) Literature-based validation score. For each DC signal, all predicted associations with Th cytokines were categorized as "new," "validated," or "contradictory."

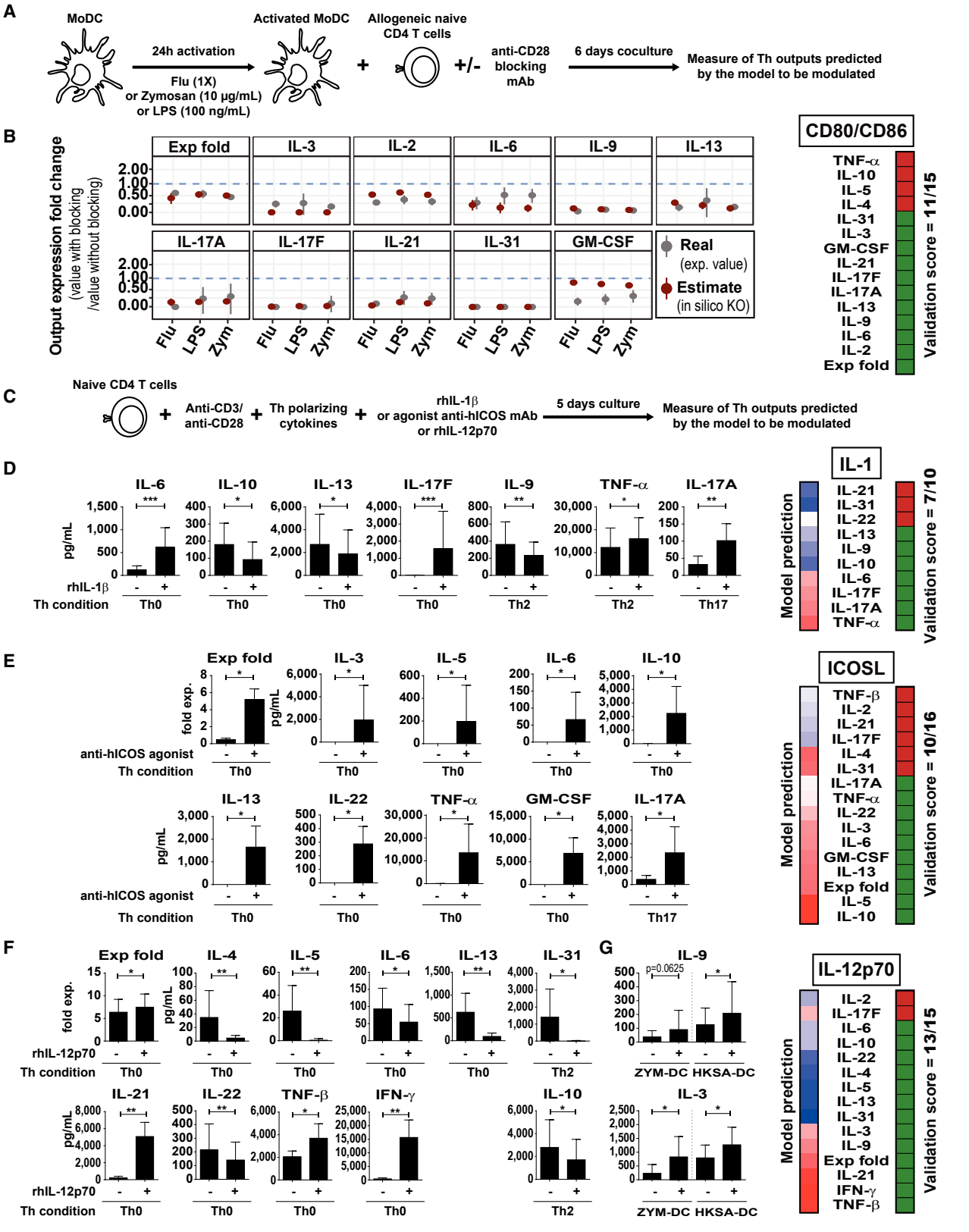

(legend on next page)

in the same cluster, implying that the model associated them with closely related DC communication signals (Figure 4B). Surprisingly, our model closely related IL-9 expression to IL-17A and IL-17F, suggesting common regulators. It also clustered IL-22 closer to the Th2 than to the Th17 cytokines. IL-21 was associated with the Th1 cytokines IL-2 and IFN-γ (Figure 4B).

The Multivariate DC-Th Model Reveals Novel Regulators of Th Cytokine Responses

We systematically compared our model results with the literature as a knowledge-based validation but also novelty assessment. We screened 178 relevant articles (STAR Methods) and extracted information regarding specific molecular control of a given Th cytokine by DC-derived signals measured in our model (Table S3). We computed a validation score based on the number of articles identifying the same associations than our model (STAR Methods). IL-12 ranked as the top DC communication signal for which our model predictions globally recapitulated existing knowledge (8 of 13 predicted associations). Among other known associations, IL-23 was positively associated with IL-17A and IL-17F, IL-10 was positively associated with IL-10 and negatively with IFN-γ, and CD40 was positively associated with IFN-γ.

However, the model also predicted 290 associations that were not described previously. Putative novel regulators were identified for all Th outputs (Table S4). The robustness of each prediction could be estimated by the value of the coefficient and by the frequency of detection of the association (Table S4). Examples of high scores were B7H3 and CD83 association with IL-4, 4-1BBL association with IL-9, ICOSL association with IL-13, and OX40L negative association with IL-22 (Table S4). Overall, literature knowledge was retrieved for 80 distinct input-output relationships presented in our model (Figure 4B); 56 were in agreement with our model, representing a global literature validation score of 70%.

Systematic and Independent Experimental Validation of Model's Predictions

We performed systematic experimental validation by selecting a subset of target inputs and systematically measuring the Th outputs selected by our model. We assessed the novelty of each validated prediction (Table S3).

First we addressed systematic validations of model predictions by blocking experiments (Figure 5A). We performed double *in silico* knockout for CD80 and CD86 under the three conditions—LPS (100 ng/mL), flu (1×), and zymosan (10 μg/mL) MoDCs—in which CD80 and CD86 were highly expressed and predicted an effect on 15 distinct Th outputs (Figure 5B), 11 of which were successfully experimentally validated (STAR Methods). The positive role of CD80 and CD86 on IL-3 and IL-31, to our knowledge, have not been described elsewhere. The predictions we failed to validate were for IL-4, IL-5, IL-10, and TNF-α (Figure S4A), all predicted to be decreased by CD80/CD86.

Then we validated the effects of three additional inputs: IL-1, ICOSL, and IL-12 used as exogenous factors (Figure 5C). First we gave the selected input together with anti CD3/CD28 signals (Th0) and systematically measured all Th outputs predicted by the model to be influenced by that input. In the absence of any effect, we gave the selected input under a Th2 (IL-4) or Th17 (IL-6, IL-1β, IL-23, and TGF-β) condition to detect additional synergistic or inhibitory effects required to validate the predicted effect. For example, it is not possible to validate the inhibition of a Th2 cytokine without significant production of this cytokine at baseline.

We focused on the ten predictions made by our model for IL-1 (Figure 5D). By adding IL-1β to the Th0 condition, we were able to detect significant upregulation of IL-6 and IL-17F and significant downregulation of IL-10 and IL-13. IL-10 downregulation and IL-6 upregulation were also significant in the Th2 context (Figure S4B). Under a Th2 condition, we validated significant upregulation of TNF-α and downregulation of IL-9 by IL-1β (Figure S4B), not seen in Th0 (Figure S4B). Under a Th17 condition, we observed a positive effect of IL-1β on IL-17A. We could not validate the predictions regarding IL-21, IL-31, and IL-22 (Figure S4B). In total, 7 of 10 predicted effects of IL-1 were validated. Interestingly, the positive role of IL-1β on induction of IL-6 by Th cells was not known (Table S3) and may suggest new biology and amplification loops in an inflammatory context.

We used a similar strategy to validate predictions regarding ICOSL using an anti-ICOS agonistic antibody. Overall, we validated 10 of 16 predictions (Figure 5E and S4C; STAR Methods). Interestingly, five of the 10 validated predictions were novel (Table S3; IL-5, IL-13, IL-3, GM-CSF, and IL-22), suggesting common pathways to induce IL-22 and Th2 responses.

Finally, we experimentally tested the predictions regarding IL-12 (Figure 5F). Adding IL-12 to the Th0 condition validated an induction of IFN-γ, IL-21, Exp Fold, and TFN-β. We also validated the inhibitory role of IL-12 on Th2 cytokine (IL-4, IL-5, and IL-13), IL-6, and IL-22 production. Using the Th2 condition, we further validated the inhibitory role of IL-12 on IL-10 and IL-31. The effects of IL-12 on TNF-β, IL-31, and IL-6 have not been described previously (Table S3).

Because our anti-CD3/CD28 system did not allow validating IL-12 effects on IL-2, IL-17F, IL-3, and IL-9 (Figure S4D), we wondered whether DC-dependent factors could affect the role

Figure 5. Independent and Systematic Experimental Validation of the Model's Prediction

(A) CD28 blocking experimental design in DC-T co-culture.

(B) Comparison of the predicted versus observed fold change following CD28 blocking; n = 6 donors.

(C) Experimental scheme of the "adding" validation procedure used in (D)–(F).

(D) DC-free validation experiment studying the effect of adding IL-1β in Th0, Th2, and Th17. Naive T cells were stimulated by anti-CD3/CD28 beads; n = 6 donors.

(E) DC-free validation experiment studying the effect of adding ICOS in Th0 and Th17. Naive T cells were stimulated by coated anti-CD3 and ICOS antibodies and soluble anti-CD28; n = 6 donors.

(F) IL-12 validation experiments in the DC-free system. Naive T cells were stimulated by anti-CD3/CD28 beads under Th0 and Th2 conditions; n = 8 donors.

(G) Validation of IL-12 predictions regarding IL-3 and IL-9. bDCs were cultured with naive CD4 T cells. IL-12 at 10 ng/mL was added for 6 days; n = 6 donors.

For (B) and (D)–(G), each panel shows the mean and SD of cytokine concentration, measured on restimulated Th supernatants (Wilcoxon test).

of IL-12 on these cytokines. We selected DC conditions with very low production of IL-12 (C51 and C55; Figure 2A) and performed a co-culture with naive T cells, adding or not adding IL-12. As a positive control, IL-12 was able to induce IFN-γ in both zymosan and HKSA conditions (Figure S4E). We did not validate the role of IL-12 on IL-2 or IL-17F regulation (data not shown). However, we validated that IL-3 was induced by IL-12 in both zymosan DCs (C51) and HKSA DCs (C54) (Figure 5G), whereas IL-9 was significantly upregulated only in HKSA DCs. Overall, we were able to experimentally validate 13 of 15 predictions regarding IL-12.

Our systematic strategy established a validated prediction of the input-output relationship in 41 of 56 cases (73.2%), 13 representing new mechanisms identified by the model. This number is similar to or higher than the computational cross-validation (Figure 4C). Predictions with higher stability selection frequencies were more validated than those with low stability selection (Figure S4F). However, the value of the model's coefficients was not statistically different between the two groups (Figure S4F), indicating that the model efficiently captured associations with low coefficient values.

Although IL-12 was the input best explained by our model, we could not validate the predicted association between IL-12 and IL-17F (Figure S4D), neither in the literature nor in our systematic experimental validation. Previous studies have shown either no effect (Volpe et al., 2008) or a negative effect (Acosta-Rodriguez et al., 2007) of IL-12 on Th17 differentiation. We hypothesized that context-dependent effects may lead to new functions of IL-12, not accomplished by IL-12 as a single agent.

A Context-Dependent Model Reveals a Role of IL-12 in Th17 Differentiation

We designed a strategy to capture context-dependent effects of one input on any given output by integrating new composite variables into the model (Figure 6A). These new input variables were based on the co-occurrence of a given input with other DC-derived communication signals (i.e., contexts). They adopted the value of the given input (for instance, IL-12) in each observation where the co-expressed DC signal was present, and they took a zero value when the co-signal was absent. We could derive 455 context-dependent variables.

The model including all context-dependent variables performed less well (higher error of prediction) than our classical MultiVarSel strategy (Figure S5A), most likely because of overfitting issues dependent on the dataset size, with a number of input variables exceeding the number of data points used to fit the model. Therefore, we derived 36 models, each one integrating the context dependencies of one input (Table S5). For each of these models, we reported the coefficient and the stability selection frequencies of each input (Table S5). To globally estimate the influence of context dependencies within our data, we quantified the number of times an input variable was selected, either "alone" or "with" another one. We derived percentages of context dependencies and represented the results either per input (Figure S5B) or per output (Figure S5C). The inputs most likely to present "context-dependent" functions were PDL1 and SLAMF3, whereas CD11a and CD70 were mostly context-independent (Figure S5B). When analyzing the outputs, the models revealed that all cytokines could be regulated by context-dependent mechanisms with relatively similar percentages (range, 0.13–0.22) (Figure S5C).

We used this strategy to explain the role of IL-12 in the control of Th17 differentiation through identification of context-dependent effects. We found that adding context-dependent variables for IL-12 improved the model predictions for IL-17F and performed equally well for IL-17A (Figure 6B). We then focused on DC-derived signals that were kept significant by the model and observed distinct associations of the new IL-12 context-dependent variables with IL-17A and IL-17F (Figure 6C), including some differentially associated with IL-17A and IL-17F, respectively. Among various contexts, we found that IL-12 in the context of IL-1, ICAM-2, or Jagged-2 was associated with IL-17F, whereas IL-12 in the context of CD70, IL-23, or LIGHT was associated with IL-17A.

As a first level of *in silico* validation, we selected a DC condition under which IL-12 was co-expressed with many of these contexts, and DC-derived signals induced IL-17A and IL-17F by responder Th cells. Zymosan (10 μg/mL) on MoDCs fulfilled these criteria (Figures 1D and 3C). To study the specific effects of IL-12 in the context of all other DC communication signals induced by zymosan, we performed *in silico* IL-12 knockout in the IL-12 context-dependent model. We compared predicted values for IL-17A and IL-17F when IL-12 was kept or not kept in the model (Figure 6D). *In silico* knockout of IL-12 diminished the production of both IL-17A and IL-17F under the zymosan (10 μg/mL) condition. As experimental validation, we performed independent DC/T cell co-culture experiments using MoDCs treated with 10 μg/mL zymosan in the presence and absence of IL-12-neutralizing antibody (Figure 6E). Blocking IL-12 significantly decreased the production of IL-17A and IL-17F, as predicted (Figure 6E), and inhibited IFN-γ production (Figure S5D). The same model predicted no effect of blocking IL-12 in Curdlan MoDCs (Figure S5E), which we validated experimentally (Figure S5F).

Synergistic Interaction between IL-12 and IL-1 Explains Induction of IL-17F without IL-17A

Our model predicted distinct roles of IL-12 on IL-17A and IL-17F production depending on the context in which IL-12 is expressed. Interestingly, IL-12, IL-1, and CD80 were the top variables almost systematically selected by the model to explain the differences between IL-17A and IL-17F (Figure 7A). This corroborated the results in Figure 6C, where we found that IL-12 in the context of IL-1 was associated with IL-17F but not IL-17A. The model estimate for a stability selection of less than 0.8 indicated that IL-12, IL-1, and CD80 were positive contributors to the differences between IL-17A and IL-17F (Figure S6A). Consequently, we hypothesized that the combination of IL-12 with IL-1 would induce IL-17F independent of IL-17A.

To experimentally validate our hypothesis, we used a DC-free Th polarization assay, allowing us to specifically study the interaction between IL-12 and IL-1 regardless of any other molecular context. Naive CD4 T cells were polyclonally activated with anti-CD3/CD28 beads and put in distinct cytokine treatments: Th0 (no cytokine) and Th2 (IL-4) as negative controls; Th17 (IL-1β+IL-23+IL-6+TGF-β) as a positive control, IL-12, IL-1β, and IL-12+IL-1β. IL-12 alone induced IFN-γ and IL-21 and inhibited Th2-related cytokines, as expected (Figure S6B). IL-12 alone induced neither IL-17F nor IL-17A, but combining IL-12

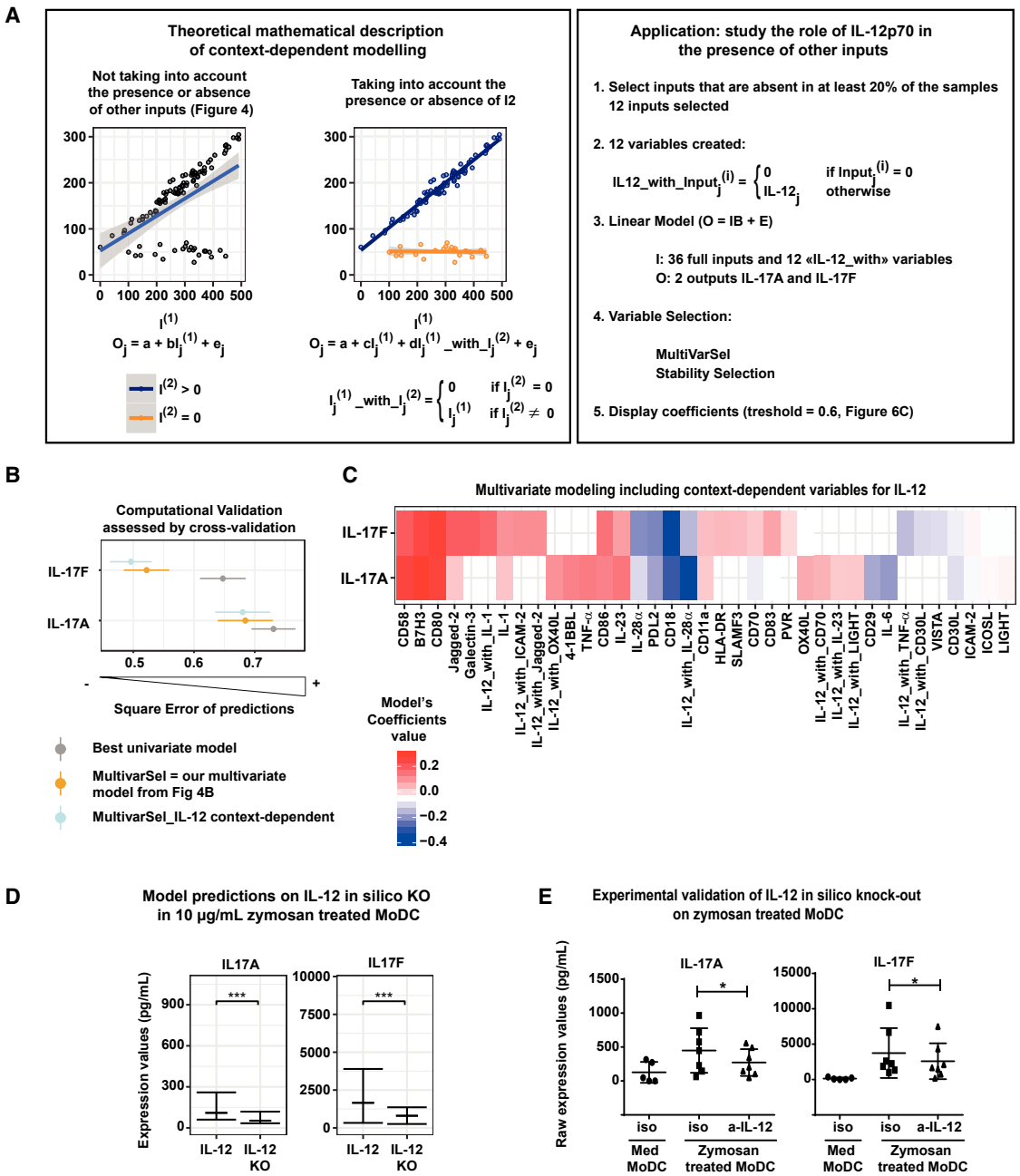

Figure 6. A Context-Dependent Model Reveals a Role of IL-12 in Th17 Differentiation

(A) Context-dependent modeling and application to IL-12. I, input; O, output.

(B) Error of prediction values obtained by 10-fold cross-validation for IL-17A and IL-17F, comparing the best univariate model (gray), MultiVarSel (yellow), and MultiVarSel with context dependencies (blue).

(C) Heatmap of the model's coefficient value of the context-dependent multivariate model explaining IL-17A and IL-17F.

(D) Model predictions regarding IL-12 *in silico* knockout (KO) under the zymosan MoDC condition for IL-17A and IL-17F values (blue) compared with experimental values in the presence of IL-12 (yellow); paired t test.

(E) Concentrations of IL-17A and IL-17F produced by Th cells after differentiation with zymosan MoDCs in the presence of anti-IL-12 neutralizing antibody or a matched isotype; n = 6 donors, paired t test.

with IL-1β dramatically induced IL-17F at levels comparable with the positive control, without a detectable amount of IL-17A, which fully validated the model predictions (Figure 7B).

This effect was specific to the IL-12+IL-1β combination IL-6, IL-23, or TGF-β alone or combined with IL-12 could not induce IL-17F expression (Figure S6C). The exact same pattern of Th

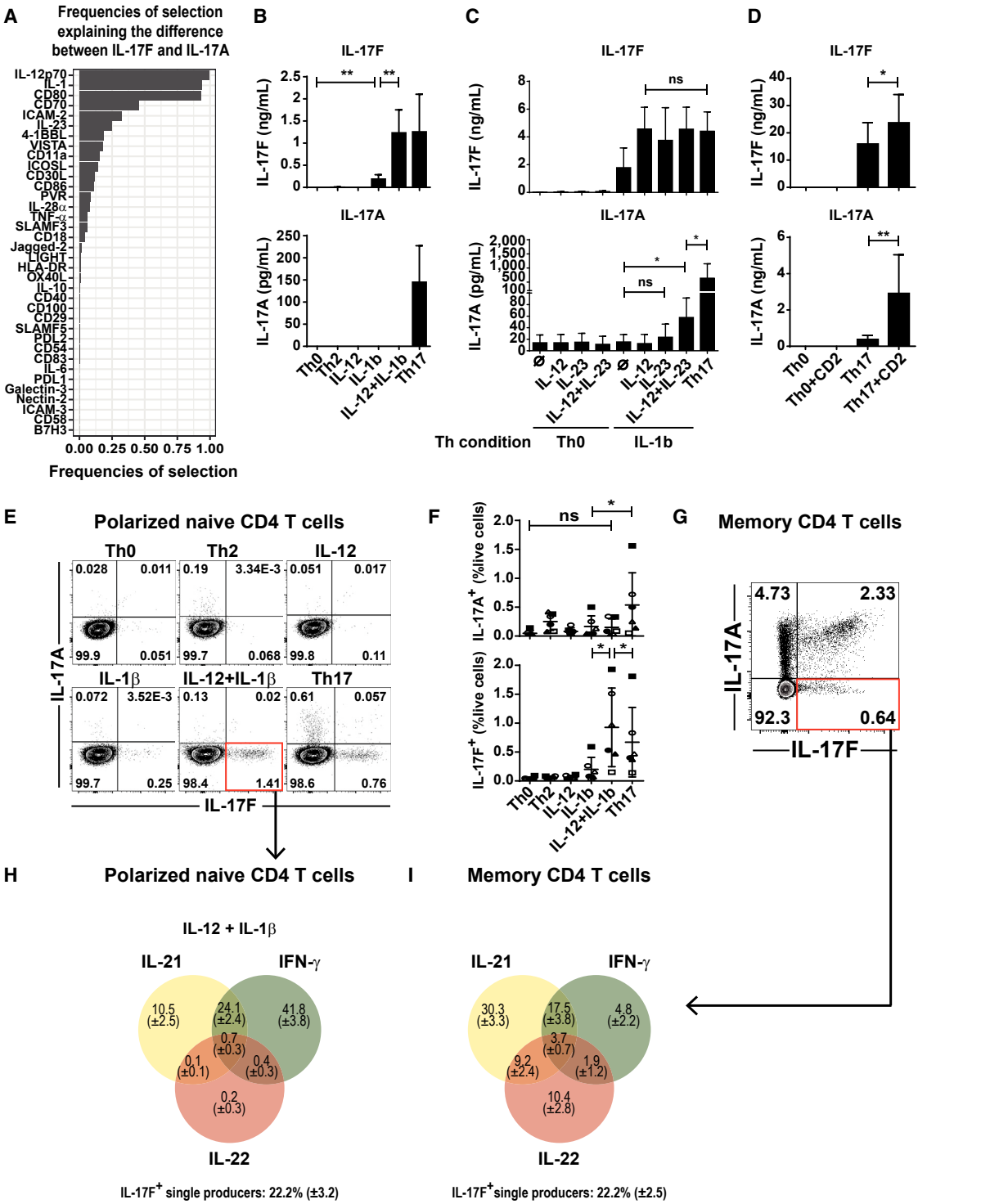

Figure 7. Synergistic Interaction of IL-12 and IL-1 Promotes IL-17F without IL-17A

(A) Stability selection frequencies of the different DC signals by a multivariate model, explaining the difference between IL-17F and IL-17A.

(B) Concentration of cytokines measured on restimulated Th supernatants. Naive CD4 T cells were differentiated for 5 days with anti-CD3/CD28 beads under the indicated conditions; n = 6 donors, paired t test.

(C) The same experimental design as in (B), with conditions as annotated; n = 6 donors, Wilcoxon test.

(D) Coated anti-CD2 and anti-CD3 together with soluble anti-CD28 were given for 5 days to naive CD4 T cells under Th0 or Th17 conditions. Cytokine concentrations were measured after 24-h restimulation on day 5. Mean and SD are shown; n = 8, Wilcoxon test.

(legend continued on next page)

cytokine expression was obtained by combining IL-1α or IL-1β with IL-12, which fit model predictions because those two variables were highly correlated (Figure S6D). The capacity of IL-12+IL-1β to induce IL-17F was resistant to the presence of other Th differentiation factors, such as IL-4 (Figure S6E). Using CellTrace Violet (CTV; Figure S6F), we could show that the production of IL-17F could not be attributed to the distinct proliferation capacity of Th cells under the IL-12+IL-1β condition.

Next we questioned whether Th cells generated under the IL-12+IL-1β condition would express transcription factors classically associated with Th17 differentiation. We measured 63 RNA transcripts by qPCR under Th0, Th2, IL-1β, IL-12, IL-12+IL-1β, and Th17 conditions (Table S6). The 63 genes included master regulators of the Th1 and Th2 subsets, such as T-bet and GATA3, respectively, and Th17 regulators, such as RORc, STAT3, BATF, and SATB1 (Ciofani et al., 2012). IL-17A and IL-17F regulation at the mRNA level mirrored the protein level (Figure S6H). IL-12+IL-1β induced significantly more RORc, BATF, and Bcl6 than IL-12 or IL-1β alone (Figure S6H), which could explain the induction of IL-17F and IL-21. Still, the levels of RORc and Bcl6 were lower in IL-12+IL-1β than under the Th17 condition (Figure S6H). T-bet was highly induced in IL-12+IL-1β in comparison with the IL-12 or Th17 conditions, indicating that Th1 differentiation was maintained and that T-bet did not inhibit IL-17F production. IL-12Rb2, a Th1 marker, was downregulated by IL-1β when added to IL-12, whereas IL-12, IL-12+IL-1β, and Th17 conditions all induced the IL-23 receptor (Figure S6H). SATB1 was specifically upregulated in IL-12+IL-1β in comparison with Th17 or IL-1β alone (Figure S6H), suggesting that it could play a role in the specific upregulation of IL-17F.

To globally assess the expression of the various Th lineage-specific factors, across IL-12- and IL-1-containing conditions, we performed a principal-component analysis (PCA) including all 63 mRNA variables (Figure S7A). Cells from the IL-12+IL-1β condition had an intermediate expression pattern between the IL-12 (Th1) and Th17 conditions. By decomposing the PCA space into vectors for each variable, we found that IL-17F, IL-23R, ICOS, and T-bet projected predominantly along the IL-12+IL-1β condition (Figure S7B), again pointing to mixed Th1/Th17 features.

We then addressed the link between IL-12 and IL-17A in various contexts. IL-12 with IL-23 was predicted to induce IL-17A but not IL-17F (Figure 6C). In a DC-free Th polarization assay, we used IL-12, IL-23, or IL-12+IL-23 and found that none of these conditions induced IL-17A (Figure 7C). We hypothesized that a third input could explain the positive link between "IL-12_with_IL-23" and IL-17A. Using an unsupervised analysis, we found IL-1 as a top variable with the highest correlation (Figure S7C). In addition, IL-12 and IL-17A positive correlation was significant specifically in the group of data points where IL-23 and IL-1 were expressed (Figures S7D and S7E) and was lost when only IL-1 or IL-23 was expressed with IL-12 (Figure S7D). Therefore, we tested whether IL-12+IL-23 would induce IL-17A in the presence of IL-1β. We validated a significant induction of IL-17A with no effect on IL-17F when IL-12 and IL-23 were given in the presence of IL-1β compared with IL-12 or IL-23 (Figure 7C). We measured IL-17A and IL-17F by qPCR and retrieved the same induction pattern (Figure S7F). Last, we could show that RORc was higher in IL-12+IL-23+IL-1β than in IL-12+IL-1β (Figure S7F).

Finally, we observed that our modeling strategy always identified CD58 as a main Th17 inducer because it positively affected both IL-17A and IL-17F (Figures 4B and 6C), an association that we had not seen during our systematic literature review (Figure 4D; Table S3). To test this hypothesis, we used an agonist anti-CD2 antibody that mimics the presence of CD58 (STAR Methods). As predicted, IL-17A and IL-17F were not induced by anti-CD2 alone under the Th0 condition. However, anti-CD2 significantly induced production of IL-17A and IL-17F under Th17 conditions (Figure 7D), which was confirmed by intracellular FACS staining (Figures S7H and S7I), with IL-17F upregulation restricted to IL-17A-positive cells (Figure S7I).

To establish the cytokine co-expression profiles of IL-12+IL-1β-treated Th cells at the single-cell level, we performed intracellular cytokine staining (Figure 7E). We confirmed that IL-12+IL-1β induced significantly more IL-17F-positive Th cells without co-production of IL-17A (Figure 7F). In naive CD4 T cells polarized with the Th17 cytokine cocktail (IL-1β, IL-6, TGF-β, and IL-23) we mainly found two subsets of Th17 cells producing either IL-17A or IL-17F, with very few cells co-producing both cytokines. To check for *in vivo* existence of those IL-17A and IL-17F single producers, we analyzed the human CD4 T cell memory compartment by intracellular FACS in healthy donor peripheral blood mononuclear cells (PBMCs). We could identify a small fraction of Th cells expressing only IL-17F in the absence of IL-17A, suggesting that this phenotype constitutes a differentiation endpoint (Figure 7G).

To gain more insight into the functional properties of these "Th17F" cells, we studied their co-production with IL-21, IFN-γ, and IL-22, all relevant to the Th17 and/or IL-12 pathways, *in vitro* (Figure S7J) and *ex vivo* (Figure S7K). Among IL-17F$^+$IL-17A$^-$ cells generated with IL-12 and IL-1β, the majority co-produced IFN-γ (41.8%), IL-21 (10.5%), or both (24.1%) (Figure 7H), reflecting a dominant role of IL-12. IL-17F$^+$/IL-17A$^-$ memory CD4 cells preferentially co-expressed IL-21 (30.3%) and IL-21 together with IFN-γ (17.5%) (Figure 7I), which matched the *in vitro* differentiated CD4 T cells. In addition, the percentage of IL-17F$^+$/IL-17A$^-$/IL-22$^-$/IL-21$^-$/IFN-γ$^-$ cells between *in vitro* IL-12+IL-1β stimulation and the *ex vivo* restimulated memory

(E) Day 5 intracellular FACS analysis of Th cells differentiated as in (B). Dot plots show a representative donor.
(F) Quantification of live total CD4 T cells producing either IL-17A or IL-17F; n = 6 donors, paired t test.
(G) Representative donor of CD4 memory T cells with intracellular FACS staining for IL-17A versus IL-17F.
(H) Venn Diagrams of IL-17F$^+$/IL17A$^-$ Th cells co-producing IL-22, IFN-γ, and IL-21 of naive CD4 T cells under the IL-12+IL-1β. IL-12+IL; mean percentage and confidence interval, n = 6 donors.
(I) Venn Diagrams of IL-17F$^+$/IL17A$^-$ Th cells co-producing IL-22, IFN-γ, and IL-21 of memory CD4 T cells stimulated for 5 h with PMA and ionomycin; mean percentage of 6 donors with confidence interval.

compartment was similar (22.2%), which indirectly supported that IL-12+IL-1β induced the emergence of IL-17F single producers.

Taken together, our results demonstrate a synergy between IL-12 and IL-1 in inducing IL-17F single-producing Th cells with possible physiopathological relevance.

DISCUSSION

Cell-cell communication may involve several tens of communication signals functioning concomitantly and possibly interacting with each other. These signals, in turn, modify many molecular and functional parameters in target cells. Such complexity cannot be captured and formalized without an integrated mathematical modeling approach. Theoretical models of Th cell differentiation have already been established (Abou-Jaoudé et al., 2015; Naldi et al., 2010) and include a large number of possible inputs to T cells. However, they suffer from three limitations: (1) they include input signals that may be expressed by diverse cell types in different anatomical locations; (2) they do not recapitulate combinations of input signals in their naturally occurring patterns and concentrations; and (3) they use prior knowledge to infer input-output relationships, which does not integrate possible context-dependencies and interactions. In parallel, data-driven models have been developed in response to predefined stimuli, such as Th17 (Yosef et al., 2013) or Th1/Th2 (Antebi et al., 2013), which do not recapitulate the integration of multiple communication signals. In our study, we applied an unbiased data-driven approach specifically designed to model DC-Th communication. Combinations and concentrations of input communication signals were measured as naturally determined by their intrinsic biological regulation. Subsequently, the input-output relationships were learned from the experimental data and integrated into any underlying context dependency and interaction, even when not described previously. This maximizes the relevance of the model and the potential for novel discoveries.

Cells can change state in response to environmental cues, a concept defined as plasticity (da Silva-Diz et al., 2018; Liu et al., 2001). Each cell state may be associated with different communication potential; i.e., different expression patterns of communication signals (Soumelis et al., 2002; Wang et al., 2014). To broadly cover the possible DC states, we used various DC-stimulatory conditions (cytokines, viruses, bacteria, fungi) at various doses and combinations and across a large number of observations (>400). This prevented us from biasing our observations toward certain quantitatively or qualitatively extreme behaviors. After the model has learned the rules from such an extended range of observations, we anticipate that it should be able to predict behaviors in situations not necessarily covered in our original dataset, as confirmed in our computational and experimental validations. This opens possibilities of application in many areas of immunology, inflammation, and immunotherapy.

RNA sequencing (RNA-seq) has offered a means of capturing the expression of many communication signals and their receptors to infer cell-cell communication between various cell types (Vento-Tormo et al., 2018). However, the RNA-to-protein correlation can be rather low (Liu et al., 2016) and varies a lot depending on the gene (Edfors et al., 2016). Consequently, RNA copies of a gene cannot be associated with a given functional output, preventing quantitative mathematical modeling. Functional response in target cells can only be estimated indirectly through surrogate activation markers, which is most often not performed. In our approach, all measurements of communication signals and output variables were done at the protein level, hence directly measuring the bioactive communication molecules with a direct link to a specific response in target cells. This ensures robustness of the modeling strategy, as evidenced by our model's ability to recapitulate most of the known relationships in DC-Th cell communication.

Modeling complex biological behaviors in a quantitative manner is challenging. In data-driven models, it relies in large parts on the choice of explanatory (input) variables, which drive the induction or regulation of output variables. Here we selected DC-derived communication molecules through exhaustive literature mining. The model was able to integrate 36 input and 18 output variables in a quantitative manner, which makes it a reference in the field. We have been able to describe patterns of DC communication molecules in a way that goes beyond the classical view of immature versus mature DCs (Banchereau and Steinman, 1998; Guermonprez et al., 2002). In fact, we showed that almost every DC stimulatory condition leads to a distinct DC state. This is a first step in defining general combinatorial rules of DC-derived communication molecules: co-expressed molecules form the basis of putative context-dependent effects. Through the large number of variables handled by the model, we identified 290 novel associations explaining major immunoregulatory cytokines, which may lead to the discovery of novel functions of known DC molecules and suggest novel therapeutic targets.

Going further into the complexity of communication, we explored context dependencies of communication signals. In verbal communication, the context may dramatically alter the meaning of an individual word. Currently, there is no systematic way to search for context dependencies in biological communication. In our modeling strategy, we devised a method that introduces context-dependent variables for a given molecule. This allows unbiased identification of context-dependent functions that would have been missed by classical regression models. For example, we identified a new function for IL-12 in promoting IL-17F production by Th cells, which was completely unexpected based on prior knowledge (Korn et al., 2009). Identifying such context dependencies before therapeutic targeting of a DC-Th communication molecule may improve the prediction of its effect.

Given that DC-Th communication is central to a large number of physiopathological conditions (Keller, 2001), we can foresee multiple applications for the model. Based on expression pattern of DC molecules, the model can predict the induced Th cytokine profile. Quantitative measurements of DC communication molecules in a given disease or in an individual patient *ex vivo* can be used to simulate the corresponding Th response. Depending on the outcome, strategies may be devised to re-orient the response toward a protective or less pathogenic profile, again through model-based predictions. Alternatively, starting from a Th profile (cytokine or groups of cytokines), the appropriate molecular targets can be manipulated through gain- or loss-of-function experiments to amplify or inhibit a given Th cytokine. Last, the model can help predict the most appropriate vaccine adjuvant to obtain

protective immunity against some microbes or to re-orient a pathogenic Th response. For example, all DC molecules positively associated in the model to Th2 responses are potential targets to decrease pathogenic Th2 allergic inflammation (Ito et al., 2005; Nakayama et al., 2017; Soumelis et al., 2002).

Using DC-Th communication as a model, we established a framework that can now be applied to other types of cell-cell communication following 5 major steps: (1) systematic perturbation of the "sender" cell to generate a diversity of communication states; (2) broad, quantitative, and protein-level measurement of communication molecules relevant to the sender cell; (3) systematic quantitative assessment of the response in "receiver" or target cells; (4) MultiVarSel modeling of the input-output relationship, which defines communication rules; (5) *in silico* and experimental validation. Currently, we believe that cell type specificities in expression of communication molecules and in their function would prevent us from generalizing our DC-Th model to other cell types. Comparing different quantitative models of cell-cell communication will ultimately tell us whether cells speak the same language (i.e., whether they express similar patterns of communication molecules) and whether the same communication molecule has the same meaning (function) when expressed by two different cell types.

STAR★METHODS

Detailed methods are provided in the online version of this paper and include the following:

- KEY RESOURCES TABLE
- LEAD CONTACT AND MATERIALS AVAILABILITY
- EXPERIMENTAL MODEL AND SUBJECT DETAILS
  - Human subjects
- METHOD DETAILS
  - PBMCs purification
  - MoDC generation and activation
  - Blood dendritic cells purification
  - $CD4^+$ T lymphocytes purification
  - Paired protein measurement in DC/T coculture
  - IL-12 blocking experiment
  - CD28 blocking experiment
  - Addition of rhIL-12p70 during DC/T coculture
  - DC-free Th cell polarization
  - ICOS agonism
  - CD2 agonism
  - Flow cytometry analysis
  - Cytokine quantification
  - Gene expression quantification
  - Anti-human ICOS monoclonal blocking antibody
- QUANTIFICATION AND STATISTICAL ANALYSIS
  - Dataset quality control – batch effect
  - Dataset quality control – T cell expansion
  - Statistical tests
  - Statistical analysis
  - Model comparison and ROC Curves
  - Modeling strategy
  - Systematic literature review
- DATA AND CODE AVAILABILITY

SUPPLEMENTAL INFORMATION

Supplemental Information can be found online at https://doi.org/10.1016/j.cell.2019.09.012.

ACKNOWLEDGMENTS

We thank the Institut Curie Cytometry platform for cell sorting, P. Gestraud and F. Coffin for advice regarding statistical analyses, and O. Lantz and N. Manel for important discussions. We wish to thank L. Pattarini, B. Fould, W. Cohen, O. Geneste, B. Lockhart, V. Blanc, and their teams from the Institut de Recherche Servier for having produced and generously shared the anti-ICOS antibody. This work was supported by funding from Agence Nationale de la Recherche: ANR-16-CE15-0024-01, ANR-10-IDEX-0001-02 PSL*, ANR-11-LABX-0043 and ANR-17-CE14-0025-02 from Center of Clinical Inverstigation IGR-Curie: CIC IGR-Curie 1428 and from Ligue contre le Cancer: EL2016.LNCC/VaS. M.G. was funded by ANRS and ARC.

AUTHOR CONTRIBUTIONS

M.G., C.T., L.K., C.C., and P.S. performed the experiments. M.G. and V.S. designed the experiments. M.P.-D. performed the statistical analysis. O.A., W.A.-J., and M.G. performed literature mining. P.H., D.T., F.B., L.S., J.C., C.L.-L., and V.S. participated in and supervised the statistical analysis. M.G. and V.S. wrote the manuscript. V.S. supervised the study.

DECLARATION OF INTERESTS

The authors declare no competing interests.

Received: February 19, 2019
Revised: June 20, 2019
Accepted: September 9, 2019
Published: October 3, 2019

REFERENCES

Abou-Jaoudé, W., Monteiro, P.T., Naldi, A., Grandclaudon, M., Soumelis, V., Chaouiya, C., and Thieffry, D. (2015). Model checking to assess T-helper cell plasticity. Front. Bioeng. Biotechnol. *2*, 86.

Acosta-Rodriguez, E.V., Napolitani, G., Lanzavecchia, A., and Sallusto, F. (2007). Interleukins 1beta and 6 but not transforming growth factor-beta are essential for the differentiation of interleukin 17-producing human T helper cells. Nat. Immunol. *8*, 942–949.

Alculumbre, S., and Pattarini, L. (2016). Purification of Human Dendritic Cell Subsets from Peripheral Blood. Methods Mol. Biol. *1423*, 153–167.

Antebi, Y.E., Reich-Zeliger, S., Hart, Y., Mayo, A., Eizenberg, I., Rimer, J., Putheti, P., Pe'er, D., and Friedman, N. (2013). Mapping differentiation under mixed culture conditions reveals a tunable continuum of T cell fates. PLoS Biol. *11*, e1001616.

Balan, S., Arnold-Schrauf, C., Abbas, A., Couespel, N., Savoret, J., Imperatore, F., Villani, A.C., Vu Manh, T.P., Bhardwaj, N., and Dalod, M. (2018). Large-Scale Human Dendritic Cell Differentiation Revealing Notch-Dependent Lineage Bifurcation and Heterogeneity. Cell Rep. *24*, 1902–1915.e6.

Banchereau, J., and Steinman, R.M. (1998). Dendritic cells and the control of immunity. Nature *392*, 245–252.

Cariani, F., and Rips, L.J. (2017). Conditionals, Context, and the Suppression Effect. Cogn. Sci. (Hauppauge) *41*, 540–589.

Chen, L., and Flies, D.B. (2013). Molecular mechanisms of T cell co-stimulation and co-inhibition. Nat. Rev. Immunol. *13*, 227–242.

Ciofani, M., Madar, A., Galan, C., Sellars, M., Mace, K., Pauli, F., Agarwal, A., Huang, W., Parkhurst, C.N., Muratet, M., et al. (2012). A validated regulatory network for Th17 cell specification. Cell *151*, 289–303.

da Silva-Diz, V., Lorenzo-Sanz, L., Bernat-Peguera, A., Lopez-Cerda, M., and Muñoz, P. (2018). Cancer cell plasticity: Impact on tumor progression and therapy response. Semin. Cancer Biol. *53*, 48–58.

Edfors, F., Danielsson, F., Hallström, B.M., Käll, L., Lundberg, E., Pontén, F., Forsström, B., and Uhlén, M. (2016). Gene-specific correlation of RNA and protein levels in human cells and tissues. Mol. Syst. Biol. *12*, 883.

Guermonprez, P., Valladeau, J., Zitvogel, L., Théry, C., and Amigorena, S. (2002). Antigen presentation and T cell stimulation by dendritic cells. Annu. Rev. Immunol. *20*, 621–667.

Ito, T., Wang, Y.H., Duramad, O., Hori, T., Delespesse, G.J., Watanabe, N., Qin, F.X., Yao, Z., Cao, W., and Liu, Y.J. (2005). TSLP-activated dendritic cells induce an inflammatory T helper type 2 cell response through OX40 ligand. J. Exp. Med. *202*, 1213–1223.

Ivanov, I.I., McKenzie, B.S., Zhou, L., Tadokoro, C.E., Lepelley, A., Lafaille, J.J., Cua, D.J., and Littman, D.R. (2006). The orphan nuclear receptor RORgammat directs the differentiation program of proinflammatory IL-17+ T helper cells. Cell *126*, 1121–1133.

Keller, R. (2001). Dendritic cells: their significance in health and disease. Immunol. Lett. *78*, 113–122.

Kintsch, W., and Mangalath, P. (2011). The construction of meaning. Top. Cogn. Sci. *3*, 346–370.

Korn, T., Bettelli, E., Oukka, M., and Kuchroo, V.K. (2009). IL-17 and Th17 Cells. Annu. Rev. Immunol. *27*, 485–517.

Liu, Y.J., Kanzler, H., Soumelis, V., and Gilliet, M. (2001). Dendritic cell lineage, plasticity and cross-regulation. Nat. Immunol. *2*, 585–589.

Liu, Y., Beyer, A., and Aebersold, R. (2016). On the Dependency of Cellular Protein Levels on mRNA Abundance. Cell *165*, 535–550.

Macagno, A., Napolitani, G., Lanzavecchia, A., and Sallusto, F. (2007). Duration, combination and timing: the signal integration model of dendritic cell activation. Trends Immunol. *28*, 227–233.

Manel, N., Unutmaz, D., and Littman, D.R. (2008). The differentiation of human T(H)-17 cells requires transforming growth factor-beta and induction of the nuclear receptor RORgammat. Nat. Immunol. *9*, 641–649.

Meinshausen, N., and Bühlmann, P. (2010). Stability selection. J. R. Stat. Soc. Series B. Stat. Methodol. *72*, 417–473.

Nakayama, T., Hirahara, K., Onodera, A., Endo, Y., Hosokawa, H., Shinoda, K., Tumes, D.J., and Okamoto, Y. (2017). Th2 Cells in Health and Disease. Annu. Rev. Immunol. *35*, 53–84.

Naldi, A., Carneiro, J., Chaouiya, C., and Thieffry, D. (2010). Diversity and plasticity of Th cell types predicted from regulatory network modelling. PLoS Comput. Biol. *6*, e1000912.

Perrot-Dockès, M., Lévy-Leduc, C., Chiquet, J., Sansonnet, L., Brégère, M., Étienne, M.P., Robin, S., and Genta-Jouve, G. (2018a). A variable selection approach in the multivariate linear model: an application to LC-MS metabolomics data. Stat. Appl. Genet. Mol. Biol. *17*, /j/sagmb.2018.17.issue-5/sagmb-2017-0077/sagmb-2017-0077.xml.

Perrot-Dockès, M., Lévy-Leduc, C., Sansonnet, L., and Chiquet, J. (2018b). Variable selection in multivariate linear models with high-dimensional covariance matrix estimation. J. Multivariate Anal. *166*, 78–97.

Soumelis, V., Reche, P.A., Kanzler, H., Yuan, W., Edward, G., Homey, B., Gilliet, M., Ho, S., Antonenko, S., Lauerma, A., et al. (2002). Human epithelial cells trigger dendritic cell mediated allergic inflammation by producing TSLP. Nat. Immunol. *3*, 673–680.

Tibshirani, R. (1996). Regression Shrinkage and Selection via the Lasso. J. R. Stat. Soc. Series B Stat. Methodol. *58*, 267–288.

Tindemans, I., Peeters, M.J.W., and Hendriks, R.W. (2017). Notch Signaling in T Helper Cell Subsets: Instructor or Unbiased Amplifier? Front. Immunol. *8*, 419.

Touzot, M., Grandclaudon, M., Cappuccio, A., Satoh, T., Martinez-Cingolani, C., Servant, N., Manel, N., and Soumelis, V. (2014). Combinatorial flexibility of cytokine function during human T helper cell differentiation. Nat. Commun. *5*, 3987.

Vento-Tormo, R., Efremova, M., Botting, R.A., Turco, M.Y., Vento-Tormo, M., Meyer, K.B., Park, J.E., Stephenson, E., Polański, K., Goncalves, A., et al. (2018). Single-cell reconstruction of the early maternal-fetal interface in humans. Nature *563*, 347–353.

Volpe, E., Servant, N., Zollinger, R., Bogiatzi, S.I., Hupé, P., Barillot, E., and Soumelis, V. (2008). A critical function for transforming growth factor-beta, interleukin 23 and proinflammatory cytokines in driving and modulating human T(H)-17 responses. Nat. Immunol. *9*, 650–657.

Wang, Y., Chen, X., Cao, W., and Shi, Y. (2014). Plasticity of mesenchymal stem cells in immunomodulation: pathological and therapeutic implications. Nat. Immunol. *15*, 1009–1016.

Yosef, N., Shalek, A.K., Gaublomme, J.T., Jin, H., Lee, Y., Awasthi, A., Wu, C., Karwacz, K., Xiao, S., Jorgolli, M., et al. (2013). Dynamic regulatory network controlling TH17 cell differentiation. Nature *496*, 461–468.

Zhu, J., Yamane, H., and Paul, W.E. (2010). Differentiation of effector CD4 T cell populations (*). Annu. Rev. Immunol. *28*, 445–489.

Zygmunt, B., and Veldhoen, M. (2011). T helper cell differentiation more than just cytokines. Adv. Immunol. *109*, 159–196.

STAR★METHODS

KEY RESOURCES TABLE

REAGENT or RESOURCE	SOURCE	IDENTIFIER
Antibodies		
FITC Mouse anti-human CD3 (Clone HIT3a)	BD	Cat# 555339; RRID:AB_395745
FITC Mouse anti-human CD14 (Clone TÜK4)	Miltenyi Biotec	Cat# 130-080-701; RRID:AB_244303
FITC Mouse anti-human CD16 (Clone NKP15)	BD	Cat# 335035
FITC Mouse anti-human CD19 (Clone LT19)	Miltenyi Biotec	Cat# 130-091-328; RRID:AB_244222
APC-Cy7 Mouse anti-human CD11c (Clone Bu15)	BioLegend	Cat# 337218; RRID:AB_10662746
PE-Cy5 Mouse anti-human CD4 (Clone 13B8.2)	Beckman Coulter	Cat# A07752
R-PE Mouse anti-human OX40L (Clone ANC10G1)	Ancell	Cat# 400-050
R-PE Mouse IgG1, κ Isotype Control (Clone MOPC31C)	Ancell	Cat# 278-050
BV711 Mouse anti-human CD54 (Clone HA58)	BD	Cat# 564078; RRID:AB_2738579
BV711 Mouse IgG1, κ Isotype Control (Clone X40)	BD	Cat# 563044
BV786 Mouse anti-human CD273 (Clone MIH18)	BD	Cat# 563843; RRID:AB_2738446
BV786 Mouse anti-human CD80 (Clone L307.4)	BD	Cat# 564159; RRID:AB_2738631
BV786 Mouse IgG1, κ Isotype Control (Clone X40)	BD	Cat# 563330
FITC Mouse anti-human CD70 (Clone Ki-24)	BD	Cat# 555834; RRID:AB_396157
FITC Mouse IgG3, κ Isotype Control (Clone J606)	BD	Cat# 555578; RRID:AB_395956
Alexa Fluor® 700 Mouse anti-human CD29 (Clone TS2/16)	BioLegend	Cat# 303020; RRID:AB_2130078
Alexa Fluor® 700 Mouse IgG1, κ Isotype Control (Clone MOPC-21)	BioLegend	Cat# 400144
APC Mouse anti-human ICAM-3 (Clone CBR-IC3/1)	BioLegend	Cat# 330011; RRID:AB_1227570
APC Mouse anti-human Jagged-2 (Clone MHJ2-523)	BioLegend	Cat# 346906 (Discontinued)
APC Mouse IgG1, κ Isotype Control (Clone MOPC-21)	BioLegend	Cat# 400121; RRID:AB_326443
BV650 Mouse anti-human CD86 (Clone IT2.2)	BioLegend	Cat# 305428; RRID:AB_2563823
BV650 Mouse IgG2b, κ Isotype Control (Clone MPC-11)	BioLegend	Cat# 400352
BV711 Mouse anti-human HLA-DR (Clone L243)	BioLegend	Cat# 307644; RRID:AB_2562913
BV711 Mouse IgG2a, κ Isotype Control (Clone MOPC-173)	BioLegend	Cat# 400272
FITC Mouse anti-human CD100 (Clone A8)	BioLegend	Cat# 328406; RRID:AB_2254362
FITC Mouse IgG1, κ Isotype Control (Clone MOPC-21)	BioLegend	Cat# 400108
FITC Mouse anti-human ICAM-2 (Clone CBR-IC2/2)	BioLegend	Cat# 328507
FITC Mouse IgG2a, κ Isotype Control (Clone MOPC-173)	BioLegend	Cat# 400209; RRID:AB_1134236
PE Mouse anti-human CD18 (Clone TS1/18)	BioLegend	Cat# 302107; RRID:AB_314225
PE Mouse anti-human Nectin-2 (Clone TX31)	BioLegend	Cat# 337410; RRID:AB_2269088
PE Mouse anti-human PVR (Clone SKII.4)	BioLegend	Cat# 337610; RRID:AB_2174019
PE Mouse IgG1, κ Isotype Control (Clone MOPC-21)	BioLegend	Cat# 400112
PE/Cy7 Mouse anti-human CD40 (Clone 5C3)	BioLegend	Cat# 334321; RRID:AB_10643414
PE/Cy7 Mouse IgG1, κ Isotype Control (Clone MOPC-21)	BioLegend	Cat# 400126; RRID:AB_326448
PE/Cy5 Mouse anti-human CD58 (Clone TS2/9)	BioLegend	Cat# 330909; RRID:AB_1227576
PE/Cy5 Mouse IgG1, κ Isotype Control (Clone MOPC-21)	BioLegend	Cat# 400117
PerCP/Cy5.5 Mouse anti-human CD83 (Clone HB15e)	BioLegend	Cat# 305320; RRID:AB_2076530
PerCP/Cy5.5 Mouse IgG1, κ Isotype Control (Clone MOPC-21)	BioLegend	Cat# 400150
Alexa Fluor® 488 Goat anti-human Galectin-3	R&D Systems	Cat# IC1154G; RRID:AB_10890949
Alexa Fluor® 488 Normal Goat IgG	R&D Systems	Cat# IC108G; RRID:AB_10890944
Alexa Fluor® 700 Mouse anti-human VISTA (Clone 730804)	R&D Systems	Cat# FAB71261N
Alexa Fluor® 700 Mouse IgG_{2B} Isotype Control (Clone 133303)	R&D Systems	Cat# IC0041N; RRID:AB_10973174
APC Mouse anti-human SLAMF3 (Clone 249936)	R&D Systems	Cat# FAB1898A; RRID:AB_2137949

(*Continued on next page*)

Continued

REAGENT or RESOURCE	SOURCE	IDENTIFIER
APC Mouse IgG_{2A} Isotype Control (Clone 20102)	R&D Systems	Cat# IC003A; RRID:AB_357243
APC Mouse anti-human 4-1BBL (Clone 282220)	R&D Systems	Cat# FAB2295A; RRID:AB_2207514
APC Mouse anti-human ICOSL (Clone 136726)	R&D Systems	Cat# FAB165A; RRID:AB_991955
APC Mouse IgG_{2B} Isotype Control (Clone 133303)	R&D Systems	Cat# IC0041A; RRID:AB_357246
FITC Mouse anti-human B7H3 (Clone 185504)	R&D Systems	Cat# FAB1027F; RRID:AB_1208024
FITC Mouse IgG_1 Isotype Control (Clone 11711)	R&D Systems	Cat# IC002F
FITC Goat anti-human SLAMF5	R&D Systems	Cat# FAB1855F (Discontinued); RRID:AB_2074764
FITC Normal Goat IgG	R&D Systems	Cat# IC108F; RRID:AB_10177332
PE Mouse anti-human LIGHT (Clone 115520)	R&D Systems	Cat# FAB664P; RRID:AB_2240851
PE Mouse IgG_1 Isotype Control (Clone 133303)	R&D Systems	Cat# IC002P; RRID:AB_357242
PE Mouse anti-human CD30L (Clone 116614)	R&D Systems	Cat# FAB1028P; RRID:AB_2207494
PE Mouse IgG2B Isotype Control (Clone 133303)	R&D Systems	Cat# IC0041P; RRID:AB_357249
PerCP Mouse anti-human CD11a (Clone CR38)	R&D Systems	Cat# FAB35951C (Discontinued); RRID:AB_10892335
PerCP Mouse IgG_{2A} Isotype Control (Clone 20102)	R&D Systems	Cat# IC003C; RRID:AB_1207937
PerCP-eFluor710 Mouse anti-human PDL1 (Clone MIH1)	ThermoFisher Scientific	Cat# 46-5983-42; RRID:AB_11041815
PerCP-eFluor710 Mouse IgG1, κ Isotype Control (Clone P3.6.2.8.1)	ThermoFisher Scientific	Cat# 46-4714-82; RRID:AB_1834453
Alexa Fluor® 488 Mouse anti-human IL-17A (Clone BL168)	BioLegend	Cat# 512308; RRID:AB_961386
Alexa Fluor® 488 Mouse IgG1, κ Isotype Control (Clone MOPC-21)	BioLegend	Cat# 400134
PE-Cy7 Rat anti-human IL-17F (Clone SHLR17)	ThermoFisher Scientific	Cat# 25-7169-42; RRID:AB_10853673
PE-Cy7 Rat IgG1, κ Isotype Control (Clone eBRG1)	ThermoFisher Scientific	Cat# 25-4301-82; RRID:AB_470198
PE Mouse anti-human IL-21 (Clone 3A3-N2)	BioLegend	Cat# 513004; RRID:AB_2249025
PE Mouse IgG1, κ Isotype Control (Clone MOPC-21)	BioLegend	Cat# 400112
eFluor 660 Mouse anti-human IL-22 (Clone 22URTI)	ThermoFisher Scientific	Cat# 50-7229-42; RRID:AB_10598650
eFluor 660 Mouse IgG1, κ Isotype Control (Clone P3.6.2.8.1)	ThermoFisher Scientific	Cat# 50-4714-82; RRID:AB_10597301
BV605 Mouse anti-human IFN-γ (Clone B27)	BD	Cat# 562974; RRID:AB_2737926
BV605 Mouse IgG1, κ Isotype Control (Clone X40)	BD	Cat# 562652; RRID:AB_2714005
Ultra-LEAF Purified anti-human CD3 Antibody (Clone OKT3)	Biolegend	Cat# 317347; RRID:AB_2571994
Ultra-LEAF Purified anti-human CD28 Antibody (Clone CD28.2)	Biolegend	Cat# 302943; RRID:AB_2616667
Mouse IgG1 kappa Isotype Control (Clone P3.6.2.8.1)	ThermoFisher Scientific	Cat# 14-4714-85; RRID:AB_470112
Human IL12 monoclonal blocking antibody (Clone B-T21)	ThermoFisher Scientific	Cat# BMS152; RRID:AB_10596494
Mouse IgG1 isotype control	R&D Systems	Cat# MAB002; RRID:AB_357344
Human CD2 monoclonal blocking antibody (Clone 299808)	R&D Systems	Cat# MAB18562
Mouse IgG2A isotype control	R&D Systems	Cat# MAB003; RRID:AB_357345
Anti-human CD28 monoclonal blocking antibody (Clone 9.3)	BioXcell	Cat# BE0248; RRID:AB_2687729
Anti-Unknown Specificity (Isotype control) Human IgG1,k	Absolute Antibody	Cat# Ab00178-10.0
Anti-human ICOS monoclonal blocking antibody	N/A	The agonist ICOS antibody was produced for research purposes from the sequence made publicly available by JOUNCE THERAPEUTICS in the patent US 2016/0304610, INC. The produced antibody corresponded to clone 37A10S713 with a human IgG1 isotype.
Biological Samples		
Human Healthy blood donors for primary MoDC, bDC, naive and memory CD4 T cells	Etablissement Français du Sang (French Blood Bank)	N/A
Human serum	Sigma-Aldrich	Cat# H4522

(*Continued on next page*)

Continued

REAGENT or RESOURCE	SOURCE	IDENTIFIER
Chemicals, Peptides and Recombinant Proteins		
Lymphoprep	StemCell Technologies	Cat# 07861
RPMI 1640 Medium, GlutaMAX Supplement	ThermoFisher Scientific	Cat# 61870010
Penicillin-Streptomycin	ThermoFisher Scientific	Cat# 15140122
Foetal Bovine Serum Research Grade	Hyclone/Perbio	Cat# CH30160.03
MEM Non-essential Amino Acids Solution (100X)	ThermoFisher Scientific	Cat# 11140050
Sodium pyruvate (100 mM)	ThermoFisher Scientific	Cat#11360070
X-VIVO 15 Chemically Defined, Serum-Free Hematopoietic Cell Medium	Ozyme	Cat# BE02-060F
HEPES Buffer	ThermoFisher Scientific	Cat# 15630056
UltraPure EDTA	ThermoFisher Scientific	Cat# 15575020
Phorbol 12-myristate 13-acetate	Sigma-Aldrich	Cat# P8139
Ionomycin calcium salt from Streptomyces conglobatus	Sigma-Aldrich	Cat# I0634
Brefeldin A Solution 1000X	ThermoFisher Scientific	Cat# 00-4506-51
Intracellular Fixation & Permeabilization Buffer Set	ThermoFisher Scientific	Cat# 88-8824-00
DAPI (4',6-Diamidino-2-Phenylindole, Dihydrochloride)	ThermoFisher Scientific	Cat# D1306
Zombie NIR Fixable Viability Kit	BioLegend	Cat# 423105
LIVE/DEAD Fixable Yellow Dead Cell Stain Kit	ThermoFisher Scientific	Cat# L34959
CellTrace Violet Cell Proliferation Kit, for flow cytometry	ThermoFisher Scientific	Cat# C34557
Recombinant human IL-1α	R&D Systems	Cat# 200-LA
Recombinant human IL-1β	Peprotech	Cat# 200-01B
Recombinant human IL-4	R&D Systems	Cat# 204-IL-010
Recombinant human IL-6	Peprotech	Cat# 200-06
Recombinant human IL-12p70	R&D Systems	Cat# 219-IL
Recombinant human IL-23	R&D Systems	Cat# 1290-IL
Recombinant human TGF-β1	Peprotech	Cat# 100-21
Recombinant human IL-4	Miltenyi Biotec	Cat# 130-093-922
Recombinant human GM-CSF	Miltenyi Biotec	Cat# 130-093-865
PAM3CSK4	Invivogen	Cat# tlrl-pms
Aluminum potassium sulfate	Invivogen	Cat# tlrl-alk
Heat-killed Staphylococcus aureus	Invivogen	Cat# tlrl-hksa
Heat-killed Candida albicans	Invivogen	Cat# tlrl-hkca
Heat-killed Listeria monocytogenes	Invivogen	Cat# tlrl-hklm
Heat-killed Streptococcus pneumoniae	Invivogen	Cat# tlrl-hksp
Poly(I:C) High molecular weight	Invivogen	Tlrl-pic
Curdlan	Invivogen	Cat# tlrl-curd
Zymosan	Sigma-Aldrich	Cat# Z4250
LPS-EB Ultrapure	Invivogen	Cat# tlrl-3pelps
Prostaglandin E2	Sigma-Aldrich	Cat# P0409
R848	Invivogen	Cat# tlrl-r848
Recombinant Human IFN-β	Preprotech	Cat# 300-02BC
Influenza A/PR/8/34 (H1N1) Allantoic Fluid	Charles River	Cat# 10100781
Recombinant human TSLP	R&D Systems	Cat# 1398-TS
Critical Commercial Assays		
EasySep Human Pan-DC Pre-Enrichment Kit	StemCell Technologies	Cat# 19251
EasySep Human Naive CD4+ T Cell Isolation Kit	StemCell Technologies	Cat# 19555
CD14 MicroBead human	Miltenyi Biotec	Cat# 130-050-201
LS columns	Miltenyi Biotec	Cat# 130-042-401

(*Continued on next page*)

Continued

REAGENT or RESOURCE	SOURCE	IDENTIFIER
Memory CD4+ T Cell Isolation Kit, human	Miltenyi Biotec	Cat# 130-091-893
Dynabeads® Human T-Activator CD3/CD28 for T Cell Expansion and Activation	ThermoFisher Scientific	Cat# 11131D
Easy 50 EasySep Magnet	StemCell Technologies	Cat# 18002
Big Easy EasySep Magnet	StemCell Technologies	Cat# 18001
QuadroMACS Starting Kit (LS)	Miltenyi Biotec	Cat# 130-091-051
BD Cytometric Bead Array (CBA) Human Soluble Protein Master Buffer Kit	BD	Cat# 558265
BD Cytometric Bead Array (CBA) Human IL-1α Flex Set	BD	Cat# 560153
BD Cytometric Bead Array (CBA) Human IL-1β Flex Set	BD	Cat# 558279
BD Cytometric Bead Array (CBA) Human IL-2 Flex Set	BD	Cat# 558270
BD Cytometric Bead Array (CBA) Human IL-3 Flex Set	BD	Cat# 558355
BD Cytometric Bead Array (CBA) Human IL-4 Flex Set	BD	Cat# 558272
BD Cytometric Bead Array (CBA) Human IL-5 Flex Set	BD	Cat# 558278
BD Cytometric Bead Array (CBA) Human IL-6 Flex Set	BD	Cat# 558276
BD Cytometric Bead Array (CBA) Human IL-9 Flex Set	BD	Cat# 558333
BD Cytometric Bead Array (CBA) Human IL-10 Flex Set	BD	Cat# 558274
BD Cytometric Bead Array (CBA) Human IL-12p70 Flex Set	BD	Cat# 558283
BD Cytometric Bead Array (CBA) Human IL-13 Flex Set	BD	Cat# 558450
BD Cytometric Bead Array (CBA) Human IL-17A Flex Set	BD	Cat# 560383
BD Cytometric Bead Array (CBA) Human IL-17F Flex Set	BD	Cat# 562151
BD Cytometric Bead Array (CBA) Human GM-CSF Flex Set	BD	Cat# 558335
BD Cytometric Bead Array (CBA) Human IFN-γ Flex Set	BD	Cat# 558269
BD Cytometric Bead Array (CBA) Human TNF-α Flex Set	BD	Cat# 558273
MILLIPLEX MAP Human TH17 Magnetic Bead Panel - Immunology Multiplex Assay IL-21, IL-22, IL-31, TNF-β	Merck Millipore	Cat# HTH17MAG-14K
MILLIPLEX MAP Human TH17 Magnetic Bead Panel - Immunology Multiplex Assay IL-23, IL-28α	Merck Millipore	Cat# HTH17MAG-14K
RNeasy Micro Kit (50)	QIAGEN	Cat# 74004
SuperScript II Reverse Transcriptase	ThermoFisher Scientific	Cat# 18064-071
Random primers	Promega	Cat# C1181
Oligo(dT)15 Primer	Promega	Cat# C1101
RNasin® Ribonuclease Inhibitors	Promega	Cat# N2515
dNTP	Promega	Cat# U1240
qPCR MasterMix Plus dTTP	Eurogentec	Cat# 05-QP2X-03+WOUN
Oligonucleotides		
RORC [Hs01076112_m1]	ThermoFisher Scientific	Cat# 4331182
TBX21 [Hs00203436_m1]	ThermoFisher Scientific	Cat# 4331182
GATA3 [Hs00231122_m1]	ThermoFisher Scientific	Cat# 4331182
RORA [Hs00536545_m1]	ThermoFisher Scientific	Cat# 4331182
FOXP3 [Hs00203958_m1]	ThermoFisher Scientific	Cat# 4331182
FOXP1 [Hs00212860_m1]	ThermoFisher Scientific	Cat# 4331182
SH2D1A [Hs00158978_m1]	ThermoFisher Scientific	Cat# 4331182
PRDM1 [Hs00153357_m1]	ThermoFisher Scientific	Cat# 4331182
PDCD1 [Hs01550088_m1]	ThermoFisher Scientific	Cat# 4331182
BTLA [Hs00699198_m1]	ThermoFisher Scientific	Cat# 4331182
HLX [Hs00172035_m1]	ThermoFisher Scientific	Cat# 4331182
IRF1 [Hs00971965_m1]	ThermoFisher Scientific	Cat# 4331182

(*Continued on next page*)

Continued

REAGENT or RESOURCE	SOURCE	IDENTIFIER
CMIP [Hs00286832_m1]	ThermoFisher Scientific	Cat# 4331182
MAF [Hs00193519_m1]	ThermoFisher Scientific	Cat# 4331182
RUNX1 [Hs00231079_m1]	ThermoFisher Scientific	Cat# 4331182
PU1 / SPI1 [Hs02786711_m1]	ThermoFisher Scientific	Cat# 4331182
CD200 [Hs01033303_m1]	ThermoFisher Scientific	Cat# 4331182
CXCL13 [Hs00757930_m1]	ThermoFisher Scientific	Cat# 4331182
IL-12RB2 [Hs00155486_m1]	ThermoFisher Scientific	Cat# 4331182
BCL6 [Hs00153368_m1]	ThermoFisher Scientific	Cat# 4331182
IRF4 [Hs00180031_m1]	ThermoFisher Scientific	Cat# 4331182
FOSL2 [Hs01050117_m1]	ThermoFisher Scientific	Cat# 4331182
BATF [Hs00232390_m1]	ThermoFisher Scientific	Cat# 4331182
KDM6B [Hs00996325_g1]	ThermoFisher Scientific	Cat# 4331182
NFKBIZ [Hs00230071_m1]	ThermoFisher Scientific	Cat# 4331182
SATB1 [Hs00962580_m1]	ThermoFisher Scientific	Cat# 4331182
BCL11B [Hs01102259_m1]	ThermoFisher Scientific	Cat# 4331182
EOMES [Hs00172872_m1]	ThermoFisher Scientific	Cat# 4331182
SKI [Hs01057032_m1]	ThermoFisher Scientific	Cat# 4331182
ATF6 [Hs00232586_m1]	ThermoFisher Scientific	Cat# 4331182
AES [Hs01081012_m1]	ThermoFisher Scientific	Cat# 4331182
CREM [Hs01582003_g1]	ThermoFisher Scientific	Cat# 4331182
DDIT3 [Hs00358796_g1]	ThermoFisher Scientific	Cat# 4331182
LEF1 [Hs01547250_m1]	ThermoFisher Scientific	Cat# 4331182
NFATC2 [Hs00905451_m1]	ThermoFisher Scientific	Cat# 4331182
ETV6 [Hs00231101_m1]	ThermoFisher Scientific	Cat# 4331182
SIRT2 [Hs01560289_m1]	ThermoFisher Scientific	Cat# 4331182
USP18 [Hs00276441_m1]	ThermoFisher Scientific	Cat# 4331182
NFATC1 [Hs00542675_m1]	ThermoFisher Scientific	Cat# 4331182
NFATC3 [Hs00190046_m1]	ThermoFisher Scientific	Cat# 4331182
SMAD3 [Hs00969210_m1]	ThermoFisher Scientific	Cat# 4331182
SMAD2 [Hs00998187_m1]	ThermoFisher Scientific	Cat# 4331182
SMAD7 [Hs00998193_m1]	ThermoFisher Scientific	Cat# 4331182
MINA [Hs01031255_m1]	ThermoFisher Scientific	Cat# 4331182
POUA2F1 [Hs01573369_m1]	ThermoFisher Scientific	Cat# 4331182
TNFRSF4/OX40 [Hs00937195_g1]	ThermoFisher Scientific	Cat# 4331182
TNFRSF8/CD30 [Hs00174277_m1]	ThermoFisher Scientific	Cat# 4331182
TIGIT [Hs00545087_m1]	ThermoFisher Scientific	Cat# 4331182
CD226/DNAM-1 [Hs00170832_m1]	ThermoFisher Scientific	Cat# 4331182
CD96 [Hs00976975_m1]	ThermoFisher Scientific	Cat# 4331182
IL17A [Hs00174383_m1]	ThermoFisher Scientific	Cat# 4331182
IL17F [Hs00369400_m1]	ThermoFisher Scientific	Cat# 4331182
STAT3 [Hs00374280_m1]	ThermoFisher Scientific	Cat# 4331182
ICOS [Hs00359999_m1]	ThermoFisher Scientific	Cat# 4331182
IL23R [Hs00332759_m1]	ThermoFisher Scientific	Cat# 4331182
AHR [Hs00169233_m1]	ThermoFisher Scientific	Cat# 4331182
IL1R2 [Hs01030384_m1]	ThermoFisher Scientific	Cat# 4331182
CCL20 [Hs01011368_m1]	ThermoFisher Scientific	Cat# 4331182
IL2RA [Hs00907779_m1]	ThermoFisher Scientific	Cat# 4331182
IL2RB [Hs01081697_m1]	ThermoFisher Scientific	Cat# 4331182

(*Continued on next page*)

Continued

REAGENT or RESOURCE	SOURCE	IDENTIFIER
IL2RG [Hs00953624_m1]	ThermoFisher Scientific	Cat# 4331182
IL17RA [Hs01064648_m1]	ThermoFisher Scientific	Cat# 4331182
CCR6 [Hs00171121_m1]	ThermoFisher Scientific	Cat# 4331182
B2M [Hs99999907_m1]	ThermoFisher Scientific	Cat# 4331182
RPL34 [Hs00241560_m1]	ThermoFisher Scientific	Cat# 4331182
Software and Algorithms		
GraphPad Prism 6 – Version 6.01	GraphPad	https://www.graphpad.com/
FlowJo V10 – Version 10.0.8	FlowJo	https://www.flowjo.com
Bioplex Manager Software	BioRad	https://www.bio-rad.com/en-cn/product/bio-plex-manager-software-standard-edition?ID=5846e84e-03a7-4599-a8ae-7ba5dd2c7684
FCAP Array – Version 3.0	BD	http://www.bdbiosciences.com/us/applications/research/bead-based-immunoassays/analysis-software/fcap-array-software-v30/p/652099
R version 3.5.2	The R Foundation	https://www.r-project.org/

LEAD CONTACT AND MATERIALS AVAILABILITY

Further information and requests for resources and reagents should be directed to and will be fulfilled by the Lead Contact, Vassili Soumelis (vassili.soumelis@curie.fr). This study did not generate new unique reagents.

EXPERIMENTAL MODEL AND SUBJECT DETAILS

Human subjects

Apheresis blood from healthy human blood donors were obtained from Etablissement Français du Sang (French Blood Establishment) after written informed consent and in conformity with Institut Curie ethical guidelines. Gender identity and age from anonymous donors were not available, but all donors were between 18 and 70 years old (age limits for blood donation in France).

METHOD DETAILS

PBMCs purification

PBMCs were isolated by centrifugation on a density gradient (Lymphoprep, Proteogenix).

MoDC generation and activation

$CD14^+$ cells were selected from PBMCs using magnetically labeled anti-CD14 Microbeads and MACS LS columns following manufacturer's instructions (MiltenyiBiotec). $CD14^+$ cells were then cultured with IL-4 (50 ng/mL) and GM-CSF (10 ng/mL) (MiltenyiBiotec) for 5 days in RPMI 1640 Medium, GlutaMAX (Life Technologies) with 10% Fetal Calf Serum. Monocyte-derived Dendritic Cells (MoDC) were activated for 24 hours using one or a combination of perturbators as described in Table S1.

Blood dendritic cells purification

A step of DC pre-enrichment was performed from PBMCs using the EasySep Human Pan-DC Pre-Enrichment kit (StemCell Technologies). Total DC were sorted on a MoFloAstrios (Beckman Coulter) as Lineage (CD3, CD14, CD16, and $CD19)^-$, $CD4^+$ (Beckman Coulter), $CD11c^+$ (BD), as described in Alculumbre and Pattarini (2016).

$CD4^+$ T lymphocytes purification

Naive $CD4^+$ T lymphocytes were purified from PBMCs using the EasySep Human Naive CD4+ T Cell Isolation Kit (StemCell Technologies). Memory $CD4^+$ T cells were purified from PBMCs using the Memory $CD4^+$ T cell isolation Kit (MiltenyiBiotec).

Paired protein measurement in DC/T coculture

After 24 hours DC or MoDC activation with DC stimuli listed in Table S1, culture supernatants were kept for cytokine analysis for IL-23, IL-28α, IL-1, IL-10, IL-12p70, IL-6, TNF-α, while cells were washed in PBS. Some cells were used for for surface staining of the

following markers: B7H3, CD30L, 4-1BBL, PDL2, VISTA, CD40, CD54, CD58, ICAM-2, ICAM-3, CD18, CD29, SLAMF5, SLAMF3, PVR, CD11a, CD100, LIGHT, Nectin-2, Jagged-2, Galectin-3, CD70, CD80, CD83, OX40L, PDL1, CD86, ICOSL and HLA-DR. And the remaining cells were put in coculture with allogeneic naive CD4 T cells, at a ratio of 1 DC for 5 T cells, in X-VIVO 15 medium (Lonza). For FACS staining, a single batch of commercially available antibodies was used across the study.After 6 days of coculture, T cells were washed and live cells were counted at the microscope using trypan blue to calculate Exp Fold. T cells were reseeded at $1x10^6$/mL and restimulated with anti-CD3/CD28 Dynabeads (LifeTechnologies). 24 hours later supernatants were collected to measure the following T cell cytokines: IL-2, IL-3, IL-4, IL-5, IL-6, IL-9, IL-10, IL-13, IL-17A, IL-17F, IL-21, IL-22, IL-31, GM-CSF, IFN-γ, TNF-α, TNF-β. In each coculture experiment, one single DC donor was coupled to a different single CD4 T cell donor. For each DC/T cell pair, the measurement of DC derived signals and Th cytokines were performed in parallel, leading to the acquisition of paired data for the 36 DC derived signals and the 18 T cell parameters measured.

IL-12 blocking experiment

For IL-12 blocking experiment, after 24 hours activation with Zymosan (10μg/mL) or curdlan (10 μg/mL), MoDC were incubated during one hour at 37°C in the presence of 20 μg/mL of anti-IL-12p70 blocking antibody or its matched isotype control. Then, naive CD4 T cells were added to the culture. Antibodies were maintained for the duration of the co-culture. After 6 days of coculture cells were washed and reseeded at $1x10^6$/mL and restimulated with anti-CD3/CD28 Dynabeads (LifeTechnologies). 24 hours later supernatants were collected to measure T cell cytokines.

CD28 blocking experiment

For CD28 blocking experiment, MoDC were first activated for 24 hours with Flu (1X), LPS (100ng/mL) or Zymosan (10 μg/mL). Then, activated DC were cocultured with allogeneic naive CD4 T cells in the presence of 5 μg/mL anti-CD28 blocking antibody or its matched isotype control (Figure 5A). Antibodies were maintained for the duration of the co-culture. After 6 days of coculture cells were washed and reseeded at $1x10^6$/mL and restimulated with anti-CD3/CD28 Dynabeads (LifeTechnologies). 24 hours later supernatants were collected to measure T cell cytokines. We systematically measured all Th outputs predicted to be associated either to CD80 or CD86 (Figure 5B). Finally, we compared the estimated (*in silico* prediction) and the real (experimental) fold change (FC) (Figure 5B). A FC higher or lower than one for a given Th output indicated an inhibitory versus inducer role of CD80/CD86, respectively.

Addition of rhIL-12p70 during DC/T coculture

Sorted myeloid-DC were activated for 24 hours with zymosan (10 μg/mL) or HKSA (MOI 1). Then, 10,000 activated DC were cocultured with 50,000 allogeneic naive CD4 T cells in the presence or absence of 10 ng/mL rhIL-12p70. After 6 days of coculture, 100,000 T cells were restimulated for 24 hours with anti-CD3/CD28 Dynabeads. Supernatants were then collected for cytokine measurements.

DC-free Th cell polarization

Naive CD4 T cells were cultured for 5 days with only anti-CD3/CD28 Dynabeads (Life Technologies) to obtain Th0 or in combination with either 10 ng/mL IL-12 (Th1), 25ng/mL IL-4 (Th2), 10 ng/mL IL-1β or IL-1α, 100 ng/mL IL-23, IL-12 plus IL-1β or a mix of IL-1β, IL-23, 1 ng/mL TGF-β and 20 ng/mL IL-6 to obtain Th17 (Peprotech) as already published (Touzot et al., 2014). At the end of the culture cells were used for intracellular staining or washed, reseeded at $1x10^6$/mL and restimulated with anti-CD3/CD28 Dynabeads (Life Technologies) for 24 hours before collecting supernatants for cytokine measure and lysing cells in RLT buffer (QIAGEN) for qPCR analysis.

ICOS agonism

For experiments with anti-ICOS antibody, prior to culture 5 μg/mL anti-CD3 (OKT3 clone, Biolegend) with 5 μg/mL anti-ICOS or matching isotype control were coated on a flat-bottom 96 well plate (TPP) and incubated overnight at 4°C. The plate was then washed 3 times with PBS before seeding 32,000 naive CD4 T cells with 1 μg/mL anti-CD28 (CD28.2 clone, Biolegend) and cytokines as described above in X-vivo medium (Lonza). After 5 days culture, T cells were counted and 100,000 cells were restimulated with anti-CD3/CD28 Dynabeads for 24 hours before collecting supernatants for cytokine measure.

We were able to induce the following Th outputs in the Th0 condition: Exp Fold, IL,3, IL-5, IL-6, IL-10, IL-13, IL-22, TNF-α and GM-CSF (Figure 5E). In a Th17 condition, we were able to demonstrate a positive effect of the ICOS pathway on the production of IL-17A (Figure 5E). All these observations were statistically significant, and validated the model predictions. However, six predictions on TNF-β, IL-2, IL-21, IL-17F, IL-4 and IL-31 could not be validated using these experimental settings (Figure S4C). For IL-17F, IL-4 and IL-31 we could not detect a significant effect of ICOS (Figure S4C), suggesting possible lack of a co-factor. However, for TNF-β, IL-2, IL-21 we found significant but opposite effects to the one predicted by the model, including the positive role of ICOSL in the induction of IL-21 (Table S3).

CD2 agonism

For experiments with anti-CD2 agonist antibody, prior to culture 5 μg/mL anti-CD3 (OKT3 clone, Biolegend) with 5 μg/mL anti-CD2 or matching isotype control were coated on a flat-bottom 96 well plate (TPP) and incubated overnight at 4°C. The plate was then washed

3 times with PBS before seeding 32,000 naive CD4 T cells with 1 μg/mL anti-CD28 (CD28.2 clone, Biolegend) and cytokines as described above in X-vivo medium (Lonza). After 5 days culture, T cells were counted and 100,000 cells were restimulated with anti-CD3/CD28 Dynabeads for 24 hours before collecting supernatants for cytokine measure.

We showed that our anti-CD2 antibody worked by studying the Exp Fold of naive T cells, cultured with anti-CD3 and CD28 with or without anti-CD2. We found that anti-CD2 significantly induced T cell Exp Fold (Figure S7G).

Flow cytometry analysis

Antibodies and matched isotypes were titrated on the relevant human PBMC population. For surface FACS analysis on activated MoDC and blood DC the complete list of antibodies and important information such as brand, final dilutions, reference, clone and colors are given in Key Resources Table. Dead cells were excluded using DAPI (Miltenyi Biotec).

For intracellular cytokine staining, naive or memory CD4 T cells were stimulated with 100 ng/mL PMA, 500 ng/mL ionomycin and 3 μg/mL Brefeldin A (ThermoFisher) for 5 hours. To exclude dead cells, CD4 T cells were stained using the LIVE/DEAD Fixable yellow dead cell stain kit, following manufacturer's instructions (LifeTechnologies). Cells were fixed and permeabilized using the IC Fix and Permeabilization buffers (ThermoFisher). Intracellular cytokines were revealed with fluorescently conjugated antibodies against IL-17A (BioLegend), IL-17F (ThermoFisher), IL-21 (BioLegend), IL-22 (ThermoFisher), and IFN-γ (BD), or matched isotype controls and acquired on a Fortessa instrument (BD).

Cytokine quantification

Cytokines were quantified in dendritic cell supernatants using CBA flex set for IL-1α, IL-1β, IL-6, IL-10, TNF-α and IL-12p70 (also named IL-12) and using Luminex for IL-23 and IL-28α. Cytokines from T cell supernatants were quantified using CBA flex set for, IL-2, IL-3, IL-4, IL-5, IL-6, IL-9, IL-10, IL-13, IL-17A, IL-17F, TNF-α, IFN-γ and GM-CSF (BD) and Luminex for IL-21, IL-22, IL-31 and TNF-β following the manufacturer's protocol.

Gene expression quantification

At the end of the 5 days Th polarization and 24 hours restimulation, total RNA was extracted from 100,000 cells using RNA easy micro kit (QIAGEN). Total RNA was retrotranscribed using Superscript II Reverse Transcriptase (ThermoFisher Scientific) in combination with random primers, Oligo(dT) and dNTP (Promega). Transcripts were then quantified by real time PCR on a 480 LightCycler Instrument (Roche). Reactions were performed using a qPCR Master Mix Plus (Eurogentec) and TaqMan assays listed in the Key Resources Table. Raw expression data (ct values) were normalized on the mean of two housekeeping genes (B2M and RPL34).

Anti-human ICOS monoclonal blocking antibody

The agonist ICOS antibody was produced for research purposes from the sequence made publicly available by JOUNCE THERAPEUTICS in the patent US 2016/0304610, INC. The produced antibody corresponded to the following sequences of the clone 37A10S713 with a human IgG1 isotype.

Heavy chain: EVQLVESGGGLVQPGGSLRLSCAASGFTFSDYWMDWVRQAPGKGLVWVSNIDEDGSITEYSPFVKGRFTISRDNAKN TLYLQMNSLRAEDTAVYYCTRWGRFGFDSWGQGTLVTVSSASTKGPSVFPLAPSSKSTSGGTAALGCLVKDYFPEPVTVSWNSGALTS GVHTFPAVLQSSGLYSLSSVVTVPSSSLGTQTYICNVNHKPSNTKVDKKVEPKSCDKTHTCPPCPAPELLGGPSVFLFPPKPKDTLMISR TPEVTCVVVDVSHEDPEVKFNWYVDGVEVHNAKTKPREEQYNSTYRVVSVLTVLHQDWLNGKEYKCKVSNKALPAPIEKTISKAKGQPR EPQVYTLPPSREEMTKNQVSLTCLVKGFYPSDIAVEWESNGQPENNYKTTPPVLDSDGSFFLYSKLTVDKSRWQQGNVFSCSVMHEAL HNHYTQKSLSLSPGK

Light chain: IVMTQSPDSLAVSLGERATINCKSSQSLLSGSFNYLTWYQQKPGQPPKLLIFYASTRHTGVPDRFSGSGSGTDFTLTISS LQAEDVAVYYCHHHYNAPPTFGPGTKVDIKRTVAAPSVFIFPPSDEQLKSGTASVVCLLNNFYPREAKVQWKVDNALQSGNSQESVTEQ DSKDSTYSLSSTLTLSKADYEKHKVYACEVTHQGLSSPVTKSFNRGEC

Classical quality controls were performed to check that the produced anti-ICOS antibody had a correct, Purity (SDS-PAGE reducing), Homogeneity (SEC-MALS) Mass (LC-MS) and binding to target (FACS).

QUANTIFICATION AND STATISTICAL ANALYSIS

Dataset quality control – batch effect

As quality control of our procedure we asked whether experimental batch effect could play a role in the differences we observed across our dataset. Selecting the 6 most frequent perturbators within our MoDC dataset we performed principal component analysis to look for batch effects related to the date of the experiments or the donor variability (Figure S1C).

Dataset quality control – T cell expansion

As a control, we could see that the Exp Fold profiles of CD4 T cells matched the activation profiles of DC observed in Figure 1C. Indeed, T cells co-cultured with either LPS-MoDC, Zymosan-MoDC or Flu-DC induced significantly more expansion than the negative Medium-DC control reflecting good quality controls of the experiments (Figure 3B).

Statistical tests

In the figure legends, n is indicated and corresponds to the number of donors used for each experiment. Paired Wilcoxon or t test were applied as detailed in figure legends to compare two groups. Significance was retained for *, $p < 0.05$.

Statistical analysis

Each variable of the dataset was transformed using first the Box-Cox transformation and then a scaling step on both the mean and the variance (using TBoCo package). For all analyses performed, cytokine values inferior to 20 pg/mL were considered as 0, as 20 pg/mL corresponds to the general detection limit of the assay. In order to cluster the inputs, outputs and the samples a hierarchical clustering approach was applied by using different criterions: Ward's criterion and Pearson correlation metric were used to cluster the inputs and the outputs, while Ward's criterion and the Euclidean metric were used to cluster the samples or DC conditions. The heatmaps were generated by using the heatmap.2 package. The correlations between the continuous variables were computed by using the Pearson correlation. All statistical tests are called ''significant'' if their p value is smaller than 0.05. The p values were corrected using Benjamini-Hochberg correction.

Boxplots represented are Tukey Boxplot, meaning that the box goes from the first to the third quartile, it is cut by the median and the whisker goes from the upper (resp. the lower) whisker extends from the third (resp. the first) quartile to the largest (resp. the smallest) value no further than 1.5 * IQR from the third (resp. The first) quartile (where IQR is the inter-quartile range, or distance between the first and third quartiles). Data beyond the end of the whiskers points and are plotted individually.

The fold change represented in Figures 5B and S4A represent the value (real or estimated) of an output in the absence of CD80 and CD86 divided by the value of the output in the same sample when CD80 and CD86 are present.

Model comparison and ROC Curves

In order to test different multivariate statistical modeling strategies, and to compare them in terms of false and true positive rates, we generated a simulated dataset that mimics the features of our DC and T cell experimental data, but for which we arbitrarily attributed a link between DC communication signals and Th cytokines, the whole strategy is detailed below.

The Figure S3A aims at assessing the performance of our modeling strategy in terms of variable selection and comparing it with other variable selection methodologies. In order to do this, we performed numerical experiment: we used the real input dataset called hereafter X, simulated a random error matrix (E) with a block covariance matrix to mimic the Th subset and a matrix of coefficients (B) to mimic the effect of the inputs on the outputs. Using these three matrices we created a new output matrix $Y = XB+E$. On this new matrix Y we applied different modeling strategies. 1) The sPLS, 2) the classical Lasso, applied to each column of Y (namely each output) independently (Lasso without covariance) 3) Our methodology, called MultivarSel, (described in the Modeling strategy section), which consists in estimating the covariance matrix of E and use it to remove the dependence between the outputs before applying the Lasso methodology (Lasso empirical covariance) 4) Lasso with real covariance matrix, the same methodology than ours, but with the real covariance matrix of E, corresponding to the internal positive control of this analysis. We also assessed stability selection by adding this analysis step to the three last methods (Lasso with stability selection and without covariance, Lasso with stability selection and empirical covariance, Lasso with stability selection and real covariance matrix). For each part of this methodology, we varied the threshold to vary the number of variables that were kept and calculated for each threshold the True Positive Rate (TPR) and the False Positive Rate (FPR). The TPR is the number of variables that have been properly identified as being relevant for explaining the response divided by the total number of explanatory variables.

We also wanted to assess the sparsity: the percentage of non-zeros in the matrix B. Namely the percentage of pairs of input-output that actually interact together. To do this, we made different scenarios with high and low sparsity (0.01 and 0.3). For all of these scenarios we simulated 1000 different Y, so we performed all this methodology 1000 times each and we calculated at each time, for each methodology and for each threshold the TPR and the FPR. We then took the mean of this TPR and FPR for each methodology and for each threshold. We also assessed the importance of the stability selection.

We can see that our MultivarSel Strategy (Lasso empirical covariance) provides better results than sPLS and Lasso without covariance. Moreover, we observed that its performance is similar to Lasso with the real covariance matrix (the positive control), which means that we greatly estimated the dependence among the outputs. We also noted that the larger the sparsity level, the smaller the differences of performance between MultivarSel (Lasso empirical covariance) and Lasso without covariance, while the differences between Lasso empirical covariance and sPLS are bigger. We can see that adding the stability selection step improves a lot the results.

Modeling strategy

In order to select the most relevant inputs for modeling the outputs, we used the linear model methodology recently developed in Perrot-Dockès et al. (2018b) which has already been successfully applied to metabolomics data in Perrot-Dockès et al. (2018a). The great advantage of such an approach is to propose a Lasso-based criterion (Tibshirani, 1996) taking into account the dependence that may exist between the outputs. The parameters involved in the criterion are chosen thanks to 10-fold cross-validation and stability selection with 1000 resampling (Meinshausen and Bühlmann, 2010). The numerical experiments were performed using the real inputs dataset. Then, in order to mimic the Th groups, a random error matrix having a blockwise constant covariance matrix was generated.

The ROC curves display the True positive rate (TPR) as a function of the False positive rate (FPR) where the TPR is the number of variables that have been properly identified as being relevant for explaining the response divided by the total number of explanatory variables. The FPR is the number of variables that have been wrongly identified as being relevant for explaining the response divided by the total number of variables that do not explain the response. To look for a context dependent role of IL-12p70 in the presence of another input we performed the same methodology but instead of modeling the outputs by using only the inputs, some new variables were added: they correspond to a combination of IL-12p70 with the other inputs. More precisely, for instance, the variable "IL-12p70 with IL-1" is equal to the value of IL-12p70 for the samples having a positive concentration in IL-1 and to zero for the samples for which the concentration in IL-1 is equal to zero.

We propose the following modeling for the outputs:

$$Y = XB + E, \tag{1}$$

where $\boldsymbol{Y}$ denotes the $\boldsymbol{n}\times\boldsymbol{q}$ output matrix, $\boldsymbol{X}$ denotes the $\boldsymbol{n}\times\boldsymbol{p}$ design matrix containing the inputs, $\boldsymbol{B}$ is an unknown $\boldsymbol{p}\times\boldsymbol{q}$ coefficient matrix and $\boldsymbol{E}$ is the $\boldsymbol{n}\times\boldsymbol{q}$ random error matrix. Here, $\boldsymbol{n}$ corresponds to the number of samples, $\boldsymbol{q}$ is the number of outputs and $\boldsymbol{p}$ denotes the number of inputs. In order to take into account the potential dependence that may exist between the outputs, we shall assume that each row $\boldsymbol{i}$ of $\boldsymbol{E}$ satisfies:

$$(\boldsymbol{E}_{i,1},\ \ldots,\boldsymbol{E}_{i,q}) \sim \boldsymbol{N}(0, \boldsymbol{\Sigma_q}), \tag{2}$$

where $\boldsymbol{\Sigma_q}$ denotes the covariance matrix of the $\boldsymbol{i}$th row of the random error matrix.

In order to select the most relevant inputs for explaining the outputs, the methodology that we propose can be summarized in the following three steps:

First step

Fitting a multiple regression model to each output to have an estimation of the error matrix: $\widehat{\boldsymbol{E}}$ and computing its empirical covariance matrix.

Second step

Using this empirical covariance matrix to remove the dependence in $\boldsymbol{E}$, namely between the outputs.

Third step

Selecting among the inputs the most relevant for explaining the outputs by applying a Lasso approach to the transformed data as explained in the second step.

First step

Residuals and covariance matrix. We obtained an ordinary least square (OLS) estimator of $\boldsymbol{B}$ by fitting a multiple regression model which is not a variable selection method. More precisely, the corresponding estimator $\widehat{\boldsymbol{B}}^{\boldsymbol{OLS}}$ is defined by

$$\widehat{B}^{OLS} = Arg\min_{\mathbf{B}}\left\{\|Y - XB\|_2^2\right\}$$

Using $\widehat{\boldsymbol{B}}^{\boldsymbol{OLS}}$ we got an estimation of $\boldsymbol{E}$: $\widehat{\boldsymbol{E}} = \boldsymbol{Y} - \boldsymbol{X}\widehat{\boldsymbol{B}}^{\boldsymbol{OLS}}$. Then, we computed the empirical covariance matrix $\widehat{\boldsymbol{\Sigma}}_{\boldsymbol{q}}$ of $\widehat{\boldsymbol{E}}$.

Second step

Transformation. Let us recall that the standard Lasso criterion, proposed by Tibshirani (1996) estimates $\boldsymbol{B}$ in the following univariate linear model:

$$\boldsymbol{Y} = \boldsymbol{XB} + \boldsymbol{E}, \tag{3}$$

by

$$\widehat{B}(\lambda) = Argmin_B\left\{\|Y - XB\|_2^2 + \lambda\|B\|_1\right\}, \tag{4}$$

where $\boldsymbol{Y}$, $\boldsymbol{B}$ and $\boldsymbol{E}$ are vectors. Usually, the components of $\boldsymbol{E}$ are assumed to be independent.

Thus, we proposed to transform Model (1) to be able to use the Lasso criterion as follows. First, we removed the dependence among the outputs:

$$Y\widehat{\Sigma}_q^{-1/2} = XB\widehat{\Sigma}_q^{-1/2} + E\widehat{\Sigma}_q^{-1/2}, \tag{5}$$

where $\widehat{\boldsymbol{\Sigma}}_{\boldsymbol{q}}^{-1/2}$ denotes the inverse of the square root of $\boldsymbol{\Sigma_q}$.

Then, we applied the ***vec*** operator which consists in stacking the columns of a matrix into a single column vector.

$$\begin{aligned} Y &= vec\left(Y\widehat{\Sigma}_q^{-1/2}\right) = vec\left(XB\widehat{\Sigma}_q^{-1/2}\right) + vec\left(E\widehat{\Sigma}_q^{-1/2}\right) \\ &= vec\left(\left(\widehat{\Sigma}_q^{-1/2}\right)' \otimes X\right)vec(B) + vec\left(E\widehat{\Sigma}_q^{-1/2}\right) \\ &= Xb + \varepsilon. \end{aligned}$$

Third step: Variable selection

Thanks to the previous transformation, the Lasso criterion can be applied to $\boldsymbol{y} = \boldsymbol{vec}(\boldsymbol{Y}\widehat{\Sigma}_{\boldsymbol{q}}^{-1/2})$. Since $\boldsymbol{B} = \mathbf{vec}(\mathbf{B})$, estimating the coefficient of $\boldsymbol{B}$ boils down to estimating the coefficients of $\boldsymbol{B}$. The parameter λ in (4) is chosen by 10-fold cross-validation followed by a stability selection step with 1000 resamplings, as proposed by Meinshausen and Bühlmann (2010).

The squared error of prediction of the different models were assessed using 10-fold cross-validation (Figures 4A, 6B, S3D, S3E, and S5A).

Systematic literature review

To assess the literature and evaluate the generated multivariate model of Figure 4B, we conducted a systematic literature review to identify articles indexed on the PubMed database by March 1st 2017, examining the effects of inputs on naive CD4+ cells.

One of three different search strategies was used to export references from the PubMed database into the reference management software EndNote.

We started by performing the first search strategy which consisted of using free text to search English language articles for the input (or any of its aliases) and the output (or any of its aliases). If the search yielded 20 or less results, the references were exported into EndNote.

If not, then we performed the second search strategy, which consisted of searching English language articles for the input (or any of its aliases) and the output (or any of its aliases), both in the title or abstract, and at least one of the following medical subject heading terms: ''cell differentiation'' or ''CD4-positive T-lymphocytes'' or ''lymphocyte activation». If the search returned 50 or less results, the references were exported into EndNote. If not, then we carried out the third search strategy which returned English language articles that had both the input (or any of its aliases) and the output (or any of its aliases) in the title or abstract, as well as indexes to both of the following medical subject heading terms: ''cell differentiation'' and ''CD4-positive T-lymphocytes.'' Results were exported into EndNote.

The electronic searches generated a total of 14,748 references that were managed through EndNote. A manual search of references from review articles and other records identified 21 additional publications that were not included in the search results. Of these 14,769 articles, 9,780 duplicates were removed, leaving 4,989 records to be screened.

Titles and abstracts were screened by 2 independent reviewers. Publications were selected for further in-depth consideration if they met all of the following inclusion criteria: 1) Journal Article, 2) Examining the effect of one input at a time, 3) Testing on naive $CD4^+$ T cells, which were defined as $CD4^+$ and $CD45RA^+$ and/or $CD45RO^-$ and/or $CD25^-$ cells. Studies were excluded from the analysis if: 1) Full-text article, Title and/or abstract were not available, 2) Methods and/or experiments and/or results were unclear or inconclusive or of low quality. Reasons for removing articles included not performing proper experimental controls, insufficient information, lack of replicates and/or statistical analysis.

The reviewers excluded 4,589 articles because they did not meet the inclusion and exclusion criteria, leaving 400 articles of which, at least, the figures and materials and methods sections were examined. Finally, 178 publications met all the inclusion criteria and underwent data extraction.

Extracted information included the PubMed identifier, the input, the output, the input's effect on naive $CD4^+$ T cells in regards to the output, the experimental context and setup (e.g., details about T cell stimulation context, input's concentration, duration…) and the organism. Data were cross-checked by the 2 reviewers, and any ambiguities were discussed and resolved through a consensus.

The Exp Fold was not included in the literature review so it was not included in the following literature validation score.

Calculation of the literature validation score: an association predicted by our model (Figure 4B) between an input and an output was considered as ''new'' if none of the 178 publications found that the input induces or inhibits the output. Absence of effect depicted in some articles was not considered relevant to assess novelty of the prediction. It was ''validated'' if at least one of the 178 publications found similar results than our model and ''contradictory'' if none of the study found the same results than our model but at least one found an opposite result. Opposite result would be an induction if the model predicted a negative coefficient or an inhibition if our model predicted a positive coefficient.

DATA AND CODE AVAILABILITY

The dataset generated during this study is available in Table S2.

All references from literature mining are listed in Table S3.

Software used for flow cytometry data analysis was FlowJo software (TreeStar).

Software used for CBA analysis was FCAP Array v3.

Software used for statistical analysis was Prism software v5 (GraphPad).

Software used for statistical analysis and modeling was R version 3.5.2.

The R packages used to perform this study are: package MultiVarSel 1.0. used for modeling (available at https://cran.r-project.org/web/packages/MultiVarSel/index.html) and package TBoCo 0.0.1 for boxcox transformation available at https://github.com/Marie-PerrotDockes/TBoCo.

This study did not generate code.

Cell

A

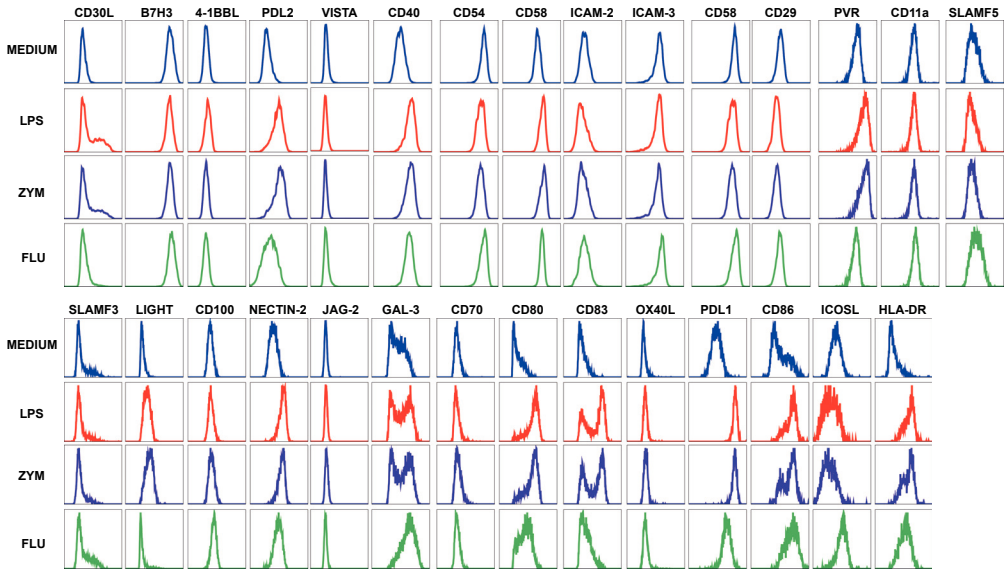

B

Comparison with Zymosan (10µg/mL)

	IL-23	IL-10	CD54	PVR
Medium	0.000	0.000	0.000	0.000
LPS (100ng/mL)	0.000	0.000	0.044	0.003
Flu (1X)	0.000	0.000	0.000	0.000

Comparison with LPS (100ng/mL)

	IL-12p70	CD83	CD30L
Medium	<0.001	<0.001	0.005
Zymosan (10µg/mL)	0.432	0.002	0.008
Flu (1X)	<0.001	0.002	0.002

Comparison with Flu (1X)

	IL-28α	ICOSL	CD18	CD100
Medium	<0.001	<0.001	<0.001	<0.001
LPS (100ng/mL)	<0.001	0.005	<0.001	0.017
Zymosan (10µg/mL)	<0.001	0.003	<0.001	0.017

Comparison with Medium

	CD86	CD80	HLA-DR
Zymosan (10µg/mL)	<0.001	<0.001	<0.001
LPS (100ng/mL)	<0.001	<0.001	<0.001
Flu (1X)	<0.001	<0.001	<0.001

C

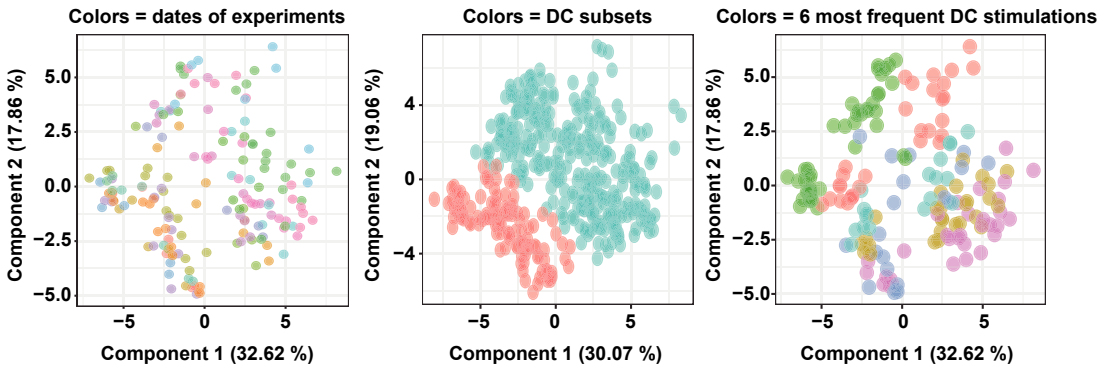

Figure S1. Descriptive Analysis of 36 DC-Derived Communication Molecules, Related to Figures 1 and 2

A) Example of raw FACS staining of MoDC communication molecules after 24 hours stimulation with Medium, LPS, Zymosan or Flu. 29 surface markers measured of one representative donor are shown. B) Statistical analysis comparing a given DC stimulation to the other 3 for each signal annotated. P values are annotated in the table, red should be considered as significant. Paired Wilcoxon test was used (n = 14). C) PCA performed either on the whole dataset (left and middle panel) or on the 6 most frequent perturbators (right panel) used across MoDC and bDC stimulations. From left to right colors respectively indicates, the dates of experiments, the DC subset, the 6 most frequent DC stimulations.

A

Input	Range (log)	% of positive observations	Coefficient of variation
IL-21	4.00	86.45	1.89
IL-10	4.00	97.43	1.78
IL-17F	4.00	75.23	1.75
IL-9	4.00	94.39	1.67
IL-5	4.00	99.53	1.07
IL-4	4.00	98.83	1.06
IL-13	4.00	97.66	0.92
IL-17A	3.00	83.18	1.77
IL-6	3.00	98.83	1.28
IFN-γ	3.00	97.20	1.08
IL-3	3.00	99.77	1.05
TNF-α	3.00	99.77	0.86
GM-CSF	3.00	100.00	0.72
IL-31	2.00	21.03	1.54
TNF-β	2.00	98.83	1.08
IL-22	2.00	57.94	0.98
IL-2	2.00	99.77	0.68
Expansion-fold	1.00	100.00	0.61

B

Comparison with Medium

	IL-2
Zymosan (10µg/mL)	0,7439
LPS (100ng/mL)	0,0535
Flu (1X)	0,0579

Comparison with Zymosan (10µg/mL)

	Expansion fold	IL-17A	IL-17F	IL-21
Medium	<0,001	<0,001	<0,001	0,0054
LPS (100ng/mL)	0,3007	0,0013	0,0127	0,1983
Flu (1X)	0,0093	<0,001	<0,001	1

Comparison with LPS (100ng/mL)

	IL-3	IL-9	IL-6	IFN-γ
Medium	0,0003	<0,001	0,2698	0,0858
Zymosan (10µg/mL)	0,082	0,5334	0,9814	0,1154
Flu (1X)	0,281	0,0072	0,1136	0,1279

	TNF-α	IL-22	IL-13	GM-CSF	TNF-β
Medium	0,3724	0,0579	0,0417	0,0008	0,1565
Zymosan (10µg/mL)	0,1823	0,2772	0,0019	<0,001	0,8342
Flu (1X)	0,1606	0,0188	0,4856	0,8391	0,0015

Comparison with Flu (1X)

	IL-4	IL-5	IL-10	IL-31
Medium	0,0584	0,0403	0,1287	0,0056
LPS (100ng/mL)	0,9769	0,504	0,1755	0,9149
Zymosan (10µg/mL)	0,0053	0,0003	0,2841	0,3998

C

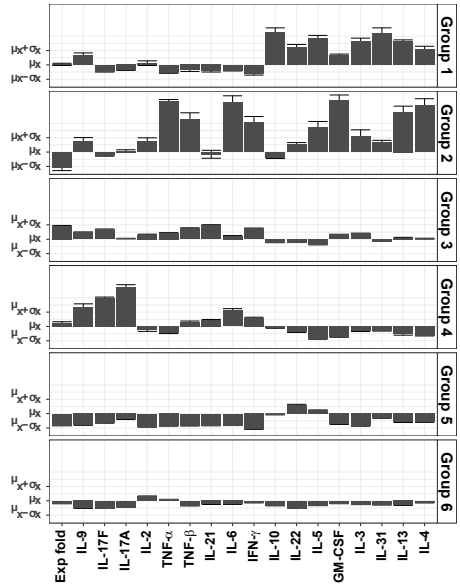

Figure S2. Mathematical Description and Statistical Analysis of Th Cytokine Profiles, Related to Figure 3

A) Table showing three key mathematical parameters of the Exp Fold and the 17 Th derived cytokines. First column: the range of expression (the number of log on which the data are expressed). Second column: the percentage of positive observations among the 428 datapoints. Third column: the coefficient of variation. Communication molecules were ranked based on their range of expression and their coefficient of variation. B) Statistical analysis comparing selected Th cytokines within the following groups: Medium-MoDC, LPS-MoDC, Zymosan-MoDC and Flu-MoDC. The statistical test used is paired Wilcoxon test on n = 14 donors. C) Expression profiles of the Exp Fold and the 17 Th derived cytokines within the six groups of DC conditions defined by hierarchical clustering. Expression data were logged transformed and scaled so as μ represents the mean and σ the SD of the expression of a given communication molecule across the whole dataset (n = 428).

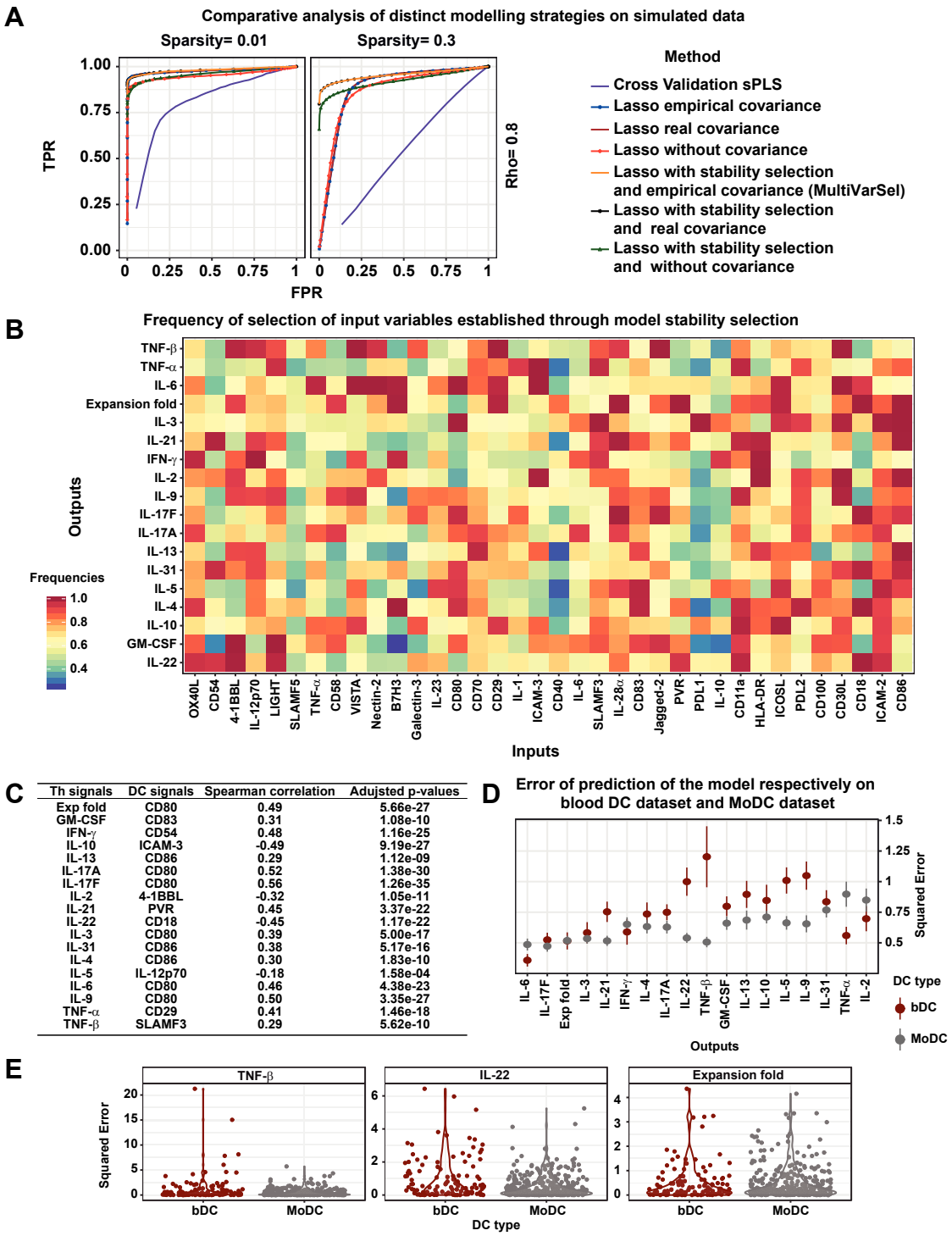

Figure S3. Multivariate Modeling Strategies Applied to Our DC-T Cell Datasets, Related to Figure 4

A) Comparative analysis of distinct modeling strategies on simulated data. Using ROC curves, we applied the annotated strategies in terms of true and false discovery. The simulated dataset mimics the features of our DC and T cell experimental data but for which we artificially attributed a link between DC signals and Th cytokines. This allowed us to compare four different types of modeling strategies (Raw, OR, MultivarSel and sPLS) and different variable selection methods (Lasso, Stability Selection and CV) by analyzing their false and true positive rates. B) Frequency of selection of input variables established through model stability selection. Stability selection was applied after our MultivarSel strategy to the full DC-T dataset (n = 428). C) Table

(legend continued on next page)

showing for each output (Th signals) the input that minimizes its mean squared error of prediction in an univariate model, with its spearman correlation coefficient and its adjusted p value. D) Error of prediction (obtained by 10-fold cross-validation) of the model respectively on blood DC dataset (n = 118) and MoDC dataset (n = 310) E) Example of distribution of the squared error of prediction per DC-type for IL-22, TNF-β and Exp Fold. Allows to see the number of data points with the highest error of prediction.

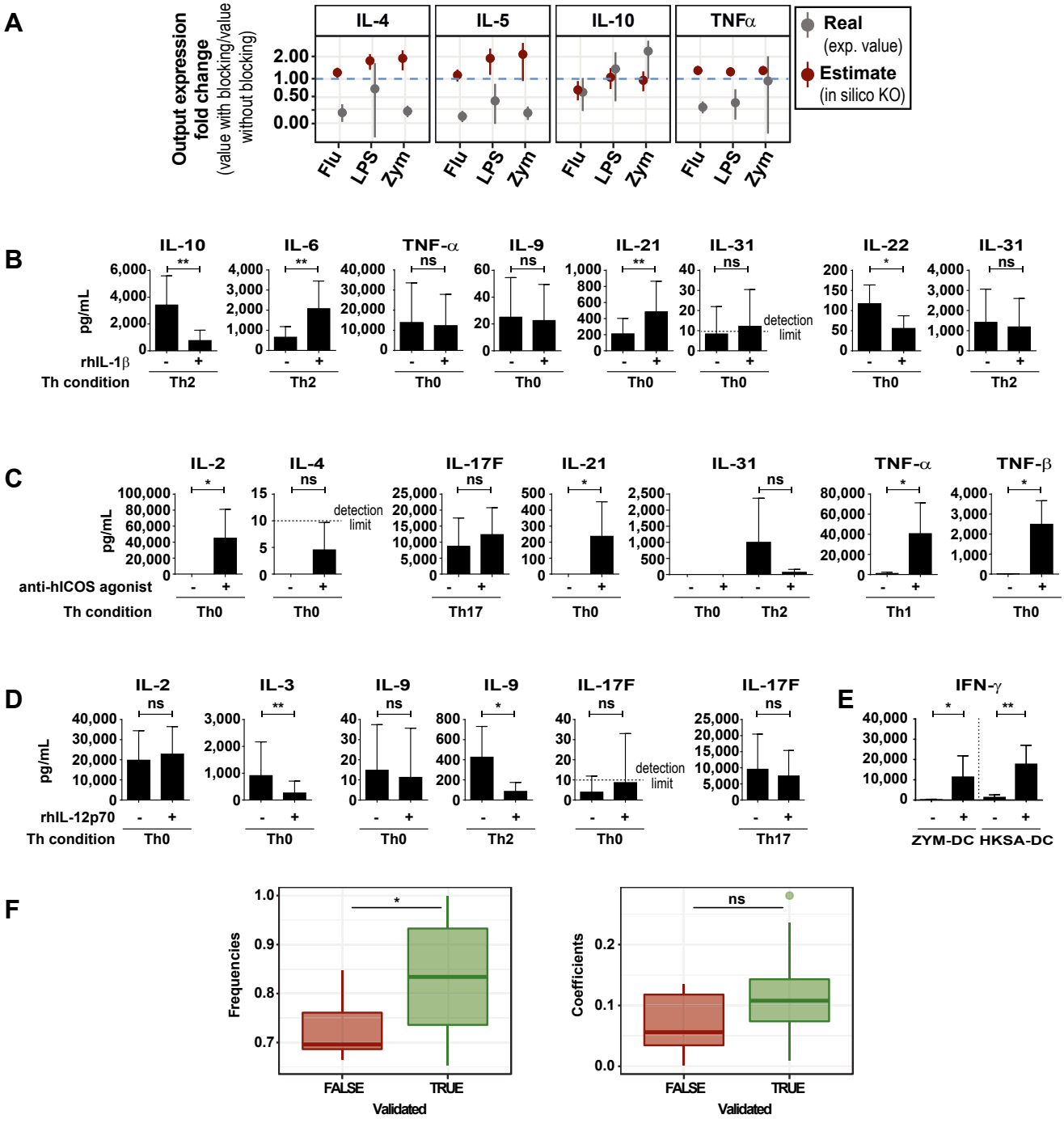

Figure S4. Complementary Th Secretion Profiles of the Tested Conditions for Systematic Model Validation, Related to Figure 5

A) Fold change of the cytokine concentration estimated versus experimentally measured for the four indicated cytokines. n = 6 independent donors B) Mean cytokine concentration and SD indicated for each condition. n = 6 C) Mean cytokine concentration and SD indicated for each condition. n = 6 D) and E) Mean cytokine concentration and SD indicated for each condition. n = 6 F) Boxplot of the coefficient and stability selection frequencies in the two conditions: True (validated predictions) and False (not validated), Wilcoxon test. Performed only for IL-12, IL-1 and ICOSL validations.

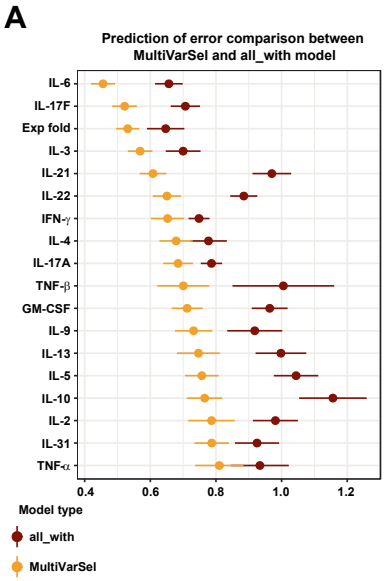

B

Intputs	Number	Number alone	Number with	Percentage
CD70	638	580	58	0.09
CD11a	673	611	62	0.09
ICOSL	609	551	58	0.10
OX40L	622	562	60	0.10
IL-28α	607	545	62	0.10
CD83	539	482	57	0.11
LIGHT	607	534	73	0.12
CD30L	606	533	73	0.12
ICAM-2	684	601	83	0.12
IL-23	389	339	50	0.13
Jagged-2	484	420	64	0.13
CD100	452	392	60	0.13
4-1BBL	482	418	64	0.13
VISTA	433	374	59	0.14
PDL2	493	420	73	0.15
IL-12p70	582	494	88	0.15
PVR	360	304	56	0.16
SLAMF3	515	433	82	0.16
TNF-α	416	346	70	0.17
CD86	569	471	98	0.17
CD80	440	362	78	0.18
HLA-DR	505	411	94	0.19
Nectin-2	316	254	62	0.20
IL-1	384	301	83	0.22
CD58	383	289	94	0.25
CD18	415	311	104	0.25
CD29	453	335	118	0.26
CD54	238	175	63	0.26
CD40	251	182	69	0.27
ICAM-3	454	325	129	0.28
IL-6	295	210	85	0.29
B7H3	432	307	125	0.29
Galectin-3	333	220	113	0.34
IL-10	241	159	82	0.34
PDL1	207	121	86	0.42
SLAFM5	217	72	145	0.67

C

Outputs	Number	Number alone	Number with	Percentage
IL-2	926	806	120	0.13
IL-4	932	802	130	0.14
IL-6	1013	865	148	0.15
IL-3	912	777	135	0.15
IL-13	741	631	110	0.15
GM-CSF	920	780	140	0.15
TNF-β	838	710	128	0.15
IL-10	1103	901	202	0.18
TNF-α	607	495	112	0.18
IL-17A	947	772	175	0.18
IL-17F	1030	839	191	0.19
IL-31	1088	884	204	0.19
IL-21	848	677	171	0.20
IL-9	955	762	193	0.20
Exp fold	1041	828	213	0.20
IL-5	773	613	160	0.21
IL-22	968	767	201	0.21
IFN-γ	682	535	147	0.22

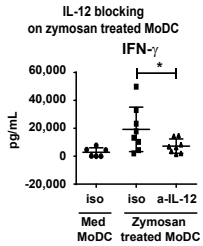

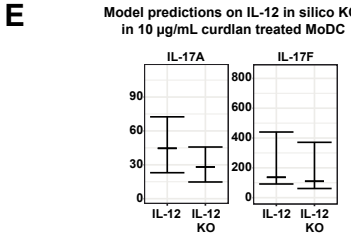

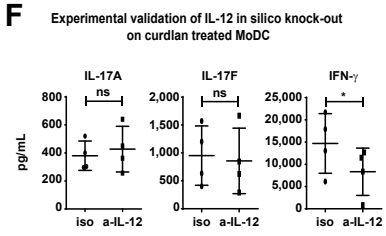

Figure S5. Quantification of Context-Dependent Input-Output Associations, Related to Figure 6

A) Prediction of error comparison between MultiVarSel and "all_with model" performed for each Th output. B) Quantification per input of the number of times it is selected as associated to an output in the 36 context-dependent models (Table S5). The total number of associations (resp. the number associations of the input alone, resp. the input with another) is represented in the column 'Number' (resp. Number alone, resp. Number with) the ratio (Number with / Number) is represented in the column 'Percentage' C) Same as panel B but per output instead of input. D) On 8 distinct donors of coculture MoDC/naive CD4 T cells experiments IL-12 was blocked using neutralizing antibody. After the coculture at day 6, Th cells were restimulated 24 hours at 1 million cells/mL and the amount of IFN-γ was determined using CBA. Paired Student's t test was applied to compare two conditions. E) Model predictions on IL-12 *in silico* KO in the condition MoDC-curdlan (10 µg/mL) for IL-17A and IL-17F values. Real values in the presence of IL-12 are compared to predicted values obtained in the absence of IL-12. F) Concentrations of IL-17A, IL-17F and IFN-γ produced by Th cells after coculture with MoDC treated with 10 µg/mL curdlan, in the presence of neutralizing antibody specific for IL-12 or matching isotype. n = 4 donors. Paired t test was performed to compare the means.

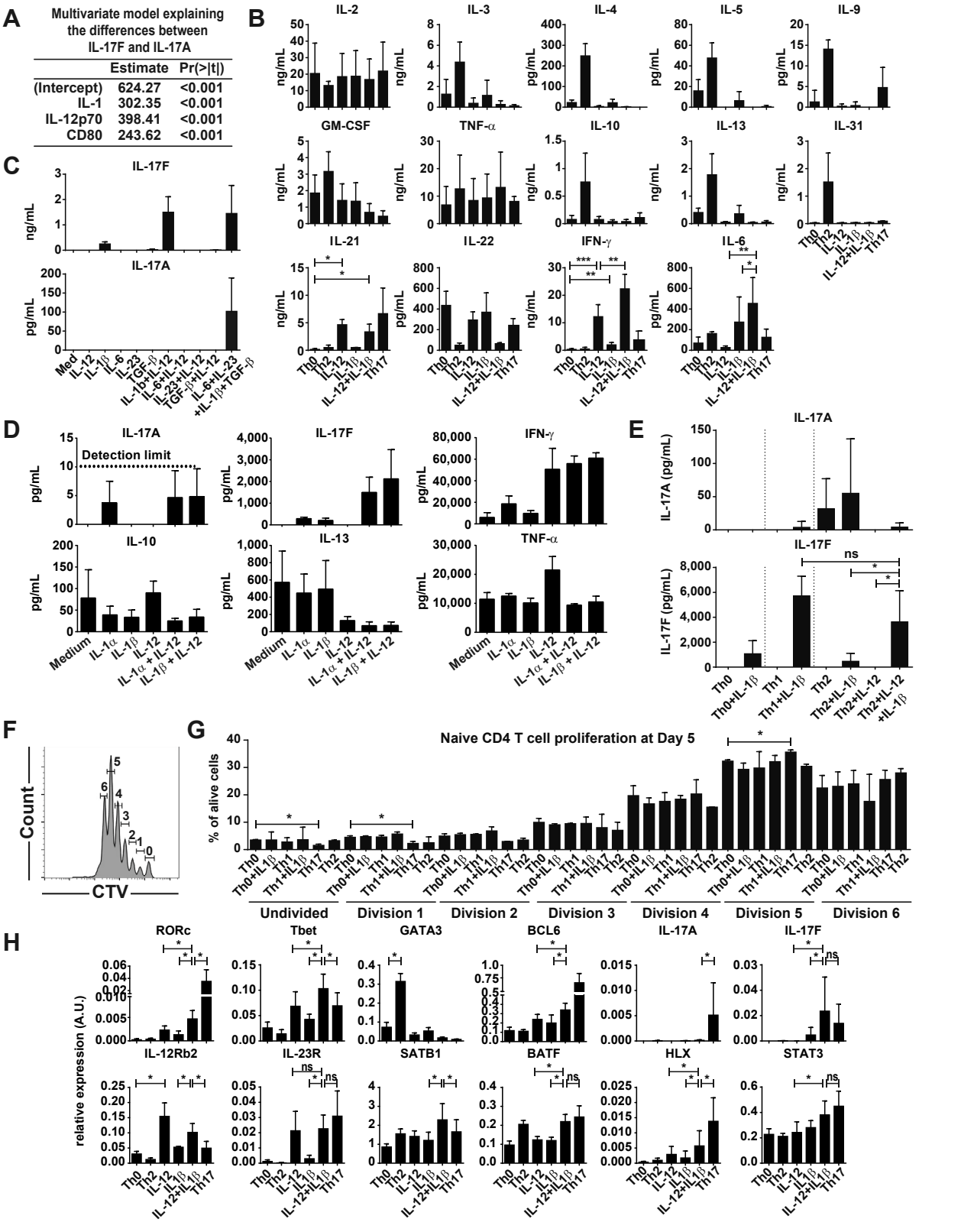

(legend on next page)

Figure S6. In-Depth Characterization of Th Cells Polarized under the IL-1+IL-12 Condition, Related to Figure 7

A) Multivariate model explaining the differences between IL-17F and IL-17A for a stability selection threshold of 0.8. B) Cytokine profiles of Th cells differentiated in distinct cytokine condition: Th0 (medium), Th2 (IL-4), IL-12, IL-1 (IL-1β), IL-12+IL-1 and Th17 (IL-6+IL-1β+TGF-β+IL-23), measured by CBA on 6 donors. Paired Student's t test was used for statistical analysis. C) IL-17A and IL-17F were measured by CBA in the supernatants of Th cells differentiated in distinct cytokine condition: Med, IL-12, IL-1β, IL-6, IL-23, TGF-β, IL-12+IL-1β, IL-6+IL-12, IL-23+IL-12, TGF-β+IL-12, IL-6+IL-23+IL-1β+TGF-β. This experiment was performed on 3 donors. D) Comparison in the same naive CD4 DC-free culture system of the effect of IL-1α and IL-1β on the production of six distinct cytokines: IFN-γ, IL-17A, IL-17F, TNF-α, IL-13, IL-10. This experiment was performed on 3 donors. E) DC-free differentiation assay performed using anti CD3/CD28 beads in the indicated cytokine conditions. n = 6, Wilcoxon test was used for statistics. F) Example of FACS CTV staining for Th proliferation assessment at day 5. G) Quantification of the % of alive cells in each peak of the CTV staining for each condition. n = 3, paired t test was performed H) qPCR expression profiles for selected genes in the following conditions Th0, Th2, IL-12, IL-1β, IL-12+IL-1β, Th17 (IL-6+IL-23+IL-1β+TGF-β). n = 6. Wilcoxon test was used.

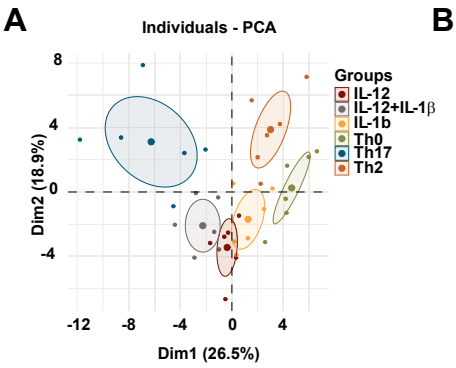

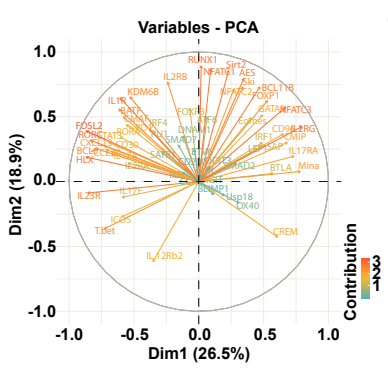

C

Inputs	Number	Correlation of IL-12 with IL-17A	p-value
IL-1	166	0.41	3.51e-08
CD70	120	0.41	3.09e-06
OX40L	181	0.39	6.44e-08
IL-6	226	0.37	1.22e-08
IL-10	207	0.36	9.06e-08
IL-23	234	0.36	1.51e-08
ICAM-2	149	0.36	7.86e-06
LIGHT	119	0.33	2.02e-04
Jagged-2	194	0.33	2.11e-06
TNF-α	205	0.31	6.30e-06
CD30L	183	0.28	9.24e-05
IL-28α	22	-0.24	2.84e-01

D

Group	Correlation of IL-12 with IL-17A	p-value
IL-23 & IL-1	0.41	3.51e-08
IL-23 & no IL-1	-0.01	9.52e-01
no IL-23 & IL-1	-0.37	2.90e-01
no IL-23 & no IL-1	-0.16	3.02e-02

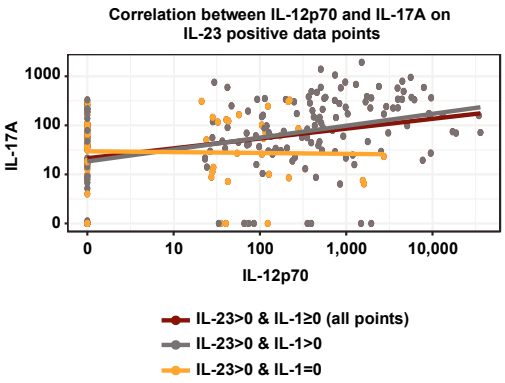

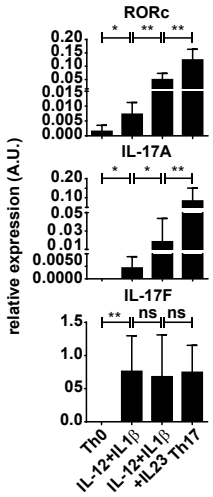

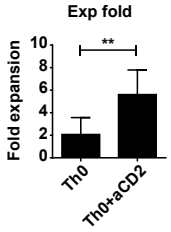

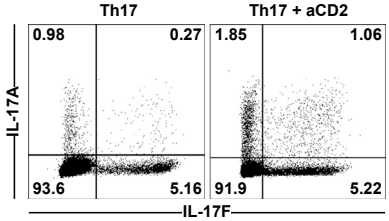

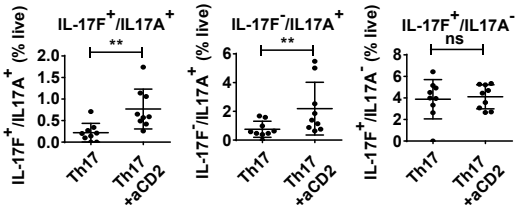

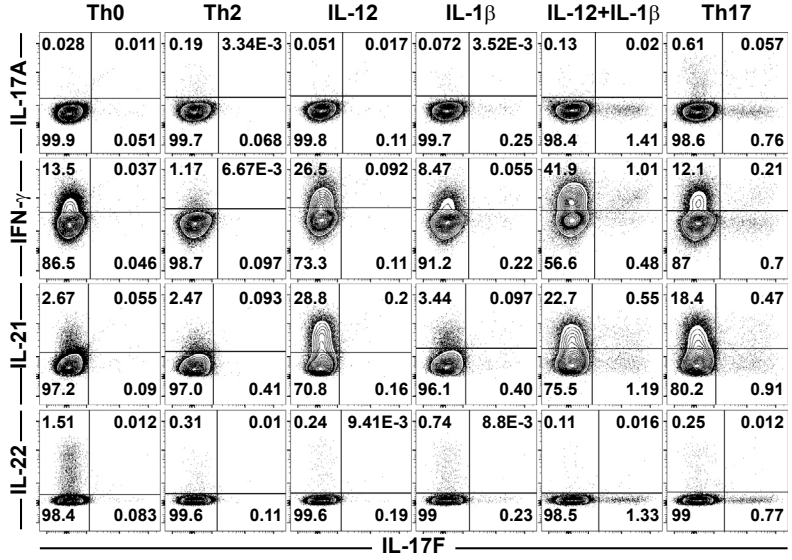

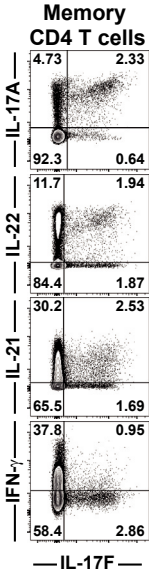

(legend on next page)

Figure S7. Detailed Description of Distinct Experimentally Validated Predictions,

A) PCA using 63 genes measured by qPCR in the 6 indicated Th conditions B) Detailed descriptions of the contribution of each 63 genes to the two first dimensions of the PCA represented in A). C) Systematic univariate analysis evaluating the Pearson correlation between IL-17A and IL-12 in the presence of IL-23 and another input (listed in the column 'Inputs') the number of samples having both of these inputs is in column 'Number'. D) Pearson correlation between IL-17A and IL-12 in the presence or absence of IL-1 and IL-23. E) Dot plot representing the correlation between IL-12 and IL-17A on IL-23 positive data points. F) qPCR measuring RORc, IL-17A and IL-17F in the indicated conditions. n = 6 independent donors. Wilcoxon test was used for statistical analysis G) Positive control showing the validation of the anti-CD2 agonist antibody through the measure of Exp Fold in the Th0 condition n = 8 H) Representative intracellular cytokine staining for IL-17A and IL-17F performed in the Th17 and Th17+anti-CD2 conditions. I) Quantification of the intracellular FACS staining performed in H) for 8 distinct donors. Wilcoxon analysis. J) Representative raw data staining of intracellular FACS for IFN-γ, IL-21, IL-22, IL-17A and IL-17F in 6 distinct conditions, Th0 (medium), Th2 (IL-4), IL-12, IL-1 (IL-1β), IL-12+IL-1 and Th17 (IL-6+IL-1β+TGF-β+IL-23) for naive CD4 culture. K) Representative raw data staining of intracellular FACS for IFN-γ, IL-21, IL-22, IL-17A and IL-17F for memory CD4 purified cells, previously isolated by magnetic sorting, and restimulated 5 hours with PMA/ionomycin.

DC Condition	Perturbators	Frequency
C1	Flu (1X) + PAM3 (1µg/mL)*MoDC	3
C2	Alum (200µg/mL) + Flu (1X)*MoDC	3
C3	Flu (1X) + HKSA (MOI 1)*MoDC	3
C4	Flu (1X) + HKCA (MOI1)*MoDC	3
C5	Flu (1X) + HKLM (MOI 1)*MoDC	3
C6	PolyIC (100µg/mL)*MoDC	2
C7	HKLM (MOI 10)*MoDC	2
C8	HKCA (MOI100)*MoDC	2
C9	GMCSF (100ng/mL)*MoDC	2
C10	Curdlan (20µg/mL)*MoDC	2
C11	Alum (200µg/mL)*MoDC	3
C12	PolyIC (50ng/mL)*MoDC	5
C13	Flu (0,1X)*MoDC	4
C14	Flu (1X)*MoDC	17
C15	Flu (0,5X)*MoDC	4
C16	PAM3 (0,1µg/mL)*MoDC	4
C17	HKSA (MOI 1)*MoDC	9
C18	PAM3 (1µg/mL)*MoDC	9
C19	Zymosan (0,1µg/mL)*MoDC	4
C20	LPS (1ng/mL)*MoDC	4
C21	Zymosan (1µg/mL) + PGE2 (1 µg/mL)*MoDC	2
C22	Zymosan (0,1µg/mL) + PGE2 (0,1µg/mL)*MoDC	2
C23	PGE2 (1 µg/mL)*MoDC	4
C24	PGE2 (0,1 µg/mL)*MoDC	2
C25	HKSA (MOI 0,1)*MoDC	4
C26	HKCA (MOI 10)*MoDC	4
C27	PGE2 (10 µg/mL)*MoDC	4
C28	R848 (10ng/mL)*MoDC	2
C29	R848 (100 ng/mL)*MoDC	2
C30	IFNb (50ng/mL)*MoDC	2
C31	GMCSF (50ng/mL)*MoDC	3
C32	HKLM (MOI 1)*MoDC	7
C33	HKCA (MOI1)*MoDC	9
C34	Med*MoDC	24
C35	HKSP (MOI1)*MoDC	3
C36	HKSA (MOI 20) + HKCA (MOI 10)*MoDC	2
C37	HKSA (MOI 1) + HKCA (MOI 1)*MoDC	2
C38	HKSA (MOI 0,1) + HKCA (MOI 0,1)*MoDC	2
C39	HKCA (MOI0,1)*MoDC	2
C40	TSLP (50ng/mL)*bDC	12
C41	PAM3 (1µg/mL)*bDC	2
C42	Curdlan (10µg/mL)*bDC	7
C43	Flu (1X)*bDC	13
C44	Med*bDC	20
C45	HKCA (MOI1)*bDC	4
C46	PAM3 (10µg/mL)*bDC	8
C47	LPS (100ng/mL)*bDC	8

C48	HKLM (MOI 1)*bDC	8
C49	GMCSF (50ng/mL)*bDC	6
C50	PolyIC (50µg/mL)*bDC	4
C51	Zymosan (10µg/mL)*bDC	8
C52	HKLM (MOI 100) *bDC	1
C53	HKSA (MOI 10)*bDC	1
C54	R848 (1µg/mL)*bDC	10
C55	HKSA (MOI 1)*bDC	6
C56	Zymosan (10µg/mL) + PGE2 (10µg/mL)*MoDC	4
C57	Curdlan (10µg/mL)*MoDC	7
C58	LPS (10ng/mL) + R848 (10ng/mL) *MoDC	2
C59	LPS (10ng/mL)*MoDC	4
C60	Zymosan (1µg/mL)*MoDC	4
C61	R848 (1µg/mL)*MoDC	10
C62	PAM3 (10µg/mL)*MoDC	10
C63	LPS (100ng/mL)*MoDC	21
C64	PAM3 (1µg/mL) + R848 (1µg/mL)*MoDC	3
C65	HKSA (MOI 20) + PAM3 (1µg/mL)*MoDC	3
C66	HKSA (MOI 20)*MoDC	7
C67	LPS (100ng/mL) + PAM3 (1µg/mL)*MoDC	3
C68	HKSA (MOI 20) + R848 (1µg/mL)*MoDC	3
C69	LPS (100ng/mL) + R848 (100 ng/mL)*MoDC	2
C70	LPS (1000ng/mL)*MoDC	4
C71	LPS (1000ng/mL) + R848 (1000ng/mL)*MoDC	2
C72	Flu (1X)+ PAM3 (10µg/mL)*MoDC	2
C73	Flu (0,5X) + PAM3 (1µg/mL)*MoDC	2
C74	Flu (0,1X) + PAM3 (0,1µg/mL)*MoDC	2
C75	Zymosan (20µg/mL)*MoDC	4
C76	Zymosan (10µg/mL)*MoDC	23
C77	LPS (100ng/mL) + R848 (1µg/mL)*MoDC	3
C78	Zymosan (10µg/mL) + PAM3 (1µg/mL)*MoDC	3
C79	Zymosan (10µg/mL) + HKSA (MOI 20)*MoDC	3
C80	LPS (100ng/mL) + Zymosan (10µg/mL) *MoDC	3
C81	LPS (100ng/mL) + HKSA (MOI 20)*MoDC	3
C82	Zymosan (10µg/mL) + R848 (1µg/mL)*MoDC	3

Table S1 Related to Figure 1: Number of data point generated per stimulation per DC subset: This table recapitulates the number of distinct data points corresponding to the biological replicates (column Frequency) generated for each DC stimulation on bDC or MoDC.

2. Appendix 2

Th diversity and response to dupilumab in patients with atopic dermatitis

Coline Trichot, Lilith Faucheux, Léa Karpf, Maximilien Grandclaudon, Lucia Pattarini, Thibault Mahévas, Marie Jachiet, Anne Saussine, Jean-David Bouaziz and Vassili Soumelis

Accepted in J. Allergy Clin. Immunol. Online ahead of print.

Letter to the Editor

T_H cell diversity and response to dupilumab in patients with atopic dermatitis

To the Editor:

We report here on a systematic assessment of T_H cell subsets and their dynamic changes in the context of dupilumab treatment, a recently approved biotherapy in atopic dermatitis (AD).

Dupilumab targets the IL-4 receptor α-chain that is common to the IL-4 and IL-13 receptors. Although the IL-4 pathway is critical for T_H2 differentiation, it may also affect other T_H pathways directly or through cross-regulation.

In this study, we used multicolor flow cytometry to measure the evolution of 8 T_H and follicular helper (T_{FH}) cell populations in the peripheral blood of patients with chronic AD before and after dupilumab, with or without concomitant treatment (as detailed in Table E1 in this article's Online Repository at www.jacionline.org). Samples were obtained from 29 patients with moderate-to-severe AD at different time points from therapy (month 0 [M0] [ie, baseline], M1, M3, M6, and ≥M12) as well as from 25 age- and sex-matched healthy subjects (see Table E2 in this article's Online Repository at www.jacionline.org). By using a validated 5-parameter surface staining[1] (see Fig E1 in this article's Online Repository at www.jacionline.org), we measured the proportions of all 8 major memory T_H and T_{FH} cell populations: T_H1, T_H2, T_H17, $T_H1/17$, $T_{FH}1$, $T_{FH}2$, $T_{FH}17$, and $T_{FH}1/17$. Patients with AD at baseline (M0) had percentages of $CXCR5^-$ (total T_H) and $CXCR5^+$ (total T_{FH}) CD4 T cells similar to those in healthy donors (HDs), with no significant variations during the course of dupilumab treatment (see Fig E2, *A* in this article's Online Repository at www.jacionline.org), supporting the importance of a detailed analysis.

Addressing the T_{FH} cell populations, $T_{FH}1$, $T_{FH}2$, and $T_{FH}1/17$ percentages were not significantly different between patients with AD at M0 and HDs, but the percentages of $T_{FH}17$ cells were lower in patients with AD than in HDs. Additionally, we did not detect any significant variation in the $T_{FH}2$, $T_{FH}17$, and $T_{FH}1/17$ cell percentages during dupilumab treatment. Only the $T_{FH}1$ cell

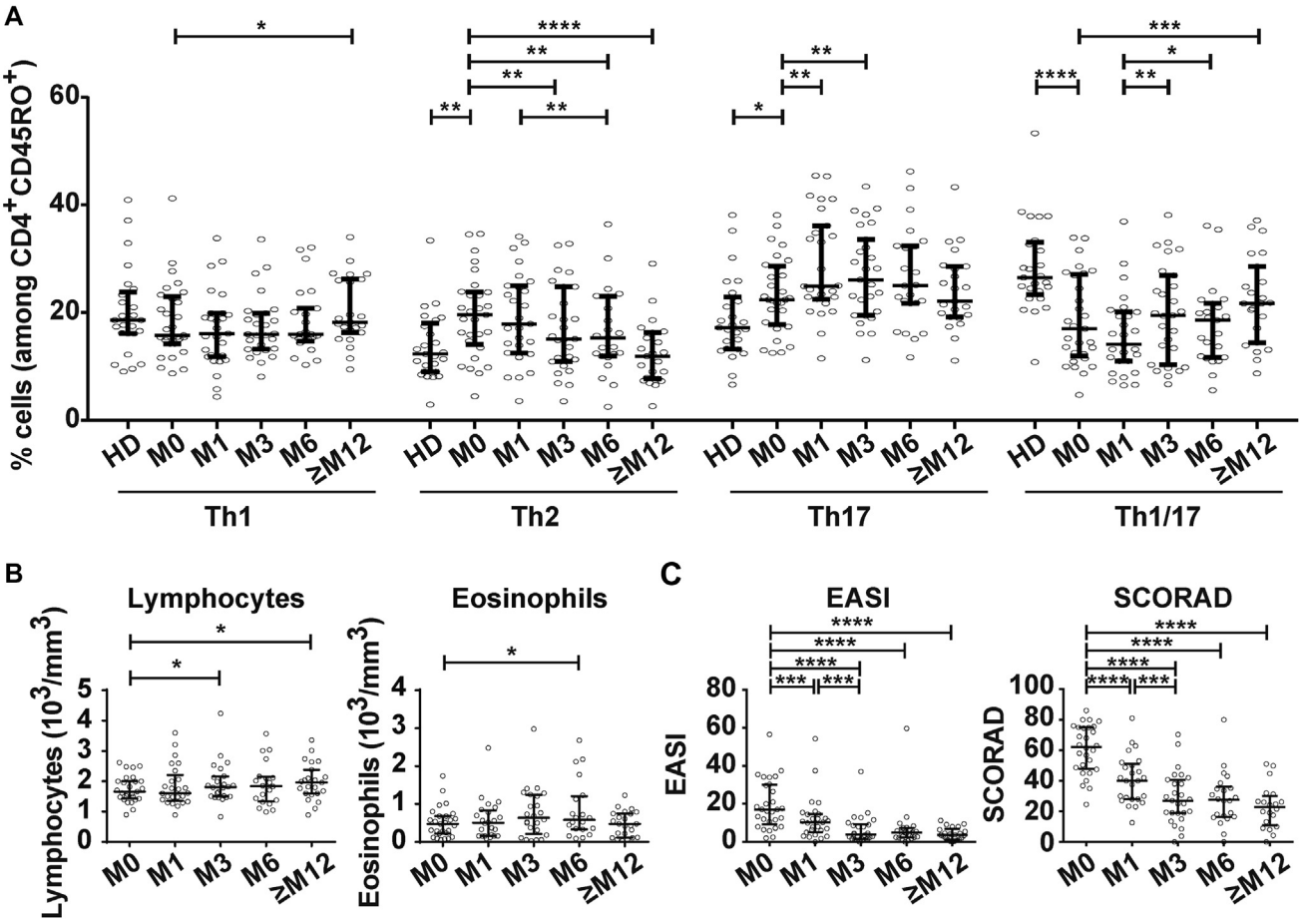

FIG 1. Systematic analysis of clinical scores and T_H cell populations in patients with AD during dupilumab treatment. **A**, Percentages of T_H1, T_H2, T_H17, and $T_H1/17$ cells among $CD4^+CD45RO^+$ cells in HDs and patients with AD at each time point during dupilumab treatment. **B**, Lymphocyte and eosinophil counts in blood at each time point. **C**, Values of EASI and SCORing Atopic Dermatitis (SCORAD) score measured by clinicians at each time point. Medians ± interquartile ranges are plotted for each graph.

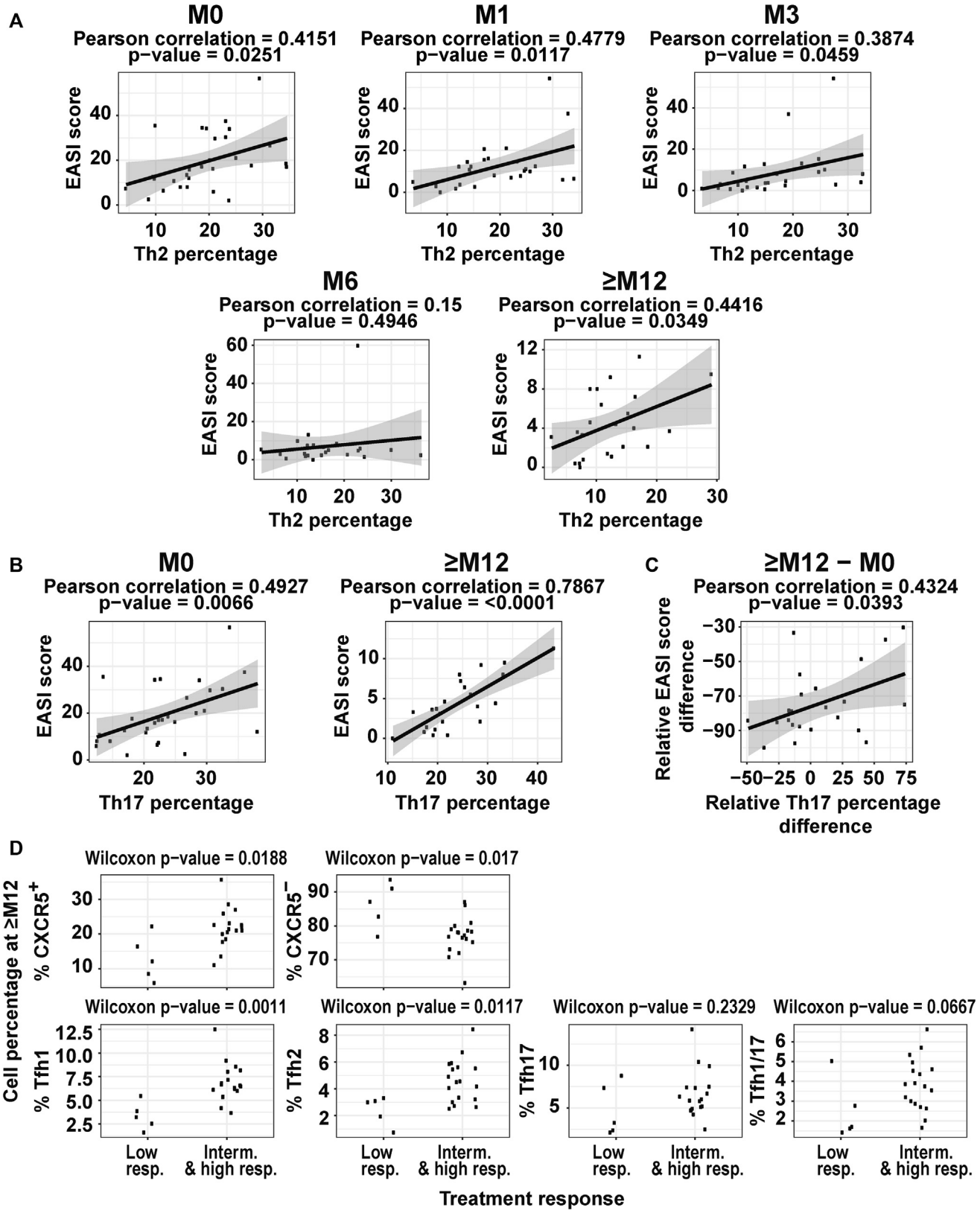

FIG 2. EASI score association with T_H2, T_H17, and T_{FH} cell percentages in patients with AD treated with dupilumab. **A**, Correlation of T_H2 cell percentage with EASI score at M0, M1, M3, M6, and M12 or longer of dupilumab treatment. **B**, Correlation of T_H17 cell percentage with EASI score at M0 and M12 or longer of dupilumab treatment. **C**, Correlation of relative difference in EASI score between M12 or longer and M0 and percentage relative difference in T_H17 between M12 or longer and M0. **D**, Comparison of $CXCR5^+$, $CXCR5^-$, $T_{FH}1$, $T_{FH}2$, $T_{FH}17$, and $T_{FH}1/17$ cell percentages at M12 or longer between low responders and high/intermediate responders.

percentages decreased between M0 and M3, but they returned to baseline levels at M12 (see Fig E2, *B*).

The biggest baseline differences and dynamic variations were measured in the T_H cell populations. When patients with AD at M0 and HDs were compared, there was no significant difference in the percentages of T_H1 cells, but higher percentages of T_H2 and T_H17 cells and lower percentages of $T_H1/17$ cells were found in patients with AD (Fig 1, *A*). Dynamically, we detected a significant increase in T_H1 and $T_H1/17$ cell percentages between M0 and M12, paralleling a gradual decrease in the percentage of T_H2 cells (Fig 1, *A*). The changes in T_H17 cell percentage were more subtle, with an initial increase (from M0 to M1 and M3) and a return to baseline at M12. The evolutions of T_H2 and T_H17 cell percentages for individual patients are also provided (see Fig E3 in this article's Online Repository at www.jacionline.org).

Among the routine blood cell count variables, the total lymphocyte counts increased slightly over the course of dupilumab treatment, whereas eosinophil counts increased from M0 to M6 and returned to baseline (Fig 1, *B*). These were minor changes as compared with the modifications in T_H subpopulations.

Other studies have measured T_H cell populations in the peripheral blood of patients with AD,[2-5] bringing new insights on the proportions of T_H subsets between skin-homing CLA^+ and CLA^- $CD4^+$ T cells. Complementarily, our study focused on the total T_H and T_{FH} subsets in circulating blood of patients with AD.

Two interesting studies used transcriptomic analysis in whole lesional skin biopsy specimens to compare baseline with 4 weeks of dupilumab treatment; they found that T_H2-associated chemokines were downregulated in response to dupilumab.[6,7] Our study significantly extends those findings by providing a detailed and dynamic analysis of T_H cell diversity in patients with AD during 12 months of dupilumab treatment.

In parallel with the immunologic variables, we monitored the baseline value and dynamics of standard clinical scores—the Eczema Area and Severity Index (EASI) and SCORing Atopic Dermatitis score—at each time point. As previously reported,[8] both scores significantly decreased from M0 to M12 during patient treatment with dupilumab (Fig 1, *C*). Administration of concomitant therapies did not influence EASI score (data not shown).

We evaluated the association between T_H cell and T_{FH} cell populations and EASI score.

The T_H2 cell percentage significantly correlated with EASI score at all time points except M6 (Fig 2, *A*). This was expected because the decrease in T_H2 cell percentage from M0 to M12 (Fig 1, *A*) paralleled the decrease in EASI score (Fig 1, *C*). It also validated blood T_H2 cells as a robust pharmacodynamic biomarker of dupilumab treatment.

Our working hypothesis was that T_H cell cross-regulation may induce more complex dynamic changes in T_H cell subsets than only changes in T_H2 cells. Indeed, T_H17 cell percentage significantly correlated with EASI score at M0 and very strongly at M12 (Pearson correlation = 0.7867) (Fig 2, *B*). Also, the correlation between relative difference in EASI score between M12 and M0 and relative difference in T_H17 cell percentage between M12 and M0 showed that the largest decreases in T_H17 cell percentages were found in patients with the largest decreases in EASI score (Fig 2, *C*). This is in line with a possible role for T_H17 cells in the physiopathology of AD.[9]

Finally, we grouped the patients according to their response to treatment: high responders displaying an improvement in their EASI score at M12 or longer of at least 85%, low responders showing a decrease in their EASI score of less than 60%, and the remaining intermediate responders. Low responders displayed significantly lower levels of $CXCR5^+$ total T_{FH} cells at M12 than did strong and intermediate responders. This difference was also identified for $T_{FH}1$ and $T_{FH}2$ cells. Conversely, low responders displayed higher levels of $CXCR5^-$ cells at M12 than did high and intermediate responders. $T_{FH}17$ and $T_{FH}1/17$ cell percentages were not significantly different between the 2 groups (Fig 2, *D*).

Reductions in CCL26 and CCL13 (T_H2-associated chemokines) expression were previously correlated with improvement in EASI score.[7] Here, we were able to show that EASI score correlated not only with T_H2 cell percentage but also with T_H17 cell percentage, and that total T_{FH}, $T_{FH}1$, and $T_{FH}2$ cell percentages could allow separation of low versus high responders.

Our detailed and systematic study further established a strong link between T_H2 cells and response to dupilumab. However, it also suggests an important role of other T_H and T_{FH} cell populations in AD physiopathology and treatment response. Although they were established on a limited number of patients, our results warrant validation in larger independent cohorts. This should set the ground for exploitation of fine-grained T_H cell subsets as biomarkers in future clinical observation studies or in the context of controlled therapeutic trials.

We wish to thank all collaborators of the Dermatology Department of Saint-Louis Hospital who contributed to sample collection and transfer to Institut Curie for analysis.

Coline Trichot, PhD[a,b]
Lilith Faucheux, MSc[b,c]
Léa Karpf, MSc[a,b]
Maximilien Grandclaudon, PhD[a]
Lucia Pattarini, PhD[a]
Martine Bagot, MD, PhD[d,e]
Thibault Mahévas, MD[d,e]
Marie Jachiet, MD[d,e]
Anne Saussine, MD[d,e]
Jean-David Bouaziz, MD, PhD[d,e]
Vassili Soumelis, MD, PhD[a,b]

From [a]the Institut Curie, PSL University, INSERM U932, Paris, France; [b]the Université de Paris, INSERM U976, Human Systemic Immunology and Inflammatory Network Team, Paris, France; [c]the Université de Paris, INSERM UMR-1153, ECSTRRA Team, Paris, France; [d]the Université de Paris, INSERM U976, Skin Immunity and Inflammation Team, Paris, France; and [e]the APHP, Dermatology Department, Hôpital Saint-Louis, Paris, France. E-mail: vassili.soumelis@aphp.fr.

Supported by grants INSERM HTE2016, Ligue Nationale contre le cancer EL2016.LNCC/VaS, ANR-10-IDEX-0001-02 PSL*, ANR-11-LABX-0043, ANR-15-CHIN-0002, ANR-17-CE14-0025-02, and CIC IGR-Curie 1428. C.T. was supported by ANRT, M.G. received support from ANRS, L.K. and L.F. are supported by a fellowship from the French Ministry of Research.

Disclosure of potential conflict of interest: The authors declare that they have no relevant conflicts of interests.

REFERENCES

1. Morita R, Schmitt N, Bentebibel SE, Ranganathan R, Bourdery L, Zurawski G, et al. Human blood CXCR5(+)CD4(+) T cells are counterparts of T follicular cells and contain specific subsets that differentially support antibody secretion. Immunity 2011;34:108-21.
2. Esaki H, Czarnowicki T, Gonzalez J, Oliva M, Talasila S, Haugh I, et al. Accelerated T-cell activation and differentiation of polar subsets characterizes early atopic dermatitis development. J Allergy Clin Immunol 2016;138:1473-7.e5.
3. Antunez C, Torres MJ, Mayorga C, Cornejo-Garcia JA, Santamaria-Babi LF, Blanca M. Different cytokine production and activation marker profiles in circulating

cutaneous-lymphocyte-associated antigen T cells from patients with acute or chronic atopic dermatitis. Clin Exper Allergy 2004;34:559-66.
4. Teraki Y, Sakurai A, Izaki S. IL-13/IL-22-coproducing T cells, a novel subset, are increased in atopic dermatitis. J Allergy Clin Immunol 2013;132:971-4.
5. Czarnowicki T, Esaki H, Gonzalez J, Malajian D, Shemer A, Noda S, et al. Early pediatric atopic dermatitis shows only a cutaneous lymphocyte antigen (CLA)(+) TH2/TH1 cell imbalance, whereas adults acquire CLA(+) TH22/TC22 cell subsets. J Allergy Clin Immunol 2015;136:941-51.e3.
6. Beck LA, Thaci D, Hamilton JD, Graham NM, Bieber T, Rocklin R, et al. Dupilumab treatment in adults with moderate-to-severe atopic dermatitis. N Engl J Med 2014;371:130-9.
7. Hamilton JD, Suarez-Farinas M, Dhingra N, Cardinale I, Li X, Kostic A, et al. Dupilumab improves the molecular signature in skin of patients with moderate-to-severe atopic dermatitis. J Allergy Clin Immunol 2014;134:1293-300.
8. Simpson EL, Bieber T, Guttman-Yassky E, Beck LA, Blauvelt A, Cork MJ, et al. Two Phase 3 trials of dupilumab versus placebo in atopic dermatitis. N Engl J Med 2016;375:2335-48.
9. Souwer Y, Szegedi K, Kapsenberg ML, de Jong EC. IL-17 and IL-22 in atopic allergic disease. Curr Opin Immunol 2010;22:821-6.

https://doi.org/10.1016/j.jaci.2020.05.037

3. Appendix 3

SARS-CoV-2 induces activation and diversification of human plasmacytoid pre-dendritic cells

Fanny Onodi, Lucie Bonnet-Madin, Léa Karpf, Laurent Meertens, Justine Poirot, Jérome Legoff, Constance Delaugerre, Ali Amara and Vassili Soumelis

Manuscript in revision at J. Exp. Med

SARS-CoV-2 induces activation and diversification of human plasmacytoid pre-dendritic cells

Fanny Onodi[1], Lucie Bonnet-Madin[2], Léa Karpf[1], Laurent Meertens[2], Justine Poirot[1], Jérome Legoff [1, 3], Constance Delaugerre[2, 3], Ali Amara[2, #] and Vassili Soumelis[1, 4, #]

[1] Université de Paris, Institut de Recherche Saint-Louis, INSERM U976, Hôpital Saint-Louis, 75010 Paris, France

[2] Université de Paris, Institut de Recherche Saint-Louis, INSERM U944 CNRS 7212, Hôpital Saint-Louis, 75010 Paris, France

[3] Laboratoire de Virologie, Hôpital Saint-Louis, APHP, 75010 Paris, France

[4] Assistance Publique-Hôpitaux de Paris (AP-HP), Hôpital Saint-Louis, Laboratoire d'Immunologie, F-75010, Paris, France

Corresponding authors: vassili.soumelis@aphp.fr; ali.amara@inserm.fr

Abstract

Several studies have analyzed antiviral immune pathways in severe COVID-19 patients. However, the initial steps of antiviral immunity are not known. Here, we have studied the interaction of isolated primary SARS-CoV-2 viral strains with human plasmacytoid pre-dendritic cells (pDC), a key player in antiviral immunity. We show that pDC are not permissive to SARS-CoV-2 infection. However, they efficiently diversified into activated P1-, P2-, and P3-pDC effector subsets in response to viral stimulation. They expressed checkpoint molecules at levels similar to influenza virus-induced activation. They rapidly produced high levels of interferon-α, interferon-λ1, IL-6, IP-10, and IL-8. Importantly, all major aspects of SARS-CoV-2-induced pDC activation were inhibited by hydroxychloroquine, including P2- and P3-pDC differentiation, the expression of maturation markers, and the production of interferon-α and inflammatory cytokines. Our results indicate that pDC may represent a major player in the first line of defense against SARS-CoV-2 infection, and call for caution in the use of hydroxychloroquine in the early treatment of the disease.

Introduction

Severe Acute Respiratory Syndrome-Coronavirus-2 (SARS-CoV-2) is the third zoonotic coronavirus that emerged in the last two decades. SARS-CoV-2 is the causative agent of coronavirus disease 2019 (COVID-19) that appeared in late 2019 in Wuhan, Hubei province in China (Nandakumar, 2020; Sheahan and Frieman, 2020). SARS-CoV-2 became rapidly pandemic, and infection have now been detected in 216 countries and territories, and is responsible for approximatively 10 million confirmed cases and 500,000 deaths as of 26 of June 2020 (WHO weekly update).

- SARS-CoV-2 infection may lead to a diversity of clinical presentations, ranging from asymptomatic or mild “flu-like” syndrome, to severe and life-threatening acute respiratory failure. Disease aggravation usually occurs after 8 to 10 days following initial symptoms (Tang et al., 2020). At this late stage, three main factors were shown to contribute to the progression and severity of the infection (Tang et al., 2020): 1) viral persistence was evidenced in the lung and systemic circulation, although it is not constant (Tang et al., 2020), 2) an excess production of pro-inflammatory cytokines, such as IL-1b and IL-6 (Tay et al., 2020; Arnaldez et al., 2020), 3) a defect in type I interferon (IFN) production, especially in critically ill patients (Tay et al., 2020; Acharya et al., 2020). Although these abnormalities were confirmed in several studies, their origin and underlying mechanisms remain mostly unknown. In particular, it is not known whether an imbalance between inflammatory cytokines and type I IFN occurs early in the disease, at the stage of the primary infection, and whether the virus itself may be responsible. To fill this gap of knowledge, it becomes essential to investigate the early innate immune response to SARS-CoV-2. Among the immune cells that are involved in innate anti-viral immunity, plasmacytoid pre-dendritic cells (pDC) play a particularly important role as the major source of type I IFN in response to viral infection (Liu, 2005). PDC can sense a large array of viruses including the coronaviruses murine hepatis virus (MHV) and the middle east respiratory syndrome coronavirus (MERS) (Scheuplein et al., 2015; Cervantes-Barragan et al., 2007), and respond by producing innate cytokines, including all forms of type I IFNs (α and β), type III IFN, and inflammatory cytokines, in particular TNF-α and IL-6 (Liu, 2005; Yin et al., 2012; Gilliet et al., 2008). However, different viruses may induce different cytokine patterns (Thomas et al., 2014), possibly creating an imbalance between IFN versus inflammatory cytokine response.

Additionally, some viruses were shown to subvert pDC functions through different mechanisms not necessarily related to productive infection. This is the case for HIV, which may induce pDC apoptosis in vitro (Meyers et al., 2007) and pDC depletion in vivo (Soumelis et al., 2001; Meera et al., 2010). Human hepatitis C virus can inhibit IFN-α production by pDC through the glycoprotein E2 binding to BDCA-2 (Florentin et al., 2012). Human papillomavirus induces very low IFN response in pDC (Bontkes et al., 2005), which may be due to impaired TLR-7 and -9 signaling (Hirsch et al., 2010). Whether SARS-CoV-2 induces efficient pDC activation, or may interfere with various biological pathways in pDC is currently unknown.

In this study, we have systematically addressed the interactions between clinical SARS-CoV-2 isolates and primary human pDC in order to reproduce the early stages of the infection. We showed that pDC are resistant to productive infection with SARS-CoV-2 strains but still mount substantial IFN responses upon viral challenge. Interestingly, pDC responded to SARS-CoV-2 by a complete activation program, including diversification into effector subsets, production of type I and type III IFN, as well as inflammatory cytokines. We also showed that hydroxychloroquine, an antimalarial drug proposed for treatment of COVID-19 patients (Das et al., 2020; Mahévas et al., 2020), inhibits SARS-CoV-2-induced pDC activation and IFN production in a dose-dependent manner. Our results establish pDC as a potential key player in innate immunity to SARS-CoV-2, and raise caution regarding pharmacological manipulation that could inhibit pDC effector functions.

Results

SARS-CoV-2 induces activation and diversification of primary human pDC

In order to efficiently recapitulate SARS-CoV-2-pDC interactions, we used two strains of SARS-CoV-2 primary isolates. Their viral genome sequences were nearly identical with 99,98% identity. Sequence comparison with reference strain Wuhan-Hu-1 (NCBI accession number NC_045512.2) showed that both strains contain a subset of mutations (C241T; C30307T; A23403G and G25563T), characteristic of the GH clade based on GISAID nomenclature. Human primary pDC were purified from healthy donor peripheral blood mononuclear cells (PBMC) by cell sorting. First, we asked whether SARS-CoV-2 was able to induce pDC activation, and diversification into IFN-producing and/or T cell stimulating effectors, as we previously described for influenza virus A (Flu) (Alculumbre et al., 2018). After 24 hours of culture, SARS-CoV-2-activated pDC efficiently diversified into P1 (PD-L1^{+}CD80^{-}), P2 (PD-L1^{+}CD80^{+}), and P3 (PD-L1^{+}CD80^{+}) pDC subsets, similar to Flu stimulation (Fig 1A). P1-, P2-, and P3-pDC were all significantly induced by SARS-CoV-2 and Flu, as compared to medium control (Fig 1B). In parallel, we observed a sharp decrease in non-activated P0-pDC (PD-L1^{-}CD80^{-}) (Fig 1A and B). SARS-CoV-2-induced pDC activation was comparable with magnetically- versus FACS-sorted pDC (Fig S1A and S1B), confirming that both methods are suitable for subsequent experiments. All main findings were confirmed on at least three independent experiments using FACS-sorted pDC, with a protocol that excluded AS-DC, a rare dendritic cell (DC) subset that shares some markers and functional features with pDC (Villani et al., 2017), based on CD2, CD5 and AXL expression (Fig S1A).

PDC activation and diversification was observed with two independent primary SARS-CoV-2 strains (Fig 1C), which both induced similar proportions of P1-P3 subsets. PDC diversification was also observed by co-culturing of pDC with SARS-CoV-2-infected Vero E6 cells with a similar efficiency than free SARS-CoV-2 (Fig

S1C). SARS-CoV-2 improved pDC viability as compared to medium condition (Fig 1D), which is compatible with subsequent effector functions.

Human pDC are not productively infected by SARS-CoV-2

Next, we asked whether SARS-CoV-2 -induced pDC activation was dependent on productive infection. We first checked whether pDC express at their cell surface ACE2, the major SARS-CoV-2 entry receptor (Hoffmann et al., 2020, 2). No significant expression was detected using an anti-ACE2-specific antibody, as compared to a low and high expression on Vero E6 and 293T-ACE2 cell lines, respectively (Fig 1E). The ability of pDC to replicate SARS-CoV-2 was then assessed. Human pDC were challenged with SARS-CoV-2 strain 220_95 at MOI of 2, and cultured for 2h, 24h or 48 h. Our results showed that pDC were refractory to SARS-CoV-2 infection, as evaluated by quantifying 1) the intracellular production of the nucleoprotein antigen (N) (Fig 1F), or the accumulation of viral RNA in SARS-CoV-2-infected cells (Fig S1D), and 2) the release of infectious progeny virus in the supernatants of infected cells using plaque assays (Fig 1G). As positive control, the permissive Vero E6 cells produced high level of the N antigen, increased viral RNA overtime (Fig S1D), and high viral titers following SARS-CoV-2 incubation (Fig 1G). Similar results were obtained with pDC isolated from three independent donors (Fig S1E). Overall, these results show that pDC are resistant to SARS-CoV-2 infection, and are efficiently activated by the virus independently of ACE2 expression. Their viability was not affected by SARS-CoV-2 challenge.

Upregulation of major immune checkpoints on SARS-CoV-2-activated pDC

Activating immune checkpoints play a key role in T cell stimulation, and serve as surrogate markers of DC differentiation (Guermonprez et al., 2002). We first

assessed the dose-dependent effect of SARS-CoV-2 on CD80 expression and subset diversification. CD80 was induced in a dose-dependent manner by SARS-CoV-2 at MOI 0.04 to 1 (Fig 2A). This was accompanied by an increase in P3-pDC subset, and a slight decrease in P1-pDC (Fig 2B). A detailed phenotypic analysis was subsequently performed on pDC after 24 and 48 hours of culture with SARS-CoV-2 (Fig 2C and Fig S2A). Diversification was observed at both time points, with a slight increase in P3-pDC at 48 hours (Fig S2A). P2- and P3-pDC significantly upregulated CD80, CD86, CCR7, and OX40L, as compared to non-activated P0-pDC, in both SARS-CoV-2 and Flu conditions (Fig 2C). PD-L1, and CD62L, an integrin that promotes lymph node homing, were both higher on P1- and P2-pDC (Fig 2C). Expression of checkpoint molecules persisted at 48h, especially the higher CD80 and CD86 expression on P3-pDC (Fig S2B).

Efficient production of type I and type III interferons by SARS-CoV-2-activated pDC

A key and defining function of pDC is their ability to produce large amounts of type I IFN (Gilliet et al., 2008). We measured the production of several cytokines at the protein level after 24 hours of culture. Both SARS-CoV-2 and Flu induced high levels of IFN-α2 and IFN-λ1, both being critical anti-viral effector cytokines (Fig 3A). IFN-α levels following SARS-CoV-2 activation reached up to 80 ng/ml, indicating a very efficient activation. The chemokine IP-10 was also significantly induced (Fig 3A), possibly due to an autocrine IFN loop (Blackwell and Krieg, 2003). Inflammatory cytokines IL-6 and IL-8 were comparably induced by SARS-CoV-2 and Flu (Fig 3A). However, TNF-α levels were marginally induced by SARS-CoV-2 as compared to Flu activation (Fig 3A). Cytokine production was maintained after 48 hours of viral activation (Fig 3B). Secreted protein levels were similar to 24h levels for most

cytokines. Interestingly, IFN-α levels raised by 3-fold between 24h and 48h for one donor (Fig 3A and B), indicating the possibility of increased production. Such strong IFN producer suggests a potential virus controller.

Because the oropharyngeal mucosa is an entry site for SARS-CoV-2, we aimed at validating our results using pDC purified from tonsils. SARS-CoV-2 induced a marked diversification of tonsillar pDC into all three activated subsets (Fig S2C). Tonsillar pDC efficiently produced IFN and inflammatory cytokines in response to SARS-CoV-2 (Fig S2D). Overall, our results establish SARS-CoV-2 as a very efficient inducer of type I and type III IFN responses. Inflammatory cytokines were induced at similar level than Flu activation, without any significant imbalance that would be suggestive of excessive inflammatory response.

SARS-CoV-2-induced pDC activation is inhibited by hydroxychloroquine

Given that SARS-CoV-2 did not infect pDC, and did not interfere with pDC activation, we asked whether pharmacological agents could modulate pDC diversification and cytokine production. Hydroxychloroquine (HCQ) is known to inhibit endosomal acidification which may diminish pDC activation (Kuznik et al., 2011, 9; Sacre et al., 2012). Additionally, it is being tested in several clinical studies as a potential treatment for COVID-19 (Das et al., 2020; Mahévas et al., 2020). Hence, we addressed its role in SARS-CoV-2-induced pDC activation. Following 24 hours of culture, we found that HCQ inhibited pDC diversification in response to SARS-CoV-2, which is similar to the decrease observed with Flu, used as a positive control (Fig 4A). In particular, P2- and P3-pDC differentiation were almost completely inhibited (Fig 4B). Inhibition of SARS-CoV-2-induced pDC diversification by HCQ was dose-dependent (Fig S3A). The significant decrease in P3-pDC was paralleled by a decrease in CD80, CD86, and CCR7 expression (Fig 4C and D). OX40-ligand

expression was not significantly affected by HCQ (Fig 4C and D). However, HCQ inhibited the appearance of an OX40-ligand^{high} pDC population (Fig S3B and S3C), which may impact subsequent T cell activation. Last, we assessed the effect of HCQ on innate pDC functions. We measured cytokine production after 24 hours of SARS-CoV-2-induced pDC activation in the presence or absence of HCQ. We found that IFN-α and λ levels were decreased by HCQ (Fig 4E). This was also the case for IL-6 and IL-8, with a much lesser impact on IP-10 (Fig 4E). Together, these results show that HCQ inhibits SARS-CoV-2-induced pDC diversification and cytokine production.

Discussion

Type I IFNs are critical cytokines that control viral replication. Several chronic viral infections were associated to poor type I IFN responses (Lee et al., 2013; Snell et al., 2017; Marsili et al., 2012; Dolganiuc et al., 2006). In COVID-19 patients, decreased serum levels of type I IFN were associated with severity in late stage infection, and increased viral load (Tay et al., 2020; Acharya et al., 2020). This raised the question as to whether SARS-CoV-2 was intrinsically capable of inducing a robust IFN response, or on the contrary could interfere with IFN production and other antiviral immune pathways. In this study, we have used primary SARS-CoV-2 isolates and human primary pDC in order to increase the relevance to a naturally occurring infection. Our results demonstrate that SARS-CoV-2 is a strong IFN inducer by efficiently stimulating primary pDC. Viral sensing was independent of the expression of the ACE2 entry receptor or the ability of the virus to replicate in pDC. However, the precise molecular mechanisms involved remain to be investigated. Both type I and type III IFNs were induced at high levels upon SARS-CoV-2 stimulation. This strongly

suggests that the defects observed in critically ill COVID-19 patients are acquired during disease evolution through secondary events, not necessarily associated to direct effect of the virus. Possible mechanisms could be related to inflammatory cytokines, such as TNF, and endogenous glucocorticoid response, both being able to promote pDC apoptosis ((Abe and Thomson, 2006). However, additional mechanisms may be involved and need to be explored in the context of severe COVID-19.

An excessive production of inflammatory cytokines, such as IL-1 β, IL-6 and TNF, was associated to COVID-19 severity (Tay et al., 2020; Arnaldez et al., 2020; Vabret et al., 2020). Their cellular source and the underlying mechanisms are currently unknown. Our results indicate that SARS-CoV-2-induced pDC activation promotes a balanced production of innate cytokines, including large amounts of type I and type III INFs, without any significant excess in inflammatory cytokines. This suggests that pDC activation may not be a causal factor of COVID-19 aggravation. In support to that, recent studies indicated that endothelial cells may be a target of SARS-CoV-2 infection, and could be at the origin of the systemic and multi-organ production of inflammatory cytokines (Pons et al., 2020). Bronchial epithelial cells could also be involved in the production of high levels of IL-6, which were not detected in the serum and in PBMC transcriptomic studies in severe COVID-19 (Wilk et al., 2020). This supports the view of pDC as being protective through an early and efficient production of antiviral cytokines, with later defects due to currently unknown mechanisms, associated with late stage aggravation. On the contrary, non-professional innate immune cells such as endothelial cells and bronchial epithelial cells may be involved in the secondary worsening of COVID-19 through the excessive and uncontrolled production of inflammatory cytokines. Several therapeutic

approaches have been explored and are currently being tested in clinical trials on COVID-19 patients (Vabret et al., 2020; Tay et al., 2020). These include antiviral agents (Yang et al., 2020), immune-modulatory molecules, such as glucocorticoids (Fernández Cruz et al., 2020), and anti-inflammatory molecules, such as HCQ (Touret and de Lamballerie, 2020; Lecuit, 2020). This latter drug was additionally shown in *in vitro* studies to interfere with SARS-CoV-2 replication (Wang et al., 2020). The difficulty in designing current and future COVID-19 treatment strategies lies in part in the complexity of the host-virus interactions. Ideally, an efficient therapy should control the excessive and potentially pathogenic inflammatory cytokine response, while preserving antiviral effector pathways in order to efficiently control viral replication. In our study, we have shown that SARS-CoV-2 effectively induced type I IFN production by pDC during initial encounter with the virus. Given the importance of IFN responses in the control of viral infections, pharmacological agents that decrease IFN production should be avoided. Our results showing that HCQ could inhibit all aspects of SARS-CoV-2-induced pDC activation call for a lot of caution in the use of that drug in the context of COVID-19. A favorable cost-benefit ratio would be expected only if a strong direct antiviral effect was demonstrated, associated with an efficient ability to control the production of pathogenic inflammatory cytokines. Else, interfering with pDC anti-viral response could contribute to a less efficient control of SARS-CoV-2 infection and subsequent worsening of the disease. Continued efforts in mapping and dissecting immune effector pathways to SARS-CoV-2 will be of major importance in order to design efficient treatment strategies adapted to each patient and stage of the infection.

Materials and methods

PDC isolation and cell culture

Buffy coats from healthy human donors were obtained from Etablissement Français du Sang, Paris, Saint-Antoine Crozatier blood bank. Peripheral blood mononuclear cells (PBMCs) were isolated through Ficoll density gradient centrifugation (Ficoll-Paque; GE Healthcare). PDC were isolated through a first step of pDC magnetic sorting (Human Plasmacytoid DC Enrichment Kit; StemCell), and subsequent flow cytometric sorting on the basis of live, lineage$^-$ (CD16, CD14, CD19, CD20, CD56 and CD3), CD11c$^-$ CD4$^+$, and CD2$^-$ CD5$^-$ cells to a 98% purity. Due to some logistic issues, alternatively frozen PBMCs from Etablissement Français du Sang, Paris, Saint Louis blood bank, were thawed and placed at 37°C for 2h for cell recovery. pDC were then magnetically sorted (Human Plasmacytoid DC Enrichment Kit; StemCell). PDC enrichment was assessed based on the cytometric sorting panel, and was ranged from 71 to 90%.

African green monkey kidney epithelial Vero E6 cells (ATCC, CRL-1586) were cultured in Dulbecco's Modified Eagle Medium (DMEM; Thermo Fisher Scientific) supplemented with 10% FBS, 1% penicillin-streptomycin, 1% GlutaMAX and 25 mM Hepes.

SARS-CoV-2 primary strain isolation and amplification

SARS-CoV-2 viruses were isolated from nasopharyngeal swab specimens collected at Service de Virologie (Hospital Saint Louis, Paris). Samples were centrifugated at 4,000 x g for 10 min then filtered using a 0.45 µM filter, and diluted 1:1 with DMEM-4% (DMEM supplemented with 4% FBS, 1% penicillin-streptomycin, 1% GlutaMAX and 25 mM Hepes). Vero E6 cells were seeded in 96-well cell culture plate (15,000 cells/well), and incubated at 37°C with 200µl of inoculum and observed daily for

cytopathogenic effects (CPE) by light microscopy. Substantial CPE were seen at 72-96 hours post inoculation. Culture supernatants were then collected, clarified by centrifugation, filtered using a 0.45 µM filter and kept at -80°C. We confirmed SARS-CoV-2 replication by RT-qPCR and whole viral genome sequences were obtained by next generation sequencing using Illumina MiSseq sequencers. Strains sequences have been deposited in the Global Initiative of Sharing All Influenza Data (GISSAID) database with accession ID EPI_ISL_469284 (220_95) and EPI_ISL_469283 (211_61). All viruses belong to the GH clade.

SARS-CoV-2 strains were further propagated on Vero E6 in DMEM-2% (DMEM supplemented with 2% FBS, 1% penicillin-streptomycin, 1% GlutaMAX and 25 mM Hepes). Viruses were passaged three times before being used for experiments. For the last passage, viruses were purified through a 20% sucrose cushion by ultracentrifugation at 80,000 x g for 2 hours at 4°C. Pellets were resuspended in HNE 1X pH7.4 (Hepes 5 mM, NaCl 150 mM, EDTA 0.1 mM), aliquoted and stored at -80°C.

Viruses titer was ascertained by plaque assays in Vero E6 cells and expressed as PFU per ml. Cells were incubated for 1 hour with 10-fold dilution of viral stocks. The inoculum was then replaced with Avicel 2.4% mixed at equal volume with DMEM supplemented with 4% FBS, 2% Glutamax, 50mM $MgCl_2$, 0.225 % of $NaHCO_3$, and incubated 3 days at 37°C before plaque counting.

Infection assays

Vero cells were plated (50,000 cell per well) in p24-well plates 4 hours before being incubated with SARS-CoV-2 diluted in DMEM-2%. Freshly purified pDC were seeded

in p96-well plates (50,000 cells per well) and incubated with SARS-CoV-2 diluted in pDCs culture medium (RPMI 1640 Medium with GlutaMAX, 10% of FBS, 1% of MEM NEAA, 1% of Sodium Pyruvate, and 1% of Penicillin/Streptomycin). At 2, 24 and 48 hour post-inoculation, Vero cells were trypsinized and transferred to p96-well plates. Vero and pDC were washed with PBS and fixed with 2% (v/v) paraformaldehyde (PFA) diluted in PBS for 15 min at room temperature. Cells were incubated for 1 hour at 4°C with 1µg/ml of anti-nucleoprotein mAb (40143-MM05; Sino Biological) diluted in permeabilization flow cytometry buffer (PBS supplemented with 5% FBS, 0.5% (w/v) saponin, 0.1% Sodium azide). After washing, cells were incubated with 1µg/ml of Alexa Fluor 488 (115-545-003; Jackson ImmunoResearch) or 647-conjugated (115-606-062; Jackson ImmunoResearch) goat anti-mouse IgG diluted in permeabilization flow cytometry buffer for 30 min at 4°C. SARS-CoV-2 infection was quantified by flow cytometry.

To quantify infectious viral particle released in the supernatants of infected cells, pDC and Vero cells were inoculated with SARS-CoV-2 as described above and incubated at 37°C for 72-hour. At indicated time points, supernatants were collected and kept at -80°C. Virus titer were then determined by plaque assay on Vero E6 cells as described above.

Kinetic of infection by qPCR assay

Vero E6 and pDC were inoculated with SARS-CoV-2 as described above. At the indicated time points, cells were washed thrice with PBS. Vero E6 were further incubated with trypsin 0.25% for 5 min at 37°C to remove cells surface bound particles. Total RNA was extracted using the RNeasy plus mini kit (Qiagen) according to manufacturer's instruction. cDNAs were generated from 80 ng total RNA by using

the Maxima First Strand Synthesis Kit following manufacturer's instruction (Thermo Fisher Scientific). Amplification products were incubated with 1 Unit of RNAse H for 20 min at 37 °C, followed by 10 min at 72°C for enzyme inactivation, and diluted 10-fold in DNAse/RNAse free water. Real time quantitative PCR was performed using a Power Syber green PCR master Mix (Fisher Thermo Scientific) on a Light Cycler 480 (Roche). The primers used for qPCR were: E_Sarbeco_F1 (5'-ACAGGTACGTTAATAGTTAATAGCGT-3'), E_Sarbeco_R2 (5'-ATATTGCAGCAGTACGCACACA-3') for viral RNA quantification. The plasmid containing the sequence corresponding to the amplified cDNA was purchased from GenScript (pUC57-2019-nCoV-PC:E; MC_0101078) and serially diluted (294 to $2.94x10^9$ genes copies/µl) to generate standard curves.

pDC activation

Freshly sorted pDC were cultured in p96-well plates at a concentration of 5.10^5 cells per ml in the presence of medium alone (RPMI 1640 Medium with GlutaMAX, 10% of FBS, 1% of MEM NEAA, 1% of Sodium Pyruvate, and 1% of Penicillin/Streptomycin), influenza virus A (Charles River, A/PR/8/34, 2µg/ml), the SARS-CoV-2 primary strain 220_95 or 211_61 at a multiplicity of infection (MOI) of 1. After 24 or 48h of culture, pDC supernatant was collected and store at -80°C for subsequent cytokine quantification. PDC were stain for flow cytometry analysis.

Flow cytometry analysis

To sort pDC, cells were stained with zombie violet or BUV fixable viability dye (Biolegend), FITC anti-CD16 (BD, clone NKP15), FITC anti-CD14 (Miltenyi, clone

TÜK4), FITC anti-CD19 (Miltenyi, clone LT19), FITC anti-CD20 (BD, clone 2H7), FITC anti-CD56 (Biolegend, clone HCD56), FITC anti-CD3 (BD, clone HIT3a), BV650 or AF700 anti-CD4 (Biolegend, clone OKT4), PE-Cy7 anti-CD11c (Biolegend, clone Bu15), APC-Vio770 anti-CD2 (Miltenyi, clone LT2), and APC anti-CD5 (BD, clone UCHT2). PDCs were gated as live, lineage$^-$ (CD16, CD14, CD19, CD20, CD56 and CD3), CD2$^-$ CD5$^-$, and CD4$^+$ CD11c$^-$ cells.

For pDC diversification and checkpoint assessment, cells were stain with zombie violet fixable viability dye (Biolegend), BV711 anti-CD123 (Biolegend, clone 6H6), PE anti-CD80 (BD, clone L307.4), PerCP efluor 710 anti-PD-L1 (eBioscience, clone MIH1), BUV737 anti-CD86 (BD, clone 2331), BV421 anti-OX40 Ligand (BD, clone ik-1), APC anti-CD62L (BD, clone DREG-56), FITC anti-CCR7 (R&D System, clone 150503).

For ACE2 cell surface expression, indicated cells were incubated with a goat anti-human ACE2 polyclonal Ab (5 µg/ml; AF933 Biotechne) in 100 µl of PBS with 0.02% NaN3 and 5% FBS for 1 h at 4°C. Cells were then washed and incubated with a Alexa 647-conjugated secondary antibody (Jackson ImmunoResearch) for 30 min at 4°C. Acquisition was performed on an Attune NxT Flow Cytometer (Thermo Fisher Scientific) or a LSR Fortessa (BD Biosciences), and analysis was done by using FlowJo software (Tree Star). Flow cytometry analysis were performed at flow cytometry core facility of IRSL (Paris, France).

Inflammatory cytokines measurement

PDC cytokine production of IFN-α2, IL-8, IL-6, IP-10 and TNF-α, was measured in culture supernatants using BD cytometric bead array (CBA), according to the

manufacturer's protocol, with a 20pg/ml detection limit. Acquisitions were performed on a LSR Fortessa (BD Biosciences), and cytokine concentrations were determined using FCAP Array Software (BD Biosciences).

The concentration of secreted IFN-λ1 was measured by enzyme-linked immunosorbent assay (ELISA) (R&D Systems, DuoSet DY7246), according to the manufacturer's instructions. The manufacturer reported no cross-reactivity nor interference with IFN-α, IFN-β 1a, IL-10Rβ, IFN-λ2 and λ3, and IL-28Rα. The optical density value (OD) of the supernatants was defined as its absolute OD value, minus the OD Absorbance from blank wells. The detection limit was 85pg/ml and all samples were run in duplicates.

Statistical analysis

Statistical analyses were performed with one-way ANOVA, Kruskall Wallis's test with Dunn's multiple comparison post-test or Mann Whitney's test, in Prism (GraphPad Software).

Author contributions

Ali Amara and Vassili Soumelis conceived the study. Fanny Onodi, Lucie Bonnet-Madin, Ali Amara and Vassili Soumelis designed the experiments. Fanny Onodi performed the pDC purification and FACS analysis with Justine Poirot. Lucie Bonnet-Madin and Laurent Meertens performed the virus strain isolation and the infection studies. Fanny Onodi and Léa Karpf performed cytokine quantification. Constance Delaugerre and Jérome Legoff performed the sequencing of the SARS-CoV-2

strains. Fanny Onodi, Ali Amara and Vassili Soumelis wrote the initial manuscript draft and other authors contributed to its editing in its final form.

Competing interest

The authors declare no competing interests.

Acknowledgments

Ali Amara's lab received fundings from the French Government's Investissement d'Avenir program, Laboratoire d'Excellence "Integrative Biology of Emerging Infectious Diseases" (grant n°ANR-10-LABX-62-IBEID), the Fondation pour la Recherche Medicale (grant FRM - EQU202003010193), the Agence Nationale de la Recherche (ANR FLASH COVID project IDISCOVR co-founded by the Foundation pour la Recherche Médicale), University of Paris (Plan de Soutien Covid-19 : RACPL20FIR01-COVID-SOUL). Vassili Soumelis' team was supported by Agence Nationale de la Recherche (ANR-17-CE15-0003, ANR-17-CE15-0003-01), and by Université de Paris « PLAN D'URGENCE COVID19». The authors thank Maud Salmona, Severine Mercier-Delarue and Tiffanie Bouillé (Laboratoire de Virologie, Hôpital Saint Louis) for SARS-CoV-2 deep sequencing, Marie Laure Chaix (Laboratoire de Virologie, Hôpital Saint Louis) for the nasopharyngeal swabs and Lauriane Goldwirt (Laboratoire de Pharmacologie Biologique, Hôpital Saint-Louis) for providing us with hydroxychloroquine. The authors thank all the "Personnel Soignant de l'Hôpital Saint-Louis" for their amazing work during the COVID-19 epidemic. Ali Amara dedicates this work to the memory of his mentor Pr Jean-Louis Virelizier (Unité d'Immunologie Virale, Institut Pasteur, Paris), who left us during the pandemic.

References

Abe, M., and A.W. Thomson. 2006. Dexamethasone preferentially suppresses plasmacytoid dendritic cell differentiation and enhances their apoptotic death. *Clin. Immunol.* 118:300–306. doi:10.1016/j.clim.2005.09.019.

Acharya, D., G. Liu, and M.U. Gack. 2020. Dysregulation of type I interferon responses in COVID-19. *Nat. Rev. Immunol.* doi:10.1038/s41577-020-0346-x.

Alculumbre, S.G., V. Saint-André, J. Di Domizio, P. Vargas, P. Sirven, P. Bost, M. Maurin, P. Maiuri, M. Wery, M.S. Roman, L. Savey, M. Touzot, B. Terrier, D. Saadoun, C. Conrad, M. Gilliet, A. Morillon, and V. Soumelis. 2018. Diversification of human plasmacytoid predendritic cells in response to a single stimulus. *Nat. Immunol.* 19:63–75. doi:10.1038/s41590-017-0012-z.

Arnaldez, F.I., S.J. O'Day, C.G. Drake, B.A. Fox, B. Fu, W.J. Urba, V. Montesarchio, J.S. Weber, H. Wei, J.M. Wigginton, and P.A. Ascierto. 2020. The Society for Immunotherapy of Cancer perspective on regulation of interleukin-6 signaling in COVID-19-related systemic inflammatory response. *J Immunother Cancer*. 8. doi:10.1136/jitc-2020-000930.

Blackwell, S.E., and A.M. Krieg. 2003. CpG-A-induced monocyte IFN-gamma-inducible protein-10 production is regulated by plasmacytoid dendritic cell-derived IFN-α. *J. Immunol.* 170:4061–4068. doi:10.4049/jimmunol.170.8.4061.

Bontkes, H.J., J.J. Ruizendaal, D. Kramer, C.J.L.M. Meijer, and E. Hooijberg. 2005. Plasmacytoid dendritic cells are present in cervical carcinoma and become activated by human papillomavirus type 16 virus-like particles. *Gynecol. Oncol.* 96:897–901. doi:10.1016/j.ygyno.2004.10.040.

Cervantes-Barragan, L., R. Züst, F. Weber, M. Spiegel, K.S. Lang, S. Akira, V. Thiel, and B. Ludewig. 2007. Control of coronavirus infection through plasmacytoid dendritic-cell-derived type I interferon. *Blood*. 109:1131–1137. doi:10.1182/blood-2006-05-023770.

Das, S., S. Bhowmick, S. Tiwari, and S. Sen. 2020. An Updated Systematic Review of the Therapeutic Role of Hydroxychloroquine in Coronavirus Disease-19 (COVID-19). *Clin Drug Investig*. 40:591–601. doi:10.1007/s40261-020-00927-1.

Dolganiuc, A., S. Chang, K. Kodys, P. Mandrekar, G. Bakis, M. Cormier, and G. Szabo. 2006. Hepatitis C virus (HCV) core protein-induced, monocyte-mediated mechanisms of reduced IFN-α and plasmacytoid dendritic cell loss in chronic HCV infection. *J. Immunol.* 177:6758–6768. doi:10.4049/jimmunol.177.10.6758.

Fernández Cruz, A., B. Ruiz-Antorán, A. Muñoz Gómez, A. Sancho López, P. Mills Sánchez, G.A. Centeno Soto, S. Blanco Alonso, L. Javaloyes Garachana, A. Galán Gómez, Á. Valencia Alijo, J. Gómez Irusta, C. Payares-Herrera, I. Morrás Torre, E. Sánchez Chica, L. Delgado Téllez de Cepeda, A. Callejas Díaz, A. Ramos Martínez, E. Múñez Rubio, C. Avendaño-Solá, and Puerta de

Hierro COVID-19 Study Group. 2020. IMPACT OF GLUCOCORTICOID TREATMENT IN SARS-COV-2 INFECTION MORTALITY: A RETROSPECTIVE CONTROLLED COHORT STUDY. *Antimicrob. Agents Chemother.* doi:10.1128/AAC.01168-20.

Florentin, J., B. Aouar, C. Dental, C. Thumann, G. Firaguay, F. Gondois-Rey, V. Soumelis, T.F. Baumert, J.A. Nunès, D. Olive, I. Hirsch, and R. Stranska. 2012. HCV glycoprotein E2 is a novel BDCA-2 ligand and acts as an inhibitor of IFN production by plasmacytoid dendritic cells. *Blood*. 120:4544–4551. doi:10.1182/blood-2012-02-413286.

Gilliet, M., W. Cao, and Y.-J. Liu. 2008. Plasmacytoid dendritic cells: sensing nucleic acids in viral infection and autoimmune diseases. *Nat. Rev. Immunol.* 8:594–606. doi:10.1038/nri2358.

Guermonprez, P., J. Valladeau, L. Zitvogel, C. Théry, and S. Amigorena. 2002. Antigen presentation and T cell stimulation by dendritic cells. *Annu. Rev. Immunol.* 20:621–667. doi:10.1146/annurev.immunol.20.100301.064828.

Hirsch, I., C. Caux, U. Hasan, N. Bendriss-Vermare, and D. Olive. 2010. Impaired Toll-like receptor 7 and 9 signaling: from chronic viral infections to cancer. *Trends Immunol.* 31:391–397. doi:10.1016/j.it.2010.07.004.

Hoffmann, M., H. Kleine-Weber, S. Schroeder, N. Krüger, T. Herrler, S. Erichsen, T.S. Schiergens, G. Herrler, N.-H. Wu, A. Nitsche, M.A. Müller, C. Drosten, and S. Pöhlmann. 2020. SARS-CoV-2 Cell Entry Depends on ACE2 and TMPRSS2 and Is Blocked by a Clinically Proven Protease Inhibitor. *Cell*. 181:271-280.e8. doi:10.1016/j.cell.2020.02.052.

Kuznik, A., M. Bencina, U. Svajger, M. Jeras, B. Rozman, and R. Jerala. 2011. Mechanism of endosomal TLR inhibition by antimalarial drugs and imidazoquinolines. *J. Immunol.* 186:4794–4804. doi:10.4049/jimmunol.1000702.

Lecuit, M. 2020. Chloroquine and COVID-19, where do we stand? *Med Mal Infect*. 50:229–230. doi:10.1016/j.medmal.2020.03.004.

Lee, M.S., C.H. Park, Y.H. Jeong, Y.-J. Kim, and S.-J. Ha. 2013. Negative regulation of type I IFN expression by OASL1 permits chronic viral infection and $CD8^+$ T-cell exhaustion. *PLoS Pathog.* 9:e1003478. doi:10.1371/journal.ppat.1003478.

Liu, Y.-J. 2005. IPC: professional type 1 interferon-producing cells and plasmacytoid dendritic cell precursors. *Annu. Rev. Immunol.* 23:275–306. doi:10.1146/annurev.immunol.23.021704.115633.

Mahévas, M., V.-T. Tran, M. Roumier, A. Chabrol, R. Paule, C. Guillaud, E. Fois, R. Lepeule, T.-A. Szwebel, F.-X. Lescure, F. Schlemmer, M. Matignon, M. Khellaf, E. Crickx, B. Terrier, C. Morbieu, P. Legendre, J. Dang, Y. Schoindre, J.-M. Pawlotsky, M. Michel, E. Perrodeau, N. Carlier, N. Roche, V. de Lastours, C. Ourghanlian, S. Kerneis, P. Ménager, L. Mouthon, E. Audureau, P. Ravaud, B. Godeau, S. Gallien, and N. Costedoat-Chalumeau. 2020. Clinical efficacy of hydroxychloroquine in patients with covid-19 pneumonia

who require oxygen: observational comparative study using routine care data. *BMJ*. 369:m1844. doi:10.1136/bmj.m1844.

Marsili, G., A.L. Remoli, M. Sgarbanti, E. Perrotti, A. Fragale, and A. Battistini. 2012. HIV-1, interferon and the interferon regulatory factor system: an interplay between induction, antiviral responses and viral evasion. *Cytokine Growth Factor Rev.* 23:255–270. doi:10.1016/j.cytogfr.2012.06.001.

Meera, S., T. Madhuri, G. Manisha, and P. Ramesh. 2010. Irreversible loss of pDCs by apoptosis during early HIV infection may be a critical determinant of immune dysfunction. *Viral Immunol.* 23:241–249. doi:10.1089/vim.2009.0112.

Meyers, J.H., J.S. Justement, C.W. Hallahan, E.T. Blair, Y.A. Sun, M.A. O'Shea, G. Roby, S. Kottilil, S. Moir, C.M. Kovacs, T.-W. Chun, and A.S. Fauci. 2007. Impact of HIV on Cell Survival and Antiviral Activity of Plasmacytoid Dendritic Cells. *PLoS ONE*. 2:e458. doi:10.1371/journal.pone.0000458.

Nandakumar, K. 2020. COVID-19: Emergence, Spread, Possible Treatments, and Global Burden. *Frontiers in Public Health*. 8:13.

Pons, S., S. Fodil, E. Azoulay, and L. Zafrani. 2020. The vascular endothelium: the cornerstone of organ dysfunction in severe SARS-CoV-2 infection. *Crit Care*. 24:353. doi:10.1186/s13054-020-03062-7.

Sacre, K., L.A. Criswell, and J.M. McCune. 2012. Hydroxychloroquine is associated with impaired interferon-α and tumor necrosis factor-α production by plasmacytoid dendritic cells in systemic lupus erythematosus. *Arthritis Res. Ther.* 14:R155. doi:10.1186/ar3895.

Scheuplein, V.A., J. Seifried, A.H. Malczyk, L. Miller, L. Höcker, J. Vergara-Alert, O. Dolnik, F. Zielecki, B. Becker, I. Spreitzer, R. König, S. Becker, Z. Waibler, and M.D. Mühlebach. 2015. High secretion of interferons by human plasmacytoid dendritic cells upon recognition of Middle East respiratory syndrome coronavirus. *J. Virol.* 89:3859–3869. doi:10.1128/JVI.03607-14.

Sheahan, T.P., and M.B. Frieman. 2020. The continued epidemic threat of SARS-CoV-2 and implications for the future of global public health. *Curr Opin Virol*. 40:37–40. doi:10.1016/j.coviro.2020.05.010.

Snell, L.M., T.L. McGaha, and D.G. Brooks. 2017. Type I Interferon in Chronic Virus Infection and Cancer. *Trends Immunol.* 38:542–557. doi:10.1016/j.it.2017.05.005.

Soumelis, V., I. Scott, F. Gheyas, D. Bouhour, G. Cozon, L. Cotte, L. Huang, J.A. Levy, and Y.J. Liu. 2001. Depletion of circulating natural type 1 interferon-producing cells in HIV-infected AIDS patients. *Blood*. 98:906–912. doi:10.1182/blood.v98.4.906.

Tang, D., P. Comish, and R. Kang. 2020. The hallmarks of COVID-19 disease. *PLoS Pathog*. 16:e1008536. doi:10.1371/journal.ppat.1008536.

Tay, M.Z., C.M. Poh, L. Rénia, P.A. MacAry, and L.F.P. Ng. 2020. The trinity of COVID-19: immunity, inflammation and intervention. *Nat. Rev. Immunol.* 20:363–374. doi:10.1038/s41577-020-0311-8.

Thomas, J.M., Z. Pos, J. Reinboth, R.Y. Wang, E. Wang, G.M. Frank, P. Lusso, G. Trinchieri, H.J. Alter, F.M. Marincola, and E. Thomas. 2014. Differential Responses of Plasmacytoid Dendritic Cells to Influenza Virus and Distinct Viral Pathogens. *Journal of Virology*. 88:10758–10766. doi:10.1128/JVI.01501-14.

Touret, F., and X. de Lamballerie. 2020. Of chloroquine and COVID-19. *Antiviral Res.* 177:104762. doi:10.1016/j.antiviral.2020.104762.

Vabret, N., G.J. Britton, C. Gruber, S. Hegde, J. Kim, M. Kuksin, R. Levantovsky, L. Malle, A. Moreira, M.D. Park, L. Pia, E. Risson, M. Saffern, B. Salomé, M. Esai Selvan, M.P. Spindler, J. Tan, V. van der Heide, J.K. Gregory, K. Alexandropoulos, N. Bhardwaj, B.D. Brown, B. Greenbaum, Z.H. Gümüş, D. Homann, A. Horowitz, A.O. Kamphorst, M.A. Curotto de Lafaille, S. Mehandru, M. Merad, R.M. Samstein, and Sinai Immunology Review Project. 2020. Immunology of COVID-19: Current State of the Science. *Immunity*. 52:910–941. doi:10.1016/j.immuni.2020.05.002.

Villani, A.-C., R. Satija, G. Reynolds, S. Sarkizova, K. Shekhar, J. Fletcher, M. Griesbeck, A. Butler, S. Zheng, S. Lazo, L. Jardine, D. Dixon, E. Stephenson, E. Nilsson, I. Grundberg, D. McDonald, A. Filby, W. Li, P.L. De Jager, O. Rozenblatt-Rosen, A.A. Lane, M. Haniffa, A. Regev, and N. Hacohen. 2017. Single-cell RNA-seq reveals new types of human blood dendritic cells, monocytes, and progenitors. *Science*. 356. doi:10.1126/science.aah4573.

Wang, M., R. Cao, L. Zhang, X. Yang, J. Liu, M. Xu, Z. Shi, Z. Hu, W. Zhong, and G. Xiao. 2020. Remdesivir and chloroquine effectively inhibit the recently emerged novel coronavirus (2019-nCoV) in vitro. *Cell Res.* 30:269–271. doi:10.1038/s41422-020-0282-0.

Wilk, A.J., A. Rustagi, N.Q. Zhao, J. Roque, G.J. Martínez-Colón, J.L. McKechnie, G.T. Ivison, T. Ranganath, R. Vergara, T. Hollis, L.J. Simpson, P. Grant, A. Subramanian, A.J. Rogers, and C.A. Blish. 2020. A single-cell atlas of the peripheral immune response in patients with severe COVID-19. *Nature Medicine*. 1–7. doi:10.1038/s41591-020-0944-y.

Yang, C.-W., T.-T. Peng, H.-Y. Hsu, Y.-Z. Lee, S.-H. Wu, W.-H. Lin, Y.-Y. Ke, T.-A. Hsu, T.-K. Yeh, W.-Z. Huang, J.-H. Lin, H.-K. Sytwu, C.-T. Chen, and S.-J. Lee. 2020. Repurposing old drugs as antiviral agents for coronaviruses. *Biomed J*. doi:10.1016/j.bj.2020.05.003.

Yin, Z., J. Dai, J. Deng, F. Sheikh, M. Natalia, T. Shih, A. Lewis-Antes, S.B. Amrute, U. Garrigues, S. Doyle, R.P. Donnelly, S.V. Kotenko, and P. Fitzgerald-Bocarsly. 2012. Type III IFNs are produced by and stimulate human plasmacytoid dendritic cells. *J. Immunol.* 189:2735–2745. doi:10.4049/jimmunol.1102038.

Figure legends

Figure 1. **SARS-CoV-2 induces activation and diversification of primary human pDC.** Sorted blood pDC from healthy donors were cultured for 24h with either Medium, SARS-CoV-2, or Influenza virus A (Flu). **(A)** Dotplot showing pDC activation and diversification through the expression of PD-L1 and CD80 into P1-, P2-, and P3-subpopulations. **(B)** Quantification of the three populations. Bars represent medians of n=5 healthy donors. *P < 0.05; **P < 0.01; Mann Whitney test. **(C)** Dotplot showing pDC activation from different strains of SARS-CoV-2 isolated from two patients. **(D)** Percentage of live pDC after 24h of culture with either Medium, SARS-CoV-2, or Influenza virus A (Flu). **(E)** Histogram of ACE2-expression on pDC, Vero E6 and 293T-ACE2 (black) compared to the isotype (light grey). **(F)** Intracellular production of SARS-CoV-2 Ribonucleoprotein in Vero E6 and pDC at 2, 24 or 48h post infection (hpi) with SARS-CoV-2. **(G)** Infectious viral titers in the supernatants of SARS-CoV-2-infected Vero E6 and pDC at 2, 24, 48 or 72h post infection (hpi).

Figure 2. **SARS-CoV-2 induces pDC activation in a dose dependent manner.** Sorted blood pDC from healthy donors were cultured for 24h with either Medium, Influenza virus A (Flu), or SARS-CoV-2 at a MOI of 0.04, 0.2, or 1. **(A)** Dotplot showing pDC activation through the expression of PD-L1 and CD80. **(B)** Quantification of the three populations. Bars represent medians of n=3 healthy donors. *P < 0.05; ns: not significant; Mann Whitney test. **(C)** PDC geometric mean (MFI) of activation markers after 24h of culture with either Medium, Influenza virus A, or SARS-CoV-2 at a MOI of 1. Histograms represent medians and bars interquartile

of n=5 healthy donors. *P < 0.05; **P < 0.01; ***P < 0.001; Kruskal-Wallis with Dunn's multiple comparison's post test.

Figure 3. **SARS-CoV-2-activated pDC produce pro-inflammatory cytokines.** Sorted blood pDC from healthy donors were cultured for 24h or 48h with either Medium, Influenza virus A (Flu), or SARS-CoV-2 at a MOI of 1. **(A)** Quantification of pro-inflammatory cytokines at 24h. Bars represent medians of n=5 healthy donors. **(B)** Quantification of pro-inflammatory cytokines at 48h. Bars represent medians of n=3 healthy donors. *P < 0.05; **P < 0.01; ns: not significant; Mann Whitney test.

Figure 4. **SARS-CoV-2-induced pDC activation is inhibited by hydroxychloroquine.** Sorted blood pDC from healthy donors were cultured for 24h with either Medium, Influenza virus A (Flu), or SARS-CoV-2 at a MOI 1 with or without the presence of hydroxychloroquine (HCQ). **(A)** Dotplot showing pDC diversification in P1-, P2-, and P3-subpopulations in the presence of HCQ. **(B)** Quantification of the three populations. **(C)** Histograms of pDC's activation markers. **(D)** Geometric mean (MFI) of activation markers. Histograms represent medians and bars interquartile of n=3 healthy donors. **(E)** Quantification of pro-inflammatory cytokines production. Bars represent medians of n=3 healthy donors. *P < 0.05; ns: not significant; Mann Whitney test.

Figure S1. **SARS-CoV-2 induces pDC activation.** Sorted blood pDC from healthy donors were cultured for 24h with either Medium, SARS-CoV-2, or Influenza virus A (Flu). **(A)** Pourcentage of pure pDC amoung live cells through different sorting strategies. **(B)** P1-, P2- and P3- diversification of fresh, fluorescent sorted pDC

versus frozen, magnetic sorted pDC with either SARS-CoV-2 or Influenza virus A (Flu) for 24h. **(C)** Dotplot of pDC activation with either free SARS-CoV-2 or pDC co-culture with SARS-CoV-2 infected cells. **(D)** Viral RNA copy number in of Vero E6 and pDC 2, 24 and 48h post infection (hpi). **(E)** Intracellular production of the nucleoprotein antigen (N) on pDC of two healthy donors.

Figure S2. **SARS-CoV-2 induces activation and diversification of tonsilar pDCs.** Sorted blood pDC from healthy donors were cultured for 48h with either Medium, SARS-CoV-2, or Influenza virus A (Flu). **(A)** Dotplot showing pDC activation and diversification through the expression of PD-L1 and CD80 at 24h and 48h. **(B)** Geometric mean (MFI) of pDC's activation markers at 48h. Histograms represent medians and bars interquartils of n=3 healthy donors. *P < 0.05; Kruskal-Wallis with Dunn's multiple comparison's post test. **(C)** Dotplot of tonsil pDC activation cultured for 24h with either Medium, SARS-CoV-2 or Influenza virus A (Flu). **(D)** Quantification of pro-inflammatory cytokines of tonsilar pDC at 24h. Histograms represent medians of n=1 healthy donors.

Figure S3. **Hydroxichloroquine inhibits SARS-CoV-2-induced pDC activation in a dose dependant manner.** Sorted blood pDC from healthy donors were cultured for 24h with either Medium, Influenza virus A (Flu), or SARS-CoV-2 at a MOI 1 with hydroxychloroquine (HCQ) or vehicule. **(A)** Dotplot of pDC diversification with increasing concentration of hydroxychloroquine (HCQ) or vehicule. **(B)** Dotplot showing OX40L and CD86 in presence or abscence of HCQ. **(C)** Pourcentage of $OX40L^{high}$ population amoung pDC. Bars represent medians of n=3 healthy donors. *P < 0.05; Mann Witney test.

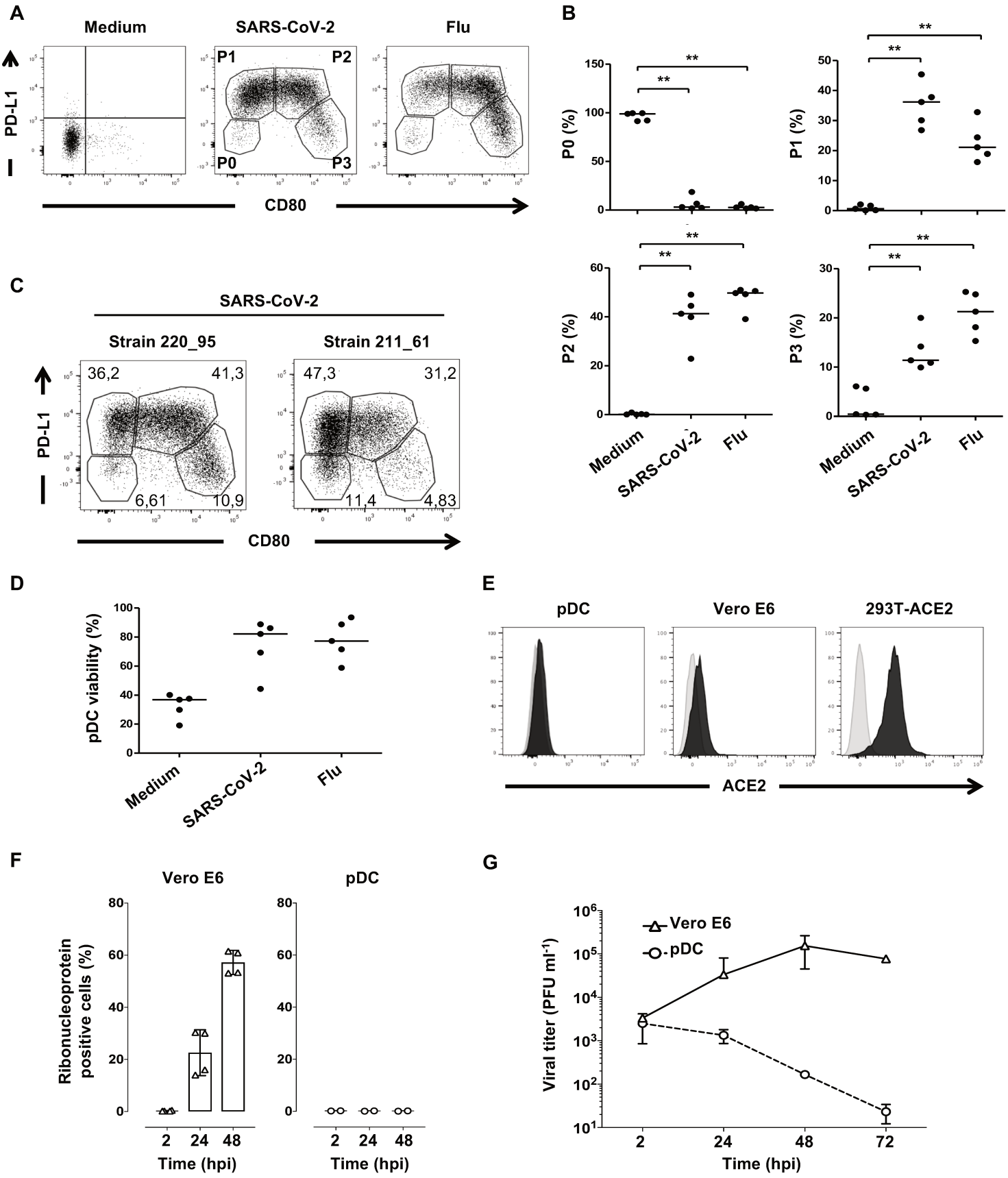
A
Medium
SARS-CoV-2
Flu
PD-L1
CD80
P0
P1
P2
P3
B
P0 (%)
P1 (%)
P2 (%)
P3 (%)
Medium
SARS-CoV-2
Flu
C
SARS-CoV-2
Strain 220_95
Strain 211_61
36,2
41,3
6,61
10,9
47,3
31,2
11,4
4,83
PD-L1
CD80
D
pDC viability (%)
Medium
SARS-CoV-2
Flu
E
pDC
Vero E6
293T-ACE2
ACE2
F
Vero E6
pDC
Ribonucleoprotein positive cells (%)
Time (hpi)
G
Vero E6
pDC
Viral titer (PFU ml-1)
Time (hpi)

Figure 1

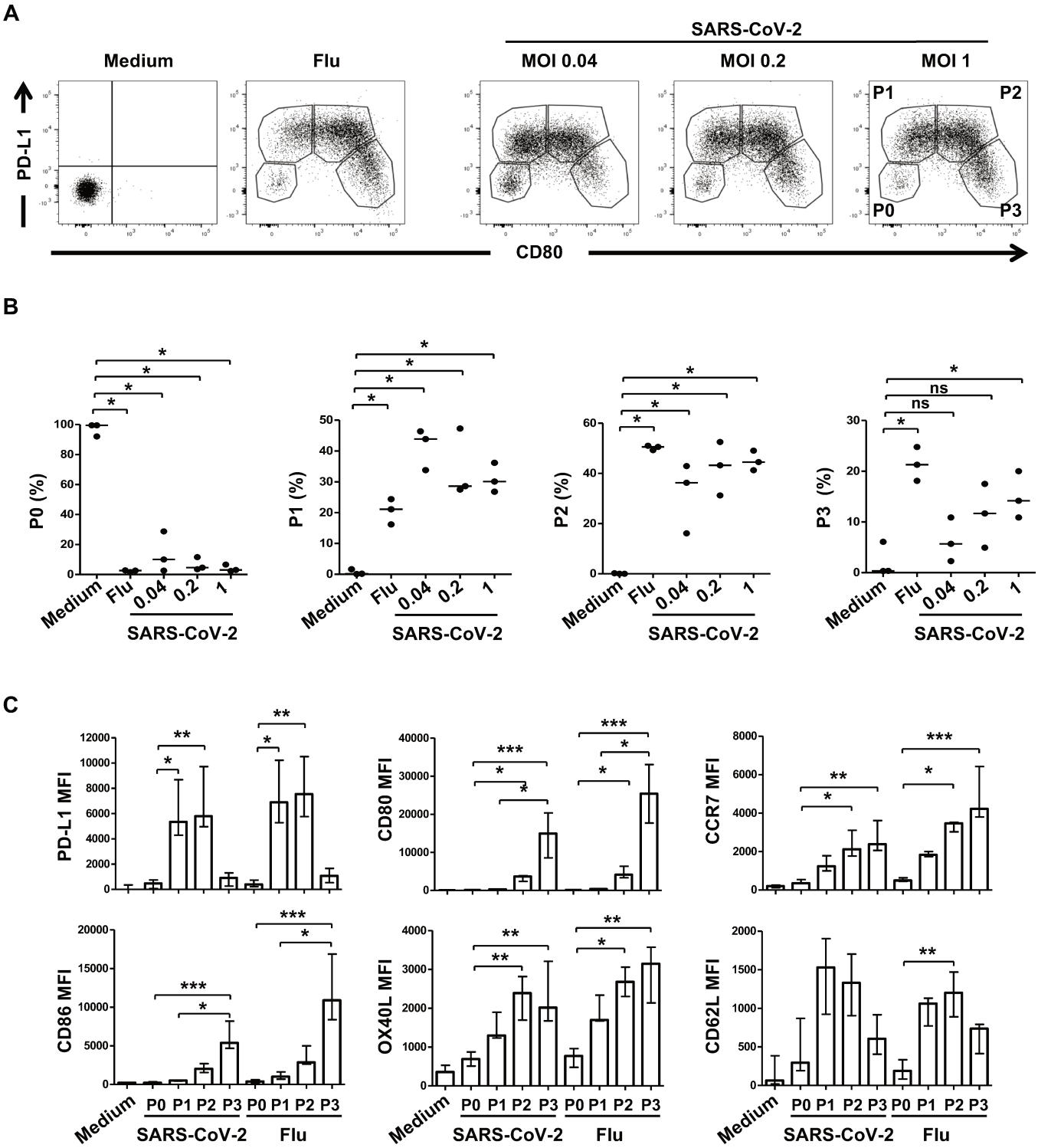
A
SARS-CoV-2
Medium
Flu
MOI 0.04
MOI 0.2
MOI 1
PD-L1
CD80
P1
P2
P0
P3
B
P0 (%)
P1 (%)
P2 (%)
P3 (%)
ns
Medium
Flu
0.04
0.2
1
SARS-CoV-2
C
PD-L1 MFI
CD80 MFI
CCR7 MFI
CD86 MFI
OX40L MFI
CD62L MFI
P0 P1 P2 P3
SARS-CoV-2
Flu

Figure 2

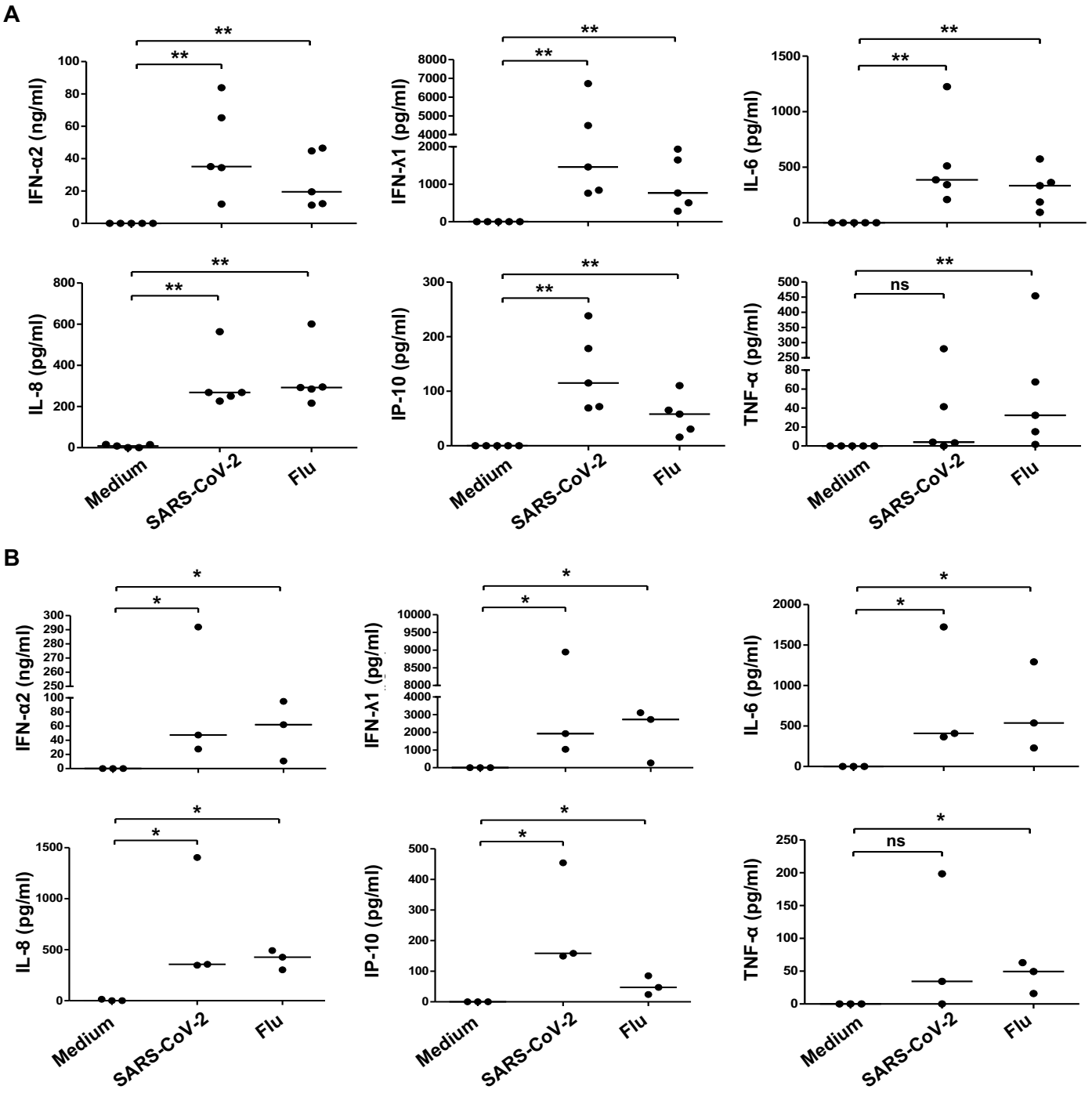
A
IFN-α2 (ng/ml)
IFN-λ1 (pg/ml)
IL-6 (pg/ml)
IL-8 (pg/ml)
IP-10 (pg/ml)
TNF-α (pg/ml)
ns
Medium
SARS-CoV-2
Flu
B
IFN-α2 (ng/ml)
IFN-λ1 (pg/ml)
IL-6 (pg/ml)
IL-8 (pg/ml)
IP-10 (pg/ml)
TNF-α (pg/ml)
ns
Medium
SARS-CoV-2
Flu

Figure 3

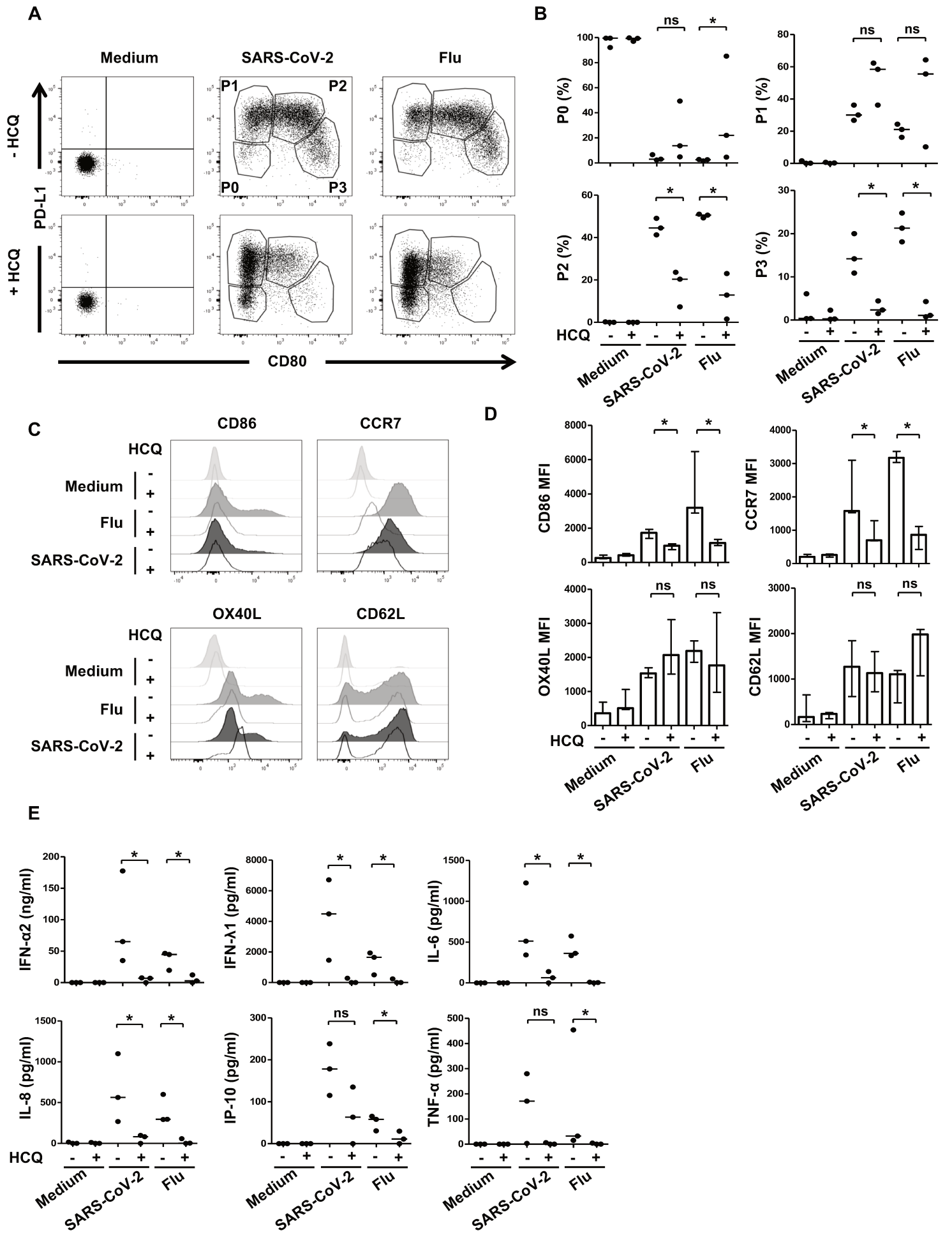
A
Medium
SARS-CoV-2
Flu
- HCQ
+ HCQ
PD-L1
CD80
P0
P1
P2
P3
B
P0 (%)
P1 (%)
P2 (%)
P3 (%)
ns
*
HCQ
Medium
SARS-CoV-2
Flu
C
CD86
CCR7
OX40L
CD62L
HCQ
Medium
Flu
SARS-CoV-2
D
CD86 MFI
CCR7 MFI
OX40L MFI
CD62L MFI
E
IFN-α2 (ng/ml)
IFN-λ1 (pg/ml)
IL-6 (pg/ml)
IL-8 (pg/ml)
IP-10 (pg/ml)
TNF-α (pg/ml)

Figure 4

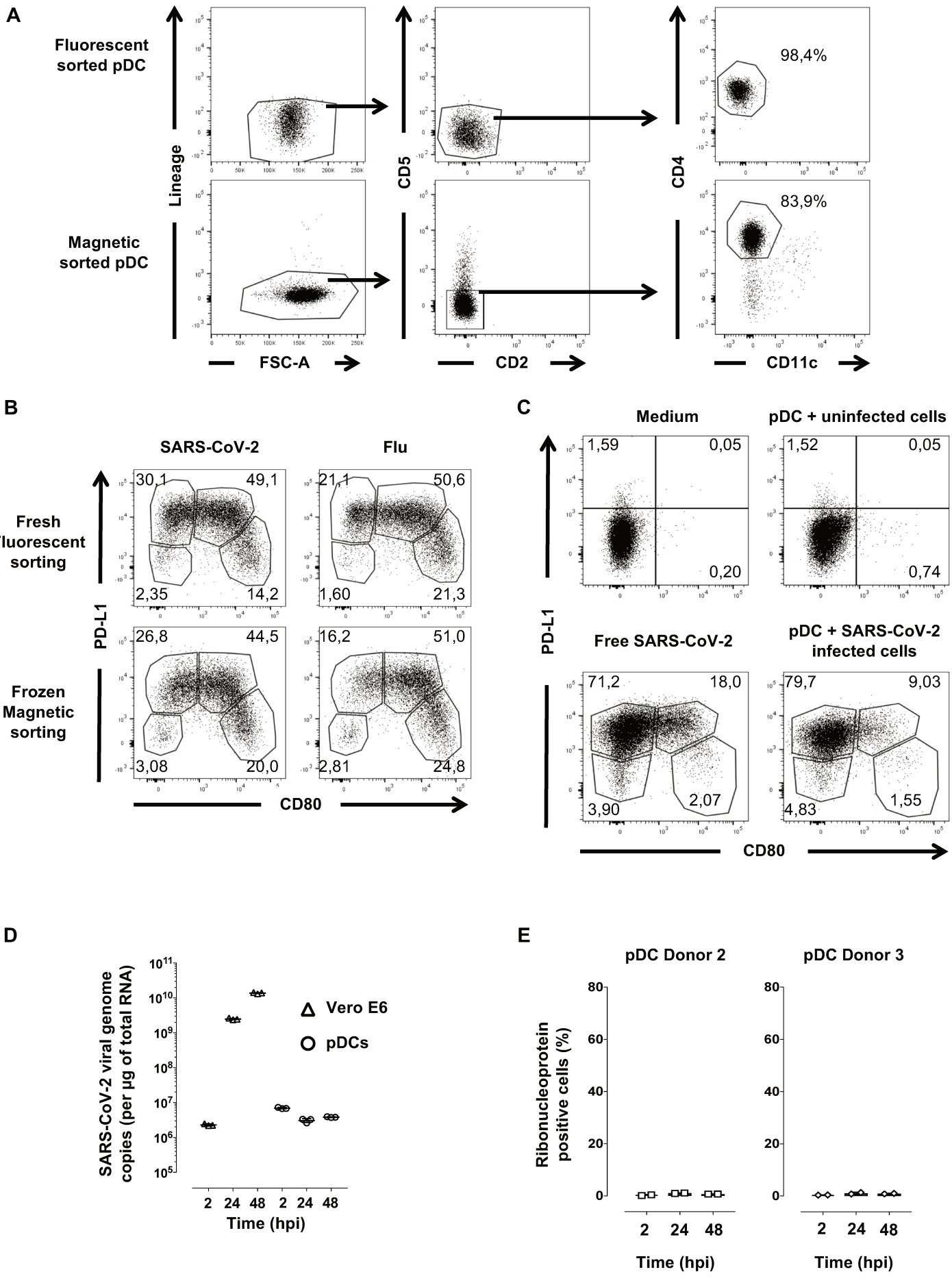
A
Fluorescent sorted pDC
Magnetic sorted pDC
Lineage
FSC-A
CD5
CD2
CD4
CD11c
98,4%
83,9%
B
SARS-CoV-2
Flu
Fresh Fluorescent sorting
Frozen Magnetic sorting
PD-L1
CD80
30,1
49,1
2,35
14,2
21,1
50,6
1,60
21,3
26,8
44,5
3,08
20,0
16,2
51,0
2,81
24,8
C
Medium
pDC + uninfected cells
Free SARS-CoV-2
pDC + SARS-CoV-2 infected cells
PD-L1
CD80
1,59
0,05
0,20
1,52
0,05
0,74
71,2
18,0
3,90
2,07
79,7
9,03
4,83
1,55
D
SARS-CoV-2 viral genome copies (per µg of total RNA)
Vero E6
pDCs
Time (hpi)
2 24 48 2 24 48
E
pDC Donor 2
pDC Donor 3
Ribonucleoprotein positive cells (%)
Time (hpi)
2 24 48

Figure 5

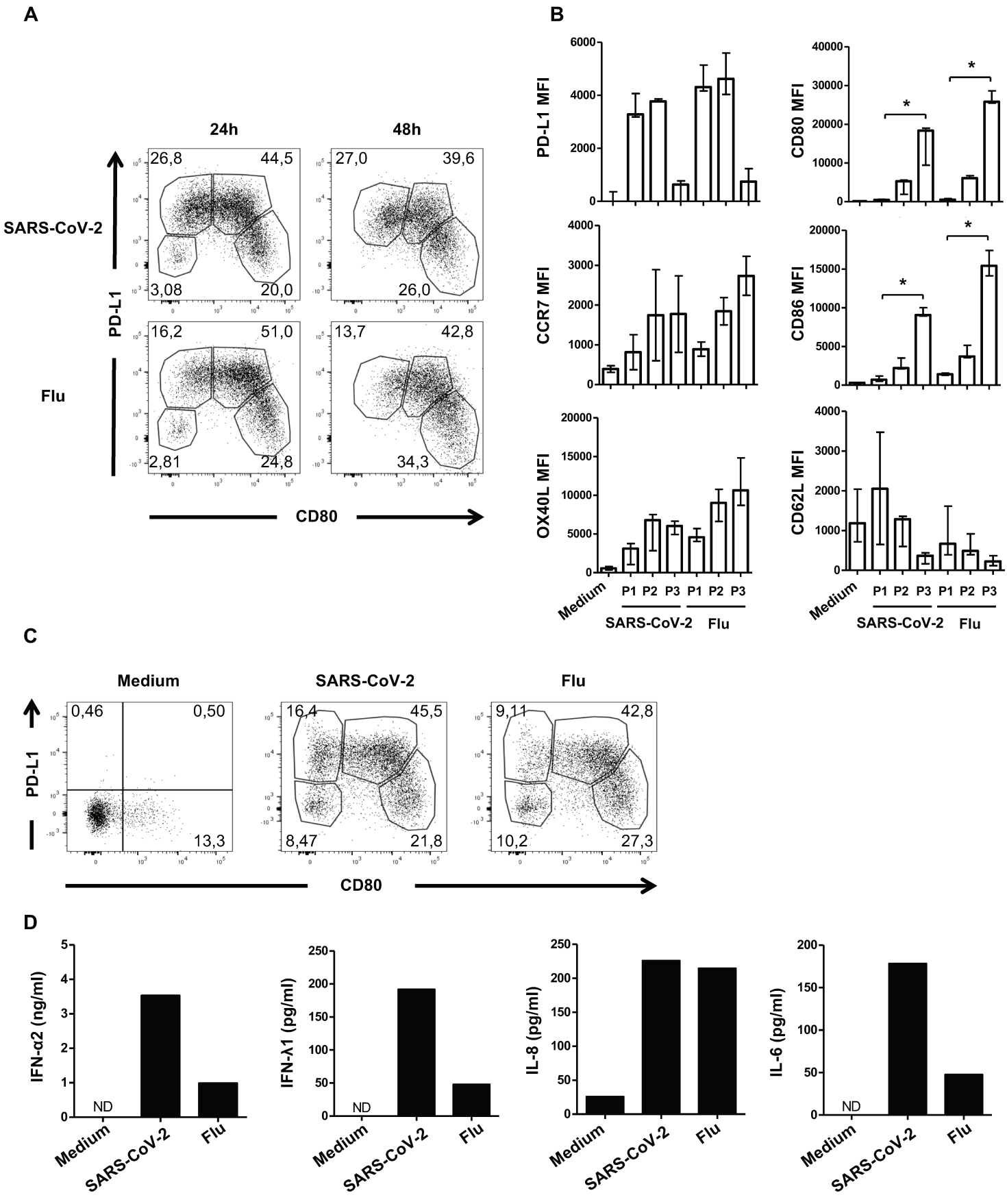
A
24h
48h
SARS-CoV-2
Flu
PD-L1
CD80
26,8
44,5
3,08
20,0
27,0
39,6
26,0
16,2
51,0
2,81
24,8
13,7
42,8
34,3
B
PD-L1 MFI
CD80 MFI
CCR7 MFI
CD86 MFI
OX40L MFI
CD62L MFI
Medium
P1 P2 P3 P1 P2 P3
SARS-CoV-2
Flu
C
Medium
SARS-CoV-2
Flu
PD-L1
CD80
0,46
0,50
13,3
16,4
45,5
8,47
21,8
9,11
42,8
10,2
27,3
D
IFN-α2 (ng/ml)
IFN-λ1 (pg/ml)
IL-8 (pg/ml)
IL-6 (pg/ml)
ND
Medium
SARS-CoV-2
Flu

Figure 6

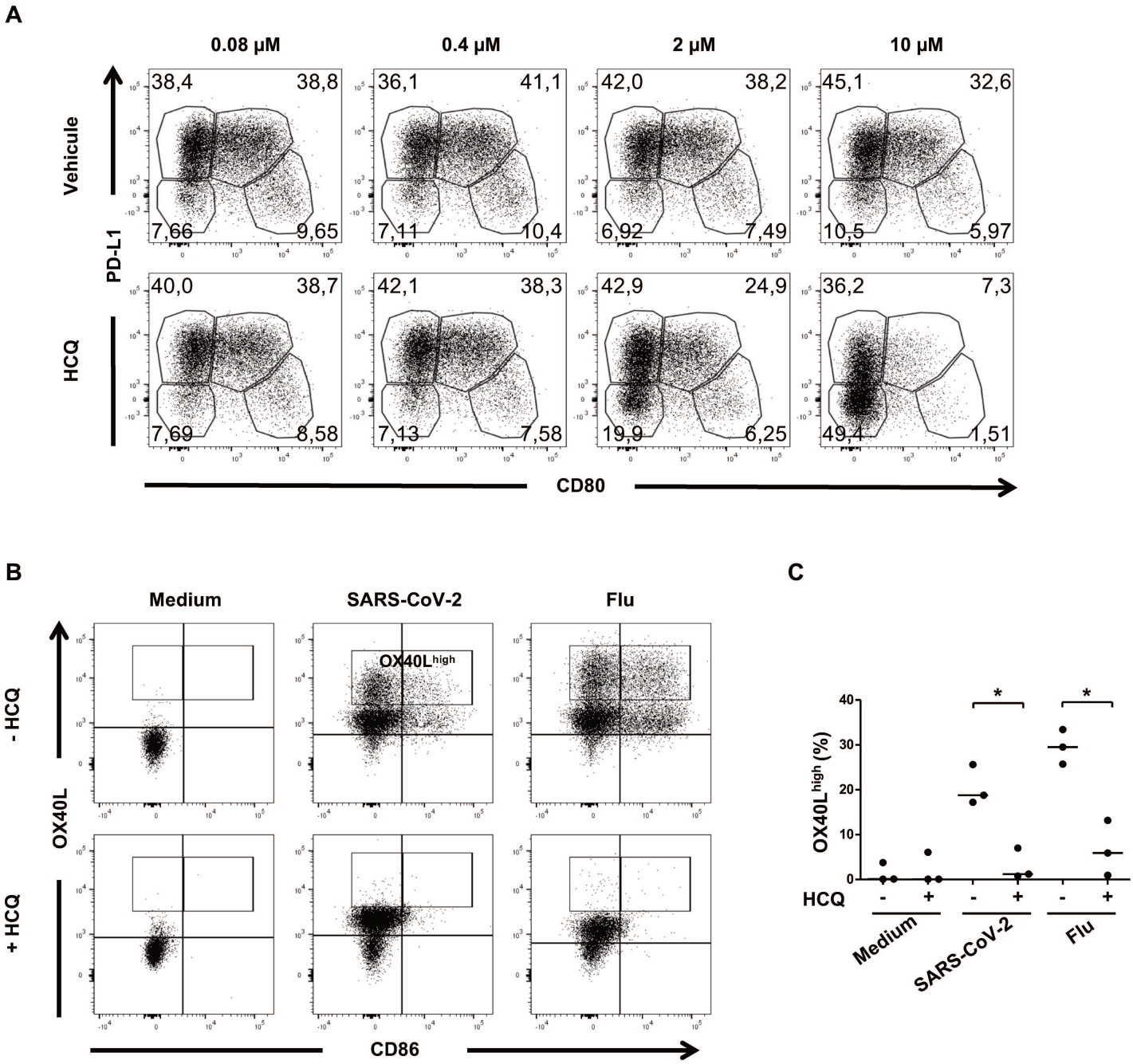
A
0.08 µM
0.4 µM
2 µM
10 µM
Vehicule
HCQ
PD-L1
CD80
38,4
38,8
7,66
9,65
36,1
41,1
7,11
10,4
42,0
38,2
6,92
7,49
45,1
32,6
10,5
5,97
40,0
38,7
7,69
8,58
42,1
38,3
7,13
7,58
42,9
24,9
19,9
6,25
36,2
7,3
49,4
1,51
B
Medium
SARS-CoV-2
Flu
- HCQ
+ HCQ
OX40L
CD86
OX40Lhigh
C
OX40Lhigh (%)
HCQ
Medium
SARS-CoV-2
Flu
*
*

Figure 7

4. Appendix 4

Inborn errors of type I IFN immunity in patients with life-threatening COVID-19

Qian Zhang, Paul Bastard*, Zhiyong Liu*, Jérémie Le Pen*, Marcela Moncada-Velez*, Jie Chen*, Masato Ogishi*, Ira K. D. Sabli*, Stephanie Hodeib*, Cecilia Korol*, Jérémie Rosain*, Kaya Bilguvar*, Junqiang Ye*, Alexandre Bolze*, Benedetta Bigio*, Rui Yang*, Andrés Augusto Arias*, Qinhua Zhou*, Yu Zhang*, Fanny Onodi, Sarantis Korniotis, Léa Karpf, Quentin Philippot, Marwa Chbihi, Lucie Bonnet-Madin, Karim Dorgham,Nikaïa Smith, William M. Schneider, Brandon S. Razooky, Hans-Heinrich Hoffmann, Eleftherios Michailidis, Leen Moens, Ji Eun Han, Lazaro Lorenzo, Lucy Bizien, Philip Meade, Anna-Lena Neehus, Aileen Camille Ugurbil, Aurélien Corneau, Gaspard Kerner, Peng Zhang, Franck Rapaport, Yoann Seeleuthner, Jeremy Manry, Cecile Masson, Yohann Schmitt, Agatha Schlüter, Tom Le Voyer, Taushif Khan, Juan Li, Jacques Fellay, Lucie Roussel, Mohammad Shahrooei, Mohammed F. Alosaimi, Davood Mansouri, Haya Al-Saud, Fahd Al-Mulla, Feras Almourfi, Saleh Zaid Al-Muhsen, Fahad Alsohime, Saeed Al Turki, Rana Hasanato, Diederik van de Beek, Andrea Biondi, Laura Rachele Bettini, Mariella D'Angio, Paolo Bonfanti, Luisa Imberti, Alessandra Sottini, Simone Paghera, Eugenia Quiros-Roldan, Camillo Rossi, Andrew J. Oler, Miranda F. Tompkins, Camille Alba, Isabelle Vandernoot, Jean-Christophe Goffard, Guillaume Smits, Isabelle Migeotte, Filomeen Haerynck, Pere Soler-Palacin, Andrea Martin-Nalda, Roger Colobran, Pierre-Emmanuel Morange, Sevgi Keles, Fatma Çölkesen, Tayfun Ozcelik, Kadriye Kart Yasar, Sevtap Senoglu, Şemsi Nur Karabela, Carlos Rodríguez-Gallego, Giuseppe Novelli, Sami Hraiech, Yacine Tandjaoui-Lambiotte, Xavier Duval, Cédric Laouénan, COVID-STORM Clinicians†, COVID Clinicians†, Imagine COVID Group†, French COVID Cohort Study Group†, CoV-Contact Cohort†, Amsterdam UMC Covid-19 Biobank†, COVID Human Genetic Effort†, NIAID-USUHS/TAGC COVID Immunity Group†, Andrew L. Snow, Clifton L. Dalgard, Joshua D. Milner, Donald C. Vinh, Trine H. Mogensen, Nico Marr, András N. Spaan, Bertrand Boisson, Stéphanie Boisson-Dupuis, Jacinta Bustamante, Anne Puel, Michael J. Ciancanelli, Isabelle Meyts, Tom Maniatis, Vassili Soumelis, Ali Amara, Michel Nussenzweig, Adolfo García-Sastre, Florian Krammer, Aurora Pujol, Darragh Duffy, Richard P. Lifton‡, Shen-Ying Zhang‡, Guy Gorochov‡, Vivien Béziat ‡, Emmanuelle Jouanguy‡, Vanessa Sancho-Shimizu‡, Charles M. Rice‡, Laurent Abel ‡, Luigi D. Notarangelo§, Aurélie Cobat§, Helen C. Su§, Jean-Laurent Casanova§¶

Zhang et al, Science 370, 422 (2020)

RESEARCH ARTICLE SUMMARY

CORONAVIRUS

Inborn errors of type I IFN immunity in patients with life-threatening COVID-19

Qian Zhang *et al.*

INTRODUCTION: Clinical outcomes of human severe acute respiratory syndrome coronavirus 2 (SARS-CoV-2) infection range from silent infection to lethal coronavirus disease 2019 (COVID-19). Epidemiological studies have identified three risk factors for severe disease: being male, being elderly, and having other medical conditions. However, interindividual clinical variability remains huge in each demographic category. Discovering the root cause and detailed molecular, cellular, and tissue- and body-level mechanisms underlying life-threatening COVID-19 is of the utmost biological and medical importance.

RATIONALE: We established the COVID Human Genetic Effort (www.covidhge.com) to test the general hypothesis that life-threatening COVID-19 in some or most patients may be caused by monogenic inborn errors of immunity to SARS-CoV-2 with incomplete or complete penetrance. We sequenced the exome or genome of 659 patients of various ancestries with life-threatening COVID-19 pneumonia and 534 subjects with asymptomatic or benign infection. We tested the specific hypothesis that inborn errors of Toll-like receptor 3 (TLR3)– and interferon regulatory factor 7 (IRF7)–dependent type I interferon (IFN) immunity that underlie life-threatening influenza pneumonia also underlie life-threatening COVID-19 pneumonia. We considered three loci identified as mutated in patients with life-threatening influenza: *TLR3*, *IRF7*, and *IRF9*. We also considered 10 loci mutated in patients with other viral illnesses but directly connected to the three core genes conferring influenza susceptibility: *TICAM1/TRIF*, *UNC93B1*, *TRAF3*, *TBK1*, *IRF3*, and *NEMO/IKBKG* from the TLR3-dependent type I IFN induction pathway, and *IFNAR1*, *IFNAR2*, *STAT1*, and *STAT2* from the IRF7- and IRF9-dependent type I IFN amplification pathway. Finally, we considered various modes of inheritance at these 13 loci.

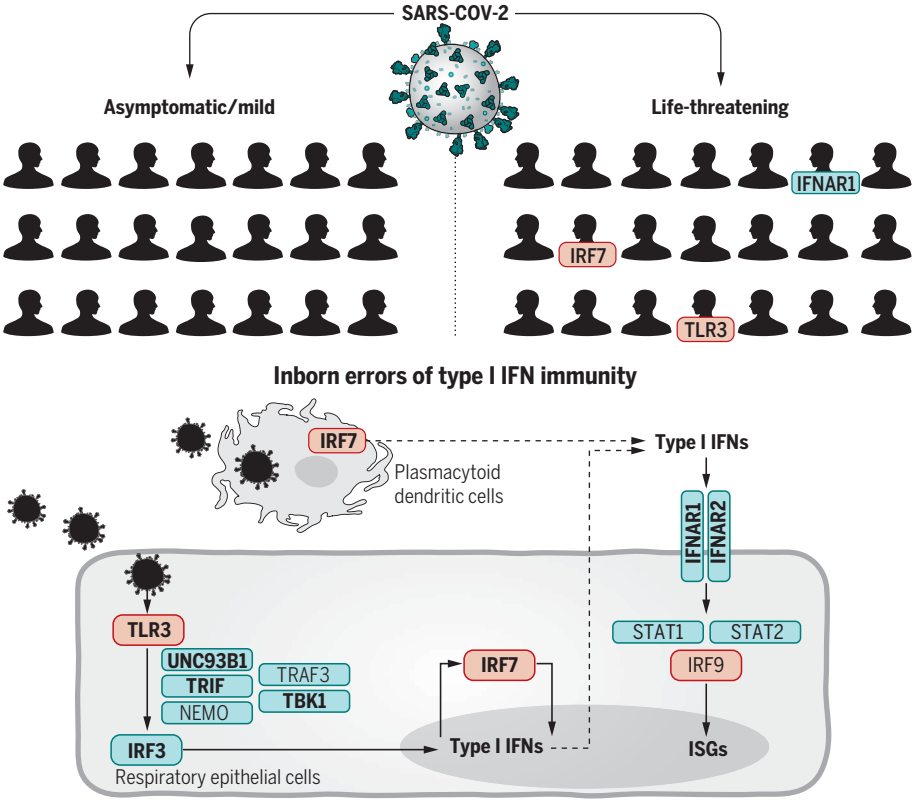

Inborn errors of TLR3- and IRF7-dependent type I IFN production and amplification underlie life-threatening COVID-19 pneumonia. Molecules in red are encoded by core genes, deleterious variants of which underlie critical influenza pneumonia with incomplete penetrance, and deleterious variants of genes encoding biochemically related molecules in blue underlie other viral illnesses. Molecules represented in bold are encoded by genes with variants that also underlie critical COVID-19 pneumonia.

RESULTS: We found an enrichment in variants predicted to be loss-of-function (pLOF), with a minor allele frequency <0.001, at the 13 candidate loci in the 659 patients with life-threatening COVID-19 pneumonia relative to the 534 subjects with asymptomatic or benign infection (P = 0.01). Experimental tests for all 118 rare nonsynonymous variants (including both pLOF and other variants) of these 13 genes found in patients with critical disease identified 23 patients (3.5%), aged 17 to 77 years, carrying 24 deleterious variants of eight genes. These variants underlie autosomal-recessive (AR) deficiencies (*IRF7* and *IFNAR1*) and autosomal-dominant (AD) deficiencies (*TLR3*, *UNC93B1*, *TICAM1*, *TBK1*, *IRF3*, *IRF7*, *IFNAR1*, and *IFNAR2*) in four and 19 patients, respectively. These patients had never been hospitalized for other life-threatening viral illness. Plasmacytoid dendritic cells from IRF7-deficient patients produced no type I IFN on infection with SARS-CoV-2, and TLR3$^{-/-}$, TLR3$^{+/-}$, IRF7$^{-/-}$, and IFNAR1$^{-/-}$ fibroblasts were susceptible to SARS-CoV-2 infection in vitro.

CONCLUSION: At least 3.5% of patients with life-threatening COVID-19 pneumonia had known (AR IRF7 and IFNAR1 deficiencies or AD TLR3, TICAM1, TBK1, and IRF3 deficiencies) or new (AD UNC93B1, IRF7, IFNAR1, and IFNAR2 deficiencies) genetic defects at eight of the 13 candidate loci involved in the TLR3- and IRF7-dependent induction and amplification of type I IFNs. This discovery reveals essential roles for both the double-stranded RNA sensor TLR3 and type I IFN cell-intrinsic immunity in the control of SARS-CoV-2 infection. Type I IFN administration may be of therapeutic benefit in selected patients, at least early in the course of SARS-CoV-2 infection. ■

The full author list and the list of affiliations is available in the full article online.
Corresponding author: Jean-Laurent Casanova (casanova@rockefeller.edu)

Cite this article as Q. Zhang *et al.*, *Science* **370**, eabd4570 (2020). DOI: 10.1126/science.abd4570

READ THE FULL ARTICLE AT
https://doi.org/10.1126/science.abd4570

RESEARCH ARTICLE

CORONAVIRUS

Inborn errors of type I IFN immunity in patients with life-threatening COVID-19

Qian Zhang[1], Paul Bastard[2,3]*, Zhiyong Liu[1]*, Jérémie Le Pen[4]*, Marcela Moncada-Velez[1]*, Jie Chen[1]*, Masato Ogishi[1]*, Ira K. D. Sabli[5]*, Stephanie Hodeib[5]*, Cecilia Korol[2]*, Jérémie Rosain[2,3]*, Kaya Bilguvar[6]*, Junqiang Ye[7]*, Alexandre Bolze[8]*, Benedetta Bigio[1]*, Rui Yang[1]*, Andrés Augusto Arias[1,9,10]*, Qinhua Zhou[1]*, Yu Zhang[11,12]*, Fanny Onodi[13], Sarantis Korniotis[13], Léa Karpf[13], Quentin Philippot[2,3], Marwa Chbihi[2,3], Lucie Bonnet-Madin[14], Karim Dorgham[15], Nikaïa Smith[16], William M. Schneider[4], Brandon S. Razooky[4], Hans-Heinrich Hoffmann[4], Eleftherios Michailidis[4], Leen Moens[17], Ji Eun Han[1], Lazaro Lorenzo[2,3], Lucy Bizien[2,3], Philip Meade[18], Anna-Lena Neehus[2,3], Aileen Camille Ugurbil[1], Aurélien Corneau[19], Gaspard Kerner[2,3], Peng Zhang[1], Franck Rapaport[1], Yoann Seeleuthner[2,3], Jeremy Manry[2,3], Cecile Masson[20], Yohann Schmitt[20], Agatha Schlüter[21], Tom Le Voyer[2,3], Taushif Khan[22], Juan Li[1], Jacques Fellay[23,24,25], Lucie Roussel[26], Mohammad Shahrooei[27,28], Mohammed F. Alosaimi[29], Davood Mansouri[30,31,32], Haya Al-Saud[33], Fahd Al-Mulla[34], Feras Almourfi[33], Saleh Zaid Al-Muhsen[35], Fahad Alsohime[29], Saeed Al Turki[36,37], Rana Hasanato[29], Diederik van de Beek[38], Andrea Biondi[39], Laura Rachele Bettini[39], Mariella D'Angio'[39], Paolo Bonfanti[40], Luisa Imberti[41], Alessandra Sottini[41], Simone Paghera[41], Eugenia Quiros-Roldan[42], Camillo Rossi[43], Andrew J. Oler[44], Miranda F. Tompkins[45], Camille Alba[45], Isabelle Vandernoot[46], Jean-Christophe Goffard[47], Guillaume Smits[46], Isabelle Migeotte[48], Filomeen Haerynck[49], Pere Soler-Palacin[50], Andrea Martin-Nalda[50], Roger Colobran[51], Pierre-Emmanuel Morange[52], Sevgi Keles[53], Fatma Çölkesen[54], Tayfun Ozcelik[55], Kadriye Kart Yasar[56], Sevtap Senoglu[56], Şemsi Nur Karabela[56], Carlos Rodríguez-Gallego[57,58], Giuseppe Novelli[59], Sami Hraiech[60], Yacine Tandjaoui-Lambiotte[61,62], Xavier Duval[63,64], Cédric Laouénan[63,64,65], COVID-STORM Clinicians†, COVID Clinicians†, Imagine COVID Group†, French COVID Cohort Study Group†, CoV-Contact Cohort†, Amsterdam UMC Covid-19 Biobank†, COVID Human Genetic Effort†, NIAID-USUHS/TAGC COVID Immunity Group†, Andrew L. Snow[66], Clifton L. Dalgard[45,67], Joshua D. Milner[68], Donald C. Vinh[26], Trine H. Mogensen[69,70], Nico Marr[22,71], András N. Spaan[1,72], Bertrand Boisson[1,2,3], Stéphanie Boisson-Dupuis[1,2,3], Jacinta Bustamante[1,2,3,73], Anne Puel[1,2,3], Michael J. Ciancanelli[1,74], Isabelle Meyts[17,75], Tom Maniatis[7,76], Vassili Soumelis[13,77], Ali Amara[14], Michel Nussenzweig[78,79], Adolfo García-Sastre[18,80,81,82], Florian Krammer[18], Aurora Pujol[21], Darragh Duffy[16], Richard P. Lifton[83,84,85]‡, Shen-Ying Zhang[1,2,3]‡, Guy Gorochov[15]‡, Vivien Béziat[1,2,3]‡, Emmanuelle Jouanguy[1,2,3]‡, Vanessa Sancho-Shimizu[5]‡, Charles M. Rice[4]‡, Laurent Abel[1,2,3]‡, Luigi D. Notarangelo[11,12]§, Aurélie Cobat[1,2,3]§, Helen C. Su[11,12]§, Jean-Laurent Casanova[1,2,3,79,86]§¶

Clinical outcome upon infection with severe acute respiratory syndrome coronavirus 2 (SARS-CoV-2) ranges from silent infection to lethal coronavirus disease 2019 (COVID-19). We have found an enrichment in rare variants predicted to be loss-of-function (LOF) at the 13 human loci known to govern Toll-like receptor 3 (TLR3)– and interferon regulatory factor 7 (IRF7)–dependent type I interferon (IFN) immunity to influenza virus in 659 patients with life-threatening COVID-19 pneumonia relative to 534 subjects with asymptomatic or benign infection. By testing these and other rare variants at these 13 loci, we experimentally defined LOF variants underlying autosomal-recessive or autosomal-dominant deficiencies in 23 patients (3.5%) 17 to 77 years of age. We show that human fibroblasts with mutations affecting this circuit are vulnerable to SARS-CoV-2. Inborn errors of TLR3- and IRF7-dependent type I IFN immunity can underlie life-threatening COVID-19 pneumonia in patients with no prior severe infection.

Severe acute respiratory syndrome coronavirus 2 (SARS-CoV-2) has already claimed at least 1 million lives, has been detected in at least 20 million people, and has probably infected at least another 200 million. The clinical manifestations range from silent infection to lethal disease, with an infection fatality rate of 0.1 to 0.9%. Three epidemiological factors increase the risk of severity: (i) increasing age, decade by decade, after the age of 50, (ii) being male, and (iii) having various underlying medical conditions (*1*). However, even taking these factors into account, there is immense inter-individual clinical variability in each demographic category considered. Following on from our human genetic studies of other severe infectious diseases (*2*, *3*), we established the COVID Human Genetic Effort (https://www.covidhge.com) to test the general hypothesis that in some patients, life-threatening coronavirus disease 2019 (COVID-19) may be caused by monogenic inborn errors of immunity to SARS-CoV-2 with incomplete or complete penetrance (*4*). We enrolled 659 patients (74.5% men and 25.5% women, 13.9% of whom died) of various ancestries between 1 month and 99 years of age (Fig. 1A). These patients were hospitalized for life-threatening pneumonia caused by SARS-CoV-2 (critical COVID-19). We sequenced their whole genome (N = 364) or exome (N = 295), and principal component analysis (PCA) on these data confirmed their ancestries (Fig. 1B).

Candidate variants at 13 human loci that govern immunity to influenza virus

We first tested the specific hypothesis that inborn errors of Toll-like receptor 3 (TLR3)– and interferon regulatory factor 7 (IRF7)–dependent type I interferon (IFN) immunity, which underlie life-threatening influenza pneumonia, may also underlie life-threatening COVID-19 pneumonia (*5*) (Fig. 2). We considered three loci previously shown to be mutated in patients with critical influenza pneumonia: *TLR3* (*6*), *IRF7* (*7*), and *IRF9* (*8*). We also considered 10 loci mutated in patients with other viral illnesses but directly connected to the three core genes conferring influenza susceptibility: *TICAM1/TRIF* (*9*), *UNC93B1* (*10*), *TRAF3* (*11*), *TBK1* (*12*), *IRF3* (*13*), and *NEMO/IKBKG* (*14*) in the TLR3-dependent type I IFN induction pathway, and *IFNAR1* (*15*), *IFNAR2* (*16*), *STAT1* (*17*), and *STAT2* (*18*) in the IRF7- and IRF9-dependent type I IFN amplification pathway. We collected both monoallelic and biallelic nonsynonymous variants with a minor allele frequency (MAF) <0.001 at all 13 loci. Twelve of the 13 candidate loci are autosomal, whereas *NEMO* is X-linked. For the latter gene, we considered only a recessive model (*19*). Autosomal-dominant (AD) inheritance has not been proven for six of the 12 autosomal loci (*UNC93B1*, *IRF7*, *IFNAR1*, *IFNAR2*, *STAT2*, and *IRF9*). Nevertheless, we considered heterozygous variants because none of the patients enrolled had been hospitalized for critical viral infections before COVID-19, raising the possibility that any underlying genetic defects that they might have display a lower penetrance for influenza and other viral illnesses than for COVID-19, which is triggered by a more virulent virus.

Enrichment of variants predicted to be LOF at the influenza susceptibility loci

We found four unrelated patients with biallelic variants of *IRF7* or *IFNAR1* (Table 1 and table S1). We also found 113 patients carrying 113 monoallelic variants at 12 loci: *TLR3* (N = 7 patients/7 variants), *UNC93B1* (N = 10/9), *TICAM1* (N = 17/15), *TRAF3* (N = 6/6), *TBK1* (N = 12/11), *IRF3* (N = 5/5), *IRF7* (N = 20/13), *IFNAR1* (N = 14/13), *IFNAR2* (N = 17/15), *STAT1* (N = 4/4), *STAT2* (N = 11/11), and *IRF9* (N = 4/4). We detected no copy number variation

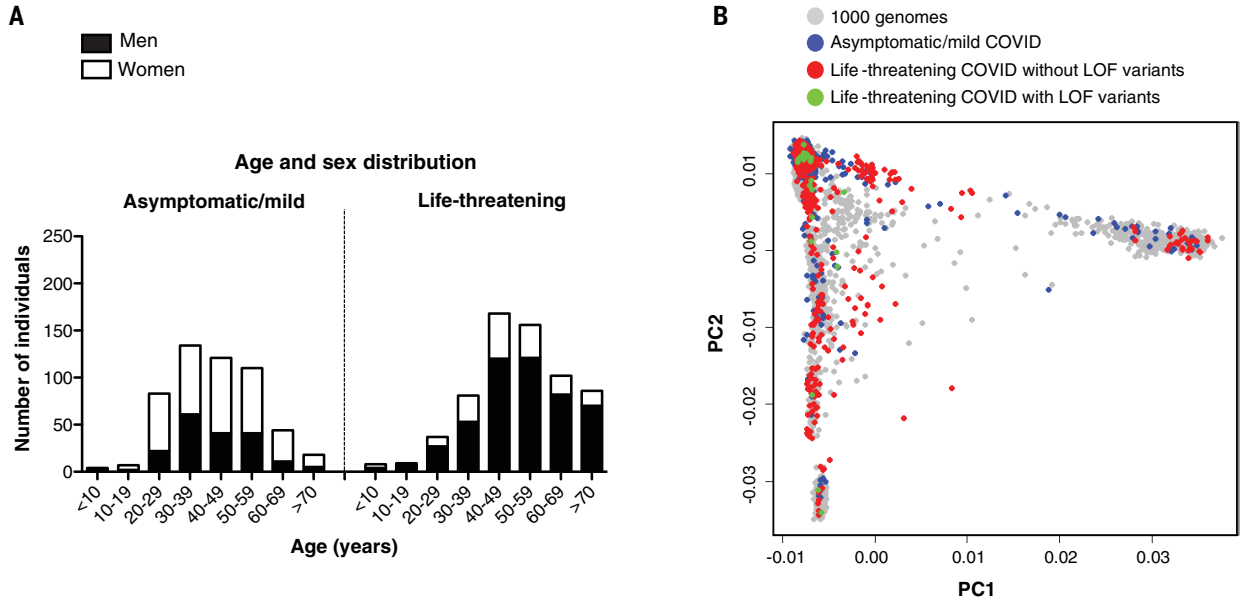

Fig. 1. Demographic and genetic data for the COVID-19 cohort. (**A**) Age and sex distribution of patients with life-threatening COVID-19. (**B**) PCA of patient (with or without LOF variants in the 13 candidate genes) and control cohorts (patients with mild or asymptomatic disease and individuals from the 1000 Genomes Project).

[1]St. Giles Laboratory of Human Genetics of Infectious Diseases, Rockefeller Branch, The Rockefeller University, New York, NY, USA. [2]Laboratory of Human Genetics of Infectious Diseases, Necker Branch, INSERM U1163, Necker Hospital for Sick Children, Paris, France. [3]University of Paris, Imagine Institute, Paris, France. [4]Laboratory of Virology and Infectious Disease, The Rockefeller University, New York, NY, USA. [5]Department of Paediatric Infectious Diseases & Virology, Imperial College London, London, UK. [6]Yale Center for Genome Analysis and Department of Genetics, Yale School of Medicine, New Haven, CT, USA. [7]Zukerman Mind Brain Behavior Institute, Columbia University, New York, NY, USA. [8]Helix, San Mateo, CA, USA. [9]Primary Immunodeficiencies Group, University of Antioquia UdeA, Medellin, Colombia. [10]School of Microbiology, University of Antioquia UdeA, Medellin, Colombia. [11]Laboratory of Clinical Immunology and Microbiology, Division of Intramural Research, NIAID, NIH, Bethesda, MD, USA. [12]NIAID Clinical Genomics Program, NIH, Bethesda, MD, USA. [13]Université de Paris, Institut de Recherche Saint-Louis, INSERM U976, Hôpital Saint-Louis, Paris, France. [14]Laboratory of Genomes & Cell Biology of Disease, INSERM U944, CNRS UMR 7212, Université de Paris, Institut de Recherche Saint-Louis, Hôpital Saint-Louis, Paris, France. [15]Sorbonne Université, Inserm, Centre d'Immunologie et des Maladies Infectieuses–Paris (CIMI PARIS), Assistance Publique-Hôpitaux de Paris (AP-HP) Hôpital Pitié-Salpêtrière, Paris, France. [16]Translational Immunology Lab, Institut Pasteur, Paris, France. [17]Laboratory for Inborn Errors of Immunity, Department of Microbiology, Immunology and Transplantation, Department of Pediatrics, University Hospitals Leuven, KU Leuven, Leuven, Belgium. [18]Department of Microbiology, Icahn School of Medicine at Mount Sinai, New York, NY, USA. [19]Sorbonne Université, UMS037, PASS, Plateforme de Cytométrie de la Pitié-Salpêtrière CyPS, Paris, France. [20]Bioinformatics Platform, Structure Fédérative de Recherche Necker, INSERM UMR1163, Université de Paris, Imagine Institute, Paris, France. [21]Neurometabolic Diseases Laboratory, IDIBELL-Hospital Duran i Reynals, CIBERER U759, and Catalan Institution of Research and Advanced Studies (ICREA), Barcelona, Spain. [22]Department of Immunology, Research Branch, Sidra Medicine, Doha, Qatar. [23]School of Life sciences, Ecole Polytechnique Fédérale de Lausanne, Lausanne, Switzerland. [24]Precision Medicine Unit, Lausanne University Hospital and University of Lausanne, Lausanne, Switzerland. [25]Swiss Institue of Bioinformatics, Lausanne, Switzerland. [26]Infectious Disease Susceptibility Program, Research Institute, McGill University Health Centre, Montréal, Québec, Canada. [27]Specialized Immunology Laboratory of Dr. Shahrooei, Sina Medical Complex, Ahvaz, Iran. [28]Department of Microbiology and Immunology, Clinical and Diagnostic Immunology, KU Leuven, Leuven, Belgium. [29]Department of Pathology and Laboratory Medicine, College of Medicine, King Saud University, Riyadh, Saudi Arabia. [30]Department of Clinical Immunology and Infectious Diseases, National Research Institute of Tuberculosis and Lung Diseases, Shahid Beheshti University of Medical Sciences, Tehran, Iran. [31]The Clinical Tuberculosis and Epidemiology Research Center, National Research Institute of, Tuberculosis and Lung Diseases (NRITLD), Masih Daneshvari Hospital, Shahid Beheshti, University of Medical Sciences, Tehran, Iran. [32]Pediatric Respiratory Diseases Research Center, National Research Institute of Tuberculosis and Lung Diseases, Shahid Beheshti, Iran. [33]National Center of Genomics Technology, King Abdulaziz City for Science and Technology, Riyadh, Saudi Arabia. [34]Dasman Diabetes Institute, Department of Genetics and Bioinformatics, Kuwait. [35]Immunology Research Laboratory, Department of Pediatrics, College of Medicine and King Saud University Medical City, King Saud University, Riyadh, Saudi Arabia. [36]Translational Pathology, Department of Pathology and Laboratory Medicine, King Abdulaziz Medical City, Misery of National Guard Health Affairs, Riyadh, Saudi Arabia. [37]Cancer & Blood Research, King Abdullah International Medical Research Center, Riyadh, Saudi Arabia. [38]Amsterdam UMC, Department of Neurology, Amsterdam Neuroscience, Amsterdam, Netherlands. [39]Pediatric Departement and Centro Tettamanti-European Reference Network PaedCan, EuroBloodNet, MetabERN-University of Milano-Bicocca-Fondazione MBBM-Ospedale, San Gerardo, Monza, Italy. [40]Department of Infectious Diseases, San Gerardo Hospital–University of Milano-Bicocca, Monza, Italy. [41]CREA Laboratory, Diagnostic Laboratory, ASST Spedali Civili di Brescia, Brescia, Italy. [42]Department of Infectious and Tropical Diseases, University of Brescia and ASST Spedali di Brescia, Brescia, Italy. [43]Chief Medical Officer, ASST Spedali Civili di Brescia, Brescia, Italy. [44]Bioinformatics and Computational Biosciences Branch, Office of Cyber Infrastructure and Computational Biology, NIAID, NIH, Bethesda, MD, USA. [45]PRIMER, Uniformed Services University of the Health Sciences, Bethesda, MD, USA. [46]Center of Human Genetics, Hôpital Erasme, Université Libre de Bruxelles, Brussels, Belgium. [47]Department of Internal Medicine, Hôpital Erasme, Université Libre de Bruxelles, Brussels, Belgium. [48]Fonds de la Recherche Scientifique (FNRS) and Center of Human Genetics, Hôpital Erasme, Université Libre de Bruxelles, Brussels, Belgium. [49]Department of Paediatric Immunology and Pulmonology, Centre for Primary Immunodeficiency Ghent (CPIG), PID Research Lab, Jeffrey Modell Diagnosis and Research Centre, Ghent University Hospital, Ghent, Belgium. [50]Pediatric Infectious Diseases and Immunodeficiencies Unit, Hospital Universitari Vall d'Hebron, Vall d'Hebron Research Institute, Vall d'Hebron Barcelona Hospital Campus, Universitat Autònoma de Barcelona (UAB), Barcelona, Catalonia, Spain. [51]Immunology Division, Genetics Department, Hospital Universitari Vall d'Hebron, Vall d'Hebron Research Institute, Vall d'Hebron Barcelona Hospital Campus, UAB, Barcelona, Catalonia, Spain. [52]Aix Marseille Univ, INSERM, INRAE, C2VN, CHU Timone, Marseille, France. [53]Necmettin Erbakan University, Meram Medical Faculty, Division of Pediatric Allergy and Immunology, Konya, Turkey. [54]Department of Infectious Diseases and Clinical Microbiology, Konya Training and Research Hospital, Konya, Turkey. [55]Department of Molecular Biology and Genetics, Bilkent University, Bilkent-Ankara, Turkey. [56]Departments of Infectious Diseases and Clinical Microbiology, Bakirkoy Dr. Sadi Konuk Training and Research Hospital, University of Health Sciences, Istanbul, Turkey. [57]Department of Immunology, Hospital Universitario de G.C. Dr. Negrín, Canarian Health System, Las Palmas de Gran Canaria, Spain. [58]University Fernando Pessoa Canarias, Las Palmas de Gran Canaria, Spain. [59]Department of Biomedicine and Prevention, University of Rome "Tor Vergata," Rome, Italy. [60]Intensive Care Unit, AP-HM, Marseille, France. [61]Avicenne Hospital Intensive Care Unit, APHP, Bobigny, INSERM U1272 Hypoxia & Lung, Paris, France. [62]PH Réanimation CHU Avicenne, Bobigny, INSERM U1272 Hypoxie & Poumon, Paris, France. [63]Université de Paris, IAME UMR-S 1137, INSERM, Paris, France. [64]Inserm CIC 1425, Paris, France. [65]AP-HP, Département Epidémiologie Biostatistiques et Recherche Clinique, Hôpital Bichat, Paris, France. [66]Department of Pharmacology & Molecular Therapeutics, Uniformed Services University of the Health Sciences, Bethesda, MD, USA. [67]Department of Anatomy, Physiology & Genetics, Uniformed Services University of the Health Sciences, Bethesda, MD, USA. [68]Division of Pediatric Allergy, Immunology and Rheumatology, Columbia University, New York, USA. [69]Department of Infectious Diseases, Aarhus University Hospital, Skejby, Denmark. [70]Department of Biomedicine, Aarhus University, Aarhus, Denmark. [71]College of Health and Life Sciences, Hamad Bin Khalifa University, Doha, Qatar. [72]Department of Medical Microbiology, Utrecht UMC, Utrecht, Netherlands. [73]Study Center for Primary Immunodeficiencies, Necker Hospital for Sick Children, Paris, France. [74]Turnstone Biologics, New York, NY, USA. [75]Department of Pediatrics, University Hospitals Leuven, KU Leuven, Leuven, Belgium. [76]New York Genome Center, New York, NY, USA. [77]AP-HP, Hôpital Saint-Louis, Laboratoire d'Immunologie, Paris, France. [78]Laboratory of Molecular Immunology, Rockefeller University, New York, NY, USA. [79]Howard Hughes Medical Institute, New York, NY, USA. [80]Department of Medicine, Division of Infectious Diseases, Icahn School of Medicine at Mount Sinai, New York, NY, USA. [81]Global Health and Emerging Pathogens Institute, Icahn School of Medicine at Mount Sinai, New York, NY, USA. [82]The Tisch Cancer Institute, Icahn School of Medicine at Mount Sinai, New York, NY, USA. [83]Laboratory of Genetics and Genomics, The Rockefeller University, New York, NY, USA. [84]Department of Genetics, Yale University School of Medicine, New Haven, CT, USA. [85]Yale Center for Genome Analysis, Yale School of Medicine, New Haven, CT, USA. [86]Pediatric Hematology and Immunology Unit, Necker Hospital for Sick Children, AP-HP, Paris, France.
*These authors contributed equally to this work.
†All collaborators and their affiliations appear at the end of this paper.
‡These authors contributed equally to this work.
§These authors contributed equally to this work.
¶Corresponding author. Email: casanova@rockefeller.edu

for these 13 genes. Unexpectedly, one of these variants has been reported in patients with life-threatening influenza pneumonia (*TLR3* p.Pro554Ser) (*6*, *20*) and another was shown to be both deleterious and dominant-negative (*IFNAR1* p.Pro335del) (*21*). Nine of the 118 biallelic or monoallelic variants were predicted to be LOF (pLOF), whereas the remaining 109 were missense or in-frame indels (table S1). In a sample of 534 controls with asymptomatic or mild SARS-CoV-2 infection, we found only one heterozygous pLOF variation with a MAF <0.001 at the 13 loci (*IRF7* p.Leu99fs). A PCA-adjusted burden test on the 12 autosomal loci revealed significant enrichment in pLOF variants in patients relative to controls [P = 0.01; odds ratio (OR) = 8.28; 95% confidence interval (CI) = 1.04 to 65.64] under an AD mode of inheritance. The same analysis performed on synonymous variants with a MAF <0.001 was not significant (P = 0.19), indicating that our ethnicity-adjusted burden test was well calibrated.

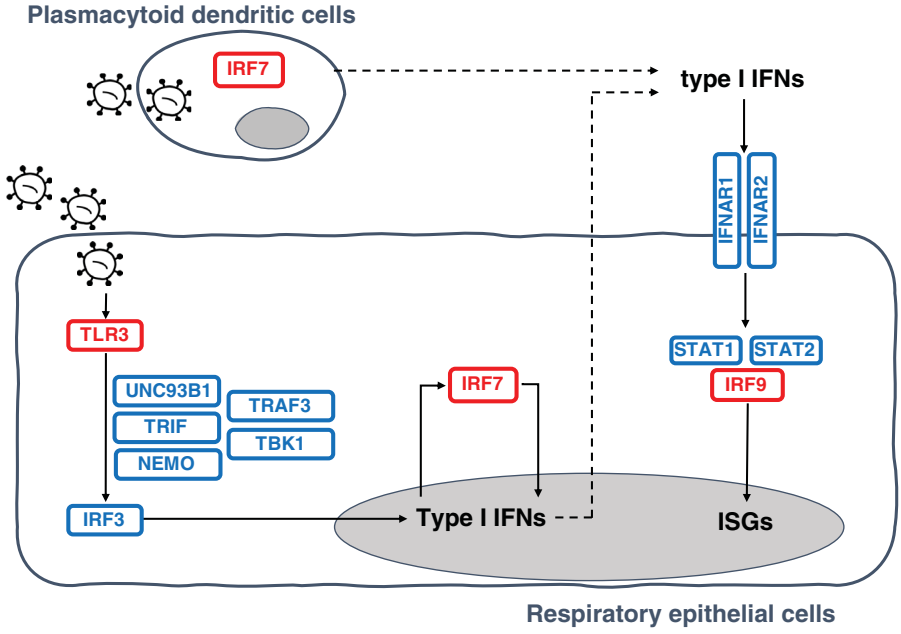

Fig. 2. Illustration of TLR3- and IRF7-dependent type I IFN production and amplification circuit. Molecules in red are encoded by core genes, deleterious variants of which underlie critical influenza pneumonia with incomplete penetrance; deleterious variants of genes encoding biochemically related molecules in blue underlie other viral illnesses. Type I IFNs also induce themselves. ISGs, interferon-stimulated genes.

Experimentally deleterious alleles at the influenza susceptibility loci in 3.5% of patients

We tested these 118 variants experimentally in ad hoc overexpression systems. We found that 24 variants of eight genes were deleterious (including all the pLOF variants) because they were loss-of-expression, LOF, or severely hypomorphic: *TLR3* (N = 4 variants), *UNC93B1* (N = 1), *TICAM1* (N = 3), *TBK1* (N = 2), *IRF3* (N = 2), *IRF7* (N = 8), *IFNAR1* (N = 3), and *IFNAR2* (N = 1) (table S1, Fig. 3, and figs. S1 to S8). Consistently, heterozygous LOF variants of *IRF3* and *IRF7* were reported in single patients with life-threatening influenza pneumonia (*22*, *23*). The remaining 94 variants were biochemically neutral. Twenty-three patients carried these 24 deleterious variants, resulting in four autosomal-recessive (AR) deficiencies (homozygosity or compound heterozygosity

Table 1. Disease-causing variants identified in patients with life-threatening COVID-19.

Gene	Inheritance	Genetic form	Genotype	Gender	Age [years]	Ancestry/residence	Outcome
TLR3	AD	Known	p.Ser339fs/WT	M	40	Spain	Survived
TLR3	AD	Known	p.Pro554Ser/WT	M	68	Italy	Survived
TLR3	AD	Known	p.Trp769*/WT	M	77	Italy	Survived
TLR3	AD	Known	p.Met870Val/WT	M	56	Colombia/Spain	Survived
UNC93B1	AD	New	p.Glu96*/WT	M	48	Venezuela/Spain	Survived
TICAM1	AD	Known	p.Thr4Ile/WT	M	49	Italy	Survived
TICAM1	AD	Known	p.Ser60Cys/WT	F	61	Vietnam/France	Survived
TICAM1	AD	Known	p.Gln392Lys/WT	F	71	Italy	Deceased
TBK1	AD	Known	p.Phe24Ser/WT	F	46	Venezuela/Spain	Survived
TBK1	AD	Known	p.Arg308*/WT	M	17	Turkey	Survived
IRF3	AD	Known	p.Glu49del/WT	F	23	Bolivia/Spain	Survived
IRF3	AD	Known	p.Asn146Lys/WT	F	60	Italy	Survived
IRF7	AR	Known	p.Pro364fs/p.Pro364fs	F	49	Italy/Belgium	Survived
IRF7	AR	Known	p.Met371Val/p.Asp117Asn	M	50	Turkey	Survived
IRF7	AD	New	p.Arg7fs/WT	M	60	Italy	Survived
IRF7	AD	New	p.Gln185*/WT	M	44	France	Survived
IRF7	AD	New	p.Pro246fs/WT	M	41	Spain	Survived
IRF7	AD	New	p.Arg369Gln/WT	M	69	Italy	Survived
IRF7	AD	New	p.Phe95Ser/WT	M	37	Turkey	Survived
IFNAR1	AR	Known	p.Trp73Cys/Trp73Cys	M	38	Turkey	Survived
IFNAR1	AR	Known	p.Ser422Arg/Ser422Arg	M	26	Pakistan/Saudi Arabia	Deceased
IFNAR1	AD	New	p.Pro335del/WT	F	23	China/Italy	Survived
IFNAR2	AD	New	p.Glu140fs/WT	F	54	Belgium	Survived

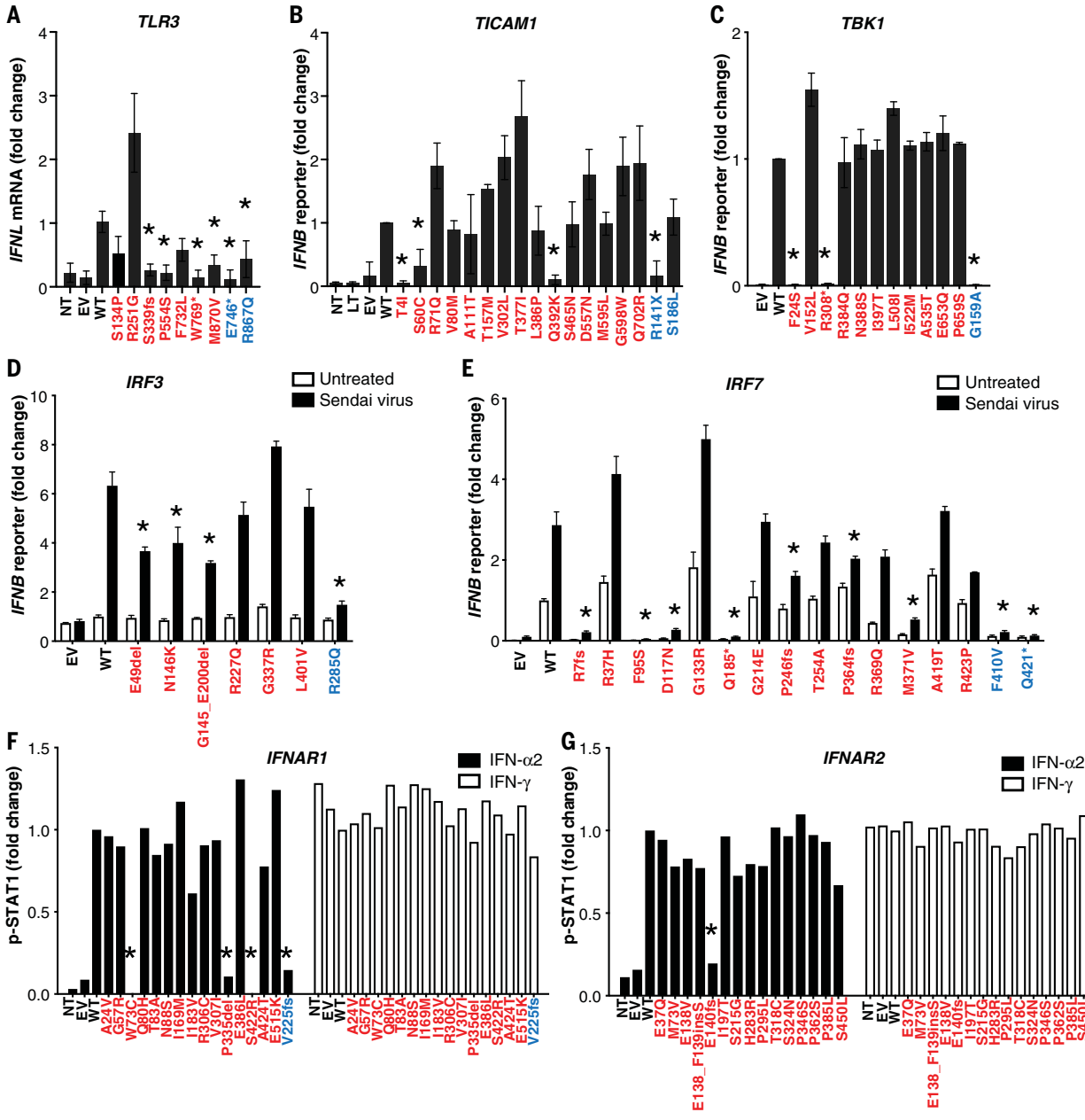

Fig. 3. Impact of *TLR3*, *TICAM1*, *TBK1*, *IRF3*, *IRF7*, *IFNAR1*, and *IFNAR2* variants on type I IFN signaling. (**A**) TLR3-deficient P2.1 fibrosarcoma cells were stably transfected with plasmids expressing WT or mutant forms of *TLR3*, and *IFNL1* mRNA levels were determined by reverse transcription quantitative PCR. *IFNL1* mRNA levels were expressed relative to the housekeeping gene *GUS* and then normalized. *IFNL1* was undetectable in unstimulated cells. The differences between variants and WT were tested using one-way ANOVA (*$P < 0.05$). (**B**) TICAM1-deficient SV40-Fib cells were transiently transfected with WT or mutant forms of *TICAM1*, together with an IFN-β luciferase reporter and a constitutively expressed reporter. Normalized luciferase induction was measured 24 hours after transfection. The differences between variants and WT were tested using one-way ANOVA (*$P < 0.05$). (**C**) HEK293T cells were transiently transfected with WT and mutant forms of *TBK1*, together with an IFN-β luciferase reporter and a constitutively expressed reporter. Normalized luciferase activity was measured 24 hours after transfection. The differences between variants and WT were tested using one-way ANOVA (*$P < 0.05$). (**D**) IRF3-deficient HEK293T cells were transiently transfected with WT and mutant forms of *IRF3*, together with an IFN-β luciferase reporter and a constitutively expressed reporter. Cells were either left untreated or infected with Sendai virus for 24 hours before the normalized measurement of luciferase activity. The differences between variants and WT were evaluated using two-way ANOVA (*$P < 0.05$). (**E**) HEK293T cells were transiently transfected with WT and mutant forms of *IRF7*, together with an IFN-β luciferase reporter and a constitutively expressed reporter. Cells were either left untreated or infected with Sendai virus for 24 hours before the normalized measurement of luciferase activity. The differences between variants and WT were tested using two-way ANOVA (*$P < 0.05$). (**F** and **G**) IFNAR1- or IFNAR2-deficient SV40-Fib cells were transiently transfected with WT or mutant forms of *IFNAR1* for 36 hours, and either left untreated or stimulated with IFN-α2 or IFN-γ. Fluorescence-activated cell sorting (FACS) staining with anti-p-STAT1 antibody and the *z*-score of the MFI were assessed. Asterisks indicate variants with MFI <50% of WT. Variants in red were identified in COVID-19 patients. Variants in blue are known deleterious variants and served as negative controls. EV, empty vector; LT, lipofectamine. Three technical repeats were performed for (A) to (E). Means and SD are shown in the columns and horizontal bars when appropriate.

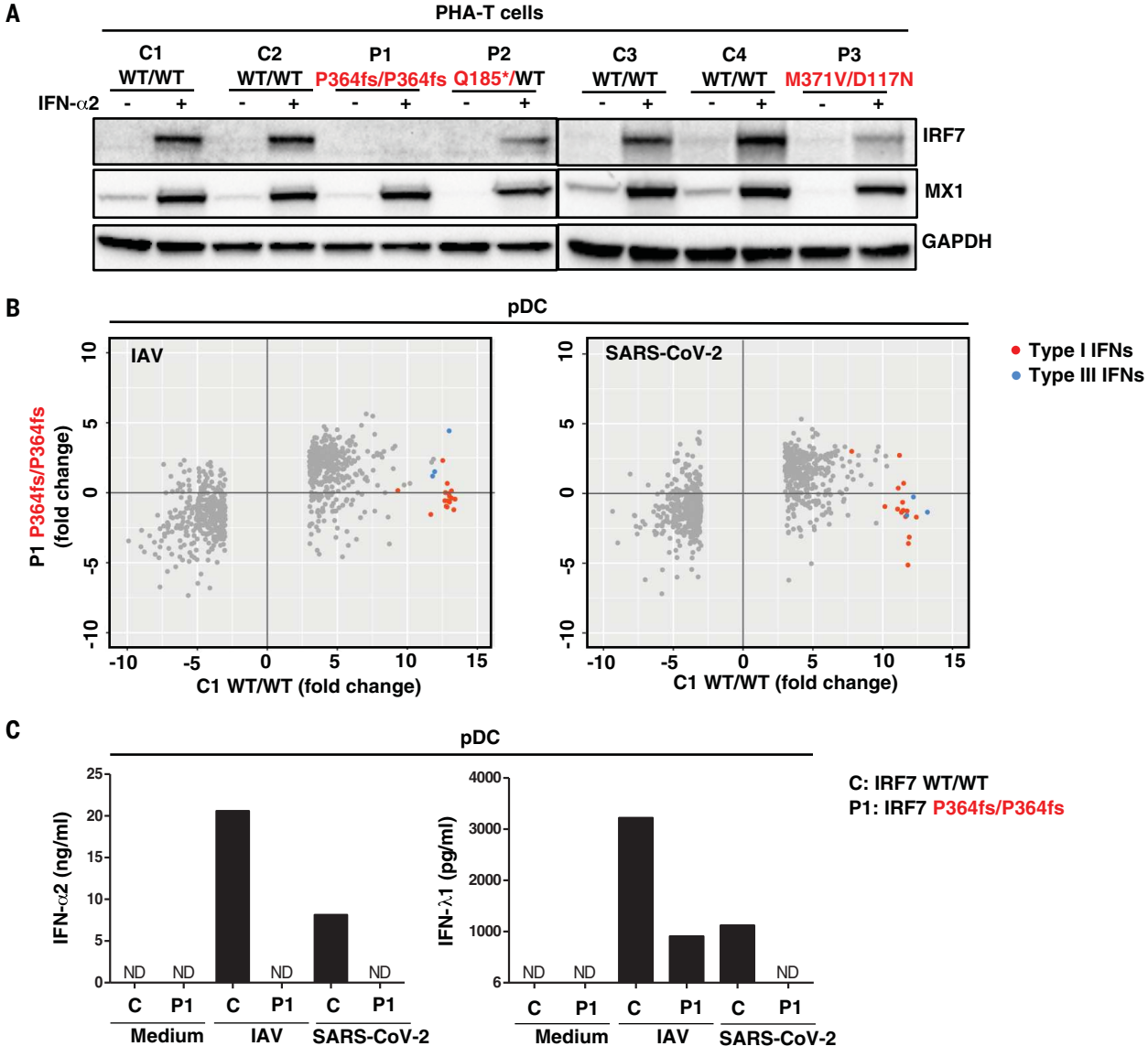

Fig. 4. Type I IFN responses in patient cells defective for IRF7. (**A**) Levels of the IRF7 protein in PHA-T cells from two patients with AR IRF7 deficiency (P1 and P3), one patient with AD IRF7 deficiency (P2), and four healthy donors (C1 to C4). Cells were either left untreated or stimulated with IFN-α2 for 24 hours, and protein levels were measured by Western blotting. MX1 was used as a positive control for IFN-α2 treatment. (**B**) pDCs isolated from an AR IRF7-deficient patient (P1) and a healthy donor (C1) were either left untreated or infected with influenza A virus (IAV) or SARS-CoV-2, and RNA-seq was performed. Genes with expression >2.5-fold higher or lower in C1 after infection are plotted as the fold change in expression. Red dots are type I IFN genes; blue dots are type III IFN genes. (**C**) pDCs isolated from healthy donor C and IRF7-deficient patient (P1) were either left untreated (Medium) or infected with IAV or SARS-CoV-2, and the production of IFN-α2 and IFN-λ1 was measured by CBA and ELISA, respectively, on the supernatant. ND, not detected.

for *IRF7*; homozygosity for *IFNAR1*) and 19 AD deficiencies. These 23 patients did not carry candidate variants at the other 417 loci known to underlie inborn errors of immunity (table S2) (*24*–*26*). These findings suggest that at least 23 (3.5%) unrelated patients of the 659 patients tested suffered from a deficiency at one of eight loci among the 13 tested: four patients with a known AR disorder (*IRF7* or *IFNAR1*) (*7*, *15*), 11 with a known AD disorder (*TLR3*, *TICAM1*, *TBK1*, or *IRF3*) (*6*, *9*, *12*, *13*, *20*), and eight with a previously unknown AD genetic disorder (*UNC93B1*, *IRF7*, *IFNAR1*, or *IFNAR2*).

Impaired TLR3- and IRF7-dependent type I immunity in patient cells in vitro

We tested cells from patients with selected genotypes and showed that PHA-driven T cell blasts (PHA-T cells) from patients with AR or AD IRF7 deficiency had low levels of IRF7 expression (Fig. 4A). We then isolated circulating plasmacytoid dendritic cells (pDCs) from a patient with AR IRF7 deficiency (fig. S9A) (*7*). These cells were present in normal proportions (fig. S9B), but they did not produce any detectable type I or III IFNs in response to SARS-CoV-2, as analyzed by cytometric bead array (CBA), enzyme-linked immunosorbent assay (ELISA), and RNA sequencing (RNA-seq) (Fig. 4, B and C). We also showed that PHA-T cells from a patient with AR IFN-α/β receptor 1 (IFNAR1) deficiency had impaired IFNAR1 expression and responses to IFN-α2 or IFN-β, and that the patient's SV40-transformed fibroblast (SV40-Fib) cells did not respond to IFN-α2 or IFN-β (Fig. 5). We then infected TLR3$^{-/-}$, TLR3$^{+/-}$, IRF7$^{-/-}$ SV40-Fib cells, and IRF7$^{-/-}$ SV40-Fib cells rescued with wild-type (WT) IRF7; IFNAR1$^{-/-}$ SV40-Fib cells, and IFNAR1$^{-/-}$ SV40-Fib cells rescued with WT

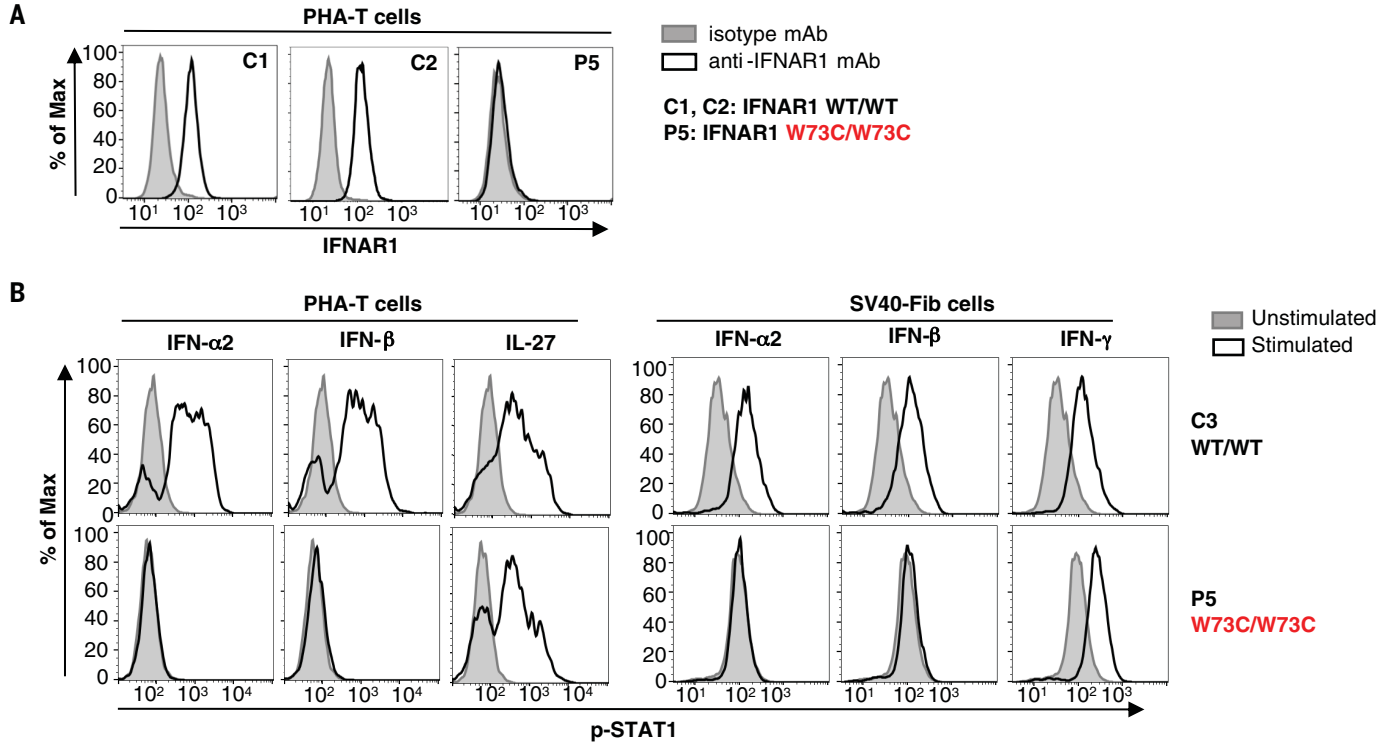

Fig. 5. Type I IFN responses in patient cells defective for IFNAR1. (**A**) FACS staining of IFNAR1 on the surface of PHA-T cells from a patient with AR IFNAR1 deficiency (P5) and healthy donors (C1 and C2). (**B**) PHA-T cells and SV40-Fib from a patient with AR IFNAR1 deficiency (P5) and a healthy donor (C3) were stimulated with IFN-α2 or IFN-β, and p-STAT1 levels were determined by FACS. Interleukin-27 stimulation served as a positive control on PHA-T cells, whereas IFN-γ stimulation served as a positive control on SV40-Fib cells.

IFNAR1, all of which were previously transduced with angiotensin-converting enzyme 2 (ACE2) and transmembrane protease, serine 2 (TMPRSS2). SARS-CoV-2 infection levels were higher in mutant cells than in cells from healthy donors, and transduction of WT *IRF7* or *IFNAR1* rescued their defects (Fig. 6). Collectively, these findings showed that AR IRF7 deficiency impaired the production of type I IFN by pDCs stimulated with SARS-CoV-2, whereas AR and AD deficiencies of TLR3 or AR deficiency of IFNAR1 impaired fibroblast-intrinsic type I IFN immunity to SARS-CoV2. They also suggest that heterozygosity for LOF variations at the other five mutated loci also underlie life-threatening COVID-19.

Impaired production of type I IFNs in patients in vivo

We tested whether these genotypes impaired the production of type I IFN in vivo during the course of SARS-CoV-2 infection. We measured the levels of the 13 types of IFN-α in the blood of patients during the acute phase of COVID-19. We found that 10 of the 23 patients with mutations for whom samples were available (one with AR IRF7 deficiency, four with AD IRF7 deficiency, one with AD TLR3 deficiency, two with AD TBK1 deficiency, one with AR IFNAR1 deficiency, and one with AD TICAM1 deficiency) had serum IFN-α levels <1 pg/ml (Fig. 7). By contrast, previously published cohorts of patients hospitalized with unexplained, severe COVID-19 had various serum IFN-α levels, significantly higher than our 10 patients [one-way analysis of variance (ANOVA), $P = 1.4 \times 10^{-7}$; Fig. 7] (*27*, *28*). Another 29 patients from our cohort displaying auto-antibodies (auto-Abs) against type I IFNs, reported in an accompanying paper, had undetectable levels of serum IFN-α (*29*). Moreover, none of the 23 patients with LOF mutations of the eight genes had detectable auto-Abs against type I IFNs (*29*), strongly suggesting that the two mechanisms of disease are similar but independent. Excluding patients with auto-Abs against type I IFN from the burden test of pLOF variants at the 12 autosomal loci strengthened the association signal ($P = 0.007$; OR = 8.97; 95% CI = 1.13 to 71.09).

Inborn errors of TLR3- and IRF7-dependent type I immunity underlie critical COVID-19

Collectively, our data suggest that at least 23 of the 659 patients with life-threatening COVID-19 pneumonia studied had known (six disorders) or new (four disorders) genetic defects at eight loci involved in the TLR3- and IRF7-dependent induction and amplification of type I IFNs. This discovery reveals the essential role of both the double-stranded RNA sensor TLR3 and type I IFN cell-intrinsic immunity in the control of SARS-CoV-2 infection in the lungs, consistent with their previously documented roles in pulmonary immunity to influenza virus (*5*–*8*). These genotypes were silent until infection with SARS-CoV-2. The most thought-provoking examples are the AR deficiencies of IRF7 and IFNAR1. AR IRF7 deficiency was diagnosed in two individuals aged 49 and 50 years, and AR IFNAR1 deficiency was diagnosed in two individuals aged 26 and 38 years, and none of the four patients had a prior history of life-threatening infections (Table 1). One patient with IRF7 deficiency was tested and was seropositive for several common viruses, including various influenza A and B viruses (figs. S10 and S11). These genetic defects therefore display incomplete penetrance for influenza respiratory distress and only manifested clinically upon infection with the more virulent SARS-CoV-2.

Conclusion

The AR form of IFNAR1 deficiency highlights the importance of type I IFN production relative to type III IFN production, which is also impaired by defects of TLR3, IRF7, and IRF9 (*5*). This conclusion is also supported by our accompanying report of neutralizing auto-Abs against type I IFNs, but not type III IFNs, in other patients with life-threatening COVID-19 pneumonia (*29*). Inborn errors of TLR3- and

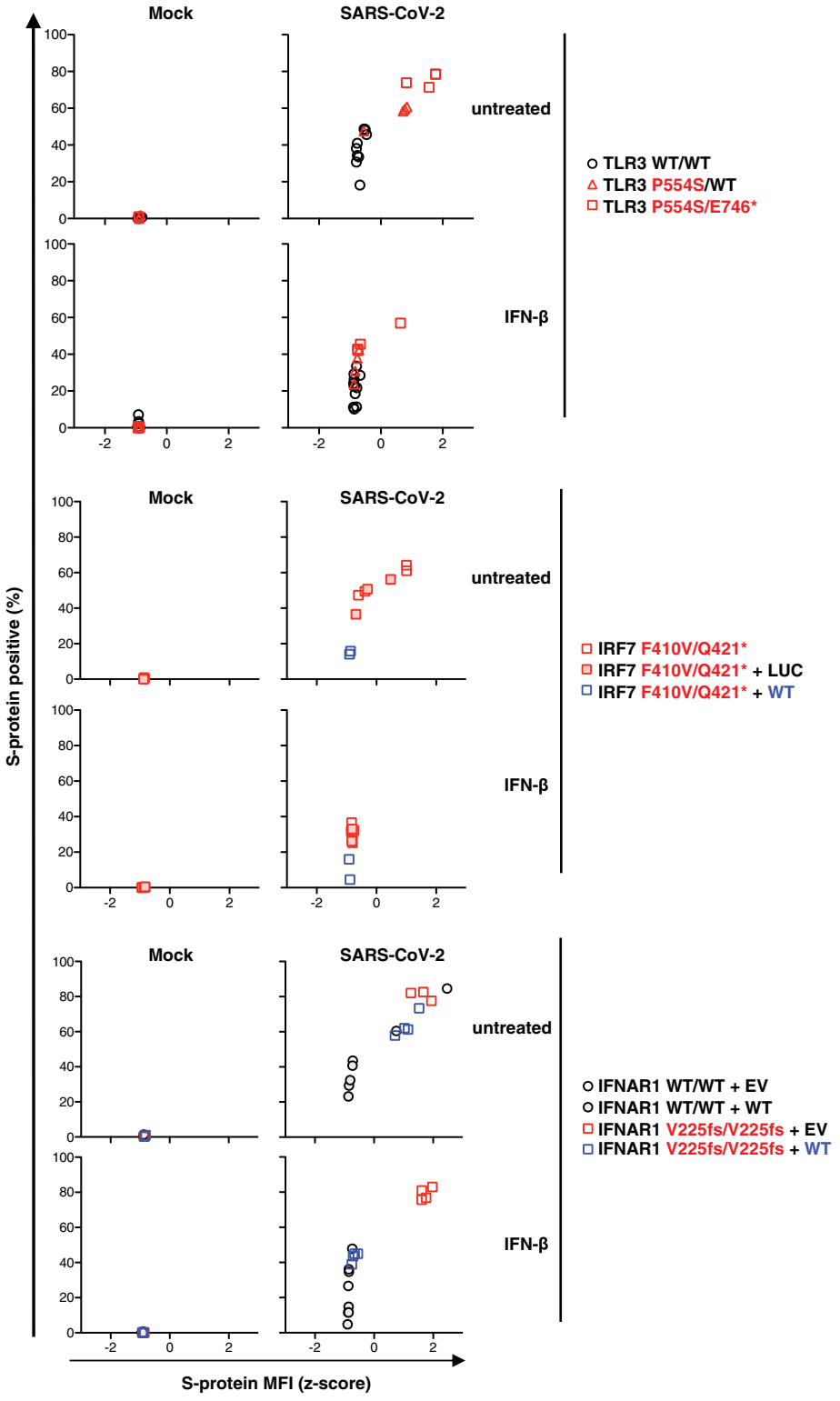

Fig. 6. Cell-intrinsic type I IFN response to SARS-CoV-2. SV40-Fib cells of TLR3$^{-/-}$, TLR3$^{+/-}$, IRF7$^{-/-}$, and IRF7$^{-/-}$ SV40-Fib cells rescued with WT IRF7; IFNAR1$^{-/-}$ SV40-Fib cells, and IFNAR1$^{-/-}$ SV40-Fib cells rescued with WT IFNAR1 were transduced with ACE2 and TMPRSS2 and then either left untreated or treated with IFN-β for 4 hours. Cells were then infected with SARS-CoV-2 (MOI = 0.5). After staining, ACE2 and viral S-protein levels were measured by high-content microscopy with gating on ACE2^{+} cells. IRF7-deficient SV40-Fib cells were previously transduced with either WT IRF7 or negative control (Luc). IFNAR1-deficient cells were previously transduced with either WT IFNAR1 or empty vector (EV).

IRF7-dependent type I IFN immunity at eight loci were found in as many as 23 patients (3.5%) of various ages (17 to 77 years) and ancestries (various nationalities from Asia, Europe, Latin America, and the Middle East) and in patients of both sexes (Table 1). Our findings suggest that there may be mutations in other type I IFN–related genes in other patients with life-threatening COVID-19 pneumonia. They also suggest that the administration of type I IFN may be of therapeutic benefit in selected patients, at least early in the course of SARS-CoV-2 infection.

Methods

Patients

We included in this study 659 patients with life-threatening COVID-19 pneumonia, defined as patients with pneumonia who developed critical disease, whether pulmonary with mechanical ventilation (CPAP, BIPAP, intubation, hi-flow oxygen), septic shock, or with any other organ damage requiring admission to the intensive care unit. Patients who developed Kawasaki-like syndrome were excluded. The age of the patients ranged from 0.1 to 99 years, with a mean age of 51.8 years (SD 15.9 years), and 25.5% of the patients were female. As controls, we enrolled 534 individuals infected with SARS-CoV-2 based on a positive polymerase chain reaction (PCR) and/or serological test and/or the presence of typical symptoms such as anosmia or ageusia after exposure to a confirmed COVID-19 case, who remained asymptomatic or developed mild, self-healing, ambulatory disease.

Next-generation sequencing

Genomic DNA was extracted from whole blood. For the 1193 patients and controls included, the whole exome (N = 687) or whole genome (N = 506) was sequenced. We used the Genome Analysis Software Kit (GATK) (version 3.4-46 or 4) best-practice pipeline to analyze our whole-exome–sequencing data (*30*). We aligned the reads obtained with the human reference genome (hg19) using the maximum exact matches algorithm in Burrows–Wheeler Aligner software (*31*). PCR duplicates were removed with Picard tools (http://broadinstitute.github.io/picard/). The GATK base quality score recalibrator was applied to correct sequencing artifacts.

All of the variants were manually curated using Integrative Genomics Viewer (IGV) and confirmed to affect the main functional protein isoform by checking the protein sequence before inclusion in further analyzes. The main functional protein isoforms were TLR3 (NM_003265), UNC93B1 (NM_030930.4), TICAM1 (NM_182919), TRAF3 (NM_145725.2), TBK1 (NM_013254.4), IRF3 (NM_001571), IRF7 (NM_001572.5), IFNAR1 (NM_000629.3), IFNAR2 (NM_001289125.3), STAT1 (NM_007315.4), STAT2

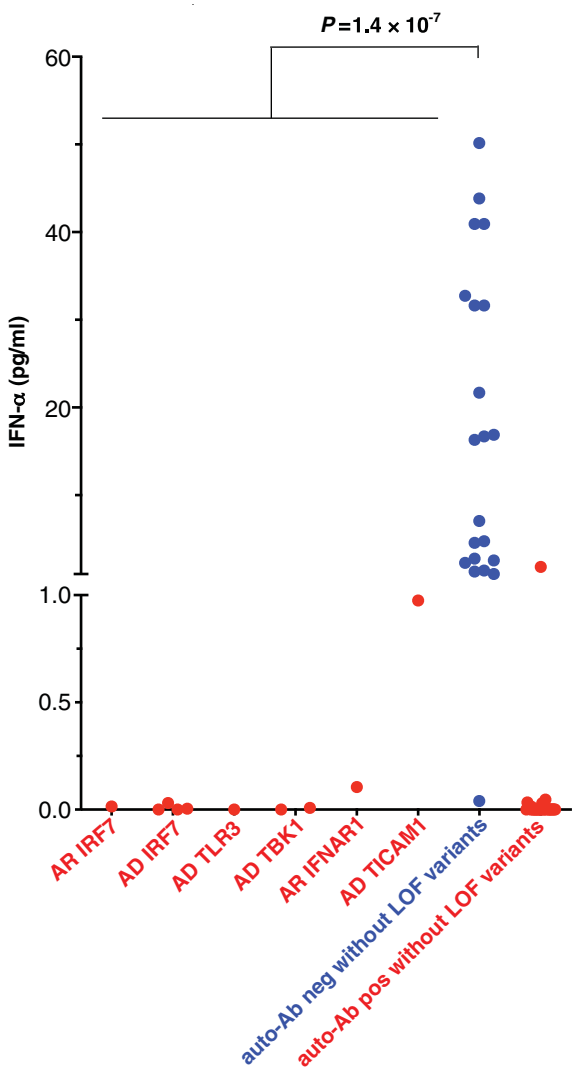

Fig. 7. In vivo type I IFN responses to SARS-CoV-2 infections. Plasma levels of 13 IFN-α were measured by Simoa. Auto-Ab(+) without LOF variants indicates COVID-19 patients with neutralizing anti-IFN-α auto-Abs in our accompanying report (*29*). *P* values indicated were evaluated using one-way ANOVA.

(NM_005419.4), and IRF9 (NM_006084.5). The analysis of IKBKG was customized to unmask the duplicated region in IKBKG using a specific pipeline previously described (*32*). We searched the next-generation–sequencing data for deletions in the 13 genes of interest using both the HMZDelFinder (*33*) and CANOES (*34*) algorithms.

Statistical analysis

We performed an enrichment analysis on our cohort of 659 patients with life-threatening COVID-19 pneumonia and 534 SARS-CoV2–infected controls, focusing on 12 autosomal IFN-related genes. We considered variants that were pLOF with a MAF <0.001 (gnomAD version 2.1.1) after experimentally demonstrating that all of the pLOF variants seen in the cases were actually LOF. We compared the proportion of individuals carrying at least one pLOF variant of the 12 autosomal genes in cases and controls by means of logistic regression with the likelihood ratio test. We accounted for the ethnic heterogeneity of the cohorts by including the first three principal components of the PCA in the logistic regression model. PC adjustment is a common and efficient strategy for accounting for different ancestries of patients and controls in the study of rare variants (*35*–*38*). We checked that our adjusted burden test was well calibrated by also performing an analysis of enrichment in rare (MAF <0.001) synonymous variants of the 12 genes. PCA was performed with Plink version 1.9 software on whole-exome– and whole-genome–sequencing data and the 1000 Genomes (1kG) Project phase 3 public database as a reference, using 27,480 exonic variants with a MAF >0.01 and a call rate >0.99. The OR was also estimated by logistic regression and adjusted for ethnic heterogeneity.

Reporter assays

Cell lines or SV40-Fib cells with known defects were transiently or stably transfected with WT, mutant variants, IFN-β- or ISRE-*firefly* luciferase reporter, and pRL-TK-*Renilla* luciferase reporter. Reporter activity was measured with the Dual-Luciferase Reporter Assay System (Promega) according to the manufacturer's instructions. *Firefly* luciferase activity was normalized against *Renilla* luciferase activity and expressed as a fold change. TRAF3-deficient human embryonic kidney (HEK) 293T cells were kindly provided by M. Romanelli (*39*).

pDC activation by SARS-CoV-2 and cytokine production

pDCs from an IRF7$^{-/-}$ patient and a healthy donor matched for age and sex were cultured in the presence of medium alone, influenza virus (A/PR/8/34, 2 μg/ml; Charles River Laboratories), or the SARS-CoV-2 primary strain 220_95 (GISAID accession ID: EPI_ISL_469284) at a multiplicity of infection (MOI) of 2. After 12 hours of culture, pDC supernatant was collected for cytokine quantification. IFN-α2 levels were measured using CBA analyzis (BD Biosciences) in accordance with the manufacturer's protocol using a 20 pg/ml detection limit. IFN-λ1 secretion was measured in an ELISA (R&D Systems, DuoSet DY7246), in accordance with the manufacturer's instructions.

SARS-CoV-2 infection in patient SV40-Fib

To make patient-derived fibroblasts permissive to SARS-CoV-2 infection, we delivered human ACE2 and TMPRSS2 cDNA to cells by lentivirus transduction using a modified SCRPSY vector (GenBank ID: KT368137.1). SARS-CoV-2 strain USA-WA1/2020 was obtained from BEI Resources. ACE2/TMPRSS2-transduced cells were either left untreated or treated with 500 U/ml IFN-β (11415-1, PBL Assay Science) 4 hours before infection. Cells were infected with SARS-CoV-2 (MOI = 0.5) for 1 hour at 37°C. After 24 hours of infection, cells were fixed and taken out of the BSL3 for staining.

After fixation, cells were stained with SARS-CoV-2 and ACE2 primary antibodies (0.5 and 1 μg/ml, respectively). Primary antibodies were as follows: for SARS-CoV-2, human monoclonal anti-spike-SARS-CoV-2 C121 antibody (*40*), and for ACE2, mouse monoclonal Alexa Fluor 488–conjugated antibody (FAB9332G-100UG, R&D Systems). Images were acquired with an ImageXpress Micro XLS microscope (Molecular Devices) using the 4× objective. MetaXpress software (Molecular Devices) was used to obtain single-cell mean fluorescence intensity (MFI) values.

Data analysis on single-cell MFI values was done in the R environment (version 4.0.2). ACE2/TMPRSS2-transduced cells were classified as ACE2 positive when the ACE2 log MFI was superior to the log mean MFI of mock-transduced cells plus 2.5 SDs. We excluded all wells with <150 ACE2-positive cells before SARS-CoV-2 scoring. ACE2-expressing cells were classified SARS-CoV-2 positive when the fluorescence intensity value was superior to

the MFI of mock-infected cells plus 4 SDs. The median SARS-CoV-2 MFI and percentage SARS-CoV-2–positive cells were calculated for each well (independent infection).

*Single-molecule array (*Simoa*)* IFN-α digital ELISA

Serum IFN-α concentrations were determined using Simoa technology, with reagents and procedures obtained from Quanterix Corporation (Quanterix SimoaTM IFNα Reagent Kit, Lexington, MA, USA). According to the manufacturer's instructions, the working dilutions were 1:2 for all sera in working volumes of 170 µl.

REFERENCES AND NOTES

1. D. M. Morens, A. S. Fauci, Emerging pandemic diseases: How we got to COVID-19. *Cell* **182**, 1077–1092 (2020). doi: 10.1016/j.cell.2020.08.021; pmid: 32846157
2. J. L. Casanova, L. Abel, Lethal Infectious Diseases as Inborn Errors of Immunity: Toward a Synthesis of the Germ and Genetic Theories. *Annu. Rev. Pathol.* (2020). pmid: 32289233
3. J. L. Casanova, L. Abel, The human genetic determinism of life-threatening infectious diseases: Genetic heterogeneity and physiological homogeneity? *Hum. Genet.* **139**, 681–694 (2020). doi: 10.1007/s00439-020-02184-w; pmid: 32462426
4. J. L. Casanova, H. C. Su; COVID Human Genetic Effort, A global effort to define the human genetics of protective immunity to SARS-CoV-2 infection. *Cell* **181**, 1194–1199 (2020). doi: 10.1016/j.cell.2020.05.016; pmid: 32405102
5. Q. Zhang, Human genetics of life-threatening influenza pneumonitis. *Hum. Genet.* **139**, 941–948 (2020). doi: 10.1007/s00439-019-02108-3; pmid: 32025908
6. H. K. Lim *et al*., Severe influenza pneumonitis in children with inherited TLR3 deficiency. *J. Exp. Med.* **216**, 2038–2056 (2019). doi: 10.1084/jem.20181621; pmid: 31217193
7. M. J. Ciancanelli *et al*., Life-threatening influenza and impaired interferon amplification in human IRF7 deficiency. *Science* **348**, 448–453 (2015). doi: 10.1126/science.aaa1578; pmid: 25814066
8. N. Hernandez *et al*., Life-threatening influenza pneumonitis in a child with inherited IRF9 deficiency. *J. Exp. Med.* **215**, 2567–2585 (2018). doi: 10.1084/jem.20180628; pmid: 30143481
9. V. Sancho-Shimizu *et al*., Herpes simplex encephalitis in children with autosomal recessive and dominant TRIF deficiency. *J. Clin. Invest.* **121**, 4889–4902 (2011). doi: 10.1172/JCI59259; pmid: 22105173
10. A. Casrouge *et al*., Herpes simplex virus encephalitis in human UNC-93B deficiency. *Science* **314**, 308–312 (2006). doi: 10.1126/science.1128346; pmid: 16973841
11. R. Pérez de Diego *et al*., Human TRAF3 adaptor molecule deficiency leads to impaired Toll-like receptor 3 response and susceptibility to herpes simplex encephalitis. *Immunity* **33**, 400–411 (2010). doi: 10.1016/j.immuni.2010.08.014; pmid: 20832341
12. M. Herman *et al*., Heterozygous TBK1 mutations impair TLR3 immunity and underlie herpes simplex encephalitis of childhood. *J. Exp. Med.* **209**, 1567–1582 (2012). doi: 10.1084/jem.20111316; pmid: 22851595
13. L. L. Andersen *et al*., Functional IRF3 deficiency in a patient with herpes simplex encephalitis. *J. Exp. Med.* **212**, 1371–1379 (2015). doi: 10.1084/jem.20142274; pmid: 26216125
14. M. Audry *et al*., NEMO is a key component of NF-κB- and IRF-3-dependent TLR3-mediated immunity to herpes simplex virus. *J. Allergy Clin. Immunol.* **128**, 610–617.e4 (2011). doi: 10.1016/j.jaci.2011.04.059; pmid: 21722947
15. N. Hernandez *et al*., Inherited IFNAR1 deficiency in otherwise healthy patients with adverse reaction to measles and yellow fever live vaccines. *J. Exp. Med.* **216**, 2057–2070 (2019). doi: 10.1084/jem.20182295; pmid: 31270247
16. C. J. Duncan *et al*., Human IFNAR2 deficiency: Lessons for antiviral immunity. *Sci. Transl. Med.* **7**, 307ra154 (2015). doi: 10.1126/scitranslmed.aac4227; pmid: 26424569
17. S. Dupuis *et al*., Impaired response to interferon-alpha/beta and lethal viral disease in human STAT1 deficiency. *Nat. Genet.* **33**, 388–391 (2003). doi: 10.1038/ng1097; pmid: 12590259
18. S. Hambleton *et al*., STAT2 deficiency and susceptibility to viral illness in humans. *Proc. Natl. Acad. Sci. U.S.A.* **110**, 3053–3058 (2013). doi: 10.1073/pnas.1220098110; pmid: 23391734
19. R. Döffinger *et al*., X-linked anhidrotic ectodermal dysplasia with immunodeficiency is caused by impaired NF-kappaB signaling. *Nat. Genet.* **27**, 277–285 (2001). doi: 10.1038/85837; pmid: 11242109
20. S. Y. Zhang *et al*., TLR3 deficiency in patients with herpes simplex encephalitis. *Science* **317**, 1522–1527 (2007). doi: 10.1126/science.1139522; pmid: 17872438
21. G. Zhang *et al*., A proline deletion in IFNAR1 impairs IFN-signaling and underlies increased resistance to tuberculosis in humans. *Nat. Commun.* **9**, 85 (2018). doi: 10.1038/s41467-017-02611-z; pmid: 29311663
22. M. M. Thomsen *et al*., Identification of an IRF3 variant and defective antiviral interferon responses in a patient with severe influenza. *Eur. J. Immunol.* **49**, 2111–2114 (2019). doi: 10.1002/eji.201848083; pmid: 31250433
23. M. M. Thomsen *et al*., Defective interferon priming and impaired antiviral responses in a patient with an IRF7 variant and severe influenza. *Med. Microbiol. Immunol. (Berl.)* **208**, 869–876 (2019). doi: 10.1007/s00430-019-00623-8; pmid: 31172279
24. S. G. Tangye *et al*., Human inborn errors of immunity: 2019 update on the classification from the International Union of Immunological Societies Expert Committee. *J. Clin. Immunol.* **40**, 24–64 (2020). doi: 10.1007/s10875-019-00737-x; pmid: 31953710
25. A. Bousfiha *et al*., Human Inborn Errors of Immunity: 2019 Update of the IUIS Phenotypical Classification. *J. Clin. Immunol.* **40**, 66–81 (2020). doi: 10.1007/s10875-020-00758-x; pmid: 32048120
26. L. D. Notarangelo, R. Bacchetta, J.-L. Casanova, H. C. Su, Human inborn errors of immunity: An expanding universe. *Sci. Immunol.* **5**, eabb1662 (2020). doi: 10.1126/sciimmunol.abb1662; pmid: 32651211
27. J. Hadjadj *et al*., Impaired type I interferon activity and inflammatory responses in severe COVID-19 patients. *Science* **369**, 718–724 (2020). doi: 10.1126/science.abc6027; pmid: 32661059
28. S. Trouillet-Assant *et al*., Type I IFN immunoprofiling in COVID-19 patients. *J. Allergy Clin. Immunol.* **146**, 206–208.e2 (2020). doi: 10.1016/j.jaci.2020.04.029; pmid: 32360285
29. P. Bastard *et al*., Auto-antibodies against type I IFNs in patients with life-threatening COVID-19. *Science* 10.1126/science.abd4585 (2020).
30. M. A. DePristo *et al*., A framework for variation discovery and genotyping using next-generation DNA sequencing data. *Nat. Genet.* **43**, 491–498 (2011). doi: 10.1038/ng.806; pmid: 21478889
31. H. Li, R. Durbin, Fast and accurate short read alignment with Burrows-Wheeler transform. *Bioinformatics* **25**, 1754–1760 (2009). doi: 10.1093/bioinformatics/btp324; pmid: 19451168
32. B. Boisson *et al*., Rescue of recurrent deep intronic mutation underlying cell type-dependent quantitative NEMO deficiency. *J. Clin. Invest.* **129**, 583–597 (2019). doi: 10.1172/JCI124011; pmid: 30422821
33. T. Gambin *et al*., Homozygous and hemizygous CNV detection from exome sequencing data in a Mendelian disease cohort. *Nucleic Acids Res.* **45**, 1633–1648 (2017). pmid: 27980096
34. D. Backenroth *et al*., CANOES: Detecting rare copy number variants from whole exome sequencing data. *Nucleic Acids Res.* **42**, e97 (2014). doi: 10.1093/nar/gku345; pmid: 24771342
35. M. Bouaziz, J. Mullaert, B. Bigio, Y. Seeleuthner, J.-L. Casanova, A. Alcais, L. Abel, A. Cobat, Controlling for human population stratification in rare variant association studies. bioRxiv 969477 [Preprint]. 28 February 2020. .doi: 10.1101/2020.02.28.969477
36. E. Persyn, R. Redon, L. Bellanger, C. Dina, The impact of a fine-scale population stratification on rare variant association test results. *PLOS ONE* **13**, e0207677 (2018). doi: 10.1371/journal.pone.0207677; pmid: 30521541
37. Y. Zhang, X. Shen, W. Pan, Adjusting for population stratification in a fine scale with principal components and sequencing data. *Genet. Epidemiol.* **37**, 787–801 (2013). doi: 10.1002/gepi.21764; pmid: 24123217
38. S. Boisson-Dupuis *et al*., Tuberculosis and impaired IL-23-dependent IFN-γ immunity in humans homozygous for a common *TYK2* missense variant. *Sci. Immunol.* **3**, eaau8714 (2018). doi: 10.1126/sciimmunol.aau8714; pmid: 30578352
39. S. Fochi *et al*., TRAF3 Is Required for NF-κB Pathway Activation Mediated by HTLV Tax Proteins. *Front. Microbiol.* **10**, 1302 (2019). doi: 10.3389/fmicb.2019.01302; pmid: 31244811
40. D. F. Robbiani *et al*., Convergent antibody responses to SARS-CoV-2 in convalescent individuals. *Nature* **584**, 437–442 (2020). doi: 10.1038/s41586-020-2456-9; pmid: 32555388
41. Q. Zhang, P. Bastard, Z. Liu, J. Le Pen, M. Moncada-Velez, J. Chen, M. Ogishi, I. K. D. Sabli, S. Hodeib, C. Korol, J. Rosain, K. Bilguvar, J. Ye, A. Bolze, B. Bigio, R. Yang, A. Augusto Arias Sierra, Q. Zhou, Y. Zhang, F. Onodi, S. Korniotis, L. Karpf, Q. Philippot, M. Chbihi, L. Bonnet-Madin, K. Dorgham, N. Smith, W. M. Schneider, B. S. Razooky, H.-H. Hoffmann, E. Michailidis, L. Moens, J. E. Han, L. Lorenzo, L. Bizien, P. Meade, A.-L. Neehus, A. C. Ugurbil, A. Corneau, G. Kerner, P. Zhang, F. Rapaport, Y. Seeleuthner, J. Manry, C. Masson, Y. Schmitt, A. Schlüter, T. Le Voyer, T. Khan, J. Li, J. Fellay, L. Roussel, M. Shahrooei, M. F. Alosaimi, D. Mansouri, H. Al-Saud, F. Al-Mulla, F. Almourfi, S. Z. Al-Muhsen, F. Alsohime, S. Al Turki, R. Hasanato, D. van de Beek, A. Biondi, L. R. Bettini, M. D'Angio, P. Bonfanti, L. Imberti, A. Sottini, S. Paghera, E. Quiros-Roldan, C. Rossi, A. J. Oler, M. F. Tompkins, C. Alba, I. Vandernoot, J.-C. Goffard, G. Smits, I. Migeotte, F. Haerynck, P. Soler-Palacin, A. Martin-Nalda, R. Colobran, P.-E. Morange, S. Keles, F. Çölkesen, T. Ozcelik, K. K. Yasar, S. Senoglu, Ş. N. Karabela, C. Rodríguez-Gallego, G. Novelli, S. Hraiech, Y. Tandjaoui-Lambiotte, X. Duval, C. Laouenan, COVID-STORM Clinicians, COVID Clinicians, Imagine COVID Group, French COVID Cohort Study Group, CoV-Contact Cohort, Amsterdam UMC Covid-19 Biobank, COVID Human Genetic Effort, NIAID-USUHS/TAGC COVID Immunity Group, A. L. Snow, C. L. Dalgard, J. Milner, D. C. Vinh, T. H. Mogensen, N. Marr, A. N. Spaan, B. Boisson, S. Boisson-Dupuis, J. Bustamante, A. Puel, M. Ciancanelli, I. Meyts, T. Maniatis, V. Soumelis, A. Amara, M. Nussenzweig, A. García-Sastre, F. Krammer, A. Pujol, D. Duffy, R. Lifton, S.-Y. Zhang, G. Gorochov, V. Béziat, E. Jouanguy, V. Sancho-Shimizu, C. M. Rice, L. Abel, L. D. Notarangelo, A. Cobat, H. C. Su, J.-L. Casanova, Detailed genotype counts for all coding variants for: Inborn errors of type I IFN immunity in patients with life-threatening COVID-19, Dryad (2020). doi: 10.5061/dryad.8pk0p2nkk

ACKNOWLEDGMENTS

We thank the patients, their families, and healthy donors for placing their trust in us; Y. Nemirowskaya, D. Papandrea, M. Woollet, D. Liu, C. Rivalain, and C. Patissier for administrative assistance; A. Adeleye, D. Bacikova, E. McGrath Martinez, A. R. Soltis, K. Dobbs, J. Danielson, H. Matthews, and S. Weber for technical and other assistance; M. M. A. Ata and F. Al Ali for their contribution to VirScan experiments; S. Elledge (Brigham and Women's Hospital and Harvard Medical School, Boston, MA) for kindly providing the VirScan phage library used in this study; A. W. Ashbrook, the BSL3 manager of the Rice laboratory assistance; M. Lazzaro, Director of Immigration and Academic Appointments, for assistance; W. Chung, K. Kiryluk, S. O'Byrne, D. Pendrick, J. Williamson, C. Andrews, and M. Disco in the J.M. lab for assistance; M. Andreoni (Tor Vergata, Italy) for his clinical contribution; and A. Novelli (Bambino Gesù Hospital, Italy) for his collaboration. We thank the GEN-COVID Multicenter study (https://sites.google.com/dbm.unisi.it/gen-covid). This study used the high-performance computational resources of the National Institutes of Health (NIH) HPC Biowulf cluster (http://hpc.nih.gov) and the Office of Cyber Infrastructure and Computational Biology (OCICB) High Performance Computing (HPC) cluster at the National Institute of Allergy and Infectious Diseases (NIAID), Bethesda, MD. The opinions and assertions expressed herein are those of the authors and are not to be construed as reflecting the views of the Uniformed Services University of the Health Sciences (USUHS) or the U.S. Department of Defense (DoD). **Funding:** This work was supported by a generous donation from the Fisher Center for Alzheimer's Research Foundation. The Laboratory of Human Genetics of Infectious Diseases is supported by the Howard Hughes Medical Institute, the Rockefeller University, the St. Giles Foundation, the NIH (R01AI088364), the National Center for Advancing Translational Sciences (NCATS), the NIH Clinical and Translational Science Award (CTSA) program (UL1 TR001866), a Fast Grant from Emergent Ventures, Mercatus Center at George Mason University, the Yale Center for Mendelian Genomics and the GSP Coordinating Center funded by the National Human Genome Research Institute (NHGRI) (UM1HG006504 and U24HG008956), the French National Research Agency (ANR) under the "Investments for the Future" program (ANR-10-IAHU-01), the Integrative Biology of Emerging Infectious Diseases Laboratory of Excellence (ANR-10-LABX-62-IBEID), the French Foundation for

Medical Research (FRM) (EQU201903007798), the FRM and ANR GENCOVID project, ANRS-COV05, the Square Foundation, Grandir–Fonds de Solidarité pour l'Enfance, the SCOR Corporate Foundation for Science, Institut National de la Santé et de la Recherche Médicale (INSERM), the University of Paris. The French COVID Cohort study group was sponsored by Inserm and supported by the REACTing consortium and by a grant from the French Ministry of Health (PHRC 20-0424). Regione Lombardia, Italy (project "Risposta immune in pazienti con COVID-19 e co-morbidità"), and the Intramural Research Program of the NIAID, NIH. The laboratory of Genomes & Cell Biology of Disease is supported by "Integrative Biology of Emerging Infectious Diseases" (grant no. ANR-10-LABX-62-IBEID), the "Fondation pour la Recherche Medicale" (grant FRM–EQU202003010193), the "Agence Nationale de la Recherche" (ANR FLASH COVID project IDISCOVR cofounded by the "Fondation pour la Recherche Médicale"), University of Paris ("Plan de Soutien Covid-19": RACPL20FIR01-COVID-SOUL). I.M. is a senior clinical investigator with the FWO Vlaanderen; I.M. and L.M. are supported by FWO G0C8517N – G0B5120N. The VS team was supported by "Agence Nationale de la Recherche" (ANR-17-CE15-0003, ANR-17-CE15-0003-01) and by Université de Paris "PLAN D'URGENCE COVID19". L.K. was supported by a fellowship from the French Ministry of Research. V.S.-S. is supported by a UKRI Future Leaders Fellowship (MR/S032304/1). S.Z.A.-M. is supported by the Elite Journals Program at King Saud University through grant no. PEJP-16-107. The J.M. laboratory is supported by Columbia University COVID biobank and grant no. UL1TR001873. Work in the Laboratory of Virology and Infectious Disease was supported by NIH grants P01AI138398-S1, 2U19AI111825, and R01AI091707-10S1; a George Mason University Fast Grant; and the G. Harold and Leila Y. Mathers Charitable Foundation. J.L.P. is supported by a European Molecular Biology Organization Long-Term Fellowship (ALTF 380-2018). Work at the Neurometabolic Diseases Laboratory received funding from the European Union's Horizon 2020 research and innovation program under grant no. 824110 (EasiGenomics grant no. COVID-19/PID12342) to A.P., and Roche and Illumina Covid Match Funds to M.G.. C.R.G. and colleagues are supported by Instituto de Salud Carlos III (COV20_01333 and COV20_01334), Spanish Ministry of Science and Innovation, with the funding of European Regional Development Fund-European Social Fund -FEDER-FSE; (RTC-2017-6471-1; AEI/FEDER, UE), and Cabildo Insular de Tenerife (CGIEU0000219140 and "Apuestas científicas del ITER para colaborar en la lucha contra la COVID-19"). D.C.V. is supported by the Fonds de la recherche en santé du Québec clinician-scientist scholar program. H.S. is adjunct faculty at the University of Pennsylvania. A.-L.N. was supported by the Foundation Bettencourt Schueller. The Amsterdam UMC Covid-19 Biobank was funded by the Netherlands Organization for Health Research and Development (ZonMw, NWO-vici 91819627), The Corona Research Fund (Amsterdam UMC), Dr. J. C. Vaillantfonds, and Amsterdam UMC. Work on COVID-19 at the A.G.-S. laboratory is partly supported by NIH supplements to grants U19AI135972, U19AI142733, and R35 HL135834, and to contract HHSN272201800048C, by a DoD supplement to grant W81XWH-20-1-0270, by DARPA project HR0011-19-2-0020, by CRIP (Center for Research on Influenza Pathogenesis), a NIAID funded Center of Excellence for Influenza Research and Surveillance (CEIRS, contract HHSN272201400008C), by an NIAID funded Collaborative Influenza Vaccine Innovation Center (SEM-CIVIC, contract 75N93019C00051) and by the generous support of the JPB Foundation, the Open Philanthropy Project (research grant 2020-215611(5384)) and anonymous donors. The Virscan analysis presented in fig. S11 was performed with financial support from Sidra Medicine. J.R.H. is supported by Biomedical Advanced Research and Development Authority under Contract (HHSO10201600031C).

Author contributions: A.G., A.A., A.A.A., A.L.S., A.-L.N., A.C., A.C., A.P., B.B., B.S.R., C.A., C.M., C.K., C.L., C.M.R., C.L.D., D.D., E.M., E.J., F.A., F.A-M., F.O., F.A., F.K., G.N., G.S., G.G., H.-H.H., H.K.A.S., H.S., I.K.D.S., I.M., J.L.P., J.R., J.E.H., J.C., J.M., J.Y., K.D., K.B., L.A., L.L.-D., L.K., L.M., L.B-M., L.B., L.D.N., M.M-V., M.C., M.O., M.C., M.N., M.F.T., M.S., M.F.A., N.M., N.S., P.B., P.M., Q.Z., Q.Z., Q.P., R.L., R.Y., S.A.T., S.Z.A-M., S.H., S.K., S.H., S.B.-D., T.K., T.M., T.H.M., V.S.-S., V.S., V.B., W.S., X.D., Y.S., and Z.L. either performed or supervised experiments, generated and analyzed data, and contributed to the manuscript. A.S., A.C.U., A.B., A.O., A.P., B.B., D.V. D.B., F.R., G.K., J.M., P.Z., S-Y.Z., T.L-V., Y.S., and Y.Z. performed computational analysis. A.S., A.N.S., A.M.-N., A.B., C.R., D.M., D.C.V., E.Q.-R., F.H., I.M., I.V., J.B., J.-C.G., L.R.B., L.R., L.I., M.D., P.B., P.S.-P., P.-E.M., R.H., R.C., S.K., S.P., T.O., Y.T.-L., K.K., S.S., J.F., and S.N.K. evaluated and recruited patients to COVID and/or control cohorts. Q.Z. and J.-L.C. wrote the manuscript. All authors edited the manuscript. J.-L.C. supervised the project. **Competing interests:** The authors declare no competing financial interests. J.-L.C. is listed as an inventor on patent application US63/055,155 filed by The Rockefeller University that encompasses aspects of this publication. R.L. is a non-executive director of Roche and its subsidiary Genentech. **Data and materials availability:** Plasma, cells, and genomic DNA are available from J.-L.C. or D.V. under a material transfer agreement with Rockfeller University/Research Institute-McGill University Health Centre. pSCRPSY_TMPRSS2-2A-NeoR_ACE2 and Huh-7.5 cells are available upon request from C.R. under a material transfer agreement with The Rockefeller University, or The Rockefeller University and Apath, LLC, respectively. Clinical data, DNA, and other patient samples are available from the Amsterdam UMC Covid-19 Biobank (D.v.d.B.) under a material transfer agreement with Amsterdam UMC. Material and reagents used are almost exclusively commercially available and nonproprietary. Requests for materals derived from human samples may be made available, subject to any underlying restrictions on such samples. J.-L.C. can make material transfer agreements available through The Rockefeller University. Detailed genotype counts for all coding variants in the genes investigated in this manuscript are available at Dryad (*41*). The whole-genome sequencing datasets used for the analyses, including critical patients and asymptomatic controls described in this manuscript, were deposited in dbGaP under accession number phs002245.v1.p1. All other data are available in the manuscript or the supplementary material. This work is licensed under a Creative Commons Attribution 4.0 International (CC BY 4.0) license, which permits unrestricted use, distribution, and reproduction in any medium, provided the original work is properly cited. To view a copy of this license, visit https://creativecommons.org/licenses/by/4.0/. This license does not apply to figures/photos/artwork or other content included in the article that is credited to a third party; obtain authorization from the rights holder before using such material.

COVID-STORM Clinicians Giuseppe Foti[1], Giacomo Bellani[1], Giuseppe Citerio[1], Ernesto Contro[1], Alberto Pesci[2], Maria Grazia Valsecchi[3], Marina Cazzaniga[4]

[1]Department of Emergency, Anesthesia and Intensive Care, School of Medicine and Surgery, University of Milano-Bicocca, San Gerardo Hospital, Monza, Italy. [2]Department of Pneumology, School of Medicine and Surgery, University of Milano-Bicocca, San Gerardo Hospital, Monza, Italy. [3]Center of Bioinformatics and Biostatistics, School of Medicine and Surgery, University of Milano-Bicocca, San Gerardo Hospital, Monza, Italy. [4]Phase I Research Center, School of Medicine and Surgery, University of Milano-Bicocca, San Gerardo Hospital, Monza, Italy.

COVID Clinicians Jorge Abad[1], Sergio Aguilera-Albesa[2], Ozge Metin Akcan[3], Ilad Alavi Darazam[4], Juan C. Aldave[5], Miquel Alfonso Ramos[6], Seyed Alireza Nadji[7], Gulsum Alkan[8], Jerome Allardet-Servent[9], Luis M. Allende[10], Laia Alsina[11], Marie-Alexandra Alyanakian[12], Blanca Amador-Borrero[13], Zahir Amoura[14], Arnau Antoli[15], Sevket Arslan[16], Sophie Assant[17], Terese Auguet[18], Axelle Azot[19], Fanny Bajolle[20], Aurélie Baldolli[21], Maite Ballester[22], Hagit Baris Feldman[23], Benoit Barrou[24], Alexandra Beurton[25], Agurtzane Bilbao[26], Geraldine Blanchard-Rohner[27], Ignacio Blanco[1], Adeline Blandinières[28], Daniel Blazquez-Gamero[29], Marketa Bloomfield[30], Mireia Bolivar-Prados[31], Raphael Borie[32], Cédric Bosteels[33], Ahmed A. Bousfiha[34], Claire Bouvattier[35], Oksana Boyarchuk[36], Maria Rita P. Bueno[37], Jacinta Bustamante[20], Juan José Cáceres Agra[38], Semra Calimli[39], Ruggero Capra[40], Maria Carrabba[41], Carlos Casasnovas[42], Marion Caseris[43], Martin Castelle[44], Francesco Castelli[45], Martín Castillo de Vera[46], Mateus V. Castro[37], Emilie Catherinot[47], Martin Chalumeau[48], Bruno Charbit[49], Matthew P. Cheng[50], Père Clavé[31], Bonaventura Clotet[51], Anna Codina[52], Fatih Colkesen[53], Fatma Çölkesen[54], Roger Colobran[55], Cloé Comarmond[56], David Dalmau[57], David Ross Darley[58], Nicolas Dauby[59], Stéphane Dauger[60], Loic de Pontual[61], Amin Dehban[62], Geoffroy Delplancq[63], Alexandre Demoule[64], Jean-Luc Diehl[65], Stephanie Dobbelaere[66], Sophie Durand[67], Waleed Eldars[68], Mohamed Elgamal[69], Marwa H. Elnagdy[70], Melike Emiroglu[71], Emine Hafize Erdeniz[72], Selma Erol Aytekin[73], Romain Euvrard[74], Recep Evcen[75], Giovanna Fabio[41], Laurence Faivre[76], Antonin Falck[43], Muriel Fartoukh[77], Morgane Faure[78], Miguel Fernandez Arquero[79], Carlos Flores[80], Bruno Francois[81], Victoria Fumadó[82], Francesca Fusco[83], Blanca Garcia Solis[84], Pascale Gaussem[85], Juana Gil-Herrera[86], Laurent Gilardin[87], Monica Girona Alarcon[88], Mònica Girona-Alarcón[88], Jean-Christophe Goffard[89], Funda Gok[90], Rafaela González-Montelongo[91], Antoine Guerder[92], Yahya Gul[93], Sukru Nail Guner[93], Marta Gut[94], Jérôme Hadjadj[95], Filomeen Haerynck[96], Rabih Halwani[97], Lennart Hammarström[98], Nevin Hatipoglu[99], Elisa Hernandez-Brito[100], Cathérine Heijmans[101], María Soledad Holanda-Peña[102], Juan Pablo Horcajada[103], Levi Hoste[104], Eric Hoste[105], Sami Hraiech[106], Linda Humbert[107], Alejandro D. Iglesias[108], Antonio Íñigo-Campos[91], Matthieu Jamme[109], María Jesús Arranz[110], Iolanda Jordan[111], Philippe Jorens[112], Fikret Kanat[113], Hasan Kapakli[114], Iskender Kara[115], Adem Karbuz[116], Kadriye Kart Yasar[117], Sevgi Keles[118], Yasemin Kendir Demirkol[119], Adam Klocperk[120], Zbigniew J. Król[121], Paul Kuentz[122], Yat Wah M. Kwan[123], Jean-Christophe Lagier[124], Bart N. Lambrecht[33], Yu-Lung Lau[125], Fleur Le Bourgeois[60], Yee-Sin Leo[126], Rafael Leon Lopez[127], Daniel Leung[125], Michael Levin[128], Michael Levy[60], Romain Lévy[20], Zhi Li[49], Agnes Linglart[129], Bart Loeys[130], José M. Lorenzo-Salazar[91], Céline Louapre[131], Catherine Lubetzki[131], Charles-Edouard Luyt[132], David C. Lye[133], Davood Mansouri[134], Majid Marjani[135], Jesus Marquez Pereira[136], Andrea Martin[137], David Martínez Pueyo[138], Javier Martinez-Picado[139], Iciar Marzana[140], Alexis Mathian[14], Larissa R. B. Matos[37], Gail V. Matthews[141], Julien Mayaux[142], Jean-Louis Mège[143], Isabelle Melki[144], Jean-François Meritet[145], Ozge Metin[146], Isabelle Meyts[147], Mehdi Mezidi[148], Isabelle Migeotte[149], Maude Millereux[150], Tristan Mirault[151], Clotilde Mircher[67], Mehdi Mirsaeidi[152], Abián Montesdeoca Melián[153], Antonio Morales Martinez[154], Pierre Morange[155], Clémence Mordacq[107], Guillaume Morelle[156], Stéphane Mouly[13], Adrián Muñoz-Barrera[91], Leslie Naesens[157], Cyril Nafati[158], João Farela Neves[159], Lisa FP. Ng[160], Yeray Novoa Medina[161], Esmeralda Nuñez Cuadros[162], J. Gonzalo Ocejo-Vinyals[163], Zerrin Orbak[164], Mehdi Oualha[20], Tayfun Özçelik[165], Qiang Pan-Hammarström[166], Christophe Parizot[142], Tiffany Pascreau[167], Estela Paz-Artal[168], Sandra Pellegrini[49], Rebeca Pérez de Diego[84], Aurélien Philippe[169], Quentin Philippot[77], Laura Planas-Serra[170], Dominique Ploin[171], Julien Poissy[172], Géraldine Poncelet[43], Marie Poulletty[173], Paul Quentric[142], Didier Raoult[143], Anne-Sophie Rebillat[67], Ismail Reisli[174], Pilar Ricart[175], Jean-Christophe Richard[176], Nadia Rivet[28], Jacques G. Rivière[177], Gemma Rocamora Blanch[15], Carlos Rodrigo[1], Carlos Rodriguez-Gallego[178], Agustí Rodríguez-Palmero[179], Carolina Soledad Romero[180], Anya Rothenbuhler[181], Flore Rozenberg[182], Maria Yolanda Ruiz del Prado[183], Joan Sabater Riera[15], Oliver Sanchez[184], Silvia Sánchez-Ramón[185], Agatha Schluter[170], Matthieu Schmidt[186], Cyril E. Schweitzer[187], Francesco Scolari[188], Anna Sediva[189], Luis M. Seijo[190], Damien Sene[13], Sevtap Senoglu[117], Mikko R. J. Seppänen[191], Alex Serra Ilovich[192], Mohammad Shahrooei[62], Hans Slabbynck[193], David M. Smadja[194], Ali Sobh[195], Xavier Solanich Moreno[15], Jordi Solé-Violán[196], Catherine Soler[197], Pere Soler-Palacín[137], Yuri Stepanovskiy[198], Annabelle Stoclin[199], Fabio Taccone[149], Yacine Tandjaoui-Lambiotte[200], Jean-Luc Taupin[201], Simon J. Tavernier[202], Benjamin Terrier[203], Caroline Thumerelle[107], Gabriele Tomasoni[204], Julie Toubiana[48], Josep Trenado Alvarez[205], Sophie Trouillet-Assant[206], Jesús Troya[207], Alessandra Tucci[208], Matilde Valeria Ursini[83], Yurdagul Uzunhan[209], Pierre Vabres[210], Juan Valencia-Ramos[211], Eva Van Braeckel[33], Stijn Van de Velde[212], Ana Maria Van Den Rym[84], Jens Van Praet[213], Isabelle Vandernoot[214], Hulya Vatansev[215], Valentina Vélez-Santamaria[42], Sébastien Viel[171], Cédric Vilain[216], Marie E. Vilaire[67], Audrey Vincent[35], Guillaume Voiriot[217], Fanny Vuotto[107], Alper Yosunkaya[90], Barnaby E. Young[126], Fatih Yucel[218], Faiez Zannad[219], Mayana Zatz[37], Alexandre Belot[220]*

[1]University Hospital and Research Institute "Germans Trias i Pujol," Badalona, Spain. [2]Navarra Health Service Hospital, Pamplona, Spain. [3]Division of Pediatric Infectious Diseases, Necmettin Erbakan University, Meram Medical Faculty, Konya, Turkey. [4]Department of Infectious Diseases, Loghman Hakim Hospital, Shahid Beheshti University of Medical Sciences, Tehran, Iran. [5]Hospital Nacional Edgardo Rebagliati Martins, Lima, Peru. [6]Parc Sanitari Sant Joan de Déu, Sant Boi de Llobregat, Spain. [7]Virology Research Center, National Institutes of Tuberculosis and Lung Diseases, Shahid Beheshti University of Medical Sciences, Tehran, Iran. [8]Division of Pediatric Infectious Diseases, Faculty of Medicine, Selcuk University, Konya, Turkey. [9]Intensive Care Unit, Hôpital Européen, Marseille, France. [10]Immunology Department, University Hospital 12 de Octubre, Research Institute imas12, and Complutense University, Madrid, Spain. [11]Clinical Immuology and Primary Immunodeficiencies Unit, Hospital Sant Joan de Déu, Barcelona, Spain. [12]Department of Biological Immunology, Necker Hospital for Sick Children, APHP and INEM, Paris, France. [13]Internal Medicine Department, Hôpital Lariboisière, APHP; Université de Paris, Paris, France. [14]Internal Medicine Department, Pitié-Salpétrière Hospital, Paris, France. [15]Hospital Universitari de Bellvitge, Barcelona, Spain. [16]Division of Clinical Immunology and Allergy, Necmettin Erbakan University, Meram Medical Faculty, Konya, Turkey. [17]Joint Research Unit, Hospices Civils de Lyon-bio Mérieux, Hospices Civils de Lyon, Lyon Sud Hospital, Lyon, France. [18]Hospital U. de Tarragona Joan XXIII, Universitat Rovira i Virgili (URV), IISPV, Tarragona, Spain. [19]Private practice, Paris, France. [20]Necker Hospital for Sick Children, AP-HP, Paris, France. [21]Department of Infectious

Diseases, CHU de Caen, Caen, France. [22]Consorcio Hospital General Universitario, Valencia, Spain. [23]The Genetics Institute, Tel Aviv Sourasky Medical Center and Sackler Faculty of Medicine, Tel Aviv University, Tel Aviv, Israel. [24]Department of Urology, Nephrology, and Transplantation, APHP-SU, Sorbonne Université, INSERM U 1082, Paris, France. [25]Service de Médecine Intensive–Réanimation et Pneumologie, APHP Hôpital Pitié–Salpêtrière, Paris, France. [26]Cruces University Hospital, Bizkaia, Spain. [27]Paediatric Immunology and Vaccinology Unit, Geneva University Hospitals and Faculty of Medicine, Geneva, Switzerland. [28]Hematology, Georges Pompidou Hospital, APHP, Paris, France. [29]Pediatric Infectious Diseases Unit, Instituto de Investigación 12 de Octubre imas12, and Hospital Universitario 12 de Octubre, Madrid, Spain. [30]Department of Immunology, Motol University Hospital, 2nd Faculty of Medicine, Charles University, Department of Pediatrics, Thomayer's Hospital, 1st Faculty of Medicine, Charles University, Prague, Czech Republic. [31]Centro de Investigación Biomédica en Red de Enfermedades Hepàticas y Digestivas (Ciberehd), Hospital de Mataró, Consorci Sanitari del Maresme, Mataró, Spain. [32]Service de Pneumologie, Hopital Bichat, APHP, Paris, France. [33]Department of Pulmonology, Ghent University Hospital, Ghent, Belgium. [34]Clinical Immunology Unit, Pediatric Infectious Disease Department, Faculty of Medicine and Pharmacy, Averroes University Hospital, LICIA Laboratoire d'Immunologie Clinique, d'Inflammation et d'Allergie, Hassann Ii University, Casablanca, Morocco. [35]Endocrinology Unit, APHP Hôpitaux Universitaires Paris-Sud, Le Kremlin-Bicêtre, France. [36]Department of Children's Diseases and Pediatric Surgery, I. Horbachevsky Ternopil National Medical University, Ternopil, Ukraine. [37]Human Genome and Stem-Cell Research Center, University of São Paulo, São Paulo, Brazil. [38]Hospital Insular, Las Palmas de Gran Canaria, Spain. [39]Division of Critical Care Medicine, Department of Anesthesiology and Reanimation, Konya State Hospital, Konya, Turkey. [40]MS Center, Spedali Civili, Brescia, Italy. [41]Fondazione IRCCS Ca' Granda Ospedale Maggiore Policlinico, Milan, Italy. [42]Bellvitge University Hospital, L'Hospitalet de Llobregat, Barcelona, Spain. [43]Hopital Robert Debré, Paris, France. [44]Pediatric Immuno-hematology Unit, Necker Enfants Malades Hospital, AP-HP, Paris, France. [45]Department of Infectious and Tropical Diseases, University of Brescia, ASST Spedali Civili di Brescia, Brescia, Italy. [46]Doctoral Health Care Center, Canarian Health System, Las Palmas de Gran Canaria, Spain. [47]Hôpital Foch, Suresnes, France. [48]Necker Hospital for Sick Children, Paris University, AP-HP, Paris, France. [49]Pasteur Institute, Paris, France. [50]McGill University Health Centre, Montreal, Canada. [51]University Hospital and Research Institute "Germans Trias i Pujol," IrsiCaixa AIDS Research Institute, UVic-UCC, Badalona, Spain. [52]Clinical Biochemistry, Pathology, Paediatric Neurology and Molecular Medicine Departments and Biobank, Institut de Recerca Sant Joan de Déu and CIBERER-ISCIII, Esplugues, Spain. [53]Division of Clinical Immunology and Allergy, Department of Internal Medicine, Necmettin Erbakan University, Meram Medical Faculty, Konya, Turkey. [54]Department of Infectious Diseases and Clinical Microbiology, Konya Training and Research Hospital, Konya, Turkey. [55]Hospital Universitari Vall d'Hebron, Barcelona, Spain. [56]Pitié-Salpêtrière Hospital, Paris, France. [57]Fundació Docència i Recerca Mútua Terrassa, Barcelona, Spain; Hospital Universitari Mutua Terrassa, Universitat de Barcelona, Terrassa, Catalonia, Spain. [58]UNSW Medicine, St. Vincent's Clinical School, and Department of Thoracic Medicine, St. Vincent's Hospital Darlinghurst, Sidney, Australia. [59]CHU Saint-Pierre, Université Libre de Bruxelles, Brussels, Belgium. [60]Pediatric Intensive Care Unit, Robert-Debré University Hospital, APHP, Paris, France. [61]Sorbonne Paris Nord, Hôpital Jean Verdier, APHP, Bondy, France. [62]Specialized Immunology Laboratory of Dr. Shahrooei, Sina Medical Complex, Ahvaz, Iran. [63]Centre de Génétique Humaine, CHU Besançon, Besançon, France. [64]Sorbonne Université Médecine and APHP Sorbonne Université Site Pitié-Salpêtrière, Paris, France. [65]Intensive Care Unit, Georges Pompidou Hospital, APHP, Paris, France. [66]Department of Pneumology, AZ Delta, Roeselare, Belgium. [67]Institut Jérôme Lejeune, Paris, France. [68]Department of Microbiology and Immunology, Faculty of Medicine, Mansoura University, Mansoura, Egypt. [69]Department of Chest, Faculty of Medicine, Mansoura University, Mansoura, Egypt. [70]Department of Medical Biochemistry and Molecular Biology, Faculty of Medicine, Mansoura University, Mansoura, Egypt. [71]Faculty of Medicine, Division of Pediatric Infectious Diseases, Selcuk University, Konya, Turkey. [72]Division of Pediatric Infectious Diseases, Ondokuz Mayıs University, Samsun, Turkey. [73]Necmettin Erbakan University, Meram Medical Faculty, Division of Pediatric Allergy and Immunology, Konya, Turkey. [74]Centre Hospitalier Fleyriat, Bourg-en-Bresse, France. [75]Division of Clinical Immunology and Allergy, Department of Internal Medicine, Necmettin Erbakan University, Meram Medical Faculty, Konya, Turkey. [76]Centre de Génétique, CHU Dijon, Dijon, France. [77]APHP Tenon Hospital, Paris, France. [78]Sorbonne Universités, UPMC University of Paris, Paris, France. [79]Department of Clinical Immunology , Hospital Clínico San Carlos, Madrid, Spain. [80]Genomics Division, Instituto Tecnológico y de Energías Renovables (ITER), Santa Cruz de Tenerife, Spain; CIBER de Enfermedades Respiratorias, Instituto de Salud Carlos III, Madrid, Spain; Research Unit, Hospital Universitario N.S. de Candelaria, Santa Cruz de Tenerife, Spain; Instituto de Tecnologías Biomédicas (ITB), Universidad de La Laguna, San Cristóbal de La Laguna, Spain. [81]CHU Limoges and Inserm CIC 1435 and UMR 1092, Limoges, France. [82]Infectious Diseases Unit, Department of Pediatrics, Hospital Sant Joan de Déu, Barcelona, Spain; Institut de Recerca Sant Joan de Déu, Spain; Universitat de Barcelona (UB), Barcelona, Spain. [83]Institute of Genetics and Biophysics "Adriano Buzzati-Traverso," IGB-CNR, Naples, Italy. [84]Laboratory of Immunogenetics of Human Diseases, IdiPAZ Institute for Health Research, La Paz Hospital, Madrid, Spain. [85]Hematology, APHP, Hopital Européen Georges Pompidou and Inserm UMR-S1140, Paris, France. [86]Hospital General Universitario and Instituto de Investigación Sanitaria "Gregorio Marañón," Madrid, Spain. [87]Bégin military Hospital, Bégin, France. [88]Pediatric Intensive Care Unit, Hospital Sant Joan de Déu, Barcelona, Spain. [89]Department of Internal Medicine, Hôpital Erasme, Université Libre de Bruxelles, Brussels, Belgium. [90]Division of Critical Care Medicine, Department of Anesthesiology and Reanimation, Necmettin Erbakan University, Meram Medical Faculty, Konya, Turkey. [91]Genomics Division, Instituto Tecnológico y de Energías Renovables (ITER), Santa Cruz de Tenerife, Spain. [92]Assistance Publique Hôpitaux de Paris, Paris, France. [93]Division of Allergy and Immunology, Necmettin Erbakan University, Meram Medical Faculty, Konya, Turkey. [94]CNAG-CRG, Centre for Genomic Regulation (CRG), Barcelona Institute of Science and Technology (BIST); Universitat Pompeu Fabra (UPF), Barcelona, Spain. [95]Department of Internal Medicine, National Reference Center for Rare Systemic Autoimmune Diseases, AP-HP, APHP-CUP, Hôpital Cochin, Paris, France. [96]Ghent University Hospital, Ghent, Belgium. [97]Sharjah Institute of Medical Research, College of Medicine, University of Sharjah, Sharjah, UAE. [98]Department of Laboratory Medicine, SE14186, Huddinge, Karolinska Institutet, Stockholm, Sweden. [99]Pediatric Infectious Diseases Unit, Bakirkoy Dr. Sadi Konuk Training and Research Hospital, University of Health Sciences, Istanbul, Turkey. [100]Department of Immunology, Hospital Universitario de Gran Canaria Dr. Negrín, Canarian Health System, Las Palmas de Gran Canaria, Spain. [101]Department of Pediatric Hemato-Oncology, Jolimont Hospital; Department of Pediatric Hemato-Oncology, HUDERF, Brussels, Belgium. [102]Intensive Care Unit, Marqués de Valdecilla Hospital, Santander, Spain. [103]Hospital del Mar, Parc de Salut Mar, Barcelona, Spain. [104]Department of Pediatric Pulmonology and Immunology, Ghent University Hospital, Ghent, Belgium. [105]Department of Intensive Care Unit, Ghent University Hospital, Ghent, Belgium. [106]Intensive Care Unit, APHM, Marseille, France. [107]CHU Lille, Lille, France. [108]Department of Pediatrics, Columbia University, New York, NY, USA. [109]Centre Hospitalier Intercommunal Poissy Saint Germain en Laye, Poissy, France. [110]Fundació Docència i Recerca Mútua Terrassa, Terrassa, Spain. [111]Hospital Sant Joan de Déu, Kids Corona Platfform, Barcelona, Spain. [112]Department of Intensive Care Unit, University Hospital Antwerp, Antwerp, Belgium. [113]Selcuk University, Faculty of Medicine, Chest Diseases Department, Konya, Turkey. [114]Division of Allergy and Immunology, Balikesir Ataturk City Hospital, Balikesir, Turkey. [115]Division of Critical Care Medicine, Selcuk University, Faculty of Medicine, Konya, Turkey. [116]Division of Pediatric Infectious Diseases, Prof. Dr. Cemil Tascıoglu City Hospital, Istanbul, Turkey. [117]Departments of Infectious Diseases and Clinical Microbiology, Bakirkoy Dr. Sadi Konuk Training and Research Hospital, University of Health Sciences, Istanbul, Turkey. [118]Meram Medical Faculty, Necmettin Erbakan University, Meram Medical Faculty, Konya, Turkey. [119]Health Sciences University, Umraniye Education and Research Hospital, Istanbul, Turkey. [120]Department of Immunology, 2nd Faculty of Medicine, Charles University and University Hospital in Motol, Prague, Czech Republic. [121]Central Clinical Hospital of Ministry of the Interior and Administration in Warsaw, Warsaw, Poland. [122]Oncobiologie Génétique Bioinformatique, PC Bio, CHU Besançon, Besançon, France. [123]Paediatric Infectious Disease Unit, Hospital Authority Infectious Disease Center, Princess Margaret Hospital, Hong Kong (Special Administrative Region), China. [124]Aix Marseille University, IRD, MEPHI, IHU Méditerranée Infection, Marseille, France. [125]Department of Paediatrics and Adolescent Medicine, The University of Hong Kong, Hong Kong, China. [126]National Centre for Infectious Diseases, Singapore. [127]Hospital Universitario Reina Sofía, Cordoba, Spain. [128]Imperial College, London, UK. [129]Endocrinology and Diabetes for Children, AP-HP, Bicêtre Paris-Saclay Hospital, Le Kremlin-Bicêtre, France. [130]Department of Medical Genetics, University Hospital Antwerp, Antwerp, Belgium. [131]Neurology Unit, APHP Pitié-Salpêtrière Hospital, Paris University, Paris, France. [132]Intensive Care Unit, APHP Pitié-Salpêtrière Hospital, Paris University, Paris, France. [133]National Centre for Infectious Diseases; Tan Tock Seng Hospital; Yong Loo Lin School of Medicine; Lee Kong Chian School of Medicine, Singapore. [134]Department of Clinical Immunology and Infectious Diseases, National Research Institute of Tuberculosis and Lung Diseases, Shahid Beheshti University of Medical Sciences, Tehran, Iran. [135]Clinical Tuberculosis and Epidemiology Research Center, National Research Institute of Tuberculosis and Lung Diseases (NRITLD), Shahid Beheshti University of Medical Sciences, Tehran, Iran. [136]Hospital Sant Joan de Déu and University of Barcelona, Barcelona, Spain. [137]Pediatric Infectious Diseases and Immunodeficiencies Unit, Hospital Universitari Vall d'Hebron, Vall d'Hebron Research Institute, Vall d'Hebron Barcelona Hospital Campus. Universitat Autònoma de Barcelona (UAB), Barcelona, Spain. [138]Hospital Universitari Mutua de Terrassa, Universitat de Barcelona, Barcelona, Spain. [139]IrsiCaixa AIDS Research Institute, ICREA, UVic-UCC, Research Institute "Germans Trias i Pujol," Badalona, Spain. [140]Department of Laboratory, Cruces University Hospital, Barakaldo, Bizkaia, Spain. [141]University of New South Wales, New South Wales, Australia. [142]APHP Pitié-Salpêtrière Hospital, Paris, France. [143]Aix-Marseille University, APHM, Marseille, France. [144]Robert Debré Hospital, Paris, France. [145]APHP Cohin Hospital, Paris, France. [146]Necmettin Erbakan University Meram Faculty of Medicine Department of Pediatric Infectious Diseases, Konya, Turkey. [147]University Hospitals Leuven, Leuven, Belgium. [148]Hospices Civils de Lyon, Hôpital de la Croix-Rousse, Lyon, France. [149]Hôpital Erasme, Brussels, Belgium. [150]CH Gonesse, Gonesse, France. [151]Vascular Medicine, Georges Pompidou Hospital, APHP, Paris, France. [152]Division of Pulmonary and Critical Care, University of Miami, Miami, FL, USA. [153]Guanarteme Health Care Center, Canarian Health System, Las Palmas de Gran Canaria, Spain. [154]Regional University Hospital of Malaga, Malaga, Spain. [155]Aix-Marseille Université, Marseille, France. [156]Department of General Paediatrics, Hôpital Bicêtre, AP-HP, University of Paris Saclay, Le Kremlin-Bicêtre, France. [157]Department of Internal Medicine, Ghent University Hospital, Ghent, Belgium. [158]CHU de La Timone, Marseille, France. [159]Centro Hospitalar Universitário de Lisboa Central, Lisbon, Portugal. [160]Infectious Diseases Horizontal Technlogy Centre, A*STAR; Singapore Immunology Network, A*STAR, Singapore. [161]Department of Pediatrics, Complejo Hospitalario Universitario Insular-Materno Infantil, Canarian Health System, Las Palmas de Gran Canaria, Spain. [162]Regional Universitary Hospital of Málaga, Málaga, Spain. [163]Hospital Universitario Marqués de Valdecilla, Santander, Spain. [164]Faculty of Medicine, Ataturk University, Erzurum, Turkey. [165]Department of Molecular Biology and Genetics, Bilkent University, Ankara, Turkey. [166]Department of Biosciences and Nutrition, Karolinska Institutet, SE14183, Stockholm, Sweden. [167]L'Hôpital Foch, Suresnes, France. [168]Department of Immunology, Hospital Universitario 12 de Octubre, Instituto de Investigación Sanitaria Hospital 12 de Octubre imas12, Madrid, Spain. [169]APHP Hôpitaux Universitaires Paris-Sud, Le Kremlin-Bicêtre, France. [170]Neurometabolic Diseases Laboratory, IDIBELL-Hospital Duran i Reynals, Barcelona; CIBERER U759, ISCiii, Madrid, Spain. [171]Hospices Civils de Lyon, Lyon, France. [172]Université de Lille, Inserm U1285, CHU Lille, Paris, France. [173]Departement of General Pediatrics, University Hospital Robert Debré, APHP, Paris, France. [174]Necmettin Erbakan University, Konya, Turkey. [175]Germans Trias i Pujol Hospital, Badalona, Spain. [176]Medical Intensive Care Unit, Hopital de la Croix-Rousse, Hospices Civils de Lyon, Lyon, France. [177]Pediatric Infectious Diseases and Immunodeficiencies Unit, Hospital Universitari Vall d'Hebron, Vall d'Hebron Research Institute, Vall d'Hebron Barcelona Hospital Campus., Barcelona, Spain. [178]Department of Immunology, Hospital Universitario de Gran Canaria Dr. Negrín, Canarian Health System, Las Palmas de Gran Canaria, Spain. University Fernando Pessoa Canarias, Las Palmas de Gran Canaria, Spain. [179]Neurometabolic Diseases Laboratory, IDIBELL-Hospital Duran i Reynals, Barcelona, Spain. [180]Consorcio Hospital General Universitario, Valencia, Spain. [181]APHP Hôpitaux Universitaires Paris-Sud, Paris, France. [182]Virology Unit, Université de Paris, Cohin Hospital, APHP, Paris, France. [183]Hospital San Pedro, Logroño, Spain. [184]Respiratory Medicine, Georges Pompidou Hospital, APHP, Paris, France. [185]Department of Immunology, Hospital Clínico San Carlos, Madrid, Spain. [186]Service de Médecine Intensive Réanimation, Institut de Cardiologie, Hopital Pitié-Salpêtrière, Paris, France. [187]CHRU de Nancy, Hôpital d'Enfants, Vandoeuvre, France. [188]Chair of Nephrology, University of Brescia, Brescia, Italy. [189]Department of Immunology, 2nd Faculty of Medicine, Charles University and Motol University Hospital, Prague,

Czech Republic. [190]Clínica Universidad de Navarra, Madrid, Spain. [191]HUS Helsinki University Hospital, Children and Adolescents, Rare Disease Center, and Inflammation Center, Adult Immunodeficiency Unit, Majakka, Helsinki, Finland. [192]Fundació Docència i Recerca Mútua Terrassa, Terrassa, Spain. [193]Department of Pulmonology, ZNA Middelheim, Antwerp, Belgium. [194]INSERM UMR-S 1140, Biosurgical Research Lab (Carpentier Foundation), Paris University and Hopital Européen Georges Pompidou, Paris, France. [195]Department of Pediatrics, Faculty of Medicine, Mansoura University, Mansoura, Egypt. [196]Critical Care Unit, Hospital Universitario de Gran Canaria Dr. Negrín, Canarian Health System, Las Palmas de Gran Canaria, Spain. [197]CHU de Saint Etienne, Saint-Priest-en-Jarez, France. [198]Shupyk National Medical Academy for Postgraduate Education, Kiev, Ukraine. [199]Gustave Roussy Cancer Campus, Villejuif, France. [200]Intensive Care Unit, Avicenne Hospital, APHP, Bobigny, France. [201]Laboratory of Immunology and Histocompatibility, Saint-Louis Hospital, Paris University, Paris, France. [202]Department of Internal Diseases and Pediatrics, Primary Immune Deficiency Research Lab, Centre for Primary Immunodeficiency Ghent, Jeffrey Modell Diagnosis and Research Centre, Ghent University Hospital, Ghent, Belgium. [203]Department of Internal Medicine, Université de Paris, INSERM, U970, PARCC, F-75015, Paris, France. [204]First Division of Anesthesiology and Critical Care Medicine, University of Brescia, ASST Spedali Civili di Brescia, Brescia, Italy. [205]Intensive Care Department, Hospital Universitari Mutua Terrassa, Universitat Barcelona, Terrassa, Spain. [206]Hospices Civils de Lyon, Lyon Sud Hospital, Lyon, France. [207]Infanta Leonor University Hospital, Madrid, Spain. [208]Hematology Department, ASST Spedali Civili di Brescia, Brescia, Italy. [209]Pneumologie, Hôpital Avicenne, APHP, INSERM U1272, Université Sorbonne Paris Nord, Bobigny, France. [210]Dermatology Unit, Laboratoire GAD, INSERM UMR1231 LNC, Université de Bourgogne, Dijon, France. [211]University Hospital of Burgos, Burgos, Spain. [212]Intensive Care Unit, M. Middelares Ghent, Ghent, Belgium. [213]Department of Nephrology and Infectiology, AZ Sint-Jan Brugge-Oostende AV, Bruges, Belgium. [214]Center of Human Genetics, Hôpital Erasme, Université Libre de Bruxelles, Brussels, Belgium. [215]Department of Chest Diseases, Necmettin Erbakan University, Meram Medical Faculty, Konya, Turkey. [216]CHU de Caen, Caen, France. [217]Sorbonne Université, Service de Médecine Intensive Réanimation, Hôpital Tenon, Assistance Publique-Hôpitaux de Paris, Paris, France. [218]General Intensive Care Unit, Konya Training and Research Hospital, Konya, Turkey. [219]CHU de Nancy, Nancy, France. [220]University of Lyon, CIRI, INSERM U1111, National Referee Centre RAISE, Pediatric Rheumatology, HFME, Hospices Civils de Lyon, Lyon, France.
*Leader of COVID Clinicians.

Imagine COVID Group Christine Bole-Feysot, Stanislas Lyonnet*, Cécile Masson, Patrick Nitschke, Aurore Pouliet, Yoann Schmitt, Frederic Tores, Mohammed Zarhrate

Imagine Institute, Université de Paris, INSERM UMR 1163, Paris, France.
*Leader of the Imagine COVID Group.

French COVID Cohort Study Group Laurent Abel[1], Claire Andrejak[2], François Angoulvant[3], Delphine Bachelet[4], Romain Basmaci[5], Sylvie Behillil[6], Marine Beluze[7], Dehbia Benkerrou[8], Krishna Bhavsar[4], François Bompart[9], Lila Bouadma[4], Maude Bouscambert[10], Mireille Caralp[11], Minerva Cervantes-Gonzalez[12], Anissa Chair[4], Alexandra Coelho[13], Camille Couffignal[4], Sandrine Couffin-Cadiergues[14], Eric D'Ortenzio[12], Charlene Da Silveira[4], Marie-Pierre Debray[4], Dominique Deplanque[15], Diane Descamps[16], Mathilde Desvallées[17], Alpha Diallo[18], Alphonsine Diouf[13], Céline Dorival[8], François Dubos[19], Xavier Duval[4], Philippine Eloy[4], Vincent VE Enouf[20], Hélène Esperou[21], Marina Esposito-Farese[4], Manuel Etienne[22], Nadia Ettalhaoui[4], Nathalie Gault[4], Alexandre Gaymard[10], Jade Ghosn[4], Tristan Gigante[23], Isabelle Gorenne[4], Jérémie Guedj[24], Alexandre Hoctin[13], Isabelle Hoffmann[4], Salma Jaafoura[21], Ouifiya Kafif[4], Florentia Kaguelidou[25], Sabina Kali[4], Antoine Khalil[4], Coralie Khan[17], Cédric Laouénan[4], Samira Laribi[4], Minh Le[4], Quentin Le Hingrat[4], Soizic Le Mestre[18], Hervé Le Nagard[24], François-Xavier Lescure[4], Yves Lévy[26], Claire Levy-Marchal[27], Bruno Lina[10], Guillaume Lingas[24], Jean Christophe Lucet[4], Denis Malvy[28], Marina Mambert[13], France Mentré[4], Noémie Mercier[18], Amina Meziane[8], Hugo Mouquet[20], Jimmy Mullaert[4], Nadège Neant[24], Marion Noret[29], Justine Pages[30], Aurélie Papadopoulos[21], Christelle Paul[18], Nathan Peiffer-Smadja[4], Ventzislava Petrov-Sanchez[18], Gilles Peytavin[4], Olivier Picone[31], Oriane Puéchal[12], Manuel Rosa-Calatrava[10], Bénédicte Rossignol[23], Patrick Rossignol[32], Carine Roy[4], Marion Schneider[4], Caroline Semaille[12], Nassima Si Mohammed[4], Lysa Tagherset[4], Coralie Tardivon[4], Marie-Capucine Tellier[4], François Téoulé[8], Olivier Terrier[10], Jean-François Timsit[4], Théo Trioux[4], Christelle Tual[33], Sarah Tubiana[4], Sylvie van der Werf[34], Noémie Vanel[35], Aurélie Veislinger[33], Benoit Visseaux[16], Aurélie Wiedemann[26], Yazdan Yazdanpanah[36]

[1]Inserm UMR 1163, Paris, France. [2]CHU Amiens, France. [3]Hôpital Necker, Paris, France. [4]Hôpital Bichat, Paris, France. [5]Hôpital Louis Mourrier, Colombes, France. [6]Institut Pasteur, Paris, France. [7]F-CRIN Partners Platform, AP-HP, Université de Paris, Paris, France. [8]Inserm UMR 1136, Paris, France. [9]Drugs for Neglected Diseases Initiative, Geneva, Switzerland. [10]Inserm UMR 1111, Lyon, France. [11]Inserm Transfert, Paris, France. [12]REACTing, Paris, France. [13]Inserm UMR 1018, Paris, France. [14]Inserm, Pôle Recherche Clinique, Paris, France. [15]CIC 1403 Inserm-CHU Lille, Paris, France. [16]Université de Paris, IAME, INSERM UMR 1137, AP-HP, University Hospital Bichat Claude Bernard, Virology, Paris, France. [17]Inserm UMR 1219, Bordeaux, France. [18]ANRS, Paris, France. [19]CHU Lille, Lille, France. [20]Pasteur Institute, Paris, France. [21]Inserm sponsor, Paris, France. [22]CHU Rouen–SMIT, Rouen, France. [23]FCRIN INI-CRCT, Nancy, France. [24]Inserm UMR 1137, Paris, France. [25]Centre d'Investigation Clinique, Inserm CIC1426, Hôpital Robert Debré, Paris, France. [26]Inserm UMR 955, Créteil, France; Vaccine Research Instiute (VRI), Paris, France. [27]F-CRIN INI-CRCT, Paris, France. [28]CHU de Bordeaux–SMIT, Bordeaux, France. [29]RENARCI, Annecy, France. [30]Hôpital Robert Debré, Paris, France. [31]Hôpital Louis Mourier–Gynécologie, Colombes, France. [32]University of Lorraine, Plurithematic Clinical Investigation Centre Inserm CIC-P; 1433, Inserm U1116, CHRU Nancy Hopitaux de Brabois, F-CRIN INI-CRCT (Cardiovascular and Renal Clinical Trialists), Nancy, France. [33]Inserm CIC-1414, Rennes, France. [34]Institut Pasteur, UMR 3569 CNRS, Université de Paris, Paris, France. [35]Hôpital la Timone, Marseille, France. [36]Bichat–SMIT, Paris, France.

CoV-Contact Cohort Loubna Alavoine[1], Karine K. A. Amat[2], Sylvie Behillil[3], Julia Bielicki[4], Patricia Bruijning[5], Charles Burdet[6], Eric Caumes[7], Charlotte Charpentier[8], Bruno Coignard[9], Yolande Costa[1], Sandrine Couffin-Cadiergues[10], Florence Damond[8], Aline Dechanet[11], Christelle Delmas[10], Diane Descamps[8], Xavier Duval[1], Jean-Luc Ecobichon[1], Vincent Enouf[3], Hélène Espérou[10], Wahiba Frezouls[1], Nadhira Houhou[11], Emila Ilic-Habensus[1], Ouifiya Kafif[11], John Kikoine[11], Quentin Le Hingrat[8], David Lebeaux[12], Anne Leclercq[1], Jonathan Lehacaut[1], Sophie Letrou[1], Bruno Lina[13], Jean-Christophe Lucet[14], Denis Malvy[15], Pauline Manchon[11], Milica Mandic[1], Mohamed Meghadecha[16], Justina Motiejunaite[17], Mariama Nouroudine[1], Valentine Piquard[11], Andreea Postolache[11], Caroline Quintin[1], Jade Rexach[1], Layidé Roufai[10], Zaven Terzian[11], Michael Thy[18], Sarah Tubiana[1], Sylvie van der Werf[3], Valérie Vignali[1], Benoit Visseaux[8], Yazdan Yazdanpanah[14]

[1]Centre d'Investigation Clinique, Inserm CIC 1425, Hôpital Bichat Claude Bernard, APHP, Paris, France. [2]IMEA Fondation Léon M'Ba, Paris, France. [3]Institut Pasteur, UMR 3569 CNRS, Université de Paris, Paris, France. [4]University of Basel Children's Hospital. [5]Julius Center for Health Sciences and Primary Care, Utrecht, Netherlands. [6]Université de Paris, IAME, Inserm UMR 1137, F-75018, Paris, France, Hôpital Bichat Claude Bernard, APHP, Paris, France. [7]Hôpital Pitiè Salpétriere, APHP, Paris. [8]Université de Paris, IAME, INSERM UMR 1137, AP-HP, University Hospital Bichat Claude Bernard, Virology, Paris, France. [9]Santé Publique France, Saint Maurice, France. [10]Pole Recherche Clinique, Inserm, Paris, France. [11]Hôpital Bichat Claude Bernard, APHP, Paris, France. [12]APHP, Paris, France. [13]Virpath Laboratory, International Center of Research in Infectiology, Lyon University, INSERM U1111, CNRS UMR 5308, ENS, UCBL, Lyon, France. [14]IAME Inserm UMR 1138, Hôpital Bichat Claude Bernard, APHP, Paris, France. [15]Service des Maladies Infectieuses et Tropicales; Groupe Pellegrin-Place Amélie-Raba-Léon, Bordeaux, France. [16]Hôpital Hotel Dieu, APHP, Paris, France. [17]Service des Explorations Fonctionnelles, Hôpital Bichat–Claude Bernard, APHP, Paris, France. [18]Center for Clinical Investigation, Assistance Publique-Hôpitaux de Paris, Bichat-Claude Bernard University Hospital, Paris, France.

Amsterdam UMC Covid-19 Biobank Michiel van Agtmael[1], Anna Geke Algera[2], Frank van Baarle[2], Diane Bax[3], Martijn Beudel[4], Harm Jan Bogaard[5], Marije Bomers[1], Lieuwe Bos[2], Michela Botta[2], Justin de Brabander[6], Godelieve de Bree[6], Matthijs C. Brouwer[4], Sanne de Bruin[2], Marianna Bugiani[7], Esther Bulle[2], Osoul Chouchane[1], Alex Cloherty[3], Paul Elbers[2], Lucas Fleuren[2], Suzanne Geerlings[1], Bart Geerts[8], Theo Geijtenbeek[9], Armand Girbes[2], Bram Goorhuis[1], Martin P. Grobusch[1], Florianne Hafkamp[9], Laura Hagens[2], Jorg Hamann[10], Vanessa Harris[1], Robert Hemke[11], Sabine M. Hermans[1], Leo Heunks[2], Markus W. Hollmann[8], Janneke Horn[2], Joppe W. Hovius[1], Menno D. de Jong[12], Rutger Koning[4], Niels van Mourik[2], Jeaninne Nellen[1], Frederique Paulus[2], Edgar Peters[1], Tom van der Poll[1], Benedikt Preckel[8], Jan M. Prins[1], Jorinde Raasveld[2], Tom Reijnders[1], Michiel Schinkel[1], Marcus J. Schultz[2], Alex Schuurman[13], Kim Sigaloff[1], Marry Smit[2], Cornelis S. Stijnis[1], Willemke Stilma[2], Charlotte Teunissen[14], Patrick Thoral[2], Anissa Tsonas[2], Marc van der Valk[1], Denise Veelo[8], Alexander P.J. Vlaar[15], Heder de Vries[2], Michèle van Vugt[1], W. Joost Wiersinga[1], Dorien Wouters[16], A. H. (Koos) Zwinderman[17], Diederik van de Beek[4]*

[1]Department of Infectious Diseases, Amsterdam UMC, Amsterdam, Netherlands. [2]Department of Intensive Care, Amsterdam UMC, Amsterdam, Netherlands. [3]Experimental Immunology, Amsterdam UMC, Amsterdam, Netherlands. [4]Department of Neurology, Amsterdam UMC, Amsterdam Neuroscience, Amsterdam, Netherlands. [5]Department of Pulmonology, Amsterdam UMC, Amsterdam, Netherlands. [6]Department of Infectious Diseases, Amsterdam UMC, Amsterdam, Netherlands. [7]Department of Pathology, Amsterdam UMC, Amsterdam, Netherlands. [8]Department of Anesthesiology, Amsterdam UMC, Amsterdam, Netherlands. [9]Department of Experimental Immunology, Amsterdam UMC, Amsterdam, Netherlands. [10]Amsterdam UMC Biobank Core Facility, Amsterdam UMC, Amsterdam, Netherlands. [11]Department of Radiology, Amsterdam UMC, Amsterdam, Netherlands. [12]Department of Medical Microbiology, Amsterdam UMC, Amsterdam, Netherlands. [13]Department of Internal Medicine, Amsterdam UMC, Amsterdam, Netherlands. [14]Neurochemical Laboratory, Amsterdam UMC, Amsterdam, Netherlands. [15]Department of Intensive Care, Amsterdam UMC, Amsterdam, Netherlands. [16]Department of Clinical Chemistry, Amsterdam UMC, Amsterdam, Netherlands. [17]Department of Clinical Epidemiology, Biostatistics and Bioinformatics, Amsterdam UMC, Amsterdam, Netherlands. [18]Department of Neurology, Amsterdam UMC, Amsterdam, Netherlands.
*Leader of the AMC Consortium.

COVID Human Genetic Effort Laurent Abel[1], Alessandro Aiuti[2], Saleh Al Muhsen[3], Fahd Al-Mulla[4], Mark S. Anderson[5], Andrés Augusto Arias[6], Hagit Baris Feldman[7], Dusan Bogunovic[8], Alexandre Bolze[9], Anastasiia Bondarenko[10], Ahmed A. Bousfiha[11], Petter Brodin[12], Yenan Bryceson[12], Carlos D. Bustamante[13], Manish Butte[14], Giorgio Casari[15], Samya Chakravorty[16], John Christodoulou[17], Elizabeth Ciralli[9], Antonio Condino-Neto[18], Megan A. Cooper[19], Clifton L. Dalgard[20], Alessia David[21], Joseph L. DeRisi[22], Murkesh Desai[23], Beth A. Drolet[24], Sara Espinosa[25], Jacques Fellay[26], Carlos Flores[27], Jose Luis Franco[28], Peter K. Gregersen[29], Filomeen Haerynck[30], David Hagin[31], Rabih Halwani[32], Jim Heath[33], Sarah E. Henrickson[34], Elena Hsieh[35], Kohsuke Imai[36], Yuval Itan[8], Timokratis Karamitros[37], Kai Kisand[38], Cheng-Lung Ku[39], Yu-Lung Lau[40], Yun Ling[41], Carrie L. Lucas[42], Tom Maniatis[43], Davoud Mansouri[44], Laszlo Marodi[45], Isabelle Meyts[46], Joshua Milner[47], Kristina Mironska[48], Trine Mogensen[49], Tomohiro Morio[50], Lisa FP. Ng[51], Luigi D. Notarangelo[52], Antonio Novelli[53], Giuseppe Novelli[54], Cliona O'Farrelly[55], Satoshi Okada[56], Tayfun Ozcelik[57], Rebeca Perez de Diego[58], Anna M. Planas[59], Carolina Prando[60], Aurora Pujol[61], Lluis Quintana-Murci[62], Laurent Renia[63], Alessandra Renieri[64], Carlos Rodríguez-Gallego[65], Vanessa Sancho-Shimizu[66], Vijay Sankaran[67], Kelly Schiabor Barrett[9], Mohammed Shahrooei[68], Andrew Snow[69], Pere Soler-Palacín[70], András N. Spaan[71], Stuart Tangye[72], Stuart Turvey[73], Furkan Uddin[74], Mohammed J. Uddin[75], Diederik van de Beek[76], Sara E. Vazquez[77], Donald C. Vinh[78], Horst von Bernuth[79], Nicole Washington[9], Pawel Zawadzki[80], Helen C. Su[52], Jean-Laurent Casanova[81]

[1]INSERM U1163, University of Paris, Imagine Institute, Paris, France. [2]San Raffaele Telethon Institute for Gene Therapy, IRCCS Ospedale San Raffaele, Milan, Italy. [3]King Saud University, Riyadh, Saudi Arabia. [4]Kuwait University, Kuwait City, Kuwait. [5]University of California, San Francisco, San Francisco, CA, USA. [6]Universidad de Antioquia, Group of Primary Immunodeficiencies, Antioquia, Colombia. [7]The Genetics Institute, Tel Aviv Sourasky Medical Center and Sackler Faculty of Medicine, Tel Aviv University, Tel Aviv, Israel. [8]Icahn School of Medicine at Mount Sinai, New York, NY, USA. [9]Helix, San Mateo, CA, USA. [10]Shupyk National Medical Academy for Postgraduate Education, Kiev, Ukraine. [11]Clinical Immunology Unit, Pediatric Infectious Disease Departement, Faculty of Medicine and Pharmacy, Averroes University Hospital; LICIA Laboratoire d'Immunologie Clinique, d'Inflammation et d'Allergie, Hassann Ii University, Casablanca, Morocco. [12]Karolinska Institute, Stockholm, Sweden. [13]Stanford University, Stanford, CA, USA. [14]University of California, Los Angeles, CA, USA. [15]Medical Genetics, IRCCS Ospedale San Raffaele, Milan, Italy. [16]Emory University Department of Pediatrics and Children's Healthcare of Atlanta, Atlanta, GA, USA. [17]Murdoch

Children's Research Institute, Victoria, Australia. [18]University of São Paulo, São Paulo, Brazil. [19]Washington University School of Medicine, St. Louis, MO, USA. [20]The American Genome Center; Uniformed Services University of the Health Sciences, Bethesda, MD, USA. [21]Centre for Bioinformatics and System Biology, Department of Life Sciences, Imperial College London, South Kensington Campus, London, UK. [22]University of California, San Francisco, CA, USA; Chan Zuckerberg Biohub, San Francisco, CA, USA. [23]Bai Jerbai Wadia Hospital for Children, Mumbai, India. [24]School of Medicine and Public Health, University of Wisconsin, Madison, WI, USA. [25]Instituto Nacional de Pediatria (National Institute of Pediatrics), Mexico City, Mexico. [26]Swiss Federal Institute of Technology Lausanne, Lausanne, Switzerland. [27]Research Unit, Hospital Universitario Nuestra Señora de Candelaria, Canarian Health System, Santa Cruz de Tenerife, Spain. [28]University of Antioquia, Medellín, Colombia. [29]Feinstein Institute for Medical Research, Northwell Health USA, Manhasset, NY, USA. [30]Department of Paediatric Immunology and Pulmonology, Centre for Primary Immunodeficiency Ghent (CPIG), PID Research Lab, Jeffrey Modell Diagnosis and Research Centre, Ghent University Hospital, Edegem, Belgium. [31]The Genetics Institute, Tel Aviv Sourasky Medical Center, Tel Aviv, Israel. [32]Sharjah Institute of Medical Research, College of Medicine, University of Sharjah, Sharjah, UAE. [33]Institute for Systems Biology, Seattle, WA, USA. [34]Children's Hospital of Philadelphia, Philadelphia, PA, USA. [35]Anschutz Medical Campus, Aurora, CO, USA. [36]Riken, Tokyo, Japan. [37]Hellenic Pasteur Institute, Athens, Greece. [38]University of Tartu, Tartu, Estonia. [39]Chang Gung University, Taoyuan County, Taiwan. [40]The University of Hong Kong, Hong Kong, China. [41]Shanghai Public Health Clinical Center, Fudan University, Shanghai, China. [42]Yale School of Medicine, New Haven, CT, USA. [43]New York Genome Center, New York, NY, USA. [44]Shahid Beheshti University of Medical Sciences, Tehran, Iran. [45]Semmelweis University Budapest, Budapest, Hungary. [46]KU Leuven, Department of Immunology, Microbiology and Transplantation, Leuven, Belgium. [47]Columbia University Medical Center, New York, NY, USA. [48]University Clinic for Children's Diseases, Skopje, North Macedonia. [49]Aarhus University, Aarhus, Denmark. [50]Tokyo Medical & Dental University Hospital, Tokyo, Japan. [51]Singapore Immunology Network, Singapore. [52]National Institute of Allergy and Infectious Diseases, National Institutes of Health, Bethesda, MD, USA. [53]Bambino Gesù Children's Hospital, Rome, Italy. [54]Department of Biomedicine and Prevention, University of Rome "Tor Vergata," Rome, Italy. [55]Trinity College, Dublin, Ireland. [56]Hiroshima University, Hiroshima, Japan. [57]Bilkent University, Ankara, Turkey. [58]Laboratory of Immunogenetics of Human Diseases, Innate Immunity Group, IdiPAZ Institute for Health Research, La Paz Hospital, Madrid, Spain. [59]IIBB-CSIC, IDIBAPS, Barcelona, Spain. [60]Faculdades Pequeno Príncipe e Instituto de Pesquisa Pelé Pequeno Príncipe, Curitiba, Brazil. [61]Neurometabolic Diseases Laboratory, IDIBELL–Hospital Duran I Reynals; Catalan Institution for Research and Advanced Studies (ICREA); CIBERER U759, ISCiii Madrid Spain, Barcelona, Spain. [62]Institut Pasteur (CNRS UMR2000) and Collège de France, Paris, France. [63]Infectious Diseases Horizontal Technology Center and Singapore Immunology Network, Agency for Science Technology (A*STAR), Singapore. [64]Medical Genetics, University of Siena, Siena, Italy; Genetica Medica, Azienda Ospedaliero-Universitaria Senese, Italy; GEN-COVID Multicenter Study. [65]Hospital Universitario de Gran Canaria Dr. Negrín, Canarian Health System, Canary Islands, Spain. [66]Imperial College London, London, UK. [67]Boston Children's Hospital, Harvard Medical School, Boston, MA, USA. [68]Saeed Pathobiology and Genetic Lab, Tehran, Iran. [69]Uniformed Services University of the Health Sciences, Bethesda, MD, USA. [70]Hospital Universitari Vall d'Hebron, Barcelona, Spain. [71]University Medical Center Utrecht, Amsterdam, The Netherlands. [72]Garvan Institute of Medical Research, Sydney, Australia. [73]The University of British Columbia, Vancouver, Canada. [74]Holy Family Red Crescent Medical College; Centre for Precision Therapeutics, NeuroGen Children's Healthcare; Genetics and Genomic Medicine Centre, NeuroGen Children's Healthcare, Dhaka, Bangladesh. [75]Mohammed Bin Rashid University of Medicine and Health Sciences, College of Medicine, Dubai, UAE; The Centre for Applied Genomics, Department of Genetics and Genome Biology, The Hospital for Sick Children, Toronto, Ontario, Canada. [76]Amsterdam UMC, University of Amsterdam, Department of Neurology, Amsterdam Neuroscience, Amsterdam, The Netherlands. [77]University of California, San Francisco, CA, USA. [78]McGill University Health Centre, Montreal, Canada. [79]Charité–Berlin University Hospital Center, Berlin, Germany. [80]Molecular Biophysics Division, Faculty of Physics, A. Mickiewicz University, Uniwersytetu Poznanskiego 2, Poznań, Poland. [81]Rockefeller University, Howard Hughes Medical Institute, Necker Hospital, New York, NY, USA.
*Leaders of the COVID Human Genetic Effort.

NIAID-USUHS/TAGC COVID Immunity Group Huie Jing[1,2], Wesley Tung[1,2], Christopher R. Luthers[3], Bradly M. Bauman[3], Samantha Shafer[2,4], Lixin Zheng[2,4], Zinan Zhang[2,4], Satoshi Kubo[2,4], Samuel D. Chauvin[2,4], Kazuyuki Meguro[1,2], Elana Shaw[1,2], Michael Lenardo[2,4], Justin Lack[5], Eric Karlins[5], Daniel M. Hupalo[7], John Rosenberger[7], Gauthaman Sukumar[7], Matthew D. Wilkerson[7], Xijun Zhang[7]

[1]Laboratory of Clinical Immunology and Microbiology, Division of Intramural Research, NIAID, NIH, Bethesda, MD, USA. [2]NIAID Clinical Genomics Program, National Institutes of Health, Bethesda, MD, USA. [3]Department of Pharmacology & Molecular Therapeutics, Uniformed Services University of the Health Sciences, Bethesda, MD, USA. [4]Laboratory of Immune System Biology, Division of Intramural Research, NIAID, NIH, Bethesda, MD, USA. [5]NIAID Collaborative Bioinformatics Resource, Frederick National Laboratory for Cancer Research, Leidos Biomedical Research, Inc., Frederick, MD, USA. [6]Bioinformatics and Computational Biosciences Branch, Office of Cyber Infrastructure and Computational Biology, NIAID, NIH, Bethesda, MD, USA. [7]The American Genome Center, Uniformed Services University of the Health Sciences, Bethesda, MD, USA.

SUPPLEMENTARY MATERIALS

science.sciencemag.org/content/370/6515/eabd4570/suppl/DC1
Materials and Methods
Figs. S1 to S11
Tables S1 and S2
References (*42* and *43*)
MDAR Reproducibility Checklist

View/request a protocol for this paper from *Bio-protocol*.

22 June 2020; accepted 16 September 2020
Published online 24 September 2020
10.1126/science.abd4570

Science

Inborn errors of type I IFN immunity in patients with life-threatening COVID-19

Qian Zhang, Paul Bastard, Zhiyong Liu, Jérémie Le Pen, Marcela Moncada-Velez, Jie Chen, Masato Ogishi, Ira K. D. Sabli, Stephanie Hodeib, Cecilia Korol, Jérémie Rosain, Kaya Bilguvar, Junqiang Ye, Alexandre Bolze, Benedetta Bigio, Rui Yang, Andrés Augusto Arias, Qinhua Zhou, Yu Zhang, Fanny Onodi, Sarantis Korniotis, Léa Karpf, Quentin Philippot, Marwa Chbihi, Lucie Bonnet-Madin, Karim Dorgham, Nikaïa Smith, William M. Schneider, Brandon S. Razooky, Hans-Heinrich Hoffmann, Eleftherios Michailidis, Leen Moens, Ji Eun Han, Lazaro Lorenzo, Lucy Bizien, Philip Meade, Anna-Lena Neehus, Aileen Camille Ugurbil, Aurélien Corneau, Gaspard Kerner, Peng Zhang, Franck Rapaport, Yoann Seeleuthner, Jeremy Manry, Cecile Masson, Yohann Schmitt, Agatha Schlüter, Tom Le Voyer, Taushif Khan, Juan Li, Jacques Fellay, Lucie Roussel, Mohammad Shahrooei, Mohammed F. Alosaimi, Davood Mansouri, Haya Al-Saud, Fahd Al-Mulla, Feras Almourfi, Saleh Zaid Al-Muhsen, Fahad Alsohime, Saeed Al Turki, Rana Hasanato, Diederik van de Beek, Andrea Biondi, Laura Rachele Bettini, Mariella D'Angio', Paolo Bonfanti, Luisa Imberti, Alessandra Sottini, Simone Paghera, Eugenia Quiros-Roldan, Camillo Rossi, Andrew J. Oler, Miranda F. Tompkins, Camille Alba, Isabelle Vandernoot, Jean-Christophe Goffard, Guillaume Smits, Isabelle Migeotte, Filomeen Haerynck, Pere Soler-Palacin, Andrea Martin-Nalda, Roger Colobran, Pierre-Emmanuel Morange, Sevgi Keles, Fatma Çölkesen, Tayfun Ozcelik, Kadriye Kart Yasar, Sevtap Senoglu, Semsi Nur Karabela, Carlos Rodríguez-Gallego, Giuseppe Novelli, Sami Hraiech, Yacine Tandjaoui-Lambiotte, Xavier Duval, Cédric Laouénan, COVID-STORM Clinicians, COVID Clinicians, Imagine COVID Group, French COVID Cohort Study Group, CoV-Contact Cohort, Amsterdam UMC Covid-19 Biobank, COVID Human Genetic Effort, NIAID-USUHS/TAGC COVID Immunity Group, Andrew L. Snow, Clifton L. Dalgard, Joshua D. Milner, Donald C. Vinh, Trine H. Mogensen, Nico Marr, András N. Spaan, Bertrand Boisson, Stéphanie Boisson-Dupuis, Jacinta Bustamante, Anne Puel, Michael J. Ciancanelli, Isabelle Meyts, Tom Maniatis, Vassili Soumelis, Ali Amara, Michel Nussenzweig, Adolfo García-Sastre, Florian Krammer, Aurora Pujol, Darragh Duffy, Richard P. Lifton, Shen-Ying Zhang, Guy Gorochov, Vivien Béziat, Emmanuelle Jouanguy, Vanessa Sancho-Shimizu, Charles M. Rice, Laurent Abel, Luigi D. Notarangelo, Aurélie Cobat, Helen C. Su and Jean-Laurent Casanova

Science **370** (6515), eabd4570.
DOI: 10.1126/science.abd4570originally published online September 24, 2020

The genetics underlying severe COVID-19

The immune system is complex and involves many genes, including those that encode cytokines known as interferons (IFNs). Individuals that lack specific IFNs can be more susceptible to infectious diseases. Furthermore, the autoantibody system dampens IFN response to prevent damage from pathogen-induced inflammation. Two studies now examine the likelihood that genetics affects the risk of severe coronavirus disease 2019 (COVID-19) through components of this system (see the Perspective by Beck and Aksentijevich). Q. Zhang *et al.* used a candidate gene approach and identified patients with severe COVID-19 who have mutations in genes involved in the regulation of type I and III IFN immunity. They found enrichment of these genes in patients and conclude that genetics may determine the clinical course of the infection. Bastard *et al.* identified individuals with high titers of neutralizing autoantibodies against type I IFN- α2 and IFN-ω in about 10% of patients with severe COVID-19 pneumonia. These autoantibodies were not found either in infected people who were asymptomatic or had milder phenotype or in healthy individuals. Together, these studies identify a means by which individuals at highest risk of life-threatening COVID-19 can be identified.

Science, this issue p. eabd4570, p. eabd4585; see also p. 404

Science (print ISSN 0036-8075; online ISSN 1095-9203) is published by the American Association for the Advancement of Science, 1200 New York Avenue NW, Washington, DC 20005. The title *Science* is a registered trademark of AAAS.

Science (print ISSN 0036-8075; online ISSN 1095-9203) is published by the American Association for the Advancement of Science, 1200 New York Avenue NW, Washington, DC 20005. The title *Science* is a registered trademark of AAAS.

5. Appendix 5

Synthèse des travaux en français

Étude systématique de la fonction contexte-dépendante de OX40 Ligand sur la polarisation des lymphocytes T CD4 auxiliaires chez l'Homme

Introduction

1) Les lymphocytes T auxiliaires : un rouage central de l'immunité adaptative

Les lymphocytes T auxiliaires (Th), également connus sous le nom de lymphocytes T CD4, sont des cellules primordiales dans l'immunité. Ce type cellulaire orchestre la réponse immunitaire adaptative et la guide en fonction du type de pathogène du non-soi rencontré. Ce manuscrit se concentrera principalement sur ces lymphocytes T auxiliaires et sur leur capacité à se polariser.

Un autre type cellulaire majeur pour le fonctionnement des lymphocytes T auxiliaires sont les cellules dendritiques (DC). Ces dernières jouent un rôle de pivot entre les systèmes immunitaires inné et adaptatif. À la rencontre d'un pathogène, détecté via de nombreux récepteurs, ces cellules professionnelles présentatrices d'antigènes capturent l'antigène, le dégradent sous forme de peptides et enfin les présentent à leur surface sur un récepteur particulier appelé complexe majeur d'histocompatibilité de classe (CMH) II [1]. Les DC migrent ensuite dans les ganglions, où les attendent les lymphocytes T CD4 naïfs, et leur présentent ce peptide. Les lymphocytes T vont ainsi s'activer et se polariser, spécifiquement au peptide présenté. Ce phénomène est décrit par la théorie des trois signaux [6]. Le premier signal consiste en l'activation du récepteur des cellules T (TCR) par le CMH II. Le deuxième est un signal de co-stimulation médié par la molécule CD28, qui accompagne le TCR. Enfin, le dernier signal est caractérisé par la sécrétion de cytokines par les cellules dendritiques, qui vont permettre la polarisation des lymphocytes T en une sous-population Th spécifique.

Dans les années 80, Mosmann et Coffman ont été les premiers à éclairer la recherche sur le concept des lymphocytes Th. Grâce à l'immunisation de souris, ils ont identifié deux clones de

lymphocytes CD4 : Th1 et Th2, et les ont caractérisés en fonction de leur sécrétion de cytokines, de leur facteurs de transcription et de leur marqueurs de surface [11,13].

Le principal rôle des lymphocytes Th1 est d'éliminer les pathogènes intracellulaires. La présence d'interleukine 12 (IL-12) est un signal clé pour la polarisation des Th1 et ils sont principalement caractérisés par l'expression du facteur de transcription T-bet et la production d'interféron gamma (IFNγ), IL-2, TNF-α et TNF-β [17,18].
Au contraire, les lymphocytes Th2 ont pour rôle d'aider à la mise en place de la production d'anticorps par les lymphocytes B et d'éliminer les pathogènes extracellulaires. Ils sont induits par la présence d'IL-4 et l'expression de GATA-3. De plus, ils sécrètent de l'IL-4, IL-5, IL-6, IL-13 and IL-31 [26,27].

Après les lymphocytes Th1 et Th2, d'autres sous-populations ont été identifiées et caractérisées. Les lymphocytes Th17 protègent principalement contre les champignons et les bactéries au niveau des muqueuses et des surfaces épithéliales et ont été décrits comme sécrétant de l'IL-17A, IL-17F, IL-21 et IL-22, et exprimant le facteur de transcription RORγt. De plus, chez l'homme, ils sont polarisés en présence d'une combinaison d'IL-1β, IL-6, IL-23 et TFG-β [38,39].
Les lymphocytes Th22 ont les mêmes fonctions que les Th17, auxquelles s'ajoute leur participation dans la réparation tissulaire. Ils expriment le facteur de transcription AHR et sont caractérisés par la production d'IL-22, en absence d'IL-17 [51,54].
De façon similaire aux Th22, les lymphocytes Th9 ont été identifiées par la production d'IL-9, en absence de production des autres cytokines Th2. Ils expriment le facteur de transcription PU.1 et sont impliqués dans le recrutement et l'activation des mastocytes [56,61].

Une autre sous-population de lymphocyte T a été découverte. Cette sous-population, appelée lymphocytes T folliculaires (Tfh), aident à la différentiation des lymphocytes B en plasmocytes et à leur commutation isotypique. Les signaux nécessaires à leur polarisation sont moins bien décrits que les autres lymphocytes Th mais ils sont caractérisés par le facteur de transcription Bcl-6 et par la sécrétion d'IL-21, IL-4, CXCL13 et CXCR5 ligand [85,90].

En parallèle de ces lymphocytes Th, une sous-population particulière a également été identifiée : les lymphocytes T CD4 régulateurs (Treg). Ceux-ci sont caractérisés par le facteur de transcription FoxP3 et induisent une tolérance nécessaire au système immunitaire [73].

2) Mécanismes sous-jacents de la polarisation des lymphocytes T auxiliaires

Les cytokines ne sont pas les seules molécules impliquées dans la polarisation des lymphocytes Th. La complexité de ces signaux peut être étudiée à différents niveaux : au niveau cellulaire et au niveau moléculaire.

Influence des cellules dendritiques sur la polarisation Th

Les DC peuvent être classifiées selon leur capacité migratoire : les DC migratoires patrouillent dans les tissus périphériques à la recherche d'antigènes, et les DC résidentes capturent les antigènes circulant directement dans les ganglions [94].

De plus, elles peuvent être séparées en deux groupes distincts : les DC conventionnelles (cDC), parmi lesquelles sont trouvées les cDC1 et les cDC2, exprimant respectivement BDCA-3 et BDCA-1), et les DC plasmacytoïdes (pDC), exprimant BDCA-4 [95,96].

Dans l'épiderme sont également spécifiquement trouvées les cellules de Langerhans.

Pour finir, on trouve les DC dérivées des monocytes (MoDCs). Elles ont tout d'abord été décrites chez la souris comme étant rares à l'état basal et recruter sur le site de l'inflammation [97]. Elles ont ensuite été retrouvées chez l'Homme dans différents contextes inflammatoires [98,99]. Il a été montré que ces MoDC pouvaient être différenciées in vitro à partir de monocytes $CD14^+$, en présence d'IL-4 et de GM-CSF [100,101].

Ces différentes populations de DC ont été montrées comme ayant un impact distinct sur la polarisation des lymphocytes Th. En effet, cDC1 et cDC2 issues de sang de donneur sain ont été décrites comme ayant un impact différent sur les Th1 et les Th2 par plusieurs études [107–109]. De plus, il a été montré que les DC isolées d'amygdales avaient un impact différent sur la polarisation Tfh [110]. Enfin, les MoDC ont été montrées comme influençant la polarisation vers Th17 et/ou Th1 [98,111].

De surcroit, le stimulus activant les DC a aussi un rôle à jouer dans le devenir de la polarisation Th. Par exemple, l'activation de plusieurs sous-populations de DC avec du lipopolysaccharide (LPS) de Escherichia coli a été montré comme induisant des lymphocytes Th1 [116,118]. En revanche, la stimulation de MoDC avec du Curdlan ou du Zymozan a été montrée comme induisant des lymphocytes Th17 [119]. Des stimuli non-dérivés de microorganismes peuvent activer les DC comme la lymphopoiétine thymique stromale (TSLP). Celle-ci a été décrite comme pro-polarisation Th2 par plusieurs équipes [121,122].

Influence de la diversité des motifs moléculaires sur la polarisation Th

Tout d'abord, le signal induit par le TCR influence la polarisation Th, de manière quantitative mais aussi qualitative. En effet, il a été démontré qu'un signal TCR fort avait plus tendance à induire des lymphocytes Th1 alors qu'un signal plus faible avait tendance à promouvoir des lymphocytes Th2. La force du signal TCR joue également sur la polarisation Th17 et Treg. Un signal TCR fort favoriserait plutôt une polarisation Th17 et un signal faible une polarisation Treg [129–131].

De plus, les molécules de co-signal, comprenant des molécules de co-stimulation et de co-inhibition, jouent aussi un rôle sur la polarisation Th. Les molécules de co-stimulation, comme leur nom l'indique, ont pour but de stimuler la réponse immunitaire, alors que les molécules de co-inhibition ont la capacité de le réguler négativement.
D'une part, ICOS est un bon exemple de molécule co-stimulatrices influençant la polarisation Th. En fonction des études, ICOS a été montrée comme pro-Th1 [141] et anti-Th1 [142–144]. En revanche, ICOS a plus clairement été classée comme pro-Th2 et pro-Tfh, en donc grandement impliquée dans l'aide aux lymphocytes B [146,148]. Les lymphocytes Th17 et Treg ont également été montrés comme impactés par ICOS [149,152]. Ainsi, l'impact de ICOS sur la polarisation Th est très complexe et sa fonction semble donc grandement dépendante du contexte dans lequel le lymphocyte T évolue.
D'autre part, TIGIT est un bon exemple de molécule co-inhibitrice influençant la polarisation Th. TIGIT a été montré comme inhibant les polarisations Th1 et Th17. En revanche, il n'aurait pas d'impact sur la polarisation Th2 [160]. Un autre article montrerait même que TIGIT promeut les lymphocytes Th2 [161]. Ainsi, peu de papiers rapportent un impact de TIGIT sur la polarisation Th, mais cela souligne malgré tout que les molécules co-inhibitrices peuvent avoir un rôle plus large qu'une simple inhibition de la réponse immunitaire.

L'intégration de signaux complexes implique de la contexte-dépendance

Il a été montré dans les parties précédentes que plusieurs signaux, d'origines et natures différentes, peuvent être impliqués dans la polarisation Th.

Le concept de contexte-dépendance dans la vie réelle peut être défini comme le fait qu'une seule et même personne peut avoir un comportement différent en fonction de l'environnement dans lequel elle se trouve, des personnes qui l'entourent etc. Ce même concept peut être appliqué à la biologie. Une cellule, une molécule peut avoir des fonctions ou des comportements différents en fonction du contexte dans lequel elle évolue.

Les cytokines exercent souvent des fonctions contexte-dépendantes. Par exemple, c'est le cas de TFG-β, qui promeut les Treg en présence d'IL-2 [168], qui promeut les Th17 en présence d'IL-1β, IL-6 et IL-23 [38], et qui promeut les Th9 en présence d'IL-4 [57]. De plus, Schmitt et al. ont montré que TFG-β en présence d'IL-12 et d'IL-23 pouvait induire plusieurs marqueurs Tfh comme CXCR5, Bcl-6 et IL-21, à partir de cellules T CD4 naïves [82]. Toujours à propos de cytokines, Touzot et al. ont exploré la contexte-dépendance de IFNα dans différents contextes de polarisation cytokinique et ont démontré que IFNα induisait des signatures transcriptionelles distinctes dans chaque contexte [169].

La fonction des molécules de checkpoints immunitaires peuvent être aussi sujet à de la contexte-dépendance. Cela peut être illustré par CD28, qui peut induire une sécrétion de cytokines quantitativement différente en fonction du stimuli d'activation des MoDC [170].

3) OX40-OX40 Ligand : biologie d'un checkpoint immunitaire co-stimulateur

La fonction de OX40-OX40 Ligand sur l'activation des lymphocytes T

OX40 a été découvert dans les années 80, puis a été cloné et séquencé pour la première fois dans les années 90. Il a ainsi été classé dans la famille des récepteurs de TNF (TNFRSF) [213,214]. OX40 Ligand (OX40L) a été découvert durant la même période [215]. Ensuite, la structure cristallographique de ce couple récepteur-ligand a été déterminée en 2006. OX40L est un homo-trimère, ce qui signifie qu'une molécule de OX40L doit se lier à trois molécules OX40 pour induire un signal [218].

OX40 est principalement exprimé par les lymphocytes T activés, CD4 et CD8, mais aussi sur les cellules NK, NKT et neutrophiles [221,224,225]. OX40L est également exprimé après activation, et principalement sur les cellules présentatrices d'antigènes (DC, lymphocyte B et macrophage) [227,228], mais également sur les cellules endothéliales vasculaires, NK et mastocytes [230,231,233]. La ligation de OX40L sur OX40 induit une signalisation dans la cellule T via la voie NFκB non canonique, parmi d'autres voies de signalisation [237]. Cela permet de réguler positivement des gènes, comme ceux codant pour Bcl-XL ou survivin (des molécules anti-apoptotique) et les cytokines Th. Au contraire, cela régule aussi négativement certains gènes, comme ceux codant pour FoxP3, CTLA-4 et TFG-β.

De plus, en termes de fonction, l'interaction OX40-OX40L va permettre d'augmenter la

prolifération, l'expansion, la polarisation et la survie des lymphocytes T CD4 [213,235]. Elle joue également un rôle dans l'adhésion et la migration des lymphocytes T [221,233,241–243].

Contrôle de la polarisation Th et de la sécrétion de cytokines par OX40L

Tout d'abord, concernant les premières sous-populations Th1 et Th2, il a été montré OX40L induit préférentiellement les lymphocytes Th2. En revanche, le contexte influe beaucoup sur la fonction de OX40L sur la polarisation Th1 [108,122,251].

Pour les lymphocytes Th17, des effets opposés de OX40L ont également été observés. Dans les modèles de souris, les avis sont très partagés, suggérant de nouveau que le contexte influe probablement sur la fonction de OX40L [256–258,262].

Concernant l'impact de OX40L sur la polarisation Th9, deux études vont dans le même sens, en démontrant que OX40L joue un rôle important dans l'induction des lymphocytes Th9 [263,264].

Pour les lymphocytes Tfh et Treg, des régulations positives et négatives par OX40L sont rapportées, démontrant encore une fois l'importance du contexte dans la fonction de la molécule [86,268,278,282].

OX40-OX40L en pathologies et essais cliniques

Différents anticorps ou protéines, visant OX40 ou OX40L, sont en développement en clinique dans plusieurs types de pathologies. De plus, en fonction de la pathologie, l'objectif va être de stimuler la voie de signalisation de OX40, ou au contraire de l'inhiber.

Tout d'abord, des anticorps antagonistes anti-OX40 sont en développement dans les cancers. Le cancer est une pathologie très complexe. Contrairement à la chimiothérapie, qui a pour but de tuer les cellules tumorales en visant les cellules se divisant rapidement, les immunothérapies vont stimuler le système immunitaire du patient, pour qu'il puisse les reconnaître et les détruire par lui-même. Pour l'instant, seules des immunothérapies visant des molécules de checkpoint immunitaires co-inhibitrices ont eu une autorisation de mise sur le marché (anti-PD-1, anti-CTLA-4) [212]. La raison pour cibler OX40 en immunothérapie vient de son aptitude à augmenter la prolifération, la migration et la survie des lymphocytes T, et leur production de cytokines. Ainsi, plusieurs anticorps monoclonaux antagonistes sont testés en essais cliniques comme MEDI6469 (NCT02274155) ou GSK3174998 (NCT02528357). En plus des anticorps, des protéines

recombinantes OX40L ont été conçues. Par exemple, MEDI6383 est testé dans les tumeurs solides avancées, seule ou en combinaison avec un anti-PD-L1 (NCT02221960).

La voie OX40-OX40L est également visée dans les allergies, mais cette fois-ci, le but est d'inhiber la fonction de ces molécules. En effet, les maladies allergiques ont rapidement été associées à la cytokine IL-4 et donc aux lymphocytes Th2 et Tfh [289,290]. Ainsi, même si la fonction de OX40L sur la polarisation Th semblerait être très dépendante du contexte, elle a été montrée comme ayant un impact positif sur ces deux sous-populations Th.
Plusieurs anticorps monoclonaux antagonistes anti-OX40 sont donc en développement dans le traitement de la maladie de dermatite atopique, comme GBR830 (NCT02683928) et KHK4083 (NCT03096223, NCT03703102). Un anti-OX40L est également testé dans le traitement l'asthme (NCT00983658).

Enfin, dans les maladies auto-immunes, il a été montré que la voie OX40-OX40L pourrait jouer un rôle dans leur exacerbation. Par exemple, dans la maladie bowel inflammatoire, classée dans les maladies gastro-intestinales, OX40 a été négativement corrélé avec l'amélioration de la maladie [296,298,299].
Malgré cela, seul un anticorps monoclonal antagoniste anti-OX40 est testé en clinique, le même que pour la dermatite atopique, KHK4083 (NCT02647866).

Objectifs

Dans l'introduction, il a été montré que les lymphocytes CD4, et leurs cytokines secrétées, jouent un rôle central dans la mise en place d'une immunité adaptative adaptée contre un pathogène. La complexité de la classification actuelle des sous-populations Th, leurs mécanismes de polarisation, et comment OX40L, un checkpoint immunitaire co-stimulateur, influe sur cette polarisation a été présenté. De plus, un point important a été de sensibilisé au fait que le contexte dans lequel une cellule, une molécule évolue, peut influencer sur son comportement ou sa fonction. Concernant l'étude des checkpoints immunitaires, beaucoup reste à faire sur la compréhension de leurs mécanismes d'action et ils ont majoritairement été étudiés individuellement, dans un contexte spécifique.
Il n'y a actuellement aucune méthode pour analyser la contexte-dépendance de la fonction d'une

molécule dans des systèmes biologiques. Ainsi, avec ce travail, plusieurs questions ont été adressées :

- Est-il possible de quantifier la contexte-dépendance de la fonction d'une molécule biologique ? Comment ?
- Quelle serait la meilleure méthode pour quantifier cette contexte-dépendance ?
- Comment les modèles statistiques peuvent s'appliquer à ce concept et à cette quantification ?

D'autres questions se sont posées :

- Comment évaluer la quantité de données nécessaires pour étudier cette contexte-dépendance ?
- Comment représenter une telle quantité de données sans perdre d'information ?
- Comment choisir les systèmes expérimentaux pour quantifier la contexte-dépendance de façon adéquate ?
- Est-ce que la contexte-dépendance vient du contexte en son ensemble ou d'un paramètre spécifique du contexte ?
- Dans cette même directive, est-il possible de disséquer le contexte pour mieux comprendre d'où vient la contexte-dépendance de la fonction de la molécule étudiée ?

Résultats

Les checkpoints immunitaires font partie d'une large diversité de signaux intégrés par les cellules T. Les checkpoints immunitaires sont connus pour jouer un rôle clé lors de l'activation et de la régulation des lymphocytes T. Cette famille comprend une trentaine de molécules et est divisée en deux catégories fonctionnelles. Les molécules co-stimulatrices, tels que CD28, ont la capacité de stimuler l'activation des lymphocytes T tandis que les molécules co-inhibitrices, tels que PD-1, jouent un rôle dans la régulation de la réponse des lymphocytes T.

Dans cette étude, nous utilisons la polarisation T auxiliaire comme modèle, pour illustrer comment les paramètres du microenvironnement peuvent avoir un impact sur les paramètres internes, tels que la fonction de biomolécule. Nous voulions explorer davantage cet aspect de contexte-

dépendance, son possible impact sur la polarisation Th et en particulier sur la sécrétion de cytokines. De plus, nous avons choisi OX40L comme un checkpoint immunitaire intéressant pour étudier ce concept. Comme présenté dans l'introduction, nous avons déjà des indices sur les fonctions d'OX40L sur la polarisation Th et la sécrétion de cytokines. Cependant, la manière dont le contexte peut influencer sa fonction n'a jamais été décrite. De plus, des outils étaient disponibles pour étudier OX40L dans nos deux systèmes expérimentaux : la protéine OX40L recombinante humaine (rhOX40L) et l'anticorps bloquant anti-OX40L humain.

Par conséquent, nous avons d'abord décidé d'utiliser une approche systématique en appliquant plusieurs contextes cytokiniques sur les lymphocytes T en présence ou en absence de rhOX40L. Pour cela, nous avons utilisé un système de culture de polarisation Th, avec des billes anti-CD3/anti-CD28 pour la stimulation du TCR et des cytokines polarisantes Th pour induire Th0 (pas de cytokine), Th1 (IL-12), Th2 (IL-4) et Th17 (IL1β + IL-6 + IL-23 + TGF-β). Une protéine rhOX40L soluble trimérique a été ajoutée à la culture pour stimuler OX40 sur les cellules T.

Dans un deuxième temps, nous avons voulu intégrer un contexte cellulaire dans nos paramètres externes appliqués aux cellules T, pour voir son impact sur la fonction OX40L. Ces contextes cellulaires sont composés de deux paramètres, le type DC et les stimuli activant les DC. Nous avons utilisé deux types de DC : des cDC2, directement isolé du sang de donneur sain, et des MoDC, différenciés par IL-4 et GM-CSF à partir de monocytes $CD14^{+}$, également isolés du sang de donneur sain. Pour étendre le nombre de contextes, chaque population a été activée à l'aide de différents stimuli, avec une large pertinence physiopathologique pour les infections bactériennes (LPS, HKSA, Curdlan) et fongiques (Zymozan), et pour les allergies (TSLP). Dans ce cas, nous avons ajouté un anticorps monoclonal antagoniste contre OX40L pour bloquer la communication DC-T via l'interaction OX40-OX40L.

Dans nos deux systèmes expérimentaux, nous avons analysé les 17 principales cytokines Th sécrétées par les lymphocytes T, en présence ou en absence d'OX40L, avec l'hypothèse que la contexte-dépendance peut se produire sur différentes cytokines. Ces cytokines sécrétées ont été mesurées dans 302 observations pour créer une grande base de données. En combinant les systèmes expérimentaux et la modélisation statistique, nous avons quantifié et évalué les fonctions contexte-dépendantes de OX40L sur la polarisation Th.

Notre stratégie de modélisation mathématique nous a permis : 1) d'identifier les cytokines pour lesquelles la contexte-dépendance d'OX40L était la plus importante dans chacun de nos systèmes,

2) de classer chaque contexte selon la contexte-dépendance d'OX40L, 3) d'identifier le paramètre le plus important influençant la contexte dépendance d'OX40L, entre le type DC et les stimuli activant les DC. Ainsi, parmi les contextes Th, Th2 apparaît comme celui qui a le plus d'influence sur la fonction OX40L, tandis que dans les contextes bDC, TSLP est de loin le plus influent. Enfin, parmi les contextes cellulaires, le type DC s'est révélé dominant dans le contrôle de la contexte-dépendance d'OX40L par rapport au stimulus activant les DC.

Pour conclure, notre modèle statistique peut être appliqué à n'importe quelle biomolécule, pour déchiffrer et quantifier sa contexte-dépendance et évaluer son impact sur sa fonction.

Discussion générale et perspectives

1) Concept de contexte-dépendance

Importance multidisciplinaire de la contexte-dépendance

Le concept de contexte-dépendance a été identifié dans de nombreux domaines scientifiques et certains articles ont tenté de mieux comprendre ses conséquences très récemment. Elle a par exemple été étudiée en génétique, écologie et même en économie [300,303–305]. Mais bien que la contexte-dépendance ait été examinée et étudiée dans de nombreux domaines, peu d'études nous permettent de la quantifier de manière complète et directe. La contexte-dépendance dans son intégralité est un problème difficile car il s'agit en réalité d'une combinaison d'un nombre incalculable de paramètres, chacun comprenant de nombreuses combinaisons de variantes. Par conséquent, une telle complexité doit être formalisée à l'aide d'une approche de modélisation mathématique intégrée.

Originalité de notre modèle statistique sur la contexte-dépendance

À propos de la polarisation Th, certaines études ont examiné l'induction de sous-populations Th dans différents contextes [82,86,122]. Cependant, à notre connaissance, aucune étude n'a évalué quantitativement la contexte-dépendance des fonctions d'une molécule, de manière systématique et dans de nombreux contextes. De plus, plus spécifiquement, les effets contexte-dépendants d'OX40L sur la polarisation Th et la sécrétion de cytokines, dans divers contextes moléculaires et cellulaires, Th n'avaient jamais été abordés.

Pour étudier les fonctions contexte-dépendants d'OX40L sur la polarisation Th, nous avons utilisé deux méthodes expérimentales, un système de polarisation Th, sans DC, et un système de co-culture de cellules T-DC. Ces derniers, ainsi que les outils pour stimuler ou inhiber OX40L, étaient très contrôlés car bien établis dans la littérature et dans l'équipe [85,86,122,169,170]. Ces systèmes expérimentaux étaient à la base de nos deux types de contextes : des contextes moléculaires, utilisant des cytokines Th polarisantes, et des contextes cellulaires. Les contextes moléculaires sont plus faciles à contrôler car ils induisent un panel très spécifique de cytokines sécrétées par les cellules T, les contextes utilisant des DC activées induisant un panel mixte de cytokines. Cependant, bien qu'il soit utile comme preuve de concept, ce type de système crée des contextes « extrêmes », dans lesquels les cytokines polarisantes sont présentes à des concentrations élevées ou pas du tout. Par conséquent, nous avons décidé d'également introduire des contextes cellulaires, dans lesquels les cellules T sont activées et polarisées par les DC. Avec les contextes cellulaires, nous avons ajouté de la complexité à nos contextes et avons essayé de nous rapprocher de la physiologie.

Pour toute cette diversité de contextes appliqués aux cellules T CD4, nous avons mesuré systématiquement une grande quantité de cytokines Th sécrétées, 17 cytokines, là où la plupart des études ne sélectionnent que peu de cytokines d'intérêt. Nous avons obtenu une base de données contenant 5046 points de données. Concernant le modèle que nous voulions établir et la taille du jeu de données généré, nous avons travaillé en étroite relation avec des biostatisticiens.

Application du modèle de contexte-dépendance

Dans nos contextes cellulaires, nous avons inclus des stimuli d'activation présentant une pertinence physiopathologique pour les bactéries (LPS, HKSA, Curdlan), les champignons (Zymozan) et les allergies (TSLP). Il aurait été intéressant d'inclure un contexte tumoral dans notre panel puisque nous travaillons sur les fonctions d'une molécule intéressante pour l'immunothérapie. Les programmes DC induits par le microenvironnement tumoral sont particuliers et peuvent favoriser ou contrôler le développement du cancer. Il existe des ressources sur les états des DC dans les tumeurs [311,312]. Cependant, ces microenvironnements tissulaires complexes, en plus d'être très variables entre les patients, sont difficiles à récapituler dans des systèmes contrôlés, et nécessitent des études dédiées. Comme expérience intéressante, les cellules T pourraient être cultivées dans des surnageants de tumeurs. Les différents contextes peuvent être définis selon plusieurs paramètres. Premièrement, il peut s'agir simplement d'un

même type de tumeur provenant de différents patients, qui ont leur propre microenvironnement tumoral. Ensuite, il est possible d'aller plus loin, y compris avec différents types de tumeurs, différents traitements de tumeurs, etc. Ce type d'analyse pourrait être une première étape pour mieux comprendre l'efficacité variable du blocage des checkpoints immunitaires.

Limitation du modèle de contexte-dépendance

Nous pouvons également nous concentrer sur les limites de notre modèle et la justification de ces limites.

Une première limitation de l'étude de la contexte-dépendance est bien sûr le nombre de contextes. Dans notre cas, nous avons d'abord décidé de prendre en compte le contexte des cytokines, car elles sont communément décrites comme étant un signal majeur en polarisation Th. Nous utilisons une protéine OX40L recombinante (rhOX40L) dans une expérience simplifiée de polarisation, sans aucune intervention de DC, en utilisant des billes anti-CD3 / anti-CD28 pour l'activation des lymphocytes T et des cytokines synthétiques pour la polarisation. Notre deuxième cadre expérimental utilisant des DC pour activer et polariser les cellules T vise à complexifier nos contextes pour se rapprocher de la réalité de la polarisation Th dans les ganglions lymphatiques. Néanmoins, l'augmentation de la complexité va de pair avec la diminution de contrôle des systèmes. Nous aurions pu faire beaucoup d'autres choix pour les contextes tels que choisir d'autres stimuli d'activation DC par exemple. Malheureusement, ajouter plus de stimuli d'activation DC aurait été difficile par rapport au nombre de DC que l'on peut obtenir à partir d'une même poche de sang.

De plus, dans les contextes cellulaires, nous n'avons inclus que deux types de DC, cDC2 et MoDC, nous aurions pu en choisir d'autres, mais encore une fois le problème du nombre de DC persiste, ainsi que celui du choix du milieu de culture par rapport au type de DC.

2) Impact de OX40L sur la sécrétion de cytokines Th et ses effets contexte-dépendants

Impact de OX40L sur les principales cytokines Th

La contexte-dépendance peut également être intéressante à considérer dans le cas de résultats paradoxaux entre différentes études. Dans le cas d'OX40L, nous avons été intéressés par IL-4 car de nombreuses études ont lié OX40L à l'allergie et aux cellules Th2 et Tfh [290]. Dans notre contexte Th2, nous avons observé une diminution de l'IL-4 en présence de la protéine rhOX40L, ainsi qu'une

diminution des cytokines Th2 IL-5 et IL-31. De manière similaire, dans notre contexte TSLP-bDC, nous avons observé une augmentation de l'IL-4 en présence de l'anticorps bloquant anti-OX40L, ce qui signifie une diminution de l'IL-4 par l'OX40L. Cependant, OX40L a été plutôt classé comme induisant les cellules Th2 dans la littérature [122,251]. Cependant, dans ces études, d'autres types de DC et milieux ont été utilisés.

Dans notre contexte Th17, nous avons remarqué qu'OX40L entrainait une régulation différente d'IL-17A et IL-17F. La concentration d'IL-17A était diminuée alors que la concentration d'IL-17F était augmentée en présence d'OX40L. À l'origine, les gènes IL17A et IL17F ont été décits comme étant régulés de manière coordonnée [325] et jusqu'à présent, seules quelques études ont rapporté une régulation différente de l'IL-17A et de l'IL-17F [131,170,326–328]. Dans le cadre de la fonction d'OX40L sur les cellules Th17, aucune étude n'avait encore rapporté une régulation différente des cytokines IL-17F et IL-17A. Nos données fournissent de nouvelles informations sur le rôle de d'OX40L sur ces cytokines. En effet, bien qu'elles aient des actions similaires voire parfois synergiques du fait d'une forte homologie, leur rôle peut également différer dans certains contextes [329–332], d'où l'intérêt d'une meilleure compréhension de leur mécanisme de sécrétion pour pouvoir les cibler individuellement.

Fonctions contexte-dépendantes d'OX40L sur les cytokines Th

Dans nos contextes Th, nous avons observé deux types de contexte-dépendance d'OX40L, qualitative et quantitative sur l'IL-22, TNF-α, IL-10 et IL-13. Parmi ces cytokines, l'IL-10 avait le score de contexte-dépendance le plus élevé, ce qui signifie qu'elle était la plus sensible, de manière quantitative, à la dépendance au contexte OX40L dans les contextes.

Dans nos contextes bDC, la contexte-dépendance d'OX40L sur IL-2, GM-CSF, IFNγ et IL-3 dépend fortement du contexte TSLP. Cela est évident parce que lorsque nous l'avons retiré de l'analyse, nous n'avons pas pu l'observer sur ces cytokines. À première vue, cela semblait cohérent car le contexte TSLP-bDC est instinctivement différent des cinq autres. C'est une cytokine inflammatoire produite dans un contexte très distinct qu'est l'allergie. Mais il s'est avéré que dans les contextes MoDC (qui n'ont pas de contexte TSLP car pas de récepteur), une contexte-dépendance a malgré tout pu être observée entre les contextes bactériens et fongiques.

Nous avons observé les types de deux dépendances contextuelles. OX40L a joué une fonction qualitative dépendante du contexte sur IL-2, GM-CSF et IFNγ. OX40L induit une diminution de ces

cytokines dans le contexte TSLP-bDC, alors qu'il induit une augmentation dans les cinq autres. De plus, OX40L a joué une fonction quantitative dépendante du contexte sur IL-3, qui a augmenté dans tous les contextes de la BDC, mais à différents niveaux.

Les cytokines affectées par la contexte-dépendance d'OX40L dans les contextes MoDC étaient principalement des cytokines Th2. OX40L a influencé différemment IL-4, IL-5, IL-31 et GM-CSF dans les différents contextes fongiques et bactériens.

Nous aurions pu également définir des comportements « contexte-indépendants » d'OX40L sur les cytokines sécrétées. Par exemple, nous n'avons observé aucune contexte-dépendance de la fonction OX40L sur la sécrétion d'IL-21. Ceci est conforme à la littérature [85,86].

3) Pertinence de la classification Th

Profil étroit versus profil mixte de sécrétion de cytokines Th

Dans notre étude, nous avons observé que les contextes Th induisaient un profil Th étroit, ce qui signifie que chaque sous-population Th sécrète principalement leurs cytokines spécifiques définissant la sous-population. Cependant, en introduisant les DC, nous avons observé que les cellules T sécrètent en fait un profil très mixte de cytokines. Bien qu'il semble qu'il y ait une dominance de certaines cytokines par rapport à d'autres dans les différents contextes, un profil mixte de cytokines de sous-populations Th distinctes est observé.

La comparaison de ces résultats de profil étroit versus mixte de cytokines sécrétées par les cellules Th avec la littérature est difficile pour plusieurs raisons :

- Les études se concentrent généralement sur des sous-populations Th spécifiques ou sur des cytokines spécifiques et n'effectuent pas d'analyse systématique de toutes les principales cytokines Th.
- Lors de l'analyse d'un large panel de cytokines, la plupart des études se penchent sur l'expression des gènes par séquençage d'ARN, alors que nous avons mesuré nos cytokines au niveau protéique, et il a été démontré par des études comparatives que les corrélations entre les niveaux d'ARNm et de protéines peuvent être relativement incertaines [338,339].

Cela peut être illustré par l'étude Cano-Gamez. Ils ont stimulé des cellules T CD4 naïves et mémoires dans un contexte de stimulation Th17 et iTreg. Pour les cellules T CD4 naïves, ils ont observé 733 gènes différemment exprimés pour seulement 455 protéines différemment exprimées entre les deux contextes. Dans la même logique, pour les cellules T CD4 mémoire, ils ont observé 42 gènes différemment exprimés et aucune protéine différemment exprimée [307].

Dans notre travail, nous avons polarisé un ensemble de cellules T CD4 naïves. Cet ensemble est en fait un mélange de nombreuses cellules T CD4 naïves spécifiques à un antigène donné, qui peuvent donc reconnaître de nombreux antigènes différents. Dans nos résultats, nous n'avons pas pris en compte la spécificité de l'antigène car nous n'avons pas ajouté d'antigène dans les contextes Th et nous étions en condition allogénique dans les contextes DC. Il pourrait être très intéressant d'identifier si les cellules T CD4 naïves spécifiques à l'antigène sécrètent un profil de cytokines plus étroit lorsqu'elles sont activées par leur antigène spécifique. En effet, le profil de sécrétion de cytokines mixtes pourrait s'expliquer par la multiplicité des clones de cellules T.

Complexité de la classification Th

Nos données fournissent des preuves supplémentaires que la majorité des cellules Th ont un degré important de plasticité. Il est important de garder à l'esprit que cette plasticité est influencée par de nombreux paramètres tels que les expressions des récepteurs des cytokines et des facteurs de transcription, la disponibilité des signaux polarisants dans le microenvironnement des lymphocytes T, etc… Cela signifie que la plasticité est considérée à un niveau « inter-sous-population », c'est-à-dire lorsque la cellule T passe d'un phénotype de sous-population Th à une autre. Nos travaux et réflexions sur le profil des cytokines mixtes nous amènent à l'idée que la plasticité pourrait même être définie à un niveau « intra-sous-population ».

En considérant tous ces aspects, le concept de plasticité peut devenir contre-intuitif car si une cellule Th est supposée être engagée dans une sous-population spécifique, alors elle ne devrait pas être plastique, sinon ce ne serait pas une sous-population spécifique.

La compréhension globale de toutes ces sous-populations Th et de leurs cytokines dérivées conduit à réexaminer leur association aux maladies. Au moment où seuls Th1 et Th2 étaient identifiés, la classification des maladies liées aux Th était binaire et liée à une sous-populations Th pathogène spécifique, c'est-à-dire Th1 ou Th2 associée à leur sécrétion spécifique de cytokines. Un exemple clair de ce fait est la sclérose en plaques. Les cellules Th1 productrices d'IFNγ ont été

décrites comme jouant un rôle majeur dans la sclérose en plaques, qui était clairement classée comme une maladie associée à Th1 [346–348]. De plus, conformément à la dichotomie Th décrite par Mossman et Coffman, les améliorations cliniques de l'EAE étaient corrélées à la diminution de l'IFNγ mais aussi à l'augmentation de l'IL-4, et les cytokines Th2 ont été décrites comme protectrices contre les cellules Th1 exacerbées [349,350]. Cependant, la découverte de Th17 a changé la vision de la sclérose en plaques et a aidé à comprendre les réponses immunitaires qui n'étaient pas expliquées par le paradigme Th1 et Th2 [351]. Après cela, les cellules Th17 ont été considérées comme jouant également un rôle central dans la maladie de la sclérose en plaques [352].

La sclérose en plaques est un exemple parmi d'autres dans lequel une maladie a été associée à une sous-population spécifique et a finalement été associée à de nombreuses sous-populations par la suite. L'évolution d'une vue bipolaire à une vue multipolaire de plusieurs sous-populations Th, impliquées différemment dans une seule pathologie, conduit à une complexité croissante de la classification Th et de l'association des cytokines Th aux maladies et aux états pathologiques. Cela soulève de nombreuses questions. D'abord liée à la maladie elle-même : une maladie est-elle associée à une sous-population Th pathogène spécifique ou à plusieurs ? Dans le second cas, comment l'identification de plusieurs sous-populations Th impliquées dans une pathologie peut aider à la compréhension et au traitement de cette maladie ?

De plus, la plasticité Th questionne la meilleure stratégie à appliquer pour traiter le patient lorsque la polarisation Th est impliquée et la manière la plus simple lorsque plusieurs sous-populations sont impliquées. Cibler les signaux dans le microenvironnement qui induisent des cellules Th pathogènes ? Cibler directement ces cellules Th pathogènes ? Cibler l'effecteur Th pathogène ? Autant de questions qui restent ouvertes sur la classification des lymphocytes Th.

BIBLIOGRAPHY

1. Förster, R., Braun, A. & Worbs, T. Lymph node homing of T cells and dendritic cells via afferent lymphatics. *Trends Immunol.* **33**, 271–280 (2012).

2. Inaba, K. *et al.* High levels of a major histocompatibility complex II-self peptide complex on dendritic cells from the T cell areas of lymph nodes. *J. Exp. Med.* **186**, 665–672 (1997).

3. Takeuchi, O. & Akira, S. Pattern recognition receptors and inflammation. *Cell* **140**, 805–820 (2010).

4. Banchereau, J. & Steinman, R. M. Dendritic cells and the control of immunity. *Nature* **392**, 245–252 (1998).

5. Summers deLuca, L. & Gommerman, J. L. Fine-tuning of dendritic cell biology by the TNF superfamily. *Nat. Rev. Immunol.* **12**, 339–351 (2012).

6. Kapsenberg, M. L. Dendritic-cell control of pathogen-driven T-cell polarization. *Nat. Rev. Immunol.* **3**, 984–993 (2003).

7. Medzhitov, R. Toll-like receptors and innate immunity. *Nat. Rev. Immunol.* **1**, 135–145 (2001).

8. Claman, H. N., Chaperon, E. A. & Triplett, R. F. Thymus-marrow cell combinations. Synergism in antibody production. *Proc. Soc. Exp. Biol. Med. Soc. Exp. Biol. Med. N. Y. N* **122**, 1167–1171 (1966).

9. Mitchell, G. F. & Miller, J. F. Cell to cell interaction in the immune response. II. The source of hemolysin-forming cells in irradiated mice given bone marrow and thymus or thoracic duct lymphocytes. *J. Exp. Med.* **128**, 821–837 (1968).

10. Cantor, H. & Boyse, E. A. Functional subclasses of T-lymphocytes bearing different Ly antigens. I. The generation of functionally distinct T-cell subclasses is a differentiative process independent of antigen. *J. Exp. Med.* **141**, 1376–1389 (1975).

11. Mosmann, T. R., Cherwinski, H., Bond, M. W., Giedlin, M. A. & Coffman, R. L. Two types of murine helper T cell clone. I. Definition according to profiles of lymphokine activities and secreted proteins. *J. Immunol. Baltim. Md 1950* **136**, 2348–2357 (1986).

12. Cherwinski, H. M., Schumacher, J. H., Brown, K. D. & Mosmann, T. R. Two types of mouse helper T cell clone. III. Further differences in lymphokine synthesis between Th1 and Th2

clones revealed by RNA hybridization, functionally monospecific bioassays, and monoclonal antibodies. *J. Exp. Med.* **166**, 1229–1244 (1987).

13. Mosmann, T. R. & Coffman, R. L. TH1 and TH2 cells: different patterns of lymphokine secretion lead to different functional properties. *Annu. Rev. Immunol.* **7**, 145–173 (1989).

14. Wu, C. *et al.* IFN-γ primes macrophage activation by increasing phosphatase and tensin homolog via downregulation of miR-3473b. *J. Immunol. Baltim. Md 1950* **193**, 3036–3044 (2014).

15. Ekkens, M. J. *et al.* Th1 and Th2 cells help CD8 T-cell responses. *Infect. Immun.* **75**, 2291–2296 (2007).

16. Durgeau, A., Virk, Y., Corgnac, S. & Mami-Chouaib, F. Recent Advances in Targeting CD8 T-Cell Immunity for More Effective Cancer Immunotherapy. *Front. Immunol.* **9**, (2018).

17. Szabo, S. J. *et al.* A novel transcription factor, T-bet, directs Th1 lineage commitment. *Cell* **100**, 655–669 (2000).

18. Szabo, S. J. *et al.* Distinct Effects of T-bet in TH1 Lineage Commitment and IFN-γ Production in CD4 and CD8 T Cells. *Science* **295**, 338–342 (2002).

19. Hibbert, L., Pflanz, S., De Waal Malefyt, R. & Kastelein, R. A. IL-27 and IFN-alpha signal via Stat1 and Stat3 and induce T-Bet and IL-12Rbeta2 in naive T cells. *J. Interferon Cytokine Res. Off. J. Int. Soc. Interferon Cytokine Res.* **23**, 513–522 (2003).

20. Usui, T. *et al.* T-bet regulates Th1 responses through essential effects on GATA-3 function rather than on IFNG gene acetylation and transcription. *J. Exp. Med.* **203**, 755–766 (2006).

21. Djuretic, I. M. *et al.* Transcription factors T-bet and Runx3 cooperate to activate Ifng and silence Il4 in T helper type 1 cells. *Nat. Immunol.* **8**, 145–153 (2007).

22. Kohu, K. *et al.* The Runx3 transcription factor augments Th1 and down-modulates Th2 phenotypes by interacting with and attenuating GATA3. *J. Immunol. Baltim. Md 1950* **183**, 7817–7824 (2009).

23. Mosmann, T. R. & Coffman, R. L. Heterogeneity of cytokine secretion patterns and functions of helper T cells. *Adv. Immunol.* **46**, 111–147 (1989).

24. Sallusto, F., Lenig, D., Mackay, C. R. & Lanzavecchia, A. Flexible programs of chemokine receptor expression on human polarized T helper 1 and 2 lymphocytes. *J. Exp. Med.* **187**, 875–883

(1998).

25. Zheng, W. & Flavell, R. A. The Transcription Factor GATA-3 Is Necessary and Sufficient for Th2 Cytokine Gene Expression in CD4 T Cells. *Cell* **89**, 587–596 (1997).

26. Ansel, K. M., Djuretic, I., Tanasa, B. & Rao, A. Regulation of Th2 differentiation and Il4 locus accessibility. *Annu. Rev. Immunol.* **24**, 607–656 (2006).

27. Zhu, J., Yamane, H., Cote-Sierra, J., Guo, L. & Paul, W. E. GATA-3 promotes Th2 responses through three different mechanisms: induction of Th2 cytokine production, selective growth of Th2 cells and inhibition of Th1 cell-specific factors. *Cell Res.* **16**, 3–10 (2006).

28. Amsen, D., Spilianakis, C. G. & Flavell, R. A. How are TH1 and TH2 effector cells made? *Curr. Opin. Immunol.* **21**, 153–160 (2009).

29. Oppmann, B. *et al.* Novel p19 protein engages IL-12p40 to form a cytokine, IL-23, with biological activities similar as well as distinct from IL-12. *Immunity* **13**, 715–725 (2000).

30. Cua, D. J. *et al.* Interleukin-23 rather than interleukin-12 is the critical cytokine for autoimmune inflammation of the brain. *Nature* **421**, 744–748 (2003).

31. Langrish, C. L. *et al.* IL-23 drives a pathogenic T cell population that induces autoimmune inflammation. *J. Exp. Med.* **201**, 233–240 (2005).

32. Veldhoen, M., Hocking, R. J., Atkins, C. J., Locksley, R. M. & Stockinger, B. TGFbeta in the context of an inflammatory cytokine milieu supports de novo differentiation of IL-17-producing T cells. *Immunity* **24**, 179–189 (2006).

33. Mangan, P. R. *et al.* Transforming growth factor-beta induces development of the T(H)17 lineage. *Nature* **441**, 231–234 (2006).

34. Wilson, N. J. *et al.* Development, cytokine profile and function of human interleukin 17-producing helper T cells. *Nat. Immunol.* **8**, 950–957 (2007).

35. Acosta-Rodriguez, E. V., Napolitani, G., Lanzavecchia, A. & Sallusto, F. Interleukins 1beta and 6 but not transforming growth factor-beta are essential for the differentiation of interleukin 17-producing human T helper cells. *Nat. Immunol.* **8**, 942–949 (2007).

36. Manel, N., Unutmaz, D. & Littman, D. R. The differentiation of human TH-17 cells requires transforming growth factor-β and induction of the nuclear receptor RORγT. *Nat. Immunol.* **9**, 641–

649 (2008).

37. Yang, L. *et al.* IL-21 and TGF-β are required for differentiation of human TH17 cells. *Nature* **454**, 350–352 (2008).

38. Volpe, E. *et al.* A critical function for transforming growth factor-beta, interleukin 23 and proinflammatory cytokines in driving and modulating human T(H)-17 responses. *Nat. Immunol.* **9**, 650–657 (2008).

39. Ivanov, I. I. *et al.* The orphan nuclear receptor RORgammat directs the differentiation program of proinflammatory IL-17+ T helper cells. *Cell* **126**, 1121–1133 (2006).

40. Yang, X. O. *et al.* T helper 17 lineage differentiation is programmed by orphan nuclear receptors ROR alpha and ROR gamma. *Immunity* **28**, 29–39 (2008).

41. Zhou, L. *et al.* IL-6 programs T(H)-17 cell differentiation by promoting sequential engagement of the IL-21 and IL-23 pathways. *Nat. Immunol.* **8**, 967–974 (2007).

42. Yang, X. O. *et al.* STAT3 regulates cytokine-mediated generation of inflammatory helper T cells. *J. Biol. Chem.* **282**, 9358–9363 (2007).

43. Acosta-Rodriguez, E. V. *et al.* Surface phenotype and antigenic specificity of human interleukin 17–producing T helper memory cells. *Nat. Immunol.* **8**, 639–646 (2007).

44. Kolls, J. K. & Lindén, A. Interleukin-17 family members and inflammation. *Immunity* **21**, 467–476 (2004).

45. Liang, S. C. *et al.* Interleukin (IL)-22 and IL-17 are coexpressed by Th17 cells and cooperatively enhance expression of antimicrobial peptides. *J. Exp. Med.* **203**, 2271–2279 (2006).

46. Laan, M. *et al.* Neutrophil recruitment by human IL-17 via C-X-C chemokine release in the airways. *J. Immunol. Baltim. Md 1950* **162**, 2347–2352 (1999).

47. Ouyang, W., Rutz, S., Crellin, N. K., Valdez, P. A. & Hymowitz, S. G. Regulation and functions of the IL-10 family of cytokines in inflammation and disease. *Annu. Rev. Immunol.* **29**, 71–109 (2011).

48. Wolk, K., Kunz, S., Asadullah, K. & Sabat, R. Cutting edge: immune cells as sources and targets of the IL-10 family members? *J. Immunol. Baltim. Md 1950* **168**, 5397–5402 (2002).

49. Ghoreschi, K. *et al.* Generation of Pathogenic Th17 Cells in the Absence of TGF-β Signaling. *Nature* **467**, 967–971 (2010).

50. Rutz, S. *et al.* Transcription factor c-Maf mediates the TGF-β-dependent suppression of IL-22 production in T(H)17 cells. *Nat. Immunol.* **12**, 1238–1245 (2011).

51. Trifari, S., Kaplan, C. D., Tran, E. H., Crellin, N. K. & Spits, H. Identification of a human helper T cell population that has abundant production of interleukin 22 and is distinct from T(H)-17, T(H)1 and T(H)2 cells. *Nat. Immunol.* **10**, 864–871 (2009).

52. Volpe, E. *et al.* Multiparametric analysis of cytokine-driven human Th17 differentiation reveals a differential regulation of IL-17 and IL-22 production. *Blood* **114**, 3610–3614 (2009).

53. Eyerich, S. *et al.* Th22 cells represent a distinct human T cell subset involved in epidermal immunity and remodeling. *J. Clin. Invest.* **119**, 3573–3585 (2009).

54. Ramirez, J.-M. *et al.* Activation of the aryl hydrocarbon receptor reveals distinct requirements for IL-22 and IL-17 production by human T helper cells. *Eur. J. Immunol.* **40**, 2450–2459 (2010).

55. Schmitt, E., Van Brandwijk, R., Fischer, H. G. & Rüde, E. Establishment of different T cell sublines using either interleukin 2 or interleukin 4 as growth factors. *Eur. J. Immunol.* **20**, 1709–1715 (1990).

56. Veldhoen, M. *et al.* Transforming growth factor-beta 'reprograms' the differentiation of T helper 2 cells and promotes an interleukin 9-producing subset. *Nat. Immunol.* **9**, 1341–1346 (2008).

57. Dardalhon, V. *et al.* IL-4 inhibits TGF-beta-induced Foxp3+ T cells and, together with TGF-beta, generates IL-9+ IL-10+ Foxp3(-) effector T cells. *Nat. Immunol.* **9**, 1347–1355 (2008).

58. Jiang, Y. *et al.* TNF-α enhances Th9 cell differentiation and antitumor immunity via TNFR2-dependent pathways. *J. Immunother. Cancer* **7**, 28 (2019).

59. Ramming, A., Druzd, D., Leipe, J., Schulze-Koops, H. & Skapenko, A. Maturation-related histone modifications in the PU.1 promoter regulate Th9-cell development. *Blood* **119**, 4665–4674 (2012).

60. Goswami, R. & Kaplan, M. H. Gcn5 is required for PU.1-dependent IL-9 induction in Th9 cells. *J. Immunol. Baltim. Md 1950* **189**, 3026–3033 (2012).

61. Chang, H.-C. *et al.* PU.1 expression delineates heterogeneity in primary Th2 cells. *Immunity* **22**, 693–703 (2005).

62. Goswami, R. *et al.* STAT6-dependent regulation of Th9 development. *J. Immunol. Baltim. Md 1950* **188**, 968–975 (2012).

63. Hadjur, S. *et al.* IL4 blockade of inducible regulatory T cell differentiation: the role of Th2 cells, Gata3 and PU.1. *Immunol. Lett.* **122**, 37–43 (2009).

64. Purwar, R. *et al.* Robust tumor immunity to melanoma mediated by interleukin-9-producing T cells. *Nat. Med.* **18**, 1248–1253 (2012).

65. Lu, Y. *et al.* Th9 cells promote antitumor immune responses in vivo. *J. Clin. Invest.* **122**, 4160–4171 (2012).

66. Zheng, S. G. *et al.* TGF-beta requires CTLA-4 early after T cell activation to induce FoxP3 and generate adaptive CD4+CD25+ regulatory cells. *J. Immunol. Baltim. Md 1950* **176**, 3321–3329 (2006).

67. Hori, S., Nomura, T. & Sakaguchi, S. Control of regulatory T cell development by the transcription factor Foxp3. *Science* **299**, 1057–1061 (2003).

68. Gottschalk, R. A., Corse, E. & Allison, J. P. TCR ligand density and affinity determine peripheral induction of Foxp3 in vivo. *J. Exp. Med.* **207**, 1701–1711 (2010).

69. Chen, W. *et al.* Conversion of peripheral CD4+CD25- naive T cells to CD4+CD25+ regulatory T cells by TGF-beta induction of transcription factor Foxp3. *J. Exp. Med.* **198**, 1875–1886 (2003).

70. Davidson, T. S., DiPaolo, R. J., Andersson, J. & Shevach, E. M. Cutting Edge: IL-2 is essential for TGF-beta-mediated induction of Foxp3+ T regulatory cells. *J. Immunol. Baltim. Md 1950* **178**, 4022–4026 (2007).

71. Schmidt, A., Éliás, S., Joshi, R. N. & Tegnér, J. In Vitro Differentiation of Human CD4+FOXP3+ Induced Regulatory T Cells (iTregs) from Naïve CD4+ T Cells Using a TGF-β-containing Protocol. *J. Vis. Exp. JoVE* (2016) doi:10.3791/55015.

72. von Boehmer, H. Mechanisms of suppression by suppressor T cells. *Nat. Immunol.* **6**, 338–344 (2005).

73. Josefowicz, S. Z., Lu, L.-F. & Rudensky, A. Y. Regulatory T cells: mechanisms of differentiation and function. *Annu. Rev. Immunol.* **30**, 531–564 (2012).

74. Chinen, T. *et al.* An essential role for the IL-2 receptor in Treg cell function. *Nat. Immunol.* **17**, 1322–1333 (2016).

75. Schaerli, P. *et al.* CXC chemokine receptor 5 expression defines follicular homing T cells with B cell helper function. *J. Exp. Med.* **192**, 1553–1562 (2000).

76. Kim, C. H. *et al.* Subspecialization of Cxcr5+ T CellsB Helper Activity Is Focused in a Germinal Center–Localized Subset of Cxcr5+ T Cells. *J. Exp. Med.* **193**, 1373–1382 (2001).

77. Johnston, R. J. *et al.* Bcl6 and Blimp-1 Are Reciprocal and Antagonistic Regulators of T Follicular Helper Cell Differentiation. *Science* **325**, 1006–1010 (2009).

78. Liu, X. *et al.* Transcription factor Achaete-Scute homologue 2 initiates T follicular helper cell development. *Nature* **507**, 513–518 (2014).

79. Suto, A. *et al.* Development and characterization of IL-21–producing CD4+ T cells. *J. Exp. Med.* **205**, 1369–1379 (2008).

80. Ma, C. S. *et al.* Early commitment of naïve human CD4+ T cells to the T follicular helper (TFH) cell lineage is induced by IL-12. *Immunol. Cell Biol.* **87**, 590–600 (2009).

81. Schmitt, N. *et al.* Human Dendritic Cells Induce the Differentiation of Interleukin-21-Producing T Follicular Helper-like Cells through Interleukin-12. *Immunity* **31**, 158–169 (2009).

82. Schmitt, N. *et al.* The cytokine TGF-β co-opts signaling via STAT3-STAT4 to promote the differentiation of human T FH cells. *Nat. Immunol.* **15**, 856–865 (2014).

83. Ballesteros-Tato, A. *et al.* Interleukin-2 inhibits germinal center formation by limiting T follicular helper cell differentiation. *Immunity* **36**, 847–856 (2012).

84. DiToro, D. *et al.* Differential IL-2 expression defines developmental fates of follicular versus nonfollicular helper T cells. *Science* **361**, (2018).

85. Pattarini, L. *et al.* TSLP-activated dendritic cells induce human T follicular helper cell differentiation through OX40-ligand. *J. Exp. Med.* **214**, 1529–1546 (2017).

86. Jacquemin, C. *et al.* OX40 Ligand Contributes to Human Lupus Pathogenesis by Promoting

T Follicular Helper Response. *Immunity* **42**, 1159–1170 (2015).

87. Choi, Y. S. *et al.* ICOS receptor instructs T follicular helper cell versus effector cell differentiation via induction of the transcriptional repressor Bcl6. *Immunity* **34**, 932–946 (2011).

88. Stone, E. L. *et al.* ICOS coreceptor signaling inactivates the transcription factor FOXO1 to promote Tfh cell differentiation. *Immunity* **42**, 239–251 (2015).

89. Kroenke, M. A. *et al.* Bcl6 and Maf cooperate to instruct human follicular helper CD4 T cell differentiation. *J. Immunol. Baltim. Md 1950* **188**, 3734–3744 (2012).

90. Yu, D. *et al.* The transcriptional repressor Bcl-6 directs T follicular helper cell lineage commitment. *Immunity* **31**, 457–468 (2009).

91. Crotty, S. Follicular helper CD4 T cells (TFH). *Annu. Rev. Immunol.* **29**, 621–663 (2011).

92. Vinuesa, C. G., Linterman, M. A., Yu, D. & MacLennan, I. C. M. Follicular Helper T Cells. *Annu. Rev. Immunol.* **34**, 335–368 (2016).

93. Schmitt, N. & Ueno, H. Regulation of Human Helper T Cell Subset Differentiation by Cytokines. *Curr. Opin. Immunol.* **34**, 130–136 (2015).

94. Merad, M. & Manz, M. G. Dendritic cell homeostasis. *Blood* **113**, 3418–3427 (2009).

95. Haniffa, M., Collin, M. & Ginhoux, F. Ontogeny and functional specialization of dendritic cells in human and mouse. *Adv. Immunol.* **120**, 1–49 (2013).

96. Dzionek, A. *et al.* BDCA-2, BDCA-3, and BDCA-4: Three Markers for Distinct Subsets of Dendritic Cells in Human Peripheral Blood. *J. Immunol.* **165**, 6037–6046 (2000).

97. León, B., López-Bravo, M. & Ardavín, C. Monocyte-derived dendritic cells formed at the infection site control the induction of protective T helper 1 responses against Leishmania. *Immunity* **26**, 519–531 (2007).

98. Segura, E. *et al.* Human Inflammatory Dendritic Cells Induce Th17 Cell Differentiation. *Immunity* **38**, 336–348 (2013).

99. Tang-Huau, T.-L. *et al.* Human in vivo-generated monocyte-derived dendritic cells and macrophages cross-present antigens through a vacuolar pathway. *Nat. Commun.* **9**, 1–12 (2018).

100. Sallusto, F. & Lanzavecchia, A. Efficient presentation of soluble antigen by cultured human

dendritic cells is maintained by granulocyte/macrophage colony-stimulating factor plus interleukin 4 and downregulated by tumor necrosis factor alpha. *J. Exp. Med.* **179**, 1109–1118 (1994).

101. Romani, N. *et al.* Proliferating dendritic cell progenitors in human blood. *J. Exp. Med.* **180**, 83–93 (1994).

102. Robbins, S. H. *et al.* Novel insights into the relationships between dendritic cell subsets in human and mouse revealed by genome-wide expression profiling. *Genome Biol.* **9**, R17 (2008).

103. Alcántara-Hernández, M. *et al.* High-Dimensional Phenotypic Mapping of Human Dendritic Cells Reveals Interindividual Variation and Tissue Specialization. *Immunity* **47**, 1037-1050.e6 (2017).

104. Yin, X. *et al.* Human Blood CD1c+ Dendritic Cells Encompass CD5high and CD5low Subsets That Differ Significantly in Phenotype, Gene Expression, and Functions. *J. Immunol. Baltim. Md 1950* **198**, 1553–1564 (2017).

105. Villani, A.-C. *et al.* Single-cell RNA-seq reveals new types of human blood dendritic cells, monocytes, and progenitors. *Science* **356**, (2017).

106. Dutertre, C.-A. *et al.* Single-Cell Analysis of Human Mononuclear Phagocytes Reveals Subset-Defining Markers and Identifies Circulating Inflammatory Dendritic Cells. *Immunity* **51**, 573-589.e8 (2019).

107. Segura, E. *et al.* Characterization of resident and migratory dendritic cells in human lymph nodes. *J. Exp. Med.* **209**, 653–660 (2012).

108. Yu, C. I. *et al.* Human CD141+ DCs induce CD4+ T cells to produce type 2 cytokines. *J. Immunol. Baltim. Md 1950* **193**, 4335–4343 (2014).

109. Jongbloed, S. L. *et al.* Human CD141+ (BDCA-3)+ dendritic cells (DCs) represent a unique myeloid DC subset that cross-presents necrotic cell antigens. *J. Exp. Med.* **207**, 1247–1260 (2010).

110. Durand, M. *et al.* Human lymphoid organ cDC2 and macrophages play complementary roles in T follicular helper responses. *J. Exp. Med.* **216**, 1561–1581 (2019).

111. Chow, K. V., Lew, A. M., Sutherland, R. M. & Zhan, Y. Monocyte-Derived Dendritic Cells Promote Th Polarization, whereas Conventional Dendritic Cells Promote Th Proliferation. *J. Immunol.* **196**, 624–636 (2016).

112. Klechevsky, E. *et al.* Functional Specializations of Human Epidermal Langerhans Cells and CD14+ Dermal Dendritic Cells. *Immunity* **29**, 497–510 (2008).

113. Furio, L., Briotet, I., Journeaux, A., Billard, H. & Péguet-Navarro, J. Human Langerhans Cells Are More Efficient Than CD14−CD1c+ Dermal Dendritic Cells at Priming Naive CD4+ T Cells. *J. Invest. Dermatol.* **130**, 1345–1354 (2010).

114. Fujita, H. *et al.* Human Langerhans cells induce distinct IL-22-producing CD4+ T cells lacking IL-17 production. *Proc. Natl. Acad. Sci. U. S. A.* **106**, 21795–21800 (2009).

115. Penel-Sotirakis, K., Simonazzi, E., Péguet-Navarro, J. & Rozières, A. Differential Capacity of Human Skin Dendritic Cells to Polarize CD4+T Cells into IL-17, IL-21 and IL-22 Producing Cells. *PLoS ONE* **7**, (2012).

116. Pulendran, B. *et al.* Lipopolysaccharides from Distinct Pathogens Induce Different Classes of Immune Responses In Vivo. *J. Immunol.* **167**, 5067–5076 (2001).

117. Dillon, S. *et al.* A Toll-Like Receptor 2 Ligand Stimulates Th2 Responses In Vivo, via Induction of Extracellular Signal-Regulated Kinase Mitogen-Activated Protein Kinase and c-Fos in Dendritic Cells. *J. Immunol.* **172**, 4733–4743 (2004).

118. Agrawal, S. *et al.* Cutting Edge: Different Toll-Like Receptor Agonists Instruct Dendritic Cells to Induce Distinct Th Responses via Differential Modulation of Extracellular Signal-Regulated Kinase-Mitogen-Activated Protein Kinase and c-Fos. *J. Immunol.* **171**, 4984–4989 (2003).

119. Agrawal, S., Gupta, S. & Agrawal, A. Human Dendritic Cells Activated via Dectin-1 Are Efficient at Priming Th17, Cytotoxic CD8 T and B Cell Responses. *PLoS ONE* **5**, (2010).

120. Reche, P. A. *et al.* Human thymic stromal lymphopoietin preferentially stimulates myeloid cells. *J. Immunol. Baltim. Md 1950* **167**, 336–343 (2001).

121. Soumelis, V. *et al.* Human epithelial cells trigger dendritic cell mediated allergic inflammation by producing TSLP. *Nat. Immunol.* **3**, 673–680 (2002).

122. Ito, T. *et al.* TSLP-activated dendritic cells induce an inflammatory T helper type 2 cell response through OX40 ligand. *J. Exp. Med.* **202**, 1213–1223 (2005).

123. Tanaka, H., Demeure, C. E., Rubio, M., Delespesse, G. & Sarfati, M. Human Monocyte–

Derived Dendritic Cells Induce Naive T Cell Differentiation into T Helper Cell Type 2 (Th2) or Th1/Th2 Effectors. *J. Exp. Med.* **192**, 405–412 (2000).

124. Extent of T cell receptor ligation can determine the functional differentiation of naive CD4+ T cells. *J. Exp. Med.* **182**, 1591–1596 (1995).

125. Tao, X., Constant, S., Jorritsma, P. & Bottomly, K. Strength of TCR signal determines the costimulatory requirements for Th1 and Th2 CD4+ T cell differentiation. *J. Immunol. Baltim. Md 1950* **159**, 5956–5963 (1997).

126. Yamane, H. & Paul, W. E. Early signaling events that underlie fate decisions of naive CD4+ T cells towards distinct T-helper cell subsets. *Immunol. Rev.* **252**, 12–23 (2013).

127. Hosken, N. A., Shibuya, K., Heath, A. W., Murphy, K. M. & O'Garra, A. The effect of antigen dose on CD4+ T helper cell phenotype development in a T cell receptor-alpha beta-transgenic model. *J. Exp. Med.* **182**, 1579–1584 (1995).

128. Boyton, R. J. & Altmann, D. M. Is selection for TCR affinity a factor in cytokine polarization? *Trends Immunol.* **23**, 526–529 (2002).

129. Turner, M. S., Kane, L. P. & Morel, P. A. Dominant role of antigen dose in CD4+Foxp3+ regulatory T cell induction and expansion. *J. Immunol. Baltim. Md 1950* **183**, 4895–4903 (2009).

130. Molinero, L. L., Miller, M. L., Evaristo, C. & Alegre, M.-L. High TCR Stimuli Prevent iTreg Differentiation in an NF-κB-Dependent Manner. *J. Immunol. Baltim. Md 1950* **186**, 4609–4617 (2011).

131. Gomez-Rodriguez, J. *et al.* Differential expression of interleukin-17A and -17F is coupled to T cell receptor signaling via inducible T cell kinase. *Immunity* **31**, 587–597 (2009).

132. Rogers, P. R. & Croft, M. CD28, Ox-40, LFA-1, and CD4 Modulation of Th1/Th2 Differentiation Is Directly Dependent on the Dose of Antigen. *J. Immunol.* **164**, 2955–2963 (2000).

133. McArthur, J. G. & Raulet, D. H. CD28-induced costimulation of T helper type 2 cells mediated by induction of responsiveness to interleukin 4. *J. Exp. Med.* **178**, 1645–1653 (1993).

134. Rulifson, I. C., Sperling, A. I., Fields, P. E., Fitch, F. W. & Bluestone, J. A. CD28 costimulation promotes the production of Th2 cytokines. *J. Immunol.* **158**, 658–665 (1997).

135. Park, H. *et al.* A distinct lineage of CD4 T cells regulates tissue inflammation by producing

interleukin 17. *Nat. Immunol.* **6**, 1133–1141 (2005).

136. Hutloff, A. *et al.* ICOS is an inducible T-cell co-stimulator structurally and functionally related to CD28. *Nature* **402**, 21–24 (1999).

137. Aicher, A. *et al.* Characterization of human inducible costimulator ligand expression and function. *J. Immunol.* (2000) doi:10.4049/jimmunol.164.9.4689.

138. Tafuri, A. *et al.* ICOS is essential for effective T-helper-cell responses. *Nature* **409**, 105–109 (2001).

139. Gonzalo, J. A. *et al.* Cutting edge: the related molecules CD28 and inducible costimulator deliver both unique and complementary signals required for optimal T cell activation. *J. Immunol. Baltim. Md 1950* **166**, 1–5 (2001).

140. Vidric, M., Bladt, A. T., Dianzani, U. & Watts, T. H. Role for inducible costimulator in control of Salmonella enterica serovar Typhimurium infection in mice. *Infect. Immun.* **74**, 1050–1061 (2006).

141. Hawiger, D. *et al.* ICOS mediates the development of insulin-dependent diabetes mellitus in nonobese diabetic mice. *J. Immunol. Baltim. Md 1950* **180**, 3140–3147 (2008).

142. Nouailles, G. *et al.* Impact of inducible co-stimulatory molecule (ICOS) on T-cell responses and protection against Mycobacterium tuberculosis infection. *Eur. J. Immunol.* **41**, 981–991 (2011).

143. Wikenheiser, D. J., Ghosh, D., Kennedy, B. & Stumhofer, J. S. The Costimulatory Molecule ICOS Regulates Host Th1 and Follicular Th Cell Differentiation in Response to Plasmodium chabaudi chabaudi AS Infection. *J. Immunol.* **196**, 778–791 (2016).

144. Rutitzky, L. I., Özkaynak, E., Rottman, J. B. & Stadecker, M. J. Disruption of the ICOS-B7RP-1 Costimulatory Pathway Leads to Enhanced Hepatic Immunopathology and Increased Gamma Interferon Production by CD4 T Cells in Murine Schistosomiasis. *Infect. Immun.* **71**, 4040–4044 (2003).

145. McAdam, A. J. *et al.* Mouse Inducible Costimulatory Molecule (ICOS) Expression Is Enhanced by CD28 Costimulation and Regulates Differentiation of CD4+ T Cells. *J. Immunol.* **165**, 5035–5040 (2000).

146. Nurieva, R. I. *et al.* Transcriptional Regulation of Th2 Differentiation by Inducible

Costimulator. *Immunity* **18**, 801–811 (2003).

147. Watanabe, M. *et al.* ICOS-Mediated Costimulation on Th2 Differentiation Is Achieved by the Enhancement of IL-4 Receptor-Mediated Signaling. *J. Immunol.* **174**, 1989–1996 (2005).

148. Weber, J. P. *et al.* ICOS maintains the T follicular helper cell phenotype by down-regulating Krüppel-like factor 2. *J. Exp. Med.* **212**, 217–233 (2015).

149. Bauquet, A. T. *et al.* Costimulatory molecule ICOS plays a critical role in the development of TH-17 and follicular T-helper cells by regulating c-Maf expression and IL-21 production. *Nat. Immunol.* **10**, 167–175 (2009).

150. Paulos, C. M. *et al.* The inducible costimulator (ICOS) is critical for the development of human T(H)17 cells. *Sci. Transl. Med.* **2**, 55ra78 (2010).

151. Akbari, O. *et al.* Antigen-specific regulatory T cells develop via the ICOS-ICOS-ligand pathway and inhibit allergen-induced airway hyperreactivity. *Nat. Med.* **8**, 1024–1032 (2002).

152. Vermeiren, J. *et al.* Human T Cell Activation by Costimulatory Signal-Deficient Allogeneic Cells Induces Inducible Costimulator-Expressing Anergic T Cells with Regulatory Cell Activity. *J. Immunol.* **172**, 5371–5378 (2004).

153. Löhning, M. *et al.* Expression of ICOS In Vivo Defines CD4+ Effector T Cells with High Inflammatory Potential and a Strong Bias for Secretion of Interleukin 10. *J. Exp. Med.* **197**, 181–193 (2003).

154. Cella, M. *et al.* Ligation of CD40 on dendritic cells triggers production of high levels of interleukin-12 and enhances T cell stimulatory capacity: T-T help via APC activation. *J. Exp. Med.* **184**, 747–752 (1996).

155. Koch, F. *et al.* High level IL-12 production by murine dendritic cells: upregulation via MHC class II and CD40 molecules and downregulation by IL-4 and IL-10. *J. Exp. Med.* **184**, 741–746 (1996).

156. Perona-Wright, G. *et al.* A pivotal role for CD40-mediated IL-6 production by dendritic cells during IL-17 induction in vivo. *J. Immunol. Baltim. Md 1950* **182**, 2808–2815 (2009).

157. Iezzi, G. *et al.* CD40-CD40L cross-talk integrates strong antigenic signals and microbial stimuli to induce development of IL-17-producing CD4+ T cells. *Proc. Natl. Acad. Sci. U. S. A.*

106, 876–881 (2009).

158. Bottino, C. *et al.* Identification of PVR (CD155) and Nectin-2 (CD112) as cell surface ligands for the human DNAM-1 (CD226) activating molecule. *J. Exp. Med.* **198**, 557–567 (2003).

159. Yu, X. *et al.* The surface protein TIGIT suppresses T cell activation by promoting the generation of mature immunoregulatory dendritic cells. *Nat. Immunol.* **10**, 48–57 (2009).

160. Joller, N. *et al.* Treg cells expressing the coinhibitory molecule TIGIT selectively inhibit proinflammatory Th1 and Th17 cell responses. *Immunity* **40**, 569–581 (2014).

161. Kourepini, E. *et al.* TIGIT Enhances Antigen-Specific Th2 Recall Responses and Allergic Disease. *J. Immunol. Baltim. Md 1950* **196**, 3570–3580 (2016).

162. Lozano, E., Dominguez-Villar, M., Kuchroo, V. & Hafler, D. A. The TIGIT/CD226 axis regulates human T cell function. *J. Immunol. Baltim. Md 1950* **188**, 3869–3875 (2012).

163. Lozano, E., Joller, N., Cao, Y., Kuchroo, V. & Hafler, D. A. The CD226/CD155 interaction regulates the pro-inflammatory (Th1/Th17)/ anti-inflammatory (Th2) balance in humans. *J. Immunol. Baltim. Md 1950* **191**, (2013).

164. Sun, X. *et al.* CD30 ligand/CD30 plays a critical role in Th17 differentiation in mice. *J. Immunol. Baltim. Md 1950* **185**, 2222–2230 (2010).

165. Sun, X. *et al.* CD30 ligand is a target for a novel biological therapy against colitis associated with Th17 responses. *J. Immunol. Baltim. Md 1950* **185**, 7671–7680 (2010).

166. Coquet, J. M. *et al.* The CD27 and CD70 costimulatory pathway inhibits effector function of T helper 17 cells and attenuates associated autoimmunity. *Immunity* **38**, 53–65 (2013).

167. Elyaman, W. *et al.* Notch receptors and Smad3 signaling cooperate in the induction of interleukin-9-producing T cells. *Immunity* **36**, 623–634 (2012).

168. Zheng, S. G., Wang, J., Wang, P., Gray, J. D. & Horwitz, D. A. IL-2 Is Essential for TGF-β to Convert Naive CD4+CD25− Cells to CD25+Foxp3+ Regulatory T Cells and for Expansion of These Cells. *J. Immunol.* **178**, 2018–2027 (2007).

169. Touzot, M. *et al.* Combinatorial flexibility of cytokine function during human T helper cell differentiation. *Nat. Commun.* **5**, 3987 (2014).

170. Grandclaudon, M. *et al.* A Quantitative Multivariate Model of Human Dendritic Cell-T Helper Cell Communication. *Cell* **179**, 432-447.e21 (2019).

171. Kalluri, R. & Zeisberg, M. Fibroblasts in cancer. *Nat. Rev. Cancer* **6**, 392–401 (2006).

172. Salmon, H. *et al.* Matrix architecture defines the preferential localization and migration of T cells into the stroma of human lung tumors. *J. Clin. Invest.* **122**, 899–910 (2012).

173. Sautès-Fridman, C., Petitprez, F., Calderaro, J. & Fridman, W. H. Tertiary lymphoid structures in the era of cancer immunotherapy. *Nat. Rev. Cancer* **19**, 307–325 (2019).

174. Hackl, H., Charoentong, P., Finotello, F. & Trajanoski, Z. Computational genomics tools for dissecting tumour-immune cell interactions. *Nat. Rev. Genet.* **17**, 441–458 (2016).

175. Schoenberger, S. P., Toes, R. E. M., van der Voort, E. I. H., Offringa, R. & Melief, C. J. M. T-cell help for cytotoxic T lymphocytes is mediated by CD40–CD40L interactions. *Nature* **393**, 480–483 (1998).

176. Yu, P., Spiotto, M. T., Lee, Y., Schreiber, H. & Fu, Y.-X. Complementary Role of CD4+ T Cells and Secondary Lymphoid Tissues for Cross-presentation of Tumor Antigen to CD8+ T Cells. *J. Exp. Med.* **197**, 985–995 (2003).

177. Shankaran, V. *et al.* IFNgamma and lymphocytes prevent primary tumour development and shape tumour immunogenicity. *Nature* **410**, 1107–1111 (2001).

178. Lai, Y.-P., Lin, C.-C., Liao, W.-J., Tang, C.-Y. & Chen, S.-C. CD4+ T Cell-Derived IL-2 Signals during Early Priming Advances Primary CD8+ T Cell Responses. *PLOS ONE* **4**, e7766 (2009).

179. Dunn, G. P., Old, L. J. & Schreiber, R. D. The three Es of cancer immunoediting. *Annu. Rev. Immunol.* **22**, 329–360 (2004).

180. Sato, T. *et al.* Interleukin 10 in the tumor microenvironment: a target for anticancer immunotherapy. *Immunol. Res.* **51**, 170–182 (2011).

181. Lebrun, J.-J. The Dual Role of TGFβ in Human Cancer: From Tumor Suppression to Cancer Metastasis. *ISRN Mol. Biol.* **2012**, 381428 (2012).

182. Francisco, L. M. *et al.* PD-L1 regulates the development, maintenance, and function of induced regulatory T cells. *J. Exp. Med.* **206**, 3015–3029 (2009).

183. Bates, G. J. *et al.* Quantification of regulatory T cells enables the identification of high-risk breast cancer patients and those at risk of late relapse. *J. Clin. Oncol. Off. J. Am. Soc. Clin. Oncol.* **24**, 5373–5380 (2006).

184. Miracco, C. *et al.* Utility of tumour-infiltrating CD25+FOXP3+ regulatory T cell evaluation in predicting local recurrence in vertical growth phase cutaneous melanoma. *Oncol. Rep.* **18**, 1115–1122 (2007).

185. Mougiakakos, D. *et al.* Intratumoral forkhead box P3-positive regulatory T cells predict poor survival in cyclooxygenase-2-positive uveal melanoma. *Cancer* **116**, 2224–2233 (2010).

186. Badoual, C. *et al.* Prognostic value of tumor-infiltrating CD4+ T-cell subpopulations in head and neck cancers. *Clin. Cancer Res. Off. J. Am. Assoc. Cancer Res.* **12**, 465–472 (2006).

187. Salama, P. *et al.* Tumor-infiltrating FOXP3+ T regulatory cells show strong prognostic significance in colorectal cancer. *J. Clin. Oncol. Off. J. Am. Soc. Clin. Oncol.* **27**, 186–192 (2009).

188. Frey, D. M. *et al.* High frequency of tumor-infiltrating FOXP3(+) regulatory T cells predicts improved survival in mismatch repair-proficient colorectal cancer patients. *Int. J. Cancer* **126**, 2635–2643 (2010).

189. Shin, E. C. *et al.* IFN-gamma induces cell death in human hepatoma cells through a TRAIL/death receptor-mediated apoptotic pathway. *Int. J. Cancer* **93**, 262–268 (2001).

190. Street, S. E. A., Trapani, J. A., MacGregor, D. & Smyth, M. J. Suppression of lymphoma and epithelial malignancies effected by interferon gamma. *J. Exp. Med.* **196**, 129–134 (2002).

191. Kortylewski, M. *et al.* Interferon-gamma-mediated growth regulation of melanoma cells: involvement of STAT1-dependent and STAT1-independent signals. *J. Invest. Dermatol.* **122**, 414–422 (2004).

192. Nastala, C. L. *et al.* Recombinant IL-12 administration induces tumor regression in association with IFN-gamma production. *J. Immunol. Baltim. Md 1950* **153**, 1697–1706 (1994).

193. Braumüller, H. *et al.* T-helper-1-cell cytokines drive cancer into senescence. *Nature* **494**, 361–365 (2013).

194. Kusuda, T. *et al.* Relative expression levels of Th1 and Th2 cytokine mRNA are independent prognostic factors in patients with ovarian cancer. *Oncol. Rep.* **13**, 1153–1158 (2005).

195. Tosolini, M. *et al.* Clinical impact of different classes of infiltrating T cytotoxic and helper cells (Th1, th2, treg, th17) in patients with colorectal cancer. *Cancer Res.* **71**, 1263–1271 (2011).

196. Hennequin, A. *et al.* Tumor infiltration by Tbet+ effector T cells and CD20+ B cells is associated with survival in gastric cancer patients. *Oncoimmunology* **5**, e1054598 (2016).

197. Bhavsar, N. A. *et al.* A peripheral circulating TH1 cytokine profile is inversely associated with prostate cancer risk in CLUE II. *Cancer Epidemiol. Biomark. Prev. Publ. Am. Assoc. Cancer Res. Cosponsored Am. Soc. Prev. Oncol.* **23**, 2561–2567 (2014).

198. Hanada, T. *et al.* IFNgamma-dependent, spontaneous development of colorectal carcinomas in SOCS1-deficient mice. *J. Exp. Med.* **203**, 1391–1397 (2006).

199. Xiao, M. *et al.* IFNgamma promotes papilloma development by up-regulating Th17-associated inflammation. *Cancer Res.* **69**, 2010–2017 (2009).

200. Bellucci, R. *et al.* Interferon-γ-induced activation of JAK1 and JAK2 suppresses tumor cell susceptibility to NK cells through upregulation of PD-L1 expression. *Oncoimmunology* **4**, e1008824 (2015).

201. Punt, S. *et al.* FoxP3+ and IL-17+ cells are correlated with improved prognosis in cervical adenocarcinoma. *Cancer Immunol. Immunother.* **64**, 745–753 (2015).

202. Lin, Y. *et al.* Interleukin-17 is a favorable prognostic marker for colorectal cancer. *Clin. Transl. Oncol.* **17**, 50–56 (2015).

203. Miyahara, Y. *et al.* Generation and regulation of human CD4+ IL-17-producing T cells in ovarian cancer. *Proc. Natl. Acad. Sci.* **105**, 15505–15510 (2008).

204. Kryczek, I., Wei, S., Szeliga, W., Vatan, L. & Zou, W. Endogenous IL-17 contributes to reduced tumor growth and metastasis. *Blood* **114**, 357–359 (2009).

205. Kryczek, I. *et al.* Phenotype, distribution, generation, and functional and clinical relevance of Th17 cells in the human tumor environments. *Blood* **114**, 1141–1149 (2009).

206. Muranski, P. *et al.* Tumor-specific Th17-polarized cells eradicate large established melanoma. *Blood* **112**, 362–373 (2008).

207. Martin-Orozco, N. *et al.* Th17 cells promote cytotoxic T cell activation in tumor immunity. *Immunity* **31**, 787–798 (2009).

208. Wang, L. *et al.* IL-17 can promote tumor growth through an IL-6–Stat3 signaling pathway. *J. Exp. Med.* **206**, 1457–1464 (2009).

209. Numasaki, M. *et al.* Interleukin-17 promotes angiogenesis and tumor growth. *Blood* **101**, 2620–2627 (2003).

210. Wu, S. *et al.* A human colonic commensal promotes colon tumorigenesis via activation of T helper type 17 T cell responses. *Nat. Med.* **15**, 1016–1022 (2009).

211. Chen, L. & Flies, D. B. Molecular mechanisms of T cell co-stimulation and co-inhibition. *Nat. Rev. Immunol.* **13**, 227–242 (2013).

212. Nakajima, M. & Tamada, K. Cancer Immunotherapy Targeting Co-signal Molecules. *Adv. Exp. Med. Biol.* **1189**, 313–326 (2019).

213. Paterson, D. J. *et al.* Antigens of activated rat T lymphocytes including a molecule of 50,000 Mr detected only on CD4 positive T blasts. *Mol. Immunol.* **24**, 1281–1290 (1987).

214. Mallett, S., Fossum, S. & Barclay, A. N. Characterization of the MRC OX40 antigen of activated CD4 positive T lymphocytes--a molecule related to nerve growth factor receptor. *EMBO J.* **9**, 1063–1068 (1990).

215. Tanaka, Y., Inoi, T., Tozawa, H., Yamamoto, N. & Hinuma, Y. A glycoprotein antigen detected with new monoclonal antibodies on the surface of human lymphocytes infected with human T-cell leukemia virus type-I (HTLV-I). *Int. J. Cancer* **36**, 549–555 (1985).

216. Godfrey, W. R., Fagnoni, F. F., Harara, M. A., Buck, D. & Engleman, E. G. Identification of a human OX-40 ligand, a costimulator of CD4+ T cells with homology to tumor necrosis factor. *J. Exp. Med.* **180**, 757–762 (1994).

217. Baum, P. R. *et al.* Molecular characterization of murine and human OX40/OX40 ligand systems: identification of a human OX40 ligand as the HTLV-1-regulated protein gp34. *EMBO J.* **13**, 3992–4001 (1994).

218. Compaan, D. M. & Hymowitz, S. G. The crystal structure of the costimulatory OX40-OX40L complex. *Struct. Lond. Engl. 1993* **14**, 1321–1330 (2006).

219. Croft, M., Benedict, C. A. & Ware, C. F. Clinical targeting of the TNF and TNFR superfamilies. *Nat. Rev. Drug Discov.* **12**, 147–168 (2013).

220. Croft, M. Control of immunity by the TNFR-related molecule OX40 (CD134). *Annu. Rev. Immunol.* **28**, 57–78 (2010).

221. Walker, L. S. *et al.* Compromised OX40 function in CD28-deficient mice is linked with failure to develop CXC chemokine receptor 5-positive CD4 cells and germinal centers. *J. Exp. Med.* **190**, 1115–1122 (1999).

222. Rogers, P. R., Song, J., Gramaglia, I., Killeen, N. & Croft, M. OX40 promotes Bcl-xL and Bcl-2 expression and is essential for long-term survival of CD4 T cells. *Immunity* **15**, 445–455 (2001).

223. Zaini, J. *et al.* OX40 ligand expressed by DCs costimulates NKT and CD4+ Th cell antitumor immunity in mice. *J. Clin. Invest.* **117**, 3330–3338 (2007).

224. Melero, I., Hirschhorn-Cymerman, D., Morales-Kastresana, A., Sanmamed, M. F. & Wolchok, J. D. Agonist Antibodies to TNFR Molecules That Costimulate T and NK Cells. *Clin. Cancer Res.* **19**, 1044–1053 (2013).

225. Baumann, R. *et al.* Functional expression of CD134 by neutrophils. *Eur. J. Immunol.* **34**, 2268–2275 (2004).

226. Ohshima, Y. *et al.* Expression and function of OX40 ligand on human dendritic cells. *J. Immunol. Baltim. Md 1950* **159**, 3838–3848 (1997).

227. Linton, P.-J. *et al.* Costimulation via OX40L expressed by B cells is sufficient to determine the extent of primary CD4 cell expansion and Th2 cytokine secretion in vivo. *J. Exp. Med.* **197**, 875–883 (2003).

228. Karulf, M., Kelly, A., Weinberg, A. D. & Gold, J. A. OX40L Regulates Inflammation and Mortality in the Innate Immune Response to Sepsis. *J. Immunol. Baltim. Md 1950* **185**, 4856–4862 (2010).

229. Maxwell, J. R. *et al.* IL-18 bridges innate and adaptive immunity through IFN-gamma and the CD134 pathway. *J. Immunol. Baltim. Md 1950* **177**, 234–245 (2006).

230. Zingoni, A. *et al.* Cross-talk between activated human NK cells and CD4+ T cells via OX40-OX40 ligand interactions. *J. Immunol. Baltim. Md 1950* **173**, 3716–3724 (2004).

231. Kashiwakura, J., Yokoi, H., Saito, H. & Okayama, Y. T cell proliferation by direct cross-

talk between OX40 ligand on human mast cells and OX40 on human T cells: comparison of gene expression profiles between human tonsillar and lung-cultured mast cells. *J. Immunol. Baltim. Md 1950* **173**, 5247–5257 (2004).

232. Krimmer, D. I. *et al.* CD40 and OX40 ligand are differentially regulated on asthmatic airway smooth muscle. *Allergy* **64**, 1074–1082 (2009).

233. Imura, A. *et al.* The human OX40/gp34 system directly mediates adhesion of activated T cells to vascular endothelial cells. *J. Exp. Med.* **183**, 2185–2195 (1996).

234. Takasawa, N. *et al.* Expression of gp34 (OX40 Ligand) and OX40 on Human T Cell Clones. *Jpn. J. Cancer Res. Gann* **92**, 377–382 (2001).

235. Soroosh, P., Ine, S., Sugamura, K. & Ishii, N. OX40-OX40 ligand interaction through T cell-T cell contact contributes to CD4 T cell longevity. *J. Immunol. Baltim. Md 1950* **176**, 5975–5987 (2006).

236. Mendel, I. & Shevach, E. M. Activated T cells express the OX40 ligand: requirements for induction and costimulatory function. *Immunology* **117**, 196–204 (2006).

237. Webb, G. J., Hirschfield, G. M. & Lane, P. J. L. OX40, OX40L and Autoimmunity: a Comprehensive Review. *Clin. Rev. Allergy Immunol.* **50**, 312–332 (2016).

238. Dannull, J. *et al.* Enhancing the immunostimulatory function of dendritic cells by transfection with mRNA encoding OX40 ligand. *Blood* **105**, 3206–3213 (2005).

239. Gramaglia, I. *et al.* The OX40 Costimulatory Receptor Determines the Development of CD4 Memory by Regulating Primary Clonal Expansion. *J. Immunol.* **165**, 3043–3050 (2000).

240. Salek-Ardakani, S. *et al.* OX40 (CD134) Controls Memory T Helper 2 Cells that Drive Lung Inflammation. *J. Exp. Med.* **198**, 315–324 (2003).

241. Obermeier, F. *et al.* OX40/OX40L interaction induces the expression of CXCR5 and contributes to chronic colitis induced by dextran sulfate sodium in mice. *Eur. J. Immunol.* **33**, 3265–3274 (2003).

242. Jourdan, P. *et al.* Cytokines and cell surface molecules independently induce CXCR4 expression on CD4+ CCR7+ human memory T cells. *J. Immunol. Baltim. Md 1950* **165**, 716–724 (2000).

243. Kotani, A., Hori, T., Matsumura, Y. & Uchiyama, T. Signaling of gp34 (OX40 ligand) induces vascular endothelial cells to produce a CC chemokine RANTES/CCL5. *Immunol. Lett.* **84**, 1–7 (2002).

244. Stüber, E., Neurath, M., Calderhead, D., Fell, H. P. & Strober, W. Cross-linking of OX40 ligand, a member of the TNF/NGF cytokine family, induces proliferation and differentiation in murine splenic B cells. *Immunity* **2**, 507–521 (1995).

245. Stüber, E. & Strober, W. The T cell-B cell interaction via OX40-OX40L is necessary for the T cell-dependent humoral immune response. *J. Exp. Med.* **183**, 979–989 (1996).

246. Ohshima, Y. *et al.* OX40 costimulation enhances interleukin-4 (IL-4) expression at priming and promotes the differentiation of naive human CD4(+) T cells into high IL-4-producing effectors. *Blood* **92**, 3338–3345 (1998).

247. Akiba, H. *et al.* Critical Contribution of Ox40 Ligand to T Helper Cell Type 2 Differentiation in Experimental Leishmaniasis. *J. Exp. Med.* **191**, 375–380 (2000).

248. So, T., Song, J., Sugie, K., Altman, A. & Croft, M. Signals from OX40 regulate nuclear factor of activated T cells c1 and T cell helper 2 lineage commitment. *Proc. Natl. Acad. Sci. U. S. A.* **103**, 3740–3745 (2006).

249. Murata, K. *et al.* Impairment of antigen-presenting cell function in mice lacking expression of OX40 ligand. *J. Exp. Med.* **191**, 365–374 (2000).

250. Jember, A. G.-H., Zuberi, R., Liu, F.-T. & Croft, M. Development of Allergic Inflammation in a Murine Model of Asthma Is Dependent on the Costimulatory Receptor Ox40. *J. Exp. Med.* **193**, 387–392 (2001).

251. Inagaki-Katashiba, N. *et al.* Statins can suppress DC-mediated Th2 responses through the repression of OX40-ligand and CCL17 expression. *Eur. J. Immunol.* **49**, 2051–2062 (2019).

252. Weinberg, A. D. *et al.* Selective depletion of myelin-reactive T cells with the anti-OX-40 antibody ameliorates autoimmune encephalomyelitis. *Nat. Med.* **2**, 183–189 (1996).

253. Ndhlovu, L. C., Ishii, N., Murata, K., Sato, T. & Sugamura, K. Critical involvement of OX40 ligand signals in the T cell priming events during experimental autoimmune encephalomyelitis. *J. Immunol. Baltim. Md 1950* **167**, 2991–2999 (2001).

254. Yoshioka, T. *et al.* Contribution of OX40/OX40 ligand interaction to the pathogenesis of rheumatoid arthritis. *Eur. J. Immunol.* **30**, 2815–2823 (2000).

255. Nakae, S. *et al.* IL-17 production from activated T cells is required for the spontaneous development of destructive arthritis in mice deficient in IL-1 receptor antagonist. *Proc. Natl. Acad. Sci. U. S. A.* **100**, 5986–5990 (2003).

256. Zhang, Z. *et al.* Activation of OX40 Augments Th17 Cytokine Expression and Antigen-Specific Uveitis. *Am. J. Pathol.* **177**, 2912–2920 (2010).

257. Xin, L. *et al.* Commensal microbes drive intestinal inflammation by IL-17–producing CD4+ T cells through ICOSL and OX40L costimulation in the absence of B7-1 and B7-2. *Proc. Natl. Acad. Sci. U. S. A.* **111**, 10672–10677 (2014).

258. Remedios, K. A. *et al.* The TNFRSF members CD27 and OX40 coordinately limit TH17 differentiation in regulatory T cells. *Sci. Immunol.* **3**, (2018).

259. Jorn Bovenschen, H. *et al.* Foxp3+ Regulatory T Cells of Psoriasis Patients Easily Differentiate into IL-17A-Producing Cells and Are Found in Lesional Skin. *J. Invest. Dermatol.* **131**, 1853–1860 (2011).

260. Hovhannisyan, Z., Treatman, J., Littman, D. R. & Mayer, L. Characterization of Interleukin-17–Producing Regulatory T Cells in Inflamed Intestinal Mucosa From Patients With Inflammatory Bowel Diseases. *Gastroenterology* **140**, 957–965 (2011).

261. Xiao, X. *et al.* The costimulatory receptor OX40 inhibits interleukin-17 expression through activation of repressive chromatin remodeling pathways. *Immunity* **44**, 1271–1283 (2016).

262. Li, J. *et al.* Negative regulation of IL-17 production by OX40/OX40L interaction. *Cell. Immunol.* **253**, 31–37 (2008).

263. Xiao, X. *et al.* OX40 signaling favors the induction of TH9 cells and airway inflammation. *Nat. Immunol.* **13**, 981–990 (2012).

264. Zhao, Y. *et al.* Dectin-1-activated dendritic cells trigger potent antitumour immunity through the induction of Th9 cells. *Nat. Commun.* **7**, (2016).

265. Flynn, S., Toellner, K.-M., Raykundalia, C., Goodall, M. & Lane, P. CD4 T Cell Cytokine Differentiation: The B Cell Activation Molecule, OX40 Ligand, Instructs CD4 T Cells to Express

Interleukin 4 and Upregulates Expression of the Chemokine Receptor, Blr-1. *J. Exp. Med.* **188**, 297–304 (1998).

266. Vogel, K. U. *et al.* Roquin Paralogs 1 and 2 Redundantly Repress the Icos and Ox40 Costimulator mRNAs and Control Follicular Helper T Cell Differentiation. *Immunity* **38**, 655–668 (2013).

267. Tahiliani, V., Hutchinson, T. E., Abboud, G., Croft, M. & Salek-Ardakani, S. OX40 Cooperates with ICOS to Amplify Follicular T Helper Cell Development and Germinal Center Reactions During Infection. *J. Immunol. Baltim. Md 1950* **198**, 218–228 (2017).

268. Boettler, T. *et al.* OX40 Facilitates Control of a Persistent Virus Infection. *PLoS Pathog.* **8**, (2012).

269. Boettler, T. *et al.* Exogenous OX40 Stimulation during Lymphocytic Choriomeningitis Virus Infection Impairs Follicular Th Cell Differentiation and Diverts CD4 T Cells into the Effector Lineage by Upregulating Blimp-1. *J. Immunol.* **191**, 5026–5035 (2013).

270. Marriott, C. L. *et al.* OX40 controls effector CD4+ T-cell expansion, not follicular T helper cell generation in acute Listeria infection. *Eur. J. Immunol.* **44**, 2437–2447 (2014).

271. Akiba, H. *et al.* The Role of ICOS in the CXCR5+ Follicular B Helper T Cell Maintenance In Vivo. *J. Immunol.* **175**, 2340–2348 (2005).

272. Montler, R. *et al.* OX40, PD-1 and CTLA-4 are selectively expressed on tumor-infiltrating T cells in head and neck cancer. *Clin. Transl. Immunol.* **5**, e70 (2016).

273. Valzasina, B. *et al.* Triggering of OX40 (CD134) on CD4+CD25+ T cells blocks their inhibitory activity: a novel regulatory role for OX40 and its comparison with GITR. *Blood* **105**, 2845–2851 (2005).

274. Vu, M. D. *et al.* OX40 costimulation turns off Foxp3+ Tregs. *Blood* **110**, 2501–2510 (2007).

275. So, T. & Croft, M. Cutting edge: OX40 inhibits TGF-beta- and antigen-driven conversion of naive CD4 T cells into CD25+Foxp3+ T cells. *J. Immunol. Baltim. Md 1950* **179**, 1427–1430 (2007).

276. Kitamura, N. *et al.* OX40 costimulation can abrogate Foxp3+ regulatory T cell-mediated suppression of antitumor immunity. *Int. J. Cancer J. Int. Cancer* **125**, 630–638 (2009).

277. Zhang, X. *et al.* OX40 Costimulation Inhibits Foxp3 Expression and Treg Induction via BATF3-Dependent and Independent Mechanisms. *Cell Rep.* **24**, 607–618 (2018).

278. Ito, T. *et al.* OX40 ligand shuts down IL-10-producing regulatory T cells. *Proc. Natl. Acad. Sci. U. S. A.* **103**, 13138–13143 (2006).

279. Voo, K. S. *et al.* Antibodies targeting human OX40 expand effector T cells and block inducible and natural regulatory T cell function. *J. Immunol. Baltim. Md 1950* **191**, (2013).

280. Griseri, T., Asquith, M., Thompson, C. & Powrie, F. OX40 is required for regulatory T cell–mediated control of colitis. *J. Exp. Med.* **207**, 699–709 (2010).

281. Polesso, F., Sarker, M., Weinberg, A. D., Murray, S. E. & Moran, A. E. OX40 Agonist Tumor Immunotherapy Does Not Impact Regulatory T Cell Suppressive Function. *J. Immunol.* **203**, 2011–2019 (2019).

282. Takeda, I. *et al.* Distinct Roles for the OX40-OX40 Ligand Interaction in Regulatory and Nonregulatory T Cells. *J. Immunol.* **172**, 3580–3589 (2004).

283. Ruby, C. E. *et al.* OX40 Agonists can drive Treg expansion if the cytokine milieu is right. *J. Immunol. Baltim. Md 1950* **183**, 4853–4857 (2009).

284. Byun, M. *et al.* Inherited human OX40 deficiency underlying classic Kaposi sarcoma of childhood. *J. Exp. Med.* **210**, 1743–1759 (2013).

285. Curti, B. D. *et al.* OX40 Is a Potent Immune-Stimulating Target in Late-Stage Cancer Patients. *Cancer Res.* **73**, 7189–7198 (2013).

286. Bell, R. B. *et al.* Neoadjuvant anti-OX40 (MEDI6469) prior to surgery in head and neck squamous cell carcinoma. *J. Clin. Oncol.* **36**, 6011–6011 (2018).

287. Fromm, G. *et al.* Agonist redirected checkpoint, PD1-Fc-OX40L, for cancer immunotherapy. *J. Immunother. Cancer* **6**, (2018).

288. Bidad, K., Nicknam, M. H. & Farid, R. A review of allergy and allergen specific immunotherapy. *Iran. J. Allergy Asthma Immunol.* **10**, 1–9 (2011).

289. Singh, V. K., Mehrotra, S. & Agarwal, S. S. The paradigm of Th1 and Th2 cytokines: its relevance to autoimmunity and allergy. *Immunol. Res.* **20**, 147–161 (1999).

290. Kubo, M. T follicular helper and TH2 cells in allergic responses. *Allergol. Int.* **66**, 377–381 (2017).

291. Ilves, T. & Harvima, I. T. OX40 ligand and OX40 are increased in atopic dermatitis lesions but do not correlate with clinical severity. *J. Eur. Acad. Dermatol. Venereol.* **27**, e197–e205 (2013).

292. Guttman-Yassky, E. *et al.* GBR 830, an anti-OX40, improves skin gene signatures and clinical scores in patients with atopic dermatitis. *J. Allergy Clin. Immunol.* **144**, 482-493.e7 (2019).

293. Gauvreau, G. M. *et al.* OX40L blockade and allergen-induced airway responses in subjects with mild asthma. *Clin. Exp. Allergy* **44**, 29–37 (2014).

294. Davidson, A. & Diamond, B. Autoimmune Diseases. *N. Engl. J. Med.* **345**, 340–350 (2001).

295. Mahmood, T. & Yang, P.-C. OX40L-OX40 Interactions: A Possible Target for Gastrointestinal Autoimmune Diseases. *North Am. J. Med. Sci.* **4**, 533–536 (2012).

296. Higgins, L. M. *et al.* Regulation of T cell activation in vitro and in vivo by targeting the OX40-OX40 ligand interaction: amelioration of ongoing inflammatory bowel disease with an OX40-IgG fusion protein, but not with an OX40 ligand-IgG fusion protein. *J. Immunol. Baltim. Md 1950* **162**, 486–493 (1999).

297. Totsuka, T. *et al.* Therapeutic effect of anti-OX40L and anti-TNF-alpha MAbs in a murine model of chronic colitis. *Am. J. Physiol. Gastrointest. Liver Physiol.* **284**, G595-603 (2003).

298. Souza, H. S., Elia, C. C., Spencer, J. & MacDonald, T. T. Expression of lymphocyte-endothelial receptor-ligand pairs, alpha4beta7/MAdCAM-1 and OX40/OX40 ligand in the colon and jejunum of patients with inflammatory bowel disease. *Gut* **45**, 856–863 (1999).

299. Stüber, E. *et al.* The expression of OX40 in immunologically mediated diseases of the gastrointestinal tract (celiac disease, Crohn's disease, ulcerative colitis). *Eur. J. Clin. Invest.* **30**, 594–599 (2000).

300. Eguchi, Y., Bilolikar, G. & Geiler-Samerotte, K. Why and how to study genetic changes with context-dependent effects. *Curr. Opin. Genet. Dev.* **58–59**, 95–102 (2019).

301. Jackson, E. K., Mi, Z., Tofovic, S. P. & Gillespie, D. G. Effect of dipeptidyl peptidase 4 inhibition on arterial blood pressure is context dependent. *Hypertens. Dallas Tex 1979* **65**, 238–249 (2015).

302. Post, R. M., Lockfeld, A., Squillace, K. M. & Contel, N. R. Drug-environment interaction: context dependency of cocaine-induced behavioral sensitization. *Life Sci.* **28**, 755–760 (1981).

303. Killen, S. S., Adriaenssens, B., Marras, S., Claireaux, G. & Cooke, S. J. Context dependency of trait repeatability and its relevance for management and conservation of fish populations. *Conserv. Physiol.* **4**, cow007 (2016).

304. Perring, M. P. *et al.* Understanding context dependency in the response of forest understorey plant communities to nitrogen deposition. *Environ. Pollut. Barking Essex 1987* **242**, 1787–1799 (2018).

305. Tymula, A. & Plassmann, H. Context-dependency in valuation. *Curr. Opin. Neurobiol.* **40**, 59–65 (2016).

306. Harrison, R., Papp, B., Pál, C., Oliver, S. G. & Delneri, D. Plasticity of genetic interactions in metabolic networks of yeast. *Proc. Natl. Acad. Sci. U. S. A.* **104**, 2307–2312 (2007).

307. Cano-Gamez, E. *et al.* Single-cell transcriptomics identifies an effectorness gradient shaping the response of CD4+ T cells to cytokines. *Nat. Commun.* **11**, (2020).

308. Zhou, H., Sehl, M. E., Sinsheimer, J. S. & Lange, K. Association screening of common and rare genetic variants by penalized regression. *Bioinforma. Oxf. Engl.* **26**, 2375–2382 (2010).

309. Fontanarosa, J. B. & Dai, Y. Using LASSO regression to detect predictive aggregate effects in genetic studies. *BMC Proc.* **5**, S69 (2011).

310. Ott, P. A., Hodi, F. S., Kaufman, H. L., Wigginton, J. M. & Wolchok, J. D. Combination immunotherapy: a road map. *J. Immunother. Cancer* **5**, 16 (2017).

311. Michea, P. *et al.* Adjustment of dendritic cells to the breast-cancer microenvironment is subset specific. *Nat. Immunol.* **19**, 885–897 (2018).

312. Dudek, A. M., Martin, S., Garg, A. D. & Agostinis, P. Immature, Semi-Mature, and Fully Mature Dendritic Cells: Toward a DC-Cancer Cells Interface That Augments Anticancer Immunity. *Front. Immunol.* **4**, 438 (2013).

313. Jenkins, R. W. *et al.* Ex Vivo Profiling of PD-1 Blockade Using Organotypic Tumor Spheroids. *Cancer Discov.* **8**, 196–215 (2018).

314. Neal, J. T. *et al.* Organoid modeling of the tumor immune microenvironment. *Cell* **175**,

1972-1988.e16 (2018).

315. Scognamiglio, G. *et al.* Patient-derived organoids as a potential model to predict response to PD-1/PD-L1 checkpoint inhibitors. *Br. J. Cancer* **121**, 979–982 (2019).

316. Francies, H. E. & Garnett, M. J. What role could organoids play in the personalization of cancer treatment? *Pharmacogenomics* **16**, 1523–1526 (2015).

317. Benien, P. & Swami, A. 3D tumor models: history, advances and future perspectives. *Future Oncol. Lond. Engl.* **10**, 1311–1327 (2014).

318. Saitakis, M. *et al.* Different TCR-induced T lymphocyte responses are potentiated by stiffness with variable sensitivity. *eLife* **6**,.

319. Granot, T. *et al.* Dendritic cells display subset and tissue-specific maturation dynamics over human life. *Immunity* **46**, 504–515 (2017).

320. Vis, M. A. M., Ito, K. & Hofmann, S. Impact of Culture Medium on Cellular Interactions in in vitro Co-culture Systems. *Front. Bioeng. Biotechnol.* **8**, (2020).

321. Brodin, P. & Davis, M. M. Human immune system variation. *Nat. Rev. Immunol.* **17**, 21–29 (2017).

322. De Jager, P. L. *et al.* ImmVar project: Insights and design considerations for future studies of 'healthy' immune variation. *Semin. Immunol.* **27**, 51–57 (2015).

323. Simon, A. K., Hollander, G. A. & McMichael, A. Evolution of the immune system in humans from infancy to old age. *Proc. Biol. Sci.* **282**, 20143085 (2015).

324. Patin, E. *et al.* Natural variation in the parameters of innate immune cells is preferentially driven by genetic factors. *Nat. Immunol.* **19**, 302–314 (2018).

325. Akimzhanov, A. M., Yang, X. O. & Dong, C. Chromatin Remodeling of Interleukin-17 (IL-17)-IL-17F Cytokine Gene Locus during Inflammatory Helper T Cell Differentiation. *J. Biol. Chem.* **282**, 5969–5972 (2007).

326. Rauen, T., Hedrich, C. M., Juang, Y.-T., Tenbrock, K. & Tsokos, G. C. cAMP-responsive element modulator (CREM)α protein induces interleukin 17A expression and mediates epigenetic alterations at the interleukin-17A gene locus in patients with systemic lupus erythematosus. *J. Biol. Chem.* **286**, 43437–43446 (2011).

327. Hedrich, C. M., Rauen, T., Kis-Toth, K., Kyttaris, V. C. & Tsokos, G. C. cAMP-responsive element modulator α (CREMα) suppresses IL-17F protein expression in T lymphocytes from patients with systemic lupus erythematosus (SLE). *J. Biol. Chem.* **287**, 4715–4725 (2012).

328. Adamik, J. *et al.* The IL17A and IL17F loci have divergent histone modifications and are differentially regulated by prostaglandin E2 in Th17 cells. *Cytokine* **64**, 404–412 (2013).

329. Ishigame, H. *et al.* Differential roles of interleukin-17A and -17F in host defense against mucoepithelial bacterial infection and allergic responses. *Immunity* **30**, 108–119 (2009).

330. Tong, Z. *et al.* A Protective Role by Interleukin-17F in Colon Tumorigenesis. *PLoS ONE* **7**, (2012).

331. Sarkar, S. *et al.* Interleukin (IL)-17A, F and AF in inflammation: a study in collagen-induced arthritis and rheumatoid arthritis. *Clin. Exp. Immunol.* **177**, 652–661 (2014).

332. Tang, C. *et al.* Suppression of IL-17F, but not of IL-17A, provides protection against colitis by inducing T reg cells through modification of the intestinal microbiota. *Nat. Immunol.* **19**, 755–765 (2018).

333. Shiomi, A. & Usui, T. Pivotal Roles of GM-CSF in Autoimmunity and Inflammation. *Mediators Inflamm.* **2015**, (2015).

334. Akamatsu, T. *et al.* Human TSLP directly enhances expansion of CD8+ T cells. *Clin. Exp. Immunol.* **154**, 98–106 (2008).

335. Wei, L., Laurence, A., Elias, K. M. & O'Shea, J. J. IL-21 is produced by Th17 cells and drives IL-17 production in a STAT3-dependent manner. *J. Biol. Chem.* **282**, 34605–34610 (2007).

336. Kunnath-Velayudhan, S. *et al.* Generation of IL-3–Secreting CD4+ T Cells by Microbial Challenge at Skin and Mucosal Barriers. *ImmunoHorizons* **3**, 161–171 (2019).

337. Sheng, W. *et al.* STAT5 programs a distinct subset of GM-CSF-producing T helper cells that is essential for autoimmune neuroinflammation. *Cell Res.* **24**, 1387–1402 (2014).

338. Kosti, I., Jain, N., Aran, D., Butte, A. J. & Sirota, M. Cross-tissue Analysis of Gene and Protein Expression in Normal and Cancer Tissues. *Sci. Rep.* **6**, (2016).

339. Vogel, C. & Marcotte, E. M. Insights into the regulation of protein abundance from proteomic and transcriptomic analyses. *Nat. Rev. Genet.* **13**, 227–232 (2012).

340. Wong, M. T. *et al.* A High-Dimensional Atlas of Human T Cell Diversity Reveals Tissue-Specific Trafficking and Cytokine Signatures. *Immunity* **45**, 442–456 (2016).

341. Akondy, R. S. *et al.* Origin and differentiation of human memory CD8 T cells after vaccination. *Nature* **552**, 362–367 (2017).

342. Wieland, D. *et al.* TCF1+ hepatitis C virus-specific CD8+ T cells are maintained after cessation of chronic antigen stimulation. *Nat. Commun.* **8**, (2017).

343. Dong, S. *et al.* Multiparameter single-cell profiling of human CD4+FOXP3+ regulatory T-cell populations in homeostatic conditions and during graft-versus-host disease. *Blood* **122**, 1802–1812 (2013).

344. Morita, R. *et al.* Human blood CXCR5(+)CD4(+) T cells are counterparts of T follicular cells and contain specific subsets that differentially support antibody secretion. *Immunity* **34**, 108–121 (2011).

345. Gowthaman, U. *et al.* Identification of a T follicular helper cell subset that drives anaphylactic IgE. *Science* **365**, (2019).

346. Ando, D. G., Clayton, J., Kono, D., Urban, J. L. & Sercarz, E. E. Encephalitogenic T cells in the B10.PL model of experimental allergic encephalomyelitis (EAE) are of the Th-1 lymphokine subtype. *Cell. Immunol.* **124**, 132–143 (1989).

347. Segal, B. M. & Shevach, E. M. IL-12 unmasks latent autoimmune disease in resistant mice. *J. Exp. Med.* **184**, 771–775 (1996).

348. Panitch, H. S., Hirsch, R. L., Haley, A. S. & Johnson, K. P. Exacerbations of multiple sclerosis in patients treated with gamma interferon. *Lancet Lond. Engl.* **1**, 893–895 (1987).

349. Racke, M. K. *et al.* Cytokine-induced immune deviation as a therapy for inflammatory autoimmune disease. *J. Exp. Med.* **180**, 1961–1966 (1994).

350. Racke, M. K. *et al.* Retinoid treatment of experimental allergic encephalomyelitis. IL-4 production correlates with improved disease course. *J. Immunol. Baltim. Md 1950* **154**, 450–458 (1995).

351. Gran, B. *et al.* Early administration of IL-12 suppresses EAE through induction of interferon-gamma. *J. Neuroimmunol.* **156**, 123–131 (2004).

352. Volpe, E., Battistini, L. & Borsellino, G. Advances in T Helper 17 Cell Biology: Pathogenic Role and Potential Therapy in Multiple Sclerosis. *Mediators Inflamm.* **2015**, 475158 (2015).

université PARIS-SACLAY

ECOLE DOCTORALE N°581
Agriculture, alimentation, biologie, environnement et santé (ABIES)

Titre : Étude systématique de la fonction contexte-dépendante de OX40 Ligand sur la polarisation des lymphocytes T auxiliaires humains

Mots clés : Contexte-dépendance, OX40 Ligand, lymphocytes T auxiliaires, modèles statistiques, cytokines, cellules dendritiques

Résumé : L'immunité adaptative est principalement orchestrée par des lymphocytes T CD4 auxiliaires. Ils ont la capacité de se polariser en plusieurs sous-populations, chacune associée à un phénotype approprié au pathogène rencontré. L'activation des lymphocytes T auxiliaires peut être régulée par des checkpoints immunitaires co-stimulateurs, tel que OX40 Ligand, ou co-inhibiteurs. Ces molécules ont été étudiées individuellement, dans des conditions spécifiques. Cependant, la contexte-dépendance pourrait expliquer une grande partie de la variabilité fonctionnelle des biomolécules. Il n'y a actuellement aucune méthode permettant d'analyser et de quantifier la contexte-dépendance d'une molécule dans plusieurs contextes et sur une réponse donnée. Mon projet de thèse a porté sur la fonction de OX40L sur la polarisation des cellules T auxiliaires, dans 4 contextes moléculaires et 11 cellulaires. Nous avons mesuré 17 cytokines T auxiliaires et développé une stratégie de modélisation statistique pour quantifier la contexte-dépendance deOX40L. Les scores de contexte-dépendance se sont révélés très variables qualitativement et quantitativement, en fonction de la cytokine et du type de contexte. Parmi les contextes Th, Th2 était le plus influent sur la fonction OX40L. Parmi les contextes DC, le type de cellules dendritique était dominant dans le contrôle de la contexte-dépendance de OX40L plutôt que le stimuli d'activation. Mon travail de thèse dévoile les complexes déterminants de la fonction de OX40L, fournit une méthode unique pour quantifier la variabilité fonctionnelle contexte-dépendante de n'importe quelle biomolécule et appuie sur le fait que la contexte-dépendance devrait être davantage prise en considération dans les études futures.

Title: Systematic study of OX40 Ligand context-dependent function on T helper cell polarization

Keywords: Context-dependency, OX40 Ligand, T helper cells, statistical modeling, cytokines, dendritic cells

Abstract: Adaptive immunity is mainly orchestrated by CD4 T helper cells. They have the ability to polarize in several subsets, each associated to a suitable phenotype for the encounter pathogen. T helper cell activation can be regulated by co-stimulator, such as OX40 Ligand, or co-inhibitor immune checkpoint molecules. These molecules have been studied individually, in specific conditions. However, context-dependency may explain large parts of the functional variability of biological molecules on a given output. Currently, there is no framework to analyze and quantify context-dependency of a molecule over multiple contexts and response outputs. My PhD project focused on OX40L function on T helper cell polarization, in 4 molecular and 11 cellular contexts. We measured 17 T helper cytokines and developed a statistical modeling strategy to quantify OX40L context-dependency on these cytokines. This revealed highly variable qualitative and quantitative context-dependency scores, depending on the output cytokine and context type. Among molecular contexts, Th2 was the most influential on OX40L function. Among cellular contexts, dendritic cell type rather than activating stimuli was dominant in controlling OX40L context-dependency. My thesis work unveils the complex determinants of OX40L function, provides a unique framework to quantify the context-dependent functional variability of any biomolecule, and supports that context-dependency should be more taken into consideration in future studies.

Université Paris-Saclay
Espace Technologique / Immeuble Discovery
Route de l'Orme aux Merisiers RD 128 / 91190 Saint-Aubin, France